ACHIEVING SPECIFICITY IN REDOX SIGNALING AND REDOX REGULATION OF PROTEIN FUNCTION

LOES VAN DAM

Achieving Specificity in Redox Signaling and Redox Regulation of Protein Function

Specificiteit in Redox-Signaaltransductie en Redoxregulatie van Eiwitfunctie

(met een samenvatting in het Nederlands)

Proefschrift

ter verkrijging van de graad van doctor aan de
Universiteit Utrecht
op gezag van de
rector magnificus, prof.dr. H.R.B.M. Kummeling,
ingevolge het besluit van het college voor promoties
in het openbaar te verdedigen op

donderdag 21 april 2022 des middags te 4.15 uur

door

Loes van Dam

geboren op 23 maart 1989
te Rotterdam

Promotor:

Prof. dr. B.M.T. Burgering

Copromotor:

Dr. T.B. Dansen

TABLE OF CONTENTS

ABBREVIATIONS

ΔC	cysteine-free mutant
-CH_2	methylene group
-S-S-	disulfide
-SOH	sulfenic acid
$^1O_2$	singlet oxygen
Å	ångström
ABC	ammonium bicarbonate
AβPP	amyloid-β protein precursor
ALS	amyotrophic lateral sclerosis
ANXA2	annexin A2
APR	aggregation prone region
ASK1	apoptosis signal-regulating kinase 1
BME, β-ME	β-mercaptoethanol
C, Cys	cysteine
CAA	chloroacetamide
CCNE	gene encoding cyclin E
CD	circular dichroism
CDKN2A	gene encoding $p16^{INK4A}$
C-SO_2H/C-SO_3H	hyperoxidized cysteine (cysteine sulfinic acid and cysteine sulfonic acid, respectively)
CDK4	cyclin-dependent kinase 4
C_P	peroxidatic cysteine
C_R	resolving cysteine
DAO, DAAO	D-amino acid oxidase
DKO21	double knockout cells for PRDX1 and PRDX2
dox	doxycyclin
DUOX	dual oxidase
DTT	dithiothreitol
ECAR	extracellular acidification rate
eNOS	endothelial nitric oxide synthase
ER	endoplasmic reticulum
ETC	electron transport chain
FDR	false discovery rate
Fe-S cluster	iron-sulphur cluster
GPX	glutathione peroxidase
Grx	glutaredoxin
GR	glutathione reductase
GSSG	oxidized glutathione
GSH	glutathione
H_2O_2	hydrogen peroxide
HA-	hemagglutinin
HAT1	histone acetyltransferase 1
HCO_4^-	peroxymonocarbonate
HMW	high molecular weight

HO•	hydroxyl radical
HOCl	hypochlorous acid
HPS	heat-shock protein
HSQC	heteronuclear single quantum coherence
IA	iodoacetamide
iBAQ	nitensity based absolute quantification
IDR	intrinsically disordered region
IP	immunoprecipitation
iNOS	inducible nitric oxide synthase
kDa	kilodalton
LEE011	ribociclib
LFQ	label-free quantification
LMCA	last mammalian common ancestor
LVCA	last vertebrate common ancestor
M	methionine
MD	molecular dynamics
MW	molecular weight
NAD	nicotinamide adenine dinucleotide
NADH	reduced form of nicotinamide adenine dinucleotide
NADP	nicotinamide adenine dinucleotide phosphate
NADPH	reduced form of nicotinamide adenine dinucleotide phosphate
NMDAR	N-methyl-D-aspartate receptor
NMR	nuclear magnetic resonance
nNOS	neuronal nitric oxide synthase
NOX	NADPH oxidase
$O_2^{\bullet-}$	superoxide
$^1O_2$	singlet molecular oxygen
O_3	ozone
OA	okadaic acid
OCR	oxygen consumption rate
$ONOO^-$	peroxinitrite
Orp1	yeast oxidant receptor peroxidase-1
OXPHOS	oxidative phosphorylation
PDI	protein disulfide isomerase
pK_a	dissociation constant
PP2A	serine-threonine phosphatase 2A
PPP	pentose-phosphate-pathway
PRDX	peroxiredoxin
PTEN	phosphatase and tensin homologue
PTM	post-translational modification
PTP	protein tyrosine phosphatase
R•	carbon-centered radicals
RAC1	Ras-related C3 botulinum toxin substrate 1

Rb	retinoblastoma
RO•	alkoxyl radical
ROO•	peroxyl radicals
ROOH	hydroperoxide
ROS	reactive oxygen species
RT	room temperature
S, Ser	serine
SAXS	small-angle x-ray scattering
SEC	size exclusion chromatography
Sit4	serine/threonine-protein phosphatase PP1-1
SOD	superoxide dismutase
SOD1	Cu,Zn-superoxide dismutase
S-GSHylated	S-glutathionylated
S-PRDXylation	S-peroxiredoxinylation
STAT3	signal transducer and activator of transcription 3
T, Thr	threonine
Tap42	type 2a phosphatase-associated protein 42, yeast homolog of α4
ThT	thioflavin T
TIGAR	TP53-inducible glycolysis and apoptosis regulator
Tip41	tap42-interacting protein of 41 kDa, yeast homolog of TIPRL
TIPRL	TOR signaling pathway regulator-like
TNPO1	transportin 1
TOR	target of rapamycin
TR	thioredoxin reductase
TRX	thioredoxin
Tsa2	thiol-specific antioxidant protein 2
UPR	unfolded protein response
UPS	ubiquitin-proteasome system
WB	western blotting
WT	wild-type

CHAPTER 1

GENERAL INTRODUCTION

GENERAL INTRODUCTION

The human body is composed of an estimated 38 trillion cells, with extremely diverse morphologies and functions [1]. To maintain integrity, organisms need to perform many different functions, carried out and coordinated by many cell types. These tasks are extraordinarily complex and diverse, ranging from growth and development, reproduction, food digestion, movement, to defense against pathogens, detoxification and even consciousness. Specialized cells like muscle-, epithelial-, germ-, bone-, liver-, neuronal cells and lymphocytes require organization primarily based on proteins to carry out their functions. Some organismal tasks can be carried out by a single cell type, but it normally requires the combined effort of several cell types acting in a coordinated manner.

On top of these diverse intrinsic functions of cells, they are subject to constant changes in the internal and external environment. Organisms and cells are viable under a set of relatively narrow conditions. Therefore, organisms continuously employ regulatory mechanisms to maintain a steady state despite changes in the environment – also known as 'homeostasis'. To maintain homeostasis, cells harness molecular mechanisms for the sensing and transduction of signals that allows them to respond to changes and allow communication between and within cells. The failure to maintain homeostasis can result in a disruption of cellular behavior and contributes to the development of diseases including cancer, neurodegenerative disease and diabetes [2].

Table 1.

ROS		Production	Radical or non-radical	Major target
Superoxide radical	$O_2^{\bullet-}$	Mitochondria (ETC) and membrane (NOXs)	Radical	Fe-S clusters, NO•, lipids
Hydrogen peroxide	H_2O_2	Superoxide ($O_2^{\bullet-}$) dismutation, enzymatic generation	Non-radical	Thiols, highly reactive with peroxiredoxins, catalase, glutathione peroxidase
Hydroxyl radical	$HO^{\bullet}$	H_2O_2 reduction in Fe2+-catalyzed Fenton reactions	Radical	Any macromolecule
Peroxyl radical	$ROO^{\bullet}$	Attack of $HO^{\bullet}$ on methylene ($-CH_2$), lipid peroxidation chain reactions	Radical	Methylene groups ($-CH_2$)
Organic hydroperoxide	ROOH	Hydrogen abstraction from lipids by peroxyl radicals ($ROO^{\bullet}$)	Non-radical	Metal ions
Alkoxyl radical	$RO^{\bullet}$	Metal-catalyzed decomposition of hydroperoxides (ROOH)	Radical	Proteins, lipids, DNA
Singlet molecular oxygen	$^1O_2$	Photoexcitation of oxygen (O_2)	Non-radical	Proteins, lipids, DNA
Electronically excited carbonyls	$R\text{-}C{=}O^*$	Photo- or chemiexcitation of carbonyl groups (R-C=O)	Non-radical	
Ozone	O_3	Photoexcitation of oxygen (O_2) in the stratosphere, antibody-catalyzed reaction of singlet oxygen with water	Non-radical	Proteins, lipids, DNA
Hypochlorous acid	HOCl	Enzymatic generation by myeloperoxidase (MPO)	Non-radical	Proteins (cys), lipids, DNA, other ROS
Peroxymonocarbonate	HCO_4^-	H_2O_2 reaction with carbon dioxide	Non-radical	Cysteine, methionine

The reversible oxidation of protein thiols by reactive oxygen species (ROS) underlies a fundamental signaling mechanism called reduction-oxidation (redox) signaling. However, the role of ROS in cellular homeostasis is dual. At physiological levels, ROS (mostly in the form of H_2O_2) act as a second messengers for redox signaling by selectively and efficiently oxidizing specific thiols on specific signaling proteins [3]. Yet at excessive levels, ROS can react non-specifically with proteins, lipids and DNA, leading to molecular damage and cytotoxicity [4]. Our understanding of ROS has dramatically changed over the past decade(s). The traditional view was that ROS production was not regulated and that ROS reacts with cellular targets randomly. The damaging actions of ROS were recognized long before it became clear that redox signaling through the reversible oxidation of protein thiols is an important signaling mechanism. Redox-dependent signaling mechanisms as well as the cysteine residues involved are well conserved throughout evolution [3,5,6]. ROS are indisputably simple molecules, which raises questions on how an appropriate cellular response downstream of redox signaling can be achieved through the selective oxidation of cysteine residues in specific proteins and not in others.

A better understanding of redox regulation allows us to understand the mechanisms of redox signaling, the biological roles of oxidative regulation in cells, and how redox-regulated pathways and processes might be linked to diseases associated with oxidative stress. Here, we will briefly introduce cysteine chemistry and the two-faced nature of ROS and we will primarily focus on the role of physiological levels of ROS in redox signaling.

REACTIVE OXYGEN SPECIES

The term reactive oxygen species (ROS) describes a group of reactive molecules containing oxygen. Especially in the cell biology literature 'ROS' is often used as an umbrella term instead of specification of the exact chemical species involved. To understand how cells respond to ROS it is important to note that there are many types of ROS, with different (thiol) reactivities, differential susceptibility to scavenging by antioxidants, different steady state intracellular concentrations, and they can be strong or weak oxidants, radical or non-radical. Because of the diversity among reactive oxygen species, ROS is a term should be avoided whenever the specific species is known.

ROS production occurs mainly as a metabolic side product of oxidative phosphorylation (OXPHOS) in the mitochondrial electron transport chain (ETC) where 85-90% of O_2 is metabolized for ATP production. The three main types of cellular ROS (H_2O_2 superoxide and hydroxyl radicals) are produced in the ETC when electrons escape during the four successive reduction steps of molecular oxygen (**Figure 1A**). In general, the more reactive a ROS species is, the shorter its half-life and the higher its toxicity, and the lower its signaling capabilities. Among the different types of ROS (**Table 1**), hydrogen peroxide (H_2O_2) has been shown to act as a messenger relevant for signal transduction [3]. There is no evidence nor likelihood that any other ROS directly mediate redox signaling, as their reactivity would simply be too high to achieve target specificity rather than random oxidation [7].

There are three main species of cellular ROS: superoxide radical ($O_2^{\bullet-}$), hydrogen peroxide (H_2O_2) and hydroxyl radical ($HO^\bullet$) which are produced during the four successive steps of 1-electron reduction (**Figure 1A**). They can further react with organic compounds, thereby forming reactive 'secondary' species. ROS can further be divided into two-electron ROS (non-radicals) and one-electron radicals (highly unstable intermediates with one or more unpaired electrons, $^\bullet$). Although this is by no means a complete overview, it contains basic information of selected ROS types. A more comprehensive overview can be found in references [8,9].

A.

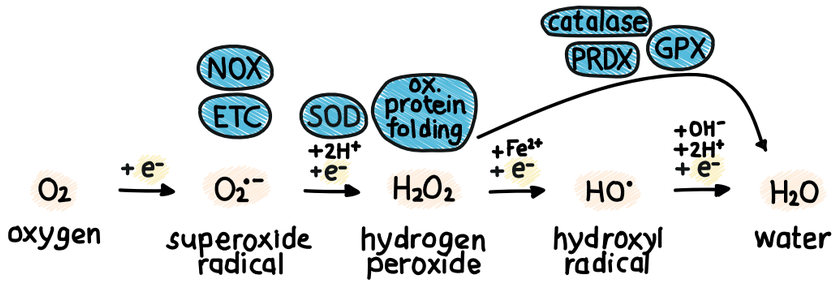

B.

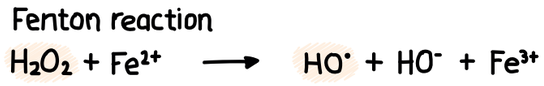

Figure 1. The chemical basis of ROS generation.
(**A**) ROS are produced from molecular oxygen, which undergoes 4 successive steps of 1-electron reduction. Enzymes or processes that can catalyze these reactions are indicated in blue. NOX: NADPH oxidase, ETC: electron transport chain, SOD: superoxide dismutase, ox. protein folding: oxidative protein folding, PRDX: peroxiredoxin, GPX: glutathione peroxidase. (**B**) H_2O_2 is converted into the highly reactive $HO^\bullet$ by the metal-catalyzed Fenton reactions.

Superoxide Anion Radical ($O_2^{\bullet-}$)

Superoxide ($O_2^{\bullet-}$) can be produced from O_2 from two main cellular sources; through leakage of electrons during mitochondrial respiration and from NADPH oxidases (NOXs) at the membrane. An estimated 1-3% of electrons escape the electron transport chain (ETC) prior to reduction of O_2 to water. The full conversion of O_2 to water involves a four-electron reduction (**Figure 1A**). However, O_2 can only react with one electron at a time a single leaking electron can thus react with O_2 to form $O_2^{\bullet-}$, which can then dismutate into H_2O_2 [8]. NOXs produce high levels of $O_2^{\bullet-}$ at the expense of NADPH, for instance during a 'respiratory burst' [10].

$O_2^{\bullet-}$ is much less reactive than $HO^\bullet$ and does not react with most biological molecules in solution. Its major target is iron-sulfur (Fe-S) clusters, thereby decomposing them and releasing free Fe^{2+} [11]. It also reacts with other radicals like nitric oxide ($NO^\bullet$), thereby forming the tyrosine-nitrating peroxynitrite ($ONOO^-$). $O_2^{\bullet-}$ has a relatively short lifetime (~50 ms) as it undergoes rapid spontaneous or superoxide dismutase (SOD)-catalyzed dismutation into O_2 and hydrogen peroxide (H_2O_2), which in turn may produce hydroxyl radical ($HO^\bullet$) [12]. As such, it is the precursor of many other types of ROS.

Hydrogen Peroxide (H_2O_2)

Hydrogen peroxide (H_2O_2) can be produced from spontaneous dismutation of superoxide ($O_2^{\bullet-}$), but also through enzymatic generation (for an overview see [13]). Enzymes that can produce cellular H_2O_2 include superoxide dismutase (SOD), NADPH oxidase 4 (NOX4) [14] and protein-disulfide isomerases (PDIs) and ERO1 during protein folding in the ER.

H_2O_2 has a relatively long lifetime of ~1 ms [12], and although it is a strong two-electron oxidant due to its high reduction potential, its high activation energy restricts its reactivity to a few targets in cells. Direct reaction is slow with (seleno)cysteine, methionine, glutathione and Fe-S clusters, although there are a few notable exceptions. Reactivity with cysteine is normally 2.9 M^{-1} s^{-1} (or ~20 M^{-1} s^{-1} when adjusted for thiolates) but in specific proteins (2-cys peroxiredoxins) this can increase up to 1-4 x 10^7 M^{-1} s^{-1} [15,16]. The reactivity of cysteines partially depends on its particular pK_a as determined by the local protein structure and environment, thereby providing a basis for selective redox signaling (see below). Because of its long lifetime and its extreme reactivity with 2-cys peroxiredoxins (see **chapter 2**), H_2O_2 is considered the main signaling ROS by means of reacting with cysteine thiols.

The plasma membrane allows limited diffusion of H_2O_2 into the cell directly, and is further facilitated by aquaporins [17]. The H_2O_2 gradient over the plasma membrane when H_2O_2 is added extracellularly is around 650-fold, with lower concentrations on the cytosolic side [18]. The toxicity of H_2O_2 at high concentrations is most likely a consequence of its reduction to the highly toxic $HO^\bullet$, catalyzed by Fe^{2+} in the Fenton reaction (**Figure 1B**) [19]. Furthermore, H_2O_2 can react with carbon dioxide, thereby producing the highly reactive peroxymonocarbonate (HCO_4^-) [20]. H_2O_2 levels are controlled through the coordinated actions of peroxiredoxins, catalase and glutathione peroxidase (see below).

Hydroxyl Radical ($HO^\bullet$)

The Hydroxyl radical ($HO^\bullet$) is the most reactive ROS, and it oxidizes most biomolecules including DNA, lipids (see below), carbohydrates and proteins. As a result, it produces stable adducts such as 8-oxo-deoxyguanosine, which causes common oxidation-derived DNA lesions in DNA.

It reacts at a rate that is close to the diffusion limit, so it acts as an unspecific oxidant. Its lifetime is very short at ~10^{-9} s [12]. $HO^\bullet$ is generated by H_2O_2 reduction in Fe^{2+}-catalyzed Fenton reactions.

Peroxyl Radical ($ROO^\bullet$)

When methylene groups (-CH_2) in polyunsaturated fatty acids are attacked by $HO^\bullet$ or $ROO^\bullet$, a hydrogen atom will be abstracted to form carbon-centered radicals ($R^\bullet$, on lipids often called lipid radical). In turn, these react rapidly with oxygen to generate peroxyl radicals ($ROO^\bullet$) [21]. In lipids this

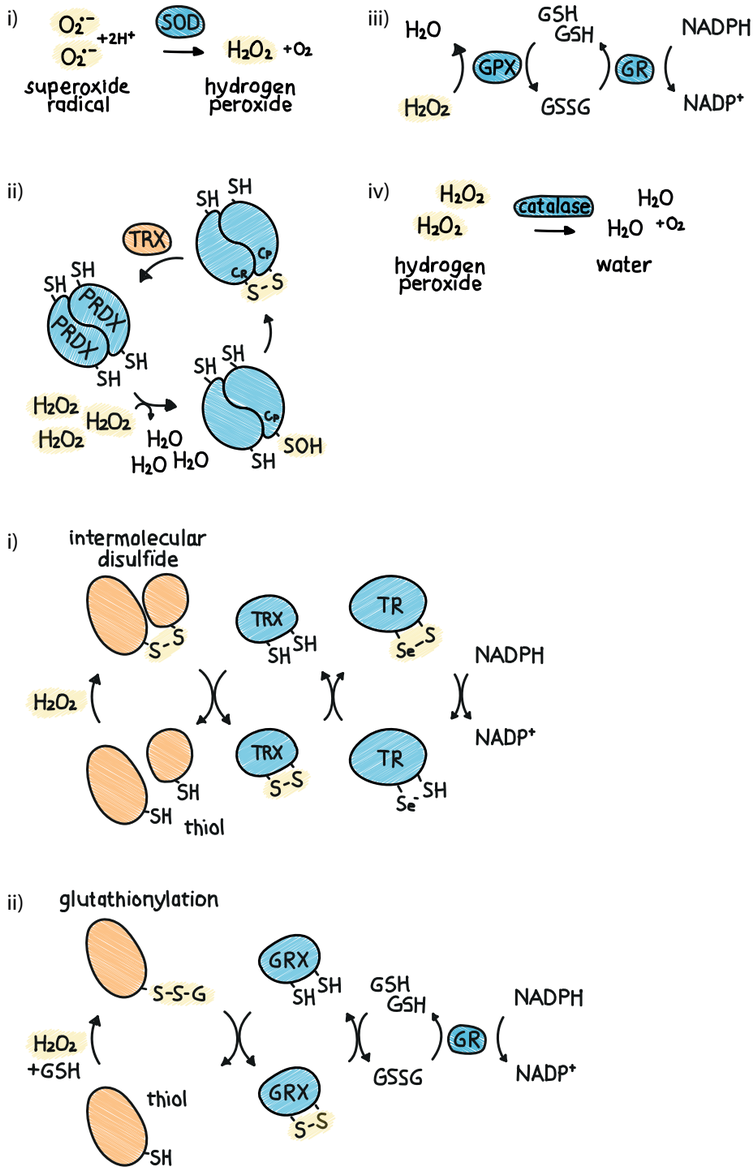

Figure 2. Scavenging systems.
(**A**) Cellular anti-oxidant systems that control H_2O_2 levels include several forms of superoxide dismutase (SOD, **i**), the peroxiredoxin system (PRDX, **ii**) glutathione peroxidase (GPX, **iii**) and peroxisomal catalase (**iv**). (**B**) Cellular disulfide reduction systems. Disulfides can be reduced by the thioredoxin system (TRX, **i**), glutathionylated proteins can be reduced by the glutaredoxin (GRX) system. Both use NADPH as a final electron donor. GSH: glutathione (reduced), GSSG: glutathione (oxidized), GR: glutathione reductase. TR: thioredoxin reductase

can cause a chain reaction, since the newly formed ROO• can again react with methylene groups in other lipids [22]. The peroxidation of lipids causes a change in the shape and fluidity of membranes, leading to permeabilization membranes. Similar short chain reactions can also take place in proteins [23].

Organic Hydroperoxide (ROOH)

(Lipid) peroxyl radicals (ROO•) can abstract hydrogen atoms from nearby polyunsaturated fatty acids and sterols such as cholesterol, thereby forming (lipid) hydroperoxide (ROOH) and a new carbon-centered (lipid) radical R•, which in turn can trigger lipid peroxidation chain reactions. They may also further react with a metal ion to generate alkoxyl radicals (RO•).

Other ROS

Other types of ROS include alkoxyl radicals (RO•), singlet molecular oxygen ($^1O_2$), electronically excited carbonyls (R-C=O*), ozone (O_3), hypochlorous acid (HOCl) and peroxymonocarbonate (HCO_4^-) and are briefly discussed below. There are several other types of reactive species such as reactive nitrogen species (e.g. nitrix oxide, NO• and peroxynitrite, $ONOO^-$), but these are not discussed here.

Alkoxyl radicals (RO•) are the result decomposition of hydroperoxides catalyzed by metal ions (e.g. iron or copper, such as in heme proteins) [24]. This occurs during lipid peroxidation and can theoretically cause amplification of lipid peroxidation reactions, although their cellular concentration is low [25]. They are stronger oxidants than ROO•, but less reactive than HO•.

Photoexcitation (such as by UV occurring in light-exposed tissues) of molecular oxygen (O_2) generates singlet oxygen ($^1O_2$) [26]. Singlet oxygen is also produced enzymatically, for instance by peroxidases, during the termination of lipid peroxidation propagation (i.e. when two peroxyl radicals react), and during reactions with ozone (O_3) [27,28].

Photoexcitation of carbonyl groups generates triplet state carbonyl (R-C=O*, where * indicates the excited state). They can also be created by chemiexcitations, for example through the encounter between two alkoxyl- or peroxyl radicals in membrane lipids [29]. A reaction with O_2 releases excited singlet oxygen [30].

Ozone (O_3) in the earth's stratosphere is known for protecting the earth from damaging radiation and as an air pollutant responsible for damaging the respiratory system, but it is also produced inside biological systems from singlet oxygen, for example in activated neutrophils [31]. Exposure of cells to ozone can cause lipid and protein peroxidation, a disruption of cellular membranes and epithelial barrier as well as DNA damage [32–34]. Ozone can react directly with biological molecules, generating singlet oxygen in the process [35]. On top of that, ozone in water slowly decomposes into HO• [36].

Myeloperoxidase (MPO) is a heme protein secreted by leukocytes, which converts H_2O_2 and Cl^- into hypochlorous acid (hypochlorite, HOCl). Hypochlorous acid is highly reactive, which is why it is considered the responsible oxidant for the killing capabilities of phagocytes against pathogens [37,38]. This is also the reason HOCl is widely used as a household disinfectant (bleach). It reacts with iron via the Fenton reaction forming HO• which makes it cytotoxic. Furthermore, it can react with other ROS like $O_2^{\bullet-}$, H_2O_2 and OH•, respectively forming OH•, $^1O_2$ and ClO. HOCl can directly oxidize cysteine thiols [39].

H_2O_2 can react with carbon dioxide to form peroxymonocarbonate (HCO_4^-). The reaction is an equilibrium which lies to the left. Although only ~1 % of H_2O_2 participates in the interaction, the product, peroxymonocarbonate (HCO_4^-), is more reactive with thiols and methionine than H_2O_2 itself [40].

ENDOGENOUS ROS GENERATION

ROS can originate from many intracellular sources. The brief overview here will mainly discuss the sources for the primary

ROS species generated by reduction of oxygen ($O2^{\bullet-}$), as well as H_2O_2 and $OH^{\bullet}$.

Mitochondrial Sources of ROS

A large part of ROS production occurs in the mitochondrial respiratory electron transport chain during oxidative phosphorylation (OXPHOS), where 85-90% of O_2 is metabolized. The inner mitochondrial membrane houses a series of electron transporters (complex I-IV) that shuttles electrons from NADH and $FADH_2$ to O_2 as the final electron acceptor. This allows proton transport into the mitochondrial intermembrane space and the resulting proton gradient drives the production of ATP using ATP synthase (complex V). Importantly, O_2 ran react prematurely with electrons 'leaking' from the electron transport chain (at complexes I and III), thereby forming superoxide ($O_2^{\bullet-}$) [41]. Up to 3% of mitochondrial oxygen consumption is reduced to form superoxide (which dismutates into H_2O_2) [42,43]. This rate may be affected by various factors such as the mitochondrial membrane potential, oxygen availability or electron flux though the respiratory chain [44–46].

NADPH Oxidases (NOXs)

The membrane-bound family of NOX enzymes produce superoxide by transferring one electron from NADPH to oxygen. The catalytic subunit of the complex contains one of seven enzymes (NOX1-5, DUOX1-2), each with varying tissue distributions and activation mechanisms. NOXs (specifically NOX2) became famous for their role in the so-called respiratory burst in activated neutrophils, which produce large amounts of ROS to inactivate microorganisms [47]. Furthermore, they have been associated with redoxomes; specialized redox-active endosomes that allow compartmentalization of H_2O_2 and localized redox signaling [48].

A wide array of extracellular signals can cause NOX activation, including cytokines, peptide growth factors, G-protein coupled receptor agonists and mechanical stretch [49]. NOX activation can be tightly controlled by the signal-mediated binding of cell-specific cofactors such as FAD and calcium [50]. The activation of NOXs and the subsequent ROS production is crucial for signal propagation in a large number of pathways [50].

Other Sources

Besides NOXs, there is a number of other enzymes that can generate ROS. Various types of oxidases generate ROS at specific subcellular locations (e.g. those localized to the endoplasmic reticulum (ER) and peroxisomes). For example, cytochrome P450 enzymes in the ER catalyze the heme-dependent oxidation of several metabolites but they can generate superoxide and H_2O_2 during 'reaction uncoupling' [51]. It is now recognized that this is not merely a by-product of metabolism but rather an important redox regulatory mechanism in adrenal corticosteroid production [52]. ROS are also produced during oxidative protein folding in the ER driven by ERO1 oxidoreductases and protein disulfide isomerases (PDI), which are responsible for structural disulfide formation in proteins but also generates H_2O_2 in the process [53,54]. Other ROS-producing enzymes include xanthine oxidase, nitric oxide synthase, cyclooxygenases and lipoxygenases. For a comprehensive overview see reference [13].

While not technically generating ROS *de novo*, superoxide dismutases (SODs) convert superoxide ($O_2^{\bullet-}$) into H_2O_2 [55]. SODs are widely distributed within tissues and cells. SOD is known as an antioxidant, but although it does scavenge toxic superoxide, it converts it to another ROS species [56]. SOD

does not necessarily increase H_2O_2 levels, since superoxide is distmutates to H_2O_2 regardless of SOD, although SOD might change the stoichiometry between $O_2^{\bullet-}$ and H_2O_2 only if the reaction prevents other reactions involving superoxide in favor of the latter[57].

ROS are also generated by exogenous factors including UV and ionizing radiation, toxins, nutrients, drugs and many more, collectively termed the 'exposome' [58,59]. The contribution of the exposome to the total cellular ROS pool is unknown due to the highly variable exposure of cells to different exposome factors.

To understand ROS biology, an important question is how much each of these ROS generating systems contribute to the total cellular pool of ROS. It was estimated that around 45% of cellular H_2O_2 in myoblasts comes from cellular respiration, 40% from NOXs and the other 15% from other ROS sources, although this may vary strongly depending on cellular context and metabolic state [60]. Furthermore, the concentration of H_2O_2 across cells is highly compartmentalized. It ranges from as low as 80 pM in the cytosol to 4 nM in the mitochondrial matrix and up to micromolars in the ER [61–63].

SCAVENGING OF INTRACELLULAR H_2O_2

Intracellular ROS levels are under tight control. As mentioned, low levels of ROS are essential for fundamental cellular processes such as proliferation, but high levels of ROS may cause random damage. Several anti-oxidant systems are in place that can decompose ROS to constrain cellular ROS levels. Firstly, several types of SODs convert $O_2^{\bullet-}$ into H_2O_2 (**Figure 2A, i**)[56]. In turn, H_2O_2 levels are tightly controlled by the combined actions of peroxiredoxins (PRDXI-VI), catalase and glutathione peroxidase (GPX), which all decompose H_2O_2 to water.

Glutathione peroxidase (GPX) catalyzes the reduction of H_2O_2 and forms oxidized glutathione (GSSG), after which glutathione reductase (GR) then recycles GSSG using NADPH (**Figure 2A, iii**) [64].

Catalase is specifically localized to peroxisomes, where it breaks down and prevents release of H_2O_2 generated by peroxisomal enzymes like acyl-CoA oxidase and D-amino acid oxidase (**Figure 2A, iv**). It may also decompose H_2O_2 from other parts of the cell [65].

Peroxiredoxins (PRDXs) are the most prominent regulators of cellular H_2O_2 levels. They are ubiquitous and highly abundant cysteine-based peroxidases, with isoforms localized to cytoplasm, mitochondria, endoplasmic reticulum (ER) and other cellular compartments [66]. Of the six isoforms in humans (PRDX1, PRDX2, PRDX3, PRDX4, PRDX5 and PRDX6), PRDX1-5 belong to the 2-cys family of peroxiredoxins. The basic structural unit of peroxiredoxins is an antiparallel homodimer, which generates a local environment that makes the active site cysteine thiol (peroxidatic cysteine, C_P-SH) extremely sensitive to H_2O_2 (**Figure 2A, ii**) [67,68]. In 2-cys peroxiredoxins, the unstable sulfenic acid intermediate (C_P-SOH) condenses with a resolving cysteine (C_R) on the C-terminal region of the other subunit of the PRDX dimer, or in case of PRDX5 the C_R on the same subunit. The disulfide is then reduced by the thioredoxin (TRX) system (see below), using NADPH as an electron donor [69].

The C_P-SOH is also sensitive to further oxidation (hyperoxidation; C_P-SO_2H), leading to the transient inactivation of peroxiredoxins mainly at higher H_2O_2 concentrations [70].

Peroxiredoxins are more abundant than GPXs, together comprising up to 1% of total soluble protein content of cells [71]. Kinetic studies revealed that the second-order rate constants for the oxidation of the PRDX C_P is 10^5-10^6 M^{-1} s^{-1}, which is up to seven orders of magnitude higher compared to cysteines described in other redox-regulated proteins [72]. Thus, peroxiredoxins are thought to scavenge more than 99% of cytosolic H_2O_2 [73]. Together, this suggests that cysteine thiols in H_2O_2 target proteins are generally outcompeted by peroxiredoxins for reaction with H_2O_2. How it is possible that H_2O_2 oxidizes these low reactive thiols in H_2O_2-sensitive proteins in the presence of peroxiredoxins is a fundamental question in redox biology.

In addition to H_2O_2 scavenging systems, cells can reduce non-structural disulfides that form between oxidized thiols in proteins. Thioredoxin (TRX) uses a thiol-disulfide exchange reaction to reduce disulfides, and TRX itself is re-

generated using by thioredoxin-reductase (TR), which in turn is reduced at the expense of NADPH (**Figure 2B, i**). TRXs reduce disulfide bonds in a wide variety of proteins [74].

The glutaredoxin system utilizes the highly abundant glutathione (GSH) to resolve protein disulfide bonds, thereby oxidizing GSH to form GSSG (**Figure 2B, ii**). Like the thioredoxin system, the glutathione system ultimately uses NADPH as an electron donor. Increasing the cellular NADPH pool thus fuels the reducing capacity of the cell [75]. It has been proposed that the main benefit of the drastically upregulated glucose metabolism in cancer cells is not to switch to glycolysis for ATP synthesis to meet a high ATP demand in tumor cells (as speculated by Warburg). Rather, it shunts glycolytic intermediates into the pentose-phosphate-pathway (PPP) for biomass synthesis and to maintain the redox balance through the supply of NADPH [76]. Both localized production of ROS and organelle-specific anti-oxidant systems result in the compartmentalization of intracellular H_2O_2 levels [77,78]. As such, redox potentials (as a measure for how reducing or oxidizing an environment is) vary greatly amongst organelles (**Figure 3**).

OXIDATIVE STRESS VERSUS REDOX SIGNALING

As mentioned, ROS have long been viewed as merely damaging side-products of metabolism. It was even posed that aging is the cumulative result of oxidative damage to cells and tissues [4]. While excessive levels of ROS cause random damage to macromolecules and oxidative stress, physiological levels of ROS are essential in the redox regulation of fundamental cellular processes. Prolonged disruption of redox homeostasis can therefore also be seen as oxidative stress. Examples of essential cellular processes that require oxidative modifications in order to function correctly include signal transduction at the plasma membrane [79], developmental processes such as morphogenesis and differentiation [80,81], cell proliferation, wound healing [82], muscle adaptation to exercise [83,84] and much more [82]. The exact boundary between oxidative stress and redox signaling is very vague. This is partially caused by the lack of tools for assessing endogenous levels of ROS, although sensitive ROS detection methods have recently been developed and are continuously being improved [74,85]. A good distinction between ROS as a signaling molecule versus ROS as oxidative stress has been proposed by Sies et al. [86].

OVERVIEW OF CYSTEINE CHEMISTRY

Despite the tight control of ROS production and antioxidant systems, changes in the cellular redox state occur continuously and these changes can result in the oxidation of cysteine residues in proteins. Proteins that are oxidized by H_2O_2 are sometimes described as 'ROS sensors', which function to provide an adequate cellular response to the changing cellular environment. As we will discuss below, and in **chapter 2** in this thesis, most so-called ROS sensors are likely not directly oxidized by H_2O_2. Redox signaling through the reversible oxidation of specific proteins is highly cell- and tissue-specific [87]. Hydrogen peroxide (H_2O_2) is considered as the major ROS in reversible cysteine oxidation (see above) [13,88].

Cysteine residues are relatively low in abundance in proteins, comprising only 2.26% of amino acids where 3.28% is expected based on the relative number of codons [89,90]. Nevertheless, cysteines participating in disulfide bonds are the most evolutionary conserved amino acids, and in cases where a disulfide bond is not conserved cysteines are replaced as pairs in 99% of cases [91]. Presumably, cysteines were introduced late in evolution [92], and proteomes of more complex organisms contain more cysteines than proteomes of more primitive organisms, suggesting an ongoing increase in cysteine content [93]. This conservation and increasing number of cysteines in our proteome suggest a selective pressure that could reflect the acquisition of cysteine-oxidation based signaling functions with the evolution of complexity [3,94].

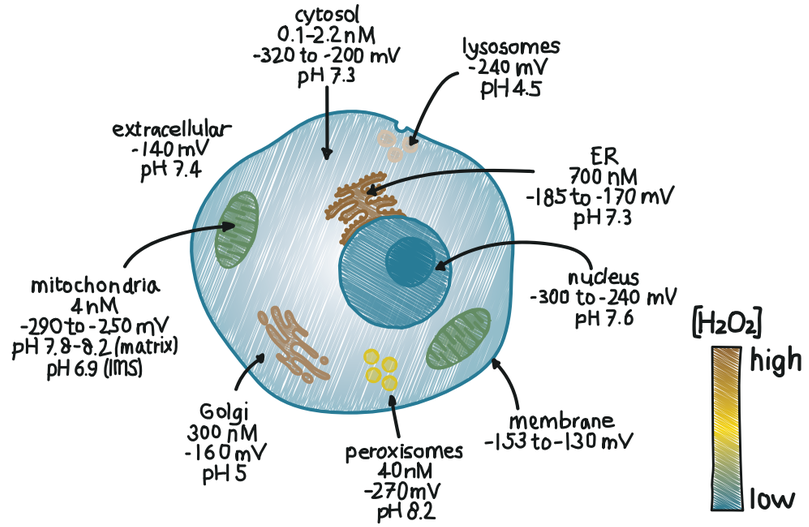

Figure 3. The cellular redox landscape.
Approximations of H_2O_2 concentrations (nM) [164], redox potentials (mV) [77,165,166] and pH [167] of subcellular compartments. Numbers vary greatly according to growth conditions and cell types [77]. Cellular mean: 10 nM [168], -160 to -260 [166,169,170]; cytosol [168,171–173]; mitochondrial matrix [77,174–180]; mitochondrial intermembrane space [178,180]; nucleus [77]; ER [63,181]; Golgi [182]; peroxisomes [104,183]; lysosomes [184]; membrane [167]; extracellular [172]. Grey/beige indicates unknown H_2O_2 levels. The order of organelles from most reducing to most oxidizing is: mitochondria, nucleus, cytoplasm, lysosome, endoplasmic reticulum, and cell membrane.

The sulfur atom makes cysteine a versatile determinant of protein structure and function, as it can adopt a variety of oxidation states (**Figure 4**). This is also the molecular basis for the critical roles that cysteines play both in enzyme catalytic sites and regulatory attributes of enzyme function. Reduced cysteines exist as either a thiol (-SH) or as a thiolate anion ($-S^-$) when it is deprotonated. The thiolate anion is prone to oxidation by H_2O_2, subsequently forming sulfenic acid (-SOH), sulfinic acid ($-SO_2H$) and sulfonic acid ($-SO_3H$) with each subsequent oxidation step. Sulfinic acid can be reduced by sulfiredoxin1 (SRX1), although this reaction is slow [95]. Sulfonic acids cannot be reduced in vivo and are considered irreversible. Sulfenic acids are short-lived and highly reactive. They readily react with other cysteine thiols to from disulfides within the same (intramolecular) or another (intermolecular) protein or with cysteines in short peptides such as glutathione (glutathionylation) (**Figure 4**).

The protonation state of a sulfur group is an important determining factor for protein thiol reactivity. Most oxidation events involve the thiolate anion as it is more nucleophilic [96]. The thiol side chain of free cysteine has a pK_a of 8.3, meaning that at physiological pH ~90% of thiols will be protonated (-SH). However, the pK_a of specific protein thiols can vary considerably, ranging from as low as 2.5 to as high as 12. Thiols in redox-sensitive proteins have a low pK_a, such as 6.5 for TRX, 5.4 for PTP1B and between 5-6 for PRDXs [15,16,97,98]. The pK_a of a thiol is influenced by its local environment. Exposed thiols have a much lower pK_a than thiols buried inside proteins on average (7.5 vs 9.5, respectively), meaning that exposed thiols exist more often in a deprotonated state. Combined with the higher accessibility of exposed thiols for H_2O_2 this means they are more easily oxidized [5]. For example, cysteines are stabilized in a deprotonated state when located in vicinity to hydrogen bond donors, within an electropositive environment, at the N-terminus of alpha

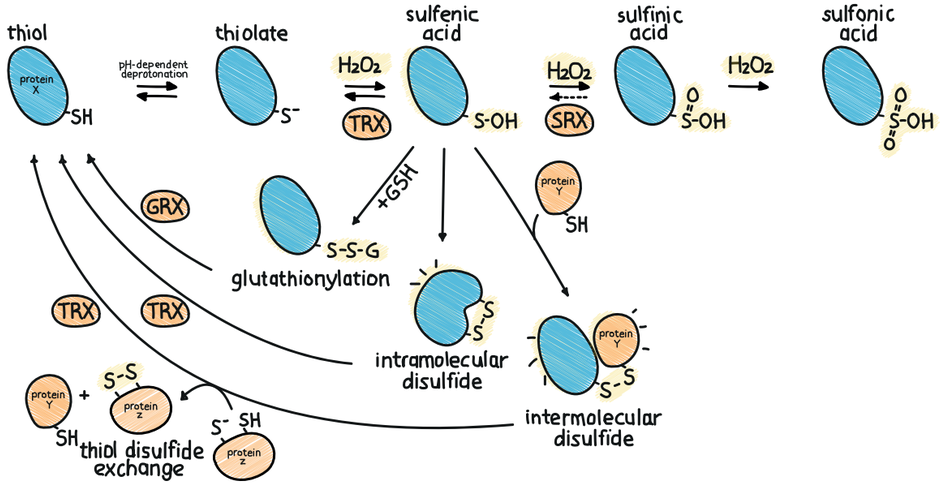

Figure 4. Overview of cysteine modifications.
Cysteine sulfur groups exist in either a thiol (-SH) or as a deprotonated thiolate anion ($-S^-$) form depending on the pK_a and local pH. A critical initial step in redox signaling is that cysteine thiolates ($-S^-$) react with H_2O_2, thereby forming the highly reactive sulfenic acid form (-SOH). Subsequent reactions with H_2O_2 form sulfinic ($-SO_2H$) and sulfonic acid ($-SO_3H$, irreversible). Sulfinic acids can be reduced anzymatically by sulfiredoxins (SRX), but sulfonic acids cannot be reduced. Sulfenic acids can react with proximal thiols and condenses into a disulfide bond (-S-S-), either intra- or intermolecularly. Disulsulfides are reduced by the thioredoxin (TRX) system or in a disulfide exchange reaction. Sulfenic acids can also form an intermolecular disulfide reaction with glutathione (GSH), a highly abundant tripeptide (Glu-Cys-Gly), a PTM that can be reduced by glutaredoxin (GRX).

helices, or when interacting with metal ions, thus enhancing their reactivity [99–101]. Another factor that influences the protonation state and reactivity of protein thiols is the local pH, which can range from 7.2 in the cytosol, nucleus and ER to 8.2 in peroxisomes and as low as 4.7 in lysosomes (**Figure 3**) [102–104].

As outlined above, cysteine residues are not equal in their ability to undergo redox modifications, thereby providing a basis for specificity in redox signaling. However, although an important determinant for reactivity, the ionization state is not the only determinant of reactivity since pH reactivity profiles for thiols do not simply correlate with their pK_a [15].

REACTIVITY AND SPECIFICITY IN REDOX SIGNALING

A conceptual problem for H_2O_2 as a second messenger is that it is unknown how it achieves the reactivity (i.e. how it reacts with low abundant targets) and specificity (i.e. reacting with specific thiols on specific proteins) required for proper signal transduction (**Figure 5**).

The first part of the problem is that it is unknown how H_2O_2 can reach its targets in cells that are rich in antioxidant proteins whose function it is to capture ROS. In contrast to most thiol-containing proteins, the most prominent thiol peroxidases, peroxiredoxins, have rate constants for the reaction with H_2O_2 more than six orders of magnitude higher, in the range of 10^6–10^8 $M^{-1}s^{-1}$ [105]. Peroxiredoxins are also highly abundant proteins, with concentrations up to three orders of magnitude higher than most redox-regulated proteins [71]. For this reason, they are expected to scavenge more than 99% of cellular H_2O_2 (**Figure 5A**) [57].

Secondly, although H_2O_2 is a strong oxidant, protein thiols in general have a low reactivity with H_2O_2. The reactivity (i.e. rate constant) of H_2O_2 with the cysteine thiolate anion ($C\text{-}S^-$) is around 20 $M^{-1}s^{-1}$ [105,106]. On top of this, most thiol-containing proteins such as $p16^{INK4A}$, are low-abundant (**Figure 5B**).

Thirdly, it is poorly understood how H_2O_2 causes the oxidation of specific redox-sensitive proteins in particular pathways in the context of virtually limitless potential targets in a cell (**Figure 5C**). Cellular stimuli are being translated in an appropriate, specific cellular response. If a general stress response is required, the source of H_2O_2 might not matter. But when H_2O_2 is the second messenger for a specific stimulus, this would require targeting of appropriate, specific pathways depending on the nature of the stimulus. As yet, what factors provide the necessary spatiotemporal precision for signal specificity is not entirely clear.

How it is possible that physiological levels of H_2O_2 lead to specific oxidation of these low reactive thiols in low abundant proteins is a fundamental question in redox biology. Several theories have been proposed to explain reactivity and specificity of otherwise unreactive cysteines that are found to be oxidized in response to redox changes. These mechanisms are visualized in **Figure 6**. Below, we discuss the proposed mechanisms and explore how these might help to overcome the reactivity and specificity challenges of H_2O_2-based signaling.

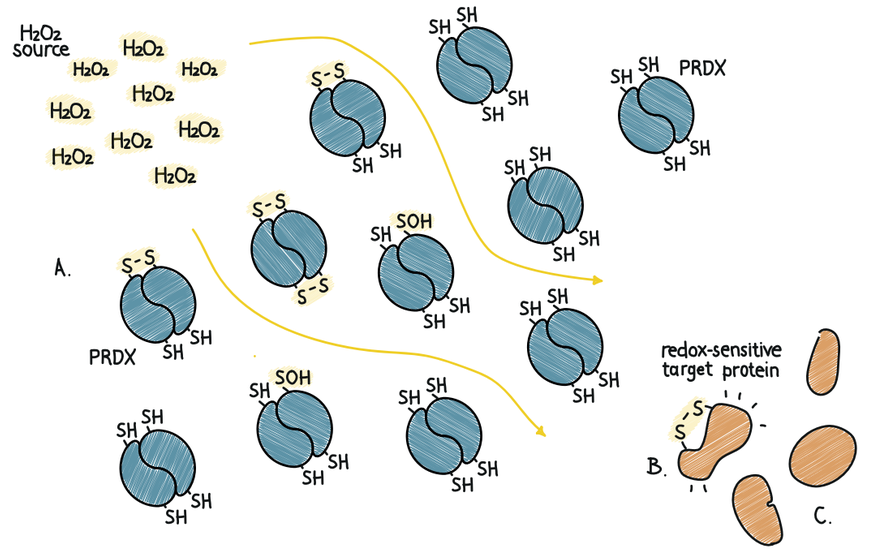

Figure 5. The redox paradox.
How is it possible that H_2O_2 achieves the required reactivity and specificity to oxidize specific protein thiols needed for proper signal transduction? There are several challenges for H_2O_2 to overcome: (**A**) Cells are rich in antioxidant proteins such as peroxiredoxins (PRDX), which have exceptional reactivity for H_2O_2 and are expected to scavenge >99% of cellular H_2O_2. (**B**) Redox-regulated thiol proteins in general showcase a low H_2O_2 reactivity and are low-abundant. (**C**) How can H_2O_2 cause oxidation of specific redox-sensitive proteins in a pool of virtually limitless options?

A) Direct Oxidation

This model assumes that H_2O_2 diffuses from its source and directly reacts with a target protein thiol to form a cysteine sulfenic acid (C-SOH) (**Figure 6A**). For this reaction to occur, a high reactivity of the targeted thiol and/or no competing reactions are required, like for instance for the oxidation of PRDXs by H_2O_2 or oxidation of some thiols in purified proteins *in vitro*. As discussed, H_2O_2 normally reacts slowly with the cysteine thiol, but variations in the direct structural context of thiols in proteins causes local changes in their pK_a, thereby affecting their protonation state. The protonation state of a sulfur group is an important determining factor for protein thiol reactivity. The pK_a of a cysteine can vary from 9.5 (for cysteines buried within a protein) to as low as 3.4, depending on the local environment [5,107].

Nonetheless, even while accounting for those local differences, a low pK_a is not sufficient to explain the oxidation of some protein thiols. For example, cysteines in peroxiredoxins, glutathione peroxidases and bacterial oxyR react with H_2O_2 many orders of magnitudes faster than can be explained by their pK_a and deprotonation state [73,108]. It was modelled that even H_2O_2 concentrations close to a site of H_2O_2 production may not be sufficient to directly oxidize protein thiols [109]. It was suggested that electrostatic and polar interactions of the cysteine thiol with the protein environment can not only contribute to lowering the pK_a but also stabilize the deprotonated state of the reaction [108]. Additionally, peroxidases like peroxiredoxins directly compete with the H_2O_2-mediated oxidation reaction. It is therefore assumed that in order for direct oxidation of thiols by H_2O_2 to take place, peroxiredoxins need to be (temporarily or locally) inactivated via the so-called "floodgate mechanism" (see B).

B) Floodgate Mechanism

In order to enable direct oxidation of thiols with modest reactivity, local H_2O_2 concentrations need to increase (transiently) to a micromolar range. Although not proven, the local inactivation of antioxidant systems such as the peroxiredoxins might facilitate this increase [110]. The local inactivation of signaling inhibitors is also observed in phosphorylation-mediated signaling, for which phosphatases need to be inactivated in order for efficient signaling to proceed [111,112]. For peroxiredoxins, inactivation can occur via two mechanisms.

i) The overoxidation of the catalytic cysteine (C_p-SO_2H or C_p-SO_3H) upon high levels of H_2O_2 inactivates the catalytic activity of peroxiredoxins (**Figure 6B**). Of note, overoxidation of peroxiredoxin is observed at high concentrations of H_2O_2, meaning that H_2O_2 levels already need to be elevated in order to facilitate a further increase. Several studies showed that H_2O_2 concentrations reached during signaling are not sufficient to hyperoxidize the C_p of peroxiredoxins [113,114]. On the other hand, overoxidation of peroxiredoxins has been shown to reflect circadian rhythm [115,116]. Furthermore, there are selective advantages that drove the evolution of peroxiredoxin overoxidation, suggesting a purpose for reversible peroxiredoxin overoxidation [117].
ii) Peroxiredoxins can also be inactivated by post-translational modifications (PTMs). For example, it is known that membrane receptor activation (including PDGF-R and EGF-R) activates SRC kinase, triggering the inactivating phosphorylation of PRDX1 at Y194. This inhibits PRDX1 catalytic activity and, together with local accumulation of activated NADPH oxidase (NOX) complexes in lipid rafts, this leads to a local increase of H_2O_2 at membranes [118–120]. A similar mechanism has been shown for H_2O_2-activated kinases MST1 and MST2 which phosphorylate PRDX1 at T90 and T183 as well as CDK1-cyclin B which phosphorylates centrosomal PRDX1 on T90 to regulate mitotic entry [121–123]. Other PTMs that seem to play a role in regulating peroxiredoxin activity include acetylation, glutathionylation and nitrosylation but how exactly they affect local peroxide concentrations is not clear [124].

Whether local inhibition of peroxiredoxins is sufficient to locally enable direct oxidation of protein thiols is unclear. It is possible that with the inactivation of peroxiredoxins, H_2O_2 is merely allowed to diffuse further from its source. In other words, protein thiols are again facing the same challenges of outcompeting peroxiredoxins at this location.

As explained, the intrinsic reactivity of protein thiols with H_2O_2 is generally low, and not much higher than that of other biomolecules. The floodgate model thus suggests that redox signaling and random oxidative damage occur simultaneously when H_2O_2 levels are high enough to cause overoxidation of peroxiredoxins. It can thus be suggested that opening the floodgate by overoxidation of peroxiredoxins may primarily occur under conditions of oxidative stress or with signaling events leading to cell death.

C) Localized Production of H_2O_2

Besides through the local inactivation of peroxiredoxins, a localized build-up of H_2O_2 can in principle also be achieved at the site of H_2O_2 production. Localized H_2O_2 production could enable direct oxidation of protein thiols (**Figure 6C**). Depending on the source of H_2O_2, oxidation of protein thiols only occurs to those that are in close proximity to that source. An example of localized H_2O_2 production is the H_2O_2 generated by NOXs, albeit via superoxide, which are localized to specific membranous compartments such as lipid rafts, the nucleus and endosomes [125]. In C. elegans zygotes, mitochondria relocate to the cellular cortex and locally increase H_2O_2 levels to promote symmetry breaking [126]. Other sites of H_2O_2 production include peroxisomes, although most H_2O_2 generated there will be broken down by catalase [65], and oxidative folding in the endoplasmic reticulum (ER), for which the H_2O_2 produced is most likely contained within the ER via recycling for oxidative folding [127–129]. Thus, cells do produce H_2O_2 at specific sites, which remains localized due to cellular compartmentalization as well as the highly abundant and reactive peroxiredoxins. Studies using sensitive genetically encoded H_2O_2 probes show that the H_2O_2 diffusion range is likely limited to a few microns [130,131]. Combining these probes with localized, inducible production of H_2O_2, for instance by targeting the H_2O_2 generating enzyme D-amino acid oxidase (DAO) to specific sites is a major tool in studying the importance of localized H_2O_2 production –and - diffusion in H_2O_2-based signaling [132]. Using this approach, it was shown that in vascular endothelial cells, nuclear H_2O_2 activates AMPK and causes phosphorylation of endothelial nitric oxide synthase (eNOS), while cytosolic or caveolae-derived H_2O_2 activates AMPK but does not cause eNOS phosphorylation [133]. Another example comes from Wnt signaling, where ROS acts in two separate pools – with seemingly opposing effects. Mitochondrial ROS resulting from the loss of TIGAR has an antiproliferative effect, whereas NOX-derived ROS induced by the upregulation of RAC1 is pro-proliferative [134]. This suggests that the cellular response to ROS depends on the ROS source, and that these cellular responses can be independently modulated in the same cell.

How much the subcellular origin of H_2O_2 affects pathways besides eNOS and Wnt signaling and whether this plays a role in different cell types is a fundamental issue for future research. Furthermore, this model does not account for differences in target thiol reactivity.

D) Redox Relay

This concept involves the initial oxidation of a highly reactive thiol in a 'redox sensor' which then catalyzes the oxidation of less favorable targets by reacting with the sulfenylated sensor or via disulfide exchange. The highly reactive sensor can be a thiol peroxidase such as peroxiredoxin, due to its exceptional reactivity with H_2O_2 and abundance. H_2O_2 first reacts with peroxiredoxin's peroxidatic cysteine (C_p), and oxidized peroxiredoxin then forms a mixed disulfide intermediate with the target protein (**Figure 6D**). Peroxiredoxin-based redox relays are recently being actively explored, and many examples have been described [135–140]. Another important observation that supports the role for peroxidases in sensing and transferring oxidative signals is that yeast cells lacking all thiol peroxidases are unable to orchestrate a transcriptional response to H_2O_2 [141]. Furthermore, it was recently shown that H_2O_2 diffusion is limited by the thioredoxin system, which points to peroxiredoxins as an initial H_2O_2 target since they utilize the thioredoxin system for their recycling [74].

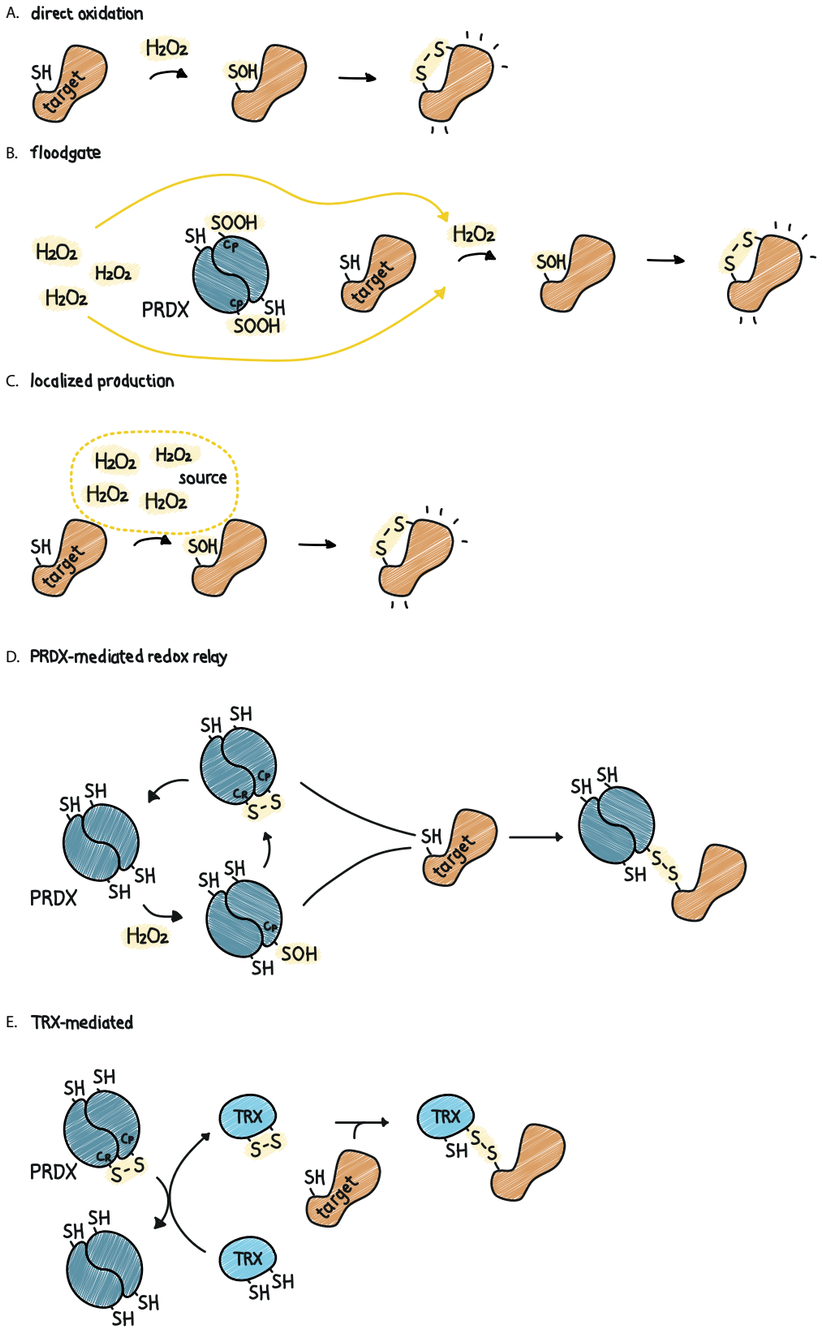

Figure 6. The different models to overcome the reactivity and specificity challenges of H_2O_2-based signaling.

Oxidized peroxiredoxins could in principle relay oxidizing equivalents to other thiols via two molecular mechanisms (**Figure 6D**). The first mechanism involves the condensation of the sulfenylated peroxidatic cysteine (C_p-SOH) of peroxiredoxins directly with the cysteine thiol of a target protein. A second possible mechanism involves a disulfide exchange reaction of the disulfide linking the peroxidatic and resolving cysteine (C_p-S-S-C_R) in oxidized peroxiredoxins with a target protein thiol. The SOH-mediated mechanism in principle only needs the peroxidatic cysteine of peroxiredoxin, whereas the S-S-mediated route is dependent on both catalytic cysteines and is limited by the activity of TRX. Of note, in the S-OH-mediated mechanism, the target protein thiol is directly competing with the peroxiredoxin resolving cysteine, requiring the target thiol to be in close proximity of the C_p-SOH. The existence of the SOH-mediated pathway is supported by data on the roGFP redox sensor, which is oxidized by Tsa2/PRDX2 with a mutated resolving cysteine [85].

Mammalian cells express five 2-cys peroxiredoxin isoforms, each with their own localization, oxidation kinetics and structural differences around their catalytic sites. A peroxiredoxin-based redox relay therefore explains not only the reactivity but could also grant selectivity in H_2O_2-dependent redox signaling.

E) TRX-mediated Oxidation

The reduction of oxidized peroxiredoxins involves the very efficient oxidation of thioredoxin (TRX) [142]. It is possible that oxidized TRX accumulates after the oxidation of peroxiredoxins, especially when the rate of TRX reduction is lower than peroxiredoxin-mediated oxidation (in which case there is also a possibility of overoxidation of peroxiredoxins, which are not a substrate for TRX), or when there is a lack of reducing power in the form of NADPH. In this state, TRX could in principle act as a thiol oxidase, thereby forming disulfide bonds in proteins instead of removing them (**Figure 6E**) [143,144]. However, it was suggested that TRX oxidase activity does not play a major role in catalyzing thiol oxidation events in the cytosol [138]. It is poorly understood whether TRX-oxidase activity is important for catalyzing protein oxidation in other compartments.

Importantly, none of the mechanisms described above are mutually exclusive and most likely act alongside each other, in parallel and/or at different locations. Furthermore, the redox potentials of the cytoplasm, nucleus, ER and mitochondria vary greatly [77]. Thus, each compartment responds differently to changes in the redox environment. Differential localization and oxidation and condensation kinetics of peroxiredoxin isoforms, combined with the different availability of target and/or adaptor proteins may determine which thiol oxidation mechanism can take place.

REDOX REGULATION OF PROTEIN STRUCTURE

The structure of a protein determines its biological function. Newly synthesized linear polypeptide chains on ribosomes are folded into 3D structures driven hydrophobic interactions, but also by van der Waals- and electrostatic interactions. Furthermore, the oxidizing environment of the ER and specialized enzymes aid the formation of disulfide bonds that ensure stabilization and assembly of native proteins that are directed for secretion of transmembrane localization. Proteins need to overcome energy barriers to reach their final, stable conformation, immanently leading to the accumulation of folding intermediates [145]. Partially folded proteins are at high risk of misfolding and aggregation, due to non-native interactions through for instance the exposure of hydrophobic residues [146].

In general, oxidative modifications on proteins result in conformational changes, which could lead to changes in protein function [3]. These redox-induced structural changes can thereby provide a molecular switch. Structural changes can also trigger partial unfolding and even aggregation of proteins. Interestingly, a large number of proteins is predicted to contain conditionally disordered regions that are redox

sensitive and thereby oxidation could play a key role the transition between folded and unfolded states [147]. In **chapter 4**, we show how the tumor suppressor protein $p16^{INK4A}$ can form β-amyloid-like fibrils under physiological conditions, triggered by the oxidation of a single cysteine residue and subsequent S-S-dependent homodimerization. In **chapter 5**, we discuss the intricate relationship between redox signaling and protein aggregation.

REDOX SIGNALING IN HEALTH AND DISEASE

Under physiological conditions, ~6-10% of protein thiols are found to be reversibly oxidized [148]. Given this large number of ROS targets, it comes as no surprise that redox modifications control a diverse set of cellular functions. Many essential cellular processes require oxidative modifications in order to function correctly. There is a large interplay with other modes of signaling and PTMs which ensures intricate signaling networks [149,150]. An elaborate description of cellular roles of redox signaling is given in refs. [13,86,151].

Given the role of redox regulation in essential cellular processes, it is not surprising that a deregulation of redox homeostasis as well as random damage due to excessive ROS levels (both leading to oxidative stress) are common pathophysiological conditions [86,152]. For example, it is known that both excessive and insufficient ROS production in mice cause neuronal problems including axonal degeneration and memory deficits, which are attributed to the redox regulation of neuronal polarity, connectivity and the modulation of neuronal networks [81,153]. Furthermore, cancer cells are known to increase both ROS production as well as reducing capacity, which is thought to contribute to increased proliferation rates, rewiring of cancer cell metabolism and stress adaptation [154–156]. Because redox imbalance is closely related to cancer, treatments based both on ROS scavenging as well as ROS overproduction are being actively explored. However, redox-based therapeutic strategies have not yet yielded promising results, and finding out the underlying mechanisms for this lack of success is of great significance [156,157]. One possibility is that most redox-based therapies act on shifting the overall redox balance in cells, thus blocking or stimulating oxidation of all redox-sensitive proteins at once. But since redox signaling involves the selective oxidation of specific redox-sensitive proteins, specifically targeting redox-sensitive proteins in cancer-related pathways is likely a more effective approach. The deregulation of redox signaling is also involved in a diverse set of pathologies involving the immune system [158], the cardiovascular system [159], insulin sensitivity [160] and aging [4,161,162].

Redox signaling is at the center of cellular homeostasis, as illustrated by the diversity and widespread character of redox-related pathologies. A deeper understanding of ROS and how they control cellular processes will allow us to unravel the mechanisms of redox signaling, the biological roles of oxidative regulation in cells, and how redox-regulated pathways and processes might be linked to diseases associated with oxidative stress.

OUTLINE OF THIS THESIS

Redox signaling is crucial for cells to maintain homeostasis. The goal of the research described in this thesis is to understand the molecular mechanisms that underlie redox signal propagation and how changes in the cellular redox state affect signaling pathways. This thesis is composed of seven chapters that can be divided into three themes. First of all, we study how the oxidation of proteins is achieved both efficiently and specifically. Secondly, we study several examples of how the oxidation of specific proteins can affect their function in important signaling pathways. Thirdly, we examine how redox regulation can affect protein aggregation.

How H_2O_2 leads to the selective and efficient oxidation of specific thiols on specific proteins is one of the most important open questions in redox biology. In **chapter 2**, we investigate peroxiredoxin-based redox relays on a proteome-wide scale, to investigate whether this may serve as a mechanism for the specific and efficient transmission of oxidative signals. We demonstrate that all 2-cys peroxiredoxin isoforms are capable of forming numerous cysteine-dependent heterodimers with target proteins, and that each peroxiredoxin isoform displays a preference for a subset of disulfide-dependent binding partners. This provides evidence that peroxiredoxins could play a role in providing not only reactivity but also selectivity in the transduction of peroxide signals to generate complex cellular signaling responses.

Chapters 3, 4 and **6** shift focus on the cysteine-dependent redox regulation of several signaling proteins. **Chapter 3** describes the PP2A regulating protein TIPRL. We show that TIPRL is highly sensitive to oxidation and forms three different disulfide-dependent homodimers involving cysteines C14 and C87 in response to endogenous levels of H_2O_2. Preliminary data suggest a role for oxidation of TIPRL in regulating phosphatase activity of PP2A-C.

Chapter 4 describes how the tumor suppressor protein $p16^{INK4A}$ can form β-amyloid-like fibrils under physiological conditions, triggered by oxidation of the single cysteine residue and subsequent S-S-dependent homodimerization. $p16^{INK4A}$ amyloid formation abolishes its function as a CDK4/6 inhibitor. We use the term 'oxaggregation' to refer to the critical dependence on a reversible disulfide cross-linked dimer as a subunit for fibril formation, which highlights the role of the cellular redox state as an important regulator of fibril formation.

Excessive ROS levels can lead to random damage of proteins, including protein unfolding and aggregation, processes that have been associated with aging. On the other hand, H_2O_2 acts as an essential second messenger and is important for healthy cell physiology. In **chapter 5** we discuss how these seemingly opposite effects of H_2O_2 as a signaling molecule and H_2O_2 as a driver of age-related protein aggregation can be united in one hypothesis. We give an overview of the literature on the intricate relationship between redox signaling and protein aggregation.

Chapter 6 describes an example of how the cellular redox state is intimately integrated with cell cycle progression [163]. We present evidence that the cell cycle regulator CDK4 and cyclin D form a temporary covalently linked complex under oxidizing conditions. This is caused by formation of a disulfide bond involving cysteine 135 in CDK4, stabilizing the otherwise hydrostatic non-covalent interaction between these proteins. Moreover, disulfide formation leads to an increased kinase activity of the CDK4-cyclin D complex. We discuss how identification of the redox sensitive C135 at the CDK4/cyclin D interface could provide a potential target for novel covalent cytostatic drugs.

Finally, in **chapter 7** I layout and summarize the work in this thesis and discuss the implications of and concepts emerging from this work.

6. Wong, J.W.H.; Ho, S.Y.W.; Hogg, P.J. Disulfide Bond Acquisition through Eukaryotic Protein Evolution. *Mol Biol Evol* **2011**, *28*, 327–334, doi:10.1093/molbev/msq194.

7. Forman, H.J.; Maiorino, M.; Ursini, F. Signaling Functions of Reactive Oxygen Species. *Biochemistry-us* **2010**, *49*, 835–842, doi:10.1021/bi9020378.

8. Halliwell, B.; Gutteridge, J.M.C. *Free Radicals in Biology and Medicine*; 2015; ISBN 9780198717478.

9. Hawkins, C.L.; Davies, M.J. Detection, Identification, and Quantification of Oxidative Protein Modifications. *J Biol Chem* **2019**, *294*, 19683–19708, doi:10.1074/jbc.rev119.006217.

10. Babior, B.M. The Respiratory Burst Oxidase. *Trends Biochem Sci* **1987**, *12*, 241–243, doi:10.1016/0968-0004(87)90118-6.

11. Hausladen, A.; Fridovich, I. Superoxide and Peroxynitrite Inactivate Aconitases, but Nitric Oxide Does Not. *J Biological Chem* **1994**, *269*, 29405–29408.

12. Zhang, L.; Wang, X.; Cueto, R.; Effi, C.; Zhang, Y.; Tan, H.; Qin, X.; Ji, Y.; Yang, X.; Wang, H. Biochemical Basis and Metabolic Interplay of Redox Regulation. *Redox Biol* **2019**, *26*, 101284, doi:10.1016/j.redox.2019.101284.

13. Sies, H.; Jones, D.P. Reactive Oxygen Species (ROS) as Pleiotropic Physiological Signalling Agents. *Nat Rev Mol Cell Biology* **2020**, 1–21, doi:10.1038/s41580-020-0230-3.

14. Nisimoto, Y.; Diebold, B.A.; Cosentino-Gomes, D.; Constentino-Gomes, D.; Lambeth, J.D. Nox4: A Hydrogen Peroxide-Generating Oxygen Sensor. *Biochemistry-us* **2014**, *53*, 5111–5120, doi:10.1021/bi500331y.

15. Winterbourn, C.C.; Metodiewa, D. Reactivity of Biologically Important Thiol Compounds with Superoxide and Hydrogen Peroxide. *Free Radical Bio Med* **1999**, *27*, 322–328, doi:10.1016/s0891-5849(99)00051-9.

16. Peskin, A.V.; Low, F.M.; Paton, L.N.; Maghzal, G.J.; Hampton, M.B.; Winterbourn, C.C. The High Reactivity of Peroxiredoxin 2 with H(2)O(2) Is Not Reflected in Its Reaction with Other Oxidants and Thiol Reagents. *J Biol Chem* **2007**, *282*, 11885 11892, doi:10.1074/jbc.m700339200.

17. Miller, E.W.; Dickinson, B.C.; Chang, C.J. Aquaporin-3 Mediates Hydrogen Peroxide Uptake to Regulate Downstream Intracellular Signaling. *Proc National Acad Sci* **2010**, *107*, 15681–15686, doi:10.1073/pnas.1005776107.

18. Huang, B.K.; Sikes, H.D. Quantifying Intracellular Hydrogen Peroxide Perturbations in Terms of Concentration. *Redox Biol* **2014**, *2*, 955 962, doi:10.1016/j.redox.2014.08.001.

19. Imlay, J.A. PATHWAYS OF OXIDATIVE DAMAGE. *Annu Rev Microbiol* **2003**, *57*, 395–418, doi:10.1146/annurev.micro.57.030502.090938.

20. Dagnell, M.; Cheng, Q.; Rizvi, S.H.M.; Pace, P.E.; Boivin, B.; Winterbourn, C.C.; Arnér, E.S.J. Bicarbonate Is Essential for Protein-Tyrosine Phosphatase 1B (PTP1B) Oxidation and Cellular Signaling through EGF-Triggered Phosphorylation Cascades. *J Biol Chem* **2019**, *294*, 12330–12338, doi:10.1074/jbc.ra119.009001.

21. O'Neill, P. The Chemical Basis of Radiation Biology. *Int J Radiat Biology Relat Stud Phys Chem Medicine* **2009**, *52*, 976–976, doi:10.1080/09553008714552571.

22. Yin, H.; Porter, N.A. New Insights Regarding the Autoxidation of Polyunsaturated Fatty Acids. *Antioxid Redox Sign* **2005**, *7*, 170–184, doi:10.1089/ars.2005.7.170.

23. Neužil, J.; Gebicki, J.M.; Stocker, R. Radical-Induced Chain Oxidation of Proteins and Its Inhibition by Chain-Breaking Antioxidants. *Biochem J* **1993**, *293*, 601–606, doi:10.1042/bj2930601.

24. Hawkins, C.L.; Davies, M.J. Generation and Propagation of Radical Reactions on Proteins. *Biochimica Et Biophysica Acta Bba - Bioenergetics* **2001**, *1504*, 196–219, doi:10.1016/s0005-2728(00)00252-8.

25. Marnett, L.J.; Wilcox, A.L. The Chemistry of Lipid Alkoxyl Radicals and Their Role in Metal-Amplified Lipid Peroxidation. *Biochem Soc Symp* **1995**, *61*, 65–72, doi:10.1042/bss0610065.

26. Davies, M.J. Reactive Species Formed on Proteins Exposed to Singlet Oxygen. *Photochem Photobio S* **2004**, *3*, 17–25, doi:10.1039/b307576c.

27. Kanofsky, J.R.; Wright, J.; Miles-Richardson, G.E.; Tauber, A.I. Biochemical Requirements for Singlet Oxygen Production by Purified Human Myeloperoxidase. *J Clin Invest* **1984**, *74*, 1489–1495, doi:10.1172/jci111562.

28. Nakano, M.; Takayama, K.; Shimizu, Y.; Tsuji, Y.; Inaba, H.; Migita, T. Spectroscopic Evidence for the Generation of Singlet Oxygen in Self-Reaction of Sec-Peroxy Radicals. *J Am Chem Soc* **1976**, *98*, 1974–1975, doi:10.1021/ja00423a060.

29. Brash, D.E.; Goncalves, L.C.P.; Bechara, E.J.H.; Group, T.E.-S.M.W. Chemiexcitation and Its Implications for Disease. *Trends Mol Med* **2018**, *24*, 527–541, doi:10.1016/j.molmed.2018.04.004.

30. Mano, C.M.; Prado, F.M.; Massari, J.; Ronsein, G.E.; Martinez, G.R.; Miyamoto, S.; Cadet, J.; Sies, H.; Medeiros, M.H.G.; Bechara, E.J.H.; et al. Excited Singlet Molecular O2 (1Δg) Is Generated Enzymatically from Excited Carbonyls in the Dark. *Sci Rep-uk* **2014**, *4*, 5938, doi:10.1038/srep05938.

31. Jr., P.W.; McDunn, J.E.; Wentworth, A.D.; Takeuchi, C.; Nieva, J.; Jones, T.; Bautista, C.; Ruedi, J.M.; Gutierrez, A.; Janda, K.D.; et al. Evidence for Antibody-Catalyzed Ozone Formation in Bacterial Killing and Inflammation. *Science* **2002**, *298*, 2195–2199, doi:10.1126/science.1077642.

32. Chen, C.; Arjomandi, M.; Balmes, J.; Tager, I.; Holland, N. Effects of Chronic and Acute Ozone Exposure on Lipid Peroxidation and Antioxidant Capacity in Healthy Young Adults. *Environ Health Persp* **2007**, *115*, 1732–1737, doi:10.1289/ehp.10294.

33. Brink, C.B.; Pretorius, A.; Niekerk, B.P.J. van; Oliver, D.W.; Venter, D.P. Studies on Cellular Resilience and Adaptation Following Acute and Repetitive Exposure to Ozone in Cultured Human Epithelial (HeLa) Cells. *Redox Rep* **2013**, *13*, 87–100, doi:10.1179/135100008x259187.

34. Hollingsworth, J.W.; Kleeberger, S.R.; Foster, W.M. Ozone and Pulmonary Innate Immunity. *Proc Am Thorac Soc* **2007**, *4*, 240–246, doi:10.1513/pats.200701-023aw.

35. Kanofsky, J.R.; Sima, P. Singlet Oxygen Production from the Reactions of Ozone with Biological Molecules. *J Biological Chem* **1991**, *266*, 9039–9042.

36. Glaze, W.H. Reaction Products of Ozone: A Review. *Environ Health Persp* **1986**, *69*, 151–157, doi:10.1289/ehp.8669151.

37. Foote, C.S.; Goyne, T.E.; Lehrer, R.I. Assessment of Chlorination by Human Neutrophils. *Nature* **1983**, *301*, 715–716, doi:10.1038/301715a0.

38. Winterbourn, C.C. Biological Reactivity and Biomarkers of the Neutrophil Oxidant, Hypochlorous Acid. *Toxicology* **2002**, *181*, 223–227, doi:10.1016/s0300-483x(02)00286-x.

39. CARR, A.C.; WINTERBOURN, C.C. Oxidation of Neutrophil Glutathione and Protein Thiols by Myeloperoxidase-Derived Hypochlorous Acid. *Biochem J* **1997**, *327*, 275–281, doi:10.1042/bj3270275.

40. Bakhmutova-Albert, E.V.; Yao, H.; Denevan, D.E.; Richardson, D.E. Kinetics and Mechanism of Peroxymonocarbonate Formation. *Inorg Chem* **2010**, *49*, 11287–11296, doi:10.1021/ic1007389.

41. Balaban, R.S.; Nemoto, S.; Finkel, T. Mitochondria, Oxidants, and Aging. *Cell* **2005**, *120*, 483–495, doi:10.1016/j.cell.2005.02.001.

42. Chance, B.; Sies, H.; Boveris, A. Hydroperoxide Metabolism in Mammalian Organs. *Physiol Rev* **1979**, *59*, 527–605, doi:10.1152/physrev.1979.59.3.527.

43. Bayne, A.-C.V.; Mockett, R.J.; Orr, W.C.; Sohal, R.S. Enhanced Catabolism of Mitochondrial Superoxide/Hydrogen Peroxide and Aging in Transgenic Drosophila. *Biochem J* **2005**, *391*, 277–284, doi:10.1042/bj20041872.

44. Mailloux, R.J.; Harper, M.-E. Mitochondrial Proticity and ROS Signaling: Lessons from the Uncoupling Proteins. *Trends Endocrinol Metabolism* **2012**, *23*, 451–458, doi:10.1016/j.tem.2012.04.004.

45. Sena, L.A.; Chandel, N.S. Physiological Roles of Mitochondrial Reactive Oxygen Species. *Mol Cell* **2012**, *48*, 158 166, doi:10.1016/j.molcel.2012.09.025.

46. Anastasiou, D.; Poulogiannis, G.; Asara, J.M.; Boxer, M.B.; Jiang, J.; Shen, M.; Bellinger, G.; Sasaki, A.T.; Locasale, J.W.; Auld, D.S.; et al. Inhibition of Pyruvate Kinase M2 by Reactive Oxygen Species Contributes to Cellular Antioxidant Responses. *Science* **2011**, *334*, 1278 1283, doi:10.1126/science.1211485.

47. Hampton, M.B.; Kettle, A.J.; Winterbourn, C.C. Inside the Neutrophil Phagosome: Oxidants, Myeloperoxidase, and Bacterial Killing. *Blood* **1998**, *92*, 3007–3017, doi:10.1182/blood.v92.9.3007.

48. Spencer, N.Y.; Engelhardt, J.F. The Basic Biology of Redoxosomes in Cytokine-Mediated Signal Transduction and Implications for Disease-Specific Therapies. *Biochemistry-us* **2014**, *53*, 1551–1564, doi:10.1021/bi401719r.

49. Prosser, B.L.; Ward, C.W.; Lederer, W.J. X-ROS Signaling: Rapid Mech-ano-Chemo Transduction in Heart. *Science* **2011**, *333*, 1440–1445, doi:10.1126/science.1202768.

50. Bedard, K.; Krause, K.-H. The NOX Family of ROS-Generating NADPH Oxidases: Physiology and Pathophysiology. *Physiol Rev* **2007**, *87*, 245–313, doi:10.1152/physrev.00044.2005.

51. White, R.E.; Coon, M.J. Oxygen Activation by Cytochrome P-450. *Annu Rev Biochem* **1980**, *49*, 315–356, doi:10.1146/annurev.bi.49.070180.001531.

52. Kil, I.S.; Lee, S.K.; Ryu, K.W.; Woo, H.A.; Hu, M.-C.; Bae, S.H.; Rhee, S.G. Feedback Control of Adrenal Steroidogenesis via H2O2-Dependent, Reversible Inactivation of Peroxiredoxin III in Mitochondria. *Mol Cell* **2012**, *46*, 584–594, doi:10.1016/j.molcel.2012.05.030.

53. Tu, B.P.; Weissman, J.S. The FAD- and O2-Dependent Reaction Cycle of Ero1-Mediated Oxidative Protein Folding in the Endoplasmic Reticulum. *Mol Cell* **2002**, *10*, 983–994, doi:10.1016/s1097-2765(02)00696-2.

54. Tu, B.P.; Weissman, J.S. Oxidative Protein Folding in Eukaryotes. *J Cell Biology* **2004**, *164*, 341–346, doi:10.1083/jcb.200311055.

55. McCord, J.M.; Fridovich, I. Superoxide Dismutase. An Enzymic Function for Erythrocuprein (Hemocuprein). *J Biological Chem* **1969**, *244*, 6049–6055.

56. Fukai, T.; Ushio-Fukai, M. Superoxide Dismutases: Role in Redox Signaling, Vascular Function, and Diseases. *Antioxid Redox Sign* **2011**, *15*, 1583–1606, doi:10.1089/ars.2011.3999.

57. Winterbourn, C.C. Biological Production, Detection, and Fate of Hydrogen Peroxide. *Antioxid Redox Sign* **2017**, *29*, ars.2017.7425, doi:10.1089/ars.2017.7425.

58. Niedzwiecki, M.M.; Walker, D.I.; Vermeulen, R.; Chadeau-Hyam, M.; Jones, D.P.; Miller, G.W. The Exposome: Molecules to Populations. *Annu Rev Pharmacol* **2018**, *59*, 1–21, doi:10.1146/annurev-pharmtox-010818-021315.

59. Yoshida, T.; Goto, S.; Kawakatsu, M.; Urata, Y.; Li, T. Mitochondrial Dysfunction, a Probable Cause of Persistent Oxidative Stress after Exposure to Ionizing Radiation. *Free Radical Res* **2012**, *46*, 147–153, doi:10.3109/10715762.2011.645207.

60. Wong, H.-S.; Benoit, B.; Brand, M.D. Mitochondrial and Cytosolic Sources of Hydrogen Peroxide in Resting C2C12 Myoblasts. *Free Radical Bio Med* **2019**, *130*, 140–150, doi:10.1016/j.freeradbiomed.2018.10.448.

61. Lim, J.B.; Huang, B.K.; Deen, W.M.; Sikes, H.D. Analysis of the Lifetime and Spatial Localization of Hydrogen Peroxide Generated in the Cytosol Using a Reduced Kinetic Model. *Free Radical Bio Med* **2015**, *89*, 47 53, doi:10.1016/j.freeradbiomed.2015.07.009.

62. Stein, K.T.; Moon, S.J.; Nguyen, A.N.; Sikes, H.D. Kinetic Modeling of H2O2 Dynamics in the Mitochondria of HeLa Cells. *Plos Comput Biol* **2020**, *16*, e1008202, doi:10.1371/journal.pcbi.1008202.

63. Gao, C.; Tian, Y.; Zhang, R.; Jing, J.; Zhang, X. Endoplasmic Reticulum-Directed Ratiometric Fluorescent Probe for Quantitive Detection of Basal H2O2. *Anal Chem* **2017**, *89*, 12945–12950, doi:10.1021/acs.analchem.7b03809.

64. Toppo, S.; Flohé, L.; Ursini, F.; Vanin, S.; Maiorino, M. Catalytic Mechanisms and Specificities of Glutathione Peroxidases: Variations of a Basic Scheme. *Biochimica Et Biophysica Acta Bba - Gen Subj* **2009**, *1790*, 1486–1500, doi:10.1016/j.bbagen.2009.04.007.

65. Bonekamp, N.A.; Völkl, A.; Fahimi, H.D.; Schrader, M. Reactive Oxygen Species and Peroxisomes: Struggling for Balance. *Biofactors* **2009**, *35*, 346–355, doi:10.1002/biof.48.

66. Wood, Z.A.; Poole, L.B.; Karplus, P.A. Peroxiredoxin Evolution and the Regulation of Hydrogen Peroxide Signaling. *Science* **2003**, *300*, 650 653, doi:10.1126/science.1080405.

67. Chae, H.Z.; Uhm, T.B.; Rhee, S.G. Dimerization of Thiol-Specific Antioxidant and the Essential Role of Cysteine 47. *Proc National Acad Sci* **1994**, *91*, 7022–7026, doi:10.1073/pnas.91.15.7022.

68. Chae, H.Z.; Chung, S.J.; Rhee, S.G. Thioredoxin-Dependent Peroxide Reductase from Yeast. *J Biol Chem* **1994**, *269*, 27670–27678, doi:10.1016/s0021-9258(18)47038-x.

69. Rhee, S.G. Overview on Peroxiredoxin. *Mol Cells* **2016**, *39*, 1 5, doi:10.14348/molcells.2016.2368.

70. Yang, K.-S.; Kang, S.W.; Woo, H.A.; Hwang, S.C.; Chae, H.Z.; Kim, K.; Rhee, S.G. Inactivation of Human Peroxiredoxin I during Catalysis as the Result of the Oxidation of the Catalytic Site Cysteine to Cysteine-Sulfinic Acid*. *J Biol Chem* **2002**, *277*, 38029–38036, doi:10.1074/jbc.m206626200.

71. Chae, H.Z.; Kim, H.J.; Kang, S.W.; Rhee, S.G. Characterization of Three Isoforms of Mammalian Peroxiredoxin That Reduce Peroxides in the Presence of Thioredoxin. *Diabetes Res Clin Pr* **1999**, *45*, 101 112, doi:10.1016/s0168-8227(99)00037-6.

72. Winterbourn, C.C.; Peskin, and A.V. Kinetic Approaches to Measuring Peroxiredoxin Reactivity. *Mol Cells* **2016**, *39*, 1 5, doi:10.14348/molcells.2016.2325.

73. Winterbourn, C.C.; Hampton, M.B. Thiol Chemistry and Specificity in Redox Signaling. *Free Radical Bio Med* **2008**, *45*, 549 561, doi:10.1016/j.freeradbiomed.2008.05.004.

74. Mishina, N.M.; Bogdanova, Y.A.; Ermakova, Y.G.; Panova, A.S.; Kotova, D.A.; Bilan, D.S.; Steinhorn, B.; Arnér, E.S.J.; Michel, T.; Belousov, V.V. Which Antioxidant System Shapes Intracellular H2O2 Gradients? *Antioxid Redox Sign* **2019**, *31*, 664–670, doi:10.1089/ars.2018.7697.

75. Hanschmann, E.-M.; Godoy, J.R.; Berndt, C.; Hudemann, C.; Lillig, C.H. Thioredoxins, Glutaredoxins, and Peroxiredoxins—Molecular Mechanisms and Health Significance: From Cofactors to Antioxidants to Redox Signaling. *Antioxid Redox Sign* **2013**, *19*, 1539–1605, doi:10.1089/ars.2012.4599.

76. Ju, H.-Q.; Lin, J.-F.; Tian, T.; Xie, D.; Xu, R.-H. NADPH Homeostasis in Cancer: Functions, Mechanisms and Therapeutic Implications. *Signal Transduct Target Ther* **2020**, *5*, 231, doi:10.1038/s41392-020-00326-0.

77. Go, Y.-M.; Jones, D.P. Redox Compartmentalization in Eukaryotic Cells. *Biochimica Et Biophysica Acta Bba - Gen Subj* **2008**, *1780*, 1273–1290, doi:10.1016/j.bbagen.2008.01.011.

78. Kaludercic, N.; Deshwal, S.; Lisa, F.D. Reactive Oxygen Species and Redox Compartmentalization. *Front Physiol* **2014**, *5*, 285, doi:10.3389/fphys.2014.00285.

79. Nordzieke, D.E.; Medraño-Fernandez, I. The Plasma Membrane: A Platform for Intra- and Intercellular Redox Signaling. *Antioxidants* **2018**, *7*, 168, doi:10.3390/antiox7110168.

80. Rampon, C.; Volovitch, M.; Joliot, A.; Vriz, S. Hydrogen Peroxide and Redox Regulation of Developments. *Antioxidants* **2018**, *7*, 159, doi:10.3390/antiox7110159.

81. Wilson, C.; Muñoz-Palma, E.; González-Billault, C. From Birth to Death: A Role for Reactive Oxygen Species in Neuronal Development. *Semin Cell Dev Biol* **2018**, *80*, 43–49, doi:10.1016/j.semcdb.2017.09.012.

82. Niethammer, P.; Grabher, C.; Look, A.T.; Mitchison, T.J. A Tissue-Scale Gradient of Hydrogen Peroxide Mediates Rapid Wound Detection in Zebrafish. *Nature* **2009**, *459*, 996–999, doi:10.1038/nature08119.

83. Trinity, J.D.; Broxterman, R.M.; Richardson, R.S. Regulation of Exercise Blood Flow: Role of Free Radicals. *Free Radical Bio Med* **2016**, *98*, 90–102, doi:10.1016/j.freeradbiomed.2016.01.017.

84. Jackson, M.J.; Stretton, C.; McArdle, A. Hydrogen Peroxide as a Signal for Skeletal Muscle Adaptations to Exercise: What Do Concentrations Tell Us about Potential Mechanisms? *Redox Biol* **2020**, *35*, 101484, doi:10.1016/j.redox.2020.101484.

85. Morgan, B.; Laer, K.V.; Owusu, T.N.E.; Ezeriņa, D.; Pastor-Flores, D.; Amponsah, P.S.; Tursch, A.; Dick, T.P. Real-Time Monitoring of Basal H2O2 Levels with Peroxiredoxin-Based Probes. *Nat Chem Biol* **2016**, *12*, 437 443, doi:10.1038/nchembio.2067.

86. Sies, H.; Berndt, C.; Jones, D.P. Oxidative Stress. *Annu Rev Biochem* **2017**, *86*, 715–748, doi:10.1146/annurev-biochem-061516-045037.

87. Xiao, H.; Jedrychowski, M.P.; Schweppe, D.K.; Huttlin, E.L.; Yu, Q.; Heppner, D.E.; Li, J.; Long, J.; Mills, E.L.; Szpyt, J.; et al. A Quantitative Tissue-Specific Landscape of Protein Redox Regulation during Aging. *Cell* **2020**, doi:10.1016/j.cell.2020.02.012.

88. D'Autréaux, B.; Toledano, M.B. ROS as Signalling Molecules: Mechanisms That Generate Specificity in ROS Homeostasis. *Nat Rev Mol Cell Bio* **2007**, *8*, 813–824, doi:10.1038/nrm2256.

89. Miseta, A.; Csutora, P. Relationship Between the Occurrence of Cysteine in Proteins and the Complexity of Organisms. *Mol Biol Evol* **2000**, *17*, 1232–1239, doi:10.1093/oxfordjournals.molbev.a026406.

90. Brooks, D.J.; Fresco, J.R. Increased Frequency of Cysteine, Tyrosine, and Phenylalanine Residues Since the Last Universal Ancestor*. *Mol Cell Proteomics* **2002**, *1*, 125–131, doi:10.1074/mcp.m100001-mcp200.

91. Thornton, J.M. Disulphide Bridges in Globular Proteins. *J Mol Biol* **1981**, *151*, 261–287, doi:10.1016/0022-2836(81)90515-5.

92. Wong, J.T.-F. A Co-Evolution Theory of the Genetic Code. *Proc National Acad Sci* **1975**, *72*, 1909–1912, doi:10.1073/pnas.72.5.1909.

93. Jordan, I.K.; Kondrashov, F.A.; Adzhubei, I.A.; Wolf, Y.I.; Koonin, E.V.; Kondrashov, A.S.; Sunyaev, S. A Universal Trend of Amino Acid Gain and Loss in Protein Evolution. *Nature* **2005**, *433*, 633–638, doi:10.1038/nature03306.

94. Jones, D.P. Redox Sensing: Orthogonal Control in Cell Cycle and Apoptosis Signalling. *J Intern Med* **2010**, *268*, 432–448, doi:10.1111/j.1365-2796.2010.02268.x.

95. Chang, T.-S.; Jeong, W.; Woo, H.A.; Lee, S.M.; Park, S.; Rhee, S.G. Characterization of Mammalian Sulfiredoxin and Its Reactivation of Hyperoxidized Peroxiredoxin through Reduction of Cysteine Sulfinic Acid in the Active Site to Cysteine*. *J Biol Chem* **2004**, *279*, 50994–51001, doi:10.1074/jbc.m409482200.

96. Poole, L.B.; Karplus, P.A.; Claiborne, A. Protein Sulfenic Acids in Redox Signaling. *Pharmacol Toxicol* **2004**, *44*, 325–347, doi:10.1146/annurev.pharmtox.44.101802.121735.

97. Goldman, R.; Stoyanovsky, D.A.; Day, B.W.; Kagan, V.E. Reduction of Phenoxyl Radicals by Thioredoxin Results in Selective Oxidation of Its SH-Groups to Disulfides. An Antioxidant Function of Thioredoxin. *Biochemistry-us* **1995**, *34*, 4765–4772, doi:10.1021/bi00014a034.

98. Denu, J.M.; Tanner, K.G. Specific and Reversible Inactivation of Protein Tyrosine Phosphatases by Hydrogen Peroxide: Evidence for a Sulfenic Acid Intermediate and Implications for Redox Regulation †. *Biochemistry-us* **1998**, *37*, 5633–5642, doi:10.1021/bi973035t.

99. Kiley, P.J.; Beinert, H. The Role of Fe–S Proteins in Sensing and Regulation in Bacteria. *Curr Opin Microbiol* **2003**, *6*, 181–185, doi:10.1016/s1369-5274(03)00039-0.

100. Roos, G.; Foloppe, N.; Messens, J. Understanding the PKa of Redox Cysteines: The Key Role of Hydrogen Bonding. *Antioxid Redox Sign* **2013**, *18*, 94 127, doi:10.1089/ars.2012.4521.

101. Kortemme, T.; Creighton, T.E. Ionisation of Cysteine Residues at the Termini of Model α-Helical Peptides. Relevance to Unusual Thiol PKa-Values in Proteins of the Thioredoxin Family. *J Mol Biol* **1995**, *253*, 799–812, doi:10.1006/jmbi.1995.0592.

102. Llopis, J.; McCaffery, J.M.; Miyawaki, A.; Farquhar, M.G.; Tsien, R.Y. Measurement of Cytosolic, Mitochondrial, and Golgi PH in Single Living Cells with Green Fluorescent Proteins. *Proc National Acad Sci* **1998**, *95*, 6803–6808, doi:10.1073/pnas.95.12.6803.

103. Casey, J.R.; Grinstein, S.; Orlowski, J. Sensors and Regulators of Intracellular PH. *Nat Rev Mol Cell Bio* **2010**, *11*, 50–61, doi:10.1038/nrm2820.

104. Dansen, T.B.; Wirtz, K.W.A.; Wanders, R.J.A.; Pap, E.H.W. Peroxisomes in Human Fibroblasts Have a Basic PH. *Nat Cell Biol* **2000**, *2*, 51–53, doi:10.1038/71375.

105. Winterbourn, C.C. The Biological Chemistry of Hydrogen Peroxide. *Methods Enzymol* **2013**, *528*, 3–25, doi:10.1016/b978-0-12-405881-1.00001-x.

106. Marinho, H.S.; Real, C.; Cyrne, L.; Soares, H.; Antunes, F. Hydrogen Peroxide Sensing, Signaling and Regulation of Transcription Factors. *Redox Biol* **2014**, *2*, 535 562, doi:10.1016/j.redox.2014.02.006.

107. Grauschopf, U.; Winther, J.R.; Korber, P.; Zander, T.; Dallinger, P.; Bardwell, J.C.A. Why Is DsbA Such an Oxidizing Disulfide Catalyst? *Cell* **1995**, *83*, 947–955, doi:10.1016/0092-8674(95)90210-4.

108. Ferrer-Sueta, G.; Manta, B.; Botti, H.; Radi, R.; Trujillo, M.; Denicola, A. Factors Affecting Protein Thiol Reactivity and Specificity in Peroxide Reduction. *Chem Res Toxicol* **2011**, *24*, 434 450, doi:10.1021/tx100413v.

109. Travasso, R.D.M.; Aidos, F.S. dos; Bayani, A.; Abranches, P.; Salvador, A. Localized Redox Relays as a Privileged Mode of Cytoplasmic Hydrogen Peroxide Signaling. *Redox Biol* **2017**, *12*, 233 245, doi:10.1016/j.redox.2017.01.003.

110. Rhee, S.G.; Woo, H.A. Multiple Functions of Peroxiredoxins: Peroxidases, Sensors and Regulators of the Intracellular Messenger H_2O_2, and Protein Chaperones. *Antioxid Redox Sign* **2011**, *15*, 781 794, doi:10.1089/ars.2010.3393.

111. Bauman, A.L.; Scott, J.D. Kinase- and Phosphatase-Anchoring Proteins: Harnessing the Dynamic Duo. *Nat Cell Biol* **2002**, *4*, E203–E206, doi:10.1038/ncb0802-e203.

112. Cordeiro, M.H.; Smith, R.J.; Saurin, A.T. A Fine Balancing Act: A Delicate Kinase-Phosphatase Equilibrium That Protects against Chromosomal Instability and Cancer. *Int J Biochem Cell Biology* **2018**, *96*, 148–156, doi:10.1016/j.biocel.2017.10.017.

113. Jarvis, R.M.; Hughes, S.M.; Ledgerwood, E.C. Peroxiredoxin 1 Functions as a Signal Peroxidase to Receive, Transduce, and Transmit Peroxide Signals in Mammalian Cells. *Free Radical Bio Med* **2012**, *53*, 1522 1530, doi:10.1016/j.freeradbiomed.2012.08.001.

114. Truong, T.H.; Carroll, K.S. Redox Regulation of Epidermal Growth Factor Receptor Signaling through Cysteine Oxidation. *Biochemistry-us* **2012**, *51*, 9954–9965, doi:10.1021/bi301441e.

115. Edgar, R.S.; Green, E.W.; Zhao, Y.; Ooijen, G. van; Olmedo, M.; Qin, X.; Xu, Y.; Pan, M.; Valekunja, U.K.; Feeney, K.A.; et al. Peroxiredoxins Are Conserved Markers of Circadian Rhythms. *Nature* **2012**, *485*, 459–464, doi:10.1038/nature11088.

116. Cho, C.-S.; Yoon, H.J.; Kim, J.Y.; Woo, H.A.; Rhee, S.G. Circadian Rhythm of Hyperoxidized Peroxiredoxin II Is Determined by Hemoglobin Autoxidation and the 20S Proteasome in Red Blood Cells. *Proc National Acad Sci* **2014**, *111*, 12043–12048, doi:10.1073/pnas.1401100111.

117. Veal, E.A.; Underwood, Z.E.; Tomalin, L.E.; Morgan, B.A.; Pillay, C.S. Hyperoxidation of Peroxiredoxins: Gain or Loss of Function? *Antioxid Redox Sign* **2017**, *28*, ars.2017.7214, doi:10.1089/ars.2017.7214.

118. Woo, H.A.; Yim, S.H.; Shin, D.H.; Kang, D.; Yu, D.-Y.; Rhee, S.G. Inactivation of Peroxiredoxin I by Phosphorylation Allows Localized H(2)O(2) Accumulation for Cell Signaling. *Cell* **2010**, *140*, 517 528, doi:10.1016/j.cell.2010.01.009.

119. Rhee, S.G.; Woo, H.A.; Kil, I.S.; Kil, I.S.; Bae, S.H. Peroxiredoxin Functions as a Peroxidase and a Regulator and Sensor of Local Peroxides. *J Biol Chem* **2012**, *287*, 4403 4410, doi:10.1074/jbc.r111.283432.

120. Panday, A.; Sahoo, M.K.; Osorio, D.; Batra, S. NADPH Oxidases: An Overview from Structure to Innate Immunity-Associated Pathologies. *Cell Mol Immunol* **2015**, *12*, 5–23, doi:10.1038/cmi.2014.89.

121. Rawat, S.J.; Creasy, C.L.; Peterson, J.R.; Chernoff, J. The Tumor Suppressor Mst1 Promotes Changes in the Cellular Redox State by Phosphorylation and Inactivation of Peroxiredoxin-1 Protein*. *J Biol Chem* **2013**, *288*, 8762–8771, doi:10.1074/jbc.m112.414524.

122. Lim, J.M.; Lee, K.S.; Woo, H.A.; Kang, D.; Rhee, S.G. Control of the Pericentrosomal H2O2 Level by Peroxiredoxin I Is Critical for Mitotic Progression. *J Cell Biology* **2015**, *210*, 23 33, doi:10.1083/jcb.201412068.

123. Chang, T.-S.; Jeong, W.; Choi, S.Y.; Yu, S.; Kang, S.W.; Rhee, S.G. Regulation of Peroxiredoxin I Activity by Cdc2-Mediated Phosphorylation. *J Biol Chem* **2002**, *277*, 25370 25376, doi:10.1074/jbc.m110432200.

124. Rhee, S.G.; Woo, H.A. Multiple Functions of 2-Cys Peroxiredoxins, I and II, and Their Regulations via Post-Translational Modifications. *Free Radical Bio Med* **2020**, *152*, 107–115, doi:10.1016/j.freeradbiomed.2020.02.028.

125. Ushio-Fukai, M. Compartmentalization of Redox Signaling Through NADPH Oxidase–Derived ROS. *Antioxid Redox Sign* **2009**, *11*, 1289–1299, doi:10.1089/ars.2008.2333.

126. Henau, S.D.; Pagès-Gallego, M.; Pannekoek, W.-J.; Dansen, T.B. Mitochondria-Derived H2O2 Promotes Symmetry Breaking of the C. Elegans Zygote. *Dev Cell* **2020**, *53*, 263-271.e6, doi:10.1016/j.devcel.2020.03.008.

127. Hansen, H.G.; Schmidt, J.D.; Søltoft, C.L.; Ramming, T.; Geertz-Hansen, H.M.; Christensen, B.; Sørensen, E.S.; Juncker, A.S.; Appenzeller-Herzog, C.; Ellgaard, L. Hyperactivity of the Ero1α Oxidase Elicits Endoplasmic Reticulum Stress but No Broad Antioxidant Response. *J Biol Chem* **2012**, *287*, 39513–39523, doi:10.1074/jbc.m112.405050.

128. Tavender, T.J.; Springate, J.J.; Bulleid, N.J. Recycling of Peroxiredoxin IV Provides a Novel Pathway for Disulphide Formation in the Endoplasmic Reticulum. *Embo J* **2010**, *29*, 4185–4197, doi:10.1038/emboj.2010.273.

129. Ramming, T.; Hansen, H.G.; Nagata, K.; Ellgaard, L.; Appenzeller-Herzog, C. GPx8 Peroxidase Prevents Leakage of H2O2 from the Endoplasmic Reticulum. *Free Radical Bio Med* **2014**, *70*, 106–116, doi:10.1016/j.freeradbiomed.2014.01.018.

130. Mishina, N.M.; Tyurin-Kuzmin, P.A.; Markvicheva, K.N.; Vorotnikov, A.V.; Tkachuk, V.A.; Laketa, V.; Schultz, C.; Lukyanov, S.; Belousov, V.V. Does Cellular Hydrogen Peroxide Diffuse or Act Locally? *Antioxid Redox Sign* **2011**, *14*, 1–7, doi:10.1089/ars.2010.3539.

131. Pak, V.V.; Ezeriņa, D.; Lyublinskaya, O.G.; Pedre, B.; Tyurin-Kuzmin, P.A.; Mishina, N.M.; Thauvin, M.; Young, D.; Wahni, K.; Gache, S.A.M.; et al. Ultrasensitive Genetically Encoded Indicator for Hydrogen Peroxide Identifies Roles for the Oxidant in Cell Migration and Mitochondrial Function. *Cell Metab* **2020**, *31*, 642-653.e6, doi:10.1016/j.cmet.2020.02.003.

132. Matlashov, M.E.; Belousov, V.V.; Enikolopov, G. How Much H2O2 Is Produced by Recombinant D-Amino Acid Oxidase in Mammalian Cells? *Antioxid Redox Sign* **2014**, *20*, 1039–1044, doi:10.1089/ars.2013.5618.

133. Saravi, S.S.S.; Eroglu, E.; Waldeck-Weiermair, M.; Sorrentino, A.; Steinhorn, B.; Belousov, V.; Michel, T. Differential Endothelial Signaling Responses Elicited by Chemogenetic H2O2 Synthesis. *Redox Biol* **2020**, *36*, 101605, doi:10.1016/j.redox.2020.101605.

134. Cheung, E.C.; Lee, P.; Ceteci, F.; Nixon, C.; Blyth, K.; Sansom, O.J.; Vousden, K.H. Opposing Effects of TIGAR- and RAC1-Derived ROS on Wnt-Driven Proliferation in the Mouse Intestine. *Gene Dev* **2016**, *30*, 52 63, doi:10.1101/gad.271130.115.

135. Delaunay, A.; Pflieger, D.; Barrault, M.-B.; Vinh, J.; Toledano, M.B. A Thiol Peroxidase Is an H2O2 Receptor and Redox-Transducer in Gene Activation. *Cell* **2002**, *111*, 471–481, doi:10.1016/s0092-8674(02)01048-6.

136. Veal, E.A.; Findlay, V.J.; Day, A.M.; Bozonet, S.M.; Evans, J.M.; Quinn, J.; Morgan, B.A. A 2-Cys Peroxiredoxin Regulates Peroxide-Induced Oxidation and Activation of a Stress-Activated MAP Kinase. *Mol Cell* **2004**, *15*, 129 139, doi:10.1016/j.molcel.2004.06.021.

137. Sobotta, M.C.; Liou, W.; cker, S.S. ouml; Talwar, D.; Oehler, M.; Ruppert, T.; Scharf, A.N.D.; Dick, T.P. Peroxiredoxin-2 and STAT3 Form a Redox Relay for H2O2 Signaling. *Nat Chem Biol* **2014**, *11*, 1 8, doi:10.1038/nchembio.1695.

138. Stöcker, S.; Maurer, M.; Ruppert, T.; Dick, T.P. A Role for 2-Cys Peroxiredoxins in Facilitating Cytosolic Protein Thiol Oxidation. *Nat Chem Biol* **2017**, *14*, doi:10.1038/nchembio.2536.

139. Brandstaedter, C.; Delahunty, C.; Schipper, S.; Rahlfs, S.; Yates, J.R.; Becker, K. The Interactome of 2-Cys Peroxiredoxins in Plasmodium Falciparum. *Sci Rep-uk* **2019**, *9*, 13542, doi:10.1038/s41598-019-49841-3.

140. Barata, A.G.; Dick, T.P. A Role for Peroxiredoxins in H2O2- and MEK-Dependent Activation of the P38 Signaling Pathway. *Redox Biol* **2020**, *28*, 101340, doi:10.1016/j.redox.2019.101340.

141. Fomenko, D.E.; Koc, A.; Agisheva, N.; Jacobsen, M.; Kaya, A.; Malinouski, M.; Rutherford, J.C.; Siu, K.-L.; Jin, D.-Y.; Winge, D.R.; et al. Thiol Peroxidases Mediate Specific Genome-Wide Regulation of Gene Expression in Response to Hydrogen Peroxide. *Proc National Acad Sci* **2011**, *108*, 2729 2734, doi:10.1073/pnas.1010721108.

142. Netto, L.E.S.; Antunes, and F. The Roles of Peroxiredoxin and Thioredoxin in Hydrogen Peroxide Sensing and in Signal Transduction. *Mol Cells* **2016**, *39*, 65 71, doi:10.14348/molcells.2016.2349.

143. Stewart, E.J.; Åslund, F.; Beckwith, J. Disulfide Bond Formation in the Escherichia Coli Cytoplasm: An in Vivo Role Reversal for the Thioredoxins. *Embo J* **1998**, *17*, 5543–5550, doi:10.1093/emboj/17.19.5543.

144. García-Santamarina, S.; Boronat, S.; Calvo, I.A.; Rodríguez-Gabriel, M.; Ayté, J.; Molina, H.; Hidalgo, E. Is Oxidized Thioredoxin a Major Trigger for Cysteine Oxidation? Clues from a Redox Proteomics Approach. *Antioxid Redox Sign* **2013**, *18*, 1549–1556, doi:10.1089/ars.2012.5037.

145. Brockwell, D.J.; Radford, S.E. Intermediates: Ubiquitous Species on Folding Energy Landscapes? *Curr Opin Struc Biol* **2007**, *17*, 30–37, doi:10.1016/j.sbi.2007.01.003.

146. Weids, A.J.; Ibstedt, S.; Tamás, M.J.; Grant, C.M. Distinct Stress Conditions Result in Aggregation of Proteins with Similar Properties. *Sci Rep-uk* **2016**, *6*, srep24554, doi:10.1038/srep24554.

147. Erdős, G.; Mészáros, B.; Reichmann, D.; Dosztányi, Z. Large-Scale Analysis of Redox-Sensitive Conditionally Disordered Protein Regions Reveals Their Widespread Nature and Key Roles in High-Level Eukaryotic Processes. *Proteomics* **2019**, *19*, 1800070, doi:10.1002/pmic.201800070.

148. Hansen, R.E.; Roth, D.; Winther, J.R. Quantifying the Global Cellular Thiol-Disulfide Status. *Proc National Acad Sci* **2009**, *106*, 422 427, doi:10.1073/pnas.0812149106.

149. Forrester, S.J.; Kikuchi, D.S.; Hernandes, M.S.; Xu, Q.; Griendling, K.K. Reactive Oxygen Species in Metabolic and Inflammatory Signaling. *Circ Res* **2018**, *122*, 877–902, doi:10.1161/circresaha.117.311401.

150. Chen, P.-H.; Chi, J.-T.; Boyce, M. Functional Crosstalk among Oxidative Stress and O-GlcNAc Signaling Pathways. *Glycobiology* **2018**, *28*, 556–564, doi:10.1093/glycob/cwy027.

151. Hornsveld, M.; Dansen, T.B. The Hallmarks of Cancer from a Redox Perspective. *Antioxid Redox Sign* **2016**, *25*, 300 325, doi:10.1089/ars.2015.6580.

152. Milkovic, L.; Gasparovic, A.C.; Cindric, M.; Mouthuy, P.-A.; Zarkovic, N. Short Overview of ROS as Cell Function Regulators and Their Implications in Therapy Concepts. *Cells* **2019**, *8*, 793, doi:10.3390/cells8080793.

153. Oswald, M.C.W.; Garnham, N.; Sweeney, S.T.; Landgraf, M. Regulation of Neuronal Development and Function by ROS. *Febs Lett* **2018**, *592*, 679–691, doi:10.1002/1873-3468.12972.

154. Kalyanaraman, B.; Cheng, G.; Hardy, M.; Ouari, O.; Bennett, B.; Zielonka, J. Teaching the Basics of Reactive Oxygen Species and Their Relevance to Cancer Biology: Mitochondrial Reactive Oxygen Species Detection, Redox Signaling, and Targeted Therapies. *Redox Biol* **2018**, *15*, 347–362, doi:10.1016/j.redox.2017.12.012.

155. Parascandolo, A.; Laukkanen, M.O. Carcinogenesis and Reactive Oxygen Species Signaling: Interaction of the NADPH Oxidase NOX1–5 and Superoxide Dismutase 1–3 Signal Transduction Pathways. *Antioxid Redox Sign* **2019**, *30*, 443–486, doi:10.1089/ars.2017.7268.

156. DeBerardinis, R.J.; Chandel, N.S. Fundamentals of Cancer Metabolism. *Sci Adv* **2016**, *2*, e1600200, doi:10.1126/sciadv.1600200.

157. Kim, J.; Kim, J.; Bae, J.-S. ROS Homeostasis and Metabolism: A Critical Liaison for Cancer Therapy. *Exp Mol Medicine* **2016**, *48*, e269–e269, doi:10.1038/emm.2016.119.

158. Nathan, C.; Cunningham-Bussel, A. Beyond Oxidative Stress: An Immunologist's Guide to Reactive Oxygen Species. *Nat Rev Immunol* **2013**, *13*, 349–361, doi:10.1038/nri3423.

159. Incalza, M.A.; D'Oria, R.; Natalicchio, A.; Perrini, S.; Laviola, L.; Giorgino, F. Oxidative Stress and Reactive Oxygen Species in Endothelial Dysfunction Associated with Cardiovascular and Metabolic Diseases. *Vasc Pharmacol* **2018**, *100*, 1–19, doi:10.1016/j.vph.2017.05.005.

160. Watson, J.D. Type 2 Diabetes as a Redox Disease. *Lancet* **2014**, *383*, 841–843, doi:10.1016/s0140-6736(13)62365-x.

161. Bazopoulou, D.; Knoefler, D.; Zheng, Y.; Ulrich, K.; Oleson, B.J.; Xie, L.; Kim, M.; Kaufmann, A.; Lee, Y.-T.; Dou, Y.; et al. Developmental ROS Individualizes Organismal Stress Resistance and Lifespan. *Nature* **2019**, *576*, 301–305, doi:10.1038/s41586-019-1814-y.

162. Golubev, A.; Hanson, A.D.; Gladyshev, V.N. A Tale of Two Concepts: Harmonizing the Free Radical and Antagonistic Pleiotropy Theories of Aging. *Antioxid Redox Sign* **2018**, *29*, 1003–1017, doi:10.1089/ars.2017.7105.

163. Burhans, W.C.; Heintz, N.H. The Cell Cycle Is a Redox Cycle: Linking Phase-Specific Targets to Cell Fate. *Free Radical Bio Med* **2009**, *47*, 1282 1293, doi:10.1016/j.freeradbiomed.2009.05.026.

164. Sies, H. Oxidative Eustress: On Constant Alert for Redox Homeostasis. *Redox Biol* **2021**, 101867, doi:10.1016/j.redox.2021.101867.

165. Meng, J.; Lv, Z.; Zhang, Y.; Wang, Y.; Qiao, X.; Sun, C.; Chen, Y.; Guo, M.; Han, W.; Ye, A.; et al. Precision Redox: The Key for Antioxidant Pharmacology. *Antioxid Redox Sign* **2021**, *34*, 1069–1082, doi:10.1089/ars.2020.8212.

166. Naviaux, R.K. Oxidative Shielding or Oxidative Stress? *J Pharmacol Exp Ther* **2012**, *342*, 608–618, doi:10.1124/jpet.112.192120.

167. Hansen, J.M.; Go, Y.-M.; Jones, D.P. Nuclear and Mitochondrial Compartmentation of Oxidative Stress and Redox Signaling. *Annu Rev Pharmacol* **2006**, *46*, 215–234, doi:10.1146/annurev.pharmtox.46.120604.141122.

168. Lyublinskaya, O.; Antunes, F. Measuring Intracellular Concentration of Hydrogen Peroxide with the Use of Genetically Encoded H2O2 Biosensor HyPer. *Redox Biol* **2019**, *24*, 101200, doi:10.1016/j.redox.2019.101200.

169. Nkabyo, Y.S.; Ziegler, T.R.; Gu, L.H.; Watson, W.H.; Jones, D.P. Glutathione and Thioredoxin Redox during Differentiation in Human Colon Epithelial (Caco-2) Cells. *Am J Physiol-gastr L* **2002**, *283*, G1352–G1359, doi:10.1152/ajpgi.00183.2002.

170. Schafer, F.Q.; Buettner, G.R. Redox Environment of the Cell as Viewed through the Redox State of the Glutathione Disulfide/Glutathione Couple. *Free Radical Bio Med* **2001**, *30*, 1191–1212, doi:10.1016/s0891-5849(01)00480-4.

171. Morgan, B.; Ezeriņa, D.; Amoako, T.N.E.; Riemer, J.; Seedorf, M.; Dick, T.P. Multiple Glutathione Disulfide Removal Pathways Mediate Cytosolic Redox Homeostasis. *Nat Chem Biol* **2013**, *9*, 119–125, doi:10.1038/nchembio.1142.

172. Jones, D.P.; Mody, V.C.; Carlson, J.L.; Lynn, M.J.; Sternberg, P. Redox Analysis of Human Plasma Allows Separation of Pro-Oxidant Events of Aging from Decline in Antioxidant Defenses. *Free Radical Bio Med* **2002**, *33*, 1290–1300, doi:10.1016/s0891-5849(02)01040-7.

173. Lim, J.B.; Langford, T.F.; Huang, B.K.; Deen, W.M.; Sikes, H.D. A Reaction-Diffusion Model of Cytosolic Hydrogen Peroxide. *Free Radical Bio Med* **2016**, *90*, 85–90, doi:10.1016/j.freeradbiomed.2015.11.005.

174. Rebrin, I.; Sohal, R.S. Comparison of Thiol Redox State of Mitochondria and Homogenates of Various Tissues between Two Strains of Mice with Different Longevities. *Exp Gerontol* **2004**, *39*, 1513–1519, doi:10.1016/j.exger.2004.08.014.

175. Shen, D.; Dalton, T.P.; Nebert, D.W.; Shertzer, H.G. Glutathione Redox State Regulates Mitochondrial Reactive OxygenProduction*. *J Biol Chem* **2005**, *280*, 25305–25312, doi:10.1074/jbc.m500095200.

176. Hu, J.; Dong, L.; Outten, C.E. The Redox Environment in the Mitochondrial Intermembrane Space Is Maintained Separately from the Cytosol and Matrix * *J Biol Chem* **2008**, *283*, 29126–29134, doi:10.1074/jbc.m803028200.

177. Matsuyama, S.; Llopis, J.; Deveraux, Q.L.; Tsien, R.Y.; Reed, J.C. Changes in Intramitochondrial and Cytosolic PH: Early Events That Modulate Caspase Activation during Apoptosis. *Nat Cell Biol* **2000**, *2*, 318–325, doi:10.1038/35014006.

178. Porcelli, A.M.; Ghelli, A.; Zanna, C.; Pinton, P.; Rizzuto, R.; Rugolo, M. PH Difference across the Outer Mitochondrial Membrane Measured with a Green Fluorescent Protein Mutant. *Biochem Bioph Res Co* **2005**, *326*, 799–804, doi:10.1016/j.bbrc.2004.11.105.

179. Abad, M.F.C.; Benedetto, G.D.; Magalhães, P.J.; Filippin, L.; Pozzan, T. Mitochondrial PH Monitored by a New Engineered Green Fluorescent Protein Mutant*. *J Biol Chem* **2004**, *279*, 11521–11529, doi:10.1074/jbc.m306766200.

180. Poburko, D.; Santo-Domingo, J.; Demaurex, N. Dynamic Regulation of the Mitochondrial Proton Gradient during Cytosolic Calcium Elevations*. *J Biological Chem* **2011**, *286*, 11672–11684, doi:10.1074/jbc.m110.159962.

181. Hwang, C.; Sinskey, A.J.; Lodish, H.F. Oxidized Redox State of Glutathione in the Endoplasmic Reticulum. *Science* **1992**, *257*, 1496–1502, doi:10.1126/science.1523409.

182. Navas, P.; Sun, I.; Crane, F.L.; Morré, D.M.; Morré, D.J. Monoascorbate Free Radical-Dependent Oxidation-Reduction Reactions of Liver Golgi Apparatus Membranes. *J Bioenerg Biomembr* **2010**, *42*, 181–187, doi:10.1007/s10863-010-9272-0.

183. Yano, T.; Oku, M.; Akeyama, N.; Itoyama, A.; Yurimoto, H.; Kuge, S.; Fujiki, Y.; Sakai, Y. A Novel Fluorescent Sensor Protein for Visualization of Redox States in the Cytoplasm and in Peroxisomes ∇ †. *Mol Cell Biol* **2010**, *30*, 3758–3766, doi:10.1128/mcb.00121-10.

184. Gille, L.; Nohl, H. The Existence of a Lysosomal Redox Chain and the Role of Ubiquinone. *Arch Biochem Biophys* **2000**, *375*, 347–354, doi:10.1006/abbi.1999.1649.

GRAPHICAL ABSTRACT

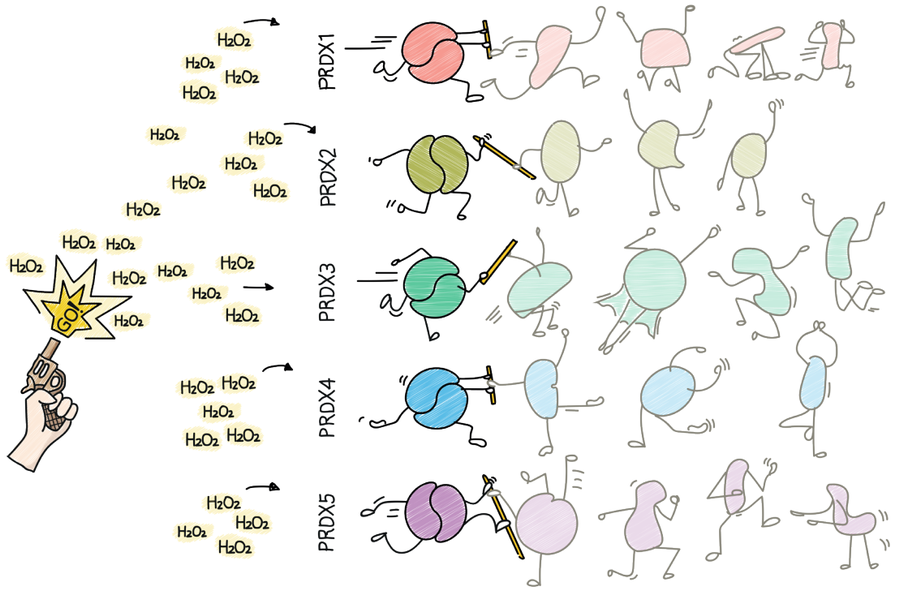

CHAPTER 2

THE HUMAN 2-CYS PEROXIREDOXINS FORM WIDESPREAD, CYSTEINE-DEPENDENT- AND ISOFORM-SPECIFIC PROTEIN-PROTEIN INTERACTIONS

Loes van Dam[1], Marc Pagès-Gallego[1], Paulien E. Polderman[1], Robert M. van Es[1], Boudewijn M. T. Burgering[1,2], Harmjan R. Vos[1] and Tobias B. Dansen[1]

[1]Center for Molecular Medicine, Molecular Cancer Research, University Medical Center Utrecht, Universiteitsweg 100, 3584CG, Utrecht, The Netherlands
[2]Oncode Institute, University Medical Center Utrecht, Universiteitsweg 100, 3584CG, Utrecht, The Netherlands.

Correspondence: t.b.dansen@umcutrecht.nl

PUBLISHED *in Antioxidants* 2021, *10*, *627*, *https://doi.org/10.3390/antiox10040627*.

KEYWORDS
redox proteomics; S-peroxiredoxinylation; peroxiredoxin; redox signaling; redox relay; hydrogen peroxide; protein thiol oxidation; cysteine sulfenic acid; thiol disulfide exchange

THE HUMAN 2-CYS PEROXIREDOXINS FORM WIDESPREAD, CYSTEINE-DEPENDENT- AND ISOFORM-SPECIFIC PROTEIN-PROTEIN INTERACTIONS

ABSTRACT

Redox signaling is controlled by the reversible oxidation of cysteine thiols, a post-translational modification triggered by H_2O_2 acting as a second messenger. However, H_2O_2 actually reacts poorly with most cysteine thiols and it is not clear how H_2O_2 discriminates between cysteines to trigger appropriate signaling cascades in the presence of dedicated H2O2 scavengers like peroxiredoxins (PRDXs). It was recently suggested that peroxiredoxins act as peroxidases and facilitate H2O2-dependent oxidation of redox-regulated proteins via disulfide exchange reactions. It is unknown how the peroxiredoxin-based relay model achieves the selective substrate targeting required for adequate cellular signaling. Using a systematic mass-spectrometry-based approach to identify cysteine-dependent interactors of the five human 2-cys peroxiredoxins, we show that all five human 2-cys peroxiredoxins can form disulfide-dependent heterodimers with a large set of proteins. Each isoform displays a preference for a subset of disulfide-dependent binding partners, and we explore isoform-specific properties that might underlie this preference. We provide evidence that peroxiredoxin-based redox relays can proceed via two distinct molecular mechanisms. Altogether, our results support the theory that peroxiredoxins could play a role in providing not only reactivity but also selectivity in the transduction of peroxide signals to generate complex cellular signaling responses.

INTRODUCTION

In order to adapt to a changing environment, cells continuously translate extracellular cues into appropriate cellular responses through cascades of protein-protein interactions and post-translational modifications known as signal transduction. A recently discovered form of signal transduction termed redox signaling, uses hydrogen peroxide (H_2O_2) as a second messenger, and proceeds through the reversible oxidation of specific cysteine thiols in proteins (for a review, see ref. [1]). To function as a reliable second messenger, H_2O_2 should be able to discriminate which cysteines it needs to oxidize specifically in order to trigger the proper signaling cascade. Although numerous H_2O_2-regulated proteins and processes have been discovered, it is unclear how exactly redox signaling achieves the required reactivity and specificity, which are fundamental requirements for coherent cellular signaling.

H_2O_2 is considered the major reactive oxygen species (ROS) for signaling because of its relative stability compared to other cellular reactive oxygen species (ROS, i.e., $O_2^{\cdot-}$ and $^{\cdot}OH$) [2]. However, this relative stability also means that H_2O_2 reacts poorly with most cysteine thiols, with rate constants ranging from 20 to 200 $M^{-1}s^{-1}$ [3–5]. Additionally, dedicated H_2O_2 scavengers like peroxiredoxins (PRDXs) are estimated to eliminate >99% of cellular H_2O_2 [6], because their catalytic cysteines react with many orders of magnitude faster with H_2O_2 than other thiols in cysteine side chains in proteins, including those found to be redox regulated. Peroxiredoxins are highly abundant and ubiquitous proteins, with isoforms localized to cytoplasm, mitochondria, ER and other cellular compartments [7]. The poor reactivity of thiols with H_2O_2 combined with the effective elimination of H_2O_2 by peroxiredoxins seems to challenge the idea that reactivity and selectivity in redox signaling can be achieved by a simple molecule like H_2O_2.

Peroxiredoxins do not only scavenge H_2O_2; in fact, oxidized 2-cys peroxiredoxins have also been shown to act as peroxidases and facilitate H_2O_2-dependent protein oxidation via disulfide exchange reactions. For example, in *S. cerevisiae,* Tsa1 and Orp1 peroxidases relay towards the Yap1 transcription factor [8] and a similar mechanism was identified for Sty1 in in *S. pombe* [9]. In mammalian cells, the ASK1 kinase and STAT3 transcription factor are oxidized by PRDX1 and PRDX2, respectively [10,11], and ER-localized PRDX4 is known to induce disulfide formation through the oxidation of protein disulfide isomerase (PDI) [12].

Others have shown a more widespread role for peroxiredoxins in H_2O_2-induced thiol oxidation [13,14] . In this so-called peroxiredoxin-based relay model, the extremely reactive peroxidatic cysteine of peroxiredoxins first reacts with H_2O_2 and subsequently the oxidized peroxiredoxin catalyzes the oxidation of low reactivity thiols in redox-regulated proteins (see Figure 1A). This mechanism could explain how so many intrinsically unreactive protein thiols can be found to be reversibly oxidized in response to H_2O_2-dependent redox signaling, despite the presence of a highly abundant and reactive H_2O_2 scavenging system.

Although the peroxiredoxin-based relay model may explain how the reactivity of H_2O_2 with protein thiols is overcome, it does not as yet explain how the selectivity in H_2O_2-dependent redox signaling is achieved. In order to produce relevant biological signals, selective substrate targeting is required to achieve proper signaling outputs. In redox signaling, this would mean that in the presence of numerous potential substrates, specific subsets of redox-regulated proteins should be oxidized dependent on, for instance, the subcellular localization or the local concentration of H_2O_2. Mammalian cells express five 2-cys peroxiredoxin isoforms, each with their own localization, oxidation kinetics and structural differences around their catalytic sites. We therefore hypothesized that reactivity and selectivity in redox signaling could also be provided by the different 2-cys peroxiredoxins.

According to this line of reasoning, peroxiredoxins would be expected to participate in temporary covalent complexes with isoform-specific subsets of target proteins, mediated by

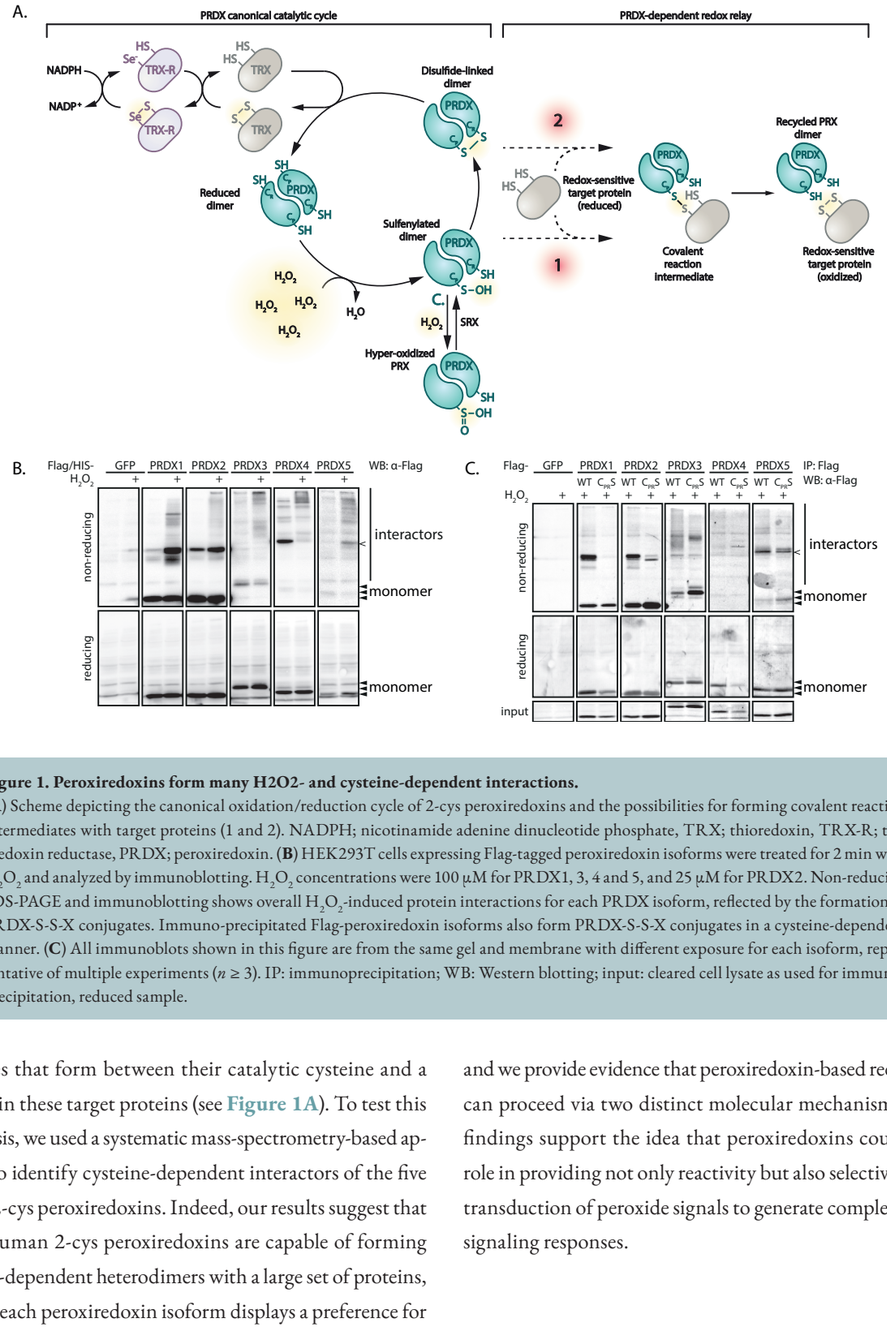

Figure 1. Peroxiredoxins form many H2O2- and cysteine-dependent interactions.
(**A**) Scheme depicting the canonical oxidation/reduction cycle of 2-cys peroxiredoxins and the possibilities for forming covalent reaction intermediates with target proteins (1 and 2). NADPH; nicotinamide adenine dinucleotide phosphate, TRX; thioredoxin, TRX-R; thioredoxin reductase, PRDX; peroxiredoxin. (**B**) HEK293T cells expressing Flag-tagged peroxiredoxin isoforms were treated for 2 min with H_2O_2 and analyzed by immunoblotting. H_2O_2 concentrations were 100 μM for PRDX1, 3, 4 and 5, and 25 μM for PRDX2. Non-reducing SDS-PAGE and immunoblotting shows overall H_2O_2-induced protein interactions for each PRDX isoform, reflected by the formation of PRDX-S-S-X conjugates. Immuno-precipitated Flag-peroxiredoxin isoforms also form PRDX-S-S-X conjugates in a cysteine-dependent manner. (**C**) All immunoblots shown in this figure are from the same gel and membrane with different exposure for each isoform, representative of multiple experiments ($n \geq 3$). IP: immunoprecipitation; WB: Western blotting; input: cleared cell lysate as used for immunoprecipitation, reduced sample.

disulfides that form between their catalytic cysteine and a cysteine in these target proteins (see Figure 1A). To test this hypothesis, we used a systematic mass-spectrometry-based approach to identify cysteine-dependent interactors of the five human 2-cys peroxiredoxins. Indeed, our results suggest that all five human 2-cys peroxiredoxins are capable of forming disulfide-dependent heterodimers with a large set of proteins, and that each peroxiredoxin isoform displays a preference for a subset of disulfide-dependent binding partners. We explore what isoform-specific properties underlie these observations and we provide evidence that peroxiredoxin-based redox relays can proceed via two distinct molecular mechanisms. These findings support the idea that peroxiredoxins could play a role in providing not only reactivity but also selectivity in the transduction of peroxide signals to generate complex cellular signaling responses.

RESULTS

All Five Human 2-cys Peroxiredoxins Have Many H_2O_2- And Cysteine-Dependent Interactors

As described above, peroxiredoxin-catalyzed cysteine oxidation proceeds through the (transient) formation of a disulfide bond between peroxiredoxins and target proteins, as has been shown for PRDX1 and PRDX2 [13]. If all human 2-cys peroxiredoxins are involved in redox relay signaling, disulfide-dependent heterodimers (i.e., PRDX-S-S-X) would be expected to be formed upon oxidation of PRDX1-5. These disulfide-dependent heterodimers would show up as PRDX-containing high-molecular weight bands upon separation on non-reducing SDS-PAGE followed by Western blotting. Indeed, a number of high-molecular weight bands containing PRDX1-5 can be detected upon a 2-min pulse of H_2O_2 (Figure 1B). These Flag-PRDX1-5-containing complexes are indeed sensitive to reduction, confirming the presence of disulfides. For PRDX1, 3, 4 and 5 we used 100 μM H_2O_2, since that concentration showed many interaction partners in another study investigating PRDX binding partners in this cell type [13]. PRDX2 shows substantial hyperoxidation at 100 μM H_2O_2 and we therefore used 25 μM H_2O_2 for the experiments using PRDX2 (Figure S1).

The covalent, disulfide-dependent heterodimeric complexes of Flag-PRDX1-5 and their interaction partners could be isolated by immunoprecipitation (Figure 1C). Mutation of the catalytic cysteines (C_P and C_R) to serine (PRDX $C_{PR}S$) abolished the formation of the majority H_2O_2-induced disulfide-dependent binding partners for all PRDX isoforms (Figure 1C), indicating that the catalytic cysteines in all 2-cys peroxiredoxins form disulfide-dependent complexes with several other proteins upon oxidation. The PRDX1–5 containing complexes migrate different distances than the disulfide dependent homodimers (for PRDX 1–4). Note that for PRDX4 and PRDX5 a band runs at about twice their MW (Figure 1B), which is also present in the $C_{PR}S$ mutant; hence this cannot be the oxidized peroxiredoxin homodimer. For PRDX5 this is not unexpected since this is the only a-typical 2-cys PRDX and forms an intramolecular rather than intermolecular disulfide upon oxidation by H_2O_2. In summary, these results show that the five 2-cys PRDX isoforms form many H_2O_2-induced, disulfide-dependent interactions that can be isolated by immunoprecipitation.

A Proteome-Wide Screen Identifies the Interactome of Human 2-cys Peroxiredoxins

Having confirmed the ability of all five 2-cys peroxiredoxins to form intermolecular disulfide-dependent complexes, we wondered about the scale of the interactome and the identities of the disulfide-dependent interacting proteins. To answer these questions, we performed an unbiased, quantitative mass-spectrometry-based screen to identify cysteine-dependent interactors for each PRDX isoform. A workflow for this screen is shown in Figure 2A. In short, cells expressing Flag-tagged PRDX were exposed to a short pulse of H_2O_2 followed by cell lysis. To prevent post-lysis oxidation and reduction, free thiols are quenched before and after lysis using N-ethylmaleimide (NEM) and iodoacetamide (IA), respectively. Flag-PRDX1-5 were pulled-down along with their interactors and subsequently exposed to a stringent high-salt wash to diminish non-covalent interactors. We then identified the interacting proteins using quantitative tandem mass spectrometry (MS/MS) followed by strict filtering and data analysis.

Figures 2B–F display scatter plots of the mean $\log_2$ intensities of the interacting proteins identified for PRDX1–5 wild-type (WT) and corresponding PRDX-$C_{PR}S$ mutants from three biological replicates. Marginal line graphs of the data distribution visualize data points that are hidden by overcrowding. Proteins interacting with both WT and mutant peroxiredoxin appear on a diagonal, while proteins interacting with only WT will have no intensity in the corresponding $C_{PR}S$ mutant and are thus visible off the diagonal. This data indicates that all five isoforms interact with a large number of proteins, and that many of those interactions are dependent on the peroxiredoxin catalytic cysteines. For most peroxiredoxin isoforms, but especially PRDX1, PRDX2 and PRDX3, the number of proteins that bind exclusively to wild-type is higher than to

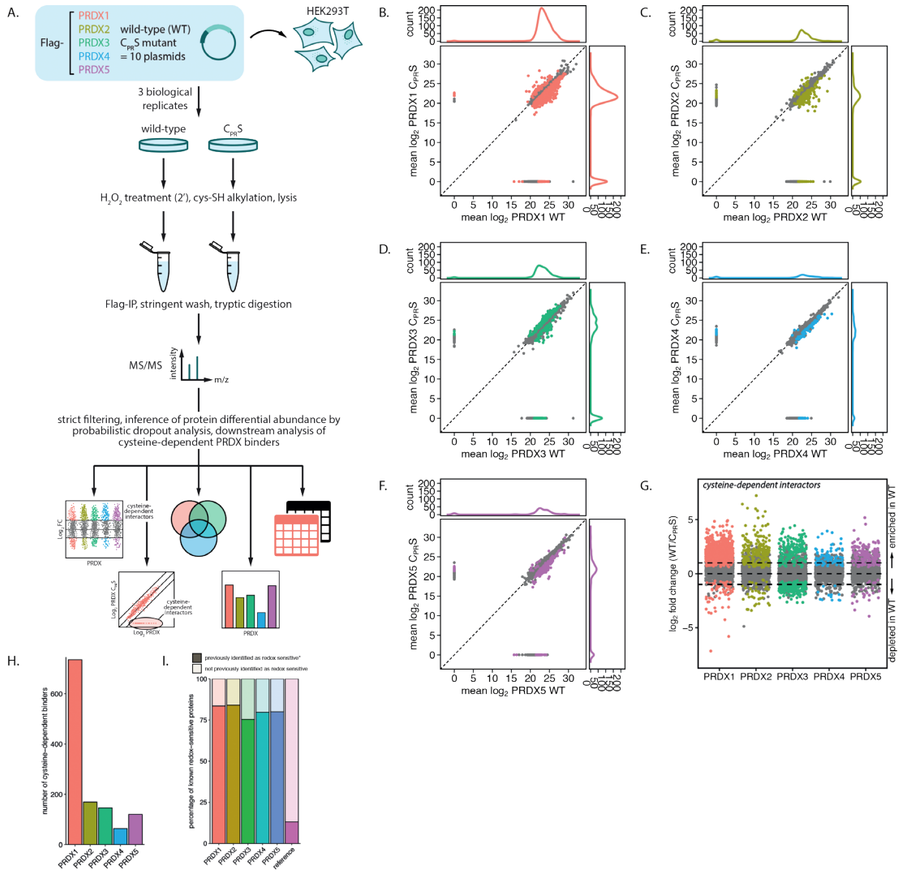

Figure 2. A proteome-wide screen to identify the interactome of human 2-cys peroxiredoxins.
(**A**) Schematic representation of our workflow. Cells expressing Flag-PRDX isoforms (either wild-type or mutant) were treated with H_2O_2 and alkylated with NEM and IA prior to and during lysis, respectively. H_2O_2 concentrations were 100 µM for PRDX1, 3, 4 and 5 and 25 µM for PRDX2. Flag-peroxiredoxins and their interacting proteins were pulled down using immobilized anti-Flag-M2 and subsequently exposed to a stringent high-salt wash and binding partners were measured by mass spectrometry. After stringent filtering we inferred protein differential abundance by probabilistic dropout modeling. PRDX; peroxiredoxin, WT; wild-type, CP; peroxidatic cysteine; CR; resolving cysteine, IP; immunoprecipitation, MS/MS; tandem mass spectrometry. (**B-F**) Marginal scatter plots for peroxiredoxins 1–5, depicting the mean log_2 LFQ intensity for both wild-type and $C_{PR}S$ mutant peroxiredoxin. Colored proteins are identified with a *p*-value <0.05, and the distribution of these proteins are also visualized in the marginal density plots. Proteins interacting with both WT and mutant peroxiredoxin appear on a diagonal, while proteins that bind only WT or the $C_{PR}S$ mutant appear along the horizontal or vertical axis, respectively, and can be found at the edges of the marginal plots. (**G**) Scatter plot of log_2 fold change between wild-type and $C_{PR}S$-peroxiredoxin isoforms. Horizontal lines are positioned at log_2 fold change of 1 and –1 (i.e., a 2-fold change). Colored proteins are identified with a *p*-value <0.05. (**H**) Number of cysteine-dependent interaction partners per peroxiredoxin isoform identified with *p*-value <0.05 and log_2 fold change >1 in our screen. (**I**) Bar chart representing the percentage of interactors per PRDX that are previously identified as redox-sensitive in a large-scale mass-spectrometry-based screen. The reference proteome contains 75071 human UniProt entries with "reference proteome" as keyword.

the corresponding mutant (visualized in the marginal plots of Figures 2B–F and Figure S2), suggesting that their interaction is cysteine-dependent. PRDX4 and PRDX5 seem to have a lower number of cysteine-dependent binders than the other isoforms. As yet we do not have a biological explanation for what the $C_{PR}S$-specific interactors would represent.

A major challenge that is inherent to mass spectrometry data analysis, especially in proteome-wide protein-protein interaction studies like these, is that not all proteins are identified or quantified in each biological replicate and sample, therefore the data contains many missing values (an average of 34% per sample) [15]. It is well known that many of these missing values are non-random and that their absence correlates with a low overall intensity. If the hypothesis that proteins bind to PRDX in a largely disulfide-dependent manner holds true, missing values are actually expected to occur more often in the PRDX-$C_{PR}S$ mutant pull-downs. Thus, non-random missing data could hold important information in this experiment. In our analysis done for Figure 2B–F we simply ignored the missing values. Although this approach produces a general picture of the data, for a detailed analysis it is not optimal. Several MS data analysis approaches replace missing values with a reasonable value (imputation). However, imputing non-random missing values can overestimate peptide abundances and obscure available information, meaning that imputed values will be considered with the same confidence as measured values. This will lead to biased results, skewing data in a sample-dependent manner. For these reasons, we reanalyzed our data using a method called proDA (inference of protein differential abundance by probabilistic dropout analysis). This method aims to combine the sigmoidal dropout curve for missing values with the information from the observed values without direct value imputation. This allows for a more robust analysis that combines both the information from measured and missing values [16].

Cysteine-dependent interactors for each PRDX are visualized by plotting the fold change in intensity for each interactor pulled down with either WT, $C_{PR}S$ or both, on a log_2 scale. In the proDA analysis, a large log_2 fold change means that the protein was detected with high abundance in the WT peroxiredoxin pulldown and with no or low abundance in $C_{PR}S$ peroxiredoxin. Specifically, the difference between means (log_2 fold change) is calculated based on the distribution of measured values and, when values are missing, the distribution of these is based on the average detection limit of the sample. To determine a suitable cutoff for our data, we randomized the data-labels a hundred times between WT and $C_{PR}S$ data and recalculated the log_2 fold change. With the randomized data, we calculate that with a log_2 fold change threshold of >0.401, 5% of the randomized data is within the 95th quantile (i.e., an FDR of 5%,); on the other hand, 25.2% of the non-randomized data are included using the same threshold. In order to increase confidence, we used a more stringent cutoff of log_2 fold change >1 (FDR of 0.02%, Figure S3). Therefore, proteins are considered to be significantly enriched when detected with at least twice the abundance (i.e., log_2 fold change >1) as compared to the average expression of a protein around the limit of detection of the experiment, and a *p*-value <0.05. A total of 1233 proteins pass these criteria as catalytic cysteine-dependent binders of peroxiredoxins (Figure 2G and Supplementary **Table S1**). Collectively, the results from our screen indicate that a large number of proteins form disulfide-dependent heterodimers with the five 2-cys peroxiredoxin isoforms.

We set out to characterize the isoform-specific interaction partners of peroxiredoxins in more detail. Specifically, we asked what proportion has previously been identified in a large-scale mass-spectrometry-based screen for redox-sensitive proteins [17]. Of the proteins identified in our screen, 80.5% contained cysteines that have previously been reported as sensitive to oxidative modification, compared to 13% in the reference proteome (Figure 2I). We also observed this enrichment for redox-sensitive proteins for each individual PRDX isoform.

Peroxiredoxin Isoforms Interact With a Specific Set of Target Proteins

The subcellular localization of the five 2-cys PRDX isoforms, as well as their reaction kinetics, are not identical, and we therefore predicted that this could be reflected in their cysteine-dependent interactomes. We therefore next asked what the extent of overlap is between cysteine-dependent binding partners of different PRDX isoforms. A quantitative analysis of the intersections between the interactomes is shown in a

matrix layout using an Upset plot (**Figure 3A**). **Figure 3B** presents the overlap in a more traditional color-coded Venn diagram. Interestingly, in this comparison we found that each peroxiredoxin isoform has a largely differential set of cysteine-dependent binding partners. This suggests that each of the peroxiredoxins catalyze the oxidation of a specific set of substrates.

Next, we investigated whether the subcellular localization of isoform-specific cysteine-dependent binding partners corresponds with the known localization of peroxiredoxin isoforms. To do so, we used SubCellBarCode [18], a resource that documents the subcellular localization of proteins in multiple cell lines. Indeed, most peroxiredoxin-binding proteins are overrepresented in the compartment where the peroxiredoxin isoform they interact with is reportedly localized (**Figure 3C**). For example, mitochondrial PRDX3, ER-localized PRDX4 and nuclear PRDX5 show an enrichment of proteins in the mitochondrial, secretory and nuclear compartments, respectively. The analysis is thus in line with the hypothesis that isoform-specific preferred localization could, at least to some extent, explain the PRDX-specificity of binding partners. A note of caution is due here since the generalizability to other cell lines is uncertain; additionally, not all databases report the same predominant localization for the peroxiredoxins [19–21]. This may vary depending on the cell state, tissue type, cell cycle and post-translational modifications (for an overview, see [22]).

PRDX1 and PRDX2 share 90% sequence similarity (**Figure 3D**) and have the same reported subcellular localization (cytoplasm), but we found approximately one third of PRDX2 interactors to overlap with PRDX1 interaction partners, suggesting that localization is apparently not the sole determinant of PRDX isoform-specific disulfide-dependent binding. Differences in the molecular interface surrounding the cysteines of the binding partners that bind the catalytic cysteine of the peroxiredoxin isoforms could be the underlying mechanism behind this specific binding. For instance, it is known that deprotonation of the cysteine thiol at physiological pH is governed by the local environment, and the thiolate is more readily oxidized [23]. Recently, it was suggested that positively charged amino acid side chains (arginine, lysine, histidine) and the N-terminus can stabilize the thiolate of a proximal cysteine [17]. We therefore investigated whether the local environment around the cysteines of peroxiredoxin isoform-specific interactors is enriched for certain amino acids that can potentially alter the reactivity of a proximal cysteine. A challenge here is that our screen does not report on which specific cysteine of a binding partner is involved in the interaction with the PRDX, and we therefore analyzed all cysteines present in the binding partner, which would likely dilute any specific motifs. To investigate the presence of characteristic molecular environments, we extracted the eight amino acids flanking all cysteine residues of cysteine-dependent interactors for each peroxiredoxin isoform. Subsequently, we examined the amino acids surrounding each cysteine and calculated the fold change in the presence of each amino acid in one peroxiredoxin compared to all other isoforms. The amino acid enrichment or depletion in possible binding sites of specific peroxiredoxin isoforms is shown in **Figure 3E–I**. In general, these calculations suggest that the local amino acid composition of interactors of a specific peroxiredoxin looks different from that of the interactors of the other peroxiredoxin isoforms. Note that this analysis is based purely on the primary sequence of the binding partners, and that a 3D structure and pinpointing which cysteine actually forms the interaction would likely reveal a clearer picture of differences in the molecular interface, but we consider that beyond the scope of this study.

The analysis of peroxiredoxin interactors described above is based on the comparison of cysteine-dependent binders to each peroxiredoxin isoform. It is possible, however, that proteins bind to one peroxiredoxin isoform in a cysteine-dependent manner, but independent of cysteines to another peroxiredoxin isoform. To analyze the peroxiredoxin-specificity for cysteine-dependent interactors with a different approach, we re-analyzed our dataset in order to identify isoform-specific interactors. For each peroxiredoxin, we fit a new probabilistic

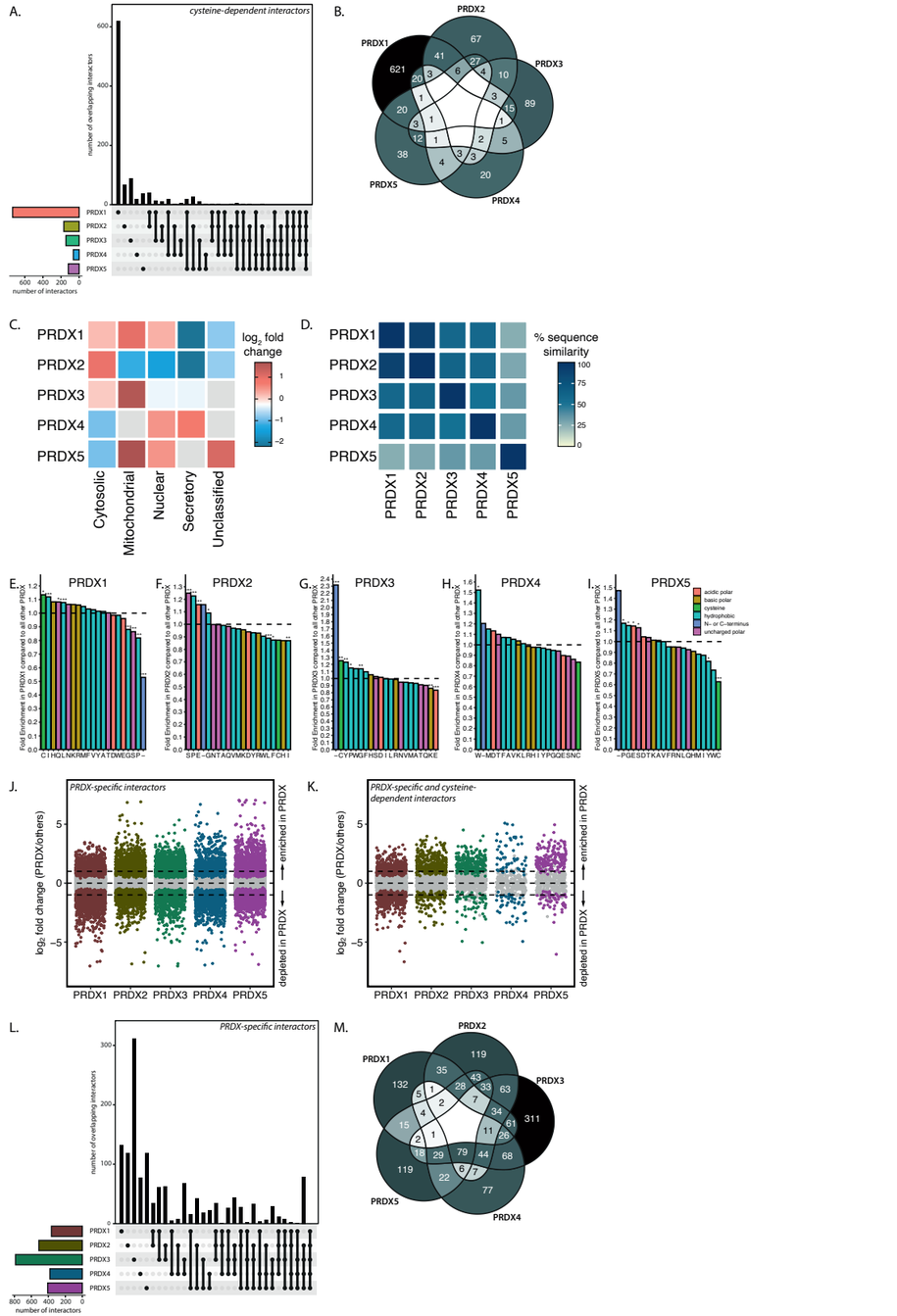

Figure 3. Peroxiredoxin isoforms interact with a specific set of target proteins. *(figure legend continues on next page)*

(**A**) UpSet plot and (**B**) Venn diagram to visualize cysteine-dependent target protein set intersections per peroxiredoxin isoform in a matrix layout. A color gradient from light (no overlap) to dark (high overlap) indicates the amount of overlap in the Venn diagram. (**C**) Localization of the top isoform-specific cysteine-dependent binders (>10-fold better binding to WT as compared to CprS) using the SubCellBarcode resource. Missing values are colored grey. (**D**) Sequence similarity for peroxiredoxins 1–5 calculated using the pairwise alignment tool EMBOSS needle. (**E-I**) Bar charts representing fold enrichment of the local amino acid composition around each cysteine in isoform-specific, cysteine-dependent peroxiredoxin interactors compared to the interactors of all other peroxiredoxin isoforms. Eight amino acids were extracted centered around each cysteine, with sequences shuffled 100 times as a control. * $p < 0.05$; ** $p < 0.01$; *** $p < 0.001$. (**J**) Scatter plot of $\log_2$ fold change comparing each peroxiredoxin isoform to all other isoforms. Horizontal lines are positioned at $\log_2$ fold change of 1 and –1 (i.e., a 2-fold change). Colored proteins are identified with Benjamini–Hochberg adjusted $p < 0.05$. (**K**) Similar to (**J**) but filtered for cysteine-dependent binders as analyzed in Figure 2G. (**L**) UpSet plot and (**M**) Venn diagram visualizing peroxiredoxin isoform-specific target protein set intersections in a matrix layout. A color gradient from light (no overlap) to dark (high overlap) indicates the amount of overlap in the Venn diagram.

dropout model using proDA, now testing which proteins are enriched in each peroxiredoxin isoform compared to the other isoforms irrespective of cysteine-dependency. Isoform-dependent interactors for each peroxiredoxin are visualized by plotting the $\log_2$ fold change in abundance comparing PRDX1–5 (i.e., the difference between the analyzed peroxiredoxin and all other isoforms on a $\log_2$ scale). Proteins that were enriched in pulldowns for one peroxiredoxin isoform (WT) but not in the other isoforms (with a log ratio of >1) are considered peroxiredoxin-specific binders. These data show a large number of proteins that bind to peroxiredoxins in an isoform-specific manner, irrespective of whether this is cysteine-dependent (**Figure 3J**). Again, we see that all PRDX isoforms have a large set of peroxiredoxin-specific interactors, which accords with our earlier observations, suggesting that each peroxiredoxin isoform has a largely differential set of cysteine-dependent binding partners (**Figure 3A,B**). Overlaying this analysis with the results obtained for cysteine-dependency in Figure 2G results in Figure 3K, which shows preferential binding partners for each PRDX isoform that do not bind to the $C_{PR}S$ mutant of that isoform. This is shown in the Upset plot and Venn diagram in Figure 3L and M, respectively.

Although we use a stringent wash buffer (containing 1 M NaCl) after the immunopurification of PRDX1–5 to enrich for disulfide-dependent covalent interactions, a large number of proteins were found to interact with the PRDX $C_{PR}S$ mutants (Supplemental **Figure S4**, light bars). The peroxiredoxin specificity of our data including both cysteine-dependent as well as -independent binders reassures that the observed interactions are not an artefact of post-lysis binding to all PRDXs or the anti-Flag coated beads in which case they would be expected to largely overlap. When we look at the top 100 proteins with the lowest *p*-values and allow them to cluster per peroxiredoxin isoform, we also observe different patterns of interacting proteins for the five PRDX isoforms (Supplemental **Figure S5**).

These results support the idea that all five peroxiredoxin isoforms bind a specific set of cysteine-dependent interactors, which could suggest that PRDX isoforms each control the oxidation of a different subset of the proteome through which redox relay signaling. The cysteine-dependent binding partners of peroxiredoxins contain a large fraction of proteins that have been reported as redox-sensitive. The localization of peroxiredoxin interactors, together with apparent differences in the local environment of interactor cysteines, could potentially explain isoform specificity.

The Peroxidatic Cysteine is Sufficient to Form Cysteine-Dependent, Peroxiredoxin-Specific Interactions

Oxidized peroxiredoxins could in principle relay oxidizing equivalents to other thiols via two molecular mechanisms. The first mechanism involves the condensation of sulfenylated peroxidatic cysteine (C_p-SOH) of peroxiredoxins directly with the cysteine thiol of a target protein (**Figure 1A**, 1). A second possible mechanism involves a disulfide exchange reaction of the disulfide between the peroxidatic and resolving cysteine (C_p-S-S-C_R) in oxidized peroxiredoxins with a target protein thiol (**Figure 1A**, 2). The SOH-mediated mechanism in principle only needs the peroxidatic cysteine of peroxiredoxin, whereas the S-S-mediated route is dependent on both catalytic cysteines.

To test which of these mechanisms is involved in the formation of S-S-dependent PRDX-target heterodimers, we performed another mass-spectrometry-based screen similar to the one described above, but now comparing C_RS mutants to the catalytic dead mutants ($C_{PR}S$) of each peroxiredoxin isoform. The C_RS mutant could in theory still relay through the (C_p-SOH) but not the C_p-S-S-C_R dependent mechanism.

Peroxiredoxin C_RS mutants of all five isoforms can still participate in disulfide-dependent interactions with many pro-

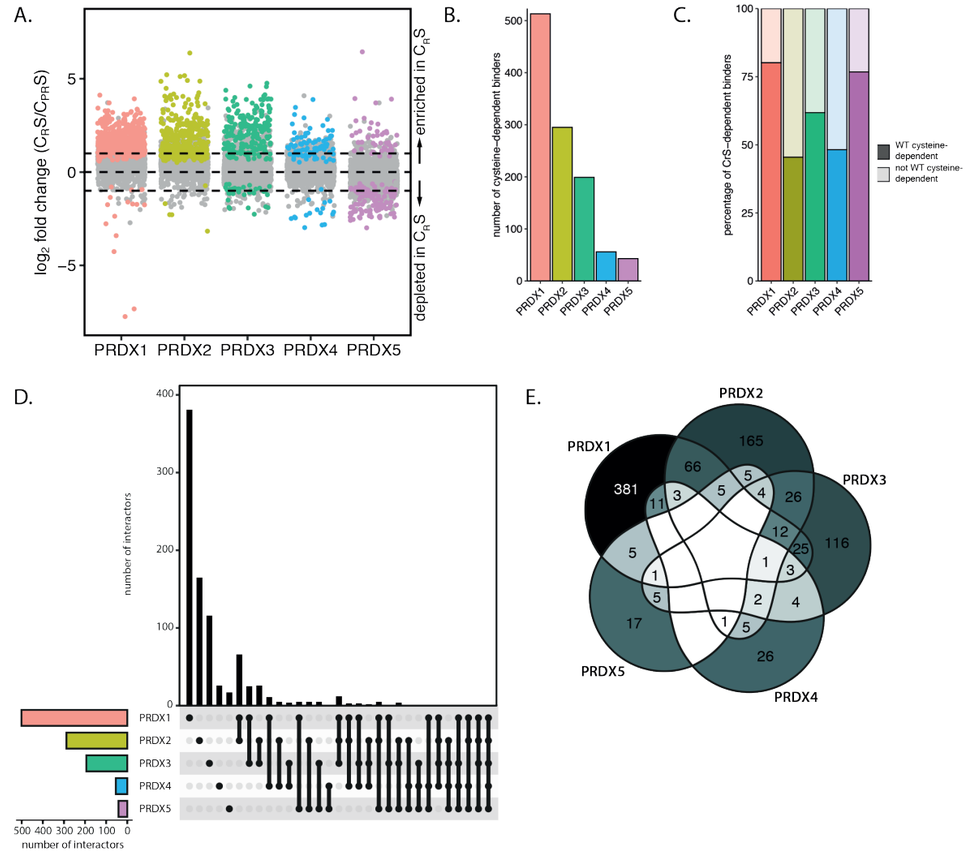

Figure 4. The peroxidatic cysteine is sufficient to form cysteine-dependent, peroxiredoxin-specific interactions.
(**A**) Scatter plot of the $\log_2$ fold change in binding of proteins to each of the C_RS-mutant peroxiredoxin isoforms compared to the $C_{PR}S$-mutant of the same peroxiredoxin isoform. Horizontal lines are positioned at $\log_2$ fold change of 1 and –1 (i.e., a 2-fold change). Colored proteins are identified with a *p*-value <0.05. (**B**) Number of peroxidatic cysteine C_p-dependent interaction partners per peroxiredoxin isoform identified with *p*-value <0.05 and $\log_2$ fold change >1 in our screen. (**C**) Bar chart representing the percentage of peroxidatic cysteine C_p-dependent binders that are also identified as cysteine-dependent binders in wild-type peroxiredoxin (Figure 2). (**D**) UpSet plot and (**E**) Venn diagram that visualize peroxidatic cysteine C_p-dependent target protein set intersections per peroxiredoxin isoform in a matrix layout. A color gradient from white (no overlap) to blue (high overlap) indicates the amount of overlap in the Venn diagram.

teins: a total of 1032 cysteine-dependent binding partners (compared to 1145 for wild-type) was identified (**Figure 4A,B** and Supplemental **Table S3**). This strongly suggests that many peroxiredoxin binding partners are capable of binding through the C_P-SOH-mediated mechanism. We then analyzed how many of the cysteine-dependent binders of PRDX-C_RS are also identified as WT cysteine-dependent binders. We found that of the proteins identified to form cysteine-dependent interactions with PRDX-C_RS, over 60% for PRDX1, PRDX3 and PRDX5 and approximately half for PRDX2 and 4, also do so using WT peroxiredoxins as bait (**Figure 4C**). When comparing peroxidatic cysteine-dependent binding partners for the five peroxiredoxin isoforms we again found that each has a largely different set of target proteins (**Figure 4D,E**). This confirms our conclusion regarding the peroxiredoxin-isoform-specific binding partners that we based on the mass-spectrometry screen comparing wild-type peroxiredoxins.

Thus, for many cysteine-dependent interactors of the peroxiredoxins, the peroxidatic cysteine suffices to mediate the interaction in the absence of the resolving catalytic cysteine. This does not mean however that the interaction cannot be established starting from C_P-S-S-C_R under normal conditions.

Peroxiredoxins Bind Target Proteins Via Two Distinct Mechanisms

We observed that cysteine-dependent heterodimerization of peroxiredoxins with many target proteins also occurs in mutants lacking the resolving cysteine. However, this might not apply to all identified interactors, and in principle, a C_P-S-S-C_R could be required for a subset of the cysteine-dependent PRDX binding partners. We questioned whether, for each PRDX, all binding partners follow the C_P-SOH-mediated mechanism, or whether some might use the C_P-S-S-C_R-mediated route. We compared cysteine-dependent binders of wild-type peroxiredoxins to cysteine-dependent binders of the C_RS mutant (**Figure 5A** and **Table S4**). Proteins that do not bind the resolving cysteine mutant C_RS, but that do bind the wild-type peroxiredoxin, likely depend on the C_P-S-S-C_R-mediated relay mechanism. We found that the majority of cysteine-dependent interactors of the WT and C_RS mutant datasets overlap. However, a number of proteins are exclusively found to interact with the WT peroxiredoxins and hence depend on a C_P-S-S-C_R mediated relay. We also identified a small number of interactors that are only pulled down with the C_RS mutant, but not with the WT peroxiredoxin.

Next, we compared the extent of C_P-S-S-C_R- and C_P-SOH-mediated binding between peroxiredoxin isoforms. As shown in **Figure 5B**, there are large differences in the distribution of the relay mechanisms between isoforms. The percentage of C_P-S-S-C_R-mediated binders ranges from 21% to 16% for PRDX2 and PRDX3, respectively, while PRDX1 and PRDX4 have 44% and 58% C_P-S-S-C_R interactors. Interestingly, as much as 73% of PRDX5 interactors follow the C_P-S-S-C_R-mechanism. It is not unlikely that the absence of the resolving cysteine may actually stabilize or facilitate disulfide formation with cysteines in other proteins.

A possible explanation as to why disulfides with binding partners are formed preferably starting from either C_P-SOH or C_P-S-S-C_R might lie in the amino acid region surrounding the cysteine in an interacting protein. Since C_P-SOH and C_P-S-S-C_R are structurally distinct, the local environment of an interacting cysteine could determine whether an interaction is favorable. We investigated whether the local environments of cysteines in interactors that preferentially bind to C_P-SOH or C_P-S-S-C_R can be distinguished. Interactors of all PRDX isoforms were separated into two groups based on their preference for either C_P-SOH or C_P-S-S-C_R-mediated interaction. For both groups, we extracted the eight amino acids flanking all cysteine residues. Using the motif-x algorithm [24], we analyzed potential motifs in each group of interactors, using the other group as a background. While both C_P-SOH and C_P-S-S-C_R-mediated interactors are enriched in the CxxC motif, a well-known motif in redox proteins (**Tables S5** and **S6**), differences in enriched motifs found in C_P-SOH and C_P-S-S-C_R-mediated interactors could be found (**Figure 5C,D**);

for example, the YCE motifs enriched in C_P-SOH-mediated interactors as compared to C_P-S-S-C_R-mediated interactors. This supports the idea that proteins might preferentially form interactions with peroxiredoxin C_P-SOH or C_P-S-S-C_R based on their local amino acid composition.

Based on these observations, we conclude that oxidized peroxiredoxins bind their interaction partners starting from the --SOH- or -S-S-state, and that a subset of interactors can only bind PRDX in the S-S state. A possible explanation for this might be found in amino acid motifs surrounding cysteine residues in the interaction partners. S-S vs. -SOH dependent relay could point to an additional level of specificity in peroxiredoxin-based interaction that may have implications for cellular redox regulation.

DISCUSSION

Peroxiredoxin-catalyzed oxidation has been suggested to answer the question as to how thiols with low intrinsic reactivity can be oxidized by low levels of H_2O_2 despite the presence of abundant and highly reactive peroxidases. Here we show that all isoforms are capable of forming numerous cysteine-dependent heterodimers. Our in-depth mass-spectrometry and complementary bioinformatics approach provides, first of all, a resource of potential 2-cys peroxiredoxin-catalyzed cysteine oxidation substrates. Many of the proteins that we identified as cysteine-dependent peroxiredoxin binders were indeed identified previously to contain redox sensitive cysteines [17]. This overlap could point at a major role for peroxiredoxins in cysteine oxidation in other proteins. It is

A.

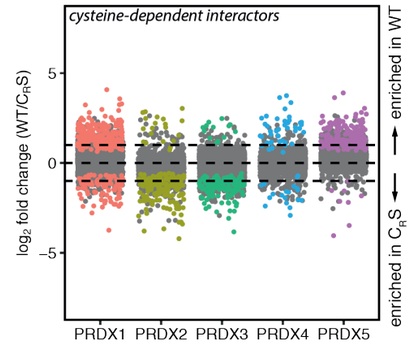

B.

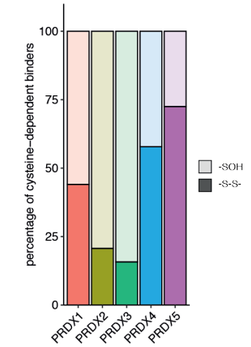

C.

Top 10 amino acid motifs in C_P SOH mediated interactors

	motif	score	fold increase
1	...YCE...	309.4	∞
2	.I..C.K..	12.9	3.4
3	Y..C...K	11.4	4.4
4	..V.C..Y.	11.4	5.8
5	....C.I.P.	11.4	4.2
6	R..AC....	10.3	2.7
7	....C.V.N	8.4	2.7
8	.R..C...T	8.4	3.8
9	...AC..A.	8.1	2.1
10	Q..EC....	7.9	2.5

D.

Top 10 amino acid motifs in C_P-S-S-C_R mediated interactors

	motif	score	fold increase
1	.C..C...F	6.5	2.5
2	....C..CG	6.4	1.9
3	..R.C..L.	5.9	1.9
4	....CP.C.	5.9	2.5
5	E..QC....	5.7	2.5
6	..T.C.V..	5.2	2.3
7	E...C..K.	4.7	2.1
8	.C..C.E..	4.6	2.3
9	...LCQ...	4.6	1.9
10	..PTC....	4.5	2.5

Figure 5. Peroxiredoxins interact via two distinct mechanisms.
(**A**) Analysis comparing cysteine-dependent interactors of wild-type and C_RS-mutant peroxiredoxins showing the $\log_2$ fold change in binding of proteins to wild-type compared to the C_RS-mutant peroxiredoxin isoforms. Horizontal lines are positioned at $\log_2$ fold change of 1 and –1 (i.e., a 2-fold change). Colored proteins are identified as cysteine-dependent binders in the analyses presented in Figure 2 and 4. (**B**) Bar chart representing the percentage of C_P-S-S-C_R-mediated and C_P-SOH cysteine-dependent interactors per peroxiredoxin isoform. Proteins interacting with the C_RS-mutant only are not included in this analysis. Local amino acid motifs around each cysteine of C_P-SOH cysteine-dependent interactors (**C**) and C_P-S-S-C_R-mediated interactors of peroxiredoxins (**D**) with sequences shuffled 100 times as a control.

not clear what follows after peroxiredoxin-dependent cysteine oxidation, but one could think of three possible scenarios following intermolecular disulfide formation between peroxiredoxin and a target protein. 1) The intermolecular disulfide could be rapidly resolved by disulfide exchange to the resolving cysteine of the peroxiredoxin, forming the canonical C_P-S-S-C_R and leaving the target reduced. 2) The intermolecular disulfide could be resolved by disulfide exchange to another cysteine in the binding protein (or protein complex), forming an intra- or intermolecular disulfide in that protein and leaving peroxiredoxin reduced. 3) The intermolecular disulfide dependent complex of peroxiredoxin and its target could represent a novel type of post-translational modification on cysteine, that for instance alters the function of the target, that we would like to coin S-peroxiredoxinylation (S-PRDXylation). Others have shown that many of the PRDX1 and PRDX2-dependent binders were also identified in a TRX-trap pull down, confirming that proteins binding to peroxiredoxin in a cysteine-dependent manner indeed become oxidized [13] . This observation probably does not exclude S-PRDXylation. Widespread S-PRDXylation could also be in accordance with the identification of many oxidation-sensitive cysteines in redox proteomics studies, as these would not distinguish S-PRDXylation from other intra- or intermolecular disulfides [25]. Besides a role as a post-translational modification impacting the function of specific proteins, widespread peroxiredoxinylation could in principle also serve as a redox buffer.

Our data furthermore provides evidence that the peroxiredoxin-dependent redox relay model could also explain how selectivity in redox signaling can be achieved. Selectivity stems from the observation that each peroxiredoxin isoform interacts with a largely specific subset of proteins. This could in part depend on isoform-specific subcellular localization, but the relatively low overlap in binders for PRDX1 and PRDX2, which share the same subcellular localization and a high sequence similarity, suggests that this is not the only determinant for binding of a protein to a specific peroxiredoxin isoform. Analysis of local structural differences surrounding the region around the cysteine of the binding protein could also contribute to selective binding of proteins to the different PRDXs. A second layer of specificity is suggested by the observation that peroxiredoxin-mediated relays can proceed through two distinct molecular mechanisms, starting from either C_P-SOH or C_P-S-S-C_R, and that peroxiredoxin isoforms and targets display varying preferences for these mechanisms. Each PRDX has different kinetics for C_P-SOH and C_P-S-S-C_R formation and reduction, and these kinetics could dictate which cysteines in target proteins can be oxidized under specific conditions. For instance, at low levels of peroxide, PRDX2 would be the first to form C_P-SOH, whereas only under conditions where TRX activity is limiting oxidized peroxiredoxin in the C_P-S-S-$C_{R\,form}$ would it be sufficiently abundant to oxidize another set of targets. Interestingly, when we look at isoform-specific differences in the frequency of C_P-SOH and C_P-S-S-C_R-mediated interactors, we find that there are large differences in the distribution of the relay mechanisms between isoforms.

A fair number of proteins seems to bind peroxiredoxins independent of its catalytic cysteines (**Figure 3L**, grey dots), despite high-salt washing. The peroxiredoxin isoform dependent specificity irrespective of cysteine-dependency suggests that these interactions are probably not artefacts of the used method. This leaves the possibility that some of these proteins could function as adaptor proteins to facilitate peroxiredoxin-dependent relays to cysteine-dependent binding proteins. Although this would need to be explored, adaptor proteins have been shown to be involved in peroxidase-dependent redox relays. For instance, Orp1-dependent Yap1 oxidation is dependent on the presence of the adapter protein Ybp1, shielding oxidized Orp1 from reduction [26,27]. Similarly, the PRDX2-STAT3 redox relay depends on association with the membrane-associated scaffold protein ANXA2 [28]. We indeed also identify ANXA2 as a PRDX2-specific and cysteine-dependent interactor in our screen (**Table S2**). It is conceivable that many more peroxiredoxin-based redox relays may proceed via the formation of ternary complexes with scaffold proteins. This would not only increase the chances that a peroxiredoxin finds a target, but would also add another level of specificity, coming from the interaction of specific peroxiredoxin isoforms with specific scaffolds for the relay of oxidation to subsets of target proteins.

Taken together, our observations regarding widespread cysteine-dependent binding of proteins to the 2-cys peroxiredoxins provides a model that could explain both the reactivity and selectivity of the extensive cysteine oxidation observed in response to low amounts of H_2O_2.

Conclusions

In conclusion, our findings suggest that all five human 2-cys peroxiredoxins can form disulfide-dependent heterodimers with a large set of proteins, and that each peroxiredoxin isoform displays a preference for a subset of disulfide-dependent binding partners. We highlight the isoform-specific characteristics that might justify this preference. Furthermore, we propose that peroxiredoxin-based redox relays can progress via one of two molecular mechanisms starting from either C_P-SOH or C_P-S-S-C_R. These findings provide a framework for peroxiredoxin biology and implicate a widespread role for peroxiredoxins in selectively transducing peroxide signals in order to generate appropriate signaling responses.

Limitations of this study

The cut-offs used in the analysis of our mass-spectrometry screen are quite stringent, and whether proteins bind only in a cysteine-dependent manner or to only a certain peroxiredoxin isoform may not be as unambiguous. Furthermore, to keep the number of mass-spectrometry samples manageable the analysis was performed at a single timepoint following a single concentration of H_2O_2 treatment. It is not unthinkable that proteins found to interact specifically to one peroxiredoxin isoform in this study will in fact interact with others when analyzed at other timepoints or H_2O_2 concentrations. The use of the H_2O_2 treated C_{PR}S mutants as a control rather than also including untreated samples for WT PRDX1–5 (for the same reason of keeping the number of mass-spectrometry samples manageable) may obscure whether proteins also bind peroxiredoxins under basal conditions, be it cysteine dependent or not. Future work will be needed to carefully validate each protein found as a cysteine-dependent peroxiredoxin interactor.

It is not unthinkable that differences in the level of overexpression of the Flag-tagged PRDX1–5 or their mutants may lead to variation in the number of proteins pulled down. In general, the C_{PR}S mutants of each PRDX1–5 isoform had very similar expression and IP efficiency as compared to their wildtype isoform counterparts (see for instance **Figure 1C**, reducing IP and input), suggesting that whether an interactor is identified as a cysteine-dependent binder is not much affected by variable expression levels. The levels of overexpression of Flag-PRDX1–5 compared to each are somewhat variable, and for his reason MS/MS data was $\log_2$-transformed followed by quantile normalization to simultaneously correct for overall protein content and IP efficiency in an attempt to lower the chance that differences in expression levels affect our analysis.

The analysis of the chemical environment of cysteines oxidized through peroxiredoxin dependent relays would greatly benefit from knowing which cysteine in a binding partner is being oxidized. Here we have analyzed all cysteines in the interactors which obviously dilutes any specific pattern. Combining peroxiredoxin-interactome screens as described here with redox proteomics or ways to keep the disulfide between peroxiredoxin and its targets intact and suitable for analysis by MS/MS in future studies could be a way to achieve this. It is difficult to unambiguously exclude that proteins no longer bind to the used peroxiredoxin mutants due to structural changes other than loss of the cysteine thiol. For the resolving cysteine mutants at least, a recent study shows that the cysteine to serine mutation has only a limited effect on the rate of oxidation of the peroxidatic cysteine in PRDX2 [29]. Characterization of the functional consequences of specific peroxiredoxin-based interactions is outside the scope of this study. However, it would be interesting to investigate the mechanisms and fate of these complexes in more detail. Additionally, further work is needed to link the mechanisms of peroxiredoxin specificity to biological cues that determine downstream signaling.

MATERIALS AND METHODS

Cell lines and culturing

HEK293T were cultured in bicarbonate-buffered DMEM, supplemented with 10% FBS (Bodinco BDC-40506-C05), 2 mM L-glutamine (Lonza, BE17-605E) and 100 U/mL penicillin-streptomycin (Lonza, DE17-602E) and kept at 37 °C and under a 6% CO^2 atmosphere. Transfections of HEK293T cells were carried out using PEI (Sigma-Aldrich, P3640) or FugeneHD reagent (Promega, E2311) following the manufacturer's instructions. After two days, cells were harvested for further analysis.

Plasmids and Reagents

Human PRDX1-5 with *att* recombination sites were cloned from cDNA using the following primers: PRDX1_att_F-5′-GGGGACAAGTTTGTACAAAAAAGCAGGCTTAATGTCTTCAGGAAATGCTAAAATTGGGC-3′, PRDX1_att_R-5′-GGGGACCACTTTGTACAAGAAAGCTGGGTCCTACTTCTGCTTGGAGAAATATTCTTTGCT-3′, PRDX2_att_F-5′-GGGGACAAGTTTGTACAAAAAAGCAGGCTTAATGGCCTCCGGTAACGC-3′, PRDX2_att_R-5′-GGGGACCACTTTGTACAAGAAAGCTGGGTTCTAATTGTGTTTGGAGAAATATTCCTTGCTGT-3′, PRDX3_att_F-5′-GGGGACAAGTTTGTACAAAAAAGCAGGCTTAATGGCGGCTGCTGTAGG-3′, PRDX3_att_R-5′-GGGGACCACTTTGTACAAGAAAGCTGGGTTCTACTGATTTACCTTCTGAAAGTACTCTTTGGAAG-3′, PRDX4_att_F-5′-GGGGACAAGTTTGTACAAAAAAGCAGGCTTAATGGAGGCGCTGCCG-3′, PRDX4_att_R-5′-GGGGACCACTTTGTACAAGAAAGCTGGGTTTTTCAGTTTATCGAAATACTTCAGCTTTCCAG-3′, PRDX5_att_F-5′-GGGGACAAGTTTGTACAAAAAAGCAGGCTTAATGGGACTAGCTGGCGTG-3′, PRDX5_att_R-5′-GGGGACCACTTTGTACAAGAAAGCTGGGTTTCAGAGCTGTGAGATGATATTGGGTG-3′. Using Gateway technology (Invitrogen) entry clones were generated. The peroxidatic and resolving cysteine mutants of PRDX1-5 were created by site-directed mutagenesis PCR using the following primers: PRDX1_C52S_F-5′-CTTTGTGTCCCCCACGGAG-3′, PRDX1_C52S._R-5′-CTCCGTGGGGGACACAAAG-3′, PRDX1_C173S_F-5′-GGGAAGTGTCCCCAGCTGG-3′, PRDX1_C173S._R-5′-CCAGCTGGGGACACTTCCC-3′, PRDX2_C51S_F-5′-TCACTTTTGTGTCTCCCACCGAGATCATCGCG-3′, PRDX2_C51S._R-5′-CGCGATGATCTCGGTGGGAGACACAAAAGTGA-3′, PRDX2_C172S_F-5′-CATGGGGAAGTTTCTCCCGCTGGCT-3′, PRDX2_C172S._R-5′-AGCCAGCGGGAGAAACTTCCCCATG-3′, PRDX3_C108S_F-5′-TCACCTTTGTGTCTCCTACAGAAATTGTTGCT-3′, PRDX3_C108S._R-5′-AGCAACAATTTCTGTAGGAGACACAAAGGTGA-3′, PRDX3_C229S_F-5′-ACACATGGAGAAGTCTCTCCAGCGAACTGGACA-3′, PRDX3_C229S_R-5′-TGTCCAGTTCGCTGGAGAGACTTCTCCATGTGT-3′, PRDX4_C124S_F-5′-ATTTCACATTTGTGTCTCCAACTGAAATTATCGCTTTTGG-3′, PRDX4_C124S._R-5′-CCAAAAGCGATAATTTCAGTTGGAGACACAAATGTGAAAT-3′, PRDX4_C245S_F-5′-GGAGAAGTCTCCCCTGCTGGCTGGAA-3′, PRDX4_C245S._R-5′-TTCCAGCCAGCAGGGGAGACTTCTCC-3′, PRDX5_C47S_F-5′-TTCACCCCTGGATCTTCCAAGACACACCTG-3′, PRDX5_C47S._R-5′-CAGGTGTGTCTTGGAAGATCCAGGGGTGAA-3′, PRDX5_C151S_F-5′-CAGGCCTCACCTCCAGCCTGGCA-3′, PRDX5_C151S._R-5′-TGCCAGGCTGGAGGTGAGGCCTG-3′. Gateway technology (Life Technologies) was used to create N-terminally tagged Flag-HIS-PRDX1-3 and 5, and C-terminally tagged PRDX4-Flag-HIS constructs (backbone pCDNA3). Furthermore, 30% H_2O_2 (Sigma 31642) was freshly diluted to a stock of 10 or 100 mM in H_2O for every experiment. Unless stated otherwise, H_2O_2 treatments were 25 µM (PRDX2) and 100 µM (other isoforms) for 2 min.

Co-immunoprecipitation experiments and Western blotting

After treatment with H_2O_2, cells were scraped in 100 mM N-ethylmaleimide (NEM, Sigma E3876) in PBS for 5 min at 37 °C to trap free thiols in their in vivo redox state during sample preparation and collected by centrifugation at 1200 rpm for 3 min. Cells were lysed using a buffer containing 50 mM Tris-HCl pH 7.5, 1% TX100, 1.5 mM $MgCl_2$, 5 mM EDTA, 100 mM NaCl, NaF, Leupeptin and Aprotinin. Furthermore, 100 mM iodoacetamide was added to the lysis buffer to prevent post-lysis cysteine oxidation and to inactivate disulfide reducing enzymes. After centrifugation at 14,000 rpm for 10 min, 5% of the supernatant was kept as input and the remaining supernatant was used for immunoprecipitation with anti-Flag-M2 affinity gel (Sigma A222). After a 2 h incubation, immunoprecipitates were washed 4 times with lysis buffer containing 1 M NaCl and samples were boiled for 5 min in sample buffer with or without the reducing agent β-mercaptoethanol. Samples were separated on a 10% polyacrylamide gel and transferred to immobilon-FL membranes before staining.

Antibodies

The following antibodies were used in this study: anti-Flag antibody and anti-Flag-M2 beads (Sigma F3165 and A222, respectively), monoclonal anti-HA antibody (12CA5) was prepared using hybridoma cell lines, anti-tubulin (Merck Millipore CP06), anti-peroxiredoxin-SO_3 (Abcam ab16830), anti-peroxiredoxin 1 (Abcam ab15571), anti-peroxiredoxin 2 (Abcam ab15572), anti-peroxiredoxin 3 (Abcam ab73349), anti-peroxiredoxin 4 (Abcam ab59542) and anti-peroxiredoxin 5 (Abcam ab16944). Detection of 2 fluorescent secondary antibodies was done simultaneously using the LI-COR Biosciences Odyssey Infrared Imaging System or the Amersham Typhoon NIR Plus Biomolecular Imager (GE Healthcare), detection of HRP-coupled secondary antibodies was performed using the FUJIFILM Luminescent Image Analyzer LAS-3000.

Mass Spectrometry Sample Preparation

For the identification of cysteine-dependent interactors the lysate of 4 × 20 cm dishes were used for each pulldown on 75 µL of Flag-M2 beads similar to the immunoprecipitation experiments described above. All immunoprecipitations were performed using three biological replicates. After washing, beads were resuspended with 8 M urea in 1 M ammonium bicarbonate (ABC), reduced and alkylated in 10 mM TCEP and 40 mM chloroacetamide (CAA) for 30 min at RT. After fourfold dilution with 1 M ABC, proteins were digested overnight on-bead with 250 ng Trypsin/LysC (Promega V5071) per sample at 37 °C. Samples were cleaned up with in-house-made C18 stagetips.

Mass Spectrometry

Mass spectrometry was performed as previously described [30]. Peptides were separated on a 30-cm pico-tip column (75 µm ID, New Objective) and were packed in-house with 3 µm aquapur gold C-18 material (Dr. Maisch) using a 140-min gradient (7–80% ACN 0.1% FA), delivered by an easy-nLC 1000 (LC120, Thermo Scientific), and electro-sprayed directly into an Orbitrap Fusion Tribrid Mass Spectrometer (Thermo Scientific). Raw files were analyzed with MaxQuant software version 1.5.2.8 with oxidation of methionine, alkylation with N-ethylmaleimide and carbamidomethylation set as variable modifications. The human protein database of UniProt was searched with both the peptide as well as the protein false discovery rate set to 1%. The mass spectrometry proteomics data were uploaded into the ProteomeXchange Consortium via the PRIDE [31] partner repository with the dataset identifier PXD024114. Downstream analysis was done using R version 4.0.2.

Data Filtering and proDA Modeling

The code used was uploaded to GitHub at https://github.com/loesoe/peroxiredoxin. In short, LFQ data from the MaxQuant proteinGroups file and corresponding protein information was used. Proteins were filtered for reverse hits and standard contaminants. Next, we selected proteins that were identified with three or more unique peptides and were

measured in at least one sample in two or more replicates. Data was log_2-transformed and normalized using quantile normalization to simultaneously correct for overall protein content and immunoprecipitation (IP) efficiency. ProDA model fitting was performed using the number of proteins in the data as the number of subsamples. To test for differential protein abundance, a proDa model was fit to compare WT against mutant for each peroxiredoxin.

Threshold cutoff calculation

To determine the cutoff for out data, we fitted a proDA model for wild-type and mutant peroxiredoxin, without considering the isoform. Next, we repeated this 100 times, but instead with randomized labels. The difference at which 5% of the randomized data was included was determined as the cutoff.

Known Redox-Sensitive Proteins

A reference proteome containing 75,071 human entries from Uniprot tagged with the keyword reference proteome was downloaded from https://www.uniprot.org/help/reference_proteome. Proteins that were previously identified in a screen for redox-sensitive proteins in human cell lines (293T and HCT116) were taken from [17].

Upset plot and Venn diagrams

To visualize the isoform-specific set of intersections we used the UpsetR package [32]. Venn diagrams were created using the Venn version 1.9 package and colored manually.

Localization Analysis

We analyzed the localization of isoform-specific interactors using the neighborhood/compartment predictions data for A431 cells from https://www.subcellbarcode.org [18]. Peroxiredoxin interactors with the highest fold change (>10-fold) were matched with their neighborhood data and their fold enrichment were calculated compared to the cell line data. Main localization of peroxiredoxin isoforms from this tool are as follows: PRDX1 PRDX2 and PRDX5, cytosol; PRDX3, mitochondria; PRDX4, unclassified.

Sequence Similarity

PRDX sequences were loaded as a FASTA file. Pairwise alignment was calculated using EMBOSS needle (https://www.ebi.ac.uk/Tools/psa/emboss_needl, accessed on 2 July 2016), which uses the Needleman–Wunsch global alignment algorithm to find the optimum global alignment. Similarity (the percentage of matches between the two aligned sequences) was plotted for each peroxiredoxin isoform pair.

AA composition and motifs

The sequences for PRDX isoform-specific interactors were retrieved from Uniprot (https://www.uniprot.org/uploadlists, accessed on 2 January 2021). Sequences were loaded using the Biostrings package, sequences were shuffled 100 times as a background using the universalmotif package. Motifs were extracted of 9 amino acids centered around each cysteine. The amino acid composition was calculated for the isoform-specific sequences, the shuffled background and total protein using the alphabetFrequency function. Fold enrichment and Benjamini–Hochberg adjusted *p*-values were calculated per peroxiredoxin isoform using the amino acid composition of all other isoforms as a control. Motifs were analyzed using motif-x (rmotifx package) using the shuffled sequences as a background [24].

SUPPLEMENTARY FIGURES AND LEGENDS

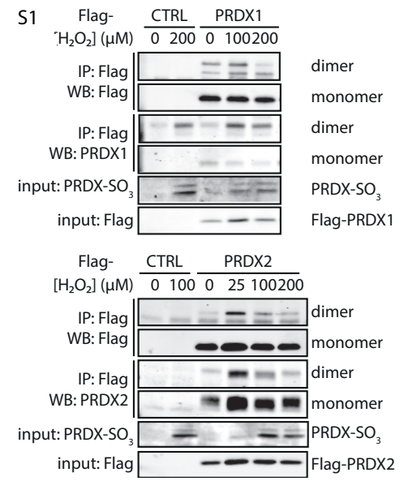

Figure S1. Immunoprecipitated Flag-PRDX Western blots.
HEK293T cells expressing Flag-tagged peroxiredoxin isoforms were treated for 2 min with H2O2 and analyzed by immunoblotting under parallel reducing and non-reducing conditions. H2O2 concentrations were as indicated. The concentrations of H2O2 applied were optimized for each PRDX isoform to yield considerable disulfide-dependent homodimerization without inducing detectable hyperoxidation (PRDX-SO3). Immunoblots shown in this figure are representative of multiple experiments (n ≥ 3). IP: immunoprecipitation; WB: Western blotting; input: cleared cell lysate as used for immunoprecipitation, reduced sample.

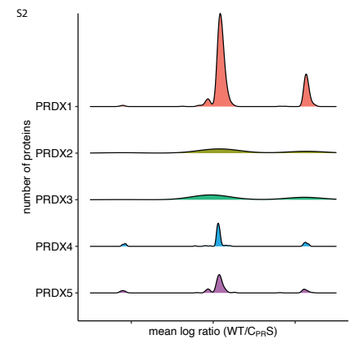

Figure S2
Ridge plot showing the density distribution centered around 0 of the mean log ratio of wild-type and C_{PR}S-peroxiredoxin, corresponding to **Figures 2B-F** (ignoring the missing values). Most PRDX isoforms show a higher density peak corresponding to WT-specific interactors (mean log ratio>0) than the peak for C_{PR}S-specific interactors (mean log ratio <0), indicating that most of the interactors are indeed cysteine-dependent binders and not false positives.

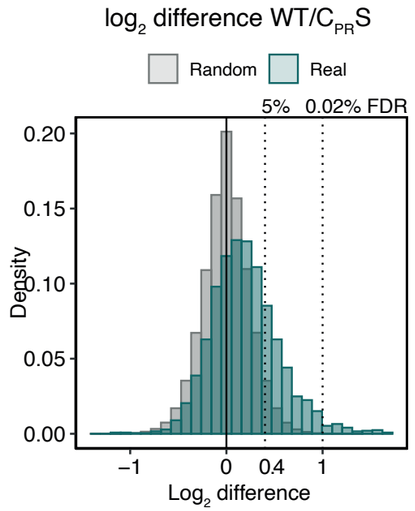

Figure S3. Log^2 fold change distribution of data presented in Figure 2G (blue curve).
Data was randomized a hundred times between wild-type and CPRS mutant peroxiredoxin data and the log2 fold change was recalculated (grey curve). With the randomized data, we calculate that at a $\log_2$ fold change threshold of >0.401, 5% of the randomized data is included (left dashed line). A more stringent cutoff of 1 includes 0.02% of randomized data (FDR; right dashed line).

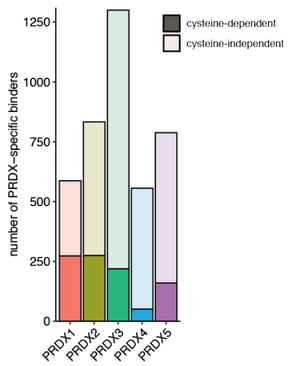

Figure S4
Bar chart depicting the number cysteine-dependent binders (as defined in Figures 2 and 4) in the set of PRDX isoform-specific binders as depicted in Figure 3J. Dark colored bars indicate proteins interacting with WT PRDXs; light bars indicate proteins interacting with PRDX $C_{PR}S$ mutants.

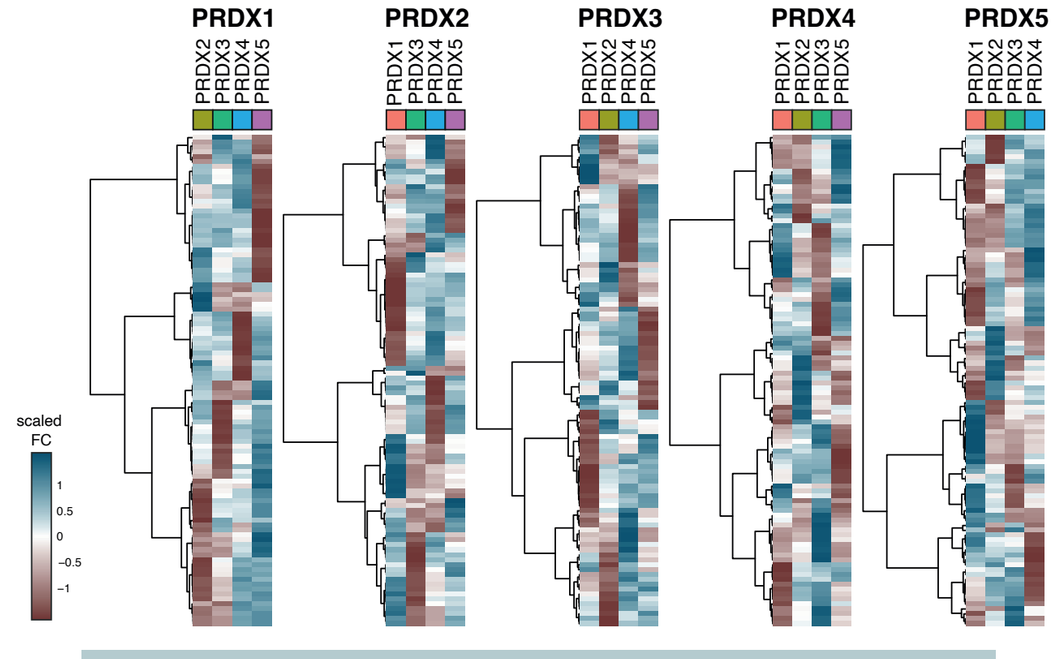

Figure S5
Heatmaps of the top 100 (based on adjusted p-value) peroxiredoxin isoform-specific binders, specified for each isoform relative to the other 4 isoforms. Heatmaps were created using the pheatmap package in R, with row scaling and Ward D2 correlation clustering.

SUPPLEMENTARY TABLES

For an online version of the tables, please follow https://doi.org/10.3390/antiox10040627#suppl_id, or see the final pages of this file (pdf only)

Table S1: Cysteine-dependent interactors (wild-type).

Table S2: Isoform-specific cysteine-dependent interactors.

Table S3: Peroxidatic cysteine-dependent interactors (C_RS).

Table S4: All cysteine-dependent interactors (wild-type and C_RS).

Table S5: Amino acid motifs in C_P-SOH-mediated interactors.

Table S6: Amino acid motifs in C_P-S-S-C_R-mediated interactors.

SUPPLEMENTARY TABLES

Table S1: cysteine-dependent interactors (wild-type)

uniprot ID	gene	protein	log ratio	p-value
PRDX1 cysteine-dependent interactors				
P15924	DSP	Desmoplakin	4,9	<0.001
Q15149	PLEC	Plectin	4,8	<0.001
Q15185	PTGES3	Prostaglandin E synthase 3	4,8	<0.001
P08559	PDHA1	Pyruvate dehydrogenase E1 component subunit alpha, somatic form, mitochondrial	4,5	<0.001
P62273	RPS29	40S ribosomal protein S29	4,4	<0.001
A0A024R4E5	HDLBP	High density lipoprotein binding protein	4,4	<0.001
Q9Y2V2	CARHSP1	Calcium-regulated heat-stable protein 1	4,4	<0.001
P55084	HADHB	Trifunctional enzyme subunit beta, mitochondrial	4,4	<0.001
P49792	RANBP2	E3 SUMO-protein ligase RanBP2	4,3	<0.001
P24666	ACP1	Low molecular weight phosphotyrosine protein phosphatase	4,3	<0.001
Q9GZT3	SLIRP	SRA stem-loop-interacting RNA-binding protein, mitochondrial	4,1	<0.001
Q15654	TRIP6	Thyroid receptor-interacting protein 6	4	<0.001
E7EX90	DCTN1	Dynactin subunit 1	4	<0.001
Q01081	U2AF1	Splicing factor U2AF 35 kDa subunit	4	0,001
Q9BY32	ITPA	Inosine triphosphate pyrophosphatase	3,9	<0.001
Q14008	CKAP5	Cytoskeleton-associated protein 5	3,8	<0.001
Q9P2J5	LARS1	Leucine--tRNA ligase, cytoplasmic	3,8	<0.001
P48047	ATP5PO	ATP synthase subunit O, mitochondrial	3,8	<0.001
Q16513	PKN2	Serine/threonine-protein kinase N2	3,7	<0.001
P30048	PRDX3	Thioredoxin-dependent peroxide reductase, mitochondrial	3,7	<0.001
A0A087WZ13	RAVER1	Ribonucleoprotein PTB-binding 1	3,7	<0.001
P39023	RPL3	60S ribosomal protein L3	3,7	<0.001
P13667	PDIA4	Protein disulfide-isomerase A4	3,6	<0.001
P61011	SRP54	Signal recognition particle 54 kDa protein	3,6	<0.001
C9JZR2	CTNND1	Catenin delta-1	3,6	<0.001
Q53H12	AGK	Acylglycerol kinase, mitochondrial	3,6	<0.001
P46940	IQGAP1	Ras GTPase-activating-like protein IQGAP1	3,5	<0.001
E3W994	CLASP2	CLIP-associating protein 2	3,5	<0.001
P62316	SNRPD2	Small nuclear ribonucleoprotein Sm D2	3,5	<0.001
P53621	COPA	Coatomer subunit alpha	3,5	<0.001
Q99615	DNAJC7	DnaJ homolog subfamily C member 7	3,5	<0.001
P62829	RPL23	60S ribosomal protein L23	3,5	<0.001
Q9UQE7	SMC3	Structural maintenance of chromosomes protein 3	3,4	<0.001
Q9H0C8	ILKAP	Integrin-linked kinase-associated serine/threonine phosphatase 2C	3,4	<0.001
Q14684	RRP1B	Ribosomal RNA processing protein 1 homolog B	3,4	<0.001
Q7Z6Z7	HUWE1	E3 ubiquitin-protein ligase HUWE1	3,4	<0.001
P31689	DNAJA1	DnaJ homolog subfamily A member 1	3,4	<0.001
Q7L2E3	DHX30	ATP-dependent RNA helicase DHX30	3,3	<0.001
E7EVH7	E7EVH7	Kinesin light chain	3,3	<0.001
Q14204	DYNC1H1	Cytoplasmic dynein 1 heavy chain 1	3,3	<0.001
Q9ULV4	CORO1C	Coronin-1C	3,3	<0.001
P63165	SUMO1	Small ubiquitin-related modifier 1	3,3	<0.001
P49790	NUP153	Nuclear pore complex protein Nup153	3,3	<0.001
P15170	GSPT1	Eukaryotic peptide chain release factor GTP-binding subunit ERF3A	3,3	<0.001
P23258	TUBG1	Tubulin gamma-1 chain	3,3	0,001
Q92879	CELF1	CUGBP Elav-like family member 1	3,2	<0.001
Q14683	SMC1A	Structural maintenance of chromosomes protein 1A	3,2	<0.001
P55809	OXCT1	Succinyl-CoA:3-ketoacid coenzyme A transferase 1, mitochondrial	3,2	<0.001
O75531	BANF1	Barrier-to-autointegration factor	3,2	0,001
O14964	HGS	Hepatocyte growth factor-regulated tyrosine kinase substrate	3,2	0,001
Q9NY93	DDX56	Probable ATP-dependent RNA helicase DDX56	3,2	0,001
O94760	DDAH1	N(G),N(G)-dimethylarginine dimethylaminohydrolase 1	3,2	0,002
Q08211	DHX9	ATP-dependent RNA helicase A	3,2	0,03
Q9C0C2	TNKS1BP1	182 kDa tankyrase-1-binding protein	3,1	<0.001
Q01082	SPTBN1	Spectrin beta chain, non-erythrocytic 1	3,1	<0.001
H3BPE1	MACF1	Microtubule-actin cross-linking factor 1, isoforms 1/2/3/5	3,1	<0.001
Q9BQG0	MYBBP1A	Myb-binding protein 1A	3,1	<0.001
Q7Z406	MYH14	Myosin-14	3,1	<0.001
P22307	SCP2	Non-specific lipid-transfer protein	3,1	<0.001
P62266	RPS23	40S ribosomal protein S23	3,1	<0.001
Q5SW79	CEP170	Centrosomal protein of 170 kDa	3,1	<0.001
Q6P1L8	MRPL14	39S ribosomal protein L14, mitochondrial	3,1	<0.001
P55735	SEC13	Protein SEC13 homolog	3,1	0,001
P21964	COMT	Catechol O-methyltransferase	3,1	0,001
Q99460	PSMD1	26S proteasome non-ATPase regulatory subunit 1	3,1	0,001
P11387	TOP1	DNA topoisomerase 1	3,1	0,002
Q5JTH9	RRP12	RRP12-like protein	3	<0.001
Q96I25	RBM17	Splicing factor 45	3	<0.001
E7ESP9	NEFM	160 kDa neurofilament protein	3	<0.001
P62851	RPS25	40S ribosomal protein S25	3	<0.001
Q13561	DCTN2	Dynactin subunit 2	3	<0.001
Q9UHI6	DDX20	Probable ATP-dependent RNA helicase DDX20	3	<0.001
Q9UNE7	STUB1	E3 ubiquitin-protein ligase CHIP	3	<0.001
Q06124	PTPN11	Tyrosine-protein phosphatase non-receptor type 11	3	<0.001
P19525	EIF2AK2	Interferon-induced, double-stranded RNA-activated protein kinase	3	0,001
Q96KB5	PBK	Lymphokine-activated killer T-cell-originated protein kinase	3	0,004
Q9HD26	GOPC	Golgi-associated PDZ and coiled-coil motif-containing protein	3	0,005
A0A0A0MRT6	ABI1	Abl interactor 1	2,9	<0.001
Q8N9T8	KRI1	Protein KRI1 homolog	2,9	<0.001
Q8N1F7	NUP93	Nuclear pore complex protein Nup93	2,9	<0.001
E9PD53	SMC4	Structural maintenance of chromosomes protein	2,9	<0.001
P46060	RANGAP1	Ran GTPase-activating protein 1	2,9	<0.001
Q99961	SH3GL1	Endophilin-A2	2,9	<0.001
Q96N67	DOCK7	Dedicator of cytokinesis protein 7	2,9	<0.001
O94979	SEC31A	Protein transport protein Sec31A	2,9	<0.001
Q9H2G2	SLK	STE20-like serine/threonine-protein kinase	2,9	<0.001
Q9H0B6	KLC2	Kinesin light chain 2	2,9	<0.001
Q9UG54	MAP3K7	Mitogen-activated protein kinase kinase kinase	2,9	<0.001
P14174	MIF	Macrophage migration inhibitory factor	2,9	0,001
P27708	CAD	CAD protein [Includes: Glutamine-dependent carbamoyl-phosphate synthase	2,9	0,004
P68133	ACTA1	Actin, alpha skeletal muscle	2,9	0,015
Q7L1Q6	BZW1	Basic leucine zipper and W2 domain-containing protein 1	2,8	<0.001
I3L2Z5	MAZ	Myc-associated zinc finger protein	2,8	<0.001
Q5JRX3	PITRM1	Presequence protease, mitochondrial	2,8	<0.001
O43837	IDH3B	Isocitrate dehydrogenase [NAD] subunit beta, mitochondrial	2,8	<0.001
P63272	SUPT4H1	Transcription elongation factor SPT4	2,8	<0.001
P57740	NUP107	Nuclear pore complex protein Nup107	2,8	<0.001
P08708	RPS17	40S ribosomal protein S17	2,8	<0.001
Q9UG63	ABCF2	ATP-binding cassette sub-family F member 2	2,8	<0.001
P48444	ARCN1	Coatomer subunit delta	2,8	<0.001
P41252	IARS1	Isoleucine--tRNA ligase, cytoplasmic	2,8	<0.001
P36915	GNL1	Guanine nucleotide-binding protein-like 1	2,8	<0.001
Q9UHB6	LIMA1	LIM domain and actin-binding protein 1	2,8	<0.001
A0A1W2PRV5	SMN2	Survival motor neuron protein	2,8	0,001
Q9BV44	THUMPD3	THUMP domain-containing protein 3	2,8	0,002
O75874	IDH1	Isocitrate dehydrogenase [NADP] cytoplasmic	2,8	0,002
O95801	TTC4	Tetratricopeptide repeat protein 4	2,8	0,004
P43897	TSFM	Elongation factor Ts, mitochondrial	2,8	0,004
Q13813	SPTAN1	Spectrin alpha chain, non-erythrocytic 1	2,8	0,005
Q5VYK3	ECPAS	Proteasome adapter and scaffold protein ECM29	2,8	0,005
Q9NR30	DDX21	Nucleolar RNA helicase 2	2,8	0,009
Q02241	KIF23	Kinesin-like protein KIF23	2,7	<0.001
P61163	ACTR1A	Alpha-centractin	2,7	<0.001
Q8WVM8	SCFD1	Sec1 family domain-containing protein 1	2,7	<0.001
P20042	EIF2S2	Eukaryotic translation initiation factor 2 subunit 2	2,7	<0.001
P83731	RPL24	60S ribosomal protein L24	2,7	<0.001
A0A2R8YDQ9	SUCLA2	Succinate--CoA ligase [ADP-forming] subunit beta, mitochondrial	2,7	<0.001
P35658	NUP214	Nuclear pore complex protein Nup214	2,7	<0.001
Q86V48	LUZP1	Leucine zipper protein 1	2,7	<0.001
O60493	SNX3	Sorting nexin-3	2,7	0,001
Q15717	ELAVL1	ELAV-like protein 1	2,7	0,003
P23919	DTYMK	Thymidylate kinase	2,7	0,003
P46013	MKI67	Proliferation marker protein Ki-67	2,7	0,003
Q92974	ARHGEF2	Rho guanine nucleotide exchange factor 2	2,7	0,003
Q15075	EEA1	Early endosome antigen 1	2,7	0,007
P06132	UROD	Uroporphyrinogen decarboxylase	2,7	0,012
Q14152	EIF3A	Eukaryotic translation initiation factor 3 subunit A	2,6	<0.001
Q6P2E9	EDC4	Enhancer of mRNA-decapping protein 4	2,6	<0.001
O75369	FLNB	Filamin-B	2,6	<0.001
Q96RP9	GFM1	Elongation factor G, mitochondrial	2,6	<0.001
Q9NR12	PDLIM7	PDZ and LIM domain protein 7	2,6	<0.001
A0A3B3IRP5	CDC73	Parafibromin	2,6	<0.001
P78344	EIF4G2	Eukaryotic translation initiation factor 4 gamma 2	2,6	<0.001
F8WB06	ATXN2	Ataxin-2	2,6	<0.001
P49207	RPL34	60S ribosomal protein L34	2,6	<0.001
P48634	PRRC2A	Protein PRRC2A	2,6	<0.001
P42704	LRPPRC	Leucine-rich PPR motif-containing protein, mitochondrial	2,6	0,001
P33991	MCM4	DNA replication licensing factor MCM4	2,6	0,001

E7ETK0	RPS24	40S ribosomal protein S24	2,6	0,003
O60762	DPM1	Dolichol-phosphate mannosyltransferase subunit 1	2,6	0,003
P29144	TPP2	Tripeptidyl-peptidase 2	2,6	0,003
P27694	RPA1	Replication protein A 70 kDa DNA-binding subunit	2,6	0,003
Q92615	LARP4B	La-related protein 4B	2,6	0,004
P13807	GYS1	Glycogen [starch] synthase, muscle	2,6	0,004
P51452	DUSP3	Dual specificity protein phosphatase 3	2,6	0,004
Q6P587	FAHD1	Acylpyruvase FAHD1, mitochondrial	2,6	0,005
O76021	RSL1D1	Ribosomal L1 domain-containing protein 1	2,6	0,008
Q9H840	GEMIN7	Gem-associated protein 7	2,6	0,01
O00425	IGF2BP3	Insulin-like growth factor 2 mRNA-binding protein 3	2,5	<0.001
F8W8I6	TIA1	Nucleolysin TIA-1 isoform p40	2,5	<0.001
A0A087WTZ5	UBXN1	UBX domain-containing protein 1	2,5	<0.001
P04637	TP53	Cellular tumor antigen p53	2,5	<0.001
P61160	ACTR2	Actin-related protein 2	2,5	<0.001
Q9UHV9	PFDN2	Prefoldin subunit 2	2,5	<0.001
Q8IWZ3	ANKHD1	Ankyrin repeat and KH domain-containing protein 1	2,5	<0.001
P00568	AK1	Adenylate kinase isoenzyme 1	2,5	<0.001
A0A087WVM4	MTHFD1L	Formyltetrahydrofolate synthetase	2,5	<0.001
M0R0F0	RPS5	40S ribosomal protein S5	2,5	<0.001
Q15042	RAB3GAP1	Rab3 GTPase-activating protein catalytic subunit	2,5	<0.001
P61081	UBE2M	NEDD8-conjugating enzyme Ubc12	2,5	<0.001
A0A0U1RRM6	ENAH	Protein enabled homolog	2,5	<0.001
P16615	ATP2A2	Sarcoplasmic/endoplasmic reticulum calcium ATPase 2	2,5	<0.001
P27824	CANX	Calnexin	2,5	0,001
P78316	NOP14	Nucleolar protein 14	2,5	0,002
P52788	SMS	Spermine synthase	2,5	0,003
P37108	SRP14	Signal recognition particle 14 kDa protein	2,5	0,003
Q6IAA8	LAMTOR1	Ragulator complex protein LAMTOR1	2,5	0,004
P08243	ASNS	Asparagine synthetase [glutamine-hydrolyzing]	2,5	0,005
A0A087X1A5	STAU1	Double-stranded RNA-binding protein Staufen homolog 1	2,5	0,005
Q8WUH6	TMEM263	Transmembrane protein 263	2,5	0,005
Q8TCG1	CIP2A	Protein CIP2A	2,5	0,006
Q9Y5Y2	NUBP2	Cytosolic Fe-S cluster assembly factor NUBP2	2,5	0,007
Q86U42	PABPN1	Polyadenylate-binding protein 2	2,5	0,007
O15446	POLR1G	DNA-directed RNA polymerase I subunit RPA34	2,5	0,008
Q8TAT6	NPLOC4	Nuclear protein localization protein 4 homolog	2,5	0,008
P07196	NEFL	Neurofilament light polypeptide	2,5	0,008
Q9Y5K6	CD2AP	CD2-associated protein	2,5	0,008
P19105	MYL12A	Myosin regulatory light chain 12A	2,5	0,012
E9PF10	NUP155	Nuclear pore complex protein Nup155	2,5	0,012
Q96J01	THOC3	THO complex subunit 3	2,5	0,015
Q14690	PDCD11	Protein RRP5 homolog	2,5	0,015
P61758	VBP1	Prefoldin subunit 3	2,5	0,015
P47897	QARS1	Glutamine--tRNA ligase	2,4	<0.001
O95782	AP2A1	AP-2 complex subunit alpha-1	2,4	<0.001
Q02252	ALDH6A1	Methylmalonate-semialdehyde dehydrogenase [acylating], mitochondrial	2,4	<0.001
Q14157	UBAP2L	Ubiquitin-associated protein 2-like	2,4	<0.001
B1AK87	CAPZB	F-actin-capping protein subunit beta	2,4	<0.001
Q14151	SAFB2	Scaffold attachment factor B2	2,4	<0.001
B7Z7F3	RANBP3	Ran-binding protein 3	2,4	0,001
P19623	SRM	Spermidine synthase	2,4	0,001
Q9H9A6	LRRC40	Leucine-rich repeat-containing protein 40	2,4	0,001
Q96PK6	RBM14	RNA-binding protein 14	2,4	0,001
P48735	IDH2	Isocitrate dehydrogenase [NADP], mitochondrial	2,4	0,002
P39748	FEN1	Flap endonuclease 1	2,4	0,003
P49841	GSK3B	Glycogen synthase kinase-3 beta	2,4	0,006
Q71UI9	H2AZ2	Histone H2A.V	2,4	0,006
A0A0C4DGX4	CUL1	Cullin-1	2,4	0,007
F5H6E2	MYO1C	Unconventional myosin-Ic	2,4	0,007
A0A2R8Y804	CTNNB1	Catenin beta-1	2,4	0,008
Q8WWH5	TRUB1	Probable tRNA pseudouridine synthase 1	2,4	0,008
Q07021	C1QBP	Complement component 1 Q subcomponent-binding protein, mitochondrial	2,4	0,008
Q16698	DECR1	2,4-dienoyl-CoA reductase, mitochondrial	2,4	0,009
P40939	HADHA	Trifunctional enzyme subunit alpha, mitochondrial	2,4	0,009
O14497	ARID1A	AT-rich interactive domain-containing protein 1A	2,4	0,01
G3V1C3	API5	Apoptosis inhibitor 5	2,4	0,011
O95373	IPO7	Importin-7	2,4	0,011
A0A3B3ISG5	IDE	Insulin-degrading enzyme	2,4	0,012
Q16204	CCDC6	Coiled-coil domain-containing protein 6	2,4	0,024
Q8N1G4	LRRC47	Leucine-rich repeat-containing protein 47	2,3	<0.001
O15160	POLR1C	DNA-directed RNA polymerases I and III subunit RPAC1	2,3	<0.001
Q99543	DNAJC2	DnaJ homolog subfamily C member 2	2,3	<0.001

P19367	HK1	Hexokinase-1	2,3	<0.001
Q07666	KHDRBS1	KH domain-containing, RNA-binding, signal transduction-associated protein 1	2,3	<0.001
Q9BSH4	TACO1	Translational activator of cytochrome c oxidase 1	2,3	<0.001
Q5TDH0	DDI2	Protein DDI1 homolog 2	2,3	<0.001
B5MCF9	PES1	Pescadillo homolog	2,3	<0.001
P46776	RPL27A	60S ribosomal protein L27a	2,3	<0.001
O75569	PRKRA	Interferon-inducible double-stranded RNA-dependent protein kinase activator A	2,3	<0.001
P13861	PRKAR2A	cAMP-dependent protein kinase type II-alpha regulatory subunit	2,3	<0.001
Q6Y7W6	GIGYF2	GRB10-interacting GYF protein 2	2,3	<0.001
O43447	PPIH	Peptidyl-prolyl cis-trans isomerase H	2,3	0,001
P43686	PSMC4	26S proteasome regulatory subunit 6B	2,3	0,001
Q16352	INA	Alpha-internexin	2,3	0,001
Q96D71	REPS1	RalBP1-associated Eps domain-containing protein 1	2,3	0,002
P42765	ACAA2	3-ketoacyl-CoA thiolase, mitochondrial	2,3	0,002
Q99959	PKP2	Plakophilin-2	2,3	0,002
O00399	DCTN6	Dynactin subunit 6	2,3	0,002
Q9Y3I0	RTCB	RNA-splicing ligase RtcB homolog	2,3	0,002
Q9Y2L1	DIS3	Exosome complex exonuclease RRP44	2,3	0,004
O75592	MYCBP2	E3 ubiquitin-protein ligase MYCBP2	2,3	0,004
P09110	ACAA1	3-ketoacyl-CoA thiolase, peroxisomal	2,3	0,008
P38432	COIL	Coilin	2,3	0,008
O95747	OXSR1	Serine/threonine-protein kinase OSR1	2,3	0,008
Q5HYI8	RABL3	Rab-like protein 3	2,3	0,009
P22626	HNRNPA2B1	Heterogeneous nuclear ribonucleoproteins A2/B1	2,3	0,01
P62318	SNRPD3	Small nuclear ribonucleoprotein Sm D3	2,3	0,011
Q9BXP5	SRRT	Serrate RNA effector molecule homolog	2,3	0,011
P50570	DNM2	Dynamin-2	2,3	0,013
Q9BQ39	DDX50	ATP-dependent RNA helicase DDX50	2,3	0,014
O43143	DHX15	Pre-mRNA-splicing factor ATP-dependent RNA helicase DHX15	2,3	0,019
Q13573	SNW1	SNW domain-containing protein 1	2,3	0,039
Q5JTZ9	AARS2	Alanine--tRNA ligase, mitochondrial	2,2	<0.001
P27144	AK4	Adenylate kinase 4, mitochondrial	2,2	<0.001
P22314	UBA1	Ubiquitin-like modifier-activating enzyme 1	2,2	<0.001
Q13509	TUBB3	Tubulin beta-3 chain	2,2	<0.001
P54578	USP14	Ubiquitin carboxyl-terminal hydrolase 14	2,2	<0.001
Q13136	PPFIA1	Liprin-alpha-1	2,2	<0.001
P30520	ADSS2	Adenylosuccinate synthetase isozyme 2	2,2	<0.001
Q99497	PARK7	Parkinson disease protein 7	2,2	<0.001
P37802	TAGLN2	Transgelin-2	2,2	<0.001
Q71RC2	LARP4	La-related protein 4	2,2	<0.001
P30153	PPP2R1A	Serine/threonine-protein phosphatase 2A 65 kDa regulatory subunit A alpha isoform	2,2	<0.001
P51114	FXR1	Fragile X mental retardation syndrome-related protein 1	2,2	<0.001
D6RBD7	EEF1E1	Eukaryotic translation elongation factor 1 epsilon-1	2,2	<0.001
P08754	GNAI3	Guanine nucleotide-binding protein G(i) subunit alpha	2,2	0,001
Q02543	RPL18A	60S ribosomal protein L18a	2,2	0,001
Q9Y6Y8	SEC23IP	SEC23-interacting protein	2,2	0,001
P28838	LAP3	Cytosol aminopeptidase	2,2	0,001
Q9NSK0	KLC4	Kinesin light chain 4	2,2	0,001
M0QXL5	FBL	rRNA 2'-O-methyltransferase fibrillarin	2,2	0,002
P35268	RPL22	60S ribosomal protein L22	2,2	0,002
Q08J23	NSUN2	RNA cytosine C(5)-methyltransferase NSUN2	2,2	0,002
Q13464	ROCK1	Rho-associated protein kinase 1	2,2	0,004
H0YDU8	PPP5C	Serine/threonine-protein phosphatase	2,2	0,01
Q92973	TNPO1	Transportin-1	2,2	0,012
Q15084	PDIA6	Protein disulfide-isomerase A6	2,2	0,012
Q15750	TAB1	TGF-beta-activated kinase 1 and MAP3K7-binding protein 1	2,2	0,012
O43660	PLRG1	Pleiotropic regulator 1	2,2	0,013
Q01813	PFKP	ATP-dependent 6-phosphofructokinase, platelet type	2,2	0,015
Q9BUQ8	DDX23	Probable ATP-dependent RNA helicase DDX23	2,2	0,016
Q13257	MAD2L1	Mitotic spindle assembly checkpoint protein MAD2A	2,2	0,019
P82921	MRPS21	28S ribosomal protein S21, mitochondrial	2,2	0,02
Q7Z434	MAVS	Mitochondrial antiviral-signaling protein	2,2	0,024
P31323	PRKAR2B	cAMP-dependent protein kinase type II-beta regulatory subunit	2,2	0,05
Q52LJ0	FAM98B	Protein FAM98B	2,1	<0.001
A0A1C7CYX9	DPYSL2	Dihydropyrimidinase-related protein 2	2,1	<0.001
Q14247	CTTN	Src substrate cortactin	2,1	<0.001
P50502	ST13	Hsc70-interacting protein	2,1	<0.001
P55795	HNRNPH2	Heterogeneous nuclear ribonucleoprotein H2	2,1	<0.001
Q8WXF1	PSPC1	Paraspeckle component 1	2,1	<0.001
Q09666	AHNAK	Neuroblast differentiation-associated protein AHNAK	2,1	<0.001
Q9BQ69	MACROD1	ADP-ribose glycohydrolase MACROD1	2,1	<0.001
B4DDF4	CNN2	Calponin	2,1	0,001
Q5T7U1	GTF3C5	General transcription factor 3C polypeptide 5	2,1	0,001

P46459	NSF	Vesicle-fusing ATPase	2,1	0,001
O76003	GLRX3	Glutaredoxin-3	2,1	0,001
A0A0A0MRM9	NOLC1	Nucleolar and coiled-body phosphoprotein 1	2,1	0,003
P00519	ABL1	Tyrosine-protein kinase ABL1	2,1	0,003
P49959	MRE11	Double-strand break repair protein MRE11	2,1	0,004
P51570	GALK1	Galactokinase	2,1	0,004
P46777	RPL5	60S ribosomal protein L5	2,1	0,005
P11388	TOP2A	DNA topoisomerase 2-alpha	2,1	0,009
P62906	RPL10A	60S ribosomal protein L10a	2,1	0,012
Q9NXH9	TRMT1	tRNA	2,1	0,012
Q9BXJ9	NAA15	N-alpha-acetyltransferase 15, NatA auxiliary subunit	2,1	0,017
B4DLN1	B4DLN1	cDNA FLJ60124, highly similar to Mitochondrial dicarboxylate carrier	2,1	0,017
Q9BT25	HAUS8	HAUS augmin-like complex subunit 8	2,1	0,018
O14654	IRS4	Insulin receptor substrate 4	2,1	0,021
O43707	ACTN4	Alpha-actinin-4	2,1	0,026
P18031	PTPN1	Tyrosine-protein phosphatase non-receptor type 1	2,1	0,027
A0A3B3IUD2	MSTO1	Protein misato homolog 1	2,1	0,036
Q53H96	PYCR3	Pyrroline-5-carboxylate reductase 3	2,1	0,042
P19022	CDH2	Cadherin-2	2,1	0,043
Q8WWK9	CKAP2	Cytoskeleton-associated protein 2	2	<0.001
Q9NZI8	IGF2BP1	Insulin-like growth factor 2 mRNA-binding protein 1	2	<0.001
P25490	YY1	Transcriptional repressor protein YY1	2	<0.001
P25325	MPST	3-mercaptopyruvate sulfurtransferase	2	<0.001
Q96AG4	LRRC59	Leucine-rich repeat-containing protein 59	2	<0.001
Q8WYP5	AHCTF1	Protein ELYS	2	<0.001
X1WI28	RPL10	60S ribosomal protein L10	2	<0.001
E7EPN9	PRRC2C	Protein PRRC2C	2	<0.001
P13804	ETFA	Electron transfer flavoprotein subunit alpha, mitochondrial	2	<0.001
E7EVA0	MAP4	Microtubule-associated protein	2	<0.001
P26640	VARS1	Valine--tRNA ligase	2	<0.001
P62280	RPS11	40S ribosomal protein S11	2	<0.001
P31942	HNRNPH3	Heterogeneous nuclear ribonucleoprotein H3	2	<0.001
Q14126	DSG2	Desmoglein-2	2	<0.001
Q9H6T3	RPAP3	RNA polymerase II-associated protein 3	2	0,001
P46063	RECQL	ATP-dependent DNA helicase Q1	2	0,001
Q9UGI8	TES	Testin	2	0,001
A0A0G2JNZ2	SCRIB	Protein scribble homolog	2	0,001
P24534	EEF1B2	Elongation factor 1-beta	2	0,001
Q86UK7	ZNF598	E3 ubiquitin-protein ligase ZNF598	2	0,001
P62258	YWHAE	14-3-3 protein epsilon	2	0,001
O75152	ZC3H11A	Zinc finger CCCH domain-containing protein 11A	2	0,002
O15305	PMM2	Phosphomannomutase 2	2	0,002
Q86Y56	DNAAF5	Dynein assembly factor 5, axonemal	2	0,002
P55265	ADAR	Double-stranded RNA-specific adenosine deaminase	2	0,002
J3QR09	RPL19	Ribosomal protein L19	2	0,002
Q99569	PKP4	Plakophilin-4	2	0,003
Q14258	TRIM25	E3 ubiquitin/ISG15 ligase TRIM25	2	0,004
A5YKK6	CNOT1	CCR4-NOT transcription complex subunit 1	2	0,008
J3KTA4	DDX5	DEAD box protein 5	2	0,01
Q9GZS1	POLR1E	DNA-directed RNA polymerase I subunit RPA49	2	0,012
P35579	MYH9	Myosin-9	2	0,018
O14744	PRMT5	Protein arginine N-methyltransferase 5	2	0,018
Q9Y2Z4	YARS2	Tyrosine--tRNA ligase, mitochondrial	2	0,019
Q86VS8	HOOK3	Protein Hook homolog 3	2	0,02
Q9UGV2	NDRG3	Protein NDRG3	2	0,02
F5GWT4	WNK1	Non-specific serine/threonine protein kinase	2	0,02
D6R938	CAMK2D	Calcium/calmodulin-dependent protein kinase	2	0,021
Q16822	PCK2	Phosphoenolpyruvate carboxykinase [GTP], mitochondrial	2	0,021
Q9GZL7	WDR12	Ribosome biogenesis protein WDR12	2	0,023
Q8NCA5	FAM98A	Protein FAM98A	2	0,024
Q92665	MRPS31	28S ribosomal protein S31, mitochondrial	2	0,025
A0A0A6YYL4	CORO7-PAM16	Coronin	2	0,025
Q13625	TP53BP2	Apoptosis-stimulating of p53 protein 2	2	0,026
Q96AC1	FERMT2	Fermitin family homolog 2	2	0,028
Q15031	LARS2	Probable leucine--tRNA ligase, mitochondrial	2	0,029
Q9BTY7	HGH1	Protein HGH1 homolog	2	0,032
Q5UIP0	RIF1	Telomere-associated protein RIF1	2	0,032
Q96DH6	MSI2	RNA-binding protein Musashi homolog 2	2	0,036
Q9HAV4	XPO5	Exportin-5	2	0,037
Q9BYG3	NIFK	MKI67 FHA domain-interacting nucleolar phosphoprotein	2	0,039
P15880	RPS2	40S ribosomal protein S2	1,9	<0.001
P52948	NUP98	Nuclear pore complex protein Nup98-Nup96	1,9	<0.001
A0A087WXM6	RPL17	60S ribosomal protein L17	1,9	<0.001

O43159	RRP8	Ribosomal RNA-processing protein 8	1,9	<0.001
Q9Y2Z0	SUGT1	Protein SGT1 homolog	1,9	<0.001
P43246	MSH2	DNA mismatch repair protein Msh2	1,9	<0.001
Q16527	CSRP2	Cysteine and glycine-rich protein 2	1,9	<0.001
P46939	UTRN	Utrophin	1,9	<0.001
Q9BV20	MRI1	Methylthioribose-1-phosphate isomerase	1,9	<0.001
Q7RTV0	PHF5A	PHD finger-like domain-containing protein 5A	1,9	<0.001
Q8ND83	SLAIN1	SLAIN motif-containing protein 1	1,9	<0.001
Q96MU7	YTHDC1	YTH domain-containing protein 1	1,9	0,001
P18615	NELFE	Negative elongation factor E	1,9	0,001
P52701	MSH6	DNA mismatch repair protein Msh6	1,9	0,001
Q9UBT2	UBA2	SUMO-activating enzyme subunit 2	1,9	0,001
O60684	KPNA6	Importin subunit alpha-7	1,9	0,002
Q8NCW5	NAXE	NAD(P)H-hydrate epimerase	1,9	0,003
Q9H0H5	RACGAP1	Rac GTPase-activating protein 1	1,9	0,005
A0A087X0K9	TJP1	Tight junction protein ZO-1	1,9	0,005
P50995	ANXA11	Annexin A11	1,9	0,005
Q9BYN8	MRPS26	28S ribosomal protein S26, mitochondrial	1,9	0,007
O75436	VPS26A	Vacuolar protein sorting-associated protein 26A	1,9	0,007
Q12849	GRSF1	G-rich sequence factor 1	1,9	0,01
O14974	PPP1R12A	Protein phosphatase 1 regulatory subunit 12A	1,9	0,011
Q9BVP2	GNL3	Guanine nucleotide-binding protein-like 3	1,9	0,011
Q9BQ67	GRWD1	Glutamate-rich WD repeat-containing protein 1	1,9	0,012
Q13144	EIF2B5	Translation initiation factor eIF-2B subunit epsilon	1,9	0,019
Q86WJ1	CHD1L	Chromodomain-helicase-DNA-binding protein 1-like	1,9	0,02
O60701	UGDH	UDP-glucose 6-dehydrogenase	1,9	0,022
Q9BR76	CORO1B	Coronin-1B	1,9	0,025
A0A087WY71	AP2M1	AP-2 complex subunit mu	1,9	0,028
Q9ULT8	HECTD1	E3 ubiquitin-protein ligase HECTD1	1,9	0,029
P50542	PEX5	Peroxisomal targeting signal 1 receptor	1,9	0,029
Q5TFE4	NT5DC1	5'-nucleotidase domain-containing protein 1	1,9	0,03
O00487	PSMD14	26S proteasome non-ATPase regulatory subunit 14	1,9	0,03
Q8WX93	PALLD	Palladin	1,9	0,031
Q13618	CUL3	Cullin-3	1,9	0,031
O15020	SPTBN2	Spectrin beta chain, non-erythrocytic 2	1,9	0,032
O00267	SUPT5H	Transcription elongation factor SPT5	1,9	0,033
Q9BVJ6	UTP14A	U3 small nucleolar RNA-associated protein 14 homolog A	1,9	0,034
O95785	WIZ	Protein Wiz	1,9	0,035
Q7L0Y3	TRMT10C	tRNA methyltransferase 10 homolog C	1,9	0,036
Q96FV9	THOC1	THO complex subunit 1	1,9	0,038
O14617	AP3D1	AP-3 complex subunit delta-1	1,9	0,038
Q14966	ZNF638	Zinc finger protein 638	1,9	0,038
Q12948	FOXC1	Forkhead box protein C1	1,9	0,04
Q2TAL8	QRICH1	Glutamine-rich protein 1	1,9	0,04
Q9NP97	DYNLRB1	Dynein light chain roadblock-type 1	1,9	0,041
Q13363	CTBP1	C-terminal-binding protein 1	1,9	0,048
O75643	SNRNP200	U5 small nuclear ribonucleoprotein 200 kDa helicase	1,9	0,049
P49368	CCT3	T-complex protein 1 subunit gamma	1,8	<0.001
Q5T6F2	UBAP2	Ubiquitin-associated protein 2	1,8	<0.001
Q10567	AP1B1	AP-1 complex subunit beta-1	1,8	<0.001
P55060	CSE1L	Exportin-2	1,8	<0.001
O75792	RNASEH2A	Ribonuclease H2 subunit A	1,8	<0.001
Q9Y490	TLN1	Talin-1	1,8	<0.001
P30084	ECHS1	Enoyl-CoA hydratase, mitochondrial	1,8	<0.001
A0A1B0GWF2	STXBP1	Syntaxin-binding protein 1	1,8	<0.001
A0A0A0MRM8	MYO6	Unconventional myosin-6	1,8	<0.001
Q6YN16	HSDL2	Hydroxysteroid dehydrogenase-like protein 2	1,8	<0.001
Q16658	FSCN1	Fascin	1,8	<0.001
P46778	RPL21	60S ribosomal protein L21	1,8	<0.001
Q13451	FKBP5	Peptidyl-prolyl cis-trans isomerase FKBP5	1,8	<0.001
Q8WUM4	PDCD6IP	Programmed cell death 6-interacting protein	1,8	<0.001
A0A1W2PPZ5	TCEA1	Transcription elongation factor A protein 1	1,8	<0.001
O95239	KIF4A	Chromosome-associated kinesin KIF4A	1,8	0,001
K4DI93	CUL4B	Cullin 4B, isoform CRA_e	1,8	0,001
Q9BRX2	PELO	Protein pelota homolog	1,8	0,001
O43390	HNRNPR	Heterogeneous nuclear ribonucleoprotein R	1,8	0,001
Q14166	TTLL12	Tubulin--tyrosine ligase-like protein 12	1,8	0,001
P61313	RPL15	60S ribosomal protein L15	1,8	0,001
P12004	PCNA	Proliferating cell nuclear antigen	1,8	0,001
H7C5E4	XRN1	5'-3' exoribonuclease 1	1,8	0,001
Q13185	CBX3	Chromobox protein homolog 3	1,8	0,001
E9PDU5	WDR6	WD repeat-containing protein 6	1,8	0,001
O95336	PGLS	6-phosphogluconolactonase	1,8	0,001

Q9NZB2	FAM120A	Constitutive coactivator of PPAR-gamma-like protein 1	1,8	0,002
Q9BUF5	TUBB6	Tubulin beta-6 chain	1,8	0,002
P26373	RPL13	60S ribosomal protein L13	1,8	0,002
Q08752	PPID	Peptidyl-prolyl cis-trans isomerase D	1,8	0,002
Q9UPN7	PPP6R1	Serine/threonine-protein phosphatase 6 regulatory subunit 1	1,8	0,003
F8W0J6	NAP1L1	Nucleosome assembly protein 1-like 1	1,8	0,003
P26368	U2AF2	Splicing factor U2AF 65 kDa subunit	1,8	0,003
Q9P0K7	RAI14	Ankycorbin	1,8	0,004
P52272	HNRNPM	Heterogeneous nuclear ribonucleoprotein M	1,8	0,004
Q9UHB9	SRP68	Signal recognition particle subunit SRP68	1,8	0,005
O95861	BPNT1	3'(2'),5'-bisphosphate nucleotidase 1	1,8	0,005
Q13595	TRA2A	Transformer-2 protein homolog alpha	1,8	0,005
P12277	CKB	Creatine kinase B-type	1,8	0,006
Q9Y6G9	DYNC1LI1	Cytoplasmic dynein 1 light intermediate chain 1	1,8	0,006
Q9BSJ8	ESYT1	Extended synaptotagmin-1	1,8	0,006
P53597	SUCLG1	Succinate--CoA ligase [ADP/GDP-forming] subunit alpha, mitochondrial	1,8	0,006
O75131	CPNE3	Copine-3	1,8	0,006
P55010	EIF5	Eukaryotic translation initiation factor 5	1,8	0,006
P52732	KIF11	Kinesin-like protein KIF11	1,8	0,007
Q15021	NCAPD2	Condensin complex subunit 1	1,8	0,009
Q14161	GIT2	ARF GTPase-activating protein GIT2	1,8	0,009
Q8IY81	FTSJ3	pre-rRNA 2'-O-ribose RNA methyltransferase FTSJ3	1,8	0,014
Q92616	GCN1	eIF-2-alpha kinase activator GCN1	1,8	0,015
O95347	SMC2	Structural maintenance of chromosomes protein 2	1,8	0,022
P25205	MCM3	DNA replication licensing factor MCM3	1,8	0,026
P53582	METAP1	Methionine aminopeptidase 1	1,8	0,027
P30154	PPP2R1B	Serine/threonine-protein phosphatase 2A 65 kDa regulatory subunit A beta isoform	1,8	0,032
Q92878	RAD50	DNA repair protein RAD50	1,8	0,032
P54920	NAPA	Alpha-soluble NSF attachment protein	1,8	0,034
Q92797	SYMPK	Symplekin	1,8	0,035
Q05048	CSTF1	Cleavage stimulation factor subunit 1	1,8	0,035
O60832	DKC1	H/ACA ribonucleoprotein complex subunit DKC1	1,8	0,036
Q06210	GFPT1	Glutamine--fructose-6-phosphate aminotransferase [isomerizing] 1	1,8	0,036
Q53EL6	PDCD4	Programmed cell death protein 4	1,8	0,043
Q9UQN3	CHMP2B	Charged multivesicular body protein 2b	1,8	0,043
E9PKP7	UBTF	Nucleolar transcription factor 1	1,8	0,046
P17252	PRKCA	Protein kinase C alpha type	1,8	0,049
A0A087WY55	VTA1	Chromosome 6 open reading frame 55, isoform CRA_b	1,7	<0.001
Q9UPQ9	TNRC6B	Trinucleotide repeat-containing gene 6B protein	1,7	<0.001
P49321	NASP	Nuclear autoantigenic sperm protein	1,7	<0.001
Q8TD19	NEK9	Serine/threonine-protein kinase Nek9	1,7	<0.001
Q86YP4	GATAD2A	Transcriptional repressor p66-alpha	1,7	<0.001
Q9H7E9	C8orf33	UPF0488 protein C8orf33	1,7	<0.001
P35221	CTNNA1	Catenin alpha-1	1,7	<0.001
Q9UQ80	PA2G4	Proliferation-associated protein 2G4	1,7	<0.001
Q7Z4H3	HDDC2	5'-deoxynucleotidase HDDC2	1,7	<0.001
P60228	EIF3E	Eukaryotic translation initiation factor 3 subunit E	1,7	0,001
Q15003	NCAPH	Condensin complex subunit 2	1,7	0,001
P62333	PSMC6	26S proteasome regulatory subunit 10B	1,7	0,001
Q9Y5A9	YTHDF2	YTH domain-containing family protein 2	1,7	0,001
P60660	MYL6	Myosin light polypeptide 6	1,7	0,001
Q15785	TOMM34	Mitochondrial import receptor subunit TOM34	1,7	0,001
Q8N163	CCAR2	Cell cycle and apoptosis regulator protein 2	1,7	0,002
C9JRJ5	LIMD1	LIM domain-containing protein 1	1,7	0,002
Q96GD0	PDXP	Pyridoxal phosphate phosphatase	1,7	0,003
P33176	KIF5B	Kinesin-1 heavy chain	1,7	0,004
P35249	RFC4	Replication factor C subunit 4	1,7	0,004
Q9NYJ8	TAB2	TGF-beta-activated kinase 1 and MAP3K7-binding protein 2	1,7	0,004
Q96F86	EDC3	Enhancer of mRNA-decapping protein 3	1,7	0,005
O60783	MRPS14	28S ribosomal protein S14, mitochondrial	1,7	0,006
P56192	MARS1	Methionine--tRNA ligase, cytoplasmic	1,7	0,006
Q9NR45	NANS	Sialic acid synthase	1,7	0,007
Q9Y237	PIN4	Peptidyl-prolyl cis-trans isomerase NIMA-interacting 4	1,7	0,007
Q00610	CLTC	Clathrin heavy chain 1	1,7	0,007
P62249	RPS16	40S ribosomal protein S16	1,7	0,007
Q1KMD3	HNRNPUL2	Heterogeneous nuclear ribonucleoprotein U-like protein 2	1,7	0,007
Q13283	G3BP1	Ras GTPase-activating protein-binding protein 1	1,7	0,01
P25685	DNAJB1	DnaJ homolog subfamily B member 1	1,7	0,013
Q9H3U1	UNC45A	Protein unc-45 homolog A	1,7	0,015
O15226	NKRF	NF-kappa-B-repressing factor	1,7	0,018
P35659	DEK	Protein DEK	1,7	0,018
Q8WTT2	NOC3L	Nucleolar complex protein 3 homolog	1,7	0,027
A0A087WVZ9	POLR2E	DNA-directed RNA polymerase II subunit E	1,7	0,027

Q9Y6A5	TACC3	Transforming acidic coiled-coil-containing protein 3	1,7	0,032
Q9H814	PHAX	Phosphorylated adapter RNA export protein	1,7	0,034
Q96G46	DUS3L	tRNA-dihydrouridine(47) synthase [NAD(P)(+)]-like	1,7	0,037
E9PB90	HK2	Hexokinase	1,7	0,04
Q86VP6	CAND1	Cullin-associated NEDD8-dissociated protein 1	1,7	0,042
Q7Z478	DHX29	ATP-dependent RNA helicase DHX29	1,7	0,043
Q4KMP7	TBC1D10B	TBC1 domain family member 10B	1,7	0,044
P29558	RBMS1	RNA-binding motif, single-stranded-interacting protein 1	1,7	0,044
Q9H845	ACAD9	Complex I assembly factor ACAD9, mitochondrial	1,7	0,045
Q9HCD5	NCOA5	Nuclear receptor coactivator 5	1,7	0,048
P78347	GTF2I	General transcription factor II-I	1,7	0,049
Q5JSZ5	PRRC2B	Protein PRRC2B	1,6	<0.001
P61158	ACTR3	Actin-related protein 3	1,6	<0.001
Q9NSD9	FARSB	Phenylalanine--tRNA ligase beta subunit	1,6	<0.001
Q00796	SORD	Sorbitol dehydrogenase	1,6	<0.001
Q14974	KPNB1	Importin subunit beta-1	1,6	<0.001
P30566	ADSL	Adenylosuccinate lyase	1,6	0,001
P38117	ETFB	Electron transfer flavoprotein subunit beta	1,6	0,001
K7EJL1	AP1M1	AP-1 complex subunit mu-1	1,6	0,001
P42166	TMPO	Lamina-associated polypeptide 2, isoform alpha	1,6	0,001
O15371	EIF3D	Eukaryotic translation initiation factor 3 subunit D	1,6	0,001
P33993	MCM7	DNA replication licensing factor MCM7	1,6	0,001
P46779	RPL28	60S ribosomal protein L28	1,6	0,002
O43264	ZW10	Centromere/kinetochore protein zw10 homolog	1,6	0,002
O00170	AIP	AH receptor-interacting protein	1,6	0,002
Q9ULX3	NOB1	RNA-binding protein NOB1	1,6	0,002
A0A0G2JH68	DIAPH1	Protein diaphanous homolog 1	1,6	0,002
M0R3C3	TECR	Very-long-chain enoyl-CoA reductase	1,6	0,002
Q9BW92	TARS2	Threonine--tRNA ligase, mitochondrial	1,6	0,003
Q9C0C9	UBE2O	(E3-independent) E2 ubiquitin-conjugating enzyme	1,6	0,004
Q15637	SF1	Splicing factor 1	1,6	0,004
P52294	KPNA1	Importin subunit alpha-5	1,6	0,004
Q15424	SAFB	Scaffold attachment factor B1	1,6	0,005
A6NDG6	PGP	Glycerol-3-phosphate phosphatase	1,6	0,005
P60174	TPI1	Triosephosphate isomerase	1,6	0,006
B4E1N1	ARMC6	Armadillo repeat-containing protein 6	1,6	0,006
Q15417	CNN3	Calponin-3	1,6	0,008
Q9UI30	TRMT112	Multifunctional methyltransferase subunit TRM112-like protein	1,6	0,008
Q9Y450	HBS1L	HBS1-like protein	1,6	0,009
P43490	NAMPT	Nicotinamide phosphoribosyltransferase	1,6	0,009
Q9BZE4	GTPBP4	Nucleolar GTP-binding protein 1	1,6	0,01
A0A087X2D5	MRPL45	39S ribosomal protein L45, mitochondrial	1,6	0,011
Q9H2P0	ADNP	Activity-dependent neuroprotector homeobox protein	1,6	0,011
Q13247	SRSF6	Serine/arginine-rich splicing factor 6	1,6	0,015
O00571	DDX3X	ATP-dependent RNA helicase DDX3X	1,6	0,015
Q9NW13	RBM28	RNA-binding protein 28	1,6	0,015
Q15813	TBCE	Tubulin-specific chaperone E	1,6	0,015
P19338	NCL	Nucleolin	1,6	0,017
O00231	PSMD11	26S proteasome non-ATPase regulatory subunit 11	1,6	0,018
Q8NB90	SPATA5	ATPase family protein 2 homolog	1,6	0,021
F8W8R3	POLD2	DNA polymerase delta subunit 2	1,6	0,024
O43719	HTATSF1	HIV Tat-specific factor 1	1,6	0,026
Q9BY77	POLDIP3	Polymerase delta-interacting protein 3	1,6	0,027
Q9H0E2	TOLLIP	Toll-interacting protein	1,6	0,044
O75150	RNF40	E3 ubiquitin-protein ligase BRE1B	1,6	0,045
Q8IWB7	WDFY1	WD repeat and FYVE domain-containing protein 1	1,6	0,046
P22102	GART	Trifunctional purine biosynthetic protein adenosine-3 [Includes: Phosphoribosylamine--glycine ligase	1,5	<0.001
Q15233	NONO	Non-POU domain-containing octamer-binding protein	1,5	<0.001
Q14669	TRIP12	E3 ubiquitin-protein ligase TRIP12	1,5	<0.001
P31948	STIP1	Stress-induced-phosphoprotein 1	1,5	<0.001
P48643	CCT5	T-complex protein 1 subunit epsilon	1,5	<0.001
P29692	EEF1D	Elongation factor 1-delta	1,5	<0.001
Q02790	FKBP4	Peptidyl-prolyl cis-trans isomerase FKBP4	1,5	0,001
P61586	RHOA	Transforming protein RhoA	1,5	0,001
O43237	DYNC1LI2	Cytoplasmic dynein 1 light intermediate chain 2	1,5	0,001
P07814	EPRS1	Bifunctional glutamate/proline--tRNA ligase	1,5	0,001
O95816	BAG2	BAG family molecular chaperone regulator 2	1,5	0,001
Q9NPI6	DCP1A	mRNA-decapping enzyme 1A	1,5	0,002
Q9BZE9	ASPSCR1	Tether containing UBX domain for GLUT4	1,5	0,003
P63241	EIF5A	Eukaryotic translation initiation factor 5A-1	1,5	0,004
P41240	CSK	Tyrosine-protein kinase CSK	1,5	0,005
Q8IWX8	CHERP	Calcium homeostasis endoplasmic reticulum protein	1,5	0,006
O75534	CSDE1	Cold shock domain-containing protein E1	1,5	0,006

O95573	ACSL3	Long-chain-fatty-acid--CoA ligase 3	1,5	0,006
Q13428	TCOF1	Treacle protein	1,5	0,006
P78371	CCT2	T-complex protein 1 subunit beta	1,5	0,006
Q9NYZ3	GTSE1	G2 and S phase-expressed protein 1	1,5	0,007
Q8IYI6	EXOC8	Exocyst complex component 8	1,5	0,009
B4DY08	HNRNPC	Heterogeneous nuclear ribonucleoproteins C1/C2	1,5	0,009
Q9NQT5	EXOSC3	Exosome complex component RRP40	1,5	0,01
P50213	IDH3A	Isocitrate dehydrogenase [NAD] subunit alpha, mitochondrial	1,5	0,014
Q9UQ35	SRRM2	Serine/arginine repetitive matrix protein 2	1,5	0,016
O43395	PRPF3	U4/U6 small nuclear ribonucleoprotein Prp3	1,5	0,018
Q02878	RPL6	60S ribosomal protein L6	1,5	0,018
O00273	DFFA	DNA fragmentation factor subunit alpha	1,5	0,019
P63010	AP2B1	AP-2 complex subunit beta	1,5	0,023
Q9BWD1	ACAT2	Acetyl-CoA acetyltransferase, cytosolic	1,5	0,023
Q9H2U1	DHX36	ATP-dependent DNA/RNA helicase DHX36	1,5	0,024
O43252	PAPSS1	Bifunctional 3'-phosphoadenosine 5'-phosphosulfate synthase 1	1,5	0,028
P48507	GCLM	Glutamate--cysteine ligase regulatory subunit	1,5	0,032
Q9HC35	EML4	Echinoderm microtubule-associated protein-like 4	1,4	<0.001
P62633	CNBP	Cellular nucleic acid-binding protein	1,4	<0.001
Q8N0X7	SPART	Spartin	1,4	<0.001
P25786	PSMA1	Proteasome subunit alpha type-1	1,4	<0.001
P40227	CCT6A	T-complex protein 1 subunit zeta	1,4	<0.001
Q5JXI8	FHL1	Four and a half LIM domains protein 1	1,4	<0.001
Q86TB9	PATL1	Protein PAT1 homolog 1	1,4	<0.001
O94826	TOMM70	Mitochondrial import receptor subunit TOM70	1,4	0,001
Q99613	EIF3C	Eukaryotic translation initiation factor 3 subunit C	1,4	0,001
Q9UJU6	DBNL	Drebrin-like protein	1,4	0,001
Q96HC4	PDLIM5	PDZ and LIM domain protein 5	1,4	0,002
Q9UNY4	TTF2	Transcription termination factor 2	1,4	0,002
P33240	CSTF2	Cleavage stimulation factor subunit 2	1,4	0,002
E9PQV9	DCUN1D5	DCN1-like protein	1,4	0,003
P42696	RBM34	RNA-binding protein 34	1,4	0,004
Q9UHD1	CHORDC1	Cysteine and histidine-rich domain-containing protein 1	1,4	0,004
A0A3B3IRI2	CTPS1	CTP synthase	1,4	0,005
Q14C86	GAPVD1	GTPase-activating protein and VPS9 domain-containing protein 1	1,4	0,005
P62244	RPS15A	40S ribosomal protein S15a	1,4	0,006
Q12904	AIMP1	Aminoacyl tRNA synthase complex-interacting multifunctional protein 1	1,4	0,007
Q9NTI5	PDS5B	Sister chromatid cohesion protein PDS5 homolog B	1,4	0,008
Q9NSV4	DIAPH3	Protein diaphanous homolog 3	1,4	0,008
P49588	AARS1	Alanine--tRNA ligase, cytoplasmic	1,4	0,009
P46783	RPS10	40S ribosomal protein S10	1,4	0,009
A0A140T9R1	FLOT1	Flotillin	1,4	0,011
Q9UKM9	RALY	RNA-binding protein Raly	1,4	0,014
P51572	BCAP31	B-cell receptor-associated protein 31	1,4	0,015
O43290	SART1	U4/U6.U5 tri-snRNP-associated protein 1	1,4	0,015
O94906	PRPF6	Pre-mRNA-processing factor 6	1,4	0,017
Q9P2R3	ANKFY1	Rabankyrin-5	1,4	0,019
O00154	ACOT7	Cytosolic acyl coenzyme A thioester hydrolase	1,4	0,027
P27540	ARNT	Aryl hydrocarbon receptor nuclear translocator	1,4	0,028
P52597	HNRNPF	Heterogeneous nuclear ribonucleoprotein F	1,4	0,028
O95453	PARN	Poly(A)-specific ribonuclease PARN	1,4	0,03
C9J4Z3	RPL37A	60S ribosomal protein L37a	1,4	0,032
Q9UKD2	MRTO4	mRNA turnover protein 4 homolog	1,4	0,033
P18583	SON	Protein SON	1,4	0,035
Q92667	AKAP1	A-kinase anchor protein 1, mitochondrial	1,4	0,042
O14980	XPO1	Exportin-1	1,4	0,049
P62913	RPL11	60S ribosomal protein L11	1,3	<0.001
Q13045	FLII	Protein flightless-1 homolog	1,3	<0.001
Q9BTE6	AARSD1	Alanyl-tRNA editing protein Aarsd1	1,3	<0.001
F6T1Q0	PDE12	2',5'-phosphodiesterase 12	1,3	0,001
Q7LBC6	KDM3B	Lysine-specific demethylase 3B	1,3	0,001
P50991	CCT4	T-complex protein 1 subunit delta	1,3	0,001
Q15365	PCBP1	Poly(rC)-binding protein 1	1,3	0,001
Q2TAM5	RELA	RELA protein	1,3	0,002
Q14677	CLINT1	Clathrin interactor 1	1,3	0,002
P57772	EEFSEC	Selenocysteine-specific elongation factor	1,3	0,003
Q5QJE6	DNTTIP2	Deoxynucleotidyltransferase terminal-interacting protein 2	1,3	0,004
Q8IWS0	PHF6	PHD finger protein 6	1,3	0,004
P09525	ANXA4	Annexin A4	1,3	0,005
Q01469	FABP5	Fatty acid-binding protein 5	1,3	0,008
P62753	RPS6	40S ribosomal protein S6	1,3	0,009
Q9Y3S2	ZNF330	Zinc finger protein 330	1,3	0,011
Q9UNM6	PSMD13	26S proteasome non-ATPase regulatory subunit 13	1,3	0,012

Q8IZ83	ALDH16A1	Aldehyde dehydrogenase family 16 member A1	1,3	0,012
A0A1B0GV47	KIF21A	Kinesin-like protein KIF21A	1,3	0,012
C9JP00	MBNL1	Muscleblind-like protein 1	1,3	0,013
P62241	RPS8	40S ribosomal protein S8	1,3	0,013
P34897	SHMT2	Serine hydroxymethyltransferase, mitochondrial	1,3	0,013
A0A2R8Y880	RBBP6	E3 ubiquitin-protein ligase RBBP6	1,3	0,014
P49736	MCM2	DNA replication licensing factor MCM2	1,3	0,018
H0Y5D5	CIZ1	Cip1-interacting zinc finger protein	1,3	0,019
Q9NWH9	SLTM	SAFB-like transcription modulator	1,3	0,019
Q13838	DDX39B	Spliceosome RNA helicase DDX39B	1,3	0,019
Q8WWQ0	PHIP	PH-interacting protein	1,3	0,021
Q9UKF6	CPSF3	Cleavage and polyadenylation specificity factor subunit 3	1,3	0,022
Q99426	TBCB	Tubulin-folding cofactor B	1,3	0,022
Q13148	TARDBP	TAR DNA-binding protein 43	1,3	0,022
P35250	RFC2	Replication factor C subunit 2	1,3	0,022
P51153	RAB13	Ras-related protein Rab-13	1,3	0,023
O94927	HAUS5	HAUS augmin-like complex subunit 5	1,3	0,023
P11177	PDHB	Pyruvate dehydrogenase E1 component subunit beta, mitochondrial	1,3	0,032
P11172	UMPS	Uridine 5'-monophosphate synthase	1,3	0,033
O75717	WDHD1	WD repeat and HMG-box DNA-binding protein 1	1,3	0,034
P09543	CNP	2',3'-cyclic-nucleotide 3'-phosphodiesterase	1,3	0,034
F2Z2T2	XPA	DNA repair protein-complementing XP-A cells	1,3	0,036
Q16543	CDC37	Hsp90 co-chaperone Cdc37	1,3	0,039
Q9BWF3	RBM4	RNA-binding protein 4	1,3	0,043
Q15154	PCM1	Pericentriolar material 1 protein	1,3	0,045
P13797	PLS3	Plastin-3	1,2	<0.001
Q9UHD8	SEPTIN9	Septin-9	1,2	0,001
P10606	COX5B	Cytochrome c oxidase subunit 5B, mitochondrial	1,2	0,003
Q92597	NDRG1	Protein NDRG1	1,2	0,004
Q13347	EIF3I	Eukaryotic translation initiation factor 3 subunit I	1,2	0,004
P36578	RPL4	60S ribosomal protein L4	1,2	0,004
A0A0C4DGA6	HLTF	Helicase-like transcription factor	1,2	0,005
Q9UMS4	PRPF19	Pre-mRNA-processing factor 19	1,2	0,007
P62701	RPS4X	40S ribosomal protein S4, X isoform	1,2	0,008
Q6PKG0	LARP1	La-related protein 1	1,2	0,008
P23246	SFPQ	Splicing factor, proline- and glutamine-rich	1,2	0,009
Q5BKZ1	ZNF326	DBIRD complex subunit ZNF326	1,2	0,012
O60884	DNAJA2	DnaJ homolog subfamily A member 2	1,2	0,012
Q8WVJ2	NUDCD2	NudC domain-containing protein 2	1,2	0,013
P55884	EIF3B	Eukaryotic translation initiation factor 3 subunit B	1,2	0,018
P62269	RPS18	40S ribosomal protein S18	1,2	0,022
O75832	PSMD10	26S proteasome non-ATPase regulatory subunit 10	1,2	0,023
G5EA36	CDC27	Cell division cycle 27, isoform CRA_c	1,2	0,027
P40937	RFC5	Replication factor C subunit 5	1,2	0,038
O43615	TIMM44	Mitochondrial import inner membrane translocase subunit TIM44	1,2	0,039
P14866	HNRNPL	Heterogeneous nuclear ribonucleoprotein L	1,2	0,045
Q13435	SF3B2	Splicing factor 3B subunit 2	1,2	0,047
P17987	TCP1	T-complex protein 1 subunit alpha	1,1	0,003
P09622	DLD	Dihydrolipoyl dehydrogenase, mitochondrial	1,1	0,003
P62195	PSMC5	26S proteasome regulatory subunit 8	1,1	0,004
Q96C36	PYCR2	Pyrroline-5-carboxylate reductase 2	1,1	0,005
O15047	SETD1A	Histone-lysine N-methyltransferase SETD1A	1,1	0,007
Q14847	LASP1	LIM and SH3 domain protein 1	1,1	0,009
P49327	FASN	Fatty acid synthase	1,1	0,009
Q15555	MAPRE2	Microtubule-associated protein RP/EB family member 2	1,1	0,014
A0A2R8Y855	SMARCE1	SWI/SNF-related matrix-associated actin-dependent regulator of chromatin subfamily E member 1	1,1	0,015
O15294	OGT	UDP-N-acetylglucosamine--peptide N-acetylglucosaminyltransferase 110 kDa subunit	1,1	0,017
Q15126	PMVK	Phosphomevalonate kinase	1,1	0,02
Q9Y5X1	SNX9	Sorting nexin-9	1,1	0,021
P45974	USP5	Ubiquitin carboxyl-terminal hydrolase 5	1,1	0,023
Q9UPT5	EXOC7	Exocyst complex component 7	1,1	0,023
P54136	RARS1	Arginine--tRNA ligase, cytoplasmic	1,1	0,024
Q32MZ4	LRRFIP1	Leucine-rich repeat flightless-interacting protein 1	1,1	0,026
Q9H0D6	XRN2	5'-3' exoribonuclease 2	1,1	0,027
P53618	COPB1	Coatomer subunit beta	1,1	0,028
P35580	MYH10	Myosin-10	1,1	0,03
Q9NVH2	INTS7	Integrator complex subunit 7	1,1	0,03
Q13907	IDI1	Isopentenyl-diphosphate Delta-isomerase 1	1,1	0,031
Q9BSD7	NTPCR	Cancer-related nucleoside-triphosphatase	1,1	0,033
O95232	LUC7L3	Luc7-like protein 3	1,1	0,033
Q9UN86	G3BP2	Ras GTPase-activating protein-binding protein 2	1,1	0,038
Q9UJC3	HOOK1	Protein Hook homolog 1	1,1	0,042
P56545	CTBP2	C-terminal-binding protein 2	1,1	0,043

A0A2R8Y5F1	TSC2	Tuberin	1,1	0,044
Q15008	PSMD6	26S proteasome non-ATPase regulatory subunit 6	1,1	0,045
Q7Z417	NUFIP2	Nuclear fragile X mental retardation-interacting protein 2	1	0,001
Q8ND24	RNF214	RING finger protein 214	1	0,008
P53396	ACLY	ATP-citrate synthase	1	0,008
Q13155	AIMP2	Aminoacyl tRNA synthase complex-interacting multifunctional protein 2	1	0,009
P38919	EIF4A3	Eukaryotic initiation factor 4A-III	1	0,01
Q9UN37	VPS4A	Vacuolar protein sorting-associated protein 4A	1	0,015
P26639	TARS1	Threonine--tRNA ligase 1, cytoplasmic	1	0,02
Q9Y613	FHOD1	FH1/FH2 domain-containing protein 1	1	0,028
P18858	LIG1	DNA ligase 1	1	0,032
P49591	SARS1	Serine--tRNA ligase, cytoplasmic	1	0,035
P62917	RPL8	60S ribosomal protein L8	1	0,037
PRDX2 cysteine-dependent interactors				
Q9BQA1	WDR77	Methylosome protein 50	7,2	<0.001
Q9NQX3	GPHN	Gephyrin [Includes: Molybdopterin adenylyltransferase	6,4	<0.001
E7EVA0	MAP4	Microtubule-associated protein	6,1	<0.001
O14744	PRMT5	Protein arginine N-methyltransferase 5	6	<0.001
Q9C0C2	TNKS1BP1	182 kDa tankyrase-1-binding protein	5,8	<0.001
P07355	ANXA2	Annexin A2	5,8	<0.001
E9PGZ1	CALD1	Caldesmon	5,3	<0.001
Q7Z434	MAVS	Mitochondrial antiviral-signaling protein	5,2	<0.001
Q96KB5	PBK	Lymphokine-activated killer T-cell-originated protein kinase	4,6	<0.001
O60664	PLIN3	Perilipin-3	4,4	<0.001
Q9UHV9	PFDN2	Prefoldin subunit 2	4,4	<0.001
Q8NC51	SERBP1	Plasminogen activator inhibitor 1 RNA-binding protein	4,4	<0.001
Q9NXV2	KCTD5	BTB/POZ domain-containing protein KCTD5	4,4	0,033
Q14247	CTTN	Src substrate cortactin	4	<0.001
O96007	MOCS2	Molybdopterin synthase catalytic subunit	4	0,014
Q9Y266	NUDC	Nuclear migration protein nudC	3,8	<0.001
Q5T6F2	UBAP2	Ubiquitin-associated protein 2	3,7	<0.001
Q9NPH2	ISYNA1	Inositol-3-phosphate synthase 1	3,6	0,001
Q9NUQ3	TXLNG	Gamma-taxilin	3,5	<0.001
Q9Y570	PPME1	Protein phosphatase methylesterase 1	3,5	<0.001
P11802	CDK4	Cyclin-dependent kinase 4	3,5	<0.001
Q13541	EIF4EBP1	Eukaryotic translation initiation factor 4E-binding protein 1	3,5	0,001
Q9Y6A5	TACC3	Transforming acidic coiled-coil-containing protein 3	3,5	0,001
Q9ULW0	TPX2	Targeting protein for Xklp2	3,5	0,002
O14965	AURKA	Aurora kinase A	3,4	<0.001
P10599	TXN	Thioredoxin	3,4	<0.001
Q5SW79	CEP170	Centrosomal protein of 170 kDa	3,4	<0.001
Q8NFC6	BOD1L1	Biorientation of chromosomes in cell division protein 1-like 1	3,3	<0.001
P61758	VBP1	Prefoldin subunit 3	3,3	0,001
Q32MZ4	LRRFIP1	Leucine-rich repeat flightless-interacting protein 1	3,2	<0.001
Q9HA64	FN3KRP	Ketosamine-3-kinase	3,1	<0.001
P46821	MAP1B	Microtubule-associated protein 1B	3,1	<0.001
P35520	CBS	Cystathionine beta-synthase	3,1	<0.001
Q9P2B4	CTTNBP2NL	CTTNBP2 N-terminal-like protein	3,1	0,001
Q16204	CCDC6	Coiled-coil domain-containing protein 6	3,1	0,004
A6NGP5	JPT2	Jupiter microtubule-associated homolog 2	3	<0.001
P52888	THOP1	Thimet oligopeptidase	3	<0.001
Q13428	TCOF1	Treacle protein	3	<0.001
Q8IYS1	PM20D2	Peptidase M20 domain-containing protein 2	3	0,001
P26599	PTBP1	Polypyrimidine tract-binding protein 1	2,9	<0.001
P40222	TXLNA	Alpha-taxilin	2,9	0,002
Q13542	EIF4EBP2	Eukaryotic translation initiation factor 4E-binding protein 2	2,9	0,024
E7EPN9	PRRC2C	Protein PRRC2C	2,8	<0.001
A0A087WTM1	ROBO1	Roundabout homolog 1	2,8	0,002
Q96F45	ZNF503	Zinc finger protein 503	2,8	0,003
P22061	PCMT1	Protein-L-isoaspartate(D-aspartate) O-methyltransferase	2,8	0,005
Q6WKZ4	RAB11FIP1	Rab11 family-interacting protein 1	2,7	0,003
Q8IWB7	WDFY1	WD repeat and FYVE domain-containing protein 1	2,7	0,004
O95104	SCAF4	SR-related and CTD-associated factor 4	2,7	0,005
P52907	CAPZA1	F-actin-capping protein subunit alpha-1	2,6	<0.001
Q9H773	DCTPP1	dCTP pyrophosphatase 1	2,6	0,001
Q9H2U2	PPA2	Inorganic pyrophosphatase 2, mitochondrial	2,6	0,002
B7Z7F3	RANBP3	Ran-binding protein 3	2,6	0,004
E7EV99	ADD1	Alpha-adducin	2,6	0,005
P30740	SERPINB1	Leukocyte elastase inhibitor	2,6	0,005
A0A0A0MRN5	OGFR	Opioid growth factor receptor	2,6	0,005
P48634	PRRC2A	Protein PRRC2A	2,5	<0.001
O60547	GMDS	GDP-mannose 4,6 dehydratase	2,5	0,005
F5H8D7	XRCC1	DNA repair protein XRCC1	2,5	0,006

P85037	FOXK1	Forkhead box protein K1	2,5	0,013
O75223	GGCT	Gamma-glutamylcyclotransferase	2,5	0,02
Q9BRP1	PDCD2L	Programmed cell death protein 2-like	2,4	0,005
Q8N3X1	FNBP4	Formin-binding protein 4	2,4	0,006
P12955	PEPD	Xaa-Pro dipeptidase	2,4	0,021
Q8N6M0	OTUD6B	Deubiquitinase OTUD6B	2,4	0,022
O15511	ARPC5	Actin-related protein 2/3 complex subunit 5	2,4	0,043
Q06124	PTPN11	Tyrosine-protein phosphatase non-receptor type 11	2,3	<0.001
Q12948	FOXC1	Forkhead box protein C1	2,3	0,002
O00629	KPNA4	Importin subunit alpha-3	2,3	0,01
O43809	NUDT21	Cleavage and polyadenylation specificity factor subunit 5	2,3	0,011
Q9H0S4	DDX47	Probable ATP-dependent RNA helicase DDX47	2,3	0,017
Q96EA4	SPDL1	Protein Spindly	2,3	0,033
A0A1B0GW38	CBL	E3 ubiquitin-protein ligase CBL	2,2	<0.001
H0YNW5	DUT	Deoxyuridine 5'-triphosphate nucleotidohydrolase	2,2	<0.001
Q16576	RBBP7	Histone-binding protein RBBP7	2,2	<0.001
Q86V48	LUZP1	Leucine zipper protein 1	2,2	<0.001
P35237	SERPINB6	Serpin B6	2,2	<0.001
P48507	GCLM	Glutamate--cysteine ligase regulatory subunit	2,2	0,002
Q9P258	RCC2	Protein RCC2	2,2	0,002
Q8TAQ2	SMARCC2	SWI/SNF complex subunit SMARCC2	2,2	0,008
O43143	DHX15	Pre-mRNA-splicing factor ATP-dependent RNA helicase DHX15	2,2	0,008
Q96IZ0	PAWR	PRKC apoptosis WT1 regulator protein	2,2	0,015
P49903	SEPHS1	Selenide, water dikinase 1	2,2	0,028
Q6FI81	CIAPIN1	Anamorsin	2,2	0,033
Q8N806	UBR7	Putative E3 ubiquitin-protein ligase UBR7	2,2	0,035
Q6PKG0	LARP1	La-related protein 1	2,1	<0.001
J3KN29	PSMD9	26S proteasome non-ATPase regulatory subunit 9	2,1	0,001
Q96K76	USP47	Ubiquitin carboxyl-terminal hydrolase 47	2,1	0,014
O60826	CCDC22	Coiled-coil domain-containing protein 22	2,1	0,019
Q99598	TSNAX	Translin-associated protein X	2,1	0,026
Q9NVP1	DDX18	ATP-dependent RNA helicase DDX18	2,1	0,029
Q8WVC2	RPS21	40S ribosomal protein S21	2,1	0,029
O00566	MPHOSPH10	U3 small nucleolar ribonucleoprotein protein MPP10	2,1	0,035
C9J0I9	ZC3HC1	Nuclear-interacting partner of ALK	2	<0.001
Q9Y3F4	STRAP	Serine-threonine kinase receptor-associated protein	2	<0.001
Q93034	CUL5	Cullin-5	2	0,001
A0AVT1	UBA6	Ubiquitin-like modifier-activating enzyme 6	2	0,003
P54646	PRKAA2	5'-AMP-activated protein kinase catalytic subunit alpha-2	2	0,006
Q6IQ49	SDE2	Replication stress response regulator SDE2	2	0,018
Q5JRA6	MIA3	Transport and Golgi organization protein 1 homolog	2	0,018
Q9ULX6	AKAP8L	A-kinase anchor protein 8-like	2	0,026
A4D1S0	KLRG2	Killer cell lectin-like receptor subfamily G member 2	2	0,043
Q9H3K6	BOLA2	BolA-like protein 2	1,9	<0.001
Q5QPM7	PSMF1	Proteasome inhibitor PI31 subunit	1,9	<0.001
Q96F86	EDC3	Enhancer of mRNA-decapping protein 3	1,9	0,002
Q15417	CNN3	Calponin-3	1,9	0,002
P10301	RRAS	Ras-related protein R-Ras	1,9	0,017
P19174	PLCG1	1-phosphatidylinositol 4,5-bisphosphate phosphodiesterase gamma-1	1,9	0,025
Q9UL15	BAG5	BAG family molecular chaperone regulator 5	1,9	0,028
Q8WYA6	CTNNBL1	Beta-catenin-like protein 1	1,9	0,038
Q5T4K5	CRTC2	CREB-regulated transcription coactivator 2	1,9	0,04
P82921	MRPS21	28S ribosomal protein S21, mitochondrial	1,9	0,04
B1AK87	CAPZB	F-actin-capping protein subunit beta	1,8	<0.001
P53985	SLC16A1	Monocarboxylate transporter 1	1,8	<0.001
Q9H3S7	PTPN23	Tyrosine-protein phosphatase non-receptor type 23	1,8	0,03
Q9BT25	HAUS8	HAUS augmin-like complex subunit 8	1,8	0,039
P49458	SRP9	Signal recognition particle 9 kDa protein	1,8	0,048
B4DDF4	CNN2	Calponin	1,7	0,008
J3QQZ9	PNPO	Pyridoxal 5'-phosphate synthase	1,7	0,016
Q13547	HDAC1	Histone deacetylase 1	1,7	0,017
Q92783	STAM	Signal transducing adapter molecule 1	1,7	0,04
Q9HCN8	SDF2L1	Stromal cell-derived factor 2-like protein 1	1,7	0,04
Q9NXF7	DCAF16	DDB1- and CUL4-associated factor 16	1,7	0,041
P11413	G6PD	Glucose-6-phosphate 1-dehydrogenase	1,6	0,001
Q9UNF1	MAGED2	Melanoma-associated antigen D2	1,6	0,001
O00273	DFFA	DNA fragmentation factor subunit alpha	1,6	0,002
Q9UHD1	CHORDC1	Cysteine and histidine-rich domain-containing protein 1	1,6	0,002
Q9C0C9	UBE2O	(E3-independent) E2 ubiquitin-conjugating enzyme	1,6	0,004
O14929	HAT1	Histone acetyltransferase type B catalytic subunit	1,6	0,008
P49790	NUP153	Nuclear pore complex protein Nup153	1,6	0,01
P63167	DYNLL1	Dynein light chain 1, cytoplasmic	1,6	0,031
Q9UQE7	SMC3	Structural maintenance of chromosomes protein 3	1,6	0,035

Q14240	EIF4A2	Eukaryotic initiation factor 4A-II	1,6	0,048
E9PGT1	TSN	Component 3 of promoter of RISC	1,6	0,048
P45985	MAP2K4	Dual specificity mitogen-activated protein kinase kinase 4	1,5	<0.001
P22314	UBA1	Ubiquitin-like modifier-activating enzyme 1	1,5	0,015
Q9UI12	ATP6V1H	V-type proton ATPase subunit H	1,4	0,001
Q9BTE6	AARSD1	Alanyl-tRNA editing protein Aarsd1	1,4	0,001
P42771	CDKN2A	Cyclin-dependent kinase inhibitor 2A	1,4	0,001
Q15365	PCBP1	Poly(rC)-binding protein 1	1,4	0,001
Q07666	KHDRBS1	KH domain-containing, RNA-binding, signal transduction-associated protein 1	1,4	0,017
Q9UN37	VPS4A	Vacuolar protein sorting-associated protein 4A	1,4	0,018
O14974	PPP1R12A	Protein phosphatase 1 regulatory subunit 12A	1,4	0,041
Q96D09	GPRASP2	G-protein coupled receptor-associated sorting protein 2	1,3	0,005
P51452	DUSP3	Dual specificity protein phosphatase 3	1,3	0,006
Q8WWK9	CKAP2	Cytoskeleton-associated protein 2	1,3	0,009
A0MZ66	SHTN1	Shootin-1	1,3	0,024
P22234	PAICS	Multifunctional protein ADE2 [Includes: Phosphoribosylaminoimidazole-succinocarboxamide synthase	1,3	0,025
Q92667	AKAP1	A-kinase anchor protein 1, mitochondrial	1,3	0,034
O75663	TIPRL	TIP41-like protein	1,3	0,036
Q9NYZ3	GTSE1	G2 and S phase-expressed protein 1	1,3	0,043
G3XAG1	ZNF512	Zinc finger protein 512	1,3	0,05
P13797	PLS3	Plastin-3	1,2	0,001
Q92945	KHSRP	Far upstream element-binding protein 2	1,2	0,003
Q9H7E9	C8orf33	UPF0488 protein C8orf33	1,2	0,008
Q96HC4	PDLIM5	PDZ and LIM domain protein 5	1,2	0,01
E9PLA9	CAPRIN1	Caprin-1	1,2	0,014
O95816	BAG2	BAG family molecular chaperone regulator 2	1,2	0,03
Q7Z6Z7	HUWE1	E3 ubiquitin-protein ligase HUWE1	1,2	0,038
Q92598	HSPH1	Heat shock protein 105 kDa	1,1	0,007
Q2NKX8	ERCC6L	DNA excision repair protein ERCC-6-like	1,1	0,014
Q86YP4	GATAD2A	Transcriptional repressor p66-alpha	1,1	0,017
Q68EM7	ARHGAP17	Rho GTPase-activating protein 17	1,1	0,021
O00170	AIP	AH receptor-interacting protein	1,1	0,031
Q92769	HDAC2	Histone deacetylase 2	1,1	0,044
Q96P47	AGAP3	Arf-GAP with GTPase, ANK repeat and PH domain-containing protein 3	1	0,007
Q13200	PSMD2	26S proteasome non-ATPase regulatory subunit 2	1	0,009
O60343	TBC1D4	TBC1 domain family member 4	1	0,018
P49321	NASP	Nuclear autoantigenic sperm protein	1	0,019
PRDX3 cysteine-dependent interactors				
F8VYE8	PPP1CC	Serine/threonine-protein phosphatase	4,4	<0.001
P05386	RPLP1	60S acidic ribosomal protein P1	4,3	<0.001
Q8N5K1	CISD2	CDGSH iron-sulfur domain-containing protein 2	4,1	<0.001
P11766	ADH5	Alcohol dehydrogenase class-3	4	<0.001
P51148	RAB5C	Ras-related protein Rab-5C	3,9	0,001
Q7L2H7	EIF3M	Eukaryotic translation initiation factor 3 subunit M	3,7	<0.001
P06132	UROD	Uroporphyrinogen decarboxylase	3,7	0,001
P40616	ARL1	ADP-ribosylation factor-like protein 1	3,6	<0.001
Q15084	PDIA6	Protein disulfide-isomerase A6	3,6	<0.001
Q6DKI1	RPL7L1	60S ribosomal protein L7-like 1	3,6	0,001
Q07820	MCL1	Induced myeloid leukemia cell differentiation protein Mcl-1	3,5	0,001
Q6IBS0	TWF2	Twinfilin-2	3,4	<0.001
H3BTA2	PPP4C	Serine/threonine-protein phosphatase	3,4	<0.001
P19022	CDH2	Cadherin-2	3,4	0,003
Q07021	C1QBP	Complement component 1 Q subcomponent-binding protein, mitochondrial	3,3	<0.001
P07355	ANXA2	Annexin A2	3,3	<0.001
P30041	PRDX6	Peroxiredoxin-6	3,3	0,001
P22061	PCMT1	Protein-L-isoaspartate(D-aspartate) O-methyltransferase	3,3	0,002
Q9NS69	TOMM22	Mitochondrial import receptor subunit TOM22 homolog	3,2	0,001
P14174	MIF	Macrophage migration inhibitory factor	3,2	0,002
Q5SZR4	TDRKH	Tudor and KH domain containing, isoform CRA_a	3,2	0,007
Q15814	TBCC	Tubulin-specific chaperone C	3,2	0,013
A0A2R8YFH5	SEC23B	Protein transport protein SEC23	3,2	0,042
Q9NWV4	CZIB	CXXC motif containing zinc binding protein	3,1	0,002
Q86WA6	BPHL	Valacyclovir hydrolase	3,1	0,003
P51809	VAMP7	Vesicle-associated membrane protein 7	3,1	0,006
Q9ULX3	NOB1	RNA-binding protein NOB1	3	0,001
Q9Y5Y2	NUBP2	Cytosolic Fe-S cluster assembly factor NUBP2	3	0,001
Q5SY16	NOL9	Polynucleotide 5'-hydroxyl-kinase NOL9	3	0,001
Q92990	GLMN	Glomulin	3	0,001
Q96EA4	SPDL1	Protein Spindly	3	0,008
Q5VW32	BROX	BRO1 domain-containing protein BROX	3	0,009
G5EA06	MRPS27	28S ribosomal protein S27, mitochondrial	3	0,025
Q92785	DPF2	Zinc finger protein ubi-d4	2,9	0,004
Q9H6R0	DHX33	ATP-dependent RNA helicase DHX33	2,9	0,027

Q9BSJ8	ESYT1	Extended synaptotagmin-1	2,8	<0.001
O43809	NUDT21	Cleavage and polyadenylation specificity factor subunit 5	2,8	0,003
B3KUS5	USP30	Ubiquitin carboxyl-terminal hydrolase	2,8	0,007
H3BRY6	INTS14	Integrator complex subunit 14	2,8	0,029
A6NDU8	C5orf51	UPF0600 protein C5orf51	2,8	0,034
P61106	RAB14	Ras-related protein Rab-14	2,7	<0.001
P78346	RPP30	Ribonuclease P protein subunit p30	2,7	0,001
Q9Y4B6	DCAF1	DDB1- and CUL4-associated factor 1	2,7	0,002
Q9UKK9	NUDT5	ADP-sugar pyrophosphatase	2,7	0,002
Q9NYK5	MRPL39	39S ribosomal protein L39, mitochondrial	2,7	0,004
F8W038	C17orf49	Chromosome 17 open reading frame 49	2,7	0,007
Q66PJ3	ARL6IP4	ADP-ribosylation factor-like protein 6-interacting protein 4	2,7	0,007
Q5JRI1	SRSF10	Serine/arginine-rich-splicing factor 10	2,7	0,036
Q7Z434	MAVS	Mitochondrial antiviral-signaling protein	2,6	<0.001
Q9Y3D0	CIAO2B	Cytosolic iron-sulfur assembly component 2B	2,6	0,005
P57076	CFAP298	Cilia- and flagella-associated protein 298	2,6	0,007
Q9NZ45	CISD1	CDGSH iron-sulfur domain-containing protein 1	2,6	0,029
Q8IYS1	PM20D2	Peptidase M20 domain-containing protein 2	2,5	0,006
Q9NP61	ARFGAP3	ADP-ribosylation factor GTPase-activating protein 3	2,5	0,006
Q9BTE1	DCTN5	Dynactin subunit 5	2,5	0,012
Q92804	TAF15	TATA-binding protein-associated factor 2N	2,5	0,017
Q9HD26	GOPC	Golgi-associated PDZ and coiled-coil motif-containing protein	2,5	0,018
C9JAW5	C9JAW5	HIG1 domain-containing protein	2,5	0,018
M0R026	ILVBL	2-hydroxyacyl-CoA lyase 2	2,4	0,002
B4DJ81	NDUFS1	NADH-ubiquinone oxidoreductase 75 kDa subunit, mitochondrial	2,4	0,003
Q15291	RBBP5	Retinoblastoma-binding protein 5	2,4	0,004
Q8IVS2	MCAT	Malonyl-CoA-acyl carrier protein transacylase, mitochondrial	2,4	0,004
D6RA00	ENOPH1	Enolase-phosphatase E1	2,4	0,004
A0A087WU06	TUBGCP3	Gamma-tubulin complex component	2,4	0,009
Q16698	DECR1	2,4-dienoyl-CoA reductase, mitochondrial	2,4	0,009
F5H008	VPS33B	Vacuolar protein sorting-associated protein 33B	2,4	0,013
Q9H9P8	L2HGDH	L-2-hydroxyglutarate dehydrogenase, mitochondrial	2,4	0,017
A0A0A0MS29	MFF	Mitochondrial fission factor	2,4	0,027
P10599	TXN	Thioredoxin	2,3	0,002
Q16718	NDUFA5	NADH dehydrogenase [ubiquinone] 1 alpha subcomplex subunit 5	2,3	0,003
Q9P287	BCCIP	BRCA2 and CDKN1A-interacting protein	2,3	0,004
Q9NP97	DYNLRB1	Dynein light chain roadblock-type 1	2,3	0,009
P54646	PRKAA2	5'-AMP-activated protein kinase catalytic subunit alpha-2	2,3	0,012
Q14161	GIT2	ARF GTPase-activating protein GIT2	2,3	0,013
O75146	HIP1R	Huntingtin-interacting protein 1-related protein	2,3	0,016
P00492	HPRT1	Hypoxanthine-guanine phosphoribosyltransferase	2,3	0,016
Q8N6M0	OTUD6B	Deubiquitinase OTUD6B	2,3	0,018
Q8WVC2	RPS21	40S ribosomal protein S21	2,3	0,022
P18669	PGAM1	Phosphoglycerate mutase 1	2,3	0,04
A0A0A0MR02	VDAC2	Outer mitochondrial membrane protein porin 2	2,2	0,001
Q8N6T3	ARFGAP1	ADP-ribosylation factor GTPase-activating protein 1	2,2	0,003
Q9BQC3	DPH2	2-(3-amino-3-carboxypropyl)histidine synthase subunit 2	2,2	0,009
Q96IU4	ABHD14B	Protein ABHD14B	2,2	0,022
O95295	SNAPIN	SNARE-associated protein Snapin	2,2	0,023
Q8N6R0	EEF1AKNMT	eEF1A lysine and N-terminal methyltransferase	2,2	0,025
Q9BYN0	SRXN1	Sulfiredoxin-1	2,2	0,044
P11802	CDK4	Cyclin-dependent kinase 4	2,1	0,001
A0A0A0MTB8	WDR36	WD repeat-containing protein 36	2,1	0,01
X6RM00	ERC1	ELKS/Rab6-interacting/CAST family member 1	2,1	0,016
P30740	SERPINB1	Leukocyte elastase inhibitor	2,1	0,017
Q13509	TUBB3	Tubulin beta-3 chain	2,1	0,017
H3BV80	RNPS1	RNA-binding protein with serine-rich domain 1	2,1	0,022
Q5T749	KPRP	Keratinocyte proline-rich protein	2,1	0,034
Q92667	AKAP1	A-kinase anchor protein 1, mitochondrial	2	0,003
Q8NBU5	ATAD1	ATPase family AAA domain-containing protein 1	2	0,011
Q96AT9	RPE	Ribulose-phosphate 3-epimerase	2	0,015
Q9UQR0	SCML2	Sex comb on midleg-like protein 2	2	0,018
Q9UHD2	TBK1	Serine/threonine-protein kinase TBK1	2	0,02
Q9HCN8	SDF2L1	Stromal cell-derived factor 2-like protein 1	2	0,022
O43815	STRN	Striatin	2	0,025
Q9BZX2	UCK2	Uridine-cytidine kinase 2	2	0,029
P04843	RPN1	Dolichyl-diphosphooligosaccharide--protein glycosyltransferase subunit 1	1,9	0,002
P62879	GNB2	Guanine nucleotide-binding protein G(I)/G(S)/G(T) subunit beta-2	1,9	0,007
Q2M2I8	AAK1	AP2-associated protein kinase 1	1,9	0,02
O75600	GCAT	2-amino-3-ketobutyrate coenzyme A ligase, mitochondrial	1,9	0,038
Q96S44	TP53RK	EKC/KEOPS complex subunit TP53RK	1,8	0,033
O15269	SPTLC1	Serine palmitoyltransferase 1	1,7	0,009
Q96BW9	TAMM41	Phosphatidate cytidylyltransferase, mitochondrial	1,7	0,027

Q96A49	SYAP1	Synapse-associated protein 1	1,7	0,033
O43237	DYNC1LI2	Cytoplasmic dynein 1 light intermediate chain 2	1,7	0,036
Q9HB71	CACYBP	Calcyclin-binding protein	1,7	0,041
Q9H974	QTRT2	Queuine tRNA-ribosyltransferase accessory subunit 2	1,7	0,048
A0A0A0MR09	PTPN9	Tyrosine-protein phosphatase non-receptor type 9	1,7	0,05
P62979	RPS27A	Ubiquitin-40S ribosomal protein S27a	1,6	0,004
Q9Y679	AUP1	Lipid droplet-regulating VLDL assembly factor AUP1	1,6	0,034
E9PJN0	ACOT8	Acyl-coenzyme A thioesterase 8	1,6	0,044
P35268	RPL22	60S ribosomal protein L22	1,6	0,045
Q8TDH9	BLOC1S5	Biogenesis of lysosome-related organelles complex 1 subunit 5	1,5	0,004
B7WPG3	HNRNPLL	Heterogeneous nuclear ribonucleoprotein L-like	1,5	0,007
O14828	SCAMP3	Secretory carrier-associated membrane protein 3	1,5	0,034
Q9H0E2	TOLLIP	Toll-interacting protein	1,5	0,037
Q14318	FKBP8	Peptidyl-prolyl cis-trans isomerase FKBP8	1,4	0,009
P27824	CANX	Calnexin	1,4	0,011
P18031	PTPN1	Tyrosine-protein phosphatase non-receptor type 1	1,4	0,026
Q9UL15	BAG5	BAG family molecular chaperone regulator 5	1,4	0,041
Q9UBE0	SAE1	SUMO-activating enzyme subunit 1	1,4	0,043
Q6PKG0	LARP1	La-related protein 1	1,3	0,009
P21964	COMT	Catechol O-methyltransferase	1,3	0,011
P62081	RPS7	40S ribosomal protein S7	1,3	0,017
P35520	CBS	Cystathionine beta-synthase	1,3	0,026
O60784	TOM1	Target of Myb protein 1	1,2	0,005
Q5QPM7	PSMF1	Proteasome inhibitor PI31 subunit	1,2	0,011
P50454	SERPINH1	Serpin H1	1,2	0,013
Q5TDH0	DDI2	Protein DDI1 homolog 2	1,2	0,014
P31040	SDHA	Succinate dehydrogenase [ubiquinone] flavoprotein subunit, mitochondrial	1,2	0,016
K7ERF1	EIF3K	Eukaryotic translation initiation factor 3 subunit K	1,2	0,024
Q9UJS0	SLC25A13	Calcium-binding mitochondrial carrier protein Aralar2	1,2	0,035
Q9H0U4	RAB1B	Ras-related protein Rab-1B	1,2	0,048
P35237	SERPINB6	Serpin B6	1,1	0,006
P62873	GNB1	Guanine nucleotide-binding protein G(I)/G(S)/G(T) subunit beta-1	1,1	0,007
Q9GZS3	WDR61	WD repeat-containing protein 61	1,1	0,012
G3V279	ERH	Enhancer of rudimentary homolog	1,1	0,022
P08240	SRPRA	Signal recognition particle receptor subunit alpha	1,1	0,023
Q14697	GANAB	Neutral alpha-glucosidase AB	1,1	0,026
H7BXI1	ESYT2	Extended synaptotagmin-2	1,1	0,047
P22695	UQCRC2	Cytochrome b-c1 complex subunit 2, mitochondrial	1	0,024
PRDX4 cysteine-dependent interactors				
I3L1P8	SLC25A11	Mitochondrial 2-oxoglutarate/malate carrier protein	3,9	<0.001
Q9BS26	ERP44	Endoplasmic reticulum resident protein 44	3,8	0,002
Q8NBS9	TXNDC5	Thioredoxin domain-containing protein 5	3,7	<0.001
Q96AC1	FERMT2	Fermitin family homolog 2	3,4	<0.001
Q9Y2R5	MRPS17	28S ribosomal protein S17, mitochondrial	3,2	0,002
F5H6E2	MYO1C	Unconventional myosin-Ic	2,8	0,003
Q9BSJ8	ESYT1	Extended synaptotagmin-1	2,7	0,002
A0A0B4J1Z1	SRSF7	Serine/arginine-rich-splicing factor 7	2,7	0,007
Q66K74	MAP1S	Microtubule-associated protein 1S	2,4	0,008
Q12797	ASPH	Aspartyl/asparaginyl beta-hydroxylase	2,3	0,002
D6RA00	ENOPH1	Enolase-phosphatase E1	2,3	0,008
P30154	PPP2R1B	Serine/threonine-protein phosphatase 2A 65 kDa regulatory subunit A beta isoform	2,3	0,012
P09110	ACAA1	3-ketoacyl-CoA thiolase, peroxisomal	2,2	0,004
P30041	PRDX6	Peroxiredoxin-6	2,2	0,012
Q92783	STAM	Signal transducing adapter molecule 1	2,2	0,015
Q96DH6	MSI2	RNA-binding protein Musashi homolog 2	2,2	0,026
F5GZS6	SLC3A2	4F2 cell-surface antigen heavy chain	2,1	0,008
Q9NW82	WDR70	WD repeat-containing protein 70	2,1	0,029
B4DJ81	NDUFS1	NADH-ubiquinone oxidoreductase 75 kDa subunit, mitochondrial	2	0,022
P42345	MTOR	Serine/threonine-protein kinase mTOR	2	0,031
Q15084	PDIA6	Protein disulfide-isomerase A6	1,9	0,029
Q93034	CUL5	Cullin-5	1,8	0,041
P22234	PAICS	Multifunctional protein ADE2 [Includes: Phosphoribosylaminoimidazole-succinocarboxamide synthase	1,7	0,003
P62249	RPS16	40S ribosomal protein S16	1,7	0,006
Q14739	LBR	Delta(14)-sterol reductase LBR	1,7	0,01
P62906	RPL10A	60S ribosomal protein L10a	1,7	0,047
C9J9K3	RPSA	40S ribosomal protein SA	1,6	0,004
Q9UHV9	PFDN2	Prefoldin subunit 2	1,6	0,005
O43809	NUDT21	Cleavage and polyadenylation specificity factor subunit 5	1,6	0,013
Q96K76	USP47	Ubiquitin carboxyl-terminal hydrolase 47	1,5	0,002
Q5SW79	CEP170	Centrosomal protein of 170 kDa	1,5	0,006
P22307	SCP2	Non-specific lipid-transfer protein	1,5	0,006
P49411	TUFM	Elongation factor Tu, mitochondrial	1,5	0,011
A0A2R8Y7S2	SMARCA4	Transcription activator BRG1	1,5	0,019

E9PGZ1	CALD1	Caldesmon	1,5	0,045
Q14697	GANAB	Neutral alpha-glucosidase AB	1,4	0,004
P60174	TPI1	Triosephosphate isomerase	1,4	0,011
Q9UQR0	SCML2	Sex comb on midleg-like protein 2	1,4	0,017
Q16513	PKN2	Serine/threonine-protein kinase N2	1,4	0,019
P10599	TXN	Thioredoxin	1,4	0,041
O14974	PPP1R12A	Protein phosphatase 1 regulatory subunit 12A	1,4	0,043
Q14152	EIF3A	Eukaryotic translation initiation factor 3 subunit A	1,4	0,046
Q86UP2	KTN1	Kinectin	1,3	0,006
Q9Y4B6	DCAF1	DDB1- and CUL4-associated factor 1	1,3	0,017
Q96I99	SUCLG2	Succinate--CoA ligase [GDP-forming] subunit beta, mitochondrial	1,3	0,033
Q13257	MAD2L1	Mitotic spindle assembly checkpoint protein MAD2A	1,3	0,038
Q9P2J5	LARS1	Leucine--tRNA ligase, cytoplasmic	1,3	0,049
P06576	ATP5F1B	ATP synthase subunit beta, mitochondrial	1,2	0,002
P06733	ENO1	Alpha-enolase	1,2	0,006
Q9BTZ2	DHRS4	Dehydrogenase/reductase SDR family member 4	1,2	0,011
P34897	SHMT2	Serine hydroxymethyltransferase, mitochondrial	1,2	0,015
P05388	RPLP0	60S acidic ribosomal protein P0	1,2	0,016
P26599	PTBP1	Polypyrimidine tract-binding protein 1	1,2	0,017
P18858	LIG1	DNA ligase 1	1,2	0,02
P18077	RPL35A	60S ribosomal protein L35a	1,2	0,024
Q9HCD5	NCOA5	Nuclear receptor coactivator 5	1,2	0,037
O15372	EIF3H	Eukaryotic translation initiation factor 3 subunit H	1,1	0,024
A0A087WY71	AP2M1	AP-2 complex subunit mu	1,1	0,024
Q12904	AIMP1	Aminoacyl tRNA synthase complex-interacting multifunctional protein 1	1,1	0,036
Q96C36	PYCR2	Pyrroline-5-carboxylate reductase 2	1	0,012
Q13347	EIF3I	Eukaryotic translation initiation factor 3 subunit I	1	0,017
P34949	MPI	Mannose-6-phosphate isomerase	1	0,022
P13489	RNH1	Ribonuclease inhibitor	1	0,036
P15880	RPS2	40S ribosomal protein S2	1	0,04
PRDX5 cysteine-dependent interactors				
P36551	CPOX	Oxygen-dependent coproporphyrinogen-III oxidase, mitochondrial	5,2	<0.001
Q96A49	SYAP1	Synapse-associated protein 1	4,6	<0.001
Q15388	TOMM20	Mitochondrial import receptor subunit TOM20 homolog	4	0,001
A0A0C4DGQ6	RPRD1A	Regulation of nuclear pre-mRNA domain-containing protein 1A	3,2	<0.001
Q9H2P9	DPH5	Diphthine methyl ester synthase	3,2	0,003
P26599	PTBP1	Polypyrimidine tract-binding protein 1	3	<0.001
Q9GZU8	PSME3IP1	PSME3-interacting protein	3	0,002
Q9BS26	ERP44	Endoplasmic reticulum resident protein 44	3	0,006
P78371	CCT2	T-complex protein 1 subunit beta	2,9	<0.001
Q8NFC6	BOD1L1	Biorientation of chromosomes in cell division protein 1-like 1	2,9	<0.001
Q53GQ0	HSD17B12	Very-long-chain 3-oxoacyl-CoA reductase	2,9	0,002
E9PGT1	TSN	Component 3 of promoter of RISC	2,8	<0.001
P63167	DYNLL1	Dynein light chain 1, cytoplasmic	2,8	0,007
O95801	TTC4	Tetratricopeptide repeat protein 4	2,7	0,005
Q6DKK2	TTC19	Tetratricopeptide repeat protein 19, mitochondrial	2,7	0,008
Q2TAM5	RELA	RELA protein	2,6	0,004
Q99598	TSNAX	Translin-associated protein X	2,5	<0.001
Q5T760	SRSF11	Serine/arginine-rich-splicing factor 11	2,5	0,006
O60664	PLIN3	Perilipin-3	2,5	0,006
Q16698	DECR1	2,4-dienoyl-CoA reductase, mitochondrial	2,5	0,007
Q10713	PMPCA	Mitochondrial-processing peptidase subunit alpha	2,5	0,008
Q16822	PCK2	Phosphoenolpyruvate carboxykinase [GTP], mitochondrial	2,5	0,016
B7Z7F3	RANBP3	Ran-binding protein 3	2,4	<0.001
Q9Y266	NUDC	Nuclear migration protein nudC	2,4	0,002
Q92990	GLMN	Glomulin	2,4	0,01
Q8N6M0	OTUD6B	Deubiquitinase OTUD6B	2,4	0,014
P85037	FOXK1	Forkhead box protein K1	2,4	0,019
Q6PID6	TTC33	Tetratricopeptide repeat protein 33	2,4	0,02
P22234	PAICS	Multifunctional protein ADE2 [Includes: Phosphoribosylaminoimidazole-succinocarboxamide synthase	2,3	<0.001
P43304	GPD2	Glycerol-3-phosphate dehydrogenase, mitochondrial	2,3	0,001
P48047	ATP5PO	ATP synthase subunit O, mitochondrial	2,3	0,001
P22061	PCMT1	Protein-L-isoaspartate(D-aspartate) O-methyltransferase	2,3	0,009
H7C128	BRD8	Bromodomain-containing protein 8	2,2	0,001
A0A0B4J1Z1	SRSF7	Serine/arginine-rich-splicing factor 7	2,2	0,029
Q9Y277	VDAC3	Voltage-dependent anion-selective channel protein 3	2,2	0,036
Q9HB71	CACYBP	Calcyclin-binding protein	2,1	<0.001
Q8N3X1	FNBP4	Formin-binding protein 4	2,1	<0.001
Q14C86	GAPVD1	GTPase-activating protein and VPS9 domain-containing protein 1	2,1	<0.001
A0A0A0MR02	VDAC2	Outer mitochondrial membrane protein porin 2	2,1	0,001
Q05655	PRKCD	Protein kinase C delta type	2,1	0,001
O00483	NDUFA4	Cytochrome c oxidase subunit NDUFA4	2,1	0,016
Q15750	TAB1	TGF-beta-activated kinase 1 and MAP3K7-binding protein 1	2,1	0,022

Q9H2U1	DHX36	ATP-dependent DNA/RNA helicase DHX36	2,1	0,024
A0A024R442	A0A024R442	>tr|A0A024R442|A0A024R442_HUMAN Aspartyl aminopeptidase, isoform CRA_b OS=Homo sapiens OX=9606 GN=DNPEP PE=1 SV=1;>sp|Q9ULA0|DNPEP_HUMAN Aspartyl aminopeptidase OS=Homo sapiens OX=9606 GN=DNPEP PE=1 SV=1;>tr|E7ETB3|E7ETB3_HUMAN Aspartyl aminopeptidase, iso	2,1	0,032
P40222	TXLNA	Alpha-taxilin	2	0,001
P43686	PSMC4	26S proteasome regulatory subunit 6B	2	0,003
Q9H773	DCTPP1	dCTP pyrophosphatase 1	2	0,005
Q9BTY7	HGH1	Protein HGH1 homolog	2	0,007
P12955	PEPD	Xaa-Pro dipeptidase	2	0,025
P62979	RPS27A	Ubiquitin-40S ribosomal protein S27a	1,9	0,001
Q9BSJ8	ESYT1	Extended synaptotagmin-1	1,9	0,002
P07355	ANXA2	Annexin A2	1,9	0,007
P30041	PRDX6	Peroxiredoxin-6	1,9	0,015
Q9H0E2	TOLLIP	Toll-interacting protein	1,9	0,016
Q9P2N5	RBM27	RNA-binding protein 27	1,9	0,028
Q5JRA6	MIA3	Transport and Golgi organization protein 1 homolog	1,9	0,03
Q6WKZ4	RAB11FIP1	Rab11 family-interacting protein 1	1,9	0,034
Q15645	TRIP13	Pachytene checkpoint protein 2 homolog	1,9	0,037
E9PJN0	ACOT8	Acyl-coenzyme A thioesterase 8	1,8	<0.001
Q8NC51	SERBP1	Plasminogen activator inhibitor 1 RNA-binding protein	1,8	0,001
F5GZS6	SLC3A2	4F2 cell-surface antigen heavy chain	1,8	0,005
P00492	HPRT1	Hypoxanthine-guanine phosphoribosyltransferase	1,8	0,012
P56385	ATP5ME	ATP synthase subunit e, mitochondrial	1,8	0,016
Q9Y6A5	TACC3	Transforming acidic coiled-coil-containing protein 3	1,8	0,016
E9PGZ1	CALD1	Caldesmon	1,8	0,019
Q9BW92	TARS2	Threonine--tRNA ligase, mitochondrial	1,8	0,019
Q15061	WDR43	WD repeat-containing protein 43	1,8	0,033
Q66PJ3	ARL6IP4	ADP-ribosylation factor-like protein 6-interacting protein 4	1,8	0,034
Q04446	GBE1	1,4-alpha-glucan-branching enzyme	1,8	0,045
A0AVT1	UBA6	Ubiquitin-like modifier-activating enzyme 6	1,7	0,005
Q9UL15	BAG5	BAG family molecular chaperone regulator 5	1,7	0,005
O43815	STRN	Striatin	1,7	0,008
E7EV99	ADD1	Alpha-adducin	1,7	0,019
Q9BQA1	WDR77	Methylosome protein 50	1,7	0,036
Q9NQX3	GPHN	Gephyrin [Includes: Molybdopterin adenylyltransferase	1,7	0,036
P14174	MIF	Macrophage migration inhibitory factor	1,7	0,045
P31689	DNAJA1	DnaJ homolog subfamily A member 1	1,6	<0.001
Q9Y570	PPME1	Protein phosphatase methylesterase 1	1,6	0,009
O14929	HAT1	Histone acetyltransferase type B catalytic subunit	1,6	0,009
O00165	HAX1	HCLS1-associated protein X-1	1,6	0,013
F8W1A4	AK2	Adenylate kinase 2, mitochondrial	1,6	0,026
Q9NT62	ATG3	Ubiquitin-like-conjugating enzyme ATG3	1,6	0,029
Q9NQP4	PFDN4	Prefoldin subunit 4	1,6	0,049
Q9BQ69	MACROD1	ADP-ribose glycohydrolase MACROD1	1,6	0,05
Q15276	RABEP1	Rab GTPase-binding effector protein 1	1,5	0,003
C9J9K3	RPSA	40S ribosomal protein SA	1,5	0,004
Q9BSD7	NTPCR	Cancer-related nucleoside-triphosphatase	1,5	0,006
Q02952	AKAP12	A-kinase anchor protein 12	1,5	0,015
Q9BRS2	RIOK1	Serine/threonine-protein kinase RIO1	1,5	0,016
Q9C0C2	TNKS1BP1	182 kDa tankyrase-1-binding protein	1,5	0,039
Q09666	AHNAK	Neuroblast differentiation-associated protein AHNAK	1,4	0,001
Q16531	DDB1	DNA damage-binding protein 1	1,4	0,003
P05386	RPLP1	60S acidic ribosomal protein P1	1,4	0,004
Q96IZ0	PAWR	PRKC apoptosis WT1 regulator protein	1,4	0,008
Q9NZL9	MAT2B	Methionine adenosyltransferase 2 subunit beta	1,4	0,015
Q8NBU5	ATAD1	ATPase family AAA domain-containing protein 1	1,4	0,016
P52888	THOP1	Thimet oligopeptidase	1,4	0,027
Q12931	TRAP1	Heat shock protein 75 kDa, mitochondrial	1,3	0,003
Q32MZ4	LRRFIP1	Leucine-rich repeat flightless-interacting protein 1	1,3	0,01
P15880	RPS2	40S ribosomal protein S2	1,3	0,012
Q13185	CBX3	Chromobox protein homolog 3	1,3	0,012
Q96RL1	UIMC1	BRCA1-A complex subunit RAP80	1,3	0,014
H7BZM7	ZPR1	Zinc finger protein ZPR1	1,2	0,003
P51665	PSMD7	26S proteasome non-ATPase regulatory subunit 7	1,2	0,006
Q9Y3F4	STRAP	Serine-threonine kinase receptor-associated protein	1,2	0,006
Q9UNM6	PSMD13	26S proteasome non-ATPase regulatory subunit 13	1,2	0,01
P04843	RPN1	Dolichyl-diphosphooligosaccharide--protein glycosyltransferase subunit 1	1,2	0,036
P46821	MAP1B	Microtubule-associated protein 1B	1,2	0,047
E9PLA9	CAPRIN1	Caprin-1	1,1	0,002
A0A087WUT6	EIF5B	Eukaryotic translation initiation factor 5B	1,1	0,008
P22570	FDXR	NADPH:adrenodoxin oxidoreductase, mitochondrial	1,1	0,008
Q9UI12	ATP6V1H	V-type proton ATPase subunit H	1,1	0,014
Q5T6F2	UBAP2	Ubiquitin-associated protein 2	1,1	0,015

E7EVA0	MAP4	Microtubule-associated protein	1,1	0,022
C9J4Z3	RPL37A	60S ribosomal protein L37a	1,1	0,041
P62195	PSMC5	26S proteasome regulatory subunit 8	1	0,005
P25398	RPS12	40S ribosomal protein S12	1	0,016
P11413	G6PD	Glucose-6-phosphate 1-dehydrogenase	1	0,036
P62333	PSMC6	26S proteasome regulatory subunit 10B	1	0,037
O14579	COPE	Coatomer subunit epsilon	1	0,038

Table S2: isoform-specific cysteine-dependent interactors

gene	uniprot ID	protein	fold change	adj. p-value	against
PRDX1 -specific interactors					
A0A075B6R9	IGKV2D-24	Probable non-functional immunoglobulin kappa variable 2D-24	2,9	0,001	PRDX2
F8W9F9	WNK2	Non-specific serine/threonine protein kinase	2,5	0,001	PRDX2
Q06830	PRDX1	Peroxiredoxin-1	2,4	0	PRDX2
O60566	BUB1B	Mitotic checkpoint serine/threonine-protein kinase BUB1 beta	2,4	0,001	PRDX2
G3V3B9	GSTZ1	Maleylacetoacetate isomerase	2,4	0,001	PRDX2
Q6NZY4	ZCCHC8	Zinc finger CCHC domain-containing protein 8	2,4	0,008	PRDX2
P30044	PRDX5	Peroxiredoxin-5, mitochondrial	2,3	0,028	PRDX2
O95218	ZRANB2	Zinc finger Ran-binding domain-containing protein 2	2,2	0,003	PRDX2
P19387	POLR2C	DNA-directed RNA polymerase II subunit RPB3	2,2	0,004	PRDX2
Q9Y3B7	MRPL11	39S ribosomal protein L11, mitochondrial	2,1	0	PRDX2
A0A3B3ITJ4	HNRNPL	Heterogeneous nuclear ribonucleoprotein L	2,1	0,004	PRDX2
O00399	DCTN6	Dynactin subunit 6	2,1	0,006	PRDX2
Q9Y3D9	MRPS23	28S ribosomal protein S23, mitochondrial	2,1	0,017	PRDX2
A0A087X1B1	IKBKG	NF-kappa-B essential modulator	2	0,009	PRDX2
P14635	CCNB1	G2/mitotic-specific cyclin-B1	2	0,01	PRDX2
Q6UWE0	LRSAM1	E3 ubiquitin-protein ligase LRSAM1	2	0,011	PRDX2
Q12929	EPS8	Epidermal growth factor receptor kinase substrate 8	1,9	0,007	PRDX2
Q16352	INA	Alpha-internexin	1,8	0	PRDX2
P07196	NEFL	Neurofilament light polypeptide	1,8	0,001	PRDX2
Q12933	TRAF2	TNF receptor-associated factor 2	1,8	0,013	PRDX2
Q13418	ILK	Integrin-linked protein kinase	1,8	0,018	PRDX2
Q96DA6	DNAJC19	Mitochondrial import inner membrane translocase subunit TIM14	1,8	0,019	PRDX2
Q99956	DUSP9	Dual specificity protein phosphatase 9	1,8	0,024	PRDX2
P42765	ACAA2	3-ketoacyl-CoA thiolase, mitochondrial	1,7	0	PRDX2
Q9H0H5	RACGAP1	Rac GTPase-activating protein 1	1,7	0	PRDX2
Q8WVC0	LEO1	RNA polymerase-associated protein LEO1	1,7	0,026	PRDX2
Q9C026	TRIM9	E3 ubiquitin-protein ligase TRIM9	1,7	0,029	PRDX2
O75616	ERAL1	GTPase Era, mitochondrial	1,7	0,036	PRDX2
Q15398	DLGAP5	Disks large-associated protein 5	1,6	0,001	PRDX2
Q9ULX3	NOB1	RNA-binding protein NOB1	1,6	0,002	PRDX2
Q9BR76	CORO1B	Coronin-1B	1,6	0,012	PRDX2
Q9BW83	IFT27	Intraflagellar transport protein 27 homolog	1,6	0,024	PRDX2
Q6R327	RICTOR	Rapamycin-insensitive companion of mTOR	1,6	0,027	PRDX2
Q96B36	AKT1S1	Proline-rich AKT1 substrate 1	1,6	0,031	PRDX2
H3BPJ9	NDUFB10	Complex I-PDSW	1,6	0,032	PRDX2
P09497	CLTB	Clathrin light chain B	1,6	0,04	PRDX2
Q92974	ARHGEF2	Rho guanine nucleotide exchange factor 2	1,5	0	PRDX2
A0A0G2JNZ2	SCRIB	Protein scribble homolog	1,5	0,001	PRDX2
Q04837	SSBP1	Single-stranded DNA-binding protein, mitochondrial	1,5	0,001	PRDX2
Q96RT1	ERBIN	Erbin	1,5	0,003	PRDX2
Q6FI81	CIAPIN1	Anamorsin	1,5	0,013	PRDX2
Q13573	SNW1	SNW domain-containing protein 1	1,5	0,02	PRDX2
Q99447	PCYT2	Ethanolamine-phosphate cytidylyltransferase	1,5	0,028	PRDX2
F5H345	HMBS	Hydroxymethylbilane synthase	1,5	0,038	PRDX2
Q13015	MLLT11	Protein AF1q	1,5	0,049	PRDX2
Q9Y5M8	SRPRB	Signal recognition particle receptor subunit beta	1,4	0	PRDX2
A0A087WW06	TTC28	Tetratricopeptide repeat protein 28	1,4	0	PRDX2
Q86Y56	DNAAF5	Dynein assembly factor 5, axonemal	1,4	0,004	PRDX2
Q8N6R0	EEF1AKNMT	eEF1A lysine and N-terminal methyltransferase	1,4	0,05	PRDX2
Q8ND24	RNF214	RING finger protein 214	1,3	0	PRDX2
P39019	RPS19	40S ribosomal protein S19	1,3	0	PRDX2
Q9UN37	VPS4A	Vacuolar protein sorting-associated protein 4A	1,3	0,002	PRDX2
Q9UJC3	HOOK1	Protein Hook homolog 1	1,3	0,003	PRDX2
A0A087WUK2	HNRNPDL	Heterogeneous nuclear ribonucleoprotein D-like	1,3	0,006	PRDX2
Q13625	TP53BP2	Apoptosis-stimulating of p53 protein 2	1,3	0,006	PRDX2
Q9Y3S2	ZNF330	Zinc finger protein 330	1,3	0,016	PRDX2
Q99569	PKP4	Plakophilin-4	1,3	0,019	PRDX2
Q5VVQ6	YOD1	Ubiquitin thioesterase OTU1	1,3	0,045	PRDX2

Q4VCS5	AMOT	Angiomotin	1,3	0,049	PRDX2
C9JRJ5	LIMD1	LIM domain-containing protein 1	1,2	0,001	PRDX2
F8WB06	ATXN2	Ataxin-2	1,2	0,003	PRDX2
P35998	PSMC2	26S proteasome regulatory subunit 7	1,2	0,004	PRDX2
A0A0A0MRM8	MYO6	Unconventional myosin-6	1,2	0,004	PRDX2
H7C5E4	XRN1	5'-3' exoribonuclease 1	1,2	0,005	PRDX2
Q92990	GLMN	Glomulin	1,2	0,006	PRDX2
Q9UG54	MAP3K7	Mitogen-activated protein kinase kinase kinase	1,2	0,013	PRDX2
Q13123	IK	Protein Red	1,2	0,023	PRDX2
Q8WTW3	COG1	Conserved oligomeric Golgi complex subunit 1	1,2	0,025	PRDX2
Q92665	MRPS31	28S ribosomal protein S31, mitochondrial	1,2	0,033	PRDX2
Q8N3C0	ASCC3	Activating signal cointegrator 1 complex subunit 3	1,2	0,034	PRDX2
A0A087X0K9	TJP1	Tight junction protein ZO-1	1,2	0,041	PRDX2
Q12955	ANK3	Ankyrin-3	1,1	0	PRDX2
P28066	PSMA5	Proteasome subunit alpha type-5	1,1	0	PRDX2
Q96S55	WRNIP1	ATPase WRNIP1	1,1	0,001	PRDX2
Q15126	PMVK	Phosphomevalonate kinase	1,1	0,002	PRDX2
Q99543	DNAJC2	DnaJ homolog subfamily C member 2	1,1	0,011	PRDX2
Q9UN86	G3BP2	Ras GTPase-activating protein-binding protein 2	1,1	0,013	PRDX2
P57740	NUP107	Nuclear pore complex protein Nup107	1,1	0,015	PRDX2
Q14126	DSG2	Desmoglein-2	1,1	0,015	PRDX2
P0DMV9	HSPA1B	Heat shock 70 kDa protein 1B	1,1	0,017	PRDX2
Q15424	SAFB	Scaffold attachment factor B1	1,1	0,017	PRDX2
Q9NQT5	EXOSC3	Exosome complex component RRP40	1,1	0,026	PRDX2
P52272	HNRNPM	Heterogeneous nuclear ribonucleoprotein M	1,1	0,029	PRDX2
O00170	AIP	AH receptor-interacting protein	1,1	0,029	PRDX2
Q9BZE4	GTPBP4	Nucleolar GTP-binding protein 1	1,1	0,03	PRDX2
Q13136	PPFIA1	Liprin-alpha-1	1,1	0,032	PRDX2
Q9H1A4	ANAPC1	Anaphase-promoting complex subunit 1	1,1	0,044	PRDX2
Q92785	DPF2	Zinc finger protein ubi-d4	1,1	0,045	PRDX2
Q13464	ROCK1	Rho-associated protein kinase 1	1,1	0,048	PRDX2
O43823	AKAP8	A-kinase anchor protein 8	1,1	0,048	PRDX2
Q96IV0	NGLY1	Peptide-N(4)-(N-acetyl-beta-glucosaminyl)asparagine amidase	1,1	0,05	PRDX2
Q13451	FKBP5	Peptidyl-prolyl cis-trans isomerase FKBP5	1	0,005	PRDX2
Q92888	ARHGEF1	Rho guanine nucleotide exchange factor 1	1	0,006	PRDX2
P43487	RANBP1	Ran-specific GTPase-activating protein	1	0,008	PRDX2
Q86VS8	HOOK3	Protein Hook homolog 3	1	0,014	PRDX2
Q9H3K6	BOLA2	BolA-like protein 2	1	0,018	PRDX2
P19022	CDH2	Cadherin-2	1	0,034	PRDX2
Q06830	PRDX1	Peroxiredoxin-1	3,1	0	PRDX3
P30044	PRDX5	Peroxiredoxin-5, mitochondrial	3,1	0,002	PRDX3
Q6WKZ4	RAB11FIP1	Rab11 family-interacting protein 1	2,7	0	PRDX3
F8W9F9	WNK2	Non-specific serine/threonine protein kinase	2,7	0	PRDX3
A0A075B6R9	IGKV2D-24	Probable non-functional immunoglobulin kappa variable 2D-24	2,7	0,002	PRDX3
G3V3B9	GSTZ1	Maleylacetoacetate isomerase	2,6	0	PRDX3
P14174	MIF	Macrophage migration inhibitory factor	2,4	0,002	PRDX3
P19387	POLR2C	DNA-directed RNA polymerase II subunit RPB3	2,4	0,002	PRDX3
O95218	ZRANB2	Zinc finger Ran-binding domain-containing protein 2	2,3	0,001	PRDX3
E7EVA0	MAP4	Microtubule-associated protein	2,3	0,02	PRDX3
Q96A10	ERVK3-1	Endogenous retrovirus group K3 member 1	2,3	0,041	PRDX3
O95831	AIFM1	Apoptosis-inducing factor 1, mitochondrial	2,2	0	PRDX3
A0A087X1B1	IKBKG	NF-kappa-B essential modulator	2,2	0,005	PRDX3
Q6UWE0	LRSAM1	E3 ubiquitin-protein ligase LRSAM1	2,2	0,006	PRDX3
O60232	ZNRD2	Protein ZNRD2	2,2	0,014	PRDX3
P21912	SDHB	Succinate dehydrogenase [ubiquinone] iron-sulfur subunit, mitochondrial	2,1	0,004	PRDX3
Q12929	EPS8	Epidermal growth factor receptor kinase substrate 8	2,1	0,004	PRDX3
P14635	CCNB1	G2/mitotic-specific cyclin-B1	2,1	0,005	PRDX3
P11802	CDK4	Cyclin-dependent kinase 4	2,1	0,006	PRDX3
Q13015	MLLT11	Protein AF1q	2,1	0,006	PRDX3
Q9Y6A5	TACC3	Transforming acidic coiled-coil-containing protein 3	2,1	0,008	PRDX3
P62273	RPS29	40S ribosomal protein S29	2,1	0,016	PRDX3
B4DDF4	CNN2	Calponin	2	0	PRDX3
Q8NC51	SERBP1	Plasminogen activator inhibitor 1 RNA-binding protein	2	0,003	PRDX3
Q13541	EIF4EBP1	Eukaryotic translation initiation factor 4E-binding protein 1	2	0,005	PRDX3
Q96DA6	DNAJC19	Mitochondrial import inner membrane translocase subunit TIM14	2	0,009	PRDX3
Q13418	ILK	Integrin-linked protein kinase	2	0,009	PRDX3
Q12948	FOXC1	Forkhead box protein C1	1,9	0,002	PRDX3
H0YNW5	DUT	Deoxyuridine 5'-triphosphate nucleotidohydrolase	1,9	0,002	PRDX3
Q8WVC0	LEO1	RNA polymerase-associated protein LEO1	1,9	0,014	PRDX3

Q9C026	TRIM9	E3 ubiquitin-protein ligase TRIM9	1,9	0,015	PRDX3
P67936	TPM4	Tropomyosin alpha-4 chain	1,9	0,025	PRDX3
Q9BW83	IFT27	Intraflagellar transport protein 27 homolog	1,8	0,012	PRDX3
P35244	RPA3	Replication protein A 14 kDa subunit	1,8	0,02	PRDX3
P09497	CLTB	Clathrin light chain B	1,8	0,021	PRDX3
A8MYK1	MRPL23	39S ribosomal protein L23, mitochondrial	1,8	0,027	PRDX3
Q8TCF1	ZFAND1	AN1-type zinc finger protein 1	1,8	0,028	PRDX3
P47985	UQCRFS1	Cytochrome b-c1 complex subunit Rieske, mitochondrial	1,7	0,004	PRDX3
Q96B36	AKT1S1	Proline-rich AKT1 substrate 1	1,7	0,016	PRDX3
Q13151	HNRNPA0	Heterogeneous nuclear ribonucleoprotein A0	1,7	0,017	PRDX3
F5H345	HMBS	Hydroxymethylbilane synthase	1,7	0,02	PRDX3
O95248	SBF1	Myotubularin-related protein 5	1,7	0,028	PRDX3
O15511	ARPC5	Actin-related protein 2/3 complex subunit 5	1,7	0,028	PRDX3
C9JAW5	C9JAW5	HIG1 domain-containing protein	1,7	0,039	PRDX3
Q9Y3D9	MRPS23	28S ribosomal protein S23, mitochondrial	1,7	0,04	PRDX3
P49914	MTHFS	5-formyltetrahydrofolate cyclo-ligase	1,7	0,049	PRDX3
Q9UN86	G3BP2	Ras GTPase-activating protein-binding protein 2	1,6	0	PRDX3
Q9Y265	RUVBL1	RuvB-like 1	1,6	0	PRDX3
A0A2R8Y811	RPS14	40S ribosomal protein S14	1,6	0	PRDX3
P35520	CBS	Cystathionine beta-synthase	1,6	0,013	PRDX3
P61758	VBP1	Prefoldin subunit 3	1,6	0,025	PRDX3
Q9H4L4	SENP3	Sentrin-specific protease 3	1,6	0,032	PRDX3
P10301	RRAS	Ras-related protein R-Ras	1,6	0,046	PRDX3
Q9H0H5	RACGAP1	Rac GTPase-activating protein 1	1,5	0	PRDX3
Q96F86	EDC3	Enhancer of mRNA-decapping protein 3	1,5	0,003	PRDX3
Q13123	IK	Protein Red	1,5	0,008	PRDX3
Q5XKP0	MICOS13	MICOS complex subunit MIC13	1,5	0,041	PRDX3
Q9P2X3	IMPACT	Protein IMPACT	1,5	0,042	PRDX3
Q16576	RBBP7	Histone-binding protein RBBP7	1,4	0,003	PRDX3
Q9NUQ3	TXLNG	Gamma-taxilin	1,4	0,005	PRDX3
Q9BR76	CORO1B	Coronin-1B	1,4	0,021	PRDX3
E9PM92	C11orf58	Small acidic protein	1,4	0,032	PRDX3
Q8NFC6	BOD1L1	Biorientation of chromosomes in cell division protein 1-like 1	1,4	0,038	PRDX3
P30041	PRDX6	Peroxiredoxin-6	1,4	0,043	PRDX3
Q9NRX4	PHPT1	14 kDa phosphohistidine phosphatase	1,3	0	PRDX3
Q9Y5M8	SRPRB	Signal recognition particle receptor subunit beta	1,3	0	PRDX3
Q6IQ49	SDE2	Replication stress response regulator SDE2	1,3	0,002	PRDX3
Q9HB71	CACYBP	Calcyclin-binding protein	1,3	0,013	PRDX3
Q16204	CCDC6	Coiled-coil domain-containing protein 6	1,3	0,038	PRDX3
Q5VVQ6	YOD1	Ubiquitin thioesterase OTU1	1,3	0,044	PRDX3
P62826	RAN	GTP-binding nuclear protein Ran	1,2	0	PRDX3
Q92974	ARHGEF2	Rho guanine nucleotide exchange factor 2	1,2	0,005	PRDX3
Q9H936	SLC25A22	Mitochondrial glutamate carrier 1	1,2	0,005	PRDX3
P0DMV9	HSPA1B	Heat shock 70 kDa protein 1B	1,2	0,007	PRDX3
A0A087WUK2	HNRNPDL	Heterogeneous nuclear ribonucleoprotein D-like	1,2	0,009	PRDX3
Q15654	TRIP6	Thyroid receptor-interacting protein 6	1,2	0,013	PRDX3
Q13356	PPIL2	RING-type E3 ubiquitin-protein ligase PPIL2	1,2	0,016	PRDX3
Q6R327	RICTOR	Rapamycin-insensitive companion of mTOR	1,2	0,017	PRDX3
Q9H840	GEMIN7	Gem-associated protein 7	1,2	0,025	PRDX3
P32119	PRDX2	Peroxiredoxin-2	1,2	0,026	PRDX3
O00399	DCTN6	Dynactin subunit 6	1,2	0,027	PRDX3
P22234	PAICS	Multifunctional protein ADE2 [Includes: Phosphoribosylaminoimidazole-succinocarboxamide synthase	1,2	0,03	PRDX3
P56385	ATP5ME	ATP synthase subunit e, mitochondrial	1,2	0,031	PRDX3
P61927	RPL37	60S ribosomal protein L37	1,2	0,031	PRDX3
H0Y4R1	IMPDH2	Inosine-5'-monophosphate dehydrogenase 2	1,2	0,04	PRDX3
P39019	RPS19	40S ribosomal protein S19	1,1	0	PRDX3
Q15181	PPA1	Inorganic pyrophosphatase	1,1	0,006	PRDX3
P82921	MRPS21	28S ribosomal protein S21, mitochondrial	1,1	0,017	PRDX3
Q07666	KHDRBS1	KH domain-containing, RNA-binding, signal transduction-associated protein 1	1,1	0,029	PRDX3
O14965	AURKA	Aurora kinase A	1,1	0,034	PRDX3
Q13247	SRSF6	Serine/arginine-rich splicing factor 6	1,1	0,041	PRDX3
P40222	TXLNA	Alpha-taxilin	1,1	0,046	PRDX3
Q9ULX3	NOB1	RNA-binding protein NOB1	1,1	0,05	PRDX3
P11586	MTHFD1	C-1-tetrahydrofolate synthase, cytoplasmic	1	0	PRDX3
O95336	PGLS	6-phosphogluconolactonase	1	0,017	PRDX3
Q15398	DLGAP5	Disks large-associated protein 5	1	0,024	PRDX3
P30044	PRDX5	Peroxiredoxin-5, mitochondrial	3,5	0,001	PRDX4
Q06830	PRDX1	Peroxiredoxin-1	3,4	0	PRDX4

H0YNW5	DUT	Deoxyuridine 5'-triphosphate nucleotidohydrolase	3,2	0	PRDX4
A0A075B6R9	IGKV2D-24	Probable non-functional immunoglobulin kappa variable 2D-24	3,1	0	PRDX4
P62273	RPS29	40S ribosomal protein S29	3,1	0,001	PRDX4
P11802	CDK4	Cyclin-dependent kinase 4	3	0	PRDX4
P06132	UROD	Uroporphyrinogen decarboxylase	3	0	PRDX4
Q13015	MLLT11	Protein AF1q	2,9	0	PRDX4
Q6FI81	CIAPIN1	Anamorsin	2,9	0	PRDX4
Q9H840	GEMIN7	Gem-associated protein 7	2,8	0	PRDX4
Q9H2P9	DPH5	Diphthine methyl ester synthase	2,6	0	PRDX4
Q6WKZ4	RAB11FIP1	Rab11 family-interacting protein 1	2,5	0	PRDX4
F8W9F9	WNK2	Non-specific serine/threonine protein kinase	2,5	0	PRDX4
Q9NP97	DYNLRB1	Dynein light chain roadblock-type 1	2,5	0	PRDX4
G3V3B9	GSTZ1	Maleylacetoacetate isomerase	2,4	0	PRDX4
P19022	CDH2	Cadherin-2	2,4	0	PRDX4
B4DDF4	CNN2	Calponin	2,4	0	PRDX4
O60566	BUB1B	Mitotic checkpoint serine/threonine-protein kinase BUB1 beta	2,4	0,001	PRDX4
P61758	VBP1	Prefoldin subunit 3	2,4	0,002	PRDX4
P56385	ATP5ME	ATP synthase subunit e, mitochondrial	2,3	0,001	PRDX4
Q9Y6A5	TACC3	Transforming acidic coiled-coil-containing protein 3	2,3	0,009	PRDX4
A0A087X2D5	MRPL45	39S ribosomal protein L45, mitochondrial	2,2	0	PRDX4
Q8WVC2	RPS21	40S ribosomal protein S21	2,2	0,001	PRDX4
Q9BTE1	DCTN5	Dynactin subunit 5	2,2	0,001	PRDX4
H3BRE8	RPAP1	RNA polymerase II-associated protein 1	2,2	0,002	PRDX4
P19387	POLR2C	DNA-directed RNA polymerase II subunit RPB3	2,2	0,002	PRDX4
P0DMV9	HSPA1B	Heat shock 70 kDa protein 1B	2,1	0	PRDX4
O95218	ZRANB2	Zinc finger Ran-binding domain-containing protein 2	2,1	0,001	PRDX4
P41250	GARS1	Glycine--tRNA ligase	2,1	0,002	PRDX4
Q9NPH2	ISYNA1	Inositol-3-phosphate synthase 1	2,1	0,003	PRDX4
P42771	CDKN2A	Cyclin-dependent kinase inhibitor 2A	2	0	PRDX4
H7BXI1	ESYT2	Extended synaptotagmin-2	2	0,002	PRDX4
Q5JRI1	SRSF10	Serine/arginine-rich-splicing factor 10	2	0,004	PRDX4
A0A087X1B1	IKBKG	NF-kappa-B essential modulator	2	0,006	PRDX4
Q6UWE0	LRSAM1	E3 ubiquitin-protein ligase LRSAM1	2	0,007	PRDX4
E9PM92	C11orf58	Small acidic protein	2	0,007	PRDX4
O60232	ZNRD2	Protein ZNRD2	2	0,018	PRDX4
Q9UN86	G3BP2	Ras GTPase-activating protein-binding protein 2	1,9	0	PRDX4
Q9BT25	HAUS8	HAUS augmin-like complex subunit 8	1,9	0	PRDX4
P34897	SHMT2	Serine hydroxymethyltransferase, mitochondrial	1,9	0	PRDX4
P22234	PAICS	Multifunctional protein ADE2 [Includes: Phosphoribosylaminoimidazole-succinocarboxamide synthase	1,9	0,001	PRDX4
Q9BPW8	NIPSNAP1	Protein NipSnap homolog 1	1,9	0,004	PRDX4
P14635	CCNB1	G2/mitotic-specific cyclin-B1	1,9	0,007	PRDX4
P85037	FOXK1	Forkhead box protein K1	1,9	0,01	PRDX4
Q96KB5	PBK	Lymphokine-activated killer T-cell-originated protein kinase	1,9	0,016	PRDX4
O14964	HGS	Hepatocyte growth factor-regulated tyrosine kinase substrate	1,8	0	PRDX4
Q12933	TRAF2	TNF receptor-associated factor 2	1,8	0,009	PRDX4
O00629	KPNA4	Importin subunit alpha-3	1,8	0,011	PRDX4
Q99956	DUSP9	Dual specificity protein phosphatase 9	1,8	0,017	PRDX4
Q9Y265	RUVBL1	RuvB-like 1	1,7	0	PRDX4
P17252	PRKCA	Protein kinase C alpha type	1,7	0,001	PRDX4
P48047	ATP5PO	ATP synthase subunit O, mitochondrial	1,7	0,01	PRDX4
Q13541	EIF4EBP1	Eukaryotic translation initiation factor 4E-binding protein 1	1,7	0,011	PRDX4
Q13418	ILK	Integrin-linked protein kinase	1,7	0,012	PRDX4
Q16186	ADRM1	Proteasomal ubiquitin receptor ADRM1	1,7	0,012	PRDX4
Q9P2B4	CTTNBP2NL	CTTNBP2 N-terminal-like protein	1,7	0,013	PRDX4
Q96DH6	MSI2	RNA-binding protein Musashi homolog 2	1,7	0,013	PRDX4
Q96DA6	DNAJC19	Mitochondrial import inner membrane translocase subunit TIM14	1,7	0,013	PRDX4
Q8WVC0	LEO1	RNA polymerase-associated protein LEO1	1,7	0,018	PRDX4
Q9C026	TRIM9	E3 ubiquitin-protein ligase TRIM9	1,7	0,021	PRDX4
Q8NFC6	BOD1L1	Biorientation of chromosomes in cell division protein 1-like 1	1,7	0,023	PRDX4
Q9HD26	GOPC	Golgi-associated PDZ and coiled-coil motif-containing protein	1,7	0,026	PRDX4
O75616	ERAL1	GTPase Era, mitochondrial	1,7	0,027	PRDX4
P14174	MIF	Macrophage migration inhibitory factor	1,7	0,028	PRDX4
Q5VUJ6	LRCH2	Leucine-rich repeat and calponin homology domain-containing protein 2	1,7	0,029	PRDX4
P67936	TPM4	Tropomyosin alpha-4 chain	1,7	0,035	PRDX4
Q9NXR7	BABAM2	BRISC and BRCA1-A complex member 2	1,7	0,04	PRDX4
Q9Y3D9	MRPS23	28S ribosomal protein S23, mitochondrial	1,7	0,04	PRDX4
Q9Y5Y2	NUBP2	Cytosolic Fe-S cluster assembly factor NUBP2	1,6	0	PRDX4
Q9ULX3	NOB1	RNA-binding protein NOB1	1,6	0,001	PRDX4

O15143	ARPC1B	Actin-related protein 2/3 complex subunit 1B	1,6	0,002	PRDX4
Q12948	FOXC1	Forkhead box protein C1	1,6	0,004	PRDX4
Q9Y5K6	CD2AP	CD2-associated protein	1,6	0,012	PRDX4
Q53H96	PYCR3	Pyrroline-5-carboxylate reductase 3	1,6	0,012	PRDX4
Q16204	CCDC6	Coiled-coil domain-containing protein 6	1,6	0,015	PRDX4
Q9BW83	IFT27	Intraflagellar transport protein 27 homolog	1,6	0,016	PRDX4
Q8NI60	COQ8A	Atypical kinase COQ8A, mitochondrial	1,6	0,017	PRDX4
Q6R327	RICTOR	Rapamycin-insensitive companion of mTOR	1,6	0,018	PRDX4
I3L2Z5	MAZ	Myc-associated zinc finger protein	1,6	0,022	PRDX4
P30041	PRDX6	Peroxiredoxin-6	1,6	0,025	PRDX4
O14617	AP3D1	AP-3 complex subunit delta-1	1,6	0,027	PRDX4
P35244	RPA3	Replication protein A 14 kDa subunit	1,6	0,029	PRDX4
P09497	CLTB	Clathrin light chain B	1,6	0,03	PRDX4
A8MYK1	MRPL23	39S ribosomal protein L23, mitochondrial	1,6	0,039	PRDX4
Q8TCF1	ZFAND1	AN1-type zinc finger protein 1	1,6	0,041	PRDX4
P53677	AP3M2	AP-3 complex subunit mu-2	1,5	0,003	PRDX4
P35520	CBS	Cystathionine beta-synthase	1,5	0,021	PRDX4
Q9BZE1	MRPL37	39S ribosomal protein L37, mitochondrial	1,5	0,022	PRDX4
U3KQC1	WDR18	WD repeat-containing protein 18	1,5	0,023	PRDX4
F5H345	HMBS	Hydroxymethylbilane synthase	1,5	0,028	PRDX4
P49903	SEPHS1	Selenide, water dikinase 1	1,5	0,038	PRDX4
P42025	ACTR1B	Beta-centractin	1,5	0,042	PRDX4
Q9NYZ3	GTSE1	G2 and S phase-expressed protein 1	1,4	0	PRDX4
P30837	ALDH1B1	Aldehyde dehydrogenase X, mitochondrial	1,4	0	PRDX4
A0A0C4DGQ6	RPRD1A	Regulation of nuclear pre-mRNA domain-containing protein 1A	1,4	0,001	PRDX4
Q9Y3B7	MRPL11	39S ribosomal protein L11, mitochondrial	1,4	0,001	PRDX4
Q96FW1	OTUB1	Ubiquitin thioesterase OTUB1	1,4	0,001	PRDX4
O95831	AIFM1	Apoptosis-inducing factor 1, mitochondrial	1,4	0,003	PRDX4
P40937	RFC5	Replication factor C subunit 5	1,4	0,003	PRDX4
Q9BWD1	ACAT2	Acetyl-CoA acetyltransferase, cytosolic	1,4	0,015	PRDX4
Q99569	PKP4	Plakophilin-4	1,4	0,015	PRDX4
A0A3B3IUD2	MSTO1	Protein misato homolog 1	1,4	0,025	PRDX4
E7EX48	NEK4	Serine/threonine-protein kinase Nek4	1,4	0,026	PRDX4
Q9UBI6	GNG12	Guanine nucleotide-binding protein G(I)/G(S)/G(O) subunit gamma-12	1,4	0,029	PRDX4
Q13573	SNW1	SNW domain-containing protein 1	1,4	0,031	PRDX4
Q8N3C0	ASCC3	Activating signal cointegrator 1 complex subunit 3	1,4	0,032	PRDX4
Q9NV56	MRGBP	MRG/MORF4L-binding protein	1,4	0,033	PRDX4
O00291	HIP1	Huntingtin-interacting protein 1	1,4	0,035	PRDX4
O94992	HEXIM1	Protein HEXIM1	1,4	0,038	PRDX4
O95248	SBF1	Myotubularin-related protein 5	1,4	0,04	PRDX4
Q6P087	RPUSD3	Mitochondrial mRNA pseudouridine synthase RPUSD3	1,4	0,04	PRDX4
G3V1Q4	SEPTIN7	Septin-7	1,4	0,045	PRDX4
Q9NPD8	UBE2T	Ubiquitin-conjugating enzyme E2 T	1,4	0,047	PRDX4
Q7L5D6	GET4	Golgi to ER traffic protein 4 homolog	1,4	0,05	PRDX4
P35232	PHB	Prohibitin	1,3	0	PRDX4
P06733	ENO1	Alpha-enolase	1,3	0	PRDX4
P62937	PPIA	Peptidyl-prolyl cis-trans isomerase A	1,3	0,001	PRDX4
Q9UN37	VPS4A	Vacuolar protein sorting-associated protein 4A	1,3	0,001	PRDX4
P43487	RANBP1	Ran-specific GTPase-activating protein	1,3	0,001	PRDX4
Q96RT1	ERBIN	Erbin	1,3	0,002	PRDX4
P31930	UQCRC1	Cytochrome b-c1 complex subunit 1, mitochondrial	1,3	0,003	PRDX4
P35998	PSMC2	26S proteasome regulatory subunit 7	1,3	0,003	PRDX4
Q6PKG0	LARP1	La-related protein 1	1,3	0,004	PRDX4
A0A087X0K9	TJP1	Tight junction protein ZO-1	1,3	0,004	PRDX4
Q14C86	GAPVD1	GTPase-activating protein and VPS9 domain-containing protein 1	1,3	0,013	PRDX4
J3KN29	PSMD9	26S proteasome non-ATPase regulatory subunit 9	1,3	0,02	PRDX4
Q96F86	EDC3	Enhancer of mRNA-decapping protein 3	1,3	0,02	PRDX4
P26599	PTBP1	Polypyrimidine tract-binding protein 1	1,3	0,025	PRDX4
P63000	RAC1	Ras-related C3 botulinum toxin substrate 1	1,3	0,026	PRDX4
P47985	UQCRFS1	Cytochrome b-c1 complex subunit Rieske, mitochondrial	1,3	0,03	PRDX4
Q13247	SRSF6	Serine/arginine-rich splicing factor 6	1,3	0,03	PRDX4
A0A3B3ITJ4	HNRNPL	Heterogeneous nuclear ribonucleoprotein L	1,3	0,031	PRDX4
P14618	PKM	Pyruvate kinase PKM	1,3	0,033	PRDX4
P43686	PSMC4	26S proteasome regulatory subunit 6B	1,3	0,033	PRDX4
Q5VVQ6	YOD1	Ubiquitin thioesterase OTU1	1,3	0,045	PRDX4
Q4VCS5	AMOT	Angiomotin	1,3	0,045	PRDX4
Q9H4L4	SENP3	Sentrin-specific protease 3	1,3	0,047	PRDX4
Q9Y5M8	SRPRB	Signal recognition particle receptor subunit beta	1,2	0	PRDX4
P11586	MTHFD1	C-1-tetrahydrofolate synthase, cytoplasmic	1,2	0	PRDX4

O95456	PSMG1	Proteasome assembly chaperone 1	1,2	0,001	PRDX4
P22695	UQCRC2	Cytochrome b-c1 complex subunit 2, mitochondrial	1,2	0,004	PRDX4
P49593	PPM1F	Protein phosphatase 1F	1,2	0,008	PRDX4
O14965	AURKA	Aurora kinase A	1,2	0,026	PRDX4
Q96B36	AKT1S1	Proline-rich AKT1 substrate 1	1,2	0,032	PRDX4
P11142	HSPA8	Heat shock cognate 71 kDa protein	1,1	0	PRDX4
P05091	ALDH2	Aldehyde dehydrogenase, mitochondrial	1,1	0,002	PRDX4
Q13347	EIF3I	Eukaryotic translation initiation factor 3 subunit I	1,1	0,004	PRDX4
Q2M1P5	KIF7	Kinesin-like protein KIF7	1,1	0,005	PRDX4
P19838	NFKB1	Nuclear factor NF-kappa-B p105 subunit	1,1	0,006	PRDX4
D6R938	CAMK2D	Calcium/calmodulin-dependent protein kinase	1,1	0,007	PRDX4
Q92974	ARHGEF2	Rho guanine nucleotide exchange factor 2	1,1	0,008	PRDX4
Q9BV44	THUMPD3	THUMP domain-containing protein 3	1,1	0,01	PRDX4
Q9UKK9	NUDT5	ADP-sugar pyrophosphatase	1,1	0,017	PRDX4
Q86WA6	BPHL	Valacyclovir hydrolase	1,1	0,02	PRDX4
Q9NXF7	DCAF16	DDB1- and CUL4-associated factor 16	1,1	0,021	PRDX4
K7EJQ8	HDHD2	Haloacid dehalogenase-like hydrolase domain-containing protein 2	1,1	0,029	PRDX4
P50542	PEX5	Peroxisomal targeting signal 1 receptor	1,1	0,03	PRDX4
O75607	NPM3	Nucleoplasmin-3	1,1	0,033	PRDX4
P21964	COMT	Catechol O-methyltransferase	1,1	0,036	PRDX4
Q6P1L8	MRPL14	39S ribosomal protein L14, mitochondrial	1,1	0,04	PRDX4
Q6DKI1	RPL7L1	60S ribosomal protein L7-like 1	1,1	0,046	PRDX4
P62195	PSMC5	26S proteasome regulatory subunit 8	1	0,003	PRDX4
Q14126	DSG2	Desmoglein-2	1	0,016	PRDX4
Q8WUM0	NUP133	Nuclear pore complex protein Nup133	1	0,016	PRDX4
Q9H223	EHD4	EH domain-containing protein 4	1	0,026	PRDX4
A0A0G2JNZ2	SCRIB	Protein scribble homolog	1	0,029	PRDX4
B1ALK7	ARHGEF7	Rho guanine nucleotide exchange factor 7	1	0,029	PRDX4
Q15398	DLGAP5	Disks large-associated protein 5	1	0,033	PRDX4
P23258	TUBG1	Tubulin gamma-1 chain	1	0,039	PRDX4
F5H008	VPS33B	Vacuolar protein sorting-associated protein 33B	1	0,04	PRDX4
Q53EL6	PDCD4	Programmed cell death protein 4	1	0,044	PRDX4
A0A075B6R9	IGKV2D-24	Probable non-functional immunoglobulin kappa variable 2D-24	3,3	0	PRDX5
Q4VCS5	AMOT	Angiomotin	3	0	PRDX5
P06132	UROD	Uroporphyrinogen decarboxylase	2,9	0	PRDX5
B4DDF4	CNN2	Calponin	2,9	0	PRDX5
Q13015	MLLT11	Protein AF1q	2,8	0,001	PRDX5
P62273	RPS29	40S ribosomal protein S29	2,8	0,003	PRDX5
Q9H840	GEMIN7	Gem-associated protein 7	2,6	0	PRDX5
Q06830	PRDX1	Peroxiredoxin-1	2,5	0	PRDX5
P19105	MYL12A	Myosin regulatory light chain 12A	2,5	0,001	PRDX5
Q9NP97	DYNLRB1	Dynein light chain roadblock-type 1	2,4	0	PRDX5
H0YNW5	DUT	Deoxyuridine 5'-triphosphate nucleotidohydrolase	2,4	0	PRDX5
F8W9F9	WNK2	Non-specific serine/threonine protein kinase	2,4	0,001	PRDX5
Q15149	PLEC	Plectin	2,4	0,004	PRDX5
Q9BR76	CORO1B	Coronin-1B	2,3	0	PRDX5
G3V3B9	GSTZ1	Maleylacetoacetate isomerase	2,3	0,001	PRDX5
P19022	CDH2	Cadherin-2	2,3	0,001	PRDX5
Q13573	SNW1	SNW domain-containing protein 1	2,3	0,002	PRDX5
O60566	BUB1B	Mitotic checkpoint serine/threonine-protein kinase BUB1 beta	2,3	0,002	PRDX5
P51570	GALK1	Galactokinase	2,2	0	PRDX5
A0A0G2JNZ2	SCRIB	Protein scribble homolog	2,2	0	PRDX5
O15143	ARPC1B	Actin-related protein 2/3 complex subunit 1B	2,2	0,001	PRDX5
Q96AC1	FERMT2	Fermitin family homolog 2	2,2	0,005	PRDX5
P42765	ACAA2	3-ketoacyl-CoA thiolase, mitochondrial	2,1	0	PRDX5
O00629	KPNA4	Importin subunit alpha-3	2,1	0,001	PRDX5
E7EPN9	PRRC2C	Protein PRRC2C	2,1	0,001	PRDX5
Q86WA6	BPHL	Valacyclovir hydrolase	2,1	0,002	PRDX5
P19387	POLR2C	DNA-directed RNA polymerase II subunit RPB3	2,1	0,004	PRDX5
Q13356	PPIL2	RING-type E3 ubiquitin-protein ligase PPIL2	2	0	PRDX5
Q9H0H5	RACGAP1	Rac GTPase-activating protein 1	2	0	PRDX5
Q9UN37	VPS4A	Vacuolar protein sorting-associated protein 4A	2	0	PRDX5
Q9BTE1	DCTN5	Dynactin subunit 5	2	0,002	PRDX5
O95218	ZRANB2	Zinc finger Ran-binding domain-containing protein 2	2	0,003	PRDX5
Q8WVC2	RPS21	40S ribosomal protein S21	2	0,003	PRDX5
Q9BZE1	MRPL37	39S ribosomal protein L37, mitochondrial	2	0,004	PRDX5
Q9Y3D9	MRPS23	28S ribosomal protein S23, mitochondrial	2	0,017	PRDX5
Q9UN86	G3BP2	Ras GTPase-activating protein-binding protein 2	1,9	0	PRDX5
P62879	GNB2	Guanine nucleotide-binding protein G(I)/G(S)/G(T) subunit beta-2	1,9	0	PRDX5

A0A087X2D5	MRPL45	39S ribosomal protein L45, mitochondrial	1,9	0,001	PRDX5
P07196	NEFL	Neurofilament light polypeptide	1,9	0,001	PRDX5
Q7L2E3	DHX30	ATP-dependent RNA helicase DHX30	1,9	0,002	PRDX5
Q6P1L8	MRPL14	39S ribosomal protein L14, mitochondrial	1,9	0,009	PRDX5
P14174	MIF	Macrophage migration inhibitory factor	1,9	0,011	PRDX5
Q6UWE0	LRSAM1	E3 ubiquitin-protein ligase LRSAM1	1,9	0,012	PRDX5
Q16822	PCK2	Phosphoenolpyruvate carboxykinase [GTP], mitochondrial	1,9	0,013	PRDX5
O60232	ZNRD2	Protein ZNRD2	1,9	0,024	PRDX5
C9J8P9	CLTA	Clathrin light chain	1,9	0,044	PRDX5
Q8TCG1	CIP2A	Protein CIP2A	1,8	0,001	PRDX5
P09110	ACAA1	3-ketoacyl-CoA thiolase, peroxisomal	1,8	0,005	PRDX5
Q5JRI1	SRSF10	Serine/arginine-rich-splicing factor 10	1,8	0,007	PRDX5
Q96DH6	MSI2	RNA-binding protein Musashi homolog 2	1,8	0,008	PRDX5
Q15477	SKIV2L	Helicase SKI2W	1,8	0,009	PRDX5
Q9BPW8	NIPSNAP1	Protein NipSnap homolog 1	1,8	0,009	PRDX5
O43347	MSI1	RNA-binding protein Musashi homolog 1	1,8	0,01	PRDX5
Q9NXH9	TRMT1	tRNA	1,8	0,012	PRDX5
C9JRJ5	LIMD1	LIM domain-containing protein 1	1,7	0	PRDX5
Q96RP9	GFM1	Elongation factor G, mitochondrial	1,7	0,002	PRDX5
Q12948	FOXC1	Forkhead box protein C1	1,7	0,002	PRDX5
Q99569	PKP4	Plakophilin-4	1,7	0,002	PRDX5
Q53H96	PYCR3	Pyrroline-5-carboxylate reductase 3	1,7	0,011	PRDX5
K7ELV2	SEH1L	Nucleoporin SEH1	1,7	0,017	PRDX5
Q9Y3B7	MRPL11	39S ribosomal protein L11, mitochondrial	1,6	0	PRDX5
Q9BT25	HAUS8	HAUS augmin-like complex subunit 8	1,6	0	PRDX5
P56545	CTBP2	C-terminal-binding protein 2	1,6	0	PRDX5
Q16352	INA	Alpha-internexin	1,6	0,001	PRDX5
P53597	SUCLG1	Succinate--CoA ligase [ADP/GDP-forming] subunit alpha, mitochondrial	1,6	0,002	PRDX5
Q6P2E9	EDC4	Enhancer of mRNA-decapping protein 4	1,6	0,003	PRDX5
Q9Y5K6	CD2AP	CD2-associated protein	1,6	0,004	PRDX5
Q8N3C0	ASCC3	Activating signal cointegrator 1 complex subunit 3	1,6	0,004	PRDX5
Q7Z406	MYH14	Myosin-14	1,6	0,005	PRDX5
O14964	HGS	Hepatocyte growth factor-regulated tyrosine kinase substrate	1,6	0,005	PRDX5
O75592	MYCBP2	E3 ubiquitin-protein ligase MYCBP2	1,6	0,005	PRDX5
Q13363	CTBP1	C-terminal-binding protein 1	1,6	0,01	PRDX5
A0A0A0MRT6	ABI1	Abl interactor 1	1,6	0,012	PRDX5
P48047	ATP5PO	ATP synthase subunit O, mitochondrial	1,6	0,013	PRDX5
Q12933	TRAF2	TNF receptor-associated factor 2	1,6	0,016	PRDX5
P42345	MTOR	Serine/threonine-protein kinase mTOR	1,6	0,017	PRDX5
Q13418	ILK	Integrin-linked protein kinase	1,6	0,021	PRDX5
Q96DA6	DNAJC19	Mitochondrial import inner membrane translocase subunit TIM14	1,6	0,022	PRDX5
Q99956	DUSP9	Dual specificity protein phosphatase 9	1,6	0,027	PRDX5
Q9C026	TRIM9	E3 ubiquitin-protein ligase TRIM9	1,6	0,035	PRDX5
P55084	HADHB	Trifunctional enzyme subunit beta, mitochondrial	1,6	0,039	PRDX5
Q5VUJ6	LRCH2	Leucine-rich repeat and calponin homology domain-containing protein 2	1,6	0,043	PRDX5
Q13526	PIN1	Peptidyl-prolyl cis-trans isomerase NIMA-interacting 1	1,5	0	PRDX5
Q96FW1	OTUB1	Ubiquitin thioesterase OTUB1	1,5	0	PRDX5
O43795	MYO1B	Unconventional myosin-Ib	1,5	0,001	PRDX5
P52272	HNRNPM	Heterogeneous nuclear ribonucleoprotein M	1,5	0,002	PRDX5
Q15398	DLGAP5	Disks large-associated protein 5	1,5	0,002	PRDX5
Q9BW92	TARS2	Threonine--tRNA ligase, mitochondrial	1,5	0,004	PRDX5
A0A087WTZ5	UBXN1	UBX domain-containing protein 1	1,5	0,006	PRDX5
P82921	MRPS21	28S ribosomal protein S21, mitochondrial	1,5	0,006	PRDX5
Q9BWD1	ACAT2	Acetyl-CoA acetyltransferase, cytosolic	1,5	0,008	PRDX5
O95785	WIZ	Protein Wiz	1,5	0,008	PRDX5
P46060	RANGAP1	Ran GTPase-activating protein 1	1,5	0,013	PRDX5
Q9Y2R4	DDX52	Probable ATP-dependent RNA helicase DDX52	1,5	0,013	PRDX5
H3BRE8	RPAP1	RNA polymerase II-associated protein 1	1,5	0,017	PRDX5
Q16186	ADRM1	Proteasomal ubiquitin receptor ADRM1	1,5	0,022	PRDX5
B1ALK7	ARHGEF7	Rho guanine nucleotide exchange factor 7	1,5	0,024	PRDX5
Q9BY32	ITPA	Inosine triphosphate pyrophosphatase	1,5	0,026	PRDX5
P16403	H1-2	Histone H1.2	1,5	0,029	PRDX5
Q8NI60	COQ8A	Atypical kinase COQ8A, mitochondrial	1,5	0,029	PRDX5
A0A3B3IUD2	MSTO1	Protein misato homolog 1	1,5	0,029	PRDX5
Q8WVC0	LEO1	RNA polymerase-associated protein LEO1	1,5	0,031	PRDX5
P17028	ZNF24	Zinc finger protein 24	1,5	0,035	PRDX5
A0A0A0MRM8	MYO6	Unconventional myosin-6	1,4	0	PRDX5
F8WB06	ATXN2	Ataxin-2	1,4	0	PRDX5
O95456	PSMG1	Proteasome assembly chaperone 1	1,4	0	PRDX5

Q9ULX3	NOB1	RNA-binding protein NOB1	1,4	0,001	PRDX5
Q86U42	PABPN1	Polyadenylate-binding protein 2	1,4	0,001	PRDX5
Q92974	ARHGEF2	Rho guanine nucleotide exchange factor 2	1,4	0,001	PRDX5
Q9Y5Y2	NUBP2	Cytosolic Fe-S cluster assembly factor NUBP2	1,4	0,002	PRDX5
Q9BSH4	TACO1	Translational activator of cytochrome c oxidase 1	1,4	0,002	PRDX5
P19838	NFKB1	Nuclear factor NF-kappa-B p105 subunit	1,4	0,002	PRDX5
Q9GZT3	SLIRP	SRA stem-loop-interacting RNA-binding protein, mitochondrial	1,4	0,003	PRDX5
P40937	RFC5	Replication factor C subunit 5	1,4	0,003	PRDX5
P23258	TUBG1	Tubulin gamma-1 chain	1,4	0,004	PRDX5
Q92888	ARHGEF1	Rho guanine nucleotide exchange factor 1	1,4	0,007	PRDX5
Q9P2B4	CTTNBP2NL	CTTNBP2 N-terminal-like protein	1,4	0,008	PRDX5
Q16513	PKN2	Serine/threonine-protein kinase N2	1,4	0,01	PRDX5
Q96PK6	RBM14	RNA-binding protein 14	1,4	0,012	PRDX5
O60783	MRPS14	28S ribosomal protein S14, mitochondrial	1,4	0,013	PRDX5
Q13247	SRSF6	Serine/arginine-rich splicing factor 6	1,4	0,019	PRDX5
Q96GD0	PDXP	Pyridoxal phosphate phosphatase	1,4	0,021	PRDX5
Q6DKI1	RPL7L1	60S ribosomal protein L7-like 1	1,4	0,026	PRDX5
Q99959	PKP2	Plakophilin-2	1,4	0,026	PRDX5
Q9BW83	IFT27	Intraflagellar transport protein 27 homolog	1,4	0,03	PRDX5
Q6R327	RICTOR	Rapamycin-insensitive companion of mTOR	1,4	0,034	PRDX5
O94760	DDAH1	N(G),N(G)-dimethylarginine dimethylaminohydrolase 1	1,4	0,042	PRDX5
P35244	RPA3	Replication protein A 14 kDa subunit	1,4	0,049	PRDX5
Q9NYZ3	GTSE1	G2 and S phase-expressed protein 1	1,3	0,001	PRDX5
Q9BSD7	NTPCR	Cancer-related nucleoside-triphosphatase	1,3	0,002	PRDX5
Q13625	TP53BP2	Apoptosis-stimulating of p53 protein 2	1,3	0,002	PRDX5
P07737	PFN1	Profilin-1	1,3	0,002	PRDX5
Q8IYI6	EXOC8	Exocyst complex component 8	1,3	0,003	PRDX5
P17252	PRKCA	Protein kinase C alpha type	1,3	0,005	PRDX5
Q96RT1	ERBIN	Erbin	1,3	0,006	PRDX5
F5H008	VPS33B	Vacuolar protein sorting-associated protein 33B	1,3	0,006	PRDX5
Q8WUM0	NUP133	Nuclear pore complex protein Nup133	1,3	0,007	PRDX5
Q13464	ROCK1	Rho-associated protein kinase 1	1,3	0,008	PRDX5
P28838	LAP3	Cytosol aminopeptidase	1,3	0,009	PRDX5
A5YKK6	CNOT1	CCR4-NOT transcription complex subunit 1	1,3	0,009	PRDX5
Q86UK7	ZNF598	E3 ubiquitin-protein ligase ZNF598	1,3	0,01	PRDX5
P48634	PRRC2A	Protein PRRC2A	1,3	0,012	PRDX5
O95373	IPO7	Importin-7	1,3	0,013	PRDX5
Q05655	PRKCD	Protein kinase C delta type	1,3	0,015	PRDX5
Q86V48	LUZP1	Leucine zipper protein 1	1,3	0,02	PRDX5
P05783	KRT18	Keratin, type I cytoskeletal 18	1,3	0,024	PRDX5
Q9Y3I0	RTCB	RNA-splicing ligase RtcB homolog	1,3	0,027	PRDX5
H3BPE1	MACF1	Microtubule-actin cross-linking factor 1, isoforms 1/2/3/5	1,3	0,034	PRDX5
Q13613	MTMR1	Myotubularin-related protein 1	1,3	0,039	PRDX5
Q01081	U2AF1	Splicing factor U2AF 35 kDa subunit	1,3	0,04	PRDX5
C9JZR2	CTNND1	Catenin delta-1	1,3	0,042	PRDX5
I3L2Z5	MAZ	Myc-associated zinc finger protein	1,3	0,049	PRDX5
P24752	ACAT1	Acetyl-CoA acetyltransferase, mitochondrial	1,2	0	PRDX5
P33240	CSTF2	Cleavage stimulation factor subunit 2	1,2	0,001	PRDX5
A0A087WW06	TTC28	Tetratricopeptide repeat protein 28	1,2	0,001	PRDX5
Q15126	PMVK	Phosphomevalonate kinase	1,2	0,001	PRDX5
P57740	NUP107	Nuclear pore complex protein Nup107	1,2	0,002	PRDX5
Q9P2R3	ANKFY1	Rabankyrin-5	1,2	0,002	PRDX5
Q16527	CSRP2	Cysteine and glycine-rich protein 2	1,2	0,003	PRDX5
Q8NCA5	FAM98A	Protein FAM98A	1,2	0,003	PRDX5
Q6P587	FAHD1	Acylpyruvase FAHD1, mitochondrial	1,2	0,004	PRDX5
A0A087WUK2	HNRNPDL	Heterogeneous nuclear ribonucleoprotein D-like	1,2	0,006	PRDX5
Q86Y56	DNAAF5	Dynein assembly factor 5, axonemal	1,2	0,007	PRDX5
P50213	IDH3A	Isocitrate dehydrogenase [NAD] subunit alpha, mitochondrial	1,2	0,008	PRDX5
Q15654	TRIP6	Thyroid receptor-interacting protein 6	1,2	0,009	PRDX5
P84103	SRSF3	Serine/arginine-rich splicing factor 3	1,2	0,013	PRDX5
Q9UNE7	STUB1	E3 ubiquitin-protein ligase CHIP	1,2	0,013	PRDX5
Q02241	KIF23	Kinesin-like protein KIF23	1,2	0,015	PRDX5
D6R938	CAMK2D	Calcium/calmodulin-dependent protein kinase	1,2	0,019	PRDX5
Q2TAL8	QRICH1	Glutamine-rich protein 1	1,2	0,021	PRDX5
Q13509	TUBB3	Tubulin beta-3 chain	1,2	0,023	PRDX5
Q9NQT5	EXOSC3	Exosome complex component RRP40	1,2	0,026	PRDX5
Q8N9T8	KRI1	Protein KRI1 homolog	1,2	0,03	PRDX5
P21912	SDHB	Succinate dehydrogenase [ubiquinone] iron-sulfur subunit, mitochondrial	1,2	0,039	PRDX5
Q8WWH5	TRUB1	Probable tRNA pseudouridine synthase 1	1,2	0,041	PRDX5

P09622	DLD	Dihydrolipoyl dehydrogenase, mitochondrial	1,1	0	PRDX5
P19525	EIF2AK2	Interferon-induced, double-stranded RNA-activated protein kinase	1,1	0	PRDX5
Q9Y5M8	SRPRB	Signal recognition particle receptor subunit beta	1,1	0	PRDX5
P39019	RPS19	40S ribosomal protein S19	1,1	0	PRDX5
Q9Y2Z4	YARS2	Tyrosine--tRNA ligase, mitochondrial	1,1	0,001	PRDX5
P58107	EPPK1	Epiplakin	1,1	0,002	PRDX5
Q9NY93	DDX56	Probable ATP-dependent RNA helicase DDX56	1,1	0,004	PRDX5
Q6P1N0	CC2D1A	Coiled-coil and C2 domain-containing protein 1A	1,1	0,005	PRDX5
P46778	RPL21	60S ribosomal protein L21	1,1	0,006	PRDX5
C9J9K3	RPSA	40S ribosomal protein SA	1,1	0,006	PRDX5
A0A2R8YDQ9	SUCLA2	Succinate--CoA ligase [ADP-forming] subunit beta, mitochondrial	1,1	0,006	PRDX5
O00442	RTCA	RNA 3'-terminal phosphate cyclase	1,1	0,008	PRDX5
P62937	PPIA	Peptidyl-prolyl cis-trans isomerase A	1,1	0,008	PRDX5
Q9P0K7	RAI14	Ankycorbin	1,1	0,011	PRDX5
Q5JSZ5	PRRC2B	Protein PRRC2B	1,1	0,012	PRDX5
Q02252	ALDH6A1	Methylmalonate-semialdehyde dehydrogenase [acylating], mitochondrial	1,1	0,014	PRDX5
Q9NQT4	EXOSC5	Exosome complex component RRP46	1,1	0,015	PRDX5
Q15750	TAB1	TGF-beta-activated kinase 1 and MAP3K7-binding protein 1	1,1	0,022	PRDX5
P50995	ANXA11	Annexin A11	1,1	0,022	PRDX5
Q92665	MRPS31	28S ribosomal protein S31, mitochondrial	1,1	0,023	PRDX5
Q12849	GRSF1	G-rich sequence factor 1	1,1	0,027	PRDX5
Q96F86	EDC3	Enhancer of mRNA-decapping protein 3	1,1	0,027	PRDX5
Q9UQ35	SRRM2	Serine/arginine repetitive matrix protein 2	1,1	0,027	PRDX5
Q9BWF3	RBM4	RNA-binding protein 4	1,1	0,028	PRDX5
Q96N67	DOCK7	Dedicator of cytokinesis protein 7	1,1	0,035	PRDX5
P00568	AK1	Adenylate kinase isoenzyme 1	1,1	0,036	PRDX5
P62266	RPS23	40S ribosomal protein S23	1,1	0,047	PRDX5
Q7KZ85	SUPT6H	Transcription elongation factor SPT6	1,1	0,048	PRDX5
P04637	TP53	Cellular tumor antigen p53	1,1	0,048	PRDX5
F2Z388	RPL35	60S ribosomal protein L35	1,1	0,049	PRDX5
P62081	RPS7	40S ribosomal protein S7	1	0,001	PRDX5
P22570	FDXR	NADPH:adrenodoxin oxidoreductase, mitochondrial	1	0,005	PRDX5
Q8WX93	PALLD	Palladin	1	0,007	PRDX5
P09525	ANXA4	Annexin A4	1	0,008	PRDX5
P35580	MYH10	Myosin-10	1	0,01	PRDX5
H7C5E4	XRN1	5'-3' exoribonuclease 1	1	0,011	PRDX5
Q13595	TRA2A	Transformer-2 protein homolog alpha	1	0,012	PRDX5
Q04837	SSBP1	Single-stranded DNA-binding protein, mitochondrial	1	0,015	PRDX5
Q12789	GTF3C1	General transcription factor 3C polypeptide 1	1	0,021	PRDX5
Q8WXF1	PSPC1	Paraspeckle component 1	1	0,022	PRDX5
P11172	UMPS	Uridine 5'-monophosphate synthase	1	0,025	PRDX5
E9PEJ4	DLAT	Acetyltransferase component of pyruvate dehydrogenase complex	1	0,026	PRDX5
Q9BQ69	MACROD1	ADP-ribose glycohydrolase MACROD1	1	0,028	PRDX5
O14965	AURKA	Aurora kinase A	1	0,031	PRDX5
O75691	UTP20	Small subunit processome component 20 homolog	1	0,038	PRDX5
P30520	ADSS2	Adenylosuccinate synthetase isozyme 2	1	0,039	PRDX5
D3YTB5	IRAK1	Interleukin-1 receptor-associated kinase 1	1	0,046	PRDX5
P45985	MAP2K4	Dual specificity mitogen-activated protein kinase kinase 4	1	0,049	PRDX5
PRDX2 -specific interactors					
P30048	PRDX3	Thioredoxin-dependent peroxide reductase, mitochondrial	5,8	0	PRDX1
P32119	PRDX2	Peroxiredoxin-2	5,7	0	PRDX1
Q9Y224	RTRAF	RNA transcription, translation and transport factor protein	5,4	0	PRDX1
P02790	HPX	Hemopexin	4,9	0	PRDX1
P62805	H4C1	Histone H4	4,1	0	PRDX1
O60506	SYNCRIP	Heterogeneous nuclear ribonucleoprotein Q	3,9	0	PRDX1
P40429	RPL13A	60S ribosomal protein L13a	3,9	0	PRDX1
P63167	DYNLL1	Dynein light chain 1, cytoplasmic	3,8	0	PRDX1
O76094	SRP72	Signal recognition particle subunit SRP72	3,7	0	PRDX1
P05386	RPLP1	60S acidic ribosomal protein P1	3,4	0	PRDX1
P00167	CYB5A	Cytochrome b5	3,3	0	PRDX1
O96007	MOCS2	Molybdopterin synthase catalytic subunit	3,3	0	PRDX1
E9PKG1	PRMT1	Protein arginine N-methyltransferase 1	3,2	0	PRDX1
P42704	LRPPRC	Leucine-rich PPR motif-containing protein, mitochondrial	3,2	0	PRDX1
P19338	NCL	Nucleolin	3,2	0	PRDX1
P63244	RACK1	Receptor of activated protein C kinase 1	3	0	PRDX1
Q9Y3D6	FIS1	Mitochondrial fission 1 protein	2,9	0	PRDX1
P62244	RPS15A	40S ribosomal protein S15a	2,9	0	PRDX1
P05387	RPLP2	60S acidic ribosomal protein P2	2,9	0	PRDX1

A0A0B4J1Z1	SRSF7	Serine/arginine-rich-splicing factor 7	2,9	0,001	PRDX1
Q6UW78	UQCC3	Ubiquinol-cytochrome-c reductase complex assembly factor 3	2,8	0	PRDX1
O00483	NDUFA4	Cytochrome c oxidase subunit NDUFA4	2,8	0	PRDX1
Q96CT7	CCDC124	Coiled-coil domain-containing protein 124	2,8	0	PRDX1
P61353	RPL27	60S ribosomal protein L27	2,7	0	PRDX1
Q92688	ANP32B	Acidic leucine-rich nuclear phosphoprotein 32 family member B	2,7	0	PRDX1
P61106	RAB14	Ras-related protein Rab-14	2,7	0,002	PRDX1
A0A3B3ISV3	COL4A1	Collagen alpha-1(IV) chain	2,6	0	PRDX1
P08758	ANXA5	Annexin A5	2,6	0	PRDX1
P68133	ACTA1	Actin, alpha skeletal muscle	2,6	0,004	PRDX1
Q9NX55	HYPK	Huntingtin-interacting protein K	2,6	0,006	PRDX1
D6RA00	ENOPH1	Enolase-phosphatase E1	2,5	0	PRDX1
B9A018	USP39	U4/U6.U5 tri-snRNP-associated protein 2	2,5	0	PRDX1
Q92769	HDAC2	Histone deacetylase 2	2,5	0	PRDX1
P12236	SLC25A6	ADP/ATP translocase 3	2,5	0	PRDX1
P26196	DDX6	Probable ATP-dependent RNA helicase DDX6	2,5	0	PRDX1
P35637	FUS	RNA-binding protein FUS	2,5	0,001	PRDX1
P18077	RPL35A	60S ribosomal protein L35a	2,4	0	PRDX1
P09211	GSTP1	Glutathione S-transferase P	2,4	0	PRDX1
G5EA06	MRPS27	28S ribosomal protein S27, mitochondrial	2,4	0,002	PRDX1
P53602	MVD	Diphosphomevalonate decarboxylase	2,4	0,002	PRDX1
Q71UI9	H2AZ2	Histone H2A.V	2,3	0	PRDX1
Q9H0U4	RAB1B	Ras-related protein Rab-1B	2,3	0	PRDX1
P36957	DLST	Dihydrolipoyllysine-residue succinyltransferase component of 2-oxoglutarate dehydrogenase complex, mitochondrial	2,3	0	PRDX1
P62750	RPL23A	60S ribosomal protein L23a	2,3	0	PRDX1
C9J4Z3	RPL37A	60S ribosomal protein L37a	2,3	0	PRDX1
P27797	CALR	Calreticulin	2,3	0	PRDX1
P15121	AKR1B1	Aldo-keto reductase family 1 member B1	2,3	0	PRDX1
Q53GQ0	HSD17B12	Very-long-chain 3-oxoacyl-CoA reductase	2,3	0,002	PRDX1
O75223	GGCT	Gamma-glutamylcyclotransferase	2,3	0,002	PRDX1
P00492	HPRT1	Hypoxanthine-guanine phosphoribosyltransferase	2,3	0,004	PRDX1
P12955	PEPD	Xaa-Pro dipeptidase	2,3	0,007	PRDX1
A0A087WTM1	ROBO1	Roundabout homolog 1	2,2	0	PRDX1
Q9H8Y8	GORASP2	Golgi reassembly-stacking protein 2	2,2	0	PRDX1
P50914	RPL14	60S ribosomal protein L14	2,2	0	PRDX1
P32969	RPL9	60S ribosomal protein L9	2,2	0	PRDX1
P51149	RAB7A	Ras-related protein Rab-7a	2,2	0	PRDX1
P19174	PLCG1	1-phosphatidylinositol 4,5-bisphosphate phosphodiesterase gamma-1	2,2	0,002	PRDX1
O15144	ARPC2	Actin-related protein 2/3 complex subunit 2	2,2	0,002	PRDX1
H3BRL3	UBFD1	Ubiquitin domain-containing protein UBFD1	2,2	0,003	PRDX1
Q13126	MTAP	S-methyl-5'-thioadenosine phosphorylase	2,2	0,004	PRDX1
P35237	SERPINB6	Serpin B6	2,1	0	PRDX1
P10301	RRAS	Ras-related protein R-Ras	2,1	0	PRDX1
P30740	SERPINB1	Leukocyte elastase inhibitor	2,1	0	PRDX1
Q15393	SF3B3	Splicing factor 3B subunit 3	2,1	0	PRDX1
Q9NS69	TOMM22	Mitochondrial import receptor subunit TOM22 homolog	2,1	0	PRDX1
Q02750	MAP2K1	Dual specificity mitogen-activated protein kinase kinase 1	2,1	0	PRDX1
P49321	NASP	Nuclear autoantigenic sperm protein	2,1	0	PRDX1
P23921	RRM1	Ribonucleoside-diphosphate reductase large subunit	2,1	0	PRDX1
Q9ULC3	RAB23	Ras-related protein Rab-23	2,1	0,002	PRDX1
O75400	PRPF40A	Pre-mRNA-processing factor 40 homolog A	2,1	0,003	PRDX1
O95104	SCAF4	SR-related and CTD-associated factor 4	2,1	0,003	PRDX1
O60547	GMDS	GDP-mannose 4,6 dehydratase	2,1	0,015	PRDX1
O00231	PSMD11	26S proteasome non-ATPase regulatory subunit 11	2	0	PRDX1
O43747	AP1G1	AP-1 complex subunit gamma-1	2	0	PRDX1
O95433	AHSA1	Activator of 90 kDa heat shock protein ATPase homolog 1	2	0	PRDX1
Q02878	RPL6	60S ribosomal protein L6	2	0	PRDX1
P15880	RPS2	40S ribosomal protein S2	2	0	PRDX1
P06730	EIF4E	Eukaryotic translation initiation factor 4E	2	0	PRDX1
P05388	RPLP0	60S acidic ribosomal protein P0	2	0	PRDX1
K7ERF1	EIF3K	Eukaryotic translation initiation factor 3 subunit K	2	0	PRDX1
P35606	COPB2	Coatomer subunit beta'	2	0,001	PRDX1
P11182	DBT	Lipoamide acyltransferase component of branched-chain alpha-keto acid dehydrogenase complex, mitochondrial	2	0,003	PRDX1
Q5SY16	NOL9	Polynucleotide 5'-hydroxyl-kinase NOL9	2	0,004	PRDX1
Q9Y570	PPME1	Protein phosphatase methylesterase 1	2	0,005	PRDX1
P00491	PNP	Purine nucleoside phosphorylase	2	0,005	PRDX1
P48147	PREP	Prolyl endopeptidase	2	0,01	PRDX1

A0AVT1	UBA6	Ubiquitin-like modifier-activating enzyme 6	2	0,021	PRDX1
P04181	OAT	Ornithine aminotransferase, mitochondrial	1,9	0	PRDX1
Q14232	EIF2B1	Translation initiation factor eIF-2B subunit alpha	1,9	0	PRDX1
Q9UJS0	SLC25A13	Calcium-binding mitochondrial carrier protein Aralar2	1,9	0	PRDX1
P53985	SLC16A1	Monocarboxylate transporter 1	1,9	0	PRDX1
O75489	NDUFS3	NADH dehydrogenase [ubiquinone] iron-sulfur protein 3, mitochondrial	1,9	0,005	PRDX1
P84085	ARF5	ADP-ribosylation factor 5	1,9	0,012	PRDX1
E9PHS0	LANCL1	Glutathione S-transferase LANCL1	1,9	0,021	PRDX1
O60664	PLIN3	Perilipin-3	1,9	0,024	PRDX1
Q7Z434	MAVS	Mitochondrial antiviral-signaling protein	1,9	0,036	PRDX1
P10599	TXN	Thioredoxin	1,9	0,043	PRDX1
Q9UBF2	COPG2	Coatomer subunit gamma-2	1,8	0	PRDX1
Q15691	MAPRE1	Microtubule-associated protein RP/EB family member 1	1,8	0	PRDX1
A6NKB8	RNPEP	Aminopeptidase B	1,8	0	PRDX1
P00387	CYB5R3	NADH-cytochrome b5 reductase 3	1,8	0	PRDX1
P23396	RPS3	40S ribosomal protein S3	1,8	0	PRDX1
P41252	IARS1	Isoleucine--tRNA ligase, cytoplasmic	1,8	0,001	PRDX1
O14980	XPO1	Exportin-1	1,8	0,002	PRDX1
Q4J6C6	PREPL	Prolyl endopeptidase-like	1,8	0,006	PRDX1
P11388	TOP2A	DNA topoisomerase 2-alpha	1,8	0,007	PRDX1
Q9NYB0	TERF2IP	Telomeric repeat-binding factor 2-interacting protein 1	1,8	0,007	PRDX1
P28288	ABCD3	ATP-binding cassette sub-family D member 3	1,8	0,009	PRDX1
E7ETZ4	BZW2	Basic leucine zipper and W2 domain-containing protein 2	1,8	0,01	PRDX1
O94925	GLS	Glutaminase kidney isoform, mitochondrial	1,8	0,012	PRDX1
E9PHN7	GSTM2	Glutathione S-transferase Mu 2	1,8	0,014	PRDX1
Q9NVP1	DDX18	ATP-dependent RNA helicase DDX18	1,8	0,015	PRDX1
P40616	ARL1	ADP-ribosylation factor-like protein 1	1,8	0,025	PRDX1
P38159	RBMX	RNA-binding motif protein, X chromosome	1,8	0,037	PRDX1
Q9P2B4	CTTNBP2NL	CTTNBP2 N-terminal-like protein	1,7	0	PRDX1
Q6PI48	DARS2	Aspartate--tRNA ligase, mitochondrial	1,7	0	PRDX1
P36542	ATP5F1C	ATP synthase subunit gamma, mitochondrial	1,7	0	PRDX1
P05141	SLC25A5	ADP/ATP translocase 2	1,7	0	PRDX1
Q5T7C4	HMGB1	High mobility group protein B1	1,7	0,001	PRDX1
P22314	UBA1	Ubiquitin-like modifier-activating enzyme 1	1,7	0,004	PRDX1
O00232	PSMD12	26S proteasome non-ATPase regulatory subunit 12	1,7	0,004	PRDX1
P27824	CANX	Calnexin	1,7	0,005	PRDX1
Q9BQG0	MYBBP1A	Myb-binding protein 1A	1,7	0,007	PRDX1
Q9ULW0	TPX2	Targeting protein for Xklp2	1,7	0,008	PRDX1
Q01085	TIAL1	Nucleolysin TIAR	1,7	0,01	PRDX1
P51398	DAP3	28S ribosomal protein S29, mitochondrial	1,7	0,014	PRDX1
Q96IU4	ABHD14B	Protein ABHD14B	1,7	0,016	PRDX1
O95163	ELP1	Elongator complex protein 1	1,7	0,017	PRDX1
Q9UBS4	DNAJB11	DnaJ homolog subfamily B member 11	1,7	0,018	PRDX1
P31153	MAT2A	S-adenosylmethionine synthase isoform type-2	1,6	0	PRDX1
P05455	SSB	Lupus La protein	1,6	0	PRDX1
P61313	RPL15	60S ribosomal protein L15	1,6	0	PRDX1
P51665	PSMD7	26S proteasome non-ATPase regulatory subunit 7	1,6	0	PRDX1
G8JLH9	STAT3	Signal transducer and activator of transcription	1,6	0	PRDX1
P53007	SLC25A1	Tricarboxylate transport protein, mitochondrial	1,6	0	PRDX1
O75821	EIF3G	Eukaryotic translation initiation factor 3 subunit G	1,6	0	PRDX1
P16435	POR	NADPH--cytochrome P450 reductase	1,6	0,003	PRDX1
P39023	RPL3	60S ribosomal protein L3	1,6	0,004	PRDX1
Q8TEX9	IPO4	Importin-4	1,6	0,006	PRDX1
Q8N3X1	FNBP4	Formin-binding protein 4	1,6	0,018	PRDX1
Q9Y4P1	ATG4B	Cysteine protease ATG4B	1,6	0,021	PRDX1
P00390	GSR	Glutathione reductase, mitochondrial	1,6	0,025	PRDX1
Q13542	EIF4EBP2	Eukaryotic translation initiation factor 4E-binding protein 2	1,6	0,025	PRDX1
Q5T4U8	RABGGTB	Geranylgeranyl transferase type-2 subunit beta	1,6	0,033	PRDX1
A6NGP5	JPT2	Jupiter microtubule-associated homolog 2	1,6	0,033	PRDX1
P51991	HNRNPA3	Heterogeneous nuclear ribonucleoprotein A3	1,6	0,037	PRDX1
Q8N806	UBR7	Putative E3 ubiquitin-protein ligase UBR7	1,6	0,047	PRDX1
P43304	GPD2	Glycerol-3-phosphate dehydrogenase, mitochondrial	1,6	0,048	PRDX1
Q9BYN0	SRXN1	Sulfiredoxin-1	1,6	0,048	PRDX1
Q6IBS0	TWF2	Twinfilin-2	1,5	0	PRDX1
Q6IQ49	SDE2	Replication stress response regulator SDE2	1,5	0	PRDX1
P38117	ETFB	Electron transfer flavoprotein subunit beta	1,5	0	PRDX1
Q9UQ80	PA2G4	Proliferation-associated protein 2G4	1,5	0	PRDX1
P61586	RHOA	Transforming protein RhoA	1,5	0	PRDX1
P43034	PAFAH1B1	Platelet-activating factor acetylhydrolase IB subunit beta	1,5	0	PRDX1

O00487	PSMD14	26S proteasome non-ATPase regulatory subunit 14	1,5	0,001	PRDX1
Q53H12	AGK	Acylglycerol kinase, mitochondrial	1,5	0,002	PRDX1
Q16531	DDB1	DNA damage-binding protein 1	1,5	0,002	PRDX1
Q9GZS3	WDR61	WD repeat-containing protein 61	1,5	0,003	PRDX1
P30101	PDIA3	Protein disulfide-isomerase A3	1,5	0,003	PRDX1
Q9NPH2	ISYNA1	Inositol-3-phosphate synthase 1	1,5	0,004	PRDX1
P52597	HNRNPF	Heterogeneous nuclear ribonucleoprotein F	1,5	0,004	PRDX1
Q5VW32	BROX	BRO1 domain-containing protein BROX	1,5	0,007	PRDX1
Q96IZ0	PAWR	PRKC apoptosis WT1 regulator protein	1,5	0,009	PRDX1
Q92621	NUP205	Nuclear pore complex protein Nup205	1,5	0,012	PRDX1
P26599	PTBP1	Polypyrimidine tract-binding protein 1	1,5	0,018	PRDX1
H3BV80	RNPS1	RNA-binding protein with serine-rich domain 1	1,5	0,023	PRDX1
Q8NI27	THOC2	THO complex subunit 2	1,5	0,024	PRDX1
P42574	CASP3	Caspase-3	1,5	0,026	PRDX1
Q9P287	BCCIP	BRCA2 and CDKN1A-interacting protein	1,5	0,029	PRDX1
E9PGT1	TSN	Component 3 of promoter of RISC	1,5	0,031	PRDX1
Q9BSJ8	ESYT1	Extended synaptotagmin-1	1,5	0,032	PRDX1
Q9H9P8	L2HGDH	L-2-hydroxyglutarate dehydrogenase, mitochondrial	1,5	0,033	PRDX1
Q8NFC6	BOD1L1	Biorientation of chromosomes in cell division protein 1-like 1	1,5	0,034	PRDX1
P07384	CAPN1	Calpain-1 catalytic subunit	1,5	0,037	PRDX1
Q9Y6Y0	IVNS1ABP	Influenza virus NS1A-binding protein	1,5	0,037	PRDX1
Q9Y277	VDAC3	Voltage-dependent anion-selective channel protein 3	1,5	0,043	PRDX1
P27694	RPA1	Replication protein A 70 kDa DNA-binding subunit	1,5	0,046	PRDX1
Q92973	TNPO1	Transportin-1	1,4	0	PRDX1
P23528	CFL1	Cofilin-1	1,4	0	PRDX1
P61247	RPS3A	40S ribosomal protein S3a	1,4	0	PRDX1
E9PN17	ATP5MG	ATP synthase subunit g, mitochondrial	1,4	0,001	PRDX1
A0A024R4M0	RPS9	40S ribosomal protein S9	1,4	0,001	PRDX1
O00203	AP3B1	AP-3 complex subunit beta-1	1,4	0,001	PRDX1
P60953	CDC42	Cell division control protein 42 homolog	1,4	0,001	PRDX1
P08133	ANXA6	Annexin A6	1,4	0,003	PRDX1
P16615	ATP2A2	Sarcoplasmic/endoplasmic reticulum calcium ATPase 2	1,4	0,004	PRDX1
Q96SB4	SRPK1	SRSF protein kinase 1	1,4	0,005	PRDX1
Q5T4K5	CRTC2	CREB-regulated transcription coactivator 2	1,4	0,006	PRDX1
G3V529	DDX24	RNA helicase	1,4	0,019	PRDX1
Q9UHQ9	CYB5R1	NADH-cytochrome b5 reductase 1	1,4	0,037	PRDX1
Q9Y2R5	MRPS17	28S ribosomal protein S17, mitochondrial	1,4	0,037	PRDX1
Q9BZK7	TBL1XR1	F-box-like/WD repeat-containing protein TBL1XR1	1,4	0,037	PRDX1
O96019	ACTL6A	Actin-like protein 6A	1,4	0,039	PRDX1
Q5JR04	MOV10	RNA helicase	1,4	0,039	PRDX1
K7EM73	CAPNS1	Calcium-activated neutral proteinase small subunit	1,4	0,04	PRDX1
O95394	PGM3	Phosphoacetylglucosamine mutase	1,3	0	PRDX1
P68104	EEF1A1	Elongation factor 1-alpha 1	1,3	0	PRDX1
P00338	LDHA	L-lactate dehydrogenase A chain	1,3	0	PRDX1
P06737	PYGL	Glycogen phosphorylase, liver form	1,3	0	PRDX1
P36578	RPL4	60S ribosomal protein L4	1,3	0	PRDX1
P08238	HSP90AB1	Heat shock protein HSP 90-beta	1,3	0	PRDX1
P52565	ARHGDIA	Rho GDP-dissociation inhibitor 1	1,3	0,001	PRDX1
E7ESY4	MTA1	Metastasis-associated protein MTA1	1,3	0,001	PRDX1
B4DLN1	B4DLN1	cDNA FLJ60124, highly similar to Mitochondrial dicarboxylate carrier	1,3	0,001	PRDX1
Q9H7D7	WDR26	WD repeat-containing protein 26	1,3	0,002	PRDX1
P61923	COPZ1	Coatomer subunit zeta-1	1,3	0,002	PRDX1
P62269	RPS18	40S ribosomal protein S18	1,3	0,002	PRDX1
Q96HC4	PDLIM5	PDZ and LIM domain protein 5	1,3	0,002	PRDX1
A0A3B3IRI2	CTPS1	CTP synthase	1,3	0,004	PRDX1
E7EV99	ADD1	Alpha-adducin	1,3	0,004	PRDX1
P56192	MARS1	Methionine--tRNA ligase, cytoplasmic	1,3	0,005	PRDX1
Q9Y678	COPG1	Coatomer subunit gamma-1	1,3	0,006	PRDX1
O75832	PSMD10	26S proteasome non-ATPase regulatory subunit 10	1,3	0,007	PRDX1
X1WI28	RPL10	60S ribosomal protein L10	1,3	0,008	PRDX1
P50502	ST13	Hsc70-interacting protein	1,3	0,013	PRDX1
Q9H0A0	NAT10	RNA cytidine acetyltransferase	1,3	0,014	PRDX1
A0A0A0MRM9	NOLC1	Nucleolar and coiled-body phosphoprotein 1	1,3	0,025	PRDX1
Q8N9Q2	SREK1IP1	Protein SREK1IP1	1,3	0,026	PRDX1
P52888	THOP1	Thimet oligopeptidase	1,3	0,032	PRDX1
Q9NUP9	LIN7C	Protein lin-7 homolog C	1,3	0,035	PRDX1
Q93008	USP9X	Probable ubiquitin carboxyl-terminal hydrolase FAF-X	1,3	0,037	PRDX1
Q9Y262	EIF3L	Eukaryotic translation initiation factor 3 subunit L	1,3	0,043	PRDX1
Q96BW9	TAMM41	Phosphatidate cytidylyltransferase, mitochondrial	1,3	0,043	PRDX1

F5GZS6	SLC3A2	4F2 cell-surface antigen heavy chain	1,3	0,047	PRDX1
P49756	RBM25	RNA-binding protein 25	1,2	0	PRDX1
P61221	ABCE1	ATP-binding cassette sub-family E member 1	1,2	0	PRDX1
Q9H3P7	ACBD3	Golgi resident protein GCP60	1,2	0,001	PRDX1
Q07020	RPL18	60S ribosomal protein L18	1,2	0,001	PRDX1
Q9NQW7	XPNPEP1	Xaa-Pro aminopeptidase 1	1,2	0,002	PRDX1
P55884	EIF3B	Eukaryotic translation initiation factor 3 subunit B	1,2	0,004	PRDX1
P62241	RPS8	40S ribosomal protein S8	1,2	0,005	PRDX1
P49736	MCM2	DNA replication licensing factor MCM2	1,2	0,005	PRDX1
P53618	COPB1	Coatomer subunit beta	1,2	0,005	PRDX1
O75531	BANF1	Barrier-to-autointegration factor	1,2	0,007	PRDX1
P15927	RPA2	Replication protein A 32 kDa subunit	1,2	0,011	PRDX1
P11387	TOP1	DNA topoisomerase 1	1,2	0,012	PRDX1
P15374	UCHL3	Ubiquitin carboxyl-terminal hydrolase isozyme L3	1,2	0,012	PRDX1
Q5QPM7	PSMF1	Proteasome inhibitor PI31 subunit	1,2	0,017	PRDX1
P49750	YLPM1	YLP motif-containing protein 1	1,2	0,019	PRDX1
P20073	ANXA7	Annexin A7	1,2	0,025	PRDX1
Q00610	CLTC	Clathrin heavy chain 1	1,2	0,026	PRDX1
P33992	MCM5	DNA replication licensing factor MCM5	1,2	0,029	PRDX1
P31689	DNAJA1	DnaJ homolog subfamily A member 1	1,2	0,031	PRDX1
A0A0A0MRN5	OGFR	Opioid growth factor receptor	1,2	0,04	PRDX1
O15269	SPTLC1	Serine palmitoyltransferase 1	1,2	0,043	PRDX1
P82663	MRPS25	28S ribosomal protein S25, mitochondrial	1,1	0	PRDX1
P62424	RPL7A	60S ribosomal protein L7a	1,1	0	PRDX1
P07900	HSP90AA1	Heat shock protein HSP 90-alpha	1,1	0	PRDX1
Q00325	SLC25A3	Phosphate carrier protein, mitochondrial	1,1	0	PRDX1
P34949	MPI	Mannose-6-phosphate isomerase	1,1	0,001	PRDX1
Q8NE71	ABCF1	ATP-binding cassette sub-family F member 1	1,1	0,001	PRDX1
E5RHG8	ELOC	Elongin-C	1,1	0,001	PRDX1
Q9Y5P6	GMPPB	Mannose-1-phosphate guanyltransferase beta	1,1	0,002	PRDX1
Q8WUH6	TMEM263	Transmembrane protein 263	1,1	0,002	PRDX1
P14324	FDPS	Farnesyl pyrophosphate synthase	1,1	0,002	PRDX1
Q15029	EFTUD2	116 kDa U5 small nuclear ribonucleoprotein component	1,1	0,003	PRDX1
Q9UMS4	PRPF19	Pre-mRNA-processing factor 19	1,1	0,003	PRDX1
Q8TAQ2	SMARCC2	SWI/SNF complex subunit SMARCC2	1,1	0,004	PRDX1
P43246	MSH2	DNA mismatch repair protein Msh2	1,1	0,005	PRDX1
Q99460	PSMD1	26S proteasome non-ATPase regulatory subunit 1	1,1	0,006	PRDX1
Q9UNM6	PSMD13	26S proteasome non-ATPase regulatory subunit 13	1,1	0,009	PRDX1
P53004	BLVRA	Biliverdin reductase A	1,1	0,012	PRDX1
Q9UI12	ATP6V1H	V-type proton ATPase subunit H	1,1	0,013	PRDX1
Q9Y3Z3	SAMHD1	Deoxynucleoside triphosphate triphosphohydrolase SAMHD1	1,1	0,013	PRDX1
Q5T760	SRSF11	Serine/arginine-rich-splicing factor 11	1,1	0,019	PRDX1
F8W6I7	HNRNPA1	Helix-destabilizing protein	1,1	0,026	PRDX1
P62333	PSMC6	26S proteasome regulatory subunit 10B	1,1	0,03	PRDX1
P34932	HSPA4	Heat shock 70 kDa protein 4	1,1	0,032	PRDX1
P26583	HMGB2	High mobility group protein B2	1,1	0,039	PRDX1
P42224	STAT1	Signal transducer and activator of transcription 1-alpha/beta	1,1	0,046	PRDX1
P62314	SNRPD1	Small nuclear ribonucleoprotein Sm D1	1,1	0,049	PRDX1
P60891	PRPS1	Ribose-phosphate pyrophosphokinase 1	1	0	PRDX1
O75396	SEC22B	Vesicle-trafficking protein SEC22b	1	0,004	PRDX1
Q9BT78	COPS4	COP9 signalosome complex subunit 4	1	0,005	PRDX1
Q14240	EIF4A2	Eukaryotic initiation factor 4A-II	1	0,011	PRDX1
O94903	PLPBP	Pyridoxal phosphate homeostasis protein	1	0,02	PRDX1
Q8IWB7	WDFY1	WD repeat and FYVE domain-containing protein 1	1	0,02	PRDX1
O00273	DFFA	DNA fragmentation factor subunit alpha	1	0,034	PRDX1
P55769	SNU13	NHP2-like protein 1	1	0,038	PRDX1
Q8NHH9	ATL2	Atlastin-2	1	0,039	PRDX1
O14965	AURKA	Aurora kinase A	1	0,044	PRDX1
Q8IYS1	PM20D2	Peptidase M20 domain-containing protein 2	1	0,046	PRDX1
P32119	PRDX2	Peroxiredoxin-2	6,8	0	PRDX3
P00167	CYB5A	Cytochrome b5	4,4	0	PRDX3
O96007	MOCS2	Molybdopterin synthase catalytic subunit	3,7	0	PRDX3
P10301	RRAS	Ras-related protein R-Ras	3,7	0	PRDX3
Q9Y224	RTRAF	RNA transcription, translation and transport factor protein	3,7	0	PRDX3
Q9Y3D6	FIS1	Mitochondrial fission 1 protein	3,2	0	PRDX3
Q96CT7	CCDC124	Coiled-coil domain-containing protein 124	3,2	0	PRDX3
Q8NFC6	BOD1L1	Biorientation of chromosomes in cell division protein 1-like 1	3	0	PRDX3
Q9Y6A5	TACC3	Transforming acidic coiled-coil-containing protein 3	3	0,001	PRDX3
Q9NX55	HYPK	Huntingtin-interacting protein K	2,9	0,003	PRDX3

E7EVA0	MAP4	Microtubule-associated protein	2,9	0,005	PRDX3
O95831	AIFM1	Apoptosis-inducing factor 1, mitochondrial	2,8	0	PRDX3
P53602	MVD	Diphosphomevalonate decarboxylase	2,8	0,001	PRDX3
Q6WKZ4	RAB11FIP1	Rab11 family-interacting protein 1	2,8	0,001	PRDX3
Q6IQ49	SDE2	Replication stress response regulator SDE2	2,7	0	PRDX3
Q9ULW0	TPX2	Targeting protein for Xklp2	2,7	0,001	PRDX3
Q96A10	ERVK3-1	Endogenous retrovirus group K3 member 1	2,7	0,024	PRDX3
H0YNW5	DUT	Deoxyuridine 5'-triphosphate nucleotidohydrolase	2,6	0	PRDX3
Q9NPH2	ISYNA1	Inositol-3-phosphate synthase 1	2,6	0	PRDX3
Q13542	EIF4EBP2	Eukaryotic translation initiation factor 4E-binding protein 2	2,6	0,002	PRDX3
P12955	PEPD	Xaa-Pro dipeptidase	2,6	0,004	PRDX3
Q9C0C2	TNKS1BP1	182 kDa tankyrase-1-binding protein	2,6	0,007	PRDX3
O60664	PLIN3	Perilipin-3	2,5	0,002	PRDX3
Q6PID6	TTC33	Tetratricopeptide repeat protein 33	2,5	0,034	PRDX3
H3BRL3	UBFD1	Ubiquitin domain-containing protein UBFD1	2,4	0	PRDX3
P47985	UQCRFS1	Cytochrome b-c1 complex subunit Rieske, mitochondrial	2,4	0	PRDX3
B7Z7F3	RANBP3	Ran-binding protein 3	2,4	0,001	PRDX3
P00491	PNP	Purine nucleoside phosphorylase	2,4	0,002	PRDX3
Q8N3X1	FNBP4	Formin-binding protein 4	2,3	0	PRDX3
Q9P2B4	CTTNBP2NL	CTTNBP2 N-terminal-like protein	2,3	0	PRDX3
Q9NUQ3	TXLNG	Gamma-taxilin	2,3	0	PRDX3
Q8NC51	SERBP1	Plasminogen activator inhibitor 1 RNA-binding protein	2,3	0,001	PRDX3
A4D1S0	KLRG2	Killer cell lectin-like receptor subfamily G member 2	2,3	0,003	PRDX3
P11802	CDK4	Cyclin-dependent kinase 4	2,3	0,004	PRDX3
P35244	RPA3	Replication protein A 14 kDa subunit	2,3	0,004	PRDX3
Q9P258	RCC2	Protein RCC2	2,2	0,001	PRDX3
Q7Z4V5	HDGFL2	Hepatoma-derived growth factor-related protein 2	2,2	0,012	PRDX3
E7EV99	ADD1	Alpha-adducin	2,1	0	PRDX3
O14965	AURKA	Aurora kinase A	2,1	0	PRDX3
Q12948	FOXC1	Forkhead box protein C1	2,1	0,001	PRDX3
P14174	MIF	Macrophage migration inhibitory factor	2,1	0,01	PRDX3
A0A087WTM1	ROBO1	Roundabout homolog 1	2	0	PRDX3
F5GZS6	SLC3A2	4F2 cell-surface antigen heavy chain	2	0,006	PRDX3
P61758	VBP1	Prefoldin subunit 3	2	0,006	PRDX3
A6NGP5	JPT2	Jupiter microtubule-associated homolog 2	2	0,007	PRDX3
P00390	GSR	Glutathione reductase, mitochondrial	2	0,009	PRDX3
O15511	ARPC5	Actin-related protein 2/3 complex subunit 5	2	0,014	PRDX3
E9PDD6	BCL2L13	Bcl-2-like protein 13	2	0,02	PRDX3
P22234	PAICS	Multifunctional protein ADE2 [Includes: Phosphoribosylaminoimidazole-succinocarboxamide synthase	1,9	0,002	PRDX3
P41250	GARS1	Glycine--tRNA ligase	1,9	0,004	PRDX3
Q13541	EIF4EBP1	Eukaryotic translation initiation factor 4E-binding protein 1	1,9	0,01	PRDX3
Q9Y266	NUDC	Nuclear migration protein nudC	1,9	0,014	PRDX3
Q8IVM0	CCDC50	Coiled-coil domain-containing protein 50	1,9	0,014	PRDX3
J3KS31	ZNF207	BUB3-interacting and GLEBS motif-containing protein ZNF207	1,9	0,032	PRDX3
A0A1B0GUC3	FTO	Alpha-ketoglutarate-dependent dioxygenase FTO	1,8	0,025	PRDX3
P40222	TXLNA	Alpha-taxilin	1,7	0,002	PRDX3
P61927	RPL37	60S ribosomal protein L37	1,7	0,005	PRDX3
Q6UW78	UQCC3	Ubiquinol-cytochrome-c reductase complex assembly factor 3	1,7	0,01	PRDX3
A0AVT1	UBA6	Ubiquitin-like modifier-activating enzyme 6	1,7	0,022	PRDX3
Q96KB5	PBK	Lymphokine-activated killer T-cell-originated protein kinase	1,7	0,027	PRDX3
P13995	MTHFD2	Bifunctional methylenetetrahydrofolate dehydrogenase/cyclohydrolase, mitochondrial [Includes: NAD-dependent methylenetetrahydrofolate dehydrogenase	1,7	0,029	PRDX3
O94903	PLPBP	Pyridoxal phosphate homeostasis protein	1,6	0	PRDX3
P26599	PTBP1	Polypyrimidine tract-binding protein 1	1,6	0,012	PRDX3
Q99598	TSNAX	Translin-associated protein X	1,6	0,014	PRDX3
Q9UHR5	SAP30BP	SAP30-binding protein	1,6	0,02	PRDX3
Q13126	MTAP	S-methyl-5'-thioadenosine phosphorylase	1,6	0,03	PRDX3
E9PGZ1	CALD1	Caldesmon	1,6	0,036	PRDX3
Q15181	PPA1	Inorganic pyrophosphatase	1,5	0	PRDX3
Q7Z2K8	GPRIN1	G protein-regulated inducer of neurite outgrowth 1	1,5	0,001	PRDX3
P31153	MAT2A	S-adenosylmethionine synthase isoform type-2	1,5	0,001	PRDX3
P62244	RPS15A	40S ribosomal protein S15a	1,5	0,003	PRDX3
Q71UI9	H2AZ2	Histone H2A.V	1,5	0,018	PRDX3
P85037	FOXK1	Forkhead box protein K1	1,5	0,022	PRDX3
Q9HA64	FN3KRP	Ketosamine-3-kinase	1,5	0,03	PRDX3
A0A087WUT6	EIF5B	Eukaryotic translation initiation factor 5B	1,4	0,001	PRDX3
Q5T4K5	CRTC2	CREB-regulated transcription coactivator 2	1,4	0,014	PRDX3
Q5T6F2	UBAP2	Ubiquitin-associated protein 2	1,4	0,018	PRDX3

Q7L2J0	MEPCE	7SK snRNA methylphosphate capping enzyme	1,4	0,021	PRDX3
Q9NUP9	LIN7C	Protein lin-7 homolog C	1,4	0,026	PRDX3
P52888	THOP1	Thimet oligopeptidase	1,4	0,028	PRDX3
Q13137	CALCOCO2	Calcium-binding and coiled-coil domain-containing protein 2	1,4	0,028	PRDX3
P49903	SEPHS1	Selenide, water dikinase 1	1,4	0,031	PRDX3
Q16204	CCDC6	Coiled-coil domain-containing protein 6	1,4	0,034	PRDX3
E9PKG1	PRMT1	Protein arginine N-methyltransferase 1	1,3	0	PRDX3
P50914	RPL14	60S ribosomal protein L14	1,3	0,001	PRDX3
Q02878	RPL6	60S ribosomal protein L6	1,3	0,008	PRDX3
Q6PKG0	LARP1	La-related protein 1	1,3	0,008	PRDX3
Q16576	RBBP7	Histone-binding protein RBBP7	1,3	0,011	PRDX3
Q9BQ61	TRIR	Telomerase RNA component interacting RNase	1,3	0,014	PRDX3
Q8N9Q2	SREK1IP1	Protein SREK1IP1	1,3	0,015	PRDX3
Q9GZS3	WDR61	WD repeat-containing protein 61	1,3	0,015	PRDX3
Q96F86	EDC3	Enhancer of mRNA-decapping protein 3	1,3	0,018	PRDX3
P62266	RPS23	40S ribosomal protein S23	1,3	0,02	PRDX3
P56385	ATP5ME	ATP synthase subunit e, mitochondrial	1,3	0,025	PRDX3
P48147	PREP	Prolyl endopeptidase	1,3	0,026	PRDX3
Q96IZ0	PAWR	PRKC apoptosis WT1 regulator protein	1,3	0,032	PRDX3
Q9Y570	PPME1	Protein phosphatase methylesterase 1	1,3	0,038	PRDX3
Q32MZ4	LRRFIP1	Leucine-rich repeat flightless-interacting protein 1	1,3	0,039	PRDX3
P40429	RPL13A	60S ribosomal protein L13a	1,2	0,001	PRDX3
P07195	LDHB	L-lactate dehydrogenase B chain	1,2	0,003	PRDX3
P34897	SHMT2	Serine hydroxymethyltransferase, mitochondrial	1,2	0,004	PRDX3
Q9BRP1	PDCD2L	Programmed cell death protein 2-like	1,2	0,006	PRDX3
J3KN29	PSMD9	26S proteasome non-ATPase regulatory subunit 9	1,2	0,011	PRDX3
P62851	RPS25	40S ribosomal protein S25	1,2	0,015	PRDX3
Q9H0U4	RAB1B	Ras-related protein Rab-1B	1,2	0,023	PRDX3
B4DDF4	CNN2	Calponin	1,2	0,031	PRDX3
O14949	UQCRQ	Cytochrome b-c1 complex subunit 8	1,2	0,046	PRDX3
P62826	RAN	GTP-binding nuclear protein Ran	1,1	0	PRDX3
Q8WUH6	TMEM263	Transmembrane protein 263	1,1	0,001	PRDX3
P18077	RPL35A	60S ribosomal protein L35a	1,1	0,004	PRDX3
P78346	RPP30	Ribonuclease P protein subunit p30	1,1	0,004	PRDX3
P62753	RPS6	40S ribosomal protein S6	1,1	0,014	PRDX3
P05388	RPLP0	60S acidic ribosomal protein P0	1,1	0,015	PRDX3
A0A0A0MRN5	OGFR	Opioid growth factor receptor	1,1	0,022	PRDX3
B1AMS2	SEPTIN6	Septin 6, isoform CRA_b	1,1	0,032	PRDX3
Q9NS69	TOMM22	Mitochondrial import receptor subunit TOM22 homolog	1,1	0,039	PRDX3
P23381	WARS1	Tryptophan--tRNA ligase, cytoplasmic	1	0,002	PRDX3
P62888	RPL30	60S ribosomal protein L30	1	0,005	PRDX3
Q9H936	SLC25A22	Mitochondrial glutamate carrier 1	1	0,019	PRDX3
Q8NCW5	NAXE	NAD(P)H-hydrate epimerase	1	0,02	PRDX3
P42771	CDKN2A	Cyclin-dependent kinase inhibitor 2A	1	0,03	PRDX3
Q9UJZ1	STOML2	Stomatin-like protein 2, mitochondrial	1	0,038	PRDX3
X1W128	RPL10	60S ribosomal protein L10	1	0,04	PRDX3
Q9Y224	RTRAF	RNA transcription, translation and transport factor protein	5,1	0	PRDX4
P32119	PRDX2	Peroxiredoxin-2	5,1	0	PRDX4
P00167	CYB5A	Cytochrome b5	4,2	0	PRDX4
H0YNW5	DUT	Deoxyuridine 5'-triphosphate nucleotidohydrolase	4	0	PRDX4
Q9NPH2	ISYNA1	Inositol-3-phosphate synthase 1	3,6	0	PRDX4
P10301	RRAS	Ras-related protein R-Ras	3,5	0	PRDX4
Q96CT7	CCDC124	Coiled-coil domain-containing protein 124	3,4	0	PRDX4
O96007	MOCS2	Molybdopterin synthase catalytic subunit	3,4	0	PRDX4
Q9P2B4	CTTNBP2NL	CTTNBP2 N-terminal-like protein	3,4	0	PRDX4
Q8NFC6	BOD1L1	Biorientation of chromosomes in cell division protein 1-like 1	3,3	0	PRDX4
P41250	GARS1	Glycine--tRNA ligase	3,3	0	PRDX4
O60664	PLIN3	Perilipin-3	3,2	0	PRDX4
P11802	CDK4	Cyclin-dependent kinase 4	3,2	0	PRDX4
Q9Y6A5	TACC3	Transforming acidic coiled-coil-containing protein 3	3,2	0,001	PRDX4
Q9Y3D6	FIS1	Mitochondrial fission 1 protein	3	0	PRDX4
Q9ULW0	TPX2	Targeting protein for Xklp2	3	0	PRDX4
Q6UW78	UQCC3	Ubiquinol-cytochrome-c reductase complex assembly factor 3	3	0	PRDX4
P61758	VBP1	Prefoldin subunit 3	2,8	0	PRDX4
P42574	CASP3	Caspase-3	2,8	0	PRDX4
Q9BPW8	NIPSNAP1	Protein NipSnap homolog 1	2,8	0	PRDX4
P26599	PTBP1	Polypyrimidine tract-binding protein 1	2,8	0	PRDX4
Q9NS69	TOMM22	Mitochondrial import receptor subunit TOM22 homolog	2,8	0	PRDX4
Q9NX55	HYPK	Huntingtin-interacting protein K	2,8	0,003	PRDX4

H3BRL3	UBFD1	Ubiquitin domain-containing protein UBFD1	2,7	0	PRDX4
B7Z7F3	RANBP3	Ran-binding protein 3	2,6	0	PRDX4
Q9H840	GEMIN7	Gem-associated protein 7	2,6	0	PRDX4
Q6WKZ4	RAB11FIP1	Rab11 family-interacting protein 1	2,6	0	PRDX4
Q8N9Q2	SREK1IP1	Protein SREK1IP1	2,6	0	PRDX4
P30740	SERPINB1	Leukocyte elastase inhibitor	2,6	0	PRDX4
A0A087WTM1	ROBO1	Roundabout homolog 1	2,6	0	PRDX4
G5EA06	MRPS27	28S ribosomal protein S27, mitochondrial	2,6	0,001	PRDX4
P53602	MVD	Diphosphomevalonate decarboxylase	2,6	0,001	PRDX4
Q96EA4	SPDL1	Protein Spindly	2,6	0,002	PRDX4
Q6PID6	TTC33	Tetratricopeptide repeat protein 33	2,6	0,026	PRDX4
Q96A10	ERVK3-1	Endogenous retrovirus group K3 member 1	2,6	0,028	PRDX4
P22234	PAICS	Multifunctional protein ADE2 [Includes: Phosphoribosylaminoimidazole-succinocarboxamide synthase	2,5	0	PRDX4
Q6IQ49	SDE2	Replication stress response regulator SDE2	2,5	0	PRDX4
P34897	SHMT2	Serine hydroxymethyltransferase, mitochondrial	2,5	0	PRDX4
E9PKG1	PRMT1	Protein arginine N-methyltransferase 1	2,5	0	PRDX4
Q13542	EIF4EBP2	Eukaryotic translation initiation factor 4E-binding protein 2	2,5	0,002	PRDX4
Q96KB5	PBK	Lymphokine-activated killer T-cell-originated protein kinase	2,5	0,002	PRDX4
P12955	PEPD	Xaa-Pro dipeptidase	2,5	0,003	PRDX4
H7BXI1	ESYT2	Extended synaptotagmin-2	2,4	0	PRDX4
O75223	GGCT	Gamma-glutamylcyclotransferase	2,4	0	PRDX4
Q9NP97	DYNLRB1	Dynein light chain roadblock-type 1	2,4	0	PRDX4
Q9H0U4	RAB1B	Ras-related protein Rab-1B	2,4	0	PRDX4
P42771	CDKN2A	Cyclin-dependent kinase inhibitor 2A	2,4	0	PRDX4
P12236	SLC25A6	ADP/ATP translocase 3	2,4	0	PRDX4
P56385	ATP5ME	ATP synthase subunit e, mitochondrial	2,4	0,001	PRDX4
P06132	UROD	Uroporphyrinogen decarboxylase	2,4	0,003	PRDX4
Q8WVC2	RPS21	40S ribosomal protein S21	2,3	0,001	PRDX4
Q9H2P9	DPH5	Diphthine methyl ester synthase	2,3	0,002	PRDX4
P49903	SEPHS1	Selenide, water dikinase 1	2,3	0,002	PRDX4
A6NGP5	JPT2	Jupiter microtubule-associated homolog 2	2,3	0,002	PRDX4
Q13126	MTAP	S-methyl-5'-thioadenosine phosphorylase	2,3	0,003	PRDX4
O14965	AURKA	Aurora kinase A	2,2	0	PRDX4
P48047	ATP5PO	ATP synthase subunit O, mitochondrial	2,2	0,001	PRDX4
Q9Y266	NUDC	Nuclear migration protein nudC	2,2	0,006	PRDX4
Q7Z4V5	HDGFL2	Hepatoma-derived growth factor-related protein 2	2,2	0,008	PRDX4
E7EV99	ADD1	Alpha-adducin	2,1	0	PRDX4
Q8N3X1	FNBP4	Formin-binding protein 4	2,1	0	PRDX4
O95831	AIFM1	Apoptosis-inducing factor 1, mitochondrial	2,1	0	PRDX4
P36542	ATP5F1C	ATP synthase subunit gamma, mitochondrial	2,1	0	PRDX4
Q9BTE1	DCTN5	Dynactin subunit 5	2,1	0,001	PRDX4
P47985	UQCRFS1	Cytochrome b-c1 complex subunit Rieske, mitochondrial	2,1	0,001	PRDX4
P00491	PNP	Purine nucleoside phosphorylase	2,1	0,002	PRDX4
P85037	FOXK1	Forkhead box protein K1	2,1	0,003	PRDX4
A0AVT1	UBA6	Ubiquitin-like modifier-activating enzyme 6	2,1	0,006	PRDX4
P07355	ANXA2	Annexin A2	2,1	0,028	PRDX4
P63000	RAC1	Ras-related C3 botulinum toxin substrate 1	2	0	PRDX4
P63167	DYNLL1	Dynein light chain 1, cytoplasmic	2	0,001	PRDX4
Q9NUP9	LIN7C	Protein lin-7 homolog C	2	0,003	PRDX4
P84085	ARF5	ADP-ribosylation factor 5	2	0,004	PRDX4
P35244	RPA3	Replication protein A 14 kDa subunit	2	0,004	PRDX4
O60547	GMDS	GDP-mannose 4,6 dehydratase	2	0,009	PRDX4
Q9HA64	FN3KRP	Ketosamine-3-kinase	2	0,009	PRDX4
P10599	TXN	Thioredoxin	2	0,028	PRDX4
Q9C0C2	TNKS1BP1	182 kDa tankyrase-1-binding protein	2	0,034	PRDX4
P62273	RPS29	40S ribosomal protein S29	2	0,038	PRDX4
P49642	PRIM1	DNA primase small subunit	1,9	0	PRDX4
Q9NUQ3	TXLNG	Gamma-taxilin	1,9	0,001	PRDX4
A0A087X2D5	MRPL45	39S ribosomal protein L45, mitochondrial	1,9	0,002	PRDX4
A4D1S0	KLRG2	Killer cell lectin-like receptor subfamily G member 2	1,9	0,002	PRDX4
P62304	SNRPE	Small nuclear ribonucleoprotein E	1,9	0,005	PRDX4
O94992	HEXIM1	Protein HEXIM1	1,9	0,005	PRDX4
Q5JRI1	SRSF10	Serine/arginine-rich-splicing factor 10	1,9	0,006	PRDX4
E9PGT1	TSN	Component 3 of promoter of RISC	1,9	0,007	PRDX4
Q9BSJ8	ESYT1	Extended synaptotagmin-1	1,9	0,008	PRDX4
P25705	ATP5F1A	ATP synthase subunit alpha, mitochondrial	1,8	0	PRDX4
Q12948	FOXC1	Forkhead box protein C1	1,8	0,001	PRDX4
Q9P258	RCC2	Protein RCC2	1,8	0,005	PRDX4

U3KQC1	WDR18	WD repeat-containing protein 18	1,8	0,005	PRDX4
P52888	THOP1	Thimet oligopeptidase	1,8	0,006	PRDX4
Q9Y4P1	ATG4B	Cysteine protease ATG4B	1,8	0,007	PRDX4
Q96DH6	MSI2	RNA-binding protein Musashi homolog 2	1,8	0,007	PRDX4
P00390	GSR	Glutathione reductase, mitochondrial	1,8	0,009	PRDX4
P54646	PRKAA2	5'-AMP-activated protein kinase catalytic subunit alpha-2	1,8	0,009	PRDX4
P61106	RAB14	Ras-related protein Rab-14	1,8	0,009	PRDX4
Q9NVJ2	ARL8B	ADP-ribosylation factor-like protein 8B	1,8	0,017	PRDX4
E9PDD6	BCL2L13	Bcl-2-like protein 13	1,8	0,023	PRDX4
P05091	ALDH2	Aldehyde dehydrogenase, mitochondrial	1,7	0	PRDX4
P31939	ATIC	Bifunctional purine biosynthesis protein ATIC	1,7	0	PRDX4
O00483	NDUFA4	Cytochrome c oxidase subunit NDUFA4	1,7	0,001	PRDX4
Q6PKG0	LARP1	La-related protein 1	1,7	0,001	PRDX4
P48147	PREP	Prolyl endopeptidase	1,7	0,003	PRDX4
Q9Y5K6	CD2AP	CD2-associated protein	1,7	0,006	PRDX4
Q9BZE1	MRPL37	39S ribosomal protein L37, mitochondrial	1,7	0,006	PRDX4
Q71UI9	H2AZ2	Histone H2A.V	1,7	0,008	PRDX4
Q16204	CCDC6	Coiled-coil domain-containing protein 6	1,7	0,011	PRDX4
Q9Y570	PPME1	Protein phosphatase methylesterase 1	1,7	0,011	PRDX4
P07384	CAPN1	Calpain-1 catalytic subunit	1,7	0,015	PRDX4
P49458	SRP9	Signal recognition particle 9 kDa protein	1,7	0,015	PRDX4
Q13541	EIF4EBP1	Eukaryotic translation initiation factor 4E-binding protein 1	1,7	0,018	PRDX4
J3KS31	ZNF207	BUB3-interacting and GLEBS motif-containing protein ZNF207	1,7	0,039	PRDX4
Q7Z434	MAVS	Mitochondrial antiviral-signaling protein	1,7	0,045	PRDX4
P35237	SERPINB6	Serpin B6	1,6	0,001	PRDX4
Q8TEX9	IPO4	Importin-4	1,6	0,001	PRDX4
Q9UJS0	SLC25A13	Calcium-binding mitochondrial carrier protein Aralar2	1,6	0,001	PRDX4
J3KN29	PSMD9	26S proteasome non-ATPase regulatory subunit 9	1,6	0,003	PRDX4
B4DDF4	CNN2	Calponin	1,6	0,003	PRDX4
Q8IYS1	PM20D2	Peptidase M20 domain-containing protein 2	1,6	0,006	PRDX4
Q32MZ4	LRRFIP1	Leucine-rich repeat flightless-interacting protein 1	1,6	0,013	PRDX4
G3V1Q4	SEPTIN7	Septin-7	1,6	0,017	PRDX4
O14949	UQCRQ	Cytochrome b-c1 complex subunit 8	1,6	0,021	PRDX4
B1AMS2	SEPTIN6	Septin 6, isoform CRA_b	1,6	0,021	PRDX4
J3KN87	J3KN87	>tr|J3KN87|J3KN87_HUMAN Serine/threonine-protein kinase Chk1 OS=Homo sapiens OX=9606 GN=CHEK1 PE=1 SV=1;>sp|O14757|CHK1_HUMAN Serine/threonine-protein kinase Chk1 OS=Homo sapiens OX=9606 GN=CHEK1 PE=1 SV=2;>tr|E7EPP6|E7EPP6_HUMAN Serine/threonine-protein k	1,6	0,022	PRDX4
P30041	PRDX6	Peroxiredoxin-6	1,6	0,028	PRDX4
A0A2R8YFH5	SEC23B	Protein transport protein SEC23	1,6	0,039	PRDX4
P51452	DUSP3	Dual specificity protein phosphatase 3	1,5	0	PRDX4
P61586	RHOA	Transforming protein RhoA	1,5	0	PRDX4
P00338	LDHA	L-lactate dehydrogenase A chain	1,5	0	PRDX4
P51149	RAB7A	Ras-related protein Rab-7a	1,5	0	PRDX4
P05141	SLC25A5	ADP/ATP translocase 2	1,5	0	PRDX4
P49593	PPM1F	Protein phosphatase 1F	1,5	0,001	PRDX4
E9PN17	ATP5MG	ATP synthase subunit g, mitochondrial	1,5	0,001	PRDX4
Q5QPM7	PSMF1	Proteasome inhibitor PI31 subunit	1,5	0,002	PRDX4
Q9GZS3	WDR61	WD repeat-containing protein 61	1,5	0,003	PRDX4
P62244	RPS15A	40S ribosomal protein S15a	1,5	0,003	PRDX4
Q9NYK5	MRPL39	39S ribosomal protein L39, mitochondrial	1,5	0,008	PRDX4
Q9H974	QTRT2	Queuine tRNA-ribosyltransferase accessory subunit 2	1,5	0,018	PRDX4
O75306	NDUFS2	NADH dehydrogenase [ubiquinone] iron-sulfur protein 2, mitochondrial	1,5	0,02	PRDX4
Q16186	ADRM1	Proteasomal ubiquitin receptor ADRM1	1,5	0,028	PRDX4
Q13190	STX5	Syntaxin-5	1,5	0,029	PRDX4
A0A1B0GUC3	FTO	Alpha-ketoglutarate-dependent dioxygenase FTO	1,5	0,03	PRDX4
P19022	CDH2	Cadherin-2	1,5	0,038	PRDX4
Q9UHV9	PFDN2	Prefoldin subunit 2	1,5	0,038	PRDX4
P61927	RPL37	60S ribosomal protein L37	1,5	0,04	PRDX4
O00487	PSMD14	26S proteasome non-ATPase regulatory subunit 14	1,4	0	PRDX4
P68104	EEF1A1	Elongation factor 1-alpha 1	1,4	0	PRDX4
O43242	PSMD3	26S proteasome non-ATPase regulatory subunit 3	1,4	0,001	PRDX4
Q9BV44	THUMPD3	THUMP domain-containing protein 3	1,4	0,001	PRDX4
P05388	RPLP0	60S acidic ribosomal protein P0	1,4	0,002	PRDX4
P68371	TUBB4B	Tubulin beta-4B chain	1,4	0,003	PRDX4
Q53EL6	PDCD4	Programmed cell death protein 4	1,4	0,004	PRDX4
Q9UKK9	NUDT5	ADP-sugar pyrophosphatase	1,4	0,004	PRDX4
J3QQZ9	PNPO	Pyridoxal 5'-phosphate synthase	1,4	0,02	PRDX4
Q96I15	SCLY	Selenocysteine lyase	1,4	0,024	PRDX4
Q99598	TSNAX	Translin-associated protein X	1,4	0,026	PRDX4

Q9Y277	VDAC3	Voltage-dependent anion-selective channel protein 3	1,4	0,027	PRDX4
Q96GK7	FAHD2A	Fumarylacetoacetate hydrolase domain-containing protein 2A	1,4	0,044	PRDX4
Q14694	USP10	Ubiquitin carboxyl-terminal hydrolase 10	1,3	0,001	PRDX4
Q92688	ANP32B	Acidic leucine-rich nuclear phosphoprotein 32 family member B	1,3	0,002	PRDX4
D6R938	CAMK2D	Calcium/calmodulin-dependent protein kinase	1,3	0,002	PRDX4
Q9BRP1	PDCD2L	Programmed cell death protein 2-like	1,3	0,003	PRDX4
Q9UHD1	CHORDC1	Cysteine and histidine-rich domain-containing protein 1	1,3	0,005	PRDX4
Q9BT25	HAUS8	HAUS augmin-like complex subunit 8	1,3	0,007	PRDX4
P63244	RACK1	Receptor of activated protein C kinase 1	1,3	0,008	PRDX4
P12235	SLC25A4	ADP/ATP translocase 1	1,3	0,02	PRDX4
Q8IVM0	CCDC50	Coiled-coil domain-containing protein 50	1,3	0,02	PRDX4
O14929	HAT1	Histone acetyltransferase type B catalytic subunit	1,3	0,024	PRDX4
Q8N6M0	OTUD6B	Deubiquitinase OTUD6B	1,3	0,035	PRDX4
P00492	HPRT1	Hypoxanthine-guanine phosphoribosyltransferase	1,3	0,042	PRDX4
Q96HS1	PGAM5	Serine/threonine-protein phosphatase PGAM5, mitochondrial	1,3	0,043	PRDX4
H0YLH3	RABGGTA	Geranylgeranyl transferase type-2 subunit alpha	1,3	0,044	PRDX4
Q92576	PHF3	PHD finger protein 3	1,3	0,047	PRDX4
Q86W42	THOC6	THO complex subunit 6 homolog	1,3	0,048	PRDX4
O95394	PGM3	Phosphoacetylglucosamine mutase	1,2	0	PRDX4
P17858	PFKL	ATP-dependent 6-phosphofructokinase, liver type	1,2	0	PRDX4
Q92769	HDAC2	Histone deacetylase 2	1,2	0,001	PRDX4
P22102	GART	Trifunctional purine biosynthetic protein adenosine-3 [Includes: Phosphoribosylamine--glycine ligase	1,2	0,001	PRDX4
P25398	RPS12	40S ribosomal protein S12	1,2	0,001	PRDX4
Q9UNM6	PSMD13	26S proteasome non-ATPase regulatory subunit 13	1,2	0,002	PRDX4
P31040	SDHA	Succinate dehydrogenase [ubiquinone] flavoprotein subunit, mitochondrial	1,2	0,002	PRDX4
P61313	RPL15	60S ribosomal protein L15	1,2	0,003	PRDX4
P22695	UQCRC2	Cytochrome b-c1 complex subunit 2, mitochondrial	1,2	0,004	PRDX4
O75400	PRPF40A	Pre-mRNA-processing factor 40 homolog A	1,2	0,004	PRDX4
O94903	PLPBP	Pyridoxal phosphate homeostasis protein	1,2	0,004	PRDX4
P49736	MCM2	DNA replication licensing factor MCM2	1,2	0,004	PRDX4
Q15738	NSDHL	Sterol-4-alpha-carboxylate 3-dehydrogenase, decarboxylating	1,2	0,006	PRDX4
O15144	ARPC2	Actin-related protein 2/3 complex subunit 2	1,2	0,007	PRDX4
P31930	UQCRC1	Cytochrome b-c1 complex subunit 1, mitochondrial	1,2	0,008	PRDX4
P21964	COMT	Catechol O-methyltransferase	1,2	0,008	PRDX4
O95373	IPO7	Importin-7	1,2	0,01	PRDX4
Q14232	EIF2B1	Translation initiation factor eIF-2B subunit alpha	1,2	0,011	PRDX4
Q9UJZ1	STOML2	Stomatin-like protein 2, mitochondrial	1,2	0,015	PRDX4
P47755	CAPZA2	F-actin-capping protein subunit alpha-2	1,2	0,017	PRDX4
P04181	OAT	Ornithine aminotransferase, mitochondrial	1,2	0,019	PRDX4
K7EJQ8	HDHD2	Haloacid dehalogenase-like hydrolase domain-containing protein 2	1,2	0,025	PRDX4
Q7L2J0	MEPCE	7SK snRNA methylphosphate capping enzyme	1,2	0,03	PRDX4
Q13177	PAK2	Serine/threonine-protein kinase PAK 2	1,2	0,032	PRDX4
O00231	PSMD11	26S proteasome non-ATPase regulatory subunit 11	1,2	0,034	PRDX4
P40222	TXLNA	Alpha-taxilin	1,2	0,035	PRDX4
Q9Y262	EIF3L	Eukaryotic translation initiation factor 3 subunit L	1,2	0,044	PRDX4
B4DLN1	B4DLN1	cDNA FLJ60124, highly similar to Mitochondrial dicarboxylate carrier	1,1	0,001	PRDX4
Q06203	PPAT	Amidophosphoribosyltransferase	1,1	0,002	PRDX4
A0A087WUT6	EIF5B	Eukaryotic translation initiation factor 5B	1,1	0,002	PRDX4
Q96BW9	TAMM41	Phosphatidate cytidylyltransferase, mitochondrial	1,1	0,003	PRDX4
P15121	AKR1B1	Aldo-keto reductase family 1 member B1	1,1	0,003	PRDX4
Q2M1P5	KIF7	Kinesin-like protein KIF7	1,1	0,004	PRDX4
P46778	RPL21	60S ribosomal protein L21	1,1	0,004	PRDX4
Q9Y5Y2	NUBP2	Cytosolic Fe-S cluster assembly factor NUBP2	1,1	0,004	PRDX4
P50914	RPL14	60S ribosomal protein L14	1,1	0,004	PRDX4
P35232	PHB	Prohibitin	1,1	0,004	PRDX4
P08574	CYC1	Cytochrome c1, heme protein, mitochondrial	1,1	0,01	PRDX4
P31153	MAT2A	S-adenosylmethionine synthase isoform type-2	1,1	0,012	PRDX4
P15880	RPS2	40S ribosomal protein S2	1,1	0,017	PRDX4
Q13618	CUL3	Cullin-3	1,1	0,017	PRDX4
P62851	RPS25	40S ribosomal protein S25	1,1	0,021	PRDX4
H0YDU8	PPP5C	Serine/threonine-protein phosphatase	1,1	0,022	PRDX4
Q5T760	SRSF11	Serine/arginine-rich-splicing factor 11	1,1	0,023	PRDX4
Q92922	SMARCC1	SWI/SNF complex subunit SMARCC1	1,1	0,027	PRDX4
Q14C86	GAPVD1	GTPase-activating protein and VPS9 domain-containing protein 1	1,1	0,034	PRDX4
A0A1B0GTG2	ALDH7A1	Alpha-aminoadipic semialdehyde dehydrogenase	1,1	0,037	PRDX4
O15143	ARPC1B	Actin-related protein 2/3 complex subunit 1B	1,1	0,038	PRDX4
P40926	MDH2	Malate dehydrogenase, mitochondrial	1	0	PRDX4
Q06210	GFPT1	Glutamine--fructose-6-phosphate aminotransferase [isomerizing] 1	1	0	PRDX4

P13639	EEF2	Elongation factor 2	1	0	PRDX4
O00303	EIF3F	Eukaryotic translation initiation factor 3 subunit F	1	0,002	PRDX4
P62888	RPL30	60S ribosomal protein L30	1	0,004	PRDX4
P62495	ETF1	Eukaryotic peptide chain release factor subunit 1	1	0,005	PRDX4
P49411	TUFM	Elongation factor Tu, mitochondrial	1	0,027	PRDX4
Q53H12	AGK	Acylglycerol kinase, mitochondrial	1	0,04	PRDX4
Q9Y224	RTRAF	RNA transcription, translation and transport factor protein	6,9	0	PRDX5
P32119	PRDX2	Peroxiredoxin-2	5,2	0	PRDX5
P00167	CYB5A	Cytochrome b5	4,1	0	PRDX5
Q96CT7	CCDC124	Coiled-coil domain-containing protein 124	3,3	0	PRDX5
O96007	MOCS2	Molybdopterin synthase catalytic subunit	3,3	0	PRDX5
P10301	RRAS	Ras-related protein R-Ras	3,3	0	PRDX5
H0YNW5	DUT	Deoxyuridine 5'-triphosphate nucleotidohydrolase	3,2	0	PRDX5
Q9P2B4	CTTNBP2NL	CTTNBP2 N-terminal-like protein	3,1	0	PRDX5
Q9Y3D6	FIS1	Mitochondrial fission 1 protein	2,9	0	PRDX5
Q6UW78	UQCC3	Ubiquinol-cytochrome-c reductase complex assembly factor 3	2,8	0	PRDX5
Q9ULW0	TPX2	Targeting protein for Xklp2	2,8	0	PRDX5
P63167	DYNLL1	Dynein light chain 1, cytoplasmic	2,7	0	PRDX5
Q9NX55	HYPK	Huntingtin-interacting protein K	2,7	0,005	PRDX5
Q9BPW8	NIPSNAP1	Protein NipSnap homolog 1	2,6	0	PRDX5
Q8N9Q2	SREK1IP1	Protein SREK1IP1	2,5	0,001	PRDX5
Q96AC1	FERMT2	Fermitin family homolog 2	2,5	0,002	PRDX5
O60664	PLIN3	Perilipin-3	2,5	0,003	PRDX5
P53602	MVD	Diphosphomevalonate decarboxylase	2,4	0,001	PRDX5
Q9H840	GEMIN7	Gem-associated protein 7	2,4	0,001	PRDX5
P55084	HADHB	Trifunctional enzyme subunit beta, mitochondrial	2,4	0,004	PRDX5
Q9NP97	DYNLRB1	Dynein light chain roadblock-type 1	2,3	0,001	PRDX5
Q6IQ49	SDE2	Replication stress response regulator SDE2	2,2	0	PRDX5
P62244	RPS15A	40S ribosomal protein S15a	2,2	0	PRDX5
Q9BZE1	MRPL37	39S ribosomal protein L37, mitochondrial	2,2	0,001	PRDX5
Q8WVC2	RPS21	40S ribosomal protein S21	2,2	0,003	PRDX5
P19105	MYL12A	Myosin regulatory light chain 12A	2,2	0,003	PRDX5
A0A0B4J1Z1	SRSF7	Serine/arginine-rich-splicing factor 7	2,2	0,004	PRDX5
Q13126	MTAP	S-methyl-5'-thioadenosine phosphorylase	2,2	0,006	PRDX5
P06132	UROD	Uroporphyrinogen decarboxylase	2,2	0,006	PRDX5
P30048	PRDX3	Thioredoxin-dependent peroxide reductase, mitochondrial	2,2	0,009	PRDX5
B4DDF4	CNN2	Calponin	2,1	0	PRDX5
Q9NS69	TOMM22	Mitochondrial import receptor subunit TOM22 homolog	2,1	0	PRDX5
P19338	NCL	Nucleolin	2,1	0	PRDX5
Q9GZS3	WDR61	WD repeat-containing protein 61	2,1	0	PRDX5
P48047	ATP5PO	ATP synthase subunit O, mitochondrial	2,1	0,002	PRDX5
Q9BYN0	SRXN1	Sulfiredoxin-1	2,1	0,018	PRDX5
O14965	AURKA	Aurora kinase A	2	0	PRDX5
O95373	IPO7	Importin-7	2	0	PRDX5
H3BRL3	UBFD1	Ubiquitin domain-containing protein UBFD1	2	0,004	PRDX5
Q9BTE1	DCTN5	Dynactin subunit 5	2	0,004	PRDX5
P00491	PNP	Purine nucleoside phosphorylase	2	0,004	PRDX5
E9PHS0	LANCL1	Glutathione S-transferase LANCL1	2	0,018	PRDX5
E9PKG1	PRMT1	Protein arginine N-methyltransferase 1	1,9	0	PRDX5
Q12948	FOXC1	Forkhead box protein C1	1,9	0,001	PRDX5
P53007	SLC25A1	Tricarboxylate transport protein, mitochondrial	1,9	0,004	PRDX5
P26599	PTBP1	Polypyrimidine tract-binding protein 1	1,9	0,004	PRDX5
P84085	ARF5	ADP-ribosylation factor 5	1,9	0,01	PRDX5
P35244	RPA3	Replication protein A 14 kDa subunit	1,9	0,01	PRDX5
P68133	ACTA1	Actin, alpha skeletal muscle	1,9	0,03	PRDX5
P15880	RPS2	40S ribosomal protein S2	1,8	0	PRDX5
P46778	RPL21	60S ribosomal protein L21	1,8	0	PRDX5
P40429	RPL13A	60S ribosomal protein L13a	1,8	0	PRDX5
A0A087WTM1	ROBO1	Roundabout homolog 1	1,8	0	PRDX5
P62266	RPS23	40S ribosomal protein S23	1,8	0,001	PRDX5
F2Z388	RPL35	60S ribosomal protein L35	1,8	0,001	PRDX5
Q96DH6	MSI2	RNA-binding protein Musashi homolog 2	1,8	0,006	PRDX5
G5EA06	MRPS27	28S ribosomal protein S27, mitochondrial	1,8	0,01	PRDX5
P62304	SNRPE	Small nuclear ribonucleoprotein E	1,8	0,013	PRDX5
Q86WA6	BPHL	Valacyclovir hydrolase	1,8	0,015	PRDX5
Q5JRI1	SRSF10	Serine/arginine-rich-splicing factor 10	1,8	0,016	PRDX5
P53597	SUCLG1	Succinate--CoA ligase [ADP/GDP-forming] subunit alpha, mitochondrial	1,7	0,001	PRDX5
P04181	OAT	Ornithine aminotransferase, mitochondrial	1,7	0,001	PRDX5
P63244	RACK1	Receptor of activated protein C kinase 1	1,7	0,001	PRDX5

Q9Y5K6	CD2AP	CD2-associated protein	1,7	0,002	PRDX5
O15143	ARPC1B	Actin-related protein 2/3 complex subunit 1B	1,7	0,018	PRDX5
P00390	GSR	Glutathione reductase, mitochondrial	1,7	0,022	PRDX5
Q15477	SKIV2L	Helicase SKI2W	1,7	0,023	PRDX5
Q13542	EIF4EBP2	Eukaryotic translation initiation factor 4E-binding protein 2	1,7	0,031	PRDX5
O95168	NDUFB4	NADH dehydrogenase [ubiquinone] 1 beta subcomplex subunit 4	1,6	0	PRDX5
Q02878	RPL6	60S ribosomal protein L6	1,6	0,001	PRDX5
A0A0U1RRM6	ENAH	Protein enabled homolog	1,6	0,001	PRDX5
O95861	BPNT1	3'(2'),5'-bisphosphate nucleotidase 1	1,6	0,003	PRDX5
P82930	MRPS34	28S ribosomal protein S34, mitochondrial	1,6	0,004	PRDX5
Q96I15	SCLY	Selenocysteine lyase	1,6	0,006	PRDX5
A0A087X2D5	MRPL45	39S ribosomal protein L45, mitochondrial	1,6	0,01	PRDX5
Q4VCS5	AMOT	Angiomotin	1,6	0,013	PRDX5
Q9Y4P1	ATG4B	Cysteine protease ATG4B	1,6	0,019	PRDX5
P16403	H1-2	Histone H1.2	1,6	0,031	PRDX5
P07384	CAPN1	Calpain-1 catalytic subunit	1,6	0,034	PRDX5
Q9NXH9	TRMT1	tRNA	1,6	0,039	PRDX5
P14174	MIF	Macrophage migration inhibitory factor	1,6	0,045	PRDX5
E9PDD6	BCL2L13	Bcl-2-like protein 13	1,6	0,045	PRDX5
Q7Z4V5	HDGFL2	Hepatoma-derived growth factor-related protein 2	1,6	0,048	PRDX5
P61313	RPL15	60S ribosomal protein L15	1,5	0	PRDX5
P36542	ATP5F1C	ATP synthase subunit gamma, mitochondrial	1,5	0	PRDX5
E9PEJ4	DLAT	Acetyltransferase component of pyruvate dehydrogenase complex	1,5	0,001	PRDX5
P35237	SERPINB6	Serpin B6	1,5	0,001	PRDX5
C9J9K3	RPSA	40S ribosomal protein SA	1,5	0,001	PRDX5
G5E9W7	MRPS22	28S ribosomal protein S22, mitochondrial	1,5	0,002	PRDX5
P63000	RAC1	Ras-related C3 botulinum toxin substrate 1	1,5	0,002	PRDX5
Q8TEX9	IPO4	Importin-4	1,5	0,002	PRDX5
P61353	RPL27	60S ribosomal protein L27	1,5	0,004	PRDX5
Q7L2J0	MEPCE	7SK snRNA methylphosphate capping enzyme	1,5	0,011	PRDX5
Q71UI9	H2AZ2	Histone H2A.V	1,5	0,022	PRDX5
Q9Y2R5	MRPS17	28S ribosomal protein S17, mitochondrial	1,5	0,028	PRDX5
Q9H7N4	SCAF1	Splicing factor, arginine/serine-rich 19	1,5	0,032	PRDX5
P42345	MTOR	Serine/threonine-protein kinase mTOR	1,5	0,035	PRDX5
G3V1Q4	SEPTIN7	Septin-7	1,5	0,038	PRDX5
Q16762	TST	Thiosulfate sulfurtransferase	1,5	0,039	PRDX5
Q6P1L8	MRPL14	39S ribosomal protein L14, mitochondrial	1,5	0,048	PRDX5
P23921	RRM1	Ribonucleoside-diphosphate reductase large subunit	1,4	0	PRDX5
P12236	SLC25A6	ADP/ATP translocase 3	1,4	0	PRDX5
P62081	RPS7	40S ribosomal protein S7	1,4	0	PRDX5
P34897	SHMT2	Serine hydroxymethyltransferase, mitochondrial	1,4	0,001	PRDX5
P50914	RPL14	60S ribosomal protein L14	1,4	0,001	PRDX5
P62750	RPL23A	60S ribosomal protein L23a	1,4	0,001	PRDX5
P51452	DUSP3	Dual specificity protein phosphatase 3	1,4	0,001	PRDX5
P62269	RPS18	40S ribosomal protein S18	1,4	0,001	PRDX5
P43897	TSFM	Elongation factor Ts, mitochondrial	1,4	0,001	PRDX5
Q9NQT4	EXOSC5	Exosome complex component RRP46	1,4	0,001	PRDX5
P22570	FDXR	NADPH:adrenodoxin oxidoreductase, mitochondrial	1,4	0,001	PRDX5
P62495	ETF1	Eukaryotic peptide chain release factor subunit 1	1,4	0,002	PRDX5
P68371	TUBB4B	Tubulin beta-4B chain	1,4	0,004	PRDX5
Q7L1Q6	BZW1	Basic leucine zipper and W2 domain-containing protein 1	1,4	0,005	PRDX5
Q96IU4	ABHD14B	Protein ABHD14B	1,4	0,006	PRDX5
O94973	AP2A2	AP-2 complex subunit alpha-2	1,4	0,007	PRDX5
P12277	CKB	Creatine kinase B-type	1,4	0,013	PRDX5
Q86XI2	NCAPG2	Condensin-2 complex subunit G2	1,4	0,024	PRDX5
P62829	RPL23	60S ribosomal protein L23	1,4	0,025	PRDX5
Q13613	MTMR1	Myotubularin-related protein 1	1,4	0,03	PRDX5
O00629	KPNA4	Importin subunit alpha-3	1,4	0,033	PRDX5
Q9UHQ9	CYB5R1	NADH-cytochrome b5 reductase 1	1,4	0,034	PRDX5
Q5VW32	BROX	BRO1 domain-containing protein BROX	1,4	0,041	PRDX5
O75306	NDUFS2	NADH dehydrogenase [ubiquinone] iron-sulfur protein 2, mitochondrial	1,4	0,046	PRDX5
P68104	EEF1A1	Elongation factor 1-alpha 1	1,3	0	PRDX5
B4DLN1	B4DLN1	cDNA FLJ60124, highly similar to Mitochondrial dicarboxylate carrier	1,3	0	PRDX5
Q8WUH6	TMEM263	Transmembrane protein 263	1,3	0	PRDX5
P05091	ALDH2	Aldehyde dehydrogenase, mitochondrial	1,3	0,001	PRDX5
Q92688	ANP32B	Acidic leucine-rich nuclear phosphoprotein 32 family member B	1,3	0,002	PRDX5
O00442	RTCA	RNA 3'-terminal phosphate cyclase	1,3	0,003	PRDX5
P11172	UMPS	Uridine 5'-monophosphate synthase	1,3	0,005	PRDX5
Q86U42	PABPN1	Polyadenylate-binding protein 2	1,3	0,005	PRDX5

A4D1S0	KLRG2	Killer cell lectin-like receptor subfamily G member 2	1,3	0,006	PRDX5
Q9NPH2	ISYNA1	Inositol-3-phosphate synthase 1	1,3	0,008	PRDX5
D6R938	CAMK2D	Calcium/calmodulin-dependent protein kinase	1,3	0,01	PRDX5
P84103	SRSF3	Serine/arginine-rich splicing factor 3	1,3	0,01	PRDX5
E9PHN7	GSTM2	Glutathione S-transferase Mu 2	1,3	0,01	PRDX5
X1WI28	RPL10	60S ribosomal protein L10	1,3	0,012	PRDX5
Q00610	CLTC	Clathrin heavy chain 1	1,3	0,016	PRDX5
O75223	GGCT	Gamma-glutamylcyclotransferase	1,3	0,016	PRDX5
Q14232	EIF2B1	Translation initiation factor eIF-2B subunit alpha	1,3	0,016	PRDX5
P48634	PRRC2A	Protein PRRC2A	1,3	0,024	PRDX5
P35606	COPB2	Coatomer subunit beta'	1,3	0,031	PRDX5
Q9Y394	DHRS7	Dehydrogenase/reductase SDR family member 7	1,3	0,035	PRDX5
E5RGR0	LYPLA1	Acyl-protein thioesterase 1	1,3	0,041	PRDX5
Q9BXW7	HDHD5	Haloacid dehalogenase-like hydrolase domain-containing 5	1,2	0	PRDX5
P09211	GSTP1	Glutathione S-transferase P	1,2	0,001	PRDX5
Q14694	USP10	Ubiquitin carboxyl-terminal hydrolase 10	1,2	0,001	PRDX5
Q6NVY1	HIBCH	3-hydroxyisobutyryl-CoA hydrolase, mitochondrial	1,2	0,001	PRDX5
P62888	RPL30	60S ribosomal protein L30	1,2	0,001	PRDX5
P61586	RHOA	Transforming protein RhoA	1,2	0,001	PRDX5
P49327	FASN	Fatty acid synthase	1,2	0,001	PRDX5
Q15645	TRIP13	Pachytene checkpoint protein 2 homolog	1,2	0,006	PRDX5
Q9Y2R9	MRPS7	28S ribosomal protein S7, mitochondrial	1,2	0,007	PRDX5
Q00688	FKBP3	Peptidyl-prolyl cis-trans isomerase FKBP3	1,2	0,008	PRDX5
O75400	PRPF40A	Pre-mRNA-processing factor 40 homolog A	1,2	0,008	PRDX5
Q14240	EIF4A2	Eukaryotic initiation factor 4A-II	1,2	0,011	PRDX5
P42771	CDKN2A	Cyclin-dependent kinase inhibitor 2A	1,2	0,014	PRDX5
Q2TAL8	QRICH1	Glutamine-rich protein 1	1,2	0,017	PRDX5
Q5T7C4	HMGB1	High mobility group protein B1	1,2	0,022	PRDX5
P51570	GALK1	Galactokinase	1,2	0,025	PRDX5
P08758	ANXA5	Annexin A5	1,2	0,025	PRDX5
Q9NTJ5	SACM1L	Phosphatidylinositol-3-phosphatase SAC1	1,2	0,03	PRDX5
Q13283	G3BP1	Ras GTPase-activating protein-binding protein 1	1,2	0,032	PRDX5
Q9BW92	TARS2	Threonine--tRNA ligase, mitochondrial	1,2	0,033	PRDX5
P05141	SLC25A5	ADP/ATP translocase 2	1,1	0	PRDX5
P36578	RPL4	60S ribosomal protein L4	1,1	0,001	PRDX5
Q9NQ88	TIGAR	Fructose-2,6-bisphosphatase TIGAR	1,1	0,001	PRDX5
Q9Y2Z4	YARS2	Tyrosine--tRNA ligase, mitochondrial	1,1	0,001	PRDX5
P17858	PFKL	ATP-dependent 6-phosphofructokinase, liver type	1,1	0,001	PRDX5
O95456	PSMG1	Proteasome assembly chaperone 1	1,1	0,003	PRDX5
Q00796	SORD	Sorbitol dehydrogenase	1,1	0,004	PRDX5
P18077	RPL35A	60S ribosomal protein L35a	1,1	0,005	PRDX5
G5EA31	SEC24C	Protein transport protein Sec24C	1,1	0,007	PRDX5
Q13595	TRA2A	Transformer-2 protein homolog alpha	1,1	0,01	PRDX5
P63010	AP2B1	AP-2 complex subunit beta	1,1	0,01	PRDX5
O43795	MYO1B	Unconventional myosin-Ib	1,1	0,012	PRDX5
Q7Z2K8	GPRIN1	G protein-regulated inducer of neurite outgrowth 1	1,1	0,017	PRDX5
Q9GZT3	SLIRP	SRA stem-loop-interacting RNA-binding protein, mitochondrial	1,1	0,021	PRDX5
Q96F45	ZNF503	Zinc finger protein 503	1,1	0,023	PRDX5
P23258	TUBG1	Tubulin gamma-1 chain	1,1	0,024	PRDX5
Q9NR45	NANS	Sialic acid synthase	1,1	0,032	PRDX5
P62879	GNB2	Guanine nucleotide-binding protein G(I)/G(S)/G(T) subunit beta-2	1,1	0,033	PRDX5
P54886	ALDH18A1	Delta-1-pyrroline-5-carboxylate synthase	1,1	0,039	PRDX5
E7ETK0	RPS24	40S ribosomal protein S24	1	0,001	PRDX5
P62701	RPS4X	40S ribosomal protein S4, X isoform	1	0,006	PRDX5
E9PN17	ATP5MG	ATP synthase subunit g, mitochondrial	1	0,011	PRDX5
Q9BT25	HAUS8	HAUS augmin-like complex subunit 8	1	0,018	PRDX5
H0YDU8	PPP5C	Serine/threonine-protein phosphatase	1	0,027	PRDX5
O00483	NDUFA4	Cytochrome c oxidase subunit NDUFA4	1	0,029	PRDX5
P62820	RAB1A	Ras-related protein Rab-1A	1	0,032	PRDX5
Q6PKG0	LARP1	La-related protein 1	1	0,038	PRDX5
Q9HAV4	XPO5	Exportin-5	1	0,038	PRDX5
O94925	GLS	Glutaminase kidney isoform, mitochondrial	1	0,04	PRDX5
A0A1B0GW38	CBL	E3 ubiquitin-protein ligase CBL	1	0,045	PRDX5
PRDX3 -specific interactors					
P62805	H4C1	Histone H4	4,9	0	PRDX1
P02790	HPX	Hemopexin	4,5	0	PRDX1
O60506	SYNCRIP	Heterogeneous nuclear ribonucleoprotein Q	4,2	0	PRDX1
O76094	SRP72	Signal recognition particle subunit SRP72	4,2	0	PRDX1
P61106	RAB14	Ras-related protein Rab-14	4	0	PRDX1

P42704	LRPPRC	Leucine-rich PPR motif-containing protein, mitochondrial	3,9	0	PRDX1
P05387	RPLP2	60S acidic ribosomal protein P2	3,4	0	PRDX1
P63167	DYNLL1	Dynein light chain 1, cytoplasmic	3,3	0	PRDX1
Q4J6C6	PREPL	Prolyl endopeptidase-like	3,3	0	PRDX1
Q14257	RCN2	Reticulocalbin-2	3,3	0	PRDX1
P40616	ARL1	ADP-ribosylation factor-like protein 1	3,1	0	PRDX1
P35637	FUS	RNA-binding protein FUS	3,1	0	PRDX1
O95163	ELP1	Elongator complex protein 1	3,1	0	PRDX1
Q15388	TOMM20	Mitochondrial import receptor subunit TOM20 homolog	3,1	0,002	PRDX1
P05386	RPLP1	60S acidic ribosomal protein P1	3	0	PRDX1
P63244	RACK1	Receptor of activated protein C kinase 1	2,9	0	PRDX1
P78417	GSTO1	Glutathione S-transferase omega-1	2,9	0	PRDX1
Q8N5K1	CISD2	CDGSH iron-sulfur domain-containing protein 2	2,9	0,003	PRDX1
P61353	RPL27	60S ribosomal protein L27	2,8	0	PRDX1
P26196	DDX6	Probable ATP-dependent RNA helicase DDX6	2,8	0	PRDX1
P35606	COPB2	Coatomer subunit beta'	2,7	0	PRDX1
P16435	POR	NADPH--cytochrome P450 reductase	2,7	0	PRDX1
Q9UBF2	COPG2	Coatomer subunit gamma-2	2,7	0	PRDX1
P40429	RPL13A	60S ribosomal protein L13a	2,7	0	PRDX1
E9PHS0	LANCL1	Glutathione S-transferase LANCL1	2,7	0,001	PRDX1
Q8N2K0	ABHD12	Lysophosphatidylserine lipase ABHD12	2,7	0,003	PRDX1
O94925	GLS	Glutaminase kidney isoform, mitochondrial	2,6	0	PRDX1
P23588	EIF4B	Eukaryotic translation initiation factor 4B	2,6	0	PRDX1
P50502	ST13	Hsc70-interacting protein	2,6	0	PRDX1
Q9UBB4	ATXN10	Ataxin-10	2,6	0	PRDX1
Q07820	MCL1	Induced myeloid leukemia cell differentiation protein Mcl-1	2,6	0,001	PRDX1
P51148	RAB5C	Ras-related protein Rab-5C	2,6	0,005	PRDX1
Q9NVP1	DDX18	ATP-dependent RNA helicase DDX18	2,5	0	PRDX1
P16615	ATP2A2	Sarcoplasmic/endoplasmic reticulum calcium ATPase 2	2,5	0	PRDX1
Q96CS3	FAF2	FAS-associated factor 2	2,5	0	PRDX1
P98194	ATP2C1	Calcium-transporting ATPase type 2C member 1	2,5	0,001	PRDX1
Q14690	PDCD11	Protein RRP5 homolog	2,5	0,001	PRDX1
P68133	ACTA1	Actin, alpha skeletal muscle	2,5	0,003	PRDX1
Q7Z434	MAVS	Mitochondrial antiviral-signaling protein	2,5	0,003	PRDX1
P11388	TOP2A	DNA topoisomerase 2-alpha	2,4	0	PRDX1
Q8TEX9	IPO4	Importin-4	2,4	0	PRDX1
Q92769	HDAC2	Histone deacetylase 2	2,4	0	PRDX1
P19338	NCL	Nucleolin	2,4	0	PRDX1
G5EA06	MRPS27	28S ribosomal protein S27, mitochondrial	2,4	0,001	PRDX1
E7ETZ4	BZW2	Basic leucine zipper and W2 domain-containing protein 2	2,4	0,001	PRDX1
Q92621	NUP205	Nuclear pore complex protein Nup205	2,3	0	PRDX1
O14980	XPO1	Exportin-1	2,3	0	PRDX1
P62314	SNRPD1	Small nuclear ribonucleoprotein Sm D1	2,3	0	PRDX1
P27797	CALR	Calreticulin	2,3	0	PRDX1
Q9H3P7	ACBD3	Golgi resident protein GCP60	2,3	0	PRDX1
Q9ULC3	RAB23	Ras-related protein Rab-23	2,3	0,001	PRDX1
Q5QNY5	PEX19	Peroxin-19	2,3	0,004	PRDX1
Q93008	USP9X	Probable ubiquitin carboxyl-terminal hydrolase FAF-X	2,2	0	PRDX1
P41252	IARS1	Isoleucine--tRNA ligase, cytoplasmic	2,2	0	PRDX1
O95373	IPO7	Importin-7	2,2	0	PRDX1
Q15393	SF3B3	Splicing factor 3B subunit 3	2,2	0	PRDX1
Q9H0A0	NAT10	RNA cytidine acetyltransferase	2,2	0	PRDX1
O75832	PSMD10	26S proteasome non-ATPase regulatory subunit 10	2,2	0	PRDX1
Q92688	ANP32B	Acidic leucine-rich nuclear phosphoprotein 32 family member B	2,2	0	PRDX1
K7ERF1	EIF3K	Eukaryotic translation initiation factor 3 subunit K	2,2	0	PRDX1
Q5SY16	NOL9	Polynucleotide 5'-hydroxyl-kinase NOL9	2,2	0,001	PRDX1
Q96EY7	PTCD3	Pentatricopeptide repeat domain-containing protein 3, mitochondrial	2,2	0,001	PRDX1
P28288	ABCD3	ATP-binding cassette sub-family D member 3	2,2	0,001	PRDX1
Q8NI27	THOC2	THO complex subunit 2	2,2	0,001	PRDX1
O96008	TOMM40	Mitochondrial import receptor subunit TOM40 homolog	2,2	0,017	PRDX1
P08758	ANXA5	Annexin A5	2,1	0	PRDX1
Q5VW32	BROX	BRO1 domain-containing protein BROX	2,1	0	PRDX1
Q5VT66	MTARC1	Mitochondrial amidoxime-reducing component 1	2,1	0	PRDX1
Q9H8Y8	GORASP2	Golgi reassembly-stacking protein 2	2,1	0	PRDX1
P06730	EIF4E	Eukaryotic translation initiation factor 4E	2,1	0	PRDX1
O00203	AP3B1	AP-3 complex subunit beta-1	2,1	0	PRDX1
P61923	COPZ1	Coatomer subunit zeta-1	2,1	0	PRDX1
Q8TC07	TBC1D15	TBC1 domain family member 15	2,1	0	PRDX1
O94826	TOMM70	Mitochondrial import receptor subunit TOM70	2,1	0	PRDX1

P43034	PAFAH1B1	Platelet-activating factor acetylhydrolase IB subunit beta	2,1	0	PRDX1
Q01085	TIAL1	Nucleolysin TIAR	2,1	0,001	PRDX1
Q9BQG0	MYBBP1A	Myb-binding protein 1A	2,1	0,001	PRDX1
B3KUS5	USP30	Ubiquitin carboxyl-terminal hydrolase	2,1	0,002	PRDX1
Q8N4V1	MMGT1	Membrane magnesium transporter 1	2,1	0,002	PRDX1
D6RA00	ENOPH1	Enolase-phosphatase E1	2,1	0,002	PRDX1
O95104	SCAF4	SR-related and CTD-associated factor 4	2,1	0,002	PRDX1
Q8N335	GPD1L	Glycerol-3-phosphate dehydrogenase 1-like protein	2,1	0,002	PRDX1
A0A3B3ISV3	COL4A1	Collagen alpha-1(IV) chain	2,1	0,002	PRDX1
Q53GQ0	HSD17B12	Very-long-chain 3-oxoacyl-CoA reductase	2,1	0,003	PRDX1
A0A0A0MS29	MFF	Mitochondrial fission factor	2,1	0,004	PRDX1
Q8N806	UBR7	Putative E3 ubiquitin-protein ligase UBR7	2,1	0,006	PRDX1
P36957	DLST	Dihydrolipoyllysine-residue succinyltransferase component of 2-oxoglutarate dehydrogenase complex, mitochondrial	2	0	PRDX1
O75381	PEX14	Peroxisomal membrane protein PEX14	2	0	PRDX1
O94874	UFL1	E3 UFM1-protein ligase 1	2	0	PRDX1
Q9Y678	COPG1	Coatomer subunit gamma-1	2	0	PRDX1
O00410	IPO5	Importin-5	2	0	PRDX1
P12236	SLC25A6	ADP/ATP translocase 3	2	0	PRDX1
P14324	FDPS	Farnesyl pyrophosphate synthase	2	0	PRDX1
Q92973	TNPO1	Transportin-1	2	0	PRDX1
P98175	RBM10	RNA-binding protein 10	2	0	PRDX1
Q9BVP2	GNL3	Guanine nucleotide-binding protein-like 3	2	0,001	PRDX1
O15269	SPTLC1	Serine palmitoyltransferase 1	2	0,001	PRDX1
O75489	NDUFS3	NADH dehydrogenase [ubiquinone] iron-sulfur protein 3, mitochondrial	2	0,002	PRDX1
Q8N6T3	ARFGAP1	ADP-ribosylation factor GTPase-activating protein 1	2	0,003	PRDX1
O15144	ARPC2	Actin-related protein 2/3 complex subunit 2	2	0,003	PRDX1
Q9NQ29	LUC7L	Putative RNA-binding protein Luc7-like 1	2	0,003	PRDX1
Q9H9P8	L2HGDH	L-2-hydroxyglutarate dehydrogenase, mitochondrial	2	0,003	PRDX1
P19174	PLCG1	1-phosphatidylinositol 4,5-bisphosphate phosphodiesterase gamma-1	2	0,003	PRDX1
Q9BSJ8	ESYT1	Extended synaptotagmin-1	2	0,003	PRDX1
P51809	VAMP7	Vesicle-associated membrane protein 7	2	0,015	PRDX1
P30048	PRDX3	Thioredoxin-dependent peroxide reductase, mitochondrial	14,7	0	PRDX1
O94905	ERLIN2	Erlin-2	1,9	0	PRDX1
P15374	UCHL3	Ubiquitin carboxyl-terminal hydrolase isozyme L3	1,9	0	PRDX1
P49321	NASP	Nuclear autoantigenic sperm protein	1,9	0	PRDX1
E7ESY4	MTA1	Metastasis-associated protein MTA1	1,9	0	PRDX1
P42166	TMPO	Lamina-associated polypeptide 2, isoform alpha	1,9	0	PRDX1
P00387	CYB5R3	NADH-cytochrome b5 reductase 3	1,9	0	PRDX1
P35237	SERPINB6	Serpin B6	1,9	0,001	PRDX1
Q9Y679	AUP1	Lipid droplet-regulating VLDL assembly factor AUP1	1,9	0,002	PRDX1
O96019	ACTL6A	Actin-like protein 6A	1,9	0,003	PRDX1
B9A018	USP39	U4/U6.U5 tri-snRNP-associated protein 2	1,9	0,003	PRDX1
Q9BZK7	TBL1XR1	F-box-like/WD repeat-containing protein TBL1XR1	1,9	0,003	PRDX1
Q5JR04	MOV10	RNA helicase	1,9	0,004	PRDX1
P51398	DAP3	28S ribosomal protein S29, mitochondrial	1,9	0,005	PRDX1
Q13190	STX5	Syntaxin-5	1,9	0,005	PRDX1
E9PKG1	PRMT1	Protein arginine N-methyltransferase 1	1,9	0,006	PRDX1
P84085	ARF5	ADP-ribosylation factor 5	1,9	0,011	PRDX1
Q9NQG6	MIEF1	Mitochondrial dynamics protein MID51	1,9	0,014	PRDX1
P13667	PDIA4	Protein disulfide-isomerase A4	1,9	0,017	PRDX1
Q14964	RAB39A	Ras-related protein Rab-39A	1,9	0,039	PRDX1
P08243	ASNS	Asparagine synthetase [glutamine-hydrolyzing]	1,8	0	PRDX1
Q9UIG0	BAZ1B	Tyrosine-protein kinase BAZ1B	1,8	0	PRDX1
O00268	TAF4	Transcription initiation factor TFIID subunit 4	1,8	0	PRDX1
P09211	GSTP1	Glutathione S-transferase P	1,8	0	PRDX1
G8JLH9	STAT3	Signal transducer and activator of transcription	1,8	0	PRDX1
Q8TC12	RDH11	Retinol dehydrogenase 11	1,8	0	PRDX1
Q9HAV4	XPO5	Exportin-5	1,8	0,001	PRDX1
O00231	PSMD11	26S proteasome non-ATPase regulatory subunit 11	1,8	0,001	PRDX1
P31689	DNAJA1	DnaJ homolog subfamily A member 1	1,8	0,001	PRDX1
O75131	CPNE3	Copine-3	1,8	0,001	PRDX1
Q5VYK3	ECPAS	Proteasome adapter and scaffold protein ECM29	1,8	0,004	PRDX1
Q9P287	BCCIP	BRCA2 and CDKN1A-interacting protein	1,8	0,006	PRDX1
O00483	NDUFA4	Cytochrome c oxidase subunit NDUFA4	1,8	0,006	PRDX1
P07384	CAPN1	Calpain-1 catalytic subunit	1,8	0,006	PRDX1
Q13951	CBFB	Core-binding factor subunit beta	1,8	0,007	PRDX1
G3V1C3	API5	Apoptosis inhibitor 5	1,8	0,007	PRDX1
Q15293	RCN1	Reticulocalbin-1	1,8	0,008	PRDX1

Q9HB07	MYG1	MYG1 exonuclease	1,8	0,008	PRDX1
P46940	IQGAP1	Ras GTPase-activating-like protein IQGAP1	1,8	0,009	PRDX1
H0Y5L2	ECHDC1	Ethylmalonyl-CoA decarboxylase	1,8	0,011	PRDX1
P56962	STX17	Syntaxin-17	1,8	0,014	PRDX1
O60502	OGA	Protein O-GlcNAcase	1,8	0,014	PRDX1
Q8NF37	LPCAT1	Lysophosphatidylcholine acyltransferase 1	1,8	0,018	PRDX1
Q9Y657	SPIN1	Spindlin-1	1,8	0,028	PRDX1
A0A0B4J1Z1	SRSF7	Serine/arginine-rich-splicing factor 7	1,8	0,034	PRDX1
O95376	ARIH2	E3 ubiquitin-protein ligase ARIH2	1,7	0	PRDX1
P11387	TOP1	DNA topoisomerase 1	1,7	0	PRDX1
O43707	ACTN4	Alpha-actinin-4	1,7	0	PRDX1
Q14232	EIF2B1	Translation initiation factor eIF-2B subunit alpha	1,7	0	PRDX1
P53618	COPB1	Coatomer subunit beta	1,7	0	PRDX1
C9J4Z3	RPL37A	60S ribosomal protein L37a	1,7	0	PRDX1
P38117	ETFB	Electron transfer flavoprotein subunit beta	1,7	0	PRDX1
O95573	ACSL3	Long-chain-fatty-acid--CoA ligase 3	1,7	0	PRDX1
Q15691	MAPRE1	Microtubule-associated protein RP/EB family member 1	1,7	0	PRDX1
Q9NV70	EXOC1	Exocyst complex component 1	1,7	0	PRDX1
P15121	AKR1B1	Aldo-keto reductase family 1 member B1	1,7	0	PRDX1
Q9UKG1	APPL1	DCC-interacting protein 13-alpha	1,7	0	PRDX1
O95292	VAPB	Vesicle-associated membrane protein-associated protein B/C	1,7	0	PRDX1
Q16531	DDB1	DNA damage-binding protein 1	1,7	0,001	PRDX1
P42224	STAT1	Signal transducer and activator of transcription 1-alpha/beta	1,7	0,002	PRDX1
G3V529	DDX24	RNA helicase	1,7	0,003	PRDX1
Q9BXJ9	NAA15	N-alpha-acetyltransferase 15, NatA auxiliary subunit	1,7	0,006	PRDX1
P22830	FECH	Ferrochelatase, mitochondrial	1,7	0,007	PRDX1
Q9Y262	EIF3L	Eukaryotic translation initiation factor 3 subunit L	1,7	0,007	PRDX1
P04844	RPN2	Dolichyl-diphosphooligosaccharide--protein glycosyltransferase subunit 2	1,7	0,01	PRDX1
D6RB59	EXOC3	Exocyst complex component 3	1,7	0,013	PRDX1
Q9NZ32	ACTR10	Actin-related protein 10	1,7	0,014	PRDX1
Q15717	ELAVL1	ELAV-like protein 1	1,7	0,014	PRDX1
Q9NWB6	ARGLU1	Arginine and glutamate-rich protein 1	1,7	0,015	PRDX1
Q96IU4	ABHD14B	Protein ABHD14B	1,7	0,016	PRDX1
Q14789	GOLGB1	Golgin subfamily B member 1	1,7	0,016	PRDX1
P35579	MYH9	Myosin-9	1,7	0,026	PRDX1
Q8N573	OXR1	Oxidation resistance protein 1	1,7	0,031	PRDX1
J3KPG2	TPT1	Translationally-controlled tumor protein	1,7	0,037	PRDX1
Q9Y3Z3	SAMHD1	Deoxynucleoside triphosphate triphosphohydrolase SAMHD1	1,6	0	PRDX1
P05455	SSB	Lupus La protein	1,6	0	PRDX1
G5EA31	SEC24C	Protein transport protein Sec24C	1,6	0	PRDX1
P23921	RRM1	Ribonucleoside-diphosphate reductase large subunit	1,6	0	PRDX1
P04181	OAT	Ornithine aminotransferase, mitochondrial	1,6	0,001	PRDX1
Q15054	POLD3	DNA polymerase delta subunit 3	1,6	0,001	PRDX1
P55769	SNU13	NHP2-like protein 1	1,6	0,001	PRDX1
Q03701	CEBPZ	CCAAT/enhancer-binding protein zeta	1,6	0,002	PRDX1
Q9Y3T9	NOC2L	Nucleolar complex protein 2 homolog	1,6	0,002	PRDX1
P33992	MCM5	DNA replication licensing factor MCM5	1,6	0,003	PRDX1
P18031	PTPN1	Tyrosine-protein phosphatase non-receptor type 1	1,6	0,004	PRDX1
P22314	UBA1	Ubiquitin-like modifier-activating enzyme 1	1,6	0,005	PRDX1
Q8WTT2	NOC3L	Nucleolar complex protein 3 homolog	1,6	0,006	PRDX1
Q96T23	RSF1	Remodeling and spacing factor 1	1,6	0,007	PRDX1
O15397	IPO8	Importin-8	1,6	0,012	PRDX1
Q5T3Q7	HEATR1	HEAT repeat-containing protein 1	1,6	0,013	PRDX1
X6RM00	ERC1	ELKS/Rab6-interacting/CAST family member 1	1,6	0,013	PRDX1
J3QRD1	ALDH3A2	Aldehyde dehydrogenase family 3 member A2	1,6	0,014	PRDX1
Q9NYB0	TERF2IP	Telomeric repeat-binding factor 2-interacting protein 1	1,6	0,014	PRDX1
H3BV80	RNPS1	RNA-binding protein with serine-rich domain 1	1,6	0,015	PRDX1
Q9Y6Y0	IVNS1ABP	Influenza virus NS1A-binding protein	1,6	0,016	PRDX1
Q14204	DYNC1H1	Cytoplasmic dynein 1 heavy chain 1	1,6	0,017	PRDX1
Q9NVI1	FANCI	Fanconi anemia group I protein	1,6	0,018	PRDX1
Q9NP72	RAB18	Ras-related protein Rab-18	1,6	0,024	PRDX1
Q01082	SPTBN1	Spectrin beta chain, non-erythrocytic 1	1,6	0,024	PRDX1
P52565	ARHGDIA	Rho GDP-dissociation inhibitor 1	1,5	0	PRDX1
P53004	BLVRA	Biliverdin reductase A	1,5	0	PRDX1
O75165	DNAJC13	DnaJ homolog subfamily C member 13	1,5	0	PRDX1
P08240	SRPRA	Signal recognition particle receptor subunit alpha	1,5	0	PRDX1
Q07020	RPL18	60S ribosomal protein L18	1,5	0	PRDX1
Q9BT78	COPS4	COP9 signalosome complex subunit 4	1,5	0	PRDX1
Q9UQ80	PA2G4	Proliferation-associated protein 2G4	1,5	0	PRDX1

Q14974	KPNB1	Importin subunit beta-1	1,5	0	PRDX1
O00299	CLIC1	Chloride intracellular channel protein 1	1,5	0	PRDX1
O60763	USO1	General vesicular transport factor p115	1,5	0	PRDX1
Q9UL25	RAB21	Ras-related protein Rab-21	1,5	0,001	PRDX1
P30101	PDIA3	Protein disulfide-isomerase A3	1,5	0,002	PRDX1
O43747	AP1G1	AP-1 complex subunit gamma-1	1,5	0,002	PRDX1
Q10713	PMPCA	Mitochondrial-processing peptidase subunit alpha	1,5	0,002	PRDX1
Q14318	FKBP8	Peptidyl-prolyl cis-trans isomerase FKBP8	1,5	0,002	PRDX1
P48735	IDH2	Isocitrate dehydrogenase [NADP], mitochondrial	1,5	0,003	PRDX1
Q86UP2	KTN1	Kinectin	1,5	0,003	PRDX1
O00505	KPNA3	Importin subunit alpha-4	1,5	0,003	PRDX1
P62750	RPL23A	60S ribosomal protein L23a	1,5	0,003	PRDX1
Q02750	MAP2K1	Dual specificity mitogen-activated protein kinase kinase 1	1,5	0,004	PRDX1
P39023	RPL3	60S ribosomal protein L3	1,5	0,004	PRDX1
P04843	RPN1	Dolichyl-diphosphooligosaccharide--protein glycosyltransferase subunit 1	1,5	0,004	PRDX1
Q15075	EEA1	Early endosome antigen 1	1,5	0,005	PRDX1
Q9NW13	RBM28	RNA-binding protein 28	1,5	0,006	PRDX1
A0A0A0MR02	VDAC2	Outer mitochondrial membrane protein porin 2	1,5	0,008	PRDX1
O60264	SMARCA5	SWI/SNF-related matrix-associated actin-dependent regulator of chromatin subfamily A member 5	1,5	0,009	PRDX1
O00232	PSMD12	26S proteasome non-ATPase regulatory subunit 12	1,5	0,011	PRDX1
P11182	DBT	Lipoamide acyltransferase component of branched-chain alpha-keto acid dehydrogenase complex, mitochondrial	1,5	0,015	PRDX1
Q9UHQ9	CYB5R1	NADH-cytochrome b5 reductase 1	1,5	0,018	PRDX1
H0YLH3	RABGGTA	Geranylgeranyl transferase type-2 subunit alpha	1,5	0,021	PRDX1
Q9UBS4	DNAJB11	DnaJ homolog subfamily B member 11	1,5	0,022	PRDX1
Q8NCM8	DYNC2H1	Cytoplasmic dynein 2 heavy chain 1	1,5	0,024	PRDX1
C9J384	CMSS1	Protein CMSS1	1,5	0,024	PRDX1
Q9Y4P1	ATG4B	Cysteine protease ATG4B	1,5	0,024	PRDX1
K7ESE9	BCAS3	Breast carcinoma-amplified sequence 3	1,5	0,025	PRDX1
P62906	RPL10A	60S ribosomal protein L10a	1,5	0,028	PRDX1
P48449	LSS	Lanosterol synthase	1,5	0,046	PRDX1
Q99459	CDC5L	Cell division cycle 5-like protein	1,5	0,049	PRDX1
Q92600	CNOT9	CCR4-NOT transcription complex subunit 9	1,4	0	PRDX1
P51665	PSMD7	26S proteasome non-ATPase regulatory subunit 7	1,4	0	PRDX1
Q96P70	IPO9	Importin-9	1,4	0	PRDX1
Q9UBU9	NXF1	Nuclear RNA export factor 1	1,4	0	PRDX1
P32969	RPL9	60S ribosomal protein L9	1,4	0	PRDX1
O76031	CLPX	ATP-dependent Clp protease ATP-binding subunit clpX-like, mitochondrial	1,4	0	PRDX1
Q5JXI8	FHL1	Four and a half LIM domains protein 1	1,4	0	PRDX1
E5RHG8	ELOC	Elongin-C	1,4	0	PRDX1
P62424	RPL7A	60S ribosomal protein L7a	1,4	0	PRDX1
Q6PI48	DARS2	Aspartate--tRNA ligase, mitochondrial	1,4	0,001	PRDX1
P53985	SLC16A1	Monocarboxylate transporter 1	1,4	0,001	PRDX1
Q15008	PSMD6	26S proteasome non-ATPase regulatory subunit 6	1,4	0,001	PRDX1
P54136	RARS1	Arginine--tRNA ligase, cytoplasmic	1,4	0,001	PRDX1
P62333	PSMC6	26S proteasome regulatory subunit 10B	1,4	0,002	PRDX1
Q9UJS0	SLC25A13	Calcium-binding mitochondrial carrier protein Aralar2	1,4	0,002	PRDX1
Q96QK1	VPS35	Vacuolar protein sorting-associated protein 35	1,4	0,002	PRDX1
Q9UHB9	SRP68	Signal recognition particle subunit SRP68	1,4	0,002	PRDX1
Q96H79	ZC3HAV1L	Zinc finger CCCH-type antiviral protein 1-like	1,4	0,002	PRDX1
O00567	NOP56	Nucleolar protein 56	1,4	0,003	PRDX1
P08133	ANXA6	Annexin A6	1,4	0,003	PRDX1
P62244	RPS15A	40S ribosomal protein S15a	1,4	0,003	PRDX1
Q15291	RBBP5	Retinoblastoma-binding protein 5	1,4	0,004	PRDX1
P20073	ANXA7	Annexin A7	1,4	0,006	PRDX1
P52597	HNRNPF	Heterogeneous nuclear ribonucleoprotein F	1,4	0,006	PRDX1
Q9P0M6	MACROH2A2	Core histone macro-H2A.2	1,4	0,008	PRDX1
O43719	HTATSF1	HIV Tat-specific factor 1	1,4	0,01	PRDX1
F8W038	C17orf49	Chromosome 17 open reading frame 49	1,4	0,015	PRDX1
Q92667	AKAP1	A-kinase anchor protein 1, mitochondrial	1,4	0,022	PRDX1
Q6UWP7	LCLAT1	Lysocardiolipin acyltransferase 1	1,4	0,024	PRDX1
O96017	CHEK2	Serine/threonine-protein kinase Chk2	1,4	0,032	PRDX1
Q12769	NUP160	Nuclear pore complex protein Nup160	1,4	0,034	PRDX1
O75400	PRPF40A	Pre-mRNA-processing factor 40 homolog A	1,4	0,034	PRDX1
A0A2Q2TH77	A0A2Q2TH77	>tr|A0A2Q2TH77|A0A2Q2TH77_HUMAN Golgin subfamily A member 2 OS=Homo sapiens OX=9606 GN=GOLGA2 PE=1 SV=1;>sp|Q08379|GOGA2_HUMAN Golgin subfamily A member 2 OS=Homo sapiens OX=9606 GN=GOLGA2 PE=1 SV=3;>tr|A0A1W2PQY5|A0A1W2PQY5_HUMAN Golgin subfamily A member	1,4	0,04	PRDX1
Q8NDI1	EHBP1	EH domain-binding protein 1	1,4	0,045	PRDX1

P78347	GTF2I	General transcription factor II-I	1,4	0,046	PRDX1
P21796	VDAC1	Voltage-dependent anion-selective channel protein 1	1,4	0,048	PRDX1
Q9Y580	RBM7	RNA-binding protein 7	1,4	0,049	PRDX1
Q6WCQ1	MPRIP	Myosin phosphatase Rho-interacting protein	1,3	0	PRDX1
Q15029	EFTUD2	116 kDa U5 small nuclear ribonucleoprotein component	1,3	0	PRDX1
Q9BRA2	TXNDC17	Thioredoxin domain-containing protein 17	1,3	0	PRDX1
P53007	SLC25A1	Tricarboxylate transport protein, mitochondrial	1,3	0	PRDX1
P34949	MPI	Mannose-6-phosphate isomerase	1,3	0	PRDX1
P17987	TCP1	T-complex protein 1 subunit alpha	1,3	0	PRDX1
A6NKB8	RNPEP	Aminopeptidase B	1,3	0	PRDX1
J3QL56	SCO1	Protein SCO1 homolog, mitochondrial	1,3	0	PRDX1
P61247	RPS3A	40S ribosomal protein S3a	1,3	0	PRDX1
P23396	RPS3	40S ribosomal protein S3	1,3	0	PRDX1
Q00325	SLC25A3	Phosphate carrier protein, mitochondrial	1,3	0	PRDX1
Q12788	TBL3	Transducin beta-like protein 3	1,3	0,001	PRDX1
P43246	MSH2	DNA mismatch repair protein Msh2	1,3	0,001	PRDX1
P60228	EIF3E	Eukaryotic translation initiation factor 3 subunit E	1,3	0,001	PRDX1
O60934	NBN	Nibrin	1,3	0,001	PRDX1
Q9UIA9	XPO7	Exportin-7	1,3	0,003	PRDX1
P18077	RPL35A	60S ribosomal protein L35a	1,3	0,004	PRDX1
Q9UI12	ATP6V1H	V-type proton ATPase subunit H	1,3	0,005	PRDX1
E9PKP7	UBTF	Nucleolar transcription factor 1	1,3	0,005	PRDX1
Q12996	CSTF3	Cleavage stimulation factor subunit 3	1,3	0,005	PRDX1
Q9Y5J1	UTP18	U3 small nucleolar RNA-associated protein 18 homolog	1,3	0,005	PRDX1
Q9Y2Q3	GSTK1	Glutathione S-transferase kappa 1	1,3	0,006	PRDX1
Q00610	CLTC	Clathrin heavy chain 1	1,3	0,008	PRDX1
O95861	BPNT1	3'(2'),5'-bisphosphate nucleotidase 1	1,3	0,009	PRDX1
O95202	LETM1	Mitochondrial proton/calcium exchanger protein	1,3	0,013	PRDX1
O15042	U2SURP	U2 snRNP-associated SURP motif-containing protein	1,3	0,015	PRDX1
P47897	QARS1	Glutamine--tRNA ligase	1,3	0,018	PRDX1
Q9Y6Y8	SEC23IP	SEC23-interacting protein	1,3	0,018	PRDX1
O00629	KPNA4	Importin subunit alpha-3	1,3	0,022	PRDX1
Q9UG63	ABCF2	ATP-binding cassette sub-family F member 2	1,3	0,023	PRDX1
Q9Y2H1	STK38L	Serine/threonine-protein kinase 38-like	1,3	0,033	PRDX1
Q96T88	UHRF1	E3 ubiquitin-protein ligase UHRF1	1,3	0,045	PRDX1
Q9BYJ9	YTHDF1	YTH domain-containing family protein 1	1,3	0,046	PRDX1
O75367	MACROH2A1	Core histone macro-H2A.1	1,3	0,046	PRDX1
Q8NBY1	STK26	Serine/threonine-protein kinase 26	1,3	0,046	PRDX1
P08572	COL4A2	Collagen alpha-2(IV) chain [Cleaved into: Canstatin]	1,3	0,046	PRDX1
Q86TI2	DPP9	Dipeptidyl peptidase 9	1,3	0,047	PRDX1
Q13439	GOLGA4	Golgin subfamily A member 4	1,3	0,049	PRDX1
P56537	EIF6	Eukaryotic translation initiation factor 6	1,2	0	PRDX1
P04899	GNAI2	Guanine nucleotide-binding protein G(i) subunit alpha-2	1,2	0	PRDX1
P51149	RAB7A	Ras-related protein Rab-7a	1,2	0	PRDX1
O75396	SEC22B	Vesicle-trafficking protein SEC22b	1,2	0,001	PRDX1
Q99613	EIF3C	Eukaryotic translation initiation factor 3 subunit C	1,2	0,001	PRDX1
Q99567	NUP88	Nuclear pore complex protein Nup88	1,2	0,003	PRDX1
Q5JY65	CRNKL1	Crooked neck-like protein 1	1,2	0,003	PRDX1
P06744	GPI	Glucose-6-phosphate isomerase	1,2	0,003	PRDX1
P31943	HNRNPH1	Heterogeneous nuclear ribonucleoprotein H	1,2	0,004	PRDX1
Q5T760	SRSF11	Serine/arginine-rich-splicing factor 11	1,2	0,005	PRDX1
Q6IBS0	TWF2	Twinfilin-2	1,2	0,006	PRDX1
O94973	AP2A2	AP-2 complex subunit alpha-2	1,2	0,007	PRDX1
P43897	TSFM	Elongation factor Ts, mitochondrial	1,2	0,008	PRDX1
O60678	PRMT3	Protein arginine N-methyltransferase 3	1,2	0,009	PRDX1
P56192	MARS1	Methionine--tRNA ligase, cytoplasmic	1,2	0,009	PRDX1
P46199	MTIF2	Translation initiation factor IF-2, mitochondrial	1,2	0,01	PRDX1
Q9H8H0	NOL11	Nucleolar protein 11	1,2	0,01	PRDX1
Q9H0E2	TOLLIP	Toll-interacting protein	1,2	0,013	PRDX1
P0DPB6	POLR1D	DNA-directed RNA polymerases I and III subunit RPAC2	1,2	0,013	PRDX1
Q53H12	AGK	Acylglycerol kinase, mitochondrial	1,2	0,015	PRDX1
O60306	AQR	RNA helicase aquarius	1,2	0,016	PRDX1
Q9Y5L0	TNPO3	Transportin-3	1,2	0,019	PRDX1
P35659	DEK	Protein DEK	1,2	0,019	PRDX1
P62979	RPS27A	Ubiquitin-40S ribosomal protein S27a	1,2	0,022	PRDX1
O75688	PPM1B	Protein phosphatase 1B	1,2	0,025	PRDX1
Q9NQG5	RPRD1B	Regulation of nuclear pre-mRNA domain-containing protein 1B	1,2	0,025	PRDX1
P23284	PPIB	Peptidyl-prolyl cis-trans isomerase B	1,2	0,026	PRDX1
P30740	SERPINB1	Leukocyte elastase inhibitor	1,2	0,027	PRDX1

P27824	CANX	Calnexin	1,2	0,032	PRDX1
Q9Y2X3	NOP58	Nucleolar protein 58	1,2	0,036	PRDX1
Q9BTT0	ANP32E	Acidic leucine-rich nuclear phosphoprotein 32 family member E	1,2	0,038	PRDX1
E7EVH7	E7EVH7	Kinesin light chain	1,2	0,045	PRDX1
M0R026	ILVBL	2-hydroxyacyl-CoA lyase 2	1,1	0	PRDX1
Q99733	NAP1L4	Nucleosome assembly protein 1-like 4	1,1	0	PRDX1
P09960	LTA4H	Leukotriene A-4 hydrolase	1,1	0	PRDX1
P05141	SLC25A5	ADP/ATP translocase 2	1,1	0	PRDX1
Q9BTX1	NDC1	Nucleoporin NDC1	1,1	0	PRDX1
Q7Z4H7	HAUS6	HAUS augmin-like complex subunit 6	1,1	0,001	PRDX1
J3QLD9	FLOT2	Flotillin	1,1	0,001	PRDX1
Q96A33	CCDC47	Coiled-coil domain-containing protein 47	1,1	0,001	PRDX1
C9J8Q5	ALDH5A1	Succinate-semialdehyde dehydrogenase	1,1	0,001	PRDX1
P49327	FASN	Fatty acid synthase	1,1	0,001	PRDX1
P07814	EPRS1	Bifunctional glutamate/proline--tRNA ligase	1,1	0,002	PRDX1
Q9NQ88	TIGAR	Fructose-2,6-bisphosphatase TIGAR	1,1	0,002	PRDX1
P31942	HNRNPH3	Heterogeneous nuclear ribonucleoprotein H3	1,1	0,004	PRDX1
E9PIF2	DDX10	RNA helicase	1,1	0,005	PRDX1
P35573	AGL	Glycogen debranching enzyme	1,1	0,006	PRDX1
O95782	AP2A1	AP-2 complex subunit alpha-1	1,1	0,006	PRDX1
O75874	IDH1	Isocitrate dehydrogenase [NADP] cytoplasmic	1,1	0,006	PRDX1
A0A024R4M0	RPS9	40S ribosomal protein S9	1,1	0,006	PRDX1
Q9UNM6	PSMD13	26S proteasome non-ATPase regulatory subunit 13	1,1	0,007	PRDX1
P52948	NUP98	Nuclear pore complex protein Nup98-Nup96	1,1	0,008	PRDX1
Q5T3I0	GPATCH4	G patch domain-containing protein 4	1,1	0,008	PRDX1
P46087	NOP2	Probable 28S rRNA	1,1	0,01	PRDX1
Q13085	ACACA	Acetyl-CoA carboxylase 1	1,1	0,011	PRDX1
Q9Y4E8	USP15	Ubiquitin carboxyl-terminal hydrolase 15	1,1	0,014	PRDX1
A0A2R8Y566	RELCH	RAB11-binding protein RELCH	1,1	0,015	PRDX1
O15226	NKRF	NF-kappa-B-repressing factor	1,1	0,015	PRDX1
Q71UM5	RPS27L	40S ribosomal protein S27-like	1,1	0,015	PRDX1
O95433	AHSA1	Activator of 90 kDa heat shock protein ATPase homolog 1	1,1	0,017	PRDX1
Q9Y371	SH3GLB1	Endophilin-B1	1,1	0,018	PRDX1
Q9BYG3	NIFK	MKI67 FHA domain-interacting nucleolar phosphoprotein	1,1	0,019	PRDX1
O14776	TCERG1	Transcription elongation regulator 1	1,1	0,02	PRDX1
P08670	VIM	Vimentin	1,1	0,023	PRDX1
P39687	ANP32A	Acidic leucine-rich nuclear phosphoprotein 32 family member A	1,1	0,024	PRDX1
P52209	PGD	6-phosphogluconate dehydrogenase, decarboxylating	1,1	0,025	PRDX1
Q99426	TBCB	Tubulin-folding cofactor B	1,1	0,025	PRDX1
P26583	HMGB2	High mobility group protein B2	1,1	0,025	PRDX1
Q96TC7	RMDN3	Regulator of microtubule dynamics protein 3	1,1	0,032	PRDX1
Q08945	SSRP1	FACT complex subunit SSRP1	1,1	0,033	PRDX1
Q6IN85	PPP4R3A	Serine/threonine-protein phosphatase 4 regulatory subunit 3A	1,1	0,034	PRDX1
Q9H0U4	RAB1B	Ras-related protein Rab-1B	1,1	0,034	PRDX1
P62258	YWHAE	14-3-3 protein epsilon	1,1	0,034	PRDX1
F8W0J6	NAP1L1	Nucleosome assembly protein 1-like 1	1,1	0,034	PRDX1
Q9C0B0	UNK	RING finger protein unkempt homolog	1,1	0,034	PRDX1
Q8IZ73	RPUSD2	RNA pseudouridylate synthase domain-containing protein 2	1,1	0,036	PRDX1
O43776	NARS1	Asparagine--tRNA ligase, cytoplasmic	1	0	PRDX1
P23528	CFL1	Cofilin-1	1	0	PRDX1
Q5H928	HSD17B10	3-hydroxyacyl-CoA dehydrogenase type-2	1	0	PRDX1
O95168	NDUFB4	NADH dehydrogenase [ubiquinone] 1 beta subcomplex subunit 4	1	0,001	PRDX1
P62136	PPP1CA	Serine/threonine-protein phosphatase PP1-alpha catalytic subunit	1	0,001	PRDX1
P68104	EEF1A1	Elongation factor 1-alpha 1	1	0,002	PRDX1
A0A087WXC5	NDUFA10	NADH dehydrogenase [ubiquinone] 1 alpha subcomplex subunit 10, mitochondrial	1	0,002	PRDX1
O75083	WDR1	WD repeat-containing protein 1	1	0,004	PRDX1
P31040	SDHA	Succinate dehydrogenase [ubiquinone] flavoprotein subunit, mitochondrial	1	0,005	PRDX1
Q9BV20	MRI1	Methylthioribose-1-phosphate isomerase	1	0,007	PRDX1
P60953	CDC42	Cell division control protein 42 homolog	1	0,008	PRDX1
P55060	CSE1L	Exportin-2	1	0,011	PRDX1
Q09161	NCBP1	Nuclear cap-binding protein subunit 1	1	0,024	PRDX1
P15927	RPA2	Replication protein A 32 kDa subunit	1	0,027	PRDX1
O00273	DFFA	DNA fragmentation factor subunit alpha	1	0,027	PRDX1
Q9NVX2	NLE1	Notchless protein homolog 1	1	0,034	PRDX1
O76003	GLRX3	Glutaredoxin-3	1	0,036	PRDX1
O60885	BRD4	Bromodomain-containing protein 4	1	0,046	PRDX1
P30048	PRDX3	Thioredoxin-dependent peroxide reductase, mitochondrial	8,9	0	PRDX2
Q15388	TOMM20	Mitochondrial import receptor subunit TOM20 homolog	3,6	0,001	PRDX2
P78417	GSTO1	Glutathione S-transferase omega-1	2,8	0	PRDX2

Q8N2K0	ABHD12	Lysophosphatidylserine lipase ABHD12	2,8	0,003	PRDX2
P30519	HMOX2	Heme oxygenase 2	2,7	0,007	PRDX2
P98175	RBM10	RNA-binding protein 10	2,6	0	PRDX2
Q8N5K1	CISD2	CDGSH iron-sulfur domain-containing protein 2	2,6	0,007	PRDX2
Q07820	MCL1	Induced myeloid leukemia cell differentiation protein Mcl-1	2,5	0	PRDX2
B3KUS5	USP30	Ubiquitin carboxyl-terminal hydrolase	2,5	0	PRDX2
A0A3B3ITJ4	HNRNPL	Heterogeneous nuclear ribonucleoprotein L	2,5	0,001	PRDX2
Q16352	INA	Alpha-internexin	2,3	0	PRDX2
Q8N6T3	ARFGAP1	ADP-ribosylation factor GTPase-activating protein 1	2,3	0,001	PRDX2
Q8N4V1	MMGT1	Membrane magnesium transporter 1	2,3	0,002	PRDX2
A0A0A0MS29	MFF	Mitochondrial fission factor	2,3	0,003	PRDX2
A0A0A0MR02	VDAC2	Outer mitochondrial membrane protein porin 2	2,2	0	PRDX2
Q14257	RCN2	Reticulocalbin-2	2,2	0,001	PRDX2
Q9Y2H1	STK38L	Serine/threonine-protein kinase 38-like	2,2	0,008	PRDX2
O96008	TOMM40	Mitochondrial import receptor subunit TOM40 homolog	2,2	0,021	PRDX2
Q13464	ROCK1	Rho-associated protein kinase 1	2,1	0	PRDX2
Q9NQG6	MIEF1	Mitochondrial dynamics protein MID51	2,1	0,01	PRDX2
Q15075	EEA1	Early endosome antigen 1	2	0	PRDX2
O75688	PPM1B	Protein phosphatase 1B	2	0,001	PRDX2
H0Y5L2	ECHDC1	Ethylmalonyl-CoA decarboxylase	2	0,008	PRDX2
P56962	STX17	Syntaxin-17	2	0,01	PRDX2
Q14789	GOLGB1	Golgin subfamily B member 1	2	0,011	PRDX2
Q9Y657	SPIN1	Spindlin-1	2	0,021	PRDX2
P51148	RAB5C	Ras-related protein Rab-5C	2	0,021	PRDX2
Q5SZR4	TDRKH	Tudor and KH domain containing, isoform CRA_a	2	0,04	PRDX2
O00268	TAF4	Transcription initiation factor TFIID subunit 4	1,9	0	PRDX2
Q9Y679	AUP1	Lipid droplet-regulating VLDL assembly factor AUP1	1,9	0,002	PRDX2
O00629	KPNA4	Importin subunit alpha-3	1,9	0,002	PRDX2
H3BPE1	MACF1	Microtubule-actin cross-linking factor 1, isoforms 1/2/3/5	1,9	0,003	PRDX2
Q8N6R0	EEF1AKNMT	eEF1A lysine and N-terminal methyltransferase	1,9	0,007	PRDX2
P57076	CFAP298	Cilia- and flagella-associated protein 298	1,9	0,01	PRDX2
Q9Y371	SH3GLB1	Endophilin-B1	1,8	0	PRDX2
Q8WTT2	NOC3L	Nucleolar complex protein 3 homolog	1,8	0,002	PRDX2
Q92667	AKAP1	A-kinase anchor protein 1, mitochondrial	1,8	0,005	PRDX2
J3QRD1	ALDH3A2	Aldehyde dehydrogenase family 3 member A2	1,8	0,009	PRDX2
Q6ZVM7	TOM1L2	TOM1-like protein 2	1,8	0,011	PRDX2
Q8TB36	GDAP1	Ganglioside-induced differentiation-associated protein 1	1,8	0,013	PRDX2
O60566	BUB1B	Mitotic checkpoint serine/threonine-protein kinase BUB1 beta	1,8	0,024	PRDX2
Q7Z3C6	ATG9A	Autophagy-related protein 9A	1,8	0,033	PRDX2
Q8TCG1	CIP2A	Protein CIP2A	1,7	0	PRDX2
Q5T3I0	GPATCH4	G patch domain-containing protein 4	1,7	0	PRDX2
Q13451	FKBP5	Peptidyl-prolyl cis-trans isomerase FKBP5	1,7	0	PRDX2
O43823	AKAP8	A-kinase anchor protein 8	1,7	0,002	PRDX2
P18031	PTPN1	Tyrosine-protein phosphatase non-receptor type 1	1,7	0,002	PRDX2
F5H008	VPS33B	Vacuolar protein sorting-associated protein 33B	1,7	0,033	PRDX2
P35580	MYH10	Myosin-10	1,6	0	PRDX2
P56182	RRP1	Ribosomal RNA processing protein 1 homolog A	1,6	0	PRDX2
Q8TC07	TBC1D15	TBC1 domain family member 15	1,6	0	PRDX2
Q4J6C6	PREPL	Prolyl endopeptidase-like	1,6	0	PRDX2
Q9UBB4	ATXN10	Ataxin-10	1,6	0	PRDX2
Q96CS3	FAF2	FAS-associated factor 2	1,6	0,001	PRDX2
K7ESE9	BCAS3	Breast carcinoma-amplified sequence 3	1,6	0,002	PRDX2
E7ESP9	NEFM	160 kDa neurofilament protein	1,6	0,006	PRDX2
Q9BVP2	GNL3	Guanine nucleotide-binding protein-like 3	1,6	0,006	PRDX2
A0A2Q2TH77	A0A2Q2TH77	>tr|A0A2Q2TH77|A0A2Q2TH77_HUMAN Golgin subfamily A member 2 OS=Homo sapiens OX=9606 GN=GOLGA2 PE=1 SV=1;>sp|Q08379|GOGA2_HUMAN Golgin subfamily A member 2 OS=Homo sapiens OX=9606 GN=GOLGA2 PE=1 SV=3;>tr|A0A1W2PQY5|A0A1W2PQY5_HUMAN Golgin subfamily A member	1,6	0,026	PRDX2
P23284	PPIB	Peptidyl-prolyl cis-trans isomerase B	1,6	0,028	PRDX2
Q96T88	UHRF1	E3 ubiquitin-protein ligase UHRF1	1,6	0,029	PRDX2
P48449	LSS	Lanosterol synthase	1,6	0,036	PRDX2
Q8ND04	SMG8	Protein SMG8	1,6	0,038	PRDX2
Q9BZG1	RAB34	Ras-related protein Rab-34	1,6	0,049	PRDX2
P42166	TMPO	Lamina-associated polypeptide 2, isoform alpha	1,5	0	PRDX2
Q6WCQ1	MPRIP	Myosin phosphatase Rho-interacting protein	1,5	0	PRDX2
O95373	IPO7	Importin-7	1,5	0,001	PRDX2
Q8IY81	FTSJ3	pre-rRNA 2'-O-ribose RNA methyltransferase FTSJ3	1,5	0,001	PRDX2
Q9NY61	AATF	Protein AATF	1,5	0,001	PRDX2
O14579	COPE	Coatomer subunit epsilon	1,5	0,001	PRDX2
O00505	KPNA3	Importin subunit alpha-4	1,5	0,002	PRDX2

Q5VT66	MTARC1	Mitochondrial amidoxime-reducing component 1	1,5	0,002	PRDX2
O60264	SMARCA5	SWI/SNF-related matrix-associated actin-dependent regulator of chromatin subfamily A member 5	1,5	0,007	PRDX2
Q9Y6Y8	SEC23IP	SEC23-interacting protein	1,5	0,009	PRDX2
P98194	ATP2C1	Calcium-transporting ATPase type 2C member 1	1,5	0,014	PRDX2
X6RCK5	DCTN3	Dynactin subunit 3	1,5	0,024	PRDX2
Q14690	PDCD11	Protein RRP5 homolog	1,5	0,032	PRDX2
Q99447	PCYT2	Ethanolamine-phosphate cytidylyltransferase	1,5	0,032	PRDX2
P46013	MKI67	Proliferation marker protein Ki-67	1,5	0,047	PRDX2
Q9Y4W2	LAS1L	Ribosomal biogenesis protein LAS1L	1,5	0,048	PRDX2
Q9BRA2	TXNDC17	Thioredoxin domain-containing protein 17	1,4	0	PRDX2
O95163	ELP1	Elongator complex protein 1	1,4	0	PRDX2
Q8TC12	RDH11	Retinol dehydrogenase 11	1,4	0	PRDX2
Q9Y4E8	USP15	Ubiquitin carboxyl-terminal hydrolase 15	1,4	0,001	PRDX2
Q15785	TOMM34	Mitochondrial import receptor subunit TOM34	1,4	0,002	PRDX2
Q6P1M0	SLC27A4	Long-chain fatty acid transport protein 4	1,4	0,003	PRDX2
O43615	TIMM44	Mitochondrial import inner membrane translocase subunit TIM44	1,4	0,003	PRDX2
Q5UIP0	RIF1	Telomere-associated protein RIF1	1,4	0,003	PRDX2
Q9P0M6	MACROH2A2	Core histone macro-H2A.2	1,4	0,004	PRDX2
P14923	JUP	Junction plakoglobin	1,4	0,004	PRDX2
O94905	ERLIN2	Erlin-2	1,4	0,005	PRDX2
C9J250	RBM6	RNA-binding protein 6	1,4	0,006	PRDX2
Q9NQ29	LUC7L	Putative RNA-binding protein Luc7-like 1	1,4	0,006	PRDX2
Q01804	OTUD4	OTU domain-containing protein 4	1,4	0,01	PRDX2
Q5T3Q7	HEATR1	HEAT repeat-containing protein 1	1,4	0,01	PRDX2
P23588	EIF4B	Eukaryotic translation initiation factor 4B	1,4	0,015	PRDX2
P29372	MPG	DNA-3-methyladenine glycosylase	1,4	0,029	PRDX2
H0YEN2	PPP6R3	Serine/threonine-protein phosphatase 6 regulatory subunit 3	1,4	0,04	PRDX2
Q676U5	ATG16L1	Autophagy-related protein 16-1	1,4	0,048	PRDX2
P46199	MTIF2	Translation initiation factor IF-2, mitochondrial	1,4	0,048	PRDX2
O94874	UFL1	E3 UFM1-protein ligase 1	1,3	0	PRDX2
P50542	PEX5	Peroxisomal targeting signal 1 receptor	1,3	0	PRDX2
Q86U86	PBRM1	Protein polybromo-1	1,3	0	PRDX2
O75165	DNAJC13	DnaJ homolog subfamily C member 13	1,3	0	PRDX2
Q9HAV7	GRPEL1	GrpE protein homolog 1, mitochondrial	1,3	0,001	PRDX2
A0A0A0MRM8	MYO6	Unconventional myosin-6	1,3	0,002	PRDX2
E9PKP7	UBTF	Nucleolar transcription factor 1	1,3	0,002	PRDX2
Q9UJC3	HOOK1	Protein Hook homolog 1	1,3	0,002	PRDX2
O15381	NVL	Nuclear valosin-containing protein-like	1,3	0,003	PRDX2
Q15843	NEDD8	NEDD8	1,3	0,004	PRDX2
Q9HB07	MYG1	MYG1 exonuclease	1,3	0,004	PRDX2
Q9Y3T9	NOC2L	Nucleolar complex protein 2 homolog	1,3	0,005	PRDX2
O60684	KPNA6	Importin subunit alpha-7	1,3	0,005	PRDX2
Q9BYN8	MRPS26	28S ribosomal protein S26, mitochondrial	1,3	0,005	PRDX2
Q15650	TRIP4	Activating signal cointegrator 1	1,3	0,006	PRDX2
Q03701	CEBPZ	CCAAT/enhancer-binding protein zeta	1,3	0,007	PRDX2
Q96QK1	VPS35	Vacuolar protein sorting-associated protein 35	1,3	0,007	PRDX2
P07196	NEFL	Neurofilament light polypeptide	1,3	0,01	PRDX2
P50502	ST13	Hsc70-interacting protein	1,3	0,01	PRDX2
Q08945	SSRP1	FACT complex subunit SSRP1	1,3	0,015	PRDX2
Q99426	TBCB	Tubulin-folding cofactor B	1,3	0,015	PRDX2
Q92665	MRPS31	28S ribosomal protein S31, mitochondrial	1,3	0,016	PRDX2
P40616	ARL1	ADP-ribosylation factor-like protein 1	1,3	0,026	PRDX2
Q7Z406	MYH14	Myosin-14	1,3	0,032	PRDX2
Q7Z4H7	HAUS6	HAUS augmin-like complex subunit 6	1,2	0	PRDX2
O76031	CLPX	ATP-dependent Clp protease ATP-binding subunit clpX-like, mitochondrial	1,2	0	PRDX2
J3QLD9	FLOT2	Flotillin	1,2	0	PRDX2
Q96S55	WRNIP1	ATPase WRNIP1	1,2	0	PRDX2
Q8NCA5	FAM98A	Protein FAM98A	1,2	0,001	PRDX2
Q9NX63	CHCHD3	MICOS complex subunit MIC19	1,2	0,001	PRDX2
O95613	PCNT	Pericentrin	1,2	0,001	PRDX2
Q9NZB2	FAM120A	Constitutive coactivator of PPAR-gamma-like protein 1	1,2	0,002	PRDX2
O94826	TOMM70	Mitochondrial import receptor subunit TOM70	1,2	0,002	PRDX2
P62314	SNRPD1	Small nuclear ribonucleoprotein Sm D1	1,2	0,002	PRDX2
G5EA36	CDC27	Cell division cycle 27, isoform CRA_c	1,2	0,002	PRDX2
A0A0D9SF70	ARFGAP2	ADP-ribosylation factor GTPase-activating protein 2	1,2	0,003	PRDX2
Q14126	DSG2	Desmoglein-2	1,2	0,004	PRDX2
P58546	MTPN	Myotrophin	1,2	0,004	PRDX2
Q9NSK0	KLC4	Kinesin light chain 4	1,2	0,005	PRDX2

Q12996	CSTF3	Cleavage stimulation factor subunit 3	1,2	0,006	PRDX2
O43707	ACTN4	Alpha-actinin-4	1,2	0,006	PRDX2
O15305	PMM2	Phosphomannomutase 2	1,2	0,006	PRDX2
Q99567	NUP88	Nuclear pore complex protein Nup88	1,2	0,006	PRDX2
Q9Y673	ALG5	Dolichyl-phosphate beta-glucosyltransferase	1,2	0,007	PRDX2
P63092	GNAS	Guanine nucleotide-binding protein G(s) subunit alpha isoforms short	1,2	0,007	PRDX2
Q96TC7	RMDN3	Regulator of microtubule dynamics protein 3	1,2	0,007	PRDX2
P42696	RBM34	RNA-binding protein 34	1,2	0,007	PRDX2
O15226	NKRF	NF-kappa-B-repressing factor	1,2	0,009	PRDX2
P19022	CDH2	Cadherin-2	1,2	0,011	PRDX2
O95376	ARIH2	E3 ubiquitin-protein ligase ARIH2	1,2	0,011	PRDX2
A0A2R8Y566	RELCH	RAB11-binding protein RELCH	1,2	0,011	PRDX2
O00291	HIP1	Huntingtin-interacting protein 1	1,2	0,011	PRDX2
O00170	AIP	AH receptor-interacting protein	1,2	0,011	PRDX2
Q15042	RAB3GAP1	Rab3 GTPase-activating protein catalytic subunit	1,2	0,011	PRDX2
P52701	MSH6	DNA mismatch repair protein Msh6	1,2	0,015	PRDX2
O75146	HIP1R	Huntingtin-interacting protein 1-related protein	1,2	0,019	PRDX2
P20042	EIF2S2	Eukaryotic translation initiation factor 2 subunit 2	1,2	0,023	PRDX2
P07947	YES1	Tyrosine-protein kinase Yes	1,2	0,023	PRDX2
O14828	SCAMP3	Secretory carrier-associated membrane protein 3	1,2	0,025	PRDX2
F8W0J6	NAP1L1	Nucleosome assembly protein 1-like 1	1,2	0,025	PRDX2
Q9BTT0	ANP32E	Acidic leucine-rich nuclear phosphoprotein 32 family member E	1,2	0,026	PRDX2
O14646	CHD1	Chromodomain-helicase-DNA-binding protein 1	1,2	0,027	PRDX2
E9PNW8	FAR1	Fatty acyl-CoA reductase	1,2	0,028	PRDX2
Q9NW13	RBM28	RNA-binding protein 28	1,2	0,032	PRDX2
Q96I51	RCC1L	RCC1-like G exchanging factor-like protein	1,2	0,033	PRDX2
Q71UM5	RPS27L	40S ribosomal protein S27-like	1,2	0,035	PRDX2
O15160	POLR1C	DNA-directed RNA polymerases I and III subunit RPAC1	1,2	0,04	PRDX2
Q9Y3B7	MRPL11	39S ribosomal protein L11, mitochondrial	1,2	0,046	PRDX2
P35251	RFC1	Replication factor C subunit 1	1,1	0	PRDX2
O43396	TXNL1	Thioredoxin-like protein 1	1,1	0	PRDX2
Q8IYB8	SUPV3L1	ATP-dependent RNA helicase SUPV3L1, mitochondrial	1,1	0	PRDX2
Q9UPT5	EXOC7	Exocyst complex component 7	1,1	0	PRDX2
B8ZZC5	GLS	Glutaminase	1,1	0,001	PRDX2
P60983	GMFB	Glia maturation factor beta	1,1	0,001	PRDX2
Q14974	KPNB1	Importin subunit beta-1	1,1	0,001	PRDX2
Q9NV70	EXOC1	Exocyst complex component 1	1,1	0,001	PRDX2
Q8N122	RPTOR	Regulatory-associated protein of mTOR	1,1	0,002	PRDX2
O75116	ROCK2	Rho-associated protein kinase 2	1,1	0,002	PRDX2
Q96EY7	PTCD3	Pentatricopeptide repeat domain-containing protein 3, mitochondrial	1,1	0,002	PRDX2
Q9UKG1	APPL1	DCC-interacting protein 13-alpha	1,1	0,002	PRDX2
Q96A33	CCDC47	Coiled-coil domain-containing protein 47	1,1	0,002	PRDX2
Q9H3P7	ACBD3	Golgi resident protein GCP60	1,1	0,003	PRDX2
Q13907	IDI1	Isopentenyl-diphosphate Delta-isomerase 1	1,1	0,004	PRDX2
Q86VS8	HOOK3	Protein Hook homolog 3	1,1	0,005	PRDX2
Q96P70	IPO9	Importin-9	1,1	0,005	PRDX2
Q13085	ACACA	Acetyl-CoA carboxylase 1	1,1	0,006	PRDX2
Q7Z7K6	CENPV	Centromere protein V	1,1	0,006	PRDX2
O00410	IPO5	Importin-5	1,1	0,006	PRDX2
Q5QJE6	DNTTIP2	Deoxynucleotidyltransferase terminal-interacting protein 2	1,1	0,006	PRDX2
P16435	POR	NADPH--cytochrome P450 reductase	1,1	0,007	PRDX2
P42765	ACAA2	3-ketoacyl-CoA thiolase, mitochondrial	1,1	0,009	PRDX2
Q04837	SSBP1	Single-stranded DNA-binding protein, mitochondrial	1,1	0,011	PRDX2
P57740	NUP107	Nuclear pore complex protein Nup107	1,1	0,013	PRDX2
Q6P996	PDXDC1	Pyridoxal-dependent decarboxylase domain-containing protein 1	1,1	0,013	PRDX2
O75691	UTP20	Small subunit processome component 20 homolog	1,1	0,017	PRDX2
Q5T4S7	UBR4	E3 ubiquitin-protein ligase UBR4	1,1	0,018	PRDX2
P16615	ATP2A2	Sarcoplasmic/endoplasmic reticulum calcium ATPase 2	1,1	0,021	PRDX2
D6RB59	EXOC3	Exocyst complex component 3	1,1	0,024	PRDX2
P62879	GNB2	Guanine nucleotide-binding protein G(I)/G(S)/G(T) subunit beta-2	1,1	0,025	PRDX2
Q14318	FKBP8	Peptidyl-prolyl cis-trans isomerase FKBP8	1,1	0,033	PRDX2
P50995	ANXA11	Annexin A11	1,1	0,033	PRDX2
Q9NQT5	EXOSC3	Exosome complex component RRP40	1,1	0,036	PRDX2
Q9H0E2	TOLLIP	Toll-interacting protein	1,1	0,036	PRDX2
Q9H6S0	YTHDC2	3'-5' RNA helicase YTHDC2	1,1	0,041	PRDX2
Q9UI30	TRMT112	Multifunctional methyltransferase subunit TRM112-like protein	1,1	0,042	PRDX2
P62979	RPS27A	Ubiquitin-40S ribosomal protein S27a	1,1	0,047	PRDX2
O43719	HTATSF1	HIV Tat-specific factor 1	1,1	0,048	PRDX2
Q8ND24	RNF214	RING finger protein 214	1	0,001	PRDX2

Q6UWP7	LCLAT1	Lysocardiolipin acyltransferase 1	1	0,001	PRDX2
Q86UP2	KTN1	Kinectin	1	0,002	PRDX2
Q9NY93	DDX56	Probable ATP-dependent RNA helicase DDX56	1	0,002	PRDX2
P56537	EIF6	Eukaryotic translation initiation factor 6	1	0,002	PRDX2
Q15555	MAPRE2	Microtubule-associated protein RP/EB family member 2	1	0,003	PRDX2
P58107	EPPK1	Epiplakin	1	0,007	PRDX2
A0A1B0GV47	KIF21A	Kinesin-like protein KIF21A	1	0,007	PRDX2
Q13951	CBFB	Core-binding factor subunit beta	1	0,011	PRDX2
Q8IWS0	PHF6	PHD finger protein 6	1	0,011	PRDX2
P53384	NUBP1	Cytosolic Fe-S cluster assembly factor NUBP1	1	0,013	PRDX2
Q93034	CUL5	Cullin-5	1	0,014	PRDX2
Q71RC2	LARP4	La-related protein 4	1	0,016	PRDX2
Q92990	GLMN	Glomulin	1	0,017	PRDX2
O43149	ZZEF1	Zinc finger ZZ-type and EF-hand domain-containing protein 1	1	0,018	PRDX2
F8VYE8	PPP1CC	Serine/threonine-protein phosphatase	1	0,022	PRDX2
P41567	EIF1	Eukaryotic translation initiation factor 1	1	0,033	PRDX2
P08670	VIM	Vimentin	1	0,038	PRDX2
Q9BZE4	GTPBP4	Nucleolar GTP-binding protein 1	1	0,038	PRDX2
O60502	OGA	Protein O-GlcNAcase	1	0,044	PRDX2
P52209	PGD	6-phosphogluconate dehydrogenase, decarboxylating	1	0,048	PRDX2
P30048	PRDX3	Thioredoxin-dependent peroxide reductase, mitochondrial	5,4	0	PRDX4
P61106	RAB14	Ras-related protein Rab-14	3,1	0	PRDX4
O00629	KPNA4	Importin subunit alpha-3	3,1	0	PRDX4
Q9Y679	AUP1	Lipid droplet-regulating VLDL assembly factor AUP1	3,1	0	PRDX4
Q8N5K1	CISD2	CDGSH iron-sulfur domain-containing protein 2	3,1	0,003	PRDX4
Q07820	MCL1	Induced myeloid leukemia cell differentiation protein Mcl-1	2,8	0,001	PRDX4
P51148	RAB5C	Ras-related protein Rab-5C	2,8	0,004	PRDX4
Q5SZR4	TDRKH	Tudor and KH domain containing, isoform CRA_a	2,8	0,007	PRDX4
P19022	CDH2	Cadherin-2	2,7	0	PRDX4
O95373	IPO7	Importin-7	2,7	0	PRDX4
O96008	TOMM40	Mitochondrial import receptor subunit TOM40 homolog	2,7	0,005	PRDX4
Q15388	TOMM20	Mitochondrial import receptor subunit TOM20 homolog	2,7	0,007	PRDX4
P30519	HMOX2	Heme oxygenase 2	2,7	0,007	PRDX4
G5EA06	MRPS27	28S ribosomal protein S27, mitochondrial	2,6	0,001	PRDX4
Q9H2P9	DPH5	Diphthine methyl ester synthase	2,6	0,001	PRDX4
P06132	UROD	Uroporphyrinogen decarboxylase	2,6	0,002	PRDX4
Q8N6T3	ARFGAP1	ADP-ribosylation factor GTPase-activating protein 1	2,5	0	PRDX4
P98194	ATP2C1	Calcium-transporting ATPase type 2C member 1	2,5	0	PRDX4
H7BXI1	ESYT2	Extended synaptotagmin-2	2,4	0	PRDX4
Q8TEX9	IPO4	Importin-4	2,4	0	PRDX4
Q9BSJ8	ESYT1	Extended synaptotagmin-1	2,4	0,001	PRDX4
Q7Z434	MAVS	Mitochondrial antiviral-signaling protein	2,4	0,006	PRDX4
Q8N4V1	MMGT1	Membrane magnesium transporter 1	2,3	0,001	PRDX4
P42574	CASP3	Caspase-3	2,3	0,003	PRDX4
A0A0A0MS29	MFF	Mitochondrial fission factor	2,3	0,003	PRDX4
A0A2R8YFH5	SEC23B	Protein transport protein SEC23	2,3	0,004	PRDX4
Q7Z3C6	ATG9A	Autophagy-related protein 9A	2,3	0,015	PRDX4
O00505	KPNA3	Importin subunit alpha-4	2,2	0	PRDX4
Q9BTE1	DCTN5	Dynactin subunit 5	2,2	0,002	PRDX4
P51809	VAMP7	Vesicle-associated membrane protein 7	2,2	0,011	PRDX4
A0A0A0MR02	VDAC2	Outer mitochondrial membrane protein porin 2	2,1	0	PRDX4
Q5VT66	MTARC1	Mitochondrial amidoxime-reducing component 1	2,1	0	PRDX4
P50542	PEX5	Peroxisomal targeting signal 1 receptor	2,1	0	PRDX4
Q96DH6	MSI2	RNA-binding protein Musashi homolog 2	2,1	0,002	PRDX4
Q92667	AKAP1	A-kinase anchor protein 1, mitochondrial	2,1	0,002	PRDX4
Q13190	STX5	Syntaxin-5	2,1	0,003	PRDX4
P84085	ARF5	ADP-ribosylation factor 5	2,1	0,007	PRDX4
Q9NQG6	MIEF1	Mitochondrial dynamics protein MID51	2,1	0,009	PRDX4
Q96EA4	SPDL1	Protein Spindly	2,1	0,014	PRDX4
P07384	CAPN1	Calpain-1 catalytic subunit	2	0,003	PRDX4
E9PHS0	LANCL1	Glutathione S-transferase LANCL1	2	0,006	PRDX4
P56962	STX17	Syntaxin-17	2	0,009	PRDX4
Q8WVC2	RPS21	40S ribosomal protein S21	2	0,009	PRDX4
P49642	PRIM1	DNA primase small subunit	1,9	0	PRDX4
Q9H0E2	TOLLIP	Toll-interacting protein	1,9	0,001	PRDX4
P18031	PTPN1	Tyrosine-protein phosphatase non-receptor type 1	1,9	0,001	PRDX4
B3KUS5	USP30	Ubiquitin carboxyl-terminal hydrolase	1,9	0,002	PRDX4
P40616	ARL1	ADP-ribosylation factor-like protein 1	1,9	0,003	PRDX4
Q9BPW8	NIPSNAP1	Protein NipSnap homolog 1	1,9	0,005	PRDX4

Q9NZ32	ACTR10	Actin-related protein 10	1,9	0,009	PRDX4
Q14789	GOLGB1	Golgin subfamily B member 1	1,9	0,01	PRDX4
Q6FI81	CIAPIN1	Anamorsin	1,9	0,013	PRDX4
A0A0A0MR09	PTPN9	Tyrosine-protein phosphatase non-receptor type 9	1,9	0,015	PRDX4
P12236	SLC25A6	ADP/ATP translocase 3	1,8	0	PRDX4
P48047	ATP5PO	ATP synthase subunit O, mitochondrial	1,8	0,007	PRDX4
Q6ZVM7	TOM1L2	TOM1-like protein 2	1,8	0,009	PRDX4
P49458	SRP9	Signal recognition particle 9 kDa protein	1,8	0,012	PRDX4
Q9NP72	RAB18	Ras-related protein Rab-18	1,8	0,015	PRDX4
O95163	ELP1	Elongator complex protein 1	1,7	0	PRDX4
Q14318	FKBP8	Peptidyl-prolyl cis-trans isomerase FKBP8	1,7	0,001	PRDX4
P31689	DNAJA1	DnaJ homolog subfamily A member 1	1,7	0,004	PRDX4
Q9NS69	TOMM22	Mitochondrial import receptor subunit TOM22 homolog	1,7	0,007	PRDX4
O14828	SCAMP3	Secretory carrier-associated membrane protein 3	1,7	0,008	PRDX4
U3KQC1	WDR18	WD repeat-containing protein 18	1,7	0,008	PRDX4
A0A3B3ITJ4	HNRNPL	Heterogeneous nuclear ribonucleoprotein L	1,7	0,01	PRDX4
P42025	ACTR1B	Beta-centractin	1,7	0,011	PRDX4
O00291	HIP1	Huntingtin-interacting protein 1	1,7	0,012	PRDX4
Q8NI60	COQ8A	Atypical kinase COQ8A, mitochondrial	1,7	0,014	PRDX4
Q16186	ADRM1	Proteasomal ubiquitin receptor ADRM1	1,7	0,014	PRDX4
Q9Y4P1	ATG4B	Cysteine protease ATG4B	1,7	0,014	PRDX4
Q9NP97	DYNLRB1	Dynein light chain roadblock-type 1	1,7	0,015	PRDX4
P30740	SERPINB1	Leukocyte elastase inhibitor	1,7	0,017	PRDX4
Q5JRI1	SRSF10	Serine/arginine-rich-splicing factor 10	1,7	0,021	PRDX4
O60566	BUB1B	Mitotic checkpoint serine/threonine-protein kinase BUB1 beta	1,7	0,023	PRDX4
Q7L5D6	GET4	Golgi to ER traffic protein 4 homolog	1,7	0,027	PRDX4
Q9NVJ2	ARL8B	ADP-ribosylation factor-like protein 8B	1,7	0,027	PRDX4
P48449	LSS	Lanosterol synthase	1,7	0,032	PRDX4
P08243	ASNS	Asparagine synthetase [glutamine-hydrolyzing]	1,6	0	PRDX4
P16435	POR	NADPH--cytochrome P450 reductase	1,6	0	PRDX4
Q8TC07	TBC1D15	TBC1 domain family member 15	1,6	0	PRDX4
Q9UBB4	ATXN10	Ataxin-10	1,6	0	PRDX4
P21964	COMT	Catechol O-methyltransferase	1,6	0,001	PRDX4
Q8TCG1	CIP2A	Protein CIP2A	1,6	0,001	PRDX4
O14964	HGS	Hepatocyte growth factor-regulated tyrosine kinase substrate	1,6	0,002	PRDX4
P04843	RPN1	Dolichyl-diphosphooligosaccharide--protein glycosyltransferase subunit 1	1,6	0,004	PRDX4
Q53H96	PYCR3	Pyrroline-5-carboxylate reductase 3	1,6	0,012	PRDX4
O95295	SNAPIN	SNARE-associated protein Snapin	1,6	0,012	PRDX4
H0YLH3	RABGGTA	Geranylgeranyl transferase type-2 subunit alpha	1,6	0,012	PRDX4
Q8NF37	LPCAT1	Lysophosphatidylcholine acyltransferase 1	1,6	0,026	PRDX4
Q9H840	GEMIN7	Gem-associated protein 7	1,6	0,033	PRDX4
Q8N573	OXR1	Oxidation resistance protein 1	1,6	0,043	PRDX4
Q9Y371	SH3GLB1	Endophilin-B1	1,5	0	PRDX4
P35232	PHB	Prohibitin	1,5	0	PRDX4
Q9Y262	EIF3L	Eukaryotic translation initiation factor 3 subunit L	1,5	0,01	PRDX4
Q9Y6Y8	SEC23IP	SEC23-interacting protein	1,5	0,013	PRDX4
Q6DKI1	RPL7L1	60S ribosomal protein L7-like 1	1,5	0,015	PRDX4
Q9BZE1	MRPL37	39S ribosomal protein L37, mitochondrial	1,5	0,019	PRDX4
Q86W42	THOC6	THO complex subunit 6 homolog	1,5	0,027	PRDX4
Q9Y580	RBM7	RNA-binding protein 7	1,5	0,031	PRDX4
Q9NUY8	TBC1D23	TBC1 domain family member 23	1,5	0,037	PRDX4
P54646	PRKAA2	5'-AMP-activated protein kinase catalytic subunit alpha-2	1,5	0,038	PRDX4
O95573	ACSL3	Long-chain-fatty-acid--CoA ligase 3	1,4	0	PRDX4
Q9UKG1	APPL1	DCC-interacting protein 13-alpha	1,4	0	PRDX4
O95292	VAPB	Vesicle-associated membrane protein-associated protein B/C	1,4	0	PRDX4
P35573	AGL	Glycogen debranching enzyme	1,4	0,001	PRDX4
Q9Y4E8	USP15	Ubiquitin carboxyl-terminal hydrolase 15	1,4	0,001	PRDX4
Q6P1M0	SLC27A4	Long-chain fatty acid transport protein 4	1,4	0,002	PRDX4
A0A0C4DGQ6	RPRD1A	Regulation of nuclear pre-mRNA domain-containing protein 1A	1,4	0,002	PRDX4
P14923	JUP	Junction plakoglobin	1,4	0,004	PRDX4
Q96CS3	FAF2	FAS-associated factor 2	1,4	0,004	PRDX4
P35237	SERPINB6	Serpin B6	1,4	0,004	PRDX4
Q53EL6	PDCD4	Programmed cell death protein 4	1,4	0,005	PRDX4
P42771	CDKN2A	Cyclin-dependent kinase inhibitor 2A	1,4	0,005	PRDX4
A0A3B3IUD2	MSTO1	Protein misato homolog 1	1,4	0,008	PRDX4
Q9BTT0	ANP32E	Acidic leucine-rich nuclear phosphoprotein 32 family member E	1,4	0,008	PRDX4
A0A0D9SF70	ARFGAP2	ADP-ribosylation factor GTPase-activating protein 2	1,4	0,009	PRDX4
P63167	DYNLL1	Dynein light chain 1, cytoplasmic	1,4	0,021	PRDX4
Q5QNY5	PEX19	Peroxin-19	1,4	0,027	PRDX4

P41250	GARS1	Glycine--tRNA ligase	1,4	0,03	PRDX4
A0A087X2D5	MRPL45	39S ribosomal protein L45, mitochondrial	1,4	0,039	PRDX4
Q6PGP7	TTC37	Tetratricopeptide repeat protein 37	1,4	0,044	PRDX4
Q9H974	QTRT2	Queuine tRNA-ribosyltransferase accessory subunit 2	1,4	0,045	PRDX4
Q9Y673	ALG5	Dolichyl-phosphate beta-glucosyltransferase	1,4	0,047	PRDX4
G5EA36	CDC27	Cell division cycle 27, isoform CRA_c	1,3	0	PRDX4
Q4J6C6	PREPL	Prolyl endopeptidase-like	1,3	0	PRDX4
E7ETZ4	BZW2	Basic leucine zipper and W2 domain-containing protein 2	1,3	0,001	PRDX4
Q5T3I0	GPATCH4	G patch domain-containing protein 4	1,3	0,001	PRDX4
D6R938	CAMK2D	Calcium/calmodulin-dependent protein kinase	1,3	0,002	PRDX4
P31930	UQCRC1	Cytochrome b-c1 complex subunit 1, mitochondrial	1,3	0,003	PRDX4
P34897	SHMT2	Serine hydroxymethyltransferase, mitochondrial	1,3	0,003	PRDX4
P51452	DUSP3	Dual specificity protein phosphatase 3	1,3	0,003	PRDX4
K7ESE9	BCAS3	Breast carcinoma-amplified sequence 3	1,3	0,003	PRDX4
A0A2Q2TH77	A0A2Q2TH77	>tr|A0A2Q2TH77|A0A2Q2TH77_HUMAN Golgin subfamily A member 2 OS=Homo sapiens OX=9606 GN=GOLGA2 PE=1 SV=1;>sp|Q08379|GOGA2_HUMAN Golgin subfamily A member 2 OS=Homo sapiens OX=9606 GN=GOLGA2 PE=1 SV=3;>tr|A0A1W2PQY5|A0A1W2PQY5_HUMAN Golgin subfamily A member	1,3	0,004	PRDX4
Q15276	RABEP1	Rab GTPase-binding effector protein 1	1,3	0,004	PRDX4
Q6UWP7	LCLAT1	Lysocardiolipin acyltransferase 1	1,3	0,004	PRDX4
O60678	PRMT3	Protein arginine N-methyltransferase 3	1,3	0,004	PRDX4
Q9NQG5	RPRD1B	Regulation of nuclear pre-mRNA domain-containing protein 1B	1,3	0,01	PRDX4
F8W0J6	NAP1L1	Nucleosome assembly protein 1-like 1	1,3	0,014	PRDX4
P19367	HK1	Hexokinase-1	1,3	0,018	PRDX4
Q9Y394	DHRS7	Dehydrogenase/reductase SDR family member 7	1,3	0,022	PRDX4
F5H008	VPS33B	Vacuolar protein sorting-associated protein 33B	1,3	0,028	PRDX4
P35606	COPB2	Coatomer subunit beta'	1,3	0,028	PRDX4
P25705	ATP5F1A	ATP synthase subunit alpha, mitochondrial	1,2	0	PRDX4
P04899	GNAI2	Guanine nucleotide-binding protein G(i) subunit alpha-2	1,2	0	PRDX4
P36542	ATP5F1C	ATP synthase subunit gamma, mitochondrial	1,2	0	PRDX4
P68104	EEF1A1	Elongation factor 1-alpha 1	1,2	0,001	PRDX4
Q96A33	CCDC47	Coiled-coil domain-containing protein 47	1,2	0,001	PRDX4
Q9BVG4	PBDC1	Protein PBDC1	1,2	0,002	PRDX4
O95168	NDUFB4	NADH dehydrogenase [ubiquinone] 1 beta subcomplex subunit 4	1,2	0,002	PRDX4
Q8IXI1	RHOT2	Mitochondrial Rho GTPase 2	1,2	0,002	PRDX4
P31040	SDHA	Succinate dehydrogenase [ubiquinone] flavoprotein subunit, mitochondrial	1,2	0,002	PRDX4
Q9UNM6	PSMD13	26S proteasome non-ATPase regulatory subunit 13	1,2	0,003	PRDX4
Q92769	HDAC2	Histone deacetylase 2	1,2	0,003	PRDX4
O14579	COPE	Coatomer subunit epsilon	1,2	0,004	PRDX4
Q14126	DSG2	Desmoglein-2	1,2	0,006	PRDX4
E9PKG1	PRMT1	Protein arginine N-methyltransferase 1	1,2	0,007	PRDX4
Q5T760	SRSF11	Serine/arginine-rich-splicing factor 11	1,2	0,009	PRDX4
Q9BT25	HAUS8	HAUS augmin-like complex subunit 8	1,2	0,014	PRDX4
P63244	RACK1	Receptor of activated protein C kinase 1	1,2	0,016	PRDX4
Q13464	ROCK1	Rho-associated protein kinase 1	1,2	0,021	PRDX4
P63000	RAC1	Ras-related C3 botulinum toxin substrate 1	1,2	0,022	PRDX4
D6REA0	GATB	Glutamyl-tRNA(Gln) amidotransferase subunit B, mitochondrial	1,2	0,039	PRDX4
O75396	SEC22B	Vesicle-trafficking protein SEC22b	1,1	0,001	PRDX4
P28288	ABCD3	ATP-binding cassette sub-family D member 3	1,1	0,002	PRDX4
C9J8Q5	ALDH5A1	Succinate-semialdehyde dehydrogenase	1,1	0,002	PRDX4
O15397	IPO8	Importin-8	1,1	0,002	PRDX4
P56545	CTBP2	C-terminal-binding protein 2	1,1	0,002	PRDX4
Q9HAV7	GRPEL1	GrpE protein homolog 1, mitochondrial	1,1	0,002	PRDX4
Q8N122	RPTOR	Regulatory-associated protein of mTOR	1,1	0,003	PRDX4
Q7Z4Q2	HEATR3	HEAT repeat-containing protein 3	1,1	0,003	PRDX4
P23526	AHCY	Adenosylhomocysteinase	1,1	0,003	PRDX4
Q9BRA2	TXNDC17	Thioredoxin domain-containing protein 17	1,1	0,004	PRDX4
Q96P70	IPO9	Importin-9	1,1	0,004	PRDX4
Q96TC7	RMDN3	Regulator of microtubule dynamics protein 3	1,1	0,006	PRDX4
Q8WUM0	NUP133	Nuclear pore complex protein Nup133	1,1	0,008	PRDX4
P63092	GNAS	Guanine nucleotide-binding protein G(s) subunit alpha isoforms short	1,1	0,01	PRDX4
Q15738	NSDHL	Sterol-4-alpha-carboxylate 3-dehydrogenase, decarboxylating	1,1	0,015	PRDX4
Q9HAV4	XPO5	Exportin-5	1,1	0,024	PRDX4
P16615	ATP2A2	Sarcoplasmic/endoplasmic reticulum calcium ATPase 2	1,1	0,024	PRDX4
Q16352	INA	Alpha-internexin	1,1	0,025	PRDX4
Q15075	EEA1	Early endosome antigen 1	1,1	0,03	PRDX4
Q9Y6I9	TEX264	Testis-expressed protein 264	1,1	0,033	PRDX4
Q9H0U4	RAB1B	Ras-related protein Rab-1B	1,1	0,036	PRDX4
P62879	GNB2	Guanine nucleotide-binding protein G(I)/G(S)/G(T) subunit beta-2	1,1	0,036	PRDX4
P53677	AP3M2	AP-3 complex subunit mu-2	1,1	0,037	PRDX4

Q9UI30	TRMT112	Multifunctional methyltransferase subunit TRM112-like protein	1,1	0,04	PRDX4
O60306	AQR	RNA helicase aquarius	1,1	0,044	PRDX4
P47755	CAPZA2	F-actin-capping protein subunit alpha-2	1,1	0,047	PRDX4
Q14C86	GAPVD1	GTPase-activating protein and VPS9 domain-containing protein 1	1,1	0,049	PRDX4
P30520	ADSS2	Adenylosuccinate synthetase isozyme 2	1,1	0,049	PRDX4
P19525	EIF2AK2	Interferon-induced, double-stranded RNA-activated protein kinase	1	0,001	PRDX4
Q92973	TNPO1	Transportin-1	1	0,002	PRDX4
P60983	GMFB	Glia maturation factor beta	1	0,003	PRDX4
Q96EY7	PTCD3	Pentatricopeptide repeat domain-containing protein 3, mitochondrial	1	0,003	PRDX4
Q6P996	PDXDC1	Pyridoxal-dependent decarboxylase domain-containing protein 1	1	0,003	PRDX4
P41240	CSK	Tyrosine-protein kinase CSK	1	0,003	PRDX4
Q8NCA5	FAM98A	Protein FAM98A	1	0,004	PRDX4
H3BTA2	PPP4C	Serine/threonine-protein phosphatase	1	0,006	PRDX4
Q13951	CBFB	Core-binding factor subunit beta	1	0,012	PRDX4
Q16718	NDUFA5	NADH dehydrogenase [ubiquinone] 1 alpha subcomplex subunit 5	1	0,012	PRDX4
O43765	SGTA	Small glutamine-rich tetratricopeptide repeat-containing protein alpha	1	0,013	PRDX4
E9PKP7	UBTF	Nucleolar transcription factor 1	1	0,021	PRDX4
Q9UJS0	SLC25A13	Calcium-binding mitochondrial carrier protein Aralar2	1	0,025	PRDX4
O15144	ARPC2	Actin-related protein 2/3 complex subunit 2	1	0,03	PRDX4
P61353	RPL27	60S ribosomal protein L27	1	0,031	PRDX4
Q03701	CEBPZ	CCAAT/enhancer-binding protein zeta	1	0,035	PRDX4
O60684	KPNA6	Importin subunit alpha-7	1	0,035	PRDX4
P15374	UCHL3	Ubiquitin carboxyl-terminal hydrolase isozyme L3	1	0,036	PRDX4
O95373	IPO7	Importin-7	3,5	0	PRDX5
O00629	KPNA4	Importin subunit alpha-3	3,3	0	PRDX5
Q9Y224	RTRAF	RNA transcription, translation and transport factor protein	3,2	0	PRDX5
Q96AC1	FERMT2	Fermitin family homolog 2	3	0	PRDX5
Q15149	PLEC	Plectin	2,9	0,001	PRDX5
Q8TCG1	CIP2A	Protein CIP2A	2,8	0	PRDX5
E9PHS0	LANCL1	Glutathione S-transferase LANCL1	2,7	0	PRDX5
P61106	RAB14	Ras-related protein Rab-14	2,7	0	PRDX5
Q07820	MCL1	Induced myeloid leukemia cell differentiation protein Mcl-1	2,7	0	PRDX5
Q8N2K0	ABHD12	Lysophosphatidylserine lipase ABHD12	2,7	0,002	PRDX5
P30519	HMOX2	Heme oxygenase 2	2,6	0,005	PRDX5
P19105	MYL12A	Myosin regulatory light chain 12A	2,5	0	PRDX5
P19022	CDH2	Cadherin-2	2,5	0	PRDX5
P06132	UROD	Uroporphyrinogen decarboxylase	2,5	0,001	PRDX5
Q8TEX9	IPO4	Importin-4	2,4	0	PRDX5
H3BPE1	MACF1	Microtubule-actin cross-linking factor 1, isoforms 1/2/3/5	2,3	0	PRDX5
Q7Z406	MYH14	Myosin-14	2,3	0	PRDX5
Q13464	ROCK1	Rho-associated protein kinase 1	2,3	0	PRDX5
B3KUS5	USP30	Ubiquitin carboxyl-terminal hydrolase	2,2	0	PRDX5
Q9Y679	AUP1	Lipid droplet-regulating VLDL assembly factor AUP1	2,2	0	PRDX5
O00505	KPNA3	Importin subunit alpha-4	2,2	0	PRDX5
P62879	GNB2	Guanine nucleotide-binding protein G(I)/G(S)/G(T) subunit beta-2	2,2	0	PRDX5
Q16352	INA	Alpha-internexin	2,2	0	PRDX5
Q8N4V1	MMGT1	Membrane magnesium transporter 1	2,2	0,001	PRDX5
Q15477	SKIV2L	Helicase SKI2W	2,2	0,001	PRDX5
P98194	ATP2C1	Calcium-transporting ATPase type 2C member 1	2,2	0,001	PRDX5
Q96DH6	MSI2	RNA-binding protein Musashi homolog 2	2,2	0,001	PRDX5
P55084	HADHB	Trifunctional enzyme subunit beta, mitochondrial	2,2	0,004	PRDX5
Q7Z434	MAVS	Mitochondrial antiviral-signaling protein	2,2	0,004	PRDX5
Q9BVP2	GNL3	Guanine nucleotide-binding protein-like 3	2,1	0	PRDX5
P40616	ARL1	ADP-ribosylation factor-like protein 1	2,1	0	PRDX5
Q9BTT0	ANP32E	Acidic leucine-rich nuclear phosphoprotein 32 family member E	2,1	0	PRDX5
O95861	BPNT1	3'(2'),5'-bisphosphate nucleotidase 1	2,1	0	PRDX5
Q9UBB4	ATXN10	Ataxin-10	2,1	0	PRDX5
P63167	DYNLL1	Dynein light chain 1, cytoplasmic	2,1	0,001	PRDX5
A0A0A0MR09	PTPN9	Tyrosine-protein phosphatase non-receptor type 9	2,1	0,001	PRDX5
Q9BTE1	DCTN5	Dynactin subunit 5	2,1	0,002	PRDX5
A0A0A0MS29	MFF	Mitochondrial fission factor	2,1	0,003	PRDX5
P51809	VAMP7	Vesicle-associated membrane protein 7	2,1	0,009	PRDX5
Q5T3Q7	HEATR1	HEAT repeat-containing protein 1	2	0	PRDX5
Q13085	ACACA	Acetyl-CoA carboxylase 1	2	0	PRDX5
G5EA31	SEC24C	Protein transport protein Sec24C	2	0	PRDX5
Q9NY93	DDX56	Probable ATP-dependent RNA helicase DDX56	2	0	PRDX5
O95163	ELP1	Elongator complex protein 1	2	0	PRDX5
Q6P2E9	EDC4	Enhancer of mRNA-decapping protein 4	2	0,001	PRDX5
Q9BZE1	MRPL37	39S ribosomal protein L37, mitochondrial	2	0,002	PRDX5

Q5VW32	BROX	BRO1 domain-containing protein BROX	2	0,003	PRDX5
H0YMZ1	PSMA4	Proteasome subunit alpha type	2	0,004	PRDX5
Q8IZ07	ANKRD13A	Ankyrin repeat domain-containing protein 13A	2	0,025	PRDX5
Q15388	TOMM20	Mitochondrial import receptor subunit TOM20 homolog	2	0,025	PRDX5
P30048	PRDX3	Thioredoxin-dependent peroxide reductase, mitochondrial	11,1	0	PRDX5
Q9P0M6	MACROH2A2	Core histone macro-H2A.2	1,9	0	PRDX5
P08670	VIM	Vimentin	1,9	0	PRDX5
O94925	GLS	Glutaminase kidney isoform, mitochondrial	1,9	0	PRDX5
Q9HAV4	XPO5	Exportin-5	1,9	0	PRDX5
P35580	MYH10	Myosin-10	1,9	0	PRDX5
E9PKP7	UBTF	Nucleolar transcription factor 1	1,9	0	PRDX5
O14579	COPE	Coatomer subunit epsilon	1,9	0	PRDX5
P35606	COPB2	Coatomer subunit beta'	1,9	0,001	PRDX5
P51570	GALK1	Galactokinase	1,9	0,001	PRDX5
P42345	MTOR	Serine/threonine-protein kinase mTOR	1,9	0,003	PRDX5
Q16762	TST	Thiosulfate sulfurtransferase	1,9	0,003	PRDX5
P46940	IQGAP1	Ras GTPase-activating-like protein IQGAP1	1,9	0,004	PRDX5
O60678	PRMT3	Protein arginine N-methyltransferase 3	1,9	0,004	PRDX5
P11388	TOP2A	DNA topoisomerase 2-alpha	1,9	0,005	PRDX5
Q14690	PDCD11	Protein RRP5 homolog	1,9	0,005	PRDX5
Q86WA6	BPHL	Valacyclovir hydrolase	1,9	0,006	PRDX5
Q6DKI1	RPL7L1	60S ribosomal protein L7-like 1	1,9	0,006	PRDX5
P84085	ARF5	ADP-ribosylation factor 5	1,9	0,007	PRDX5
P46013	MKI67	Proliferation marker protein Ki-67	1,9	0,008	PRDX5
Q9NQG6	MIEF1	Mitochondrial dynamics protein MID51	1,9	0,009	PRDX5
P56962	STX17	Syntaxin-17	1,9	0,009	PRDX5
Q7Z3C6	ATG9A	Autophagy-related protein 9A	1,9	0,014	PRDX5
Q5VT66	MTARC1	Mitochondrial amidoxime-reducing component 1	1,8	0	PRDX5
O94905	ERLIN2	Erlin-2	1,8	0	PRDX5
P08240	SRPRA	Signal recognition particle receptor subunit alpha	1,8	0	PRDX5
O95168	NDUFB4	NADH dehydrogenase [ubiquinone] 1 beta subcomplex subunit 4	1,8	0	PRDX5
Q6WCQ1	MPRIP	Myosin phosphatase Rho-interacting protein	1,8	0	PRDX5
Q9NW13	RBM28	RNA-binding protein 28	1,8	0,001	PRDX5
Q02880	TOP2B	DNA topoisomerase 2-beta	1,8	0,002	PRDX5
Q96RP9	GFM1	Elongation factor G, mitochondrial	1,8	0,002	PRDX5
Q9Y6Y8	SEC23IP	SEC23-interacting protein	1,8	0,002	PRDX5
K7ESE9	BCAS3	Breast carcinoma-amplified sequence 3	1,8	0,002	PRDX5
E7EVH7	E7EVH7	Kinesin light chain	1,8	0,003	PRDX5
Q4VCS5	AMOT	Angiomotin	1,8	0,003	PRDX5
P07384	CAPN1	Calpain-1 catalytic subunit	1,8	0,004	PRDX5
Q13951	CBFB	Core-binding factor subunit beta	1,8	0,005	PRDX5
Q9BPW8	NIPSNAP1	Protein NipSnap homolog 1	1,8	0,006	PRDX5
P42704	LRPPRC	Leucine-rich PPR motif-containing protein, mitochondrial	1,8	0,006	PRDX5
G5EA06	MRPS27	28S ribosomal protein S27, mitochondrial	1,8	0,006	PRDX5
O60502	OGA	Protein O-GlcNAcase	1,8	0,009	PRDX5
Q8WVC2	RPS21	40S ribosomal protein S21	1,8	0,009	PRDX5
Q14789	GOLGB1	Golgin subfamily B member 1	1,8	0,01	PRDX5
P68133	ACTA1	Actin, alpha skeletal muscle	1,8	0,019	PRDX5
O96008	TOMM40	Mitochondrial import receptor subunit TOM40 homolog	1,8	0,033	PRDX5
Q9BYN0	SRXN1	Sulfiredoxin-1	1,8	0,038	PRDX5
Q15075	EEA1	Early endosome antigen 1	1,7	0	PRDX5
O94973	AP2A2	AP-2 complex subunit alpha-2	1,7	0	PRDX5
Q9GZT3	SLIRP	SRA stem-loop-interacting RNA-binding protein, mitochondrial	1,7	0	PRDX5
O15381	NVL	Nuclear valosin-containing protein-like	1,7	0	PRDX5
Q6P996	PDXDC1	Pyridoxal-dependent decarboxylase domain-containing protein 1	1,7	0	PRDX5
P58107	EPPK1	Epiplakin	1,7	0	PRDX5
P04899	GNAI2	Guanine nucleotide-binding protein G(i) subunit alpha-2	1,7	0	PRDX5
P56545	CTBP2	C-terminal-binding protein 2	1,7	0	PRDX5
P50995	ANXA11	Annexin A11	1,7	0,001	PRDX5
P53597	SUCLG1	Succinate--CoA ligase [ADP/GDP-forming] subunit alpha, mitochondrial	1,7	0,001	PRDX5
P18031	PTPN1	Tyrosine-protein phosphatase non-receptor type 1	1,7	0,001	PRDX5
Q8WTT2	NOC3L	Nucleolar complex protein 3 homolog	1,7	0,003	PRDX5
P09110	ACAA1	3-ketoacyl-CoA thiolase, peroxisomal	1,7	0,005	PRDX5
P48047	ATP5PO	ATP synthase subunit O, mitochondrial	1,7	0,006	PRDX5
Q53H96	PYCR3	Pyrroline-5-carboxylate reductase 3	1,7	0,007	PRDX5
C9JZR2	CTNND1	Catenin delta-1	1,7	0,008	PRDX5
P78316	NOP14	Nucleolar protein 14	1,7	0,008	PRDX5
Q6ZVM7	TOM1L2	TOM1-like protein 2	1,7	0,01	PRDX5
Q9NP72	RAB18	Ras-related protein Rab-18	1,7	0,015	PRDX5

Q9H6R0	DHX33	ATP-dependent RNA helicase DHX33	1,7	0,015	PRDX5
P15924	DSP	Desmoplakin	1,7	0,016	PRDX5
Q9NZ45	CISD1	CDGSH iron-sulfur domain-containing protein 1	1,7	0,04	PRDX5
Q8N5K1	CISD2	CDGSH iron-sulfur domain-containing protein 2	1,7	0,047	PRDX5
P52948	NUP98	Nuclear pore complex protein Nup98-Nup96	1,6	0	PRDX5
Q5UIP0	RIF1	Telomere-associated protein RIF1	1,6	0	PRDX5
Q5T3I0	GPATCH4	G patch domain-containing protein 4	1,6	0	PRDX5
Q86U42	PABPN1	Polyadenylate-binding protein 2	1,6	0	PRDX5
O75439	PMPCB	Mitochondrial-processing peptidase subunit beta	1,6	0	PRDX5
P43897	TSFM	Elongation factor Ts, mitochondrial	1,6	0	PRDX5
A0A0D9SF70	ARFGAP2	ADP-ribosylation factor GTPase-activating protein 2	1,6	0	PRDX5
B8ZZC5	GLS	Glutaminase	1,6	0	PRDX5
O00410	IPO5	Importin-5	1,6	0	PRDX5
Q9Y2R9	MRPS7	28S ribosomal protein S7, mitochondrial	1,6	0	PRDX5
P16435	POR	NADPH--cytochrome P450 reductase	1,6	0	PRDX5
E9PFR3	PPP2R5D	Serine/threonine-protein phosphatase 2A 56 kDa regulatory subunit	1,6	0	PRDX5
O95573	ACSL3	Long-chain-fatty-acid--CoA ligase 3	1,6	0	PRDX5
Q8TC07	TBC1D15	TBC1 domain family member 15	1,6	0	PRDX5
Q9NQ88	TIGAR	Fructose-2,6-bisphosphatase TIGAR	1,6	0	PRDX5
A0A087X1A5	STAU1	Double-stranded RNA-binding protein Staufen homolog 1	1,6	0	PRDX5
D6RB59	EXOC3	Exocyst complex component 3	1,6	0,001	PRDX5
E9PF10	NUP155	Nuclear pore complex protein Nup155	1,6	0,001	PRDX5
Q03701	CEBPZ	CCAAT/enhancer-binding protein zeta	1,6	0,001	PRDX5
P63244	RACK1	Receptor of activated protein C kinase 1	1,6	0,001	PRDX5
O43615	TIMM44	Mitochondrial import inner membrane translocase subunit TIM44	1,6	0,001	PRDX5
O75691	UTP20	Small subunit processome component 20 homolog	1,6	0,001	PRDX5
P14923	JUP	Junction plakoglobin	1,6	0,001	PRDX5
P61353	RPL27	60S ribosomal protein L27	1,6	0,002	PRDX5
F5H008	VPS33B	Vacuolar protein sorting-associated protein 33B	1,6	0,003	PRDX5
Q9BW92	TARS2	Threonine--tRNA ligase, mitochondrial	1,6	0,003	PRDX5
Q9H3U1	UNC45A	Protein unc-45 homolog A	1,6	0,003	PRDX5
Q9NTJ5	SACM1L	Phosphatidylinositol-3-phosphatase SAC1	1,6	0,003	PRDX5
Q9UHI6	DDX20	Probable ATP-dependent RNA helicase DDX20	1,6	0,004	PRDX5
Q7L2E3	DHX30	ATP-dependent RNA helicase DHX30	1,6	0,007	PRDX5
Q5VYK3	ECPAS	Proteasome adapter and scaffold protein ECM29	1,6	0,008	PRDX5
Q9Y2R4	DDX52	Probable ATP-dependent RNA helicase DDX52	1,6	0,008	PRDX5
P53007	SLC25A1	Tricarboxylate transport protein, mitochondrial	1,6	0,01	PRDX5
P08559	PDHA1	Pyruvate dehydrogenase E1 component subunit alpha, somatic form, mitochondrial	1,6	0,012	PRDX5
Q8TB36	GDAP1	Ganglioside-induced differentiation-associated protein 1	1,6	0,013	PRDX5
Q01082	SPTBN1	Spectrin beta chain, non-erythrocytic 1	1,6	0,016	PRDX5
Q16186	ADRM1	Proteasomal ubiquitin receptor ADRM1	1,6	0,016	PRDX5
Q9Y4P1	ATG4B	Cysteine protease ATG4B	1,6	0,016	PRDX5
Q13813	SPTAN1	Spectrin alpha chain, non-erythrocytic 1	1,6	0,021	PRDX5
Q5JRI1	SRSF10	Serine/arginine-rich-splicing factor 10	1,6	0,022	PRDX5
O60566	BUB1B	Mitotic checkpoint serine/threonine-protein kinase BUB1 beta	1,6	0,024	PRDX5
K7ELV2	SEH1L	Nucleoporin SEH1	1,6	0,025	PRDX5
H3BRY6	INTS14	Integrator complex subunit 14	1,6	0,027	PRDX5
P42765	ACAA2	3-ketoacyl-CoA thiolase, mitochondrial	1,5	0	PRDX5
P08243	ASNS	Asparagine synthetase [glutamine-hydrolyzing]	1,5	0	PRDX5
Q9UN37	VPS4A	Vacuolar protein sorting-associated protein 4A	1,5	0	PRDX5
A0A0A0MRM8	MYO6	Unconventional myosin-6	1,5	0	PRDX5
Q9Y2Q3	GSTK1	Glutathione S-transferase kappa 1	1,5	0	PRDX5
P49327	FASN	Fatty acid synthase	1,5	0	PRDX5
Q92973	TNPO1	Transportin-1	1,5	0	PRDX5
P19525	EIF2AK2	Interferon-induced, double-stranded RNA-activated protein kinase	1,5	0	PRDX5
Q9Y371	SH3GLB1	Endophilin-B1	1,5	0,001	PRDX5
O15226	NKRF	NF-kappa-B-repressing factor	1,5	0,001	PRDX5
Q9Y4E8	USP15	Ubiquitin carboxyl-terminal hydrolase 15	1,5	0,003	PRDX5
P04181	OAT	Ornithine aminotransferase, mitochondrial	1,5	0,003	PRDX5
Q13363	CTBP1	C-terminal-binding protein 1	1,5	0,004	PRDX5
O60264	SMARCA5	SWI/SNF-related matrix-associated actin-dependent regulator of chromatin subfamily A member 5	1,5	0,004	PRDX5
P82930	MRPS34	28S ribosomal protein S34, mitochondrial	1,5	0,005	PRDX5
Q92616	GCN1	eIF-2-alpha kinase activator GCN1	1,5	0,006	PRDX5
Q9Y394	DHRS7	Dehydrogenase/reductase SDR family member 7	1,5	0,008	PRDX5
A0A3B3IUD2	MSTO1	Protein misato homolog 1	1,5	0,01	PRDX5
Q9UHQ9	CYB5R1	NADH-cytochrome b5 reductase 1	1,5	0,012	PRDX5
P07947	YES1	Tyrosine-protein kinase Yes	1,5	0,013	PRDX5
P42694	HELZ	Probable helicase with zinc finger domain	1,5	0,013	PRDX5

H0YLH3	RABGGTA	Geranylgeranyl transferase type-2 subunit alpha	1,5	0,014	PRDX5
Q13561	DCTN2	Dynactin subunit 2	1,5	0,015	PRDX5
Q8NI60	COQ8A	Atypical kinase COQ8A, mitochondrial	1,5	0,016	PRDX5
A0A0A0MRT6	ABI1	Abl interactor 1	1,5	0,016	PRDX5
P31327	CPS1	Carbamoyl-phosphate synthase [ammonia], mitochondrial	1,5	0,017	PRDX5
Q9NP97	DYNLRB1	Dynein light chain roadblock-type 1	1,5	0,018	PRDX5
O15143	ARPC1B	Actin-related protein 2/3 complex subunit 1B	1,5	0,019	PRDX5
Q14204	DYNC1H1	Cytoplasmic dynein 1 heavy chain 1	1,5	0,021	PRDX5
A0A2R8YFH5	SEC23B	Protein transport protein SEC23	1,5	0,026	PRDX5
Q9NXH9	TRMT1	tRNA	1,5	0,028	PRDX5
Q7L5D6	GET4	Golgi to ER traffic protein 4 homolog	1,5	0,028	PRDX5
O43347	MSI1	RNA-binding protein Musashi homolog 1	1,5	0,029	PRDX5
Q9H840	GEMIN7	Gem-associated protein 7	1,5	0,034	PRDX5
Q99459	CDC5L	Cell division cycle 5-like protein	1,5	0,04	PRDX5
Q9NY61	AATF	Protein AATF	1,4	0	PRDX5
E7ETZ4	BZW2	Basic leucine zipper and W2 domain-containing protein 2	1,4	0	PRDX5
Q9HAV7	GRPEL1	GrpE protein homolog 1, mitochondrial	1,4	0	PRDX5
P50542	PEX5	Peroxisomal targeting signal 1 receptor	1,4	0	PRDX5
Q4J6C6	PREPL	Prolyl endopeptidase-like	1,4	0	PRDX5
Q99798	ACO2	Aconitate hydratase, mitochondrial	1,4	0	PRDX5
O76031	CLPX	ATP-dependent Clp protease ATP-binding subunit clpX-like, mitochondrial	1,4	0	PRDX5
A0A0U1RRM6	ENAH	Protein enabled homolog	1,4	0,001	PRDX5
Q9BSH4	TACO1	Translational activator of cytochrome c oxidase 1	1,4	0,001	PRDX5
O60684	KPNA6	Importin subunit alpha-7	1,4	0,001	PRDX5
P54136	RARS1	Arginine--tRNA ligase, cytoplasmic	1,4	0,001	PRDX5
Q8WUM0	NUP133	Nuclear pore complex protein Nup133	1,4	0,002	PRDX5
Q8WXF1	PSPC1	Paraspeckle component 1	1,4	0,002	PRDX5
G5E9W7	MRPS22	28S ribosomal protein S22, mitochondrial	1,4	0,002	PRDX5
Q12849	GRSF1	G-rich sequence factor 1	1,4	0,002	PRDX5
O15397	IPO8	Importin-8	1,4	0,002	PRDX5
Q93034	CUL5	Cullin-5	1,4	0,002	PRDX5
A0A0G2JNZ2	SCRIB	Protein scribble homolog	1,4	0,002	PRDX5
Q92621	NUP205	Nuclear pore complex protein Nup205	1,4	0,002	PRDX5
P11172	UMPS	Uridine 5'-monophosphate synthase	1,4	0,003	PRDX5
Q7L1Q6	BZW1	Basic leucine zipper and W2 domain-containing protein 1	1,4	0,003	PRDX5
Q9Y678	COPG1	Coatomer subunit gamma-1	1,4	0,003	PRDX5
P84103	SRSF3	Serine/arginine-rich splicing factor 3	1,4	0,003	PRDX5
B7Z6D5	DDX27	RNA helicase	1,4	0,004	PRDX5
Q00610	CLTC	Clathrin heavy chain 1	1,4	0,004	PRDX5
P52209	PGD	6-phosphogluconate dehydrogenase, decarboxylating	1,4	0,004	PRDX5
P04843	RPN1	Dolichyl-diphosphooligosaccharide--protein glycosyltransferase subunit 1	1,4	0,004	PRDX5
D6R938	CAMK2D	Calcium/calmodulin-dependent protein kinase	1,4	0,005	PRDX5
O14980	XPO1	Exportin-1	1,4	0,006	PRDX5
P19367	HK1	Hexokinase-1	1,4	0,006	PRDX5
P33992	MCM5	DNA replication licensing factor MCM5	1,4	0,006	PRDX5
Q5JTH9	RRP12	RRP12-like protein	1,4	0,006	PRDX5
Q6P1M0	SLC27A4	Long-chain fatty acid transport protein 4	1,4	0,006	PRDX5
P07196	NEFL	Neurofilament light polypeptide	1,4	0,007	PRDX5
Q96IU4	ABHD14B	Protein ABHD14B	1,4	0,007	PRDX5
Q6P2Q9	PRPF8	Pre-mRNA-processing-splicing factor 8	1,4	0,007	PRDX5
Q9HB07	MYG1	MYG1 exonuclease	1,4	0,007	PRDX5
Q15061	WDR43	WD repeat-containing protein 43	1,4	0,009	PRDX5
Q7Z4Q2	HEATR3	HEAT repeat-containing protein 3	1,4	0,01	PRDX5
Q9Y262	EIF3L	Eukaryotic translation initiation factor 3 subunit L	1,4	0,012	PRDX5
Q5JRX3	PITRM1	Presequence protease, mitochondrial	1,4	0,012	PRDX5
Q14684	RRP1B	Ribosomal RNA processing protein 1 homolog B	1,4	0,018	PRDX5
Q9NWB6	ARGLU1	Arginine and glutamate-rich protein 1	1,4	0,021	PRDX5
O00411	POLRMT	DNA-directed RNA polymerase, mitochondrial	1,4	0,024	PRDX5
Q96KM6	ZNF512B	Zinc finger protein 512B	1,4	0,026	PRDX5
O60306	AQR	RNA helicase aquarius	1,4	0,029	PRDX5
P23284	PPIB	Peptidyl-prolyl cis-trans isomerase B	1,4	0,03	PRDX5
Q86W42	THOC6	THO complex subunit 6 homolog	1,4	0,031	PRDX5
Q9Y580	RBM7	RNA-binding protein 7	1,4	0,033	PRDX5
Q96L92	SNX27	Sorting nexin-27	1,4	0,034	PRDX5
O75146	HIP1R	Huntingtin-interacting protein 1-related protein	1,4	0,039	PRDX5
Q6P1N0	CC2D1A	Coiled-coil and C2 domain-containing protein 1A	1,3	0	PRDX5
Q8N335	GPD1L	Glycerol-3-phosphate dehydrogenase 1-like protein	1,3	0	PRDX5
Q8NCA5	FAM98A	Protein FAM98A	1,3	0	PRDX5
P26196	DDX6	Probable ATP-dependent RNA helicase DDX6	1,3	0	PRDX5

A0A2R8Y855	SMARCE1	SWI/SNF-related matrix-associated actin-dependent regulator of chromatin subfamily E member 1	1,3	0,001	PRDX5
Q14137	BOP1	Ribosome biogenesis protein BOP1	1,3	0,001	PRDX5
P55060	CSE1L	Exportin-2	1,3	0,001	PRDX5
J3QLD9	FLOT2	Flotillin	1,3	0,001	PRDX5
Q9NV70	EXOC1	Exocyst complex component 1	1,3	0,001	PRDX5
A1X283	SH3PXD2B	SH3 and PX domain-containing protein 2B	1,3	0,001	PRDX5
P35237	SERPINB6	Serpin B6	1,3	0,002	PRDX5
P62495	ETF1	Eukaryotic peptide chain release factor subunit 1	1,3	0,002	PRDX5
Q15785	TOMM34	Mitochondrial import receptor subunit TOM34	1,3	0,002	PRDX5
P50213	IDH3A	Isocitrate dehydrogenase [NAD] subunit alpha, mitochondrial	1,3	0,002	PRDX5
Q96EY7	PTCD3	Pentatricopeptide repeat domain-containing protein 3, mitochondrial	1,3	0,002	PRDX5
Q8N122	RPTOR	Regulatory-associated protein of mTOR	1,3	0,002	PRDX5
P23258	TUBG1	Tubulin gamma-1 chain	1,3	0,003	PRDX5
Q9P0K7	RAI14	Ankycorbin	1,3	0,003	PRDX5
P82933	MRPS9	28S ribosomal protein S9, mitochondrial	1,3	0,003	PRDX5
Q02252	ALDH6A1	Methylmalonate-semialdehyde dehydrogenase [acylating], mitochondrial	1,3	0,003	PRDX5
O00567	NOP56	Nucleolar protein 56	1,3	0,003	PRDX5
A5YKK6	CNOT1	CCR4-NOT transcription complex subunit 1	1,3	0,004	PRDX5
Q14258	TRIM25	E3 ubiquitin/ISG15 ligase TRIM25	1,3	0,004	PRDX5
Q9BYN8	MRPS26	28S ribosomal protein S26, mitochondrial	1,3	0,004	PRDX5
Q96N67	DOCK7	Dedicator of cytokinesis protein 7	1,3	0,006	PRDX5
P35659	DEK	Protein DEK	1,3	0,007	PRDX5
P48735	IDH2	Isocitrate dehydrogenase [NADP], mitochondrial	1,3	0,007	PRDX5
Q02241	KIF23	Kinesin-like protein KIF23	1,3	0,007	PRDX5
Q8TEM1	NUP210	Nuclear pore membrane glycoprotein 210	1,3	0,007	PRDX5
Q13190	STX5	Syntaxin-5	1,3	0,009	PRDX5
O14964	HGS	Hepatocyte growth factor-regulated tyrosine kinase substrate	1,3	0,01	PRDX5
Q7KZ85	SUPT6H	Transcription elongation factor SPT6	1,3	0,012	PRDX5
E7ESP9	NEFM	160 kDa neurofilament protein	1,3	0,015	PRDX5
Q86XI2	NCAPG2	Condensin-2 complex subunit G2	1,3	0,017	PRDX5
A0A087WZ13	RAVER1	Ribonucleoprotein PTB-binding 1	1,3	0,02	PRDX5
Q96GD0	PDXP	Pyridoxal phosphate phosphatase	1,3	0,023	PRDX5
O14974	PPP1R12A	Protein phosphatase 1 regulatory subunit 12A	1,3	0,024	PRDX5
Q9BXJ9	NAA15	N-alpha-acetyltransferase 15, NatA auxiliary subunit	1,3	0,024	PRDX5
P62318	SNRPD3	Small nuclear ribonucleoprotein Sm D3	1,3	0,024	PRDX5
Q99959	PKP2	Plakophilin-2	1,3	0,027	PRDX5
Q9Y2R5	MRPS17	28S ribosomal protein S17, mitochondrial	1,3	0,03	PRDX5
F8W108	ARID2	AT-rich interactive domain-containing protein 2	1,3	0,031	PRDX5
Q92878	RAD50	DNA repair protein RAD50	1,3	0,034	PRDX5
Q15058	KIF14	Kinesin-like protein KIF14	1,3	0,037	PRDX5
P42025	ACTR1B	Beta-centractin	1,3	0,038	PRDX5
Q9Y5L0	TNPO3	Transportin-3	1,3	0,039	PRDX5
Q96MW1	CCDC43	Coiled-coil domain-containing protein 43	1,3	0,04	PRDX5
Q969Z0	TBRG4	FAST kinase domain-containing protein 4	1,3	0,046	PRDX5
Q6PGP7	TTC37	Tetratricopeptide repeat protein 37	1,3	0,047	PRDX5
O75643	SNRNP200	U5 small nuclear ribonucleoprotein 200 kDa helicase	1,3	0,048	PRDX5
P48449	LSS	Lanosterol synthase	1,3	0,049	PRDX5
P60983	GMFB	Glia maturation factor beta	1,2	0	PRDX5
Q9BSJ2	TUBGCP2	Gamma-tubulin complex component 2	1,2	0	PRDX5
Q9UPT5	EXOC7	Exocyst complex component 7	1,2	0	PRDX5
Q15555	MAPRE2	Microtubule-associated protein RP/EB family member 2	1,2	0	PRDX5
O95613	PCNT	Pericentrin	1,2	0	PRDX5
Q5H928	HSD17B10	3-hydroxyacyl-CoA dehydrogenase type-2	1,2	0	PRDX5
Q9BTW9	TBCD	Tubulin-specific chaperone D	1,2	0	PRDX5
Q9P2R3	ANKFY1	Rabankyrin-5	1,2	0,001	PRDX5
P35249	RFC4	Replication factor C subunit 4	1,2	0,001	PRDX5
A0A140T9R1	FLOT1	Flotillin	1,2	0,001	PRDX5
Q5QJE6	DNTTIP2	Deoxynucleotidyltransferase terminal-interacting protein 2	1,2	0,002	PRDX5
P35573	AGL	Glycogen debranching enzyme	1,2	0,002	PRDX5
P57740	NUP107	Nuclear pore complex protein Nup107	1,2	0,002	PRDX5
P56182	RRP1	Ribosomal RNA processing protein 1 homolog A	1,2	0,002	PRDX5
Q5JTZ9	AARS2	Alanine--tRNA ligase, mitochondrial	1,2	0,003	PRDX5
Q8TEQ6	GEMIN5	Gem-associated protein 5	1,2	0,003	PRDX5
P63092	GNAS	Guanine nucleotide-binding protein G(s) subunit alpha isoforms short	1,2	0,003	PRDX5
Q9Y2H6	FNDC3A	Fibronectin type-III domain-containing protein 3A	1,2	0,003	PRDX5
P51452	DUSP3	Dual specificity protein phosphatase 3	1,2	0,003	PRDX5
Q9BSD7	NTPCR	Cancer-related nucleoside-triphosphatase	1,2	0,003	PRDX5
Q5T4S7	UBR4	E3 ubiquitin-protein ligase UBR4	1,2	0,004	PRDX5

O43795	MYO1B	Unconventional myosin-Ib	1,2	0,004	PRDX5
Q9Y3T9	NOC2L	Nucleolar complex protein 2 homolog	1,2	0,004	PRDX5
Q15031	LARS2	Probable leucine--tRNA ligase, mitochondrial	1,2	0,004	PRDX5
Q00688	FKBP3	Peptidyl-prolyl cis-trans isomerase FKBP3	1,2	0,005	PRDX5
Q09666	AHNAK	Neuroblast differentiation-associated protein AHNAK	1,2	0,005	PRDX5
P09543	CNP	2',3'-cyclic-nucleotide 3'-phosphodiesterase	1,2	0,006	PRDX5
Q15042	RAB3GAP1	Rab3 GTPase-activating protein catalytic subunit	1,2	0,006	PRDX5
Q96QK1	VPS35	Vacuolar protein sorting-associated protein 35	1,2	0,006	PRDX5
P25685	DNAJB1	DnaJ homolog subfamily B member 1	1,2	0,006	PRDX5
Q8WYP5	AHCTF1	Protein ELYS	1,2	0,008	PRDX5
Q92665	MRPS31	28S ribosomal protein S31, mitochondrial	1,2	0,008	PRDX5
Q8IWX8	CHERP	Calcium homeostasis endoplasmic reticulum protein	1,2	0,009	PRDX5
D6REA0	GATB	Glutamyl-tRNA(Gln) amidotransferase subunit B, mitochondrial	1,2	0,009	PRDX5
P16615	ATP2A2	Sarcoplasmic/endoplasmic reticulum calcium ATPase 2	1,2	0,009	PRDX5
A0A0A0MRJ0	CDC42BPA	Non-specific serine/threonine protein kinase	1,2	0,01	PRDX5
P19338	NCL	Nucleolin	1,2	0,01	PRDX5
P30520	ADSS2	Adenylosuccinate synthetase isozyme 2	1,2	0,011	PRDX5
P52701	MSH6	DNA mismatch repair protein Msh6	1,2	0,013	PRDX5
Q8WVM8	SCFD1	Sec1 family domain-containing protein 1	1,2	0,018	PRDX5
O14828	SCAMP3	Secretory carrier-associated membrane protein 3	1,2	0,018	PRDX5
Q9NU22	MDN1	Midasin	1,2	0,019	PRDX5
O00566	MPHOSPH10	U3 small nucleolar ribonucleoprotein protein MPP10	1,2	0,021	PRDX5
A0A3B3ITJ4	HNRNPL	Heterogeneous nuclear ribonucleoprotein L	1,2	0,022	PRDX5
P49642	PRIM1	DNA primase small subunit	1,2	0,039	PRDX5
Q5TG40	DMAP1	DNA methyltransferase 1-associated protein 1	1,2	0,044	PRDX5
P46060	RANGAP1	Ran GTPase-activating protein 1	1,2	0,045	PRDX5
Q9H2M9	RAB3GAP2	Rab3 GTPase-activating protein non-catalytic subunit	1,1	0	PRDX5
O94874	UFL1	E3 UFM1-protein ligase 1	1,1	0	PRDX5
O95292	VAPB	Vesicle-associated membrane protein-associated protein B/C	1,1	0	PRDX5
Q6UWP7	LCLAT1	Lysocardiolipin acyltransferase 1	1,1	0	PRDX5
Q6P3W7	SCYL2	SCY1-like protein 2	1,1	0	PRDX5
Q8TC12	RDH11	Retinol dehydrogenase 11	1,1	0	PRDX5
O75396	SEC22B	Vesicle-trafficking protein SEC22b	1,1	0,001	PRDX5
P35221	CTNNA1	Catenin alpha-1	1,1	0,001	PRDX5
P23919	DTYMK	Thymidylate kinase	1,1	0,001	PRDX5
O14530	TXNDC9	Thioredoxin domain-containing protein 9	1,1	0,001	PRDX5
C9JRJ5	LIMD1	LIM domain-containing protein 1	1,1	0,001	PRDX5
Q6P9B6	MEAK7	MTOR-associated protein MEAK7	1,1	0,001	PRDX5
Q96A33	CCDC47	Coiled-coil domain-containing protein 47	1,1	0,001	PRDX5
E9PS17	SCYL1	N-terminal kinase-like protein	1,1	0,001	PRDX5
Q14166	TTLL12	Tubulin--tyrosine ligase-like protein 12	1,1	0,002	PRDX5
Q6NVY1	HIBCH	3-hydroxyisobutyryl-CoA hydrolase, mitochondrial	1,1	0,002	PRDX5
P68104	EEF1A1	Elongation factor 1-alpha 1	1,1	0,002	PRDX5
Q8IXI1	RHOT2	Mitochondrial Rho GTPase 2	1,1	0,003	PRDX5
Q96P70	IPO9	Importin-9	1,1	0,003	PRDX5
Q4G0F5	VPS26B	Vacuolar protein sorting-associated protein 26B	1,1	0,004	PRDX5
P63010	AP2B1	AP-2 complex subunit beta	1,1	0,004	PRDX5
Q8IWC1	MAP7D3	MAP7 domain-containing protein 3	1,1	0,004	PRDX5
A0A3B3IS71	RB1	Retinoblastoma-associated protein	1,1	0,004	PRDX5
A0A2R8YDQ9	SUCLA2	Succinate--CoA ligase [ADP-forming] subunit beta, mitochondrial	1,1	0,004	PRDX5
A0A1B0GV47	KIF21A	Kinesin-like protein KIF21A	1,1	0,004	PRDX5
Q01968	OCRL	Inositol polyphosphate 5-phosphatase OCRL	1,1	0,005	PRDX5
Q9NZL4	HSPBP1	Hsp70-binding protein 1	1,1	0,006	PRDX5
Q10713	PMPCA	Mitochondrial-processing peptidase subunit alpha	1,1	0,006	PRDX5
P33993	MCM7	DNA replication licensing factor MCM7	1,1	0,006	PRDX5
Q8IX01	SUGP2	SURP and G-patch domain-containing protein 2	1,1	0,007	PRDX5
Q8IY81	FTSJ3	pre-rRNA 2'-O-ribose RNA methyltransferase FTSJ3	1,1	0,007	PRDX5
Q9BPX3	NCAPG	Condensin complex subunit 3	1,1	0,007	PRDX5
P53618	COPB1	Coatomer subunit beta	1,1	0,007	PRDX5
Q9Y237	PIN4	Peptidyl-prolyl cis-trans isomerase NIMA-interacting 4	1,1	0,007	PRDX5
P46778	RPL21	60S ribosomal protein L21	1,1	0,007	PRDX5
Q9BYG3	NIFK	MKI67 FHA domain-interacting nucleolar phosphoprotein	1,1	0,008	PRDX5
Q9BXY0	MAK16	Protein MAK16 homolog	1,1	0,008	PRDX5
P55735	SEC13	Protein SEC13 homolog	1,1	0,009	PRDX5
Q16512	PKN1	Serine/threonine-protein kinase N1	1,1	0,009	PRDX5
O76094	SRP72	Signal recognition particle subunit SRP72	1,1	0,01	PRDX5
Q7L0Y3	TRMT10C	tRNA methyltransferase 10 homolog C	1,1	0,011	PRDX5
Q9NSK0	KLC4	Kinesin light chain 4	1,1	0,012	PRDX5
Q8IYI6	EXOC8	Exocyst complex component 8	1,1	0,013	PRDX5

Q14240	EIF4A2	Eukaryotic initiation factor 4A-II	1,1	0,014	PRDX5
Q9BQ69	MACROD1	ADP-ribose glycohydrolase MACROD1	1,1	0,016	PRDX5
P78344	EIF4G2	Eukaryotic translation initiation factor 4 gamma 2	1,1	0,016	PRDX5
Q14318	FKBP8	Peptidyl-prolyl cis-trans isomerase FKBP8	1,1	0,017	PRDX5
Q8N3C0	ASCC3	Activating signal cointegrator 1 complex subunit 3	1,1	0,017	PRDX5
Q9UFC0	LRWD1	Leucine-rich repeat and WD repeat-containing protein 1	1,1	0,018	PRDX5
Q9ULX6	AKAP8L	A-kinase anchor protein 8-like	1,1	0,019	PRDX5
Q05655	PRKCD	Protein kinase C delta type	1,1	0,019	PRDX5
Q5T7U1	GTF3C5	General transcription factor 3C polypeptide 5	1,1	0,021	PRDX5
Q9BUF5	TUBB6	Tubulin beta-6 chain	1,1	0,021	PRDX5
P33176	KIF5B	Kinesin-1 heavy chain	1,1	0,022	PRDX5
Q8N9T8	KRI1	Protein KRI1 homolog	1,1	0,023	PRDX5
E7EVI4	TACC1	Transforming acidic coiled-coil-containing protein 1	1,1	0,024	PRDX5
P00568	AK1	Adenylate kinase isoenzyme 1	1,1	0,024	PRDX5
Q08945	SSRP1	FACT complex subunit SSRP1	1,1	0,024	PRDX5
P08754	GNAI3	Guanine nucleotide-binding protein G(i) subunit alpha	1,1	0,025	PRDX5
Q5SY16	NOL9	Polynucleotide 5'-hydroxyl-kinase NOL9	1,1	0,026	PRDX5
O75436	VPS26A	Vacuolar protein sorting-associated protein 26A	1,1	0,027	PRDX5
P48507	GCLM	Glutamate--cysteine ligase regulatory subunit	1,1	0,029	PRDX5
F2Z388	RPL35	60S ribosomal protein L35	1,1	0,03	PRDX5
Q9H0E2	TOLLIP	Toll-interacting protein	1,1	0,03	PRDX5
Q9NQT5	EXOSC3	Exosome complex component RRP40	1,1	0,031	PRDX5
Q99961	SH3GL1	Endophilin-A2	1,1	0,037	PRDX5
Q9UG63	ABCF2	ATP-binding cassette sub-family F member 2	1,1	0,038	PRDX5
H3BTL2	BCKDK	Protein-serine/threonine kinase	1,1	0,038	PRDX5
P49458	SRP9	Signal recognition particle 9 kDa protein	1,1	0,039	PRDX5
P47897	QARS1	Glutamine--tRNA ligase	1,1	0,039	PRDX5
A0A087WU06	TUBGCP3	Gamma-tubulin complex component	1,1	0,039	PRDX5
Q9HCD5	NCOA5	Nuclear receptor coactivator 5	1,1	0,041	PRDX5
O60783	MRPS14	28S ribosomal protein S14, mitochondrial	1,1	0,047	PRDX5
G8JLH9	STAT3	Signal transducer and activator of transcription	1	0	PRDX5
P11498	PC	Pyruvate carboxylase, mitochondrial	1	0	PRDX5
Q6IAA8	LAMTOR1	Ragulator complex protein LAMTOR1	1	0	PRDX5
P41240	CSK	Tyrosine-protein kinase CSK	1	0,001	PRDX5
Q96SK2	TMEM209	Transmembrane protein 209	1	0,001	PRDX5
Q9BRA2	TXNDC17	Thioredoxin domain-containing protein 17	1	0,002	PRDX5
O00203	AP3B1	AP-3 complex subunit beta-1	1	0,002	PRDX5
Q86VS8	HOOK3	Protein Hook homolog 3	1	0,002	PRDX5
Q13451	FKBP5	Peptidyl-prolyl cis-trans isomerase FKBP5	1	0,003	PRDX5
Q9H3P7	ACBD3	Golgi resident protein GCP60	1	0,003	PRDX5
Q9UPN9	TRIM33	E3 ubiquitin-protein ligase TRIM33	1	0,003	PRDX5
Q9NQT4	EXOSC5	Exosome complex component RRP46	1	0,004	PRDX5
Q15650	TRIP4	Activating signal cointegrator 1	1	0,005	PRDX5
Q12788	TBL3	Transducin beta-like protein 3	1	0,005	PRDX5
Q8IWZ3	ANKHD1	Ankyrin repeat and KH domain-containing protein 1	1	0,006	PRDX5
Q12769	NUP160	Nuclear pore complex protein Nup160	1	0,006	PRDX5
Q16527	CSRP2	Cysteine and glycine-rich protein 2	1	0,007	PRDX5
P23921	RRM1	Ribonucleoside-diphosphate reductase large subunit	1	0,007	PRDX5
Q92600	CNOT9	CCR4-NOT transcription complex subunit 9	1	0,009	PRDX5
Q9UHB9	SRP68	Signal recognition particle subunit SRP68	1	0,009	PRDX5
P21964	COMT	Catechol O-methyltransferase	1	0,012	PRDX5
P00519	ABL1	Tyrosine-protein kinase ABL1	1	0,014	PRDX5
Q8NI27	THOC2	THO complex subunit 2	1	0,015	PRDX5
P61163	ACTR1A	Alpha-centractin	1	0,015	PRDX5
Q9BQ39	DDX50	ATP-dependent RNA helicase DDX50	1	0,015	PRDX5
Q96RQ3	MCCC1	Methylcrotonoyl-CoA carboxylase subunit alpha, mitochondrial	1	0,017	PRDX5
O75150	RNF40	E3 ubiquitin-protein ligase BRE1B	1	0,024	PRDX5
Q9UNX4	WDR3	WD repeat-containing protein 3	1	0,025	PRDX5
Q14232	EIF2B1	Translation initiation factor eIF-2B subunit alpha	1	0,027	PRDX5
F8W0J6	NAP1L1	Nucleosome assembly protein 1-like 1	1	0,039	PRDX5
Q99569	PKP4	Plakophilin-4	1	0,039	PRDX5
Q5T760	SRSF11	Serine/arginine-rich-splicing factor 11	1	0,039	PRDX5
Q9Y5K6	CD2AP	CD2-associated protein	1	0,046	PRDX5
O75131	CPNE3	Copine-3	1	0,047	PRDX5
P12277	CKB	Creatine kinase B-type	1	0,049	PRDX5
PRDX4 -specific interactors					
P30048	PRDX3	Thioredoxin-dependent peroxide reductase, mitochondrial	9,3	0	PRDX1
P13667	PDIA4	Protein disulfide-isomerase A4	6,7	0	PRDX1
Q15084	PDIA6	Protein disulfide-isomerase A6	5,1	0	PRDX1

P27797	CALR	Calreticulin	5,1	0	PRDX1
P30101	PDIA3	Protein disulfide-isomerase A3	4,4	0	PRDX1
P62805	H4C1	Histone H4	4,1	0	PRDX1
O76094	SRP72	Signal recognition particle subunit SRP72	4	0	PRDX1
P02790	HPX	Hemopexin	3,9	0	PRDX1
Q12797	ASPH	Aspartyl/asparaginyl beta-hydroxylase	3,8	0	PRDX1
Q9NYU2	UGGT1	UDP-glucose:glycoprotein glucosyltransferase 1	3,8	0	PRDX1
P07237	P4HB	Protein disulfide-isomerase	3,8	0	PRDX1
P27824	CANX	Calnexin	3,8	0	PRDX1
O60506	SYNCRIP	Heterogeneous nuclear ribonucleoprotein Q	3,7	0	PRDX1
P42704	LRPPRC	Leucine-rich PPR motif-containing protein, mitochondrial	3,7	0	PRDX1
Q14257	RCN2	Reticulocalbin-2	3,6	0	PRDX1
A0A087X054	HYOU1	Hypoxia up-regulated protein 1	3,5	0	PRDX1
P11047	LAMC1	Laminin subunit gamma-1	3,3	0	PRDX1
P05387	RPLP2	60S acidic ribosomal protein P2	3,3	0	PRDX1
P11021	HSPA5	Endoplasmic reticulum chaperone BiP	3,3	0	PRDX1
P35637	FUS	RNA-binding protein FUS	3,2	0	PRDX1
Q13217	DNAJC3	DnaJ homolog subfamily C member 3	3,2	0	PRDX1
O00469	PLOD2	Procollagen-lysine,2-oxoglutarate 5-dioxygenase 2	3,2	0,001	PRDX1
Q9BS26	ERP44	Endoplasmic reticulum resident protein 44	3,2	0,016	PRDX1
P40429	RPL13A	60S ribosomal protein L13a	3,1	0	PRDX1
P05386	RPLP1	60S acidic ribosomal protein P1	3	0	PRDX1
Q9UBS4	DNAJB11	DnaJ homolog subfamily B member 11	2,9	0	PRDX1
P98175	RBM10	RNA-binding protein 10	2,9	0	PRDX1
P78417	GSTO1	Glutathione S-transferase omega-1	2,7	0	PRDX1
C9J4Z3	RPL37A	60S ribosomal protein L37a	2,7	0	PRDX1
P14625	HSP90B1	Endoplasmin	2,7	0	PRDX1
B9A018	USP39	U4/U6.U5 tri-snRNP-associated protein 2	2,6	0	PRDX1
P23588	EIF4B	Eukaryotic translation initiation factor 4B	2,6	0	PRDX1
P19338	NCL	Nucleolin	2,6	0	PRDX1
P50454	SERPINH1	Serpin H1	2,6	0	PRDX1
Q9BZQ6	EDEM3	ER degradation-enhancing alpha-mannosidase-like protein 3	2,6	0,001	PRDX1
D6RBV2	LMAN2	Vesicular integral-membrane protein VIP36	2,6	0,002	PRDX1
P62314	SNRPD1	Small nuclear ribonucleoprotein Sm D1	2,5	0	PRDX1
P18077	RPL35A	60S ribosomal protein L35a	2,5	0	PRDX1
O00268	TAF4	Transcription initiation factor TFIID subunit 4	2,5	0	PRDX1
P12109	COL6A1	Collagen alpha-1(VI) chain	2,5	0,002	PRDX1
Q9UBF2	COPG2	Coatomer subunit gamma-2	2,4	0	PRDX1
Q8TEM1	NUP210	Nuclear pore membrane glycoprotein 210	2,4	0,001	PRDX1
Q15293	RCN1	Reticulocalbin-1	2,4	0,001	PRDX1
Q9Y680	FKBP7	Peptidyl-prolyl cis-trans isomerase FKBP7	2,4	0,003	PRDX1
Q15459	SF3A1	Splicing factor 3A subunit 1	2,4	0,049	PRDX1
P49257	LMAN1	Protein ERGIC-53	2,3	0,001	PRDX1
P36957	DLST	Dihydrolipoyllysine-residue succinyltransferase component of 2-oxoglutarate dehydrogenase complex, mitochondrial	2,2	0	PRDX1
Q02750	MAP2K1	Dual specificity mitogen-activated protein kinase kinase 1	2,1	0	PRDX1
Q9H8Y8	GORASP2	Golgi reassembly-stacking protein 2	2,1	0	PRDX1
P06730	EIF4E	Eukaryotic translation initiation factor 4E	2,1	0	PRDX1
Q9UIG0	BAZ1B	Tyrosine-protein kinase BAZ1B	2,1	0	PRDX1
P31942	HNRNPH3	Heterogeneous nuclear ribonucleoprotein H3	2,1	0	PRDX1
P26196	DDX6	Probable ATP-dependent RNA helicase DDX6	2,1	0	PRDX1
Q13257	MAD2L1	Mitotic spindle assembly checkpoint protein MAD2A	2,1	0,001	PRDX1
Q8NI27	THOC2	THO complex subunit 2	2,1	0,001	PRDX1
Q9BQG0	MYBBP1A	Myb-binding protein 1A	2,1	0,001	PRDX1
Q8IXB1	DNAJC10	DnaJ homolog subfamily C member 10	2,1	0,002	PRDX1
Q5SY16	NOL9	Polynucleotide 5'-hydroxyl-kinase NOL9	2,1	0,002	PRDX1
P55268	LAMB2	Laminin subunit beta-2	2,1	0,003	PRDX1
P53350	PLK1	Serine/threonine-protein kinase PLK1	2,1	0,025	PRDX1
P09972	ALDOC	Fructose-bisphosphate aldolase C	2,1	0,048	PRDX1
P13674	P4HA1	Prolyl 4-hydroxylase subunit alpha-1	2	0	PRDX1
O75821	EIF3G	Eukaryotic translation initiation factor 3 subunit G	2	0	PRDX1
Q4J6C6	PREPL	Prolyl endopeptidase-like	2	0,001	PRDX1
D6RA00	ENOPH1	Enolase-phosphatase E1	2	0,003	PRDX1
P11388	TOP2A	DNA topoisomerase 2-alpha	2	0,003	PRDX1
Q13162	PRDX4	Peroxiredoxin-4	11,3	0	PRDX1
Q9H0A0	NAT10	RNA cytidine acetyltransferase	1,9	0	PRDX1
P50502	ST13	Hsc70-interacting protein	1,9	0	PRDX1
P55769	SNU13	NHP2-like protein 1	1,9	0	PRDX1
O75832	PSMD10	26S proteasome non-ATPase regulatory subunit 10	1,9	0	PRDX1

Q9Y3Z3	SAMHD1	Deoxynucleoside triphosphate triphosphohydrolase SAMHD1	1,9	0	PRDX1
O00203	AP3B1	AP-3 complex subunit beta-1	1,9	0	PRDX1
Q96H79	ZC3HAV1L	Zinc finger CCCH-type antiviral protein 1-like	1,9	0	PRDX1
P14324	FDPS	Farnesyl pyrophosphate synthase	1,9	0	PRDX1
G3V529	DDX24	RNA helicase	1,9	0,001	PRDX1
Q9ULC3	RAB23	Ras-related protein Rab-23	1,9	0,003	PRDX1
P11182	DBT	Lipoamide acyltransferase component of branched-chain alpha-keto acid dehydrogenase complex, mitochondrial	1,9	0,004	PRDX1
O94925	GLS	Glutaminase kidney isoform, mitochondrial	1,9	0,006	PRDX1
P63167	DYNLL1	Dynein light chain 1, cytoplasmic	1,9	0,019	PRDX1
A0A0B4J1Z1	SRSF7	Serine/arginine-rich-splicing factor 7	1,9	0,028	PRDX1
P38159	RBMX	RNA-binding motif protein, X chromosome	1,9	0,029	PRDX1
P11387	TOP1	DNA topoisomerase 1	1,8	0	PRDX1
P49321	NASP	Nuclear autoantigenic sperm protein	1,8	0	PRDX1
P53985	SLC16A1	Monocarboxylate transporter 1	1,8	0	PRDX1
P40938	RFC3	Replication factor C subunit 3	1,8	0	PRDX1
O75688	PPM1B	Protein phosphatase 1B	1,8	0,001	PRDX1
P52597	HNRNPF	Heterogeneous nuclear ribonucleoprotein F	1,8	0,001	PRDX1
Q92621	NUP205	Nuclear pore complex protein Nup205	1,8	0,002	PRDX1
Q93008	USP9X	Probable ubiquitin carboxyl-terminal hydrolase FAF-X	1,8	0,002	PRDX1
O95104	SCAF4	SR-related and CTD-associated factor 4	1,8	0,006	PRDX1
C9J384	CMSS1	Protein CMSS1	1,8	0,009	PRDX1
Q9NQ29	LUC7L	Putative RNA-binding protein Luc7-like 1	1,8	0,009	PRDX1
P62750	RPL23A	60S ribosomal protein L23a	1,7	0	PRDX1
P52565	ARHGDIA	Rho GDP-dissociation inhibitor 1	1,7	0	PRDX1
E9PIF2	DDX10	RNA helicase	1,7	0	PRDX1
Q15691	MAPRE1	Microtubule-associated protein RP/EB family member 1	1,7	0	PRDX1
Q15393	SF3B3	Splicing factor 3B subunit 3	1,7	0,002	PRDX1
Q09028	RBBP4	Histone-binding protein RBBP4	1,7	0,002	PRDX1
P41252	IARS1	Isoleucine--tRNA ligase, cytoplasmic	1,7	0,002	PRDX1
P08758	ANXA5	Annexin A5	1,7	0,003	PRDX1
P22307	SCP2	Non-specific lipid-transfer protein	1,7	0,003	PRDX1
Q01085	TIAL1	Nucleolysin TIAR	1,7	0,007	PRDX1
Q9Y2H1	STK38L	Serine/threonine-protein kinase 38-like	1,7	0,007	PRDX1
P63244	RACK1	Receptor of activated protein C kinase 1	1,7	0,01	PRDX1
P04844	RPN2	Dolichyl-diphosphooligosaccharide--protein glycosyltransferase subunit 2	1,7	0,013	PRDX1
P61353	RPL27	60S ribosomal protein L27	1,7	0,016	PRDX1
E9PFZ2	CP	Ceruloplasmin	1,7	0,024	PRDX1
P35579	MYH9	Myosin-9	1,7	0,026	PRDX1
Q53GQ0	HSD17B12	Very-long-chain 3-oxoacyl-CoA reductase	1,7	0,028	PRDX1
Q15291	RBBP5	Retinoblastoma-binding protein 5	1,6	0	PRDX1
Q14697	GANAB	Neutral alpha-glucosidase AB	1,6	0	PRDX1
O60934	NBN	Nibrin	1,6	0	PRDX1
P09211	GSTP1	Glutathione S-transferase P	1,6	0	PRDX1
P32969	RPL9	60S ribosomal protein L9	1,6	0	PRDX1
P43034	PAFAH1B1	Platelet-activating factor acetylhydrolase IB subunit beta	1,6	0	PRDX1
P34949	MPI	Mannose-6-phosphate isomerase	1,6	0	PRDX1
P62424	RPL7A	60S ribosomal protein L7a	1,6	0	PRDX1
P56192	MARS1	Methionine--tRNA ligase, cytoplasmic	1,6	0,001	PRDX1
Q16531	DDB1	DNA damage-binding protein 1	1,6	0,001	PRDX1
O43747	AP1G1	AP-1 complex subunit gamma-1	1,6	0,001	PRDX1
Q01831	XPC	DNA repair protein complementing XP-C cells	1,6	0,001	PRDX1
O43852	CALU	Calumenin	1,6	0,002	PRDX1
Q96T23	RSF1	Remodeling and spacing factor 1	1,6	0,008	PRDX1
Q5VW32	BROX	BRO1 domain-containing protein BROX	1,6	0,008	PRDX1
P46821	MAP1B	Microtubule-associated protein 1B	1,6	0,013	PRDX1
O75367	MACROH2A1	Core histone macro-H2A.1	1,6	0,015	PRDX1
Q9BZK7	TBL1XR1	F-box-like/WD repeat-containing protein TBL1XR1	1,6	0,016	PRDX1
Q01082	SPTBN1	Spectrin beta chain, non-erythrocytic 1	1,6	0,026	PRDX1
P07942	LAMB1	Laminin subunit beta-1	1,6	0,027	PRDX1
Q9NVP1	DDX18	ATP-dependent RNA helicase DDX18	1,6	0,038	PRDX1
Q9BYN0	SRXN1	Sulfiredoxin-1	1,6	0,041	PRDX1
O15372	EIF3H	Eukaryotic translation initiation factor 3 subunit H	1,5	0	PRDX1
P38117	ETFB	Electron transfer flavoprotein subunit beta	1,5	0	PRDX1
O94826	TOMM70	Mitochondrial import receptor subunit TOM70	1,5	0	PRDX1
Q68E01	INTS3	Integrator complex subunit 3	1,5	0	PRDX1
A0A2R8YD50	HSD17B4	Peroxisomal multifunctional enzyme type 2	1,5	0	PRDX1
O00299	CLIC1	Chloride intracellular channel protein 1	1,5	0	PRDX1
P61247	RPS3A	40S ribosomal protein S3a	1,5	0	PRDX1

O60763	USO1	General vesicular transport factor p115	1,5	0	PRDX1
O95376	ARIH2	E3 ubiquitin-protein ligase ARIH2	1,5	0,001	PRDX1
Q15054	POLD3	DNA polymerase delta subunit 3	1,5	0,001	PRDX1
Q9Y678	COPG1	Coatomer subunit gamma-1	1,5	0,001	PRDX1
O95433	AHSA1	Activator of 90 kDa heat shock protein ATPase homolog 1	1,5	0,002	PRDX1
Q9Y2X3	NOP58	Nucleolar protein 58	1,5	0,01	PRDX1
A0A3B3ISV3	COL4A1	Collagen alpha-1(IV) chain	1,5	0,019	PRDX1
O96019	ACTL6A	Actin-like protein 6A	1,5	0,02	PRDX1
Q9NYB0	TERF2IP	Telomeric repeat-binding factor 2-interacting protein 1	1,5	0,021	PRDX1
P19174	PLCG1	1-phosphatidylinositol 4,5-bisphosphate phosphodiesterase gamma-1	1,5	0,029	PRDX1
Q9UKN8	GTF3C4	General transcription factor 3C polypeptide 4	1,5	0,032	PRDX1
P11717	IGF2R	Cation-independent mannose-6-phosphate receptor	1,5	0,037	PRDX1
P27694	RPA1	Replication protein A 70 kDa DNA-binding subunit	1,5	0,049	PRDX1
Q2TAY7	SMU1	WD40 repeat-containing protein SMU1	1,4	0	PRDX1
P42166	TMPO	Lamina-associated polypeptide 2, isoform alpha	1,4	0	PRDX1
J3QQW9	SUZ12	Polycomb protein SUZ12	1,4	0	PRDX1
Q5T9A4	ATAD3B	ATPase family AAA domain-containing protein 3B	1,4	0	PRDX1
Q5H928	HSD17B10	3-hydroxyacyl-CoA dehydrogenase type-2	1,4	0	PRDX1
P53618	COPB1	Coatomer subunit beta	1,4	0,001	PRDX1
Q9Y5J1	UTP18	U3 small nucleolar RNA-associated protein 18 homolog	1,4	0,001	PRDX1
Q8IWB7	WDFY1	WD repeat and FYVE domain-containing protein 1	1,4	0,001	PRDX1
P62244	RPS15A	40S ribosomal protein S15a	1,4	0,004	PRDX1
P16615	ATP2A2	Sarcoplasmic/endoplasmic reticulum calcium ATPase 2	1,4	0,004	PRDX1
P26583	HMGB2	High mobility group protein B2	1,4	0,008	PRDX1
P33992	MCM5	DNA replication licensing factor MCM5	1,4	0,008	PRDX1
P20073	ANXA7	Annexin A7	1,4	0,008	PRDX1
P39023	RPL3	60S ribosomal protein L3	1,4	0,01	PRDX1
O43719	HTATSF1	HIV Tat-specific factor 1	1,4	0,013	PRDX1
O14980	XPO1	Exportin-1	1,4	0,015	PRDX1
O00232	PSMD12	26S proteasome non-ATPase regulatory subunit 12	1,4	0,015	PRDX1
P35606	COPB2	Coatomer subunit beta'	1,4	0,016	PRDX1
Q5VYK3	ECPAS	Proteasome adapter and scaffold protein ECM29	1,4	0,027	PRDX1
O76021	RSL1D1	Ribosomal L1 domain-containing protein 1	1,4	0,03	PRDX1
P31327	CPS1	Carbamoyl-phosphate synthase [ammonia], mitochondrial	1,4	0,032	PRDX1
Q8N335	GPD1L	Glycerol-3-phosphate dehydrogenase 1-like protein	1,4	0,035	PRDX1
P39748	FEN1	Flap endonuclease 1	1,4	0,042	PRDX1
P78347	GTF2I	General transcription factor II-I	1,4	0,045	PRDX1
Q86TI2	DPP9	Dipeptidyl peptidase 9	1,4	0,046	PRDX1
Q9Y383	LUC7L2	Putative RNA-binding protein Luc7-like 2	1,3	0	PRDX1
Q9UQ80	PA2G4	Proliferation-associated protein 2G4	1,3	0	PRDX1
Q8NFH5	NUP35	Nucleoporin NUP35	1,3	0	PRDX1
Q12788	TBL3	Transducin beta-like protein 3	1,3	0,001	PRDX1
P49916	LIG3	DNA ligase 3	1,3	0,001	PRDX1
Q9H3P7	ACBD3	Golgi resident protein GCP60	1,3	0,001	PRDX1
K7ERF1	EIF3K	Eukaryotic translation initiation factor 3 subunit K	1,3	0,001	PRDX1
P29401	TKT	Transketolase	1,3	0,001	PRDX1
P62877	RBX1	E3 ubiquitin-protein ligase RBX1	1,3	0,001	PRDX1
P53004	BLVRA	Biliverdin reductase A	1,3	0,002	PRDX1
P61923	COPZ1	Coatomer subunit zeta-1	1,3	0,002	PRDX1
Q96HC4	PDLIM5	PDZ and LIM domain protein 5	1,3	0,002	PRDX1
P62241	RPS8	40S ribosomal protein S8	1,3	0,003	PRDX1
O00116	AGPS	Alkyldihydroxyacetonephosphate synthase, peroxisomal	1,3	0,004	PRDX1
Q92688	ANP32B	Acidic leucine-rich nuclear phosphoprotein 32 family member B	1,3	0,004	PRDX1
J3KMX5	RPS13	40S ribosomal protein S13	1,3	0,01	PRDX1
O94874	UFL1	E3 UFM1-protein ligase 1	1,3	0,01	PRDX1
P48735	IDH2	Isocitrate dehydrogenase [NADP], mitochondrial	1,3	0,015	PRDX1
P62979	RPS27A	Ubiquitin-40S ribosomal protein S27a	1,3	0,017	PRDX1
O75131	CPNE3	Copine-3	1,3	0,018	PRDX1
Q92769	HDAC2	Histone deacetylase 2	1,3	0,027	PRDX1
O95163	ELP1	Elongator complex protein 1	1,3	0,048	PRDX1
Q8ND82	ZNF280C	Zinc finger protein 280C	1,2	0	PRDX1
G8JLH9	STAT3	Signal transducer and activator of transcription	1,2	0	PRDX1
E5RHG8	ELOC	Elongin-C	1,2	0	PRDX1
P52594	AGFG1	Arf-GAP domain and FG repeat-containing protein 1	1,2	0	PRDX1
Q5JXI8	FHL1	Four and a half LIM domains protein 1	1,2	0	PRDX1
Q13112	CHAF1B	Chromatin assembly factor 1 subunit B	1,2	0	PRDX1
Q07020	RPL18	60S ribosomal protein L18	1,2	0,001	PRDX1
Q92600	CNOT9	CCR4-NOT transcription complex subunit 9	1,2	0,001	PRDX1
P15121	AKR1B1	Aldo-keto reductase family 1 member B1	1,2	0,001	PRDX1

E7ESY4	MTA1	Metastasis-associated protein MTA1	1,2	0,003	PRDX1
Q15008	PSMD6	26S proteasome non-ATPase regulatory subunit 6	1,2	0,004	PRDX1
M0QY97	ZC3H4	Zinc finger CCCH domain-containing protein 4	1,2	0,006	PRDX1
P55795	HNRNPH2	Heterogeneous nuclear ribonucleoprotein H2	1,2	0,006	PRDX1
Q9UKM9	RALY	RNA-binding protein Raly	1,2	0,007	PRDX1
Q02878	RPL6	60S ribosomal protein L6	1,2	0,01	PRDX1
Q09161	NCBP1	Nuclear cap-binding protein subunit 1	1,2	0,01	PRDX1
P49750	YLPM1	YLP motif-containing protein 1	1,2	0,01	PRDX1
O95202	LETM1	Mitochondrial proton/calcium exchanger protein	1,2	0,019	PRDX1
Q86UP2	KTN1	Kinectin	1,2	0,022	PRDX1
P42224	STAT1	Signal transducer and activator of transcription 1-alpha/beta	1,2	0,026	PRDX1
Q9Y3T9	NOC2L	Nucleolar complex protein 2 homolog	1,2	0,028	PRDX1
Q9Y5V3	MAGED1	Melanoma-associated antigen D1	1,1	0,001	PRDX1
Q9UBU9	NXF1	Nuclear RNA export factor 1	1,1	0,002	PRDX1
Q9NTI5	PDS5B	Sister chromatid cohesion protein PDS5 homolog B	1,1	0,003	PRDX1
Q9BT78	COPS4	COP9 signalosome complex subunit 4	1,1	0,004	PRDX1
P53007	SLC25A1	Tricarboxylate transport protein, mitochondrial	1,1	0,004	PRDX1
P23921	RRM1	Ribonucleoside-diphosphate reductase large subunit	1,1	0,006	PRDX1
P05455	SSB	Lupus La protein	1,1	0,006	PRDX1
P27144	AK4	Adenylate kinase 4, mitochondrial	1,1	0,007	PRDX1
A0A024R4M0	RPS9	40S ribosomal protein S9	1,1	0,007	PRDX1
P31943	HNRNPH1	Heterogeneous nuclear ribonucleoprotein H	1,1	0,009	PRDX1
O43390	HNRNPR	Heterogeneous nuclear ribonucleoprotein R	1,1	0,012	PRDX1
Q96CS3	FAF2	FAS-associated factor 2	1,1	0,013	PRDX1
P50914	RPL14	60S ribosomal protein L14	1,1	0,013	PRDX1
Q9UHB9	SRP68	Signal recognition particle subunit SRP68	1,1	0,015	PRDX1
Q9UI12	ATP6V1H	V-type proton ATPase subunit H	1,1	0,019	PRDX1
P08133	ANXA6	Annexin A6	1,1	0,022	PRDX1
Q71UM5	RPS27L	40S ribosomal protein S27-like	1,1	0,025	PRDX1
O76003	GLRX3	Glutaredoxin-3	1,1	0,026	PRDX1
P39687	ANP32A	Acidic leucine-rich nuclear phosphoprotein 32 family member A	1,1	0,026	PRDX1
Q96SB4	SRPK1	SRSF protein kinase 1	1,1	0,029	PRDX1
P16435	POR	NADPH--cytochrome P450 reductase	1,1	0,03	PRDX1
F8W6I7	HNRNPA1	Helix-destabilizing protein	1,1	0,031	PRDX1
O75381	PEX14	Peroxisomal membrane protein PEX14	1,1	0,037	PRDX1
P06748	NPM1	Nucleophosmin	1,1	0,039	PRDX1
Q99426	TBCB	Tubulin-folding cofactor B	1,1	0,045	PRDX1
Q9NW13	RBM28	RNA-binding protein 28	1,1	0,048	PRDX1
P78406	RAE1	mRNA export factor	1	0,001	PRDX1
Q14974	KPNB1	Importin subunit beta-1	1	0,002	PRDX1
Q86VM9	ZC3H18	Zinc finger CCCH domain-containing protein 18	1	0,005	PRDX1
Q9Y5P6	GMPPB	Mannose-1-phosphate guanyltransferase beta	1	0,005	PRDX1
P45973	CBX5	Chromobox protein homolog 5	1	0,008	PRDX1
O00410	IPO5	Importin-5	1	0,008	PRDX1
C9JRT6	NUB1	NEDD8 ultimate buster 1	1	0,009	PRDX1
P43897	TSFM	Elongation factor Ts, mitochondrial	1	0,022	PRDX1
Q9Y2Q3	GSTK1	Glutathione S-transferase kappa 1	1	0,026	PRDX1
Q9BQ52	ELAC2	Zinc phosphodiesterase ELAC protein 2	1	0,031	PRDX1
P43490	NAMPT	Nicotinamide phosphoribosyltransferase	1	0,046	PRDX1
Q13162	PRDX4	Peroxiredoxin-4	9,7	0	PRDX2
P13667	PDIA4	Protein disulfide-isomerase A4	5,9	0	PRDX2
Q12797	ASPH	Aspartyl/asparaginyl beta-hydroxylase	4,2	0	PRDX2
Q9NYU2	UGGT1	UDP-glucose:glycoprotein glucosyltransferase 1	4	0	PRDX2
Q15084	PDIA6	Protein disulfide-isomerase A6	3,9	0	PRDX2
P07237	P4HB	Protein disulfide-isomerase	3,9	0	PRDX2
P30048	PRDX3	Thioredoxin-dependent peroxide reductase, mitochondrial	3,6	0	PRDX2
P98175	RBM10	RNA-binding protein 10	3,5	0	PRDX2
Q13217	DNAJC3	DnaJ homolog subfamily C member 3	3,4	0	PRDX2
P11021	HSPA5	Endoplasmic reticulum chaperone BiP	3,4	0	PRDX2
A0A087X054	HYOU1	Hypoxia up-regulated protein 1	3,3	0	PRDX2
O00469	PLOD2	Procollagen-lysine,2-oxoglutarate 5-dioxygenase 2	3,3	0,001	PRDX2
P11047	LAMC1	Laminin subunit gamma-1	3,1	0	PRDX2
Q9BS26	ERP44	Endoplasmic reticulum resident protein 44	3,1	0,02	PRDX2
P30101	PDIA3	Protein disulfide-isomerase A3	2,9	0	PRDX2
P27797	CALR	Calreticulin	2,8	0	PRDX2
D6RBV2	LMAN2	Vesicular integral-membrane protein VIP36	2,8	0,001	PRDX2
Q9BZQ6	EDEM3	ER degradation-enhancing alpha-mannosidase-like protein 3	2,8	0,001	PRDX2
P78417	GSTO1	Glutathione S-transferase omega-1	2,7	0	PRDX2
P12109	COL6A1	Collagen alpha-1(VI) chain	2,7	0,001	PRDX2

O75688	PPM1B	Protein phosphatase 1B	2,6	0	PRDX2
P50454	SERPINH1	Serpin H1	2,6	0	PRDX2
O00268	TAF4	Transcription initiation factor TFIID subunit 4	2,6	0	PRDX2
Q9Y2H1	STK38L	Serine/threonine-protein kinase 38-like	2,6	0,002	PRDX2
Q9Y680	FKBP7	Peptidyl-prolyl cis-trans isomerase FKBP7	2,6	0,002	PRDX2
Q14257	RCN2	Reticulocalbin-2	2,5	0	PRDX2
Q8TEM1	NUP210	Nuclear pore membrane glycoprotein 210	2,5	0	PRDX2
P49257	LMAN1	Protein ERGIC-53	2,5	0,001	PRDX2
P55268	LAMB2	Laminin subunit beta-2	2,3	0,002	PRDX2
P27824	CANX	Calnexin	2,2	0	PRDX2
P09972	ALDOC	Fructose-bisphosphate aldolase C	2,1	0,046	PRDX2
Q15424	SAFB	Scaffold attachment factor B1	2	0	PRDX2
Q13257	MAD2L1	Mitotic spindle assembly checkpoint protein MAD2A	2	0,002	PRDX2
P14625	HSP90B1	Endoplasmin	1,9	0	PRDX2
O00399	DCTN6	Dynactin subunit 6	1,9	0,011	PRDX2
E9PFZ2	CP	Ceruloplasmin	1,9	0,013	PRDX2
Q12929	EPS8	Epidermal growth factor receptor kinase substrate 8	1,8	0,01	PRDX2
P57076	CFAP298	Cilia- and flagella-associated protein 298	1,8	0,011	PRDX2
P07942	LAMB1	Laminin subunit beta-1	1,8	0,015	PRDX2
P11717	IGF2R	Cation-independent mannose-6-phosphate receptor	1,8	0,021	PRDX2
O43852	CALU	Calumenin	1,7	0,001	PRDX2
Q5RKV6	EXOSC6	Exosome complex component MTR3	1,7	0,006	PRDX2
Q9UKN8	GTF3C4	General transcription factor 3C polypeptide 4	1,7	0,018	PRDX2
Q9HAU5	UPF2	Regulator of nonsense transcripts 2	1,7	0,019	PRDX2
P13674	P4HA1	Prolyl 4-hydroxylase subunit alpha-1	1,6	0,003	PRDX2
Q32P28	P3H1	Prolyl 3-hydroxylase 1	1,6	0,014	PRDX2
P09110	ACAA1	3-ketoacyl-CoA thiolase, peroxisomal	1,6	0,015	PRDX2
Q8IXB1	DNAJC10	DnaJ homolog subfamily C member 10	1,5	0,002	PRDX2
P23588	EIF4B	Eukaryotic translation initiation factor 4B	1,5	0,011	PRDX2
P67809	YBX1	Y-box-binding protein 1	1,5	0,034	PRDX2
H0YEN2	PPP6R3	Serine/threonine-protein phosphatase 6 regulatory subunit 3	1,5	0,036	PRDX2
Q8N6R0	EEF1AKNMT	eEF1A lysine and N-terminal methyltransferase	1,5	0,037	PRDX2
P62314	SNRPD1	Small nuclear ribonucleoprotein Sm D1	1,4	0	PRDX2
Q15020	SART3	Squamous cell carcinoma antigen recognized by T-cells 3	1,4	0,001	PRDX2
Q99504	EYA3	Eyes absent homolog 3	1,4	0,001	PRDX2
P56182	RRP1	Ribosomal RNA processing protein 1 homolog A	1,4	0,001	PRDX2
Q9H0H5	RACGAP1	Rac GTPase-activating protein 1	1,4	0,002	PRDX2
O00116	AGPS	Alkyldihydroxyacetonephosphate synthase, peroxisomal	1,4	0,004	PRDX2
O00170	AIP	AH receptor-interacting protein	1,4	0,005	PRDX2
E7ESP9	NEFM	160 kDa neurofilament protein	1,4	0,017	PRDX2
O60934	NBN	Nibrin	1,3	0	PRDX2
A6NHR9	SMCHD1	Structural maintenance of chromosomes flexible hinge domain-containing protein 1	1,3	0	PRDX2
Q9UIG0	BAZ1B	Tyrosine-protein kinase BAZ1B	1,3	0,001	PRDX2
Q04837	SSBP1	Single-stranded DNA-binding protein, mitochondrial	1,3	0,002	PRDX2
Q01831	XPC	DNA repair protein complementing XP-C cells	1,3	0,003	PRDX2
P42696	RBM34	RNA-binding protein 34	1,3	0,005	PRDX2
Q9UBE0	SAE1	SUMO-activating enzyme subunit 1	1,3	0,012	PRDX2
P22307	SCP2	Non-specific lipid-transfer protein	1,3	0,014	PRDX2
Q14676	MDC1	Mediator of DNA damage checkpoint protein 1	1,3	0,034	PRDX2
P40938	RFC3	Replication factor C subunit 3	1,2	0	PRDX2
P25786	PSMA1	Proteasome subunit alpha type-1	1,2	0,001	PRDX2
B8ZZC5	GLS	Glutaminase	1,2	0,001	PRDX2
Q68E01	INTS3	Integrator complex subunit 3	1,2	0,002	PRDX2
P49916	LIG3	DNA ligase 3	1,2	0,003	PRDX2
P31942	HNRNPH3	Heterogeneous nuclear ribonucleoprotein H3	1,2	0,004	PRDX2
Q9UBS4	DNAJB11	DnaJ homolog subfamily B member 11	1,2	0,004	PRDX2
P18583	SON	Protein SON	1,2	0,008	PRDX2
O94906	PRPF6	Pre-mRNA-processing factor 6	1,2	0,009	PRDX2
M0QY97	ZC3H4	Zinc finger CCCH domain-containing protein 4	1,2	0,009	PRDX2
Q16352	INA	Alpha-internexin	1,2	0,012	PRDX2
Q9BZE4	GTPBP4	Nucleolar GTP-binding protein 1	1,2	0,013	PRDX2
Q02241	KIF23	Kinesin-like protein KIF23	1,2	0,015	PRDX2
P05783	KRT18	Keratin, type I cytoskeletal 18	1,2	0,021	PRDX2
Q99426	TBCB	Tubulin-folding cofactor B	1,2	0,023	PRDX2
O14646	CHD1	Chromodomain-helicase-DNA-binding protein 1	1,2	0,027	PRDX2
Q9Y3D0	CIAO2B	Cytosolic iron-sulfur assembly component 2B	1,2	0,031	PRDX2
O75152	ZC3H11A	Zinc finger CCCH domain-containing protein 11A	1,2	0,042	PRDX2
Q9NVI7	ATAD3A	ATPase family AAA domain-containing protein 3A	1,1	0	PRDX2
Q96KR1	ZFR	Zinc finger RNA-binding protein	1,1	0,003	PRDX2

Q15785	TOMM34	Mitochondrial import receptor subunit TOM34	1,1	0,011	PRDX2
Q8IY81	FTSJ3	pre-rRNA 2'-O-ribose RNA methyltransferase FTSJ3	1,1	0,011	PRDX2
C9J384	CMSS1	Protein CMSS1	1,1	0,014	PRDX2
Q9NQ29	LUC7L	Putative RNA-binding protein Luc7-like 1	1,1	0,017	PRDX2
Q8N163	CCAR2	Cell cycle and apoptosis regulator protein 2	1,1	0,021	PRDX2
Q9Y2T2	AP3M1	AP-3 complex subunit mu-1	1,1	0,023	PRDX2
P52701	MSH6	DNA mismatch repair protein Msh6	1,1	0,027	PRDX2
P07196	NEFL	Neurofilament light polypeptide	1,1	0,03	PRDX2
C9J250	RBM6	RNA-binding protein 6	1,1	0,032	PRDX2
P62979	RPS27A	Ubiquitin-40S ribosomal protein S27a	1,1	0,033	PRDX2
Q71UM5	RPS27L	40S ribosomal protein S27-like	1,1	0,045	PRDX2
P04792	HSPB1	Heat shock protein beta-1	1	0	PRDX2
P02545	LMNA	Prelamin-A/C [Cleaved into: Lamin-A/C	1	0,001	PRDX2
Q9BY42	RTF2	Replication termination factor 2	1	0,004	PRDX2
Q13451	FKBP5	Peptidyl-prolyl cis-trans isomerase FKBP5	1	0,006	PRDX2
Q9NZB2	FAM120A	Constitutive coactivator of PPAR-gamma-like protein 1	1	0,007	PRDX2
A0A0A0MRM8	MYO6	Unconventional myosin-6	1	0,013	PRDX2
Q96H79	ZC3HAV1L	Zinc finger CCCH-type antiviral protein 1-like	1	0,013	PRDX2
P42765	ACAA2	3-ketoacyl-CoA thiolase, mitochondrial	1	0,017	PRDX2
Q15042	RAB3GAP1	Rab3 GTPase-activating protein catalytic subunit	1	0,023	PRDX2
O95376	ARIH2	E3 ubiquitin-protein ligase ARIH2	1	0,027	PRDX2
Q9P0M6	MACROH2A2	Core histone macro-H2A.2	1	0,046	PRDX2
Q15084	PDIA6	Protein disulfide-isomerase A6	4,9	0	PRDX3
P13667	PDIA4	Protein disulfide-isomerase A4	4,8	0	PRDX3
Q9NYU2	UGGT1	UDP-glucose:glycoprotein glucosyltransferase 1	4,2	0	PRDX3
P11047	LAMC1	Laminin subunit gamma-1	4	0	PRDX3
O00469	PLOD2	Procollagen-lysine,2-oxoglutarate 5-dioxygenase 2	3,9	0	PRDX3
P07237	P4HB	Protein disulfide-isomerase	3,9	0	PRDX3
A0A087X054	HYOU1	Hypoxia up-regulated protein 1	3,9	0	PRDX3
Q12797	ASPH	Aspartyl/asparaginyl beta-hydroxylase	3,6	0	PRDX3
P11021	HSPA5	Endoplasmic reticulum chaperone BiP	3,5	0	PRDX3
P30101	PDIA3	Protein disulfide-isomerase A3	2,9	0	PRDX3
Q13217	DNAJC3	DnaJ homolog subfamily C member 3	2,9	0	PRDX3
P12109	COL6A1	Collagen alpha-1(VI) chain	2,9	0,002	PRDX3
P50454	SERPINH1	Serpin H1	2,8	0	PRDX3
P27797	CALR	Calreticulin	2,8	0	PRDX3
Q9BS26	ERP44	Endoplasmic reticulum resident protein 44	2,8	0,047	PRDX3
Q9Y680	FKBP7	Peptidyl-prolyl cis-trans isomerase FKBP7	2,7	0,002	PRDX3
P27824	CANX	Calnexin	2,6	0	PRDX3
P09972	ALDOC	Fructose-bisphosphate aldolase C	2,6	0,016	PRDX3
P14625	HSP90B1	Endoplasmin	2,4	0	PRDX3
D6RBV2	LMAN2	Vesicular integral-membrane protein VIP36	2,4	0,006	PRDX3
P55268	LAMB2	Laminin subunit beta-2	2,2	0,001	PRDX3
Q13257	MAD2L1	Mitotic spindle assembly checkpoint protein MAD2A	2,1	0,002	PRDX3
E9PFZ2	CP	Ceruloplasmin	2,1	0,012	PRDX3
Q12929	EPS8	Epidermal growth factor receptor kinase substrate 8	2	0,008	PRDX3
P07942	LAMB1	Laminin subunit beta-1	2	0,013	PRDX3
Q13162	PRDX4	Peroxiredoxin-4	11	0	PRDX3
Q8IXB1	DNAJC10	DnaJ homolog subfamily C member 10	1,9	0	PRDX3
Q9BZQ6	EDEM3	ER degradation-enhancing alpha-mannosidase-like protein 3	1,9	0,012	PRDX3
Q9UKN8	GTF3C4	General transcription factor 3C polypeptide 4	1,9	0,015	PRDX3
P11717	IGF2R	Cation-independent mannose-6-phosphate receptor	1,9	0,018	PRDX3
P32119	PRDX2	Peroxiredoxin-2	1,8	0,002	PRDX3
Q8NBJ5	COLGALT1	Procollagen galactosyltransferase 1	1,7	0,031	PRDX3
Q16576	RBBP7	Histone-binding protein RBBP7	1,6	0,002	PRDX3
Q13151	HNRNPA0	Heterogeneous nuclear ribonucleoprotein A0	1,6	0,035	PRDX3
Q8TEM1	NUP210	Nuclear pore membrane glycoprotein 210	1,5	0,001	PRDX3
P13674	P4HA1	Prolyl 4-hydroxylase subunit alpha-1	1,5	0,002	PRDX3
A0A2R8Y811	RPS14	40S ribosomal protein S14	1,4	0	PRDX3
Q9UBS4	DNAJB11	DnaJ homolog subfamily B member 11	1,4	0	PRDX3
P62753	RPS6	40S ribosomal protein S6	1,4	0,003	PRDX3
P06748	NPM1	Nucleophosmin	1,4	0,017	PRDX3
Q14696	MESD	LRP chaperone MESD	1,4	0,045	PRDX3
Q14697	GANAB	Neutral alpha-glucosidase AB	1,3	0,003	PRDX3
P62280	RPS11	40S ribosomal protein S11	1,3	0,004	PRDX3
O00116	AGPS	Alkyldihydroxyacetonephosphate synthase, peroxisomal	1,3	0,006	PRDX3
P18077	RPL35A	60S ribosomal protein L35a	1,2	0,003	PRDX3
P49257	LMAN1	Protein ERGIC-53	1,2	0,01	PRDX3
Q15424	SAFB	Scaffold attachment factor B1	1,2	0,014	PRDX3

O43852	CALU	Calumenin	1,2	0,014	PRDX3
O75821	EIF3G	Eukaryotic translation initiation factor 3 subunit G	1,1	0,003	PRDX3
Q9H0H5	RACGAP1	Rac GTPase-activating protein 1	1,1	0,008	PRDX3
Q9HCN8	SDF2L1	Stromal cell-derived factor 2-like protein 1	1,1	0,011	PRDX3
Q15020	SART3	Squamous cell carcinoma antigen recognized by T-cells 3	1,1	0,015	PRDX3
P18124	RPL7	60S ribosomal protein L7	1,1	0,032	PRDX3
P13667	PDIA4	Protein disulfide-isomerase A4	6	0	PRDX5
P30048	PRDX3	Thioredoxin-dependent peroxide reductase, mitochondrial	5,7	0	PRDX5
Q15084	PDIA6	Protein disulfide-isomerase A6	5	0	PRDX5
A0A087X054	HYOU1	Hypoxia up-regulated protein 1	4,2	0	PRDX5
Q12797	ASPH	Aspartyl/asparaginyl beta-hydroxylase	3,9	0	PRDX5
Q9NYU2	UGGT1	UDP-glucose:glycoprotein glucosyltransferase 1	3,8	0	PRDX5
O00469	PLOD2	Procollagen-lysine,2-oxoglutarate 5-dioxygenase 2	3,7	0	PRDX5
P07237	P4HB	Protein disulfide-isomerase	3,5	0	PRDX5
P11047	LAMC1	Laminin subunit gamma-1	3,4	0	PRDX5
P50454	SERPINH1	Serpin H1	3,4	0	PRDX5
P11021	HSPA5	Endoplasmic reticulum chaperone BiP	3,2	0	PRDX5
Q13217	DNAJC3	DnaJ homolog subfamily C member 3	2,9	0	PRDX5
Q8TEM1	NUP210	Nuclear pore membrane glycoprotein 210	2,9	0	PRDX5
P30101	PDIA3	Protein disulfide-isomerase A3	2,8	0	PRDX5
Q9BS26	ERP44	Endoplasmic reticulum resident protein 44	2,8	0,036	PRDX5
Q9BZQ6	EDEM3	ER degradation-enhancing alpha-mannosidase-like protein 3	2,7	0,001	PRDX5
D6RBV2	LMAN2	Vesicular integral-membrane protein VIP36	2,7	0,002	PRDX5
P12109	COL6A1	Collagen alpha-1(VI) chain	2,6	0,001	PRDX5
P49257	LMAN1	Protein ERGIC-53	2,4	0,001	PRDX5
Q9Y680	FKBP7	Peptidyl-prolyl cis-trans isomerase FKBP7	2,4	0,002	PRDX5
P27824	CANX	Calnexin	2,2	0	PRDX5
P55268	LAMB2	Laminin subunit beta-2	2,2	0,002	PRDX5
P09110	ACAA1	3-ketoacyl-CoA thiolase, peroxisomal	2,1	0,001	PRDX5
Q96AC1	FERMT2	Fermitin family homolog 2	2,1	0,011	PRDX5
Q9BYN0	SRXN1	Sulfiredoxin-1	2,1	0,016	PRDX5
P22307	SCP2	Non-specific lipid-transfer protein	2	0	PRDX5
Q7Z406	MYH14	Myosin-14	2	0,001	PRDX5
Q13162	PRDX4	Peroxiredoxin-4	10,2	0	PRDX5
P27797	CALR	Calreticulin	1,9	0	PRDX5
Q8IXB1	DNAJC10	DnaJ homolog subfamily C member 10	1,9	0,001	PRDX5
Q13257	MAD2L1	Mitotic spindle assembly checkpoint protein MAD2A	1,9	0,002	PRDX5
P19105	MYL12A	Myosin regulatory light chain 12A	1,9	0,011	PRDX5
Q15149	PLEC	Plectin	1,9	0,025	PRDX5
P05783	KRT18	Keratin, type I cytoskeletal 18	1,8	0,003	PRDX5
E9PFZ2	CP	Ceruloplasmin	1,8	0,022	PRDX5
Q9Y224	RTRAF	RNA transcription, translation and transport factor protein	1,8	0,027	PRDX5
P55084	HADHB	Trifunctional enzyme subunit beta, mitochondrial	1,8	0,034	PRDX5
B8ZZC5	GLS	Glutaminase	1,7	0	PRDX5
P14625	HSP90B1	Endoplasmin	1,7	0	PRDX5
Q9BW92	TARS2	Threonine--tRNA ligase, mitochondrial	1,7	0,003	PRDX5
P31327	CPS1	Carbamoyl-phosphate synthase [ammonia], mitochondrial	1,7	0,012	PRDX5
G3V5X4	SYNE2	Nesprin-2	1,7	0,022	PRDX5
Q01082	SPTBN1	Spectrin beta chain, non-erythrocytic 1	1,7	0,025	PRDX5
Q9H0H5	RACGAP1	Rac GTPase-activating protein 1	1,6	0	PRDX5
Q4VCS5	AMOT	Angiomotin	1,6	0,012	PRDX5
Q96KM6	ZNF512B	Zinc finger protein 512B	1,6	0,025	PRDX5
P07942	LAMB1	Laminin subunit beta-1	1,6	0,025	PRDX5
P42704	LRPPRC	Leucine-rich PPR motif-containing protein, mitochondrial	1,6	0,025	PRDX5
P42345	MTOR	Serine/threonine-protein kinase mTOR	1,6	0,026	PRDX5
Q13813	SPTAN1	Spectrin alpha chain, non-erythrocytic 1	1,6	0,034	PRDX5
P46013	MKI67	Proliferation marker protein Ki-67	1,6	0,035	PRDX5
P43897	TSFM	Elongation factor Ts, mitochondrial	1,5	0	PRDX5
A0A2R8YDQ9	SUCLA2	Succinate--CoA ligase [ADP-forming] subunit beta, mitochondrial	1,5	0	PRDX5
Q9NY93	DDX56	Probable ATP-dependent RNA helicase DDX56	1,5	0	PRDX5
Q5H928	HSD17B10	3-hydroxyacyl-CoA dehydrogenase type-2	1,5	0	PRDX5
Q02241	KIF23	Kinesin-like protein KIF23	1,5	0,003	PRDX5
P53597	SUCLG1	Succinate--CoA ligase [ADP/GDP-forming] subunit alpha, mitochondrial	1,5	0,004	PRDX5
Q9P0M6	MACROH2A2	Core histone macro-H2A.2	1,5	0,005	PRDX5
Q5JRX3	PITRM1	Presequence protease, mitochondrial	1,5	0,007	PRDX5
Q6P2E9	EDC4	Enhancer of mRNA-decapping protein 4	1,5	0,008	PRDX5
Q5VW32	BROX	BRO1 domain-containing protein BROX	1,5	0,04	PRDX5
P53007	SLC25A1	Tricarboxylate transport protein, mitochondrial	1,5	0,04	PRDX5
Q15477	SKIV2L	Helicase SKI2W	1,5	0,044	PRDX5

P27144	AK4	Adenylate kinase 4, mitochondrial	1,4	0	PRDX5
P98175	RBM10	RNA-binding protein 10	1,4	0	PRDX5
A0A2R8YD50	HSD17B4	Peroxisomal multifunctional enzyme type 2	1,4	0	PRDX5
P42765	ACAA2	3-ketoacyl-CoA thiolase, mitochondrial	1,4	0,001	PRDX5
Q9BSH4	TACO1	Translational activator of cytochrome c oxidase 1	1,4	0,002	PRDX5
Q02252	ALDH6A1	Methylmalonate-semialdehyde dehydrogenase [acylating], mitochondrial	1,4	0,002	PRDX5
Q5JTZ9	AARS2	Alanine--tRNA ligase, mitochondrial	1,4	0,002	PRDX5
Q8IYI6	EXOC8	Exocyst complex component 8	1,4	0,003	PRDX5
Q12849	GRSF1	G-rich sequence factor 1	1,4	0,003	PRDX5
P19338	NCL	Nucleolin	1,4	0,005	PRDX5
Q92616	GCN1	eIF-2-alpha kinase activator GCN1	1,4	0,013	PRDX5
Q15061	WDR43	WD repeat-containing protein 43	1,4	0,019	PRDX5
Q7L2E3	DHX30	ATP-dependent RNA helicase DHX30	1,4	0,027	PRDX5
O75367	MACROH2A1	Core histone macro-H2A.1	1,4	0,034	PRDX5
Q16762	TST	Thiosulfate sulfurtransferase	1,4	0,04	PRDX5
P11388	TOP2A	DNA topoisomerase 2-alpha	1,4	0,042	PRDX5
Q9Y2Q3	GSTK1	Glutathione S-transferase kappa 1	1,3	0,002	PRDX5
A0A0A0MRM8	MYO6	Unconventional myosin-6	1,3	0,003	PRDX5
P13674	P4HA1	Prolyl 4-hydroxylase subunit alpha-1	1,3	0,006	PRDX5
Q9NW13	RBM28	RNA-binding protein 28	1,3	0,012	PRDX5
P82930	MRPS34	28S ribosomal protein S34, mitochondrial	1,3	0,025	PRDX5
Q13356	PPIL2	RING-type E3 ubiquitin-protein ligase PPIL2	1,3	0,03	PRDX5
P04792	HSPB1	Heat shock protein beta-1	1,2	0	PRDX5
P30084	ECHS1	Enoyl-CoA hydratase, mitochondrial	1,2	0,002	PRDX5
P18077	RPL35A	60S ribosomal protein L35a	1,2	0,003	PRDX5
G5EA31	SEC24C	Protein transport protein Sec24C	1,2	0,003	PRDX5
Q9Y2R9	MRPS7	28S ribosomal protein S7, mitochondrial	1,2	0,004	PRDX5
P35580	MYH10	Myosin-10	1,2	0,004	PRDX5
O94925	GLS	Glutaminase kidney isoform, mitochondrial	1,2	0,017	PRDX5
Q13509	TUBB3	Tubulin beta-3 chain	1,2	0,023	PRDX5
P33992	MCM5	DNA replication licensing factor MCM5	1,2	0,024	PRDX5
P07196	NEFL	Neurofilament light polypeptide	1,2	0,035	PRDX5
Q9HCD5	NCOA5	Nuclear receptor coactivator 5	1,2	0,036	PRDX5
Q9H3U1	UNC45A	Protein unc-45 homolog A	1,2	0,044	PRDX5
Q9UBS4	DNAJB11	DnaJ homolog subfamily B member 11	1,1	0,001	PRDX5
Q9UBQ7	GRHPR	Glyoxylate reductase/hydroxypyruvate reductase	1,1	0,002	PRDX5
Q96KR1	ZFR	Zinc finger RNA-binding protein	1,1	0,003	PRDX5
O15381	NVL	Nuclear valosin-containing protein-like	1,1	0,004	PRDX5
P31942	HNRNPH3	Heterogeneous nuclear ribonucleoprotein H3	1,1	0,005	PRDX5
Q13085	ACACA	Acetyl-CoA carboxylase 1	1,1	0,005	PRDX5
Q9GZT3	SLIRP	SRA stem-loop-interacting RNA-binding protein, mitochondrial	1,1	0,011	PRDX5
P18583	SON	Protein SON	1,1	0,016	PRDX5
A0A0G2JNZ2	SCRIB	Protein scribble homolog	1,1	0,016	PRDX5
A0A0U1RRM6	ENAH	Protein enabled homolog	1,1	0,016	PRDX5
E9PEJ4	DLAT	Acetyltransferase component of pyruvate dehydrogenase complex	1,1	0,016	PRDX5
G5E9W7	MRPS22	28S ribosomal protein S22, mitochondrial	1,1	0,019	PRDX5
O43615	TIMM44	Mitochondrial import inner membrane translocase subunit TIM44	1,1	0,022	PRDX5
Q05655	PRKCD	Protein kinase C delta type	1,1	0,023	PRDX5
Q14258	TRIM25	E3 ubiquitin/ISG15 ligase TRIM25	1,1	0,023	PRDX5
Q9BQ69	MACROD1	ADP-ribose glycohydrolase MACROD1	1,1	0,024	PRDX5
P25685	DNAJB1	DnaJ homolog subfamily B member 1	1,1	0,025	PRDX5
P62879	GNB2	Guanine nucleotide-binding protein G(I)/G(S)/G(T) subunit beta-2	1,1	0,026	PRDX5
O95861	BPNT1	3'(2'),5'-bisphosphate nucleotidase 1	1,1	0,031	PRDX5
Q13464	ROCK1	Rho-associated protein kinase 1	1,1	0,034	PRDX5
P50995	ANXA11	Annexin A11	1,1	0,034	PRDX5
Q5JTH9	RRP12	RRP12-like protein	1,1	0,035	PRDX5
P51570	GALK1	Galactokinase	1,1	0,042	PRDX5
Q00610	CLTC	Clathrin heavy chain 1	1,1	0,046	PRDX5
Q99798	ACO2	Aconitate hydratase, mitochondrial	1	0,001	PRDX5
Q15555	MAPRE2	Microtubule-associated protein RP/EB family member 2	1	0,002	PRDX5
P78406	RAE1	mRNA export factor	1	0,002	PRDX5
P40429	RPL13A	60S ribosomal protein L13a	1	0,005	PRDX5
O60701	UGDH	UDP-glucose 6-dehydrogenase	1	0,008	PRDX5
Q09666	AHNAK	Neuroblast differentiation-associated protein AHNAK	1	0,014	PRDX5
O75439	PMPCB	Mitochondrial-processing peptidase subunit beta	1	0,016	PRDX5
P55795	HNRNPH2	Heterogeneous nuclear ribonucleoprotein H2	1	0,017	PRDX5
Q15042	RAB3GAP1	Rab3 GTPase-activating protein catalytic subunit	1	0,023	PRDX5
Q16352	INA	Alpha-internexin	1	0,032	PRDX5
Q8WYP5	AHCTF1	Protein ELYS	1	0,036	PRDX5

P52701	MSH6	DNA mismatch repair protein Msh6	1	0,04	PRDX5
P48735	IDH2	Isocitrate dehydrogenase [NADP], mitochondrial	1	0,041	PRDX5
P60174	TPI1	Triosephosphate isomerase	1	0,043	PRDX5
PRDX5 -specific interactors					
O94776	MTA2	Metastasis-associated protein MTA2	7	0	PRDX1
P49366	DHPS	Deoxyhypusine synthase	6,6	0	PRDX1
Q92769	HDAC2	Histone deacetylase 2	5	0	PRDX1
Q5QNY5	PEX19	Peroxin-19	4,9	0	PRDX1
P61289	PSME3	Proteasome activator complex subunit 3	4,6	0,001	PRDX1
Q09028	RBBP4	Histone-binding protein RBBP4	4,5	0	PRDX1
P05386	RPLP1	60S acidic ribosomal protein P1	4,1	0	PRDX1
P62805	H4C1	Histone H4	4,1	0	PRDX1
P63151	PPP2R2A	Serine/threonine-protein phosphatase 2A 55 kDa regulatory subunit B alpha isoform	3,9	0	PRDX1
O14744	PRMT5	Protein arginine N-methyltransferase 5	3,8	0	PRDX1
Q16576	RBBP7	Histone-binding protein RBBP7	3,7	0	PRDX1
P30048	PRDX3	Thioredoxin-dependent peroxide reductase, mitochondrial	3,6	0	PRDX1
P41250	GARS1	Glycine--tRNA ligase	3,6	0	PRDX1
P02790	HPX	Hemopexin	3,6	0,001	PRDX1
O00165	HAX1	HCLS1-associated protein X-1	3,5	0	PRDX1
Q9NQP4	PFDN4	Prefoldin subunit 4	3,5	0	PRDX1
H0YEN2	PPP6R3	Serine/threonine-protein phosphatase 6 regulatory subunit 3	3,5	0	PRDX1
H0Y4R1	IMPDH2	Inosine-5'-monophosphate dehydrogenase 2	3,5	0	PRDX1
P62258	YWHAE	14-3-3 protein epsilon	3,5	0	PRDX1
O60506	SYNCRIP	Heterogeneous nuclear ribonucleoprotein Q	3,4	0	PRDX1
Q13547	HDAC1	Histone deacetylase 1	3,3	0	PRDX1
P27797	CALR	Calreticulin	3,3	0	PRDX1
P10599	TXN	Thioredoxin	3,2	0	PRDX1
O76094	SRP72	Signal recognition particle subunit SRP72	3,2	0	PRDX1
P05387	RPLP2	60S acidic ribosomal protein P2	3,2	0	PRDX1
Q9BQA1	WDR77	Methylosome protein 50	3,2	0,002	PRDX1
Q9GZU8	PSME3IP1	PSME3-interacting protein	3,1	0	PRDX1
P48147	PREP	Prolyl endopeptidase	3,1	0	PRDX1
P67936	TPM4	Tropomyosin alpha-4 chain	3,1	0	PRDX1
P22234	PAICS	Multifunctional protein ADE2 [Includes: Phosphoribosylaminoimidazole-succinocarboxamide synthase	3,1	0	PRDX1
Q9BSJ8	ESYT1	Extended synaptotagmin-1	3	0	PRDX1
Q14257	RCN2	Reticulocalbin-2	3	0	PRDX1
Q6DKK2	TTC19	Tetratricopeptide repeat protein 19, mitochondrial	3	0,001	PRDX1
Q96BR5	COA7	Cytochrome c oxidase assembly factor 7	3	0,001	PRDX1
P54619	PRKAG1	5'-AMP-activated protein kinase subunit gamma-1	3	0,001	PRDX1
A0A024R442	A0A024R442	>tr|A0A024R442|A0A024R442_HUMAN Aspartyl aminopeptidase, isoform CRA_b OS=Homo sapiens OX=9606 GN=DNPEP PE=1 SV=1;>sp|Q9ULA0|DNPEP_HUMAN Aspartyl aminopeptidase OS=Homo sapiens OX=9606 GN=DNPEP PE=1 SV=1;>tr|E7ETB3|E7ETB3_HUMAN Aspartyl aminopeptidase, iso	2,9	0	PRDX1
Q8N806	UBR7	Putative E3 ubiquitin-protein ligase UBR7	2,9	0	PRDX1
P20839	IMPDH1	Inosine-5'-monophosphate dehydrogenase 1	2,9	0	PRDX1
Q96EW2	HSPBAP1	HSPB1-associated protein 1	2,9	0	PRDX1
P49321	NASP	Nuclear autoantigenic sperm protein	2,9	0	PRDX1
P53985	SLC16A1	Monocarboxylate transporter 1	2,9	0	PRDX1
A0A1C7CYX9	DPYSL2	Dihydropyrimidinase-related protein 2	2,8	0	PRDX1
Q15008	PSMD6	26S proteasome non-ATPase regulatory subunit 6	2,8	0	PRDX1
E7ESY4	MTA1	Metastasis-associated protein MTA1	2,8	0	PRDX1
P23526	AHCY	Adenosylhomocysteinase	2,8	0	PRDX1
Q96DB5	RMDN1	Regulator of microtubule dynamics protein 1	2,8	0,001	PRDX1
Q96RS6	NUDCD1	NudC domain-containing protein 1	2,7	0	PRDX1
Q9UEY8	ADD3	Gamma-adducin	2,7	0	PRDX1
P22314	UBA1	Ubiquitin-like modifier-activating enzyme 1	2,7	0	PRDX1
O43143	DHX15	Pre-mRNA-splicing factor ATP-dependent RNA helicase DHX15	2,6	0	PRDX1
Q9UHV9	PFDN2	Prefoldin subunit 2	2,6	0	PRDX1
Q5T4U8	RABGGTB	Geranylgeranyl transferase type-2 subunit beta	2,6	0	PRDX1
P78417	GSTO1	Glutathione S-transferase omega-1	2,6	0	PRDX1
Q15276	RABEP1	Rab GTPase-binding effector protein 1	2,6	0	PRDX1
P31153	MAT2A	S-adenosylmethionine synthase isoform type-2	2,6	0	PRDX1
O75821	EIF3G	Eukaryotic translation initiation factor 3 subunit G	2,6	0	PRDX1
P23528	CFL1	Cofilin-1	2,6	0	PRDX1
A0A2U3TZY2	CLPB	Caseinolytic peptidase B protein homolog	2,6	0,001	PRDX1
P54646	PRKAA2	5'-AMP-activated protein kinase catalytic subunit alpha-2	2,5	0	PRDX1
Q9BPU6	DPYSL5	Dihydropyrimidinase-related protein 5	2,5	0	PRDX1
Q13200	PSMD2	26S proteasome non-ATPase regulatory subunit 2	2,5	0	PRDX1
B9A018	USP39	U4/U6.U5 tri-snRNP-associated protein 2	2,4	0	PRDX1

P23588	EIF4B	Eukaryotic translation initiation factor 4B	2,4	0	PRDX1
Q16531	DDB1	DNA damage-binding protein 1	2,4	0	PRDX1
P00492	HPRT1	Hypoxanthine-guanine phosphoribosyltransferase	2,4	0,001	PRDX1
Q15459	SF3A1	Splicing factor 3A subunit 1	2,4	0,038	PRDX1
J3QQZ9	PNPO	Pyridoxal 5'-phosphate synthase	2,3	0	PRDX1
P78371	CCT2	T-complex protein 1 subunit beta	2,3	0	PRDX1
A0A0A0MR02	VDAC2	Outer mitochondrial membrane protein porin 2	2,3	0	PRDX1
O00268	TAF4	Transcription initiation factor TFIID subunit 4	2,3	0	PRDX1
P35637	FUS	RNA-binding protein FUS	2,3	0,001	PRDX1
P38159	RBMX	RNA-binding motif protein, X chromosome	2,3	0,005	PRDX1
Q32MZ4	LRRFIP1	Leucine-rich repeat flightless-interacting protein 1	2,2	0	PRDX1
P27348	YWHAQ	14-3-3 protein theta	2,2	0	PRDX1
Q9C0C9	UBE2O	(E3-independent) E2 ubiquitin-conjugating enzyme	2,2	0	PRDX1
Q13177	PAK2	Serine/threonine-protein kinase PAK 2	2,2	0	PRDX1
Q9Y3F4	STRAP	Serine-threonine kinase receptor-associated protein	2,2	0	PRDX1
Q9ULC3	RAB23	Ras-related protein Rab-23	2,2	0,001	PRDX1
P42704	LRPPRC	Leucine-rich PPR motif-containing protein, mitochondrial	2,2	0,001	PRDX1
P12955	PEPD	Xaa-Pro dipeptidase	2,2	0,004	PRDX1
P43304	GPD2	Glycerol-3-phosphate dehydrogenase, mitochondrial	2,2	0,004	PRDX1
O00232	PSMD12	26S proteasome non-ATPase regulatory subunit 12	2,1	0	PRDX1
Q96RG2	PASK	PAS domain-containing serine/threonine-protein kinase	2,1	0	PRDX1
P15374	UCHL3	Ubiquitin carboxyl-terminal hydrolase isozyme L3	2,1	0	PRDX1
Q9H8Y8	GORASP2	Golgi reassembly-stacking protein 2	2,1	0	PRDX1
Q96HC4	PDLIM5	PDZ and LIM domain protein 5	2,1	0	PRDX1
P40429	RPL13A	60S ribosomal protein L13a	2,1	0	PRDX1
P45973	CBX5	Chromobox protein homolog 5	2,1	0	PRDX1
A0A087WT45	GRIPAP1	GRIP1-associated protein 1	2,1	0,002	PRDX1
O00231	PSMD11	26S proteasome non-ATPase regulatory subunit 11	2	0	PRDX1
P62979	RPS27A	Ubiquitin-40S ribosomal protein S27a	2	0	PRDX1
P36957	DLST	Dihydrolipoyllysine-residue succinyltransferase component of 2-oxoglutarate dehydrogenase complex, mitochondrial	2	0	PRDX1
P31689	DNAJA1	DnaJ homolog subfamily A member 1	2	0	PRDX1
Q02750	MAP2K1	Dual specificity mitogen-activated protein kinase kinase 1	2	0	PRDX1
C9J4Z3	RPL37A	60S ribosomal protein L37a	2	0	PRDX1
Q93009	USP7	Ubiquitin carboxyl-terminal hydrolase 7	2	0	PRDX1
P61221	ABCE1	ATP-binding cassette sub-family E member 1	2	0	PRDX1
E5KLJ9	OPA1	Dynamin-like 120 kDa protein, form S1	2	0,003	PRDX1
E9PGT1	TSN	Component 3 of promoter of RISC	2	0,003	PRDX1
H7C3C4	SLC4A7	Anion exchange protein	2	0,004	PRDX1
P52788	SMS	Spermine synthase	2	0,007	PRDX1
H0YKU1	TMOD3	Tropomodulin-3	2	0,008	PRDX1
P30044	PRDX5	Peroxiredoxin-5, mitochondrial	10,1	0	PRDX1
O43852	CALU	Calumenin	1,9	0	PRDX1
Q9UBF2	COPG2	Coatomer subunit gamma-2	1,9	0	PRDX1
O95433	AHSA1	Activator of 90 kDa heat shock protein ATPase homolog 1	1,9	0	PRDX1
P34932	HSPA4	Heat shock 70 kDa protein 4	1,9	0	PRDX1
Q4J6C6	PREPL	Prolyl endopeptidase-like	1,9	0,001	PRDX1
Q13564	NAE1	NEDD8-activating enzyme E1 regulatory subunit	1,9	0,001	PRDX1
P62314	SNRPD1	Small nuclear ribonucleoprotein Sm D1	1,9	0,001	PRDX1
Q13185	CBX3	Chromobox protein homolog 3	1,9	0,001	PRDX1
Q9Y478	PRKAB1	5'-AMP-activated protein kinase subunit beta-1	1,9	0,004	PRDX1
P30041	PRDX6	Peroxiredoxin-6	1,9	0,005	PRDX1
Q96KB5	PBK	Lymphokine-activated killer T-cell-originated protein kinase	1,9	0,01	PRDX1
J3KPG2	TPT1	Translationally-controlled tumor protein	1,9	0,017	PRDX1
Q96A49	SYAP1	Synapse-associated protein 1	1,9	0,023	PRDX1
P61981	YWHAG	14-3-3 protein gamma	1,8	0	PRDX1
P06730	EIF4E	Eukaryotic translation initiation factor 4E	1,8	0	PRDX1
Q99460	PSMD1	26S proteasome non-ATPase regulatory subunit 1	1,8	0	PRDX1
E9PLK3	NPEPPS	Aminopeptidase	1,8	0	PRDX1
Q9BRP1	PDCD2L	Programmed cell death protein 2-like	1,8	0	PRDX1
Q15393	SF3B3	Splicing factor 3B subunit 3	1,8	0,001	PRDX1
Q8WXD5	GEMIN6	Gem-associated protein 6	1,8	0,001	PRDX1
Q9UBS4	DNAJB11	DnaJ homolog subfamily B member 11	1,8	0,005	PRDX1
Q8N3X1	FNBP4	Formin-binding protein 4	1,8	0,006	PRDX1
O00483	NDUFA4	Cytochrome c oxidase subunit NDUFA4	1,8	0,009	PRDX1
Q15293	RCN1	Reticulocalbin-1	1,8	0,009	PRDX1
P12814	ACTN1	Alpha-actinin-1	1,8	0,012	PRDX1
Q9NVP1	DDX18	ATP-dependent RNA helicase DDX18	1,8	0,013	PRDX1
P62333	PSMC6	26S proteasome regulatory subunit 10B	1,7	0	PRDX1

P50502	ST13	Hsc70-interacting protein	1,7	0,001	PRDX1
P27824	CANX	Calnexin	1,7	0,004	PRDX1
P52888	THOP1	Thimet oligopeptidase	1,7	0,005	PRDX1
P46821	MAP1B	Microtubule-associated protein 1B	1,7	0,007	PRDX1
X6RM00	ERC1	ELKS/Rab6-interacting/CAST family member 1	1,7	0,009	PRDX1
Q9UHY1	NRBP1	Nuclear receptor-binding protein	1,7	0,009	PRDX1
O96019	ACTL6A	Actin-like protein 6A	1,7	0,01	PRDX1
D6RA00	ENOPH1	Enolase-phosphatase E1	1,7	0,012	PRDX1
B4DHR0	RABEP2	Rab GTPase-binding effector protein 2	1,7	0,013	PRDX1
Q53GQ0	HSD17B12	Very-long-chain 3-oxoacyl-CoA reductase	1,7	0,032	PRDX1
Q96CS3	FAF2	FAS-associated factor 2	1,6	0	PRDX1
Q9UJS0	SLC25A13	Calcium-binding mitochondrial carrier protein Aralar2	1,6	0	PRDX1
O00487	PSMD14	26S proteasome non-ATPase regulatory subunit 14	1,6	0	PRDX1
E9PIF2	DDX10	RNA helicase	1,6	0	PRDX1
P52565	ARHGDIA	Rho GDP-dissociation inhibitor 1	1,6	0	PRDX1
P61923	COPZ1	Coatomer subunit zeta-1	1,6	0	PRDX1
P98175	RBM10	RNA-binding protein 10	1,6	0	PRDX1
Q9UQ80	PA2G4	Proliferation-associated protein 2G4	1,6	0	PRDX1
Q8NE71	ABCF1	ATP-binding cassette sub-family F member 1	1,6	0	PRDX1
P34949	MPI	Mannose-6-phosphate isomerase	1,6	0	PRDX1
P26196	DDX6	Probable ATP-dependent RNA helicase DDX6	1,6	0	PRDX1
O43164	PJA2	E3 ubiquitin-protein ligase Praja-2	1,6	0,001	PRDX1
O15212	PFDN6	Prefoldin subunit 6	1,6	0,001	PRDX1
B1AK87	CAPZB	F-actin-capping protein subunit beta	1,6	0,002	PRDX1
O75688	PPM1B	Protein phosphatase 1B	1,6	0,004	PRDX1
P29218	IMPA1	Inositol monophosphatase 1	1,6	0,014	PRDX1
A0A087WXS7	A0A087WXS7	>tr|A0A087WXS7|A0A087WXS7_HUMAN ATPase ASNA1 OS=Homo sapiens OX=9606 GN=ASNA1 PE=1 SV=1;>sp|O43681|ASNA_HUMAN ATPase ASNA1 OS=Homo sapiens OX=9606 GN=ASNA1 PE=1 SV=2;>tr|K7ERW9|K7ERW9_HUMAN Arsenical pump-driving ATPase (Fragment) OS=Homo sapiens OX=9606 G	1,6	0,03	PRDX1
O15372	EIF3H	Eukaryotic translation initiation factor 3 subunit H	1,5	0	PRDX1
Q9UIG0	BAZ1B	Tyrosine-protein kinase BAZ1B	1,5	0	PRDX1
K7ERF1	EIF3K	Eukaryotic translation initiation factor 3 subunit K	1,5	0	PRDX1
Q96D09	GPRASP2	G-protein coupled receptor-associated sorting protein 2	1,5	0	PRDX1
P06737	PYGL	Glycogen phosphorylase, liver form	1,5	0	PRDX1
Q15029	EFTUD2	116 kDa U5 small nuclear ribonucleoprotein component	1,5	0	PRDX1
P63104	YWHAZ	14-3-3 protein zeta/delta	1,5	0	PRDX1
E5RHG8	ELOC	Elongin-C	1,5	0	PRDX1
P30101	PDIA3	Protein disulfide-isomerase A3	1,5	0,001	PRDX1
O75832	PSMD10	26S proteasome non-ATPase regulatory subunit 10	1,5	0,001	PRDX1
O00273	DFFA	DNA fragmentation factor subunit alpha	1,5	0,002	PRDX1
O43747	AP1G1	AP-1 complex subunit gamma-1	1,5	0,002	PRDX1
Q6IN85	PPP4R3A	Serine/threonine-protein phosphatase 4 regulatory subunit 3A	1,5	0,005	PRDX1
Q96T23	RSF1	Remodeling and spacing factor 1	1,5	0,01	PRDX1
H7C128	BRD8	Bromodomain-containing protein 8	1,5	0,012	PRDX1
Q9HA64	FN3KRP	Ketosamine-3-kinase	1,5	0,017	PRDX1
Q9P287	BCCIP	BRCA2 and CDKN1A-interacting protein	1,5	0,018	PRDX1
Q13033	STRN3	Striatin-3	1,5	0,022	PRDX1
Q9NQ29	LUC7L	Putative RNA-binding protein Luc7-like 1	1,5	0,023	PRDX1
P19174	PLCG1	1-phosphatidylinositol 4,5-bisphosphate phosphodiesterase gamma-1	1,5	0,024	PRDX1
Q86TI2	DPP9	Dipeptidyl peptidase 9	1,5	0,027	PRDX1
Q9NTK5	OLA1	Obg-like ATPase 1	1,5	0,031	PRDX1
P28288	ABCD3	ATP-binding cassette sub-family D member 3	1,5	0,034	PRDX1
O15144	ARPC2	Actin-related protein 2/3 complex subunit 2	1,5	0,035	PRDX1
Q9Y277	VDAC3	Voltage-dependent anion-selective channel protein 3	1,5	0,044	PRDX1
Q9UL15	BAG5	BAG family molecular chaperone regulator 5	1,5	0,046	PRDX1
Q15691	MAPRE1	Microtubule-associated protein RP/EB family member 1	1,4	0	PRDX1
P15121	AKR1B1	Aldo-keto reductase family 1 member B1	1,4	0	PRDX1
E9PMI6	CLNS1A	Chloride channel, nucleotide sensitive 1A	1,4	0	PRDX1
Q92598	HSPH1	Heat shock protein 105 kDa	1,4	0	PRDX1
P60900	PSMA6	Proteasome subunit alpha type-6	1,4	0	PRDX1
Q8IWB7	WDFY1	WD repeat and FYVE domain-containing protein 1	1,4	0,001	PRDX1
H7BZM7	ZPR1	Zinc finger protein ZPR1	1,4	0,001	PRDX1
P45974	USP5	Ubiquitin carboxyl-terminal hydrolase 5	1,4	0,001	PRDX1
O43707	ACTN4	Alpha-actinin-4	1,4	0,002	PRDX1
E7EV99	ADD1	Alpha-adducin	1,4	0,002	PRDX1
Q9H0A0	NAT10	RNA cytidine acetyltransferase	1,4	0,006	PRDX1
F8W038	C17orf49	Chromosome 17 open reading frame 49	1,4	0,008	PRDX1
P42574	CASP3	Caspase-3	1,4	0,025	PRDX1
Q99598	TSNAX	Translin-associated protein X	1,4	0,029	PRDX1

Q01085	TIAL1	Nucleolysin TIAR	1,4	0,033	PRDX1
Q9NZL9	MAT2B	Methionine adenosyltransferase 2 subunit beta	1,4	0,037	PRDX1
Q9UKN8	GTF3C4	General transcription factor 3C polypeptide 4	1,4	0,045	PRDX1
Q8N999	C12orf29	Uncharacterized protein C12orf29	1,4	0,047	PRDX1
P32969	RPL9	60S ribosomal protein L9	1,3	0	PRDX1
Q9NSD9	FARSB	Phenylalanine--tRNA ligase beta subunit	1,3	0	PRDX1
Q9Y383	LUC7L2	Putative RNA-binding protein Luc7-like 2	1,3	0	PRDX1
P05023	ATP1A1	Sodium/potassium-transporting ATPase subunit alpha-1	1,3	0	PRDX1
A6NKB8	RNPEP	Aminopeptidase B	1,3	0	PRDX1
P61247	RPS3A	40S ribosomal protein S3a	1,3	0	PRDX1
P62424	RPL7A	60S ribosomal protein L7a	1,3	0	PRDX1
P60953	CDC42	Cell division control protein 42 homolog	1,3	0,001	PRDX1
Q68E01	INTS3	Integrator complex subunit 3	1,3	0,001	PRDX1
F8VVL1	DENR	Density-regulated protein	1,3	0,002	PRDX1
Q92688	ANP32B	Acidic leucine-rich nuclear phosphoprotein 32 family member B	1,3	0,003	PRDX1
P18077	RPL35A	60S ribosomal protein L35a	1,3	0,003	PRDX1
O00186	STXBP3	Syntaxin-binding protein 3	1,3	0,005	PRDX1
P16615	ATP2A2	Sarcoplasmic/endoplasmic reticulum calcium ATPase 2	1,3	0,005	PRDX1
P08133	ANXA6	Annexin A6	1,3	0,005	PRDX1
Q15291	RBBP5	Retinoblastoma-binding protein 5	1,3	0,005	PRDX1
P49750	YLPM1	YLP motif-containing protein 1	1,3	0,005	PRDX1
P55769	SNU13	NHP2-like protein 1	1,3	0,006	PRDX1
O75381	PEX14	Peroxisomal membrane protein PEX14	1,3	0,011	PRDX1
P41252	IARS1	Isoleucine--tRNA ligase, cytoplasmic	1,3	0,018	PRDX1
P08758	ANXA5	Annexin A5	1,3	0,022	PRDX1
A0A0D9SG77	UBE3A	Ubiquitin-protein ligase E3A	1,3	0,039	PRDX1
E9PJN0	ACOT8	Acyl-coenzyme A thioesterase 8	1,3	0,04	PRDX1
P63244	RACK1	Receptor of activated protein C kinase 1	1,3	0,045	PRDX1
Q9NYB0	TERF2IP	Telomeric repeat-binding factor 2-interacting protein 1	1,3	0,045	PRDX1
A0A3B3ISV3	COL4A1	Collagen alpha-1(IV) chain	1,3	0,049	PRDX1
Q13131	PRKAA1	5'-AMP-activated protein kinase catalytic subunit alpha-1	1,3	0,05	PRDX1
P40938	RFC3	Replication factor C subunit 3	1,2	0	PRDX1
O00299	CLIC1	Chloride intracellular channel protein 1	1,2	0	PRDX1
P00387	CYB5R3	NADH-cytochrome b5 reductase 3	1,2	0	PRDX1
Q9Y5V3	MAGED1	Melanoma-associated antigen D1	1,2	0	PRDX1
P51149	RAB7A	Ras-related protein Rab-7a	1,2	0	PRDX1
O60763	USO1	General vesicular transport factor p115	1,2	0	PRDX1
P23396	RPS3	40S ribosomal protein S3	1,2	0	PRDX1
C9J2Y9	POLR2B	DNA-directed RNA polymerase subunit beta	1,2	0,001	PRDX1
Q3ZCQ8	TIMM50	Mitochondrial import inner membrane translocase subunit TIM50	1,2	0,001	PRDX1
Q9H3P7	ACBD3	Golgi resident protein GCP60	1,2	0,001	PRDX1
P51665	PSMD7	26S proteasome non-ATPase regulatory subunit 7	1,2	0,001	PRDX1
C9J0I9	ZC3HC1	Nuclear-interacting partner of ALK	1,2	0,001	PRDX1
P43034	PAFAH1B1	Platelet-activating factor acetylhydrolase IB subunit beta	1,2	0,001	PRDX1
P14324	FDPS	Farnesyl pyrophosphate synthase	1,2	0,001	PRDX1
Q8ND82	ZNF280C	Zinc finger protein 280C	1,2	0,001	PRDX1
P09211	GSTP1	Glutathione S-transferase P	1,2	0,001	PRDX1
P62877	RBX1	E3 ubiquitin-protein ligase RBX1	1,2	0,002	PRDX1
Q07020	RPL18	60S ribosomal protein L18	1,2	0,002	PRDX1
P25490	YY1	Transcriptional repressor protein YY1	1,2	0,003	PRDX1
Q96H79	ZC3HAV1L	Zinc finger CCCH-type antiviral protein 1-like	1,2	0,004	PRDX1
Q9Y3Z3	SAMHD1	Deoxynucleoside triphosphate triphosphohydrolase SAMHD1	1,2	0,005	PRDX1
Q01831	XPC	DNA repair protein complementing XP-C cells	1,2	0,005	PRDX1
P55884	EIF3B	Eukaryotic translation initiation factor 3 subunit B	1,2	0,005	PRDX1
Q9UI12	ATP6V1H	V-type proton ATPase subunit H	1,2	0,006	PRDX1
Q9Y5J1	UTP18	U3 small nucleolar RNA-associated protein 18 homolog	1,2	0,006	PRDX1
Q15843	NEDD8	NEDD8	1,2	0,008	PRDX1
P56192	MARS1	Methionine--tRNA ligase, cytoplasmic	1,2	0,009	PRDX1
P19338	NCL	Nucleolin	1,2	0,015	PRDX1
Q9H0U4	RAB1B	Ras-related protein Rab-1B	1,2	0,017	PRDX1
Q96RL1	UIMC1	BRCA1-A complex subunit RAP80	1,2	0,03	PRDX1
P30740	SERPINB1	Leukocyte elastase inhibitor	1,2	0,033	PRDX1
Q93008	USP9X	Probable ubiquitin carboxyl-terminal hydrolase FAF-X	1,2	0,037	PRDX1
O75369	FLNB	Filamin-B	1,2	0,041	PRDX1
E7EMC7	SQSTM1	Sequestosome-1	1,2	0,046	PRDX1
Q00325	SLC25A3	Phosphate carrier protein, mitochondrial	1,1	0	PRDX1
P11310	ACADM	Medium-chain specific acyl-CoA dehydrogenase, mitochondrial	1,1	0	PRDX1
Q96CX2	KCTD12	BTB/POZ domain-containing protein KCTD12	1,1	0	PRDX1
J3QQW9	SUZ12	Polycomb protein SUZ12	1,1	0,001	PRDX1

O60934	NBN	Nibrin	1,1	0,002	PRDX1
O94826	TOMM70	Mitochondrial import receptor subunit TOM70	1,1	0,002	PRDX1
P45954	ACADSB	Short/branched chain specific acyl-CoA dehydrogenase, mitochondrial	1,1	0,002	PRDX1
O94992	HEXIM1	Protein HEXIM1	1,1	0,003	PRDX1
P12236	SLC25A6	ADP/ATP translocase 3	1,1	0,003	PRDX1
P42166	TMPO	Lamina-associated polypeptide 2, isoform alpha	1,1	0,004	PRDX1
P43246	MSH2	DNA mismatch repair protein Msh2	1,1	0,004	PRDX1
P53004	BLVRA	Biliverdin reductase A	1,1	0,006	PRDX1
A0A0C4DGX4	CUL1	Cullin-1	1,1	0,01	PRDX1
O95376	ARIH2	E3 ubiquitin-protein ligase ARIH2	1,1	0,014	PRDX1
Q9UL25	RAB21	Ras-related protein Rab-21	1,1	0,015	PRDX1
O60784	TOM1	Target of Myb protein 1	1,1	0,02	PRDX1
Q15054	POLD3	DNA polymerase delta subunit 3	1,1	0,02	PRDX1
Q8IZ73	RPUSD2	RNA pseudouridylate synthase domain-containing protein 2	1,1	0,031	PRDX1
Q96SB4	SRPK1	SRSF protein kinase 1	1,1	0,033	PRDX1
P16435	POR	NADPH--cytochrome P450 reductase	1,1	0,035	PRDX1
G3V529	DDX24	RNA helicase	1,1	0,044	PRDX1
P09960	LTA4H	Leukotriene A-4 hydrolase	1	0	PRDX1
Q99623	PHB2	Prohibitin-2	1	0,001	PRDX1
Q99613	EIF3C	Eukaryotic translation initiation factor 3 subunit C	1	0,002	PRDX1
Q9NQW7	XPNPEP1	Xaa-Pro aminopeptidase 1	1	0,005	PRDX1
P07195	LDHB	L-lactate dehydrogenase B chain	1	0,006	PRDX1
Q9BY42	RTF2	Replication termination factor 2	1	0,007	PRDX1
Q9UPN7	PPP6R1	Serine/threonine-protein phosphatase 6 regulatory subunit 1	1	0,008	PRDX1
Q6PI48	DARS2	Aspartate--tRNA ligase, mitochondrial	1	0,012	PRDX1
O00203	AP3B1	AP-3 complex subunit beta-1	1	0,013	PRDX1
O76003	GLRX3	Glutaredoxin-3	1	0,035	PRDX1
F8W1A4	AK2	Adenylate kinase 2, mitochondrial	1	0,043	PRDX1
P20073	ANXA7	Annexin A7	1	0,047	PRDX1
P49366	DHPS	Deoxyhypusine synthase	6,9	0	PRDX2
O94776	MTA2	Metastasis-associated protein MTA2	6,7	0	PRDX2
H0YEN2	PPP6R3	Serine/threonine-protein phosphatase 6 regulatory subunit 3	4,1	0	PRDX2
Q16576	RBBP7	Histone-binding protein RBBP7	3,8	0	PRDX2
P63151	PPP2R2A	Serine/threonine-protein phosphatase 2A 55 kDa regulatory subunit B alpha isoform	3,7	0	PRDX2
Q5QNY5	PEX19	Peroxin-19	3,7	0	PRDX2
H0Y4R1	IMPDH2	Inosine-5'-monophosphate dehydrogenase 2	3,7	0	PRDX2
P67936	TPM4	Tropomyosin alpha-4 chain	3,6	0	PRDX2
Q13547	HDAC1	Histone deacetylase 1	3,6	0	PRDX2
Q96BR5	COA7	Cytochrome c oxidase assembly factor 7	3,5	0	PRDX2
O00165	HAX1	HCLS1-associated protein X-1	3,4	0	PRDX2
Q09028	RBBP4	Histone-binding protein RBBP4	3,4	0	PRDX2
P61289	PSME3	Proteasome activator complex subunit 3	3,4	0,023	PRDX2
Q96EW2	HSPBAP1	HSPB1-associated protein 1	3,1	0	PRDX2
Q9GZU8	PSME3IP1	PSME3-interacting protein	3	0	PRDX2
A0A0A0MR02	VDAC2	Outer mitochondrial membrane protein porin 2	3	0	PRDX2
Q96RS6	NUDCD1	NudC domain-containing protein 1	2,9	0	PRDX2
Q9NQP4	PFDN4	Prefoldin subunit 4	2,9	0	PRDX2
P62258	YWHAE	14-3-3 protein epsilon	2,9	0	PRDX2
A0A1C7CYX9	DPYSL2	Dihydropyrimidinase-related protein 2	2,8	0	PRDX2
O14744	PRMT5	Protein arginine N-methyltransferase 5	2,8	0,011	PRDX2
P23526	AHCY	Adenosylhomocysteinase	2,7	0	PRDX2
Q6DKK2	TTC19	Tetratricopeptide repeat protein 19, mitochondrial	2,7	0,003	PRDX2
P20839	IMPDH1	Inosine-5'-monophosphate dehydrogenase 1	2,6	0	PRDX2
Q96DB5	RMDN1	Regulator of microtubule dynamics protein 1	2,6	0,002	PRDX2
P78417	GSTO1	Glutathione S-transferase omega-1	2,5	0	PRDX2
Q15276	RABEP1	Rab GTPase-binding effector protein 1	2,5	0	PRDX2
P41250	GARS1	Glycine--tRNA ligase	2,4	0	PRDX2
P22234	PAICS	Multifunctional protein ADE2 [Includes: Phosphoribosylaminoimidazole-succinocarboxamide synthase	2,4	0	PRDX2
P78371	CCT2	T-complex protein 1 subunit beta	2,4	0	PRDX2
O75688	PPM1B	Protein phosphatase 1B	2,4	0	PRDX2
P27348	YWHAQ	14-3-3 protein theta	2,4	0	PRDX2
Q92769	HDAC2	Histone deacetylase 2	2,4	0	PRDX2
O00268	TAF4	Transcription initiation factor TFIID subunit 4	2,3	0	PRDX2
P60900	PSMA6	Proteasome subunit alpha type-6	2,2	0,002	PRDX2
H7C3C4	SLC4A7	Anion exchange protein	2,2	0,003	PRDX2
H0YKU1	TMOD3	Tropomodulin-3	2,2	0,006	PRDX2
P98175	RBM10	RNA-binding protein 10	2,1	0	PRDX2
Q9Y478	PRKAB1	5'-AMP-activated protein kinase subunit beta-1	2,1	0,003	PRDX2

O43143	DHX15	Pre-mRNA-splicing factor ATP-dependent RNA helicase DHX15	2,1	0,004	PRDX2
A0A2U3TZY2	CLPB	Caseinolytic peptidase B protein homolog	2,1	0,004	PRDX2
P52788	SMS	Spermine synthase	2,1	0,008	PRDX2
O43852	CALU	Calumenin	2	0	PRDX2
H7BZM7	ZPR1	Zinc finger protein ZPR1	2	0	PRDX2
F8W1A4	AK2	Adenylate kinase 2, mitochondrial	2	0,005	PRDX2
P12814	ACTN1	Alpha-actinin-1	2	0,009	PRDX2
P30044	PRDX5	Peroxiredoxin-5, mitochondrial	12,4	0	PRDX2
Q9C0C9	UBE2O	(E3-independent) E2 ubiquitin-conjugating enzyme	1,9	0	PRDX2
P31946	YWHAB	14-3-3 protein beta/alpha	1,9	0	PRDX2
Q9BPU6	DPYSL5	Dihydropyrimidinase-related protein 5	1,9	0	PRDX2
P45973	CBX5	Chromobox protein homolog 5	1,9	0	PRDX2
P30041	PRDX6	Peroxiredoxin-6	1,9	0,012	PRDX2
P61981	YWHAG	14-3-3 protein gamma	1,8	0	PRDX2
Q15008	PSMD6	26S proteasome non-ATPase regulatory subunit 6	1,8	0	PRDX2
Q13200	PSMD2	26S proteasome non-ATPase regulatory subunit 2	1,8	0	PRDX2
P11142	HSPA8	Heat shock cognate 71 kDa protein	1,8	0	PRDX2
O43164	PJA2	E3 ubiquitin-protein ligase Praja-2	1,8	0,001	PRDX2
P54646	PRKAA2	5'-AMP-activated protein kinase catalytic subunit alpha-2	1,8	0,001	PRDX2
J3QQZ9	PNPO	Pyridoxal 5'-phosphate synthase	1,8	0,001	PRDX2
P62979	RPS27A	Ubiquitin-40S ribosomal protein S27a	1,8	0,001	PRDX2
Q14257	RCN2	Reticulocalbin-2	1,8	0,003	PRDX2
Q96RG2	PASK	PAS domain-containing serine/threonine-protein kinase	1,8	0,003	PRDX2
Q96B36	AKT1S1	Proline-rich AKT1 substrate 1	1,8	0,015	PRDX2
O00399	DCTN6	Dynactin subunit 6	1,8	0,018	PRDX2
A0A087WXS7	A0A087WXS7	>tr|A0A087WXS7|A0A087WXS7_HUMAN ATPase ASNA1 OS=Homo sapiens OX=9606 GN=ASNA1 PE=1 SV=1;>sp|O43681|ASNA_HUMAN ATPase ASNA1 OS=Homo sapiens OX=9606 GN=ASNA1 PE=1 SV=2;>tr|K7ERW9|K7ERW9_HUMAN Arsenical pump-driving ATPase (Fragment) OS=Homo sapiens OX=9606 G	1,8	0,023	PRDX2
Q9UHV9	PFDN2	Prefoldin subunit 2	1,8	0,024	PRDX2
P63104	YWHAZ	14-3-3 protein zeta/delta	1,7	0	PRDX2
A0A024R442	A0A024R442	>tr|A0A024R442|A0A024R442_HUMAN Aspartyl aminopeptidase, isoform CRA_b OS=Homo sapiens OX=9606 GN=DNPEP PE=1 SV=1;>sp|Q9ULA0|DNPEP_HUMAN Aspartyl aminopeptidase OS=Homo sapiens OX=9606 GN=DNPEP PE=1 SV=1;>tr|E7ETB3|E7ETB3_HUMAN Aspartyl aminopeptidase, iso	1,7	0,005	PRDX2
Q9NTK5	OLA1	Obg-like ATPase 1	1,7	0,022	PRDX2
Q9NV56	MRGBP	MRG/MORF4L-binding protein	1,7	0,025	PRDX2
B4DHR0	RABEP2	Rab GTPase-binding effector protein 2	1,7	0,025	PRDX2
Q13131	PRKAA1	5'-AMP-activated protein kinase catalytic subunit alpha-1	1,7	0,03	PRDX2
E9PLK3	NPEPPS	Aminopeptidase	1,6	0	PRDX2
Q93009	USP7	Ubiquitin carboxyl-terminal hydrolase 7	1,6	0	PRDX2
P28066	PSMA5	Proteasome subunit alpha type-5	1,6	0	PRDX2
O15212	PFDN6	Prefoldin subunit 6	1,6	0,001	PRDX2
Q32MZ4	LRRFIP1	Leucine-rich repeat flightless-interacting protein 1	1,6	0,012	PRDX2
Q9UKN8	GTF3C4	General transcription factor 3C polypeptide 4	1,6	0,033	PRDX2
P57076	CFAP298	Cilia- and flagella-associated protein 298	1,6	0,038	PRDX2
C9J0I9	ZC3HC1	Nuclear-interacting partner of ALK	1,5	0	PRDX2
E7ESY4	MTA1	Metastasis-associated protein MTA1	1,5	0	PRDX2
Q15424	SAFB	Scaffold attachment factor B1	1,5	0,001	PRDX2
Q15843	NEDD8	NEDD8	1,5	0,001	PRDX2
Q9UBE0	SAE1	SUMO-activating enzyme subunit 1	1,5	0,004	PRDX2
Q9UEY8	ADD3	Gamma-adducin	1,5	0,011	PRDX2
A0A087X0K9	TJP1	Tight junction protein ZO-1	1,5	0,011	PRDX2
Q5RKV6	EXOSC6	Exosome complex component MTR3	1,5	0,012	PRDX2
A0A087WT45	GRIPAP1	GRIP1-associated protein 1	1,5	0,017	PRDX2
P67809	YBX1	Y-box-binding protein 1	1,5	0,035	PRDX2
Q9BSJ8	ESYT1	Extended synaptotagmin-1	1,5	0,037	PRDX2
Q8N6R0	EEF1AKNMT	eEF1A lysine and N-terminal methyltransferase	1,5	0,04	PRDX2
Q9BY42	RTF2	Replication termination factor 2	1,4	0	PRDX2
P35998	PSMC2	26S proteasome regulatory subunit 7	1,4	0,001	PRDX2
Q9Y3F4	STRAP	Serine-threonine kinase receptor-associated protein	1,4	0,002	PRDX2
Q13185	CBX3	Chromobox protein homolog 3	1,4	0,021	PRDX2
H7C128	BRD8	Bromodomain-containing protein 8	1,4	0,031	PRDX2
Q8N806	UBR7	Putative E3 ubiquitin-protein ligase UBR7	1,3	0,032	PRDX2
P15104	GLUL	Glutamine synthetase	1,2	0	PRDX2
P23528	CFL1	Cofilin-1	1,2	0	PRDX2
P12270	TPR	Nucleoprotein TPR	1,2	0	PRDX2
Q96D09	GPRASP2	G-protein coupled receptor-associated sorting protein 2	1,2	0,001	PRDX2
P62191	PSMC1	26S proteasome regulatory subunit 4	1,2	0,001	PRDX2
Q9UPN7	PPP6R1	Serine/threonine-protein phosphatase 6 regulatory subunit 1	1,2	0,008	PRDX2

E5KLJ9	OPA1	Dynamin-like 120 kDa protein, form S1	1,2	0,011	PRDX2
Q13564	NAE1	NEDD8-activating enzyme E1 regulatory subunit	1,2	0,025	PRDX2
P23588	EIF4B	Eukaryotic translation initiation factor 4B	1,2	0,039	PRDX2
O14545	TRAFD1	TRAF-type zinc finger domain-containing protein 1	1,1	0	PRDX2
Q3ZCQ8	TIMM50	Mitochondrial import inner membrane translocase subunit TIM50	1,1	0,001	PRDX2
Q9NX63	CHCHD3	MICOS complex subunit MIC19	1,1	0,001	PRDX2
C9J2Y9	POLR2B	DNA-directed RNA polymerase subunit beta	1,1	0,003	PRDX2
P25786	PSMA1	Proteasome subunit alpha type-1	1,1	0,003	PRDX2
O15355	PPM1G	Protein phosphatase 1G	1,1	0,008	PRDX2
Q9BTE6	AARSD1	Alanyl-tRNA editing protein Aarsd1	1,1	0,011	PRDX2
Q9NXF7	DCAF16	DDB1- and CUL4-associated factor 16	1,1	0,013	PRDX2
Q99504	EYA3	Eyes absent homolog 3	1,1	0,015	PRDX2
P48147	PREP	Prolyl endopeptidase	1,1	0,031	PRDX2
P29218	IMPA1	Inositol monophosphatase 1	1,1	0,031	PRDX2
Q8N999	C12orf29	Uncharacterized protein C12orf29	1,1	0,035	PRDX2
Q13177	PAK2	Serine/threonine-protein kinase PAK 2	1,1	0,039	PRDX2
O00429	DNM1L	Dynamin-1-like protein	1,1	0,047	PRDX2
P20020	ATP2B1	Plasma membrane calcium-transporting ATPase 1	1	0,003	PRDX2
Q68E01	INTS3	Integrator complex subunit 3	1	0,012	PRDX2
Q96K76	USP47	Ubiquitin carboxyl-terminal hydrolase 47	1	0,016	PRDX2
P53985	SLC16A1	Monocarboxylate transporter 1	1	0,02	PRDX2
O60784	TOM1	Target of Myb protein 1	1	0,022	PRDX2
P49588	AARS1	Alanine--tRNA ligase, cytoplasmic	1	0,033	PRDX2
X6RM00	ERC1	ELKS/Rab6-interacting/CAST family member 1	1	0,035	PRDX2
O94776	MTA2	Metastasis-associated protein MTA2	7	0	PRDX3
P49366	DHPS	Deoxyhypusine synthase	7	0	PRDX3
P61289	PSME3	Proteasome activator complex subunit 3	5	0	PRDX3
Q16576	RBBP7	Histone-binding protein RBBP7	5	0	PRDX3
P67936	TPM4	Tropomyosin alpha-4 chain	4,9	0	PRDX3
H0Y4R1	IMPDH2	Inosine-5'-monophosphate dehydrogenase 2	4,6	0	PRDX3
P41250	GARS1	Glycine--tRNA ligase	4,3	0	PRDX3
P22234	PAICS	Multifunctional protein ADE2 [Includes: Phosphoribosylaminoimidazole-succinocarboxamide synthase	4,3	0	PRDX3
O14744	PRMT5	Protein arginine N-methyltransferase 5	3,9	0	PRDX3
Q9NQP4	PFDN4	Prefoldin subunit 4	3,7	0	PRDX3
Q96BR5	COA7	Cytochrome c oxidase assembly factor 7	3,6	0	PRDX3
Q09028	RBBP4	Histone-binding protein RBBP4	3,6	0	PRDX3
O00165	HAX1	HCLS1-associated protein X-1	3,4	0	PRDX3
E7EVA0	MAP4	Microtubule-associated protein	3,4	0,001	PRDX3
P20839	IMPDH1	Inosine-5'-monophosphate dehydrogenase 1	3,3	0	PRDX3
P30041	PRDX6	Peroxiredoxin-6	3,3	0	PRDX3
Q9GZU8	PSME3IP1	PSME3-interacting protein	3,2	0	PRDX3
Q96EW2	HSPBAP1	HSPB1-associated protein 1	3,2	0	PRDX3
Q96RS6	NUDCD1	NudC domain-containing protein 1	3,1	0	PRDX3
Q9UEY8	ADD3	Gamma-adducin	3,1	0	PRDX3
Q96KB5	PBK	Lymphokine-activated killer T-cell-originated protein kinase	3,1	0	PRDX3
Q9UHV9	PFDN2	Prefoldin subunit 2	3	0	PRDX3
Q13547	HDAC1	Histone deacetylase 1	3	0	PRDX3
Q6DKK2	TTC19	Tetratricopeptide repeat protein 19, mitochondrial	3	0,001	PRDX3
P63151	PPP2R2A	Serine/threonine-protein phosphatase 2A 55 kDa regulatory subunit B alpha isoform	3	0,001	PRDX3
O43143	DHX15	Pre-mRNA-splicing factor ATP-dependent RNA helicase DHX15	2,9	0	PRDX3
Q32MZ4	LRRFIP1	Leucine-rich repeat flightless-interacting protein 1	2,9	0	PRDX3
J3QQZ9	PNPO	Pyridoxal 5'-phosphate synthase	2,9	0	PRDX3
A0A024R442	A0A024R442	>tr|A0A024R442|A0A024R442_HUMAN Aspartyl aminopeptidase, isoform CRA_b OS=Homo sapiens OX=9606 GN=DNPEP PE=1 SV=1;>sp|Q9ULA0|DNPEP_HUMAN Aspartyl aminopeptidase OS=Homo sapiens OX=9606 GN=DNPEP PE=1 SV=1;>tr|E7ETB3|E7ETB3_HUMAN Aspartyl aminopeptidase, iso	2,7	0	PRDX3
Q8NFC6	BOD1L1	Biorientation of chromosomes in cell division protein 1-like 1	2,7	0	PRDX3
H0YEN2	PPP6R3	Serine/threonine-protein phosphatase 6 regulatory subunit 3	2,7	0	PRDX3
P10599	TXN	Thioredoxin	2,7	0,002	PRDX3
Q99598	TSNAX	Translin-associated protein X	2,6	0	PRDX3
Q5QNY5	PEX19	Peroxin-19	2,6	0	PRDX3
Q9C0C9	UBE2O	(E3-independent) E2 ubiquitin-conjugating enzyme	2,5	0	PRDX3
P31153	MAT2A	S-adenosylmethionine synthase isoform type-2	2,5	0	PRDX3
Q92769	HDAC2	Histone deacetylase 2	2,5	0	PRDX3
A0A2U3TZY2	CLPB	Caseinolytic peptidase B protein homolog	2,5	0,001	PRDX3
A0A087WT45	GRIPAP1	GRIP1-associated protein 1	2,5	0,001	PRDX3
P12955	PEPD	Xaa-Pro dipeptidase	2,5	0,002	PRDX3
Q9C0C2	TNKS1BP1	182 kDa tankyrase-1-binding protein	2,5	0,005	PRDX3
Q9BQA1	WDR77	Methylosome protein 50	2,5	0,008	PRDX3

Q8N3X1	FNBP4	Formin-binding protein 4	2,4	0	PRDX3
P62258	YWHAE	14-3-3 protein epsilon	2,4	0	PRDX3
P48147	PREP	Prolyl endopeptidase	2,4	0	PRDX3
H7C3C4	SLC4A7	Anion exchange protein	2,4	0,001	PRDX3
Q96DB5	RMDN1	Regulator of microtubule dynamics protein 1	2,4	0,003	PRDX3
Q9BPU6	DPYSL5	Dihydropyrimidinase-related protein 5	2,3	0	PRDX3
Q9Y478	PRKAB1	5'-AMP-activated protein kinase subunit beta-1	2,3	0,001	PRDX3
Q8NC51	SERBP1	Plasminogen activator inhibitor 1 RNA-binding protein	2,3	0,001	PRDX3
H0YKU1	TMOD3	Tropomodulin-3	2,3	0,002	PRDX3
P36551	CPOX	Oxygen-dependent coproporphyrinogen-III oxidase, mitochondrial	2,3	0,034	PRDX3
O95831	AIFM1	Apoptosis-inducing factor 1, mitochondrial	2,2	0	PRDX3
Q15276	RABEP1	Rab GTPase-binding effector protein 1	2,2	0	PRDX3
P23526	AHCY	Adenosylhomocysteinase	2,2	0	PRDX3
E7EV99	ADD1	Alpha-adducin	2,1	0	PRDX3
Q9BRP1	PDCD2L	Programmed cell death protein 2-like	2,1	0	PRDX3
Q9NT62	ATG3	Ubiquitin-like-conjugating enzyme ATG3	2,1	0,001	PRDX3
Q9HA64	FN3KRP	Ketosamine-3-kinase	2,1	0,002	PRDX3
Q13131	PRKAA1	5'-AMP-activated protein kinase catalytic subunit alpha-1	2,1	0,004	PRDX3
P52788	SMS	Spermine synthase	2,1	0,004	PRDX3
A0A0C4DGB5	CAST	Calpain inhibitor	2,1	0,006	PRDX3
P54646	PRKAA2	5'-AMP-activated protein kinase catalytic subunit alpha-2	2	0	PRDX3
O15212	PFDN6	Prefoldin subunit 6	2	0	PRDX3
Q9Y3F4	STRAP	Serine-threonine kinase receptor-associated protein	2	0	PRDX3
Q96D09	GPRASP2	G-protein coupled receptor-associated sorting protein 2	2	0	PRDX3
P29218	IMPA1	Inositol monophosphatase 1	2	0,004	PRDX3
Q9Y266	NUDC	Nuclear migration protein nudC	2	0,006	PRDX3
P30044	PRDX5	Peroxiredoxin-5, mitochondrial	13,2	0	PRDX3
A0A1C7CYX9	DPYSL2	Dihydropyrimidinase-related protein 2	1,9	0	PRDX3
Q15181	PPA1	Inorganic pyrophosphatase	1,9	0	PRDX3
Q13200	PSMD2	26S proteasome non-ATPase regulatory subunit 2	1,9	0	PRDX3
F5GZS6	SLC3A2	4F2 cell-surface antigen heavy chain	1,9	0,006	PRDX3
Q96B36	AKT1S1	Proline-rich AKT1 substrate 1	1,9	0,006	PRDX3
A0A087WXS7	A0A087WXS7	>tr|A0A087WXS7|A0A087WXS7_HUMAN ATPase ASNA1 OS=Homo sapiens OX=9606 GN=ASNA1 PE=1 SV=1;>sp|O43681|ASNA_HUMAN ATPase ASNA1 OS=Homo sapiens OX=9606 GN=ASNA1 PE=1 SV=2;>tr|K7ERW9|K7ERW9_HUMAN Arsenical pump-driving ATPase (Fragment) OS=Homo sapiens OX=9606 G	1,9	0,008	PRDX3
Q9NTK5	OLA1	Obg-like ATPase 1	1,9	0,008	PRDX3
Q13177	PAK2	Serine/threonine-protein kinase PAK 2	1,8	0	PRDX3
Q13564	NAE1	NEDD8-activating enzyme E1 regulatory subunit	1,8	0	PRDX3
B7Z7F3	RANBP3	Ran-binding protein 3	1,8	0,004	PRDX3
F8W1A4	AK2	Adenylate kinase 2, mitochondrial	1,8	0,004	PRDX3
P54619	PRKAG1	5'-AMP-activated protein kinase subunit gamma-1	1,8	0,005	PRDX3
P61758	VBP1	Prefoldin subunit 3	1,8	0,005	PRDX3
H7C128	BRD8	Bromodomain-containing protein 8	1,8	0,006	PRDX3
Q9H773	DCTPP1	dCTP pyrophosphatase 1	1,8	0,007	PRDX3
Q8IVM0	CCDC50	Coiled-coil domain-containing protein 50	1,8	0,011	PRDX3
Q9UKN8	GTF3C4	General transcription factor 3C polypeptide 4	1,8	0,012	PRDX3
Q9BRS2	RIOK1	Serine/threonine-protein kinase RIO1	1,8	0,012	PRDX3
Q6WKZ4	RAB11FIP1	Rab11 family-interacting protein 1	1,8	0,016	PRDX3
O43164	PJA2	E3 ubiquitin-protein ligase Praja-2	1,7	0	PRDX3
Q5T4U8	RABGGTB	Geranylgeranyl transferase type-2 subunit beta	1,7	0,003	PRDX3
E9PGT1	TSN	Component 3 of promoter of RISC	1,7	0,005	PRDX3
P52888	THOP1	Thimet oligopeptidase	1,7	0,005	PRDX3
P85037	FOXK1	Forkhead box protein K1	1,7	0,006	PRDX3
Q8N999	C12orf29	Uncharacterized protein C12orf29	1,7	0,012	PRDX3
B1ANM7	FAF1	FAS-associated factor 1	1,7	0,019	PRDX3
Q9Y6A5	TACC3	Transforming acidic coiled-coil-containing protein 3	1,7	0,022	PRDX3
Q96HC4	PDLIM5	PDZ and LIM domain protein 5	1,6	0	PRDX3
P07195	LDHB	L-lactate dehydrogenase B chain	1,6	0	PRDX3
O75821	EIF3G	Eukaryotic translation initiation factor 3 subunit G	1,6	0	PRDX3
H7BZM7	ZPR1	Zinc finger protein ZPR1	1,6	0	PRDX3
P23528	CFL1	Cofilin-1	1,6	0	PRDX3
P32119	PRDX2	Peroxiredoxin-2	1,6	0,002	PRDX3
Q9HB71	CACYBP	Calcyclin-binding protein	1,6	0,002	PRDX3
B4DHR0	RABEP2	Rab GTPase-binding effector protein 2	1,6	0,013	PRDX3
P11802	CDK4	Cyclin-dependent kinase 4	1,6	0,021	PRDX3
P53985	SLC16A1	Monocarboxylate transporter 1	1,5	0	PRDX3
P45973	CBX5	Chromobox protein homolog 5	1,5	0	PRDX3
E5KLJ9	OPA1	Dynamin-like 120 kDa protein, form S1	1,5	0	PRDX3
Q9NSD9	FARSB	Phenylalanine--tRNA ligase beta subunit	1,5	0	PRDX3

P23381	WARS1	Tryptophan--tRNA ligase, cytoplasmic	1,5	0	PRDX3
O43852	CALU	Calumenin	1,5	0,001	PRDX3
P60900	PSMA6	Proteasome subunit alpha type-6	1,5	0,001	PRDX3
O94992	HEXIM1	Protein HEXIM1	1,5	0,002	PRDX3
P27348	YWHAQ	14-3-3 protein theta	1,5	0,005	PRDX3
Q12929	EPS8	Epidermal growth factor receptor kinase substrate 8	1,5	0,03	PRDX3
Q13541	EIF4EBP1	Eukaryotic translation initiation factor 4E-binding protein 1	1,5	0,03	PRDX3
O95825	CRYZL1	Quinone oxidoreductase-like protein 1	1,5	0,034	PRDX3
E9PLK3	NPEPPS	Aminopeptidase	1,4	0	PRDX3
Q9NXF7	DCAF16	DDB1- and CUL4-associated factor 16	1,4	0,001	PRDX3
P61981	YWHAG	14-3-3 protein gamma	1,4	0,001	PRDX3
Q15008	PSMD6	26S proteasome non-ATPase regulatory subunit 6	1,4	0,001	PRDX3
P40222	TXLNA	Alpha-taxilin	1,4	0,004	PRDX3
P47985	UQCRFS1	Cytochrome b-c1 complex subunit Rieske, mitochondrial	1,4	0,008	PRDX3
P78371	CCT2	T-complex protein 1 subunit beta	1,4	0,011	PRDX3
Q9P258	RCC2	Protein RCC2	1,4	0,016	PRDX3
F8VXG7	SCAF11	Protein SCAF11	1,4	0,035	PRDX3
E5RGS4	PFDN1	Prefoldin subunit 1	1,4	0,045	PRDX3
C9J0I9	ZC3HC1	Nuclear-interacting partner of ALK	1,3	0	PRDX3
F8VVL1	DENR	Density-regulated protein	1,3	0	PRDX3
A0A2R8Y811	RPS14	40S ribosomal protein S14	1,3	0	PRDX3
Q3ZCQ8	TIMM50	Mitochondrial import inner membrane translocase subunit TIM50	1,3	0	PRDX3
P61221	ABCE1	ATP-binding cassette sub-family E member 1	1,3	0	PRDX3
Q06203	PPAT	Amidophosphoribosyltransferase	1,3	0,001	PRDX3
Q9NUQ3	TXLNG	Gamma-taxilin	1,3	0,004	PRDX3
P06748	NPM1	Nucleophosmin	1,3	0,014	PRDX3
Q9NPH2	ISYNA1	Inositol-3-phosphate synthase 1	1,3	0,017	PRDX3
P78356	PIP4K2B	Phosphatidylinositol 5-phosphate 4-kinase type-2 beta	1,3	0,035	PRDX3
P62191	PSMC1	26S proteasome regulatory subunit 4	1,2	0	PRDX3
P63104	YWHAZ	14-3-3 protein zeta/delta	1,2	0	PRDX3
Q9Y230	RUVBL2	RuvB-like 2	1,2	0	PRDX3
Q93009	USP7	Ubiquitin carboxyl-terminal hydrolase 7	1,2	0	PRDX3
Q9UHY1	NRBP1	Nuclear receptor-binding protein	1,2	0	PRDX3
P62826	RAN	GTP-binding nuclear protein Ran	1,2	0	PRDX3
Q9Y265	RUVBL1	RuvB-like 1	1,2	0,001	PRDX3
Q96RL1	UIMC1	BRCA1-A complex subunit RAP80	1,2	0,011	PRDX3
Q9UBE0	SAE1	SUMO-activating enzyme subunit 1	1,2	0,015	PRDX3
P43304	GPD2	Glycerol-3-phosphate dehydrogenase, mitochondrial	1,2	0,022	PRDX3
Q9NV56	MRGBP	MRG/MORF4L-binding protein	1,2	0,031	PRDX3
P11142	HSPA8	Heat shock cognate 71 kDa protein	1,1	0	PRDX3
P54578	USP14	Ubiquitin carboxyl-terminal hydrolase 14	1,1	0,002	PRDX3
Q92598	HSPH1	Heat shock protein 105 kDa	1,1	0,002	PRDX3
P55072	VCP	Transitional endoplasmic reticulum ATPase	1,1	0,006	PRDX3
P34932	HSPA4	Heat shock 70 kDa protein 4	1,1	0,012	PRDX3
A0A087X0K9	TJP1	Tight junction protein ZO-1	1,1	0,016	PRDX3
P05386	RPLP1	60S acidic ribosomal protein P1	1,1	0,016	PRDX3
O00487	PSMD14	26S proteasome non-ATPase regulatory subunit 14	1	0,004	PRDX3
P49321	NASP	Nuclear autoantigenic sperm protein	1	0,018	PRDX3
P31946	YWHAB	14-3-3 protein beta/alpha	1	0,025	PRDX3
Q9UKK9	NUDT5	ADP-sugar pyrophosphatase	1	0,028	PRDX3
Q96RG2	PASK	PAS domain-containing serine/threonine-protein kinase	1	0,035	PRDX3
Q9BRX5	GINS3	DNA replication complex GINS protein PSF3	1	0,037	PRDX3
Q13185	CBX3	Chromobox protein homolog 3	1	0,046	PRDX3
O94776	MTA2	Metastasis-associated protein MTA2	7	0	PRDX4
P49366	DHPS	Deoxyhypusine synthase	6,8	0	PRDX4
P41250	GARS1	Glycine--tRNA ligase	5,7	0	PRDX4
P61289	PSME3	Proteasome activator complex subunit 3	5,5	0	PRDX4
P22234	PAICS	Multifunctional protein ADE2 [Includes: Phosphoribosylaminoimidazole-succinocarboxamide synthase	5	0	PRDX4
P63151	PPP2R2A	Serine/threonine-protein phosphatase 2A 55 kDa regulatory subunit B alpha isoform	4,9	0	PRDX4
P67936	TPM4	Tropomyosin alpha-4 chain	4,8	0	PRDX4
H0Y4R1	IMPDH2	Inosine-5'-monophosphate dehydrogenase 2	4,2	0	PRDX4
Q5QNY5	PEX19	Peroxin-19	4	0	PRDX4
Q96KB5	PBK	Lymphokine-activated killer T-cell-originated protein kinase	3,9	0	PRDX4
Q92769	HDAC2	Histone deacetylase 2	3,7	0	PRDX4
O00165	HAX1	HCLS1-associated protein X-1	3,6	0	PRDX4
O14744	PRMT5	Protein arginine N-methyltransferase 5	3,6	0,001	PRDX4
Q96BR5	COA7	Cytochrome c oxidase assembly factor 7	3,5	0	PRDX4
P30041	PRDX6	Peroxiredoxin-6	3,5	0	PRDX4

P54646	PRKAA2	5'-AMP-activated protein kinase catalytic subunit alpha-2	3,5	0	PRDX4
Q9NQP4	PFDN4	Prefoldin subunit 4	3,5	0	PRDX4
Q15276	RABEP1	Rab GTPase-binding effector protein 1	3,5	0	PRDX4
Q9GZU8	PSME3IP1	PSME3-interacting protein	3,4	0	PRDX4
Q9BSJ8	ESYT1	Extended synaptotagmin-1	3,4	0	PRDX4
Q13547	HDAC1	Histone deacetylase 1	3,4	0	PRDX4
Q16576	RBBP7	Histone-binding protein RBBP7	3,4	0	PRDX4
P10599	TXN	Thioredoxin	3,3	0	PRDX4
Q9UHV9	PFDN2	Prefoldin subunit 2	3,3	0	PRDX4
P23526	AHCY	Adenosylhomocysteinase	3,3	0	PRDX4
O43143	DHX15	Pre-mRNA-splicing factor ATP-dependent RNA helicase DHX15	3,2	0	PRDX4
Q32MZ4	LRRFIP1	Leucine-rich repeat flightless-interacting protein 1	3,2	0	PRDX4
J3QQZ9	PNPO	Pyridoxal 5'-phosphate synthase	3,2	0	PRDX4
Q6DKK2	TTC19	Tetratricopeptide repeat protein 19, mitochondrial	3,2	0,001	PRDX4
A0A024R442	A0A024R442	>tr|A0A024R442|A0A024R442_HUMAN Aspartyl aminopeptidase, isoform CRA_b OS=Homo sapiens OX=9606 GN=DNPEP PE=1 SV=1;>sp|Q9ULA0|DNPEP_ HUMAN Aspartyl aminopeptidase OS=Homo sapiens OX=9606 GN=DNPEP PE=1 SV=1;>tr|E7ETB3|E7ETB3_HUMAN Aspartyl aminopeptidase, iso	3,1	0	PRDX4
Q8NFC6	BOD1L1	Biorientation of chromosomes in cell division protein 1-like 1	3	0	PRDX4
Q96EW2	HSPBAP1	HSPB1-associated protein 1	3	0	PRDX4
P20839	IMPDH1	Inosine-5'-monophosphate dehydrogenase 1	3	0	PRDX4
Q96DB5	RMDN1	Regulator of microtubule dynamics protein 1	3	0,001	PRDX4
A0A0A0MR02	VDAC2	Outer mitochondrial membrane protein porin 2	2,9	0	PRDX4
Q9BQA1	WDR77	Methylosome protein 50	2,9	0,003	PRDX4
P42574	CASP3	Caspase-3	2,8	0	PRDX4
Q09028	RBBP4	Histone-binding protein RBBP4	2,8	0	PRDX4
P48147	PREP	Prolyl endopeptidase	2,8	0	PRDX4
Q96A49	SYAP1	Synapse-associated protein 1	2,8	0,001	PRDX4
A0A2U3TZY2	CLPB	Caseinolytic peptidase B protein homolog	2,8	0,001	PRDX4
P61758	VBP1	Prefoldin subunit 3	2,6	0	PRDX4
O15212	PFDN6	Prefoldin subunit 6	2,6	0	PRDX4
H0YEN2	PPP6R3	Serine/threonine-protein phosphatase 6 regulatory subunit 3	2,6	0	PRDX4
P11802	CDK4	Cyclin-dependent kinase 4	2,6	0,001	PRDX4
P54619	PRKAG1	5'-AMP-activated protein kinase subunit gamma-1	2,6	0,001	PRDX4
O94992	HEXIM1	Protein HEXIM1	2,5	0	PRDX4
P62258	YWHAE	14-3-3 protein epsilon	2,5	0	PRDX4
Q9HA64	FN3KRP	Ketosamine-3-kinase	2,5	0,001	PRDX4
Q6FI81	CIAPIN1	Anamorsin	2,5	0,001	PRDX4
P12955	PEPD	Xaa-Pro dipeptidase	2,5	0,002	PRDX4
Q96RS6	NUDCD1	NudC domain-containing protein 1	2,4	0	PRDX4
H7BXI1	ESYT2	Extended synaptotagmin-2	2,4	0	PRDX4
Q99598	TSNAX	Translin-associated protein X	2,4	0	PRDX4
A0A1C7CYX9	DPYSL2	Dihydropyrimidinase-related protein 2	2,4	0	PRDX4
Q9C0C9	UBE2O	(E3-independent) E2 ubiquitin-conjugating enzyme	2,4	0	PRDX4
E9PGT1	TSN	Component 3 of promoter of RISC	2,4	0,001	PRDX4
Q9UEY8	ADD3	Gamma-adducin	2,3	0	PRDX4
Q8N3X1	FNBP4	Formin-binding protein 4	2,3	0	PRDX4
Q13564	NAE1	NEDD8-activating enzyme E1 regulatory subunit	2,3	0	PRDX4
Q13177	PAK2	Serine/threonine-protein kinase PAK 2	2,3	0	PRDX4
Q9Y3F4	STRAP	Serine-threonine kinase receptor-associated protein	2,3	0	PRDX4
Q9BRP1	PDCD2L	Programmed cell death protein 2-like	2,3	0	PRDX4
Q9NPH2	ISYNA1	Inositol-3-phosphate synthase 1	2,3	0,001	PRDX4
P85037	FOXK1	Forkhead box protein K1	2,3	0,001	PRDX4
A0A087WT45	GRIPAP1	GRIP1-associated protein 1	2,3	0,001	PRDX4
Q9Y266	NUDC	Nuclear migration protein nudC	2,3	0,004	PRDX4
P78371	CCT2	T-complex protein 1 subunit beta	2,2	0	PRDX4
F8W1A4	AK2	Adenylate kinase 2, mitochondrial	2,2	0,001	PRDX4
Q5T4U8	RABGGTB	Geranylgeranyl transferase type-2 subunit beta	2,2	0,002	PRDX4
Q13131	PRKAA1	5'-AMP-activated protein kinase catalytic subunit alpha-1	2,2	0,005	PRDX4
Q96EA4	SPDL1	Protein Spindly	2,2	0,008	PRDX4
E7EV99	ADD1	Alpha-adducin	2,1	0	PRDX4
P31153	MAT2A	S-adenosylmethionine synthase isoform type-2	2,1	0	PRDX4
Q13200	PSMD2	26S proteasome non-ATPase regulatory subunit 2	2,1	0	PRDX4
H7C3C4	SLC4A7	Anion exchange protein	2,1	0,001	PRDX4
Q9NT62	ATG3	Ubiquitin-like-conjugating enzyme ATG3	2,1	0,001	PRDX4
P52888	THOP1	Thimet oligopeptidase	2,1	0,001	PRDX4
P60900	PSMA6	Proteasome subunit alpha type-6	2,1	0,001	PRDX4
Q9Y478	PRKAB1	5'-AMP-activated protein kinase subunit beta-1	2,1	0,002	PRDX4
H0YKU1	TMOD3	Tropomodulin-3	2,1	0,004	PRDX4
A0A0C4DGB5	CAST	Calpain inhibitor	2,1	0,005	PRDX4

H7BZM7	ZPR1	Zinc finger protein ZPR1	2	0	PRDX4
P11142	HSPA8	Heat shock cognate 71 kDa protein	2	0	PRDX4
Q9H974	QTRT2	Queuine tRNA-ribosyltransferase accessory subunit 2	2	0,002	PRDX4
Q96RG2	PASK	PAS domain-containing serine/threonine-protein kinase	2	0,003	PRDX4
B7Z7F3	RANBP3	Ran-binding protein 3	2	0,003	PRDX4
P49903	SEPHS1	Selenide, water dikinase 1	2	0,006	PRDX4
P52788	SMS	Spermine synthase	2	0,009	PRDX4
P30044	PRDX5	Peroxiredoxin-5, mitochondrial	13,5	0	PRDX4
P49593	PPM1F	Protein phosphatase 1F	1,9	0	PRDX4
Q9BPU6	DPYSL5	Dihydropyrimidinase-related protein 5	1,9	0	PRDX4
E9PLK3	NPEPPS	Aminopeptidase	1,9	0	PRDX4
P23528	CFL1	Cofilin-1	1,9	0	PRDX4
P31689	DNAJA1	DnaJ homolog subfamily A member 1	1,9	0,001	PRDX4
P27348	YWHAQ	14-3-3 protein theta	1,9	0,001	PRDX4
Q8N806	UBR7	Putative E3 ubiquitin-protein ligase UBR7	1,9	0,001	PRDX4
E5KLJ9	OPA1	Dynamin-like 120 kDa protein, form S1	1,9	0,001	PRDX4
Q9NV56	MRGBP	MRG/MORF4L-binding protein	1,9	0,002	PRDX4
O43164	PJA2	E3 ubiquitin-protein ligase Praja-2	1,9	0,004	PRDX4
Q9Y6A5	TACC3	Transforming acidic coiled-coil-containing protein 3	1,9	0,032	PRDX4
Q9C0C2	TNKS1BP1	182 kDa tankyrase-1-binding protein	1,9	0,046	PRDX4
B1AK87	CAPZB	F-actin-capping protein subunit beta	1,8	0	PRDX4
P22314	UBA1	Ubiquitin-like modifier-activating enzyme 1	1,8	0,003	PRDX4
H7C128	BRD8	Bromodomain-containing protein 8	1,8	0,007	PRDX4
Q9H773	DCTPP1	dCTP pyrophosphatase 1	1,8	0,012	PRDX4
Q9BV44	THUMPD3	THUMP domain-containing protein 3	1,7	0	PRDX4
E7ESY4	MTA1	Metastasis-associated protein MTA1	1,7	0	PRDX4
Q96D09	GPRASP2	G-protein coupled receptor-associated sorting protein 2	1,7	0	PRDX4
P31946	YWHAB	14-3-3 protein beta/alpha	1,7	0,001	PRDX4
P43304	GPD2	Glycerol-3-phosphate dehydrogenase, mitochondrial	1,7	0,008	PRDX4
A0A087WXS7	A0A087WXS7	>tr|A0A087WXS7|A0A087WXS7_HUMAN ATPase ASNA1 OS=Homo sapiens OX=9606 GN=ASNA1 PE=1 SV=1;>sp|O43681|ASNA_HUMAN ATPase ASNA1 OS=Homo sapiens OX=9606 GN=ASNA1 PE=1 SV=2;>tr|K7ERW9|K7ERW9_ HUMAN Arsenical pump-driving ATPase (Fragment) OS=Homo sapiens OX=9606 G	1,7	0,017	PRDX4
Q9UL15	BAG5	BAG family molecular chaperone regulator 5	1,7	0,027	PRDX4
A0A087X0K9	TJP1	Tight junction protein ZO-1	1,6	0	PRDX4
Q15738	NSDHL	Sterol-4-alpha-carboxylate 3-dehydrogenase, decarboxylating	1,6	0	PRDX4
Q15008	PSMD6	26S proteasome non-ATPase regulatory subunit 6	1,6	0	PRDX4
Q9NXF7	DCAF16	DDB1- and CUL4-associated factor 16	1,6	0,001	PRDX4
P30740	SERPINB1	Leukocyte elastase inhibitor	1,6	0,019	PRDX4
Q9BRS2	RIOK1	Serine/threonine-protein kinase RIO1	1,6	0,024	PRDX4
B4DHR0	RABEP2	Rab GTPase-binding effector protein 2	1,6	0,032	PRDX4
Q6WKZ4	RAB11FIP1	Rab11 family-interacting protein 1	1,6	0,033	PRDX4
A0AVT1	UBA6	Ubiquitin-like modifier-activating enzyme 6	1,6	0,04	PRDX4
Q96K76	USP47	Ubiquitin carboxyl-terminal hydrolase 47	1,5	0	PRDX4
E9PMI6	CLNS1A	Chloride channel, nucleotide sensitive 1A	1,5	0	PRDX4
Q06203	PPAT	Amidophosphoribosyltransferase	1,5	0	PRDX4
Q92598	HSPH1	Heat shock protein 105 kDa	1,5	0	PRDX4
O00487	PSMD14	26S proteasome non-ATPase regulatory subunit 14	1,5	0	PRDX4
P62191	PSMC1	26S proteasome regulatory subunit 4	1,5	0	PRDX4
Q13033	STRN3	Striatin-3	1,5	0	PRDX4
P63104	YWHAZ	14-3-3 protein zeta/delta	1,5	0	PRDX4
P34932	HSPA4	Heat shock 70 kDa protein 4	1,5	0,001	PRDX4
Q9UKK9	NUDT5	ADP-sugar pyrophosphatase	1,5	0,001	PRDX4
P35998	PSMC2	26S proteasome regulatory subunit 7	1,5	0,001	PRDX4
A0A0C4DGQ6	RPRD1A	Regulation of nuclear pre-mRNA domain-containing protein 1A	1,5	0,002	PRDX4
O95831	AIFM1	Apoptosis-inducing factor 1, mitochondrial	1,5	0,003	PRDX4
Q13185	CBX3	Chromobox protein homolog 3	1,5	0,006	PRDX4
O95295	SNAPIN	SNARE-associated protein Snapin	1,5	0,011	PRDX4
U3KQC1	WDR18	WD repeat-containing protein 18	1,5	0,017	PRDX4
Q8N6T3	ARFGAP1	ADP-ribosylation factor GTPase-activating protein 1	1,5	0,018	PRDX4
P00492	HPRT1	Hypoxanthine-guanine phosphoribosyltransferase	1,5	0,019	PRDX4
Q8N999	C12orf29	Uncharacterized protein C12orf29	1,5	0,025	PRDX4
J3KN87	J3KN87	>tr|J3KN87|J3KN87_HUMAN Serine/threonine-protein kinase Chk1 OS=Homo sapiens OX=9606 GN=CHEK1 PE=1 SV=1;>sp|O14757|CHK1_HUMAN Serine/ threonine-protein kinase Chk1 OS=Homo sapiens OX=9606 GN=CHEK1 PE=1 SV=2;>tr|E7EPP6|E7EPP6_HUMAN Serine/threonine-protein k	1,5	0,032	PRDX4
P29966	MARCKS	Myristoylated alanine-rich C-kinase substrate	1,5	0,046	PRDX4
Q3ZCQ8	TIMM50	Mitochondrial import inner membrane translocase subunit TIM50	1,4	0	PRDX4
Q9NSD9	FARSB	Phenylalanine--tRNA ligase beta subunit	1,4	0	PRDX4
Q93009	USP7	Ubiquitin carboxyl-terminal hydrolase 7	1,4	0	PRDX4

P61981	YWHAG	14-3-3 protein gamma	1,4	0,001	PRDX4
P31930	UQCRC1	Cytochrome b-c1 complex subunit 1, mitochondrial	1,4	0,001	PRDX4
P29218	IMPA1	Inositol monophosphatase 1	1,4	0,004	PRDX4
Q14C86	GAPVD1	GTPase-activating protein and VPS9 domain-containing protein 1	1,4	0,008	PRDX4
B1ANM7	FAF1	FAS-associated factor 1	1,4	0,039	PRDX4
Q9Y277	VDAC3	Voltage-dependent anion-selective channel protein 3	1,4	0,043	PRDX4
P31939	ATIC	Bifunctional purine biosynthesis protein ATIC	1,3	0	PRDX4
Q9Y230	RUVBL2	RuvB-like 2	1,3	0	PRDX4
P23381	WARS1	Tryptophan--tRNA ligase, cytoplasmic	1,3	0	PRDX4
P15104	GLUL	Glutamine synthetase	1,3	0	PRDX4
Q9Y265	RUVBL1	RuvB-like 1	1,3	0,001	PRDX4
C9J0I9	ZC3HC1	Nuclear-interacting partner of ALK	1,3	0,001	PRDX4
P22695	UQCRC2	Cytochrome b-c1 complex subunit 2, mitochondrial	1,3	0,003	PRDX4
Q9UJS0	SLC25A13	Calcium-binding mitochondrial carrier protein Aralar2	1,3	0,004	PRDX4
P0DMV9	HSPA1B	Heat shock 70 kDa protein 1B	1,3	0,006	PRDX4
Q9UHD1	CHORDC1	Cysteine and histidine-rich domain-containing protein 1	1,3	0,009	PRDX4
Q96B36	AKT1S1	Proline-rich AKT1 substrate 1	1,3	0,012	PRDX4
Q9H0U4	RAB1B	Ras-related protein Rab-1B	1,3	0,016	PRDX4
J3KN29	PSMD9	26S proteasome non-ATPase regulatory subunit 9	1,3	0,02	PRDX4
P12814	ACTN1	Alpha-actinin-1	1,3	0,035	PRDX4
Q16204	CCDC6	Coiled-coil domain-containing protein 6	1,3	0,043	PRDX4
P78356	PIP4K2B	Phosphatidylinositol 5-phosphate 4-kinase type-2 beta	1,3	0,045	PRDX4
P25705	ATP5F1A	ATP synthase subunit alpha, mitochondrial	1,2	0	PRDX4
P05023	ATP1A1	Sodium/potassium-transporting ATPase subunit alpha-1	1,2	0	PRDX4
Q8WXD5	GEMIN6	Gem-associated protein 6	1,2	0	PRDX4
P20020	ATP2B1	Plasma membrane calcium-transporting ATPase 1	1,2	0,001	PRDX4
P34897	SHMT2	Serine hydroxymethyltransferase, mitochondrial	1,2	0,005	PRDX4
K7EJQ8	HDHD2	Haloacid dehalogenase-like hydrolase domain-containing protein 2	1,2	0,009	PRDX4
P42771	CDKN2A	Cyclin-dependent kinase inhibitor 2A	1,2	0,01	PRDX4
Q5QPM7	PSMF1	Proteasome inhibitor PI31 subunit	1,2	0,013	PRDX4
P62333	PSMC6	26S proteasome regulatory subunit 10B	1,2	0,014	PRDX4
P15374	UCHL3	Ubiquitin carboxyl-terminal hydrolase isozyme L3	1,2	0,014	PRDX4
Q8IVM0	CCDC50	Coiled-coil domain-containing protein 50	1,2	0,032	PRDX4
O00231	PSMD11	26S proteasome non-ATPase regulatory subunit 11	1,2	0,032	PRDX4
Q13045	FLII	Protein flightless-1 homolog	1,1	0	PRDX4
Q9Y285	FARSA	Phenylalanine--tRNA ligase alpha subunit	1,1	0	PRDX4
P11310	ACADM	Medium-chain specific acyl-CoA dehydrogenase, mitochondrial	1,1	0	PRDX4
P36871	PGM1	Phosphoglucomutase-1	1,1	0,001	PRDX4
P61221	ABCE1	ATP-binding cassette sub-family E member 1	1,1	0,001	PRDX4
P06733	ENO1	Alpha-enolase	1,1	0,002	PRDX4
P62195	PSMC5	26S proteasome regulatory subunit 8	1,1	0,002	PRDX4
P00338	LDHA	L-lactate dehydrogenase A chain	1,1	0,002	PRDX4
Q9BTE6	AARSD1	Alanyl-tRNA editing protein Aarsd1	1,1	0,004	PRDX4
P45973	CBX5	Chromobox protein homolog 5	1,1	0,005	PRDX4
O43242	PSMD3	26S proteasome non-ATPase regulatory subunit 3	1,1	0,006	PRDX4
P07195	LDHB	L-lactate dehydrogenase B chain	1,1	0,007	PRDX4
Q15181	PPA1	Inorganic pyrophosphatase	1,1	0,008	PRDX4
P55072	VCP	Transitional endoplasmic reticulum ATPase	1,1	0,009	PRDX4
P53985	SLC16A1	Monocarboxylate transporter 1	1,1	0,009	PRDX4
O95453	PARN	Poly(A)-specific ribonuclease PARN	1,1	0,01	PRDX4
P05386	RPLP1	60S acidic ribosomal protein P1	1,1	0,015	PRDX4
P52907	CAPZA1	F-actin-capping protein subunit alpha-1	1,1	0,017	PRDX4
Q9HB71	CACYBP	Calcyclin-binding protein	1,1	0,022	PRDX4
P49321	NASP	Nuclear autoantigenic sperm protein	1,1	0,023	PRDX4
Q99536	VAT1	Synaptic vesicle membrane protein VAT-1 homolog	1	0,001	PRDX4
O60884	DNAJA2	DnaJ homolog subfamily A member 2	1	0,001	PRDX4
Q99460	PSMD1	26S proteasome non-ATPase regulatory subunit 1	1	0,003	PRDX4
Q8NBU5	ATAD1	ATPase family AAA domain-containing protein 1	1	0,029	PRDX4

Table S3: peroxidatic cysteine-dependent interactors ($C_R S$)

uniprot ID	gene	protein	log ratio	p-value
PRDX1 cysteine-dependent interactors				
Q53H12	AGK	Acylglycerol kinase, mitochondrial	4,1	<0.001
O75531	BANF1	Barrier-to-autointegration factor	3,9	<0.001
P27824	CANX	Calnexin	3,7	<0.001
P22061	PCMT1	Protein-L-isoaspartate(D-aspartate) O-methyltransferase	3,4	0,001
P68133	ACTA1	Actin, alpha skeletal muscle	3,4	0,006
A0A024R4E5	HDLBP	High density lipoprotein binding protein	3,3	<0.001
P55084	HADHB	Trifunctional enzyme subunit beta, mitochondrial	3,3	<0.001
Q9NY93	DDX56	Probable ATP-dependent RNA helicase DDX56	3,3	0,001
Q9Y6A5	TACC3	Transforming acidic coiled-coil-containing protein 3	3,2	<0.001
Q9UHV9	PFDN2	Prefoldin subunit 2	3,2	<0.001
P55735	SEC13	Protein SEC13 homolog	3,2	0,001
P43897	TSFM	Elongation factor Ts, mitochondrial	3,2	0,001
P21964	COMT	Catechol O-methyltransferase	3,2	0,001
P62316	SNRPD2	Small nuclear ribonucleoprotein Sm D2	3,1	<0.001
P53621	COPA	Coatomer subunit alpha	3,1	<0.001
Q6P587	FAHD1	Acylpyruvase FAHD1, mitochondrial	3,1	0,001
Q01081	U2AF1	Splicing factor U2AF 35 kDa subunit	3,1	0,006
Q9P2J5	LARS1	Leucine--tRNA ligase, cytoplasmic	3	<0.001
P06132	UROD	Uroporphyrinogen decarboxylase	3	0,009
B7Z7F3	RANBP3	Ran-binding protein 3	2,9	<0.001
Q16513	PKN2	Serine/threonine-protein kinase N2	2,9	0,003
Q15654	TRIP6	Thyroid receptor-interacting protein 6	2,9	0,003
O00148	DDX39A	ATP-dependent RNA helicase DDX39A	2,9	0,008
P35268	RPL22	60S ribosomal protein L22	2,8	<0.001
C9JZR2	CTNND1	Catenin delta-1	2,8	<0.001
P62829	RPL23	60S ribosomal protein L23	2,8	<0.001
Q86V48	LUZP1	Leucine zipper protein 1	2,8	<0.001
P24666	ACP1	Low molecular weight phosphotyrosine protein phosphatase	2,8	0,001
Q9C0C2	TNKS1BP1	182 kDa tankyrase-1-binding protein	2,8	0,001
O14744	PRMT5	Protein arginine N-methyltransferase 5	2,8	0,002
Q96DH6	MSI2	RNA-binding protein Musashi homolog 2	2,8	0,003
Q15149	PLEC	Plectin	2,8	0,004
E7ETK0	RPS24	40S ribosomal protein S24	2,8	0,004
P39023	RPL3	60S ribosomal protein L3	2,7	<0.001
Q7Z406	MYH14	Myosin-14	2,7	<0.001
Q06124	PTPN11	Tyrosine-protein phosphatase non-receptor type 11	2,7	<0.001
Q9UHB6	LIMA1	LIM domain and actin-binding protein 1	2,7	<0.001
P52788	SMS	Spermine synthase	2,7	0,001
P27694	RPA1	Replication protein A 70 kDa DNA-binding subunit	2,7	0,002
Q9Y262	EIF3L	Eukaryotic translation initiation factor 3 subunit L	2,7	0,013
A0A087WTZ5	UBXN1	UBX domain-containing protein 1	2,6	<0.001
O94979	SEC31A	Protein transport protein Sec31A	2,6	<0.001
P48634	PRRC2A	Protein PRRC2A	2,6	<0.001
P31689	DNAJA1	DnaJ homolog subfamily A member 1	2,6	<0.001
E7EX90	DCTN1	Dynactin subunit 1	2,6	0,002
P51452	DUSP3	Dual specificity protein phosphatase 3	2,6	0,004
Q9GZT3	SLIRP	SRA stem-loop-interacting RNA-binding protein, mitochondrial	2,6	0,005
Q99460	PSMD1	26S proteasome non-ATPase regulatory subunit 1	2,6	0,005
Q6WKZ4	RAB11FIP1	Rab11 family-interacting protein 1	2,6	0,006
Q5VYK3	ECPAS	Proteasome adapter and scaffold protein ECM29	2,6	0,007
Q96AC1	FERMT2	Fermitin family homolog 2	2,6	0,009
O43143	DHX15	Pre-mRNA-splicing factor ATP-dependent RNA helicase DHX15	2,6	0,009
O95373	IPO7	Importin-7	2,6	0,01
Q8IWZ3	ANKHD1	Ankyrin repeat and KH domain-containing protein 1	2,5	<0.001
P22314	UBA1	Ubiquitin-like modifier-activating enzyme 1	2,5	<0.001
P48444	ARCN1	Coatomer subunit delta	2,5	<0.001
P62258	YWHAE	14-3-3 protein epsilon	2,5	<0.001
Q13185	CBX3	Chromobox protein homolog 3	2,5	<0.001
Q15075	EEA1	Early endosome antigen 1	2,5	0,01
P11387	TOP1	DNA topoisomerase 1	2,5	0,011
Q5SW79	CEP170	Centrosomal protein of 170 kDa	2,4	<0.001
Q9BSH4	TACO1	Translational activator of cytochrome c oxidase 1	2,4	<0.001
P15170	GSPT1	Eukaryotic peptide chain release factor GTP-binding subunit ERF3A	2,4	<0.001
P16615	ATP2A2	Sarcoplasmic/endoplasmic reticulum calcium ATPase 2	2,4	<0.001
Q14204	DYNC1H1	Cytoplasmic dynein 1 heavy chain 1	2,4	0,001
P15924	DSP	Desmoplakin	2,4	0,002
O95747	OXSR1	Serine/threonine-protein kinase OSR1	2,4	0,005
Q6IAA8	LAMTOR1	Ragulator complex protein LAMTOR1	2,4	0,006

P08559	PDHA1	Pyruvate dehydrogenase E1 component subunit alpha, somatic form, mitochondrial	2,4	0,006
Q9Y5Y2	NUBP2	Cytosolic Fe-S cluster assembly factor NUBP2	2,4	0,009
Q12948	FOXC1	Forkhead box protein C1	2,4	0,011
Q8TAT6	NPLOC4	Nuclear protein localization protein 4 homolog	2,4	0,014
Q5T7U1	GTF3C5	General transcription factor 3C polypeptide 5	2,3	<0.001
Q7Z6Z7	HUWE1	E3 ubiquitin-protein ligase HUWE1	2,3	<0.001
Q14247	CTTN	Src substrate cortactin	2,3	<0.001
Q9UHB9	SRP68	Signal recognition particle subunit SRP68	2,3	0,001
Q9BQ67	GRWD1	Glutamate-rich WD repeat-containing protein 1	2,3	0,002
A0A087WZ13	RAVER1	Ribonucleoprotein PTB-binding 1	2,3	0,003
P19525	EIF2AK2	Interferon-induced, double-stranded RNA-activated protein kinase	2,3	0,009
A0A087X1A5	STAU1	Double-stranded RNA-binding protein Staufen homolog 1	2,3	0,011
Q9NP97	DYNLRB1	Dynein light chain roadblock-type 1	2,3	0,014
P27708	CAD	CAD protein [Includes: Glutamine-dependent carbamoyl-phosphate synthase	2,3	0,017
Q9BYG3	NIFK	MKI67 FHA domain-interacting nucleolar phosphoprotein	2,3	0,02
Q15061	WDR43	WD repeat-containing protein 43	2,3	0,025
E5RGR0	LYPLA1	Acyl-protein thioesterase 1	2,3	0,049
P41252	IARS1	Isoleucine--tRNA ligase, cytoplasmic	2,2	<0.001
P35658	NUP214	Nuclear pore complex protein Nup214	2,2	<0.001
Q9UG54	MAP3K7	Mitogen-activated protein kinase kinase kinase	2,2	<0.001
P55809	OXCT1	Succinyl-CoA:3-ketoacid coenzyme A transferase 1, mitochondrial	2,2	0,001
Q14684	RRP1B	Ribosomal RNA processing protein 1 homolog B	2,2	0,002
P39748	FEN1	Flap endonuclease 1	2,2	0,007
P37108	SRP14	Signal recognition particle 14 kDa protein	2,2	0,008
F5H6E2	MYO1C	Unconventional myosin-Ic	2,2	0,01
P13807	GYS1	Glycogen [starch] synthase, muscle	2,2	0,013
Q8WUH6	TMEM263	Transmembrane protein 263	2,2	0,015
O43795	MYO1B	Unconventional myosin-Ib	2,2	0,016
O75663	TIPRL	TIP41-like protein	2,2	0,018
P49792	RANBP2	E3 SUMO-protein ligase RanBP2	2,2	0,03
E9PF10	NUP155	Nuclear pore complex protein Nup155	2,2	0,032
E9PDU5	WDR6	WD repeat-containing protein 6	2,1	<0.001
Q5T6F2	UBAP2	Ubiquitin-associated protein 2	2,1	<0.001
P22307	SCP2	Non-specific lipid-transfer protein	2,1	0,001
Q9Y6Y8	SEC23IP	SEC23-interacting protein	2,1	0,001
Q09666	AHNAK	Neuroblast differentiation-associated protein AHNAK	2,1	0,001
Q9BSJ8	ESYT1	Extended synaptotagmin-1	2,1	0,002
O75436	VPS26A	Vacuolar protein sorting-associated protein 26A	2,1	0,003
Q9UQE7	SMC3	Structural maintenance of chromosomes protein 3	2,1	0,007
P35579	MYH9	Myosin-9	2,1	0,012
Q92797	SYMPK	Symplekin	2,1	0,015
O75874	IDH1	Isocitrate dehydrogenase [NADP] cytoplasmic	2,1	0,018
Q4KMP7	TBC1D10B	TBC1 domain family member 10B	2,1	0,019
Q7L0Y3	TRMT10C	tRNA methyltransferase 10 homolog C	2,1	0,02
Q16822	PCK2	Phosphoenolpyruvate carboxykinase [GTP], mitochondrial	2,1	0,021
Q07021	C1QBP	Complement component 1 Q subcomponent-binding protein, mitochondrial	2,1	0,021
P29144	TPP2	Tripeptidyl-peptidase 2	2,1	0,023
Q15645	TRIP13	Pachytene checkpoint protein 2 homolog	2,1	0,025
Q8NCA5	FAM98A	Protein FAM98A	2,1	0,026
P50542	PEX5	Peroxisomal targeting signal 1 receptor	2,1	0,028
Q9HD26	GOPC	Golgi-associated PDZ and coiled-coil motif-containing protein	2,1	0,048
Q9Y2R4	DDX52	Probable ATP-dependent RNA helicase DDX52	2,1	0,049
Q9UNE7	STUB1	E3 ubiquitin-protein ligase CHIP	2	<0.001
Q14166	TTLL12	Tubulin--tyrosine ligase-like protein 12	2	<0.001
Q32MZ4	LRRFIP1	Leucine-rich repeat flightless-interacting protein 1	2	<0.001
Q14157	UBAP2L	Ubiquitin-associated protein 2-like	2	<0.001
P63272	SUPT4H1	Transcription elongation factor SPT4	2	0,001
P08708	RPS17	40S ribosomal protein S17	2	0,001
P30520	ADSS2	Adenylosuccinate synthetase isozyme 2	2	0,001
A0A087WVM4	MTHFD1L	Formyltetrahydrofolate synthetase	2	0,001
Q9ULV4	CORO1C	Coronin-1C	2	0,002
P61011	SRP54	Signal recognition particle 54 kDa protein	2	0,005
Q9UKD2	MRTO4	mRNA turnover protein 4 homolog	2	0,005
Q14683	SMC1A	Structural maintenance of chromosomes protein 1A	2	0,005
P42704	LRPPRC	Leucine-rich PPR motif-containing protein, mitochondrial	2	0,007
Q9H0C8	ILKAP	Integrin-linked kinase-associated serine/threonine phosphatase 2C	2	0,007
O14929	HAT1	Histone acetyltransferase type B catalytic subunit	2	0,008
Q86VP6	CAND1	Cullin-associated NEDD8-dissociated protein 1	2	0,014
P11388	TOP2A	DNA topoisomerase 2-alpha	2	0,015
P30048	PRDX3	Thioredoxin-dependent peroxide reductase, mitochondrial	2	0,016
Q13144	EIF2B5	Translation initiation factor eIF-2B subunit epsilon	2	0,017
P34949	MPI	Mannose-6-phosphate isomerase	2	0,018
O43660	PLRG1	Pleiotropic regulator 1	2	0,024

Q15750	TAB1	TGF-beta-activated kinase 1 and MAP3K7-binding protein 1	2	0,026
P23258	TUBG1	Tubulin gamma-1 chain	2	0,029
G3V1C3	API5	Apoptosis inhibitor 5	2	0,035
Q9H840	GEMIN7	Gem-associated protein 7	2	0,048
Q16204	CCDC6	Coiled-coil domain-containing protein 6	2	0,048
P19105	MYL12A	Myosin regulatory light chain 12A	2	0,049
Q9NXF7	DCAF16	DDB1- and CUL4-associated factor 16	1,9	<0.001
E7EVA0	MAP4	Microtubule-associated protein	1,9	<0.001
Q9UHD1	CHORDC1	Cysteine and histidine-rich domain-containing protein 1	1,9	<0.001
P49321	NASP	Nuclear autoantigenic sperm protein	1,9	<0.001
A0A087X0M4	SLC4A1AP	Kanadaptin	1,9	<0.001
Q7LBC6	KDM3B	Lysine-specific demethylase 3B	1,9	<0.001
A0A0U1RRM6	ENAH	Protein enabled homolog	1,9	<0.001
P48643	CCT5	T-complex protein 1 subunit epsilon	1,9	<0.001
Q8ND83	SLAIN1	SLAIN motif-containing protein 1	1,9	<0.001
O60784	TOM1	Target of Myb protein 1	1,9	0,001
P00568	AK1	Adenylate kinase isoenzyme 1	1,9	0,001
Q96GD0	PDXP	Pyridoxal phosphate phosphatase	1,9	0,001
O75832	PSMD10	26S proteasome non-ATPase regulatory subunit 10	1,9	0,001
P57740	NUP107	Nuclear pore complex protein Nup107	1,9	0,002
P46459	NSF	Vesicle-fusing ATPase	1,9	0,002
P48047	ATP5PO	ATP synthase subunit O, mitochondrial	1,9	0,003
O43837	IDH3B	Isocitrate dehydrogenase [NAD] subunit beta, mitochondrial	1,9	0,004
P33991	MCM4	DNA replication licensing factor MCM4	1,9	0,007
E7ESP9	NEFM	160 kDa neurofilament protein	1,9	0,008
Q9Y3I0	RTCB	RNA-splicing ligase RtcB homolog	1,9	0,008
O43719	HTATSF1	HIV Tat-specific factor 1	1,9	0,009
O00399	DCTN6	Dynactin subunit 6	1,9	0,01
Q9Y2L1	DIS3	Exosome complex exonuclease RRP44	1,9	0,015
Q9Y2V2	CARHSP1	Calcium-regulated heat-stable protein 1	1,9	0,015
H3BPE1	MACF1	Microtubule-actin cross-linking factor 1, isoforms 1/2/3/5	1,9	0,016
Q9NQ88	TIGAR	Fructose-2,6-bisphosphatase TIGAR	1,9	0,027
P09110	ACAA1	3-ketoacyl-CoA thiolase, peroxisomal	1,9	0,028
P23919	DTYMK	Thymidylate kinase	1,9	0,029
E9PLK3	NPEPPS	Aminopeptidase	1,9	0,031
P46940	IQGAP1	Ras GTPase-activating-like protein IQGAP1	1,9	0,034
P40939	HADHA	Trifunctional enzyme subunit alpha, mitochondrial	1,9	0,038
Q8NFC6	BOD1L1	Biorientation of chromosomes in cell division protein 1-like 1	1,9	0,039
P40222	TXLNA	Alpha-taxilin	1,9	0,041
E9PKP7	UBTF	Nucleolar transcription factor 1	1,9	0,043
O00487	PSMD14	26S proteasome non-ATPase regulatory subunit 14	1,9	0,045
P62333	PSMC6	26S proteasome regulatory subunit 10B	1,8	<0.001
E7EPN9	PRRC2C	Protein PRRC2C	1,8	<0.001
B1AK87	CAPZB	F-actin-capping protein subunit beta	1,8	<0.001
Q9BQ69	MACROD1	ADP-ribose glycohydrolase MACROD1	1,8	<0.001
Q14126	DSG2	Desmoglein-2	1,8	<0.001
P46776	RPL27A	60S ribosomal protein L27a	1,8	<0.001
P13861	PRKAR2A	cAMP-dependent protein kinase type II-alpha regulatory subunit	1,8	<0.001
Q13428	TCOF1	Treacle protein	1,8	0,001
A0A3B3IRI2	CTPS1	CTP synthase	1,8	0,001
P62753	RPS6	40S ribosomal protein S6	1,8	0,001
A0A3B3IRP5	CDC73	Parafibromin	1,8	0,002
P11802	CDK4	Cyclin-dependent kinase 4	1,8	0,003
B4DDF4	CNN2	Calponin	1,8	0,003
Q9UPN7	PPP6R1	Serine/threonine-protein phosphatase 6 regulatory subunit 1	1,8	0,003
P43490	NAMPT	Nicotinamide phosphoribosyltransferase	1,8	0,003
P49790	NUP153	Nuclear pore complex protein Nup153	1,8	0,004
Q13561	DCTN2	Dynactin subunit 2	1,8	0,005
Q9BZE4	GTPBP4	Nucleolar GTP-binding protein 1	1,8	0,005
O00154	ACOT7	Cytosolic acyl coenzyme A thioester hydrolase	1,8	0,006
M0QXL5	FBL	rRNA 2'-O-methyltransferase fibrillarin	1,8	0,008
Q6P2E9	EDC4	Enhancer of mRNA-decapping protein 4	1,8	0,008
Q14152	EIF3A	Eukaryotic translation initiation factor 3 subunit A	1,8	0,009
Q9BVP2	GNL3	Guanine nucleotide-binding protein-like 3	1,8	0,013
Q99959	PKP2	Plakophilin-2	1,8	0,017
Q14008	CKAP5	Cytoskeleton-associated protein 5	1,8	0,017
P25205	MCM3	DNA replication licensing factor MCM3	1,8	0,022
Q9NQX3	GPHN	Gephyrin [Includes: Molybdopterin adenylyltransferase	1,8	0,026
P82673	MRPS35	28S ribosomal protein S35, mitochondrial	1,8	0,03
P52594	AGFG1	Arf-GAP domain and FG repeat-containing protein 1	1,8	0,034
Q15084	PDIA6	Protein disulfide-isomerase A6	1,8	0,036
Q6P9B6	MEAK7	MTOR-associated protein MEAK7	1,8	0,036
Q9BR76	CORO1B	Coronin-1B	1,8	0,037

O60832	DKC1	H/ACA ribonucleoprotein complex subunit DKC1	1,8	0,037
Q92973	TNPO1	Transportin-1	1,8	0,04
P30154	PPP2R1B	Serine/threonine-protein phosphatase 2A 65 kDa regulatory subunit A beta isoform	1,8	0,041
O76021	RSL1D1	Ribosomal L1 domain-containing protein 1	1,8	0,05
Q6PKG0	LARP1	La-related protein 1	1,7	<0.001
Q9BV20	MRI1	Methylthioribose-1-phosphate isomerase	1,7	<0.001
Q9H7E9	C8orf33	UPF0488 protein C8orf33	1,7	<0.001
Q00796	SORD	Sorbitol dehydrogenase	1,7	<0.001
Q9H0B6	KLC2	Kinesin light chain 2	1,7	0,001
X1WI28	RPL10	60S ribosomal protein L10	1,7	0,001
P30566	ADSL	Adenylosuccinate lyase	1,7	0,001
Q99497	PARK7	Parkinson disease protein 7	1,7	0,002
P51553	IDH3G	Isocitrate dehydrogenase [NAD] subunit gamma, mitochondrial	1,7	0,002
P12004	PCNA	Proliferating cell nuclear antigen	1,7	0,002
P50502	ST13	Hsc70-interacting protein	1,7	0,002
Q99615	DNAJC7	DnaJ homolog subfamily C member 7	1,7	0,003
O60684	KPNA6	Importin subunit alpha-7	1,7	0,004
Q14694	USP10	Ubiquitin carboxyl-terminal hydrolase 10	1,7	0,004
Q15417	CNN3	Calponin-3	1,7	0,005
Q9UG63	ABCF2	ATP-binding cassette sub-family F member 2	1,7	0,006
Q9UHI6	DDX20	Probable ATP-dependent RNA helicase DDX20	1,7	0,006
O00178	GTPBP1	GTP-binding protein 1	1,7	0,006
O15160	POLR1C	DNA-directed RNA polymerases I and III subunit RPAC1	1,7	0,006
P46060	RANGAP1	Ran GTPase-activating protein 1	1,7	0,012
Q92667	AKAP1	A-kinase anchor protein 1, mitochondrial	1,7	0,014
Q8IY81	FTSJ3	pre-rRNA 2'-O-ribose RNA methyltransferase FTSJ3	1,7	0,016
Q12849	GRSF1	G-rich sequence factor 1	1,7	0,018
P42765	ACAA2	3-ketoacyl-CoA thiolase, mitochondrial	1,7	0,022
O75533	SF3B1	Splicing factor 3B subunit 1	1,7	0,029
A0A0A0MRT6	ABI1	Abl interactor 1	1,7	0,03
Q9Y2X3	NOP58	Nucleolar protein 58	1,7	0,032
P14174	MIF	Macrophage migration inhibitory factor	1,7	0,035
P62906	RPL10A	60S ribosomal protein L10a	1,7	0,043
Q9UGV2	NDRG3	Protein NDRG3	1,7	0,045
Q96P70	IPO9	Importin-9	1,7	0,048
Q3ZCQ8	TIMM50	Mitochondrial import inner membrane translocase subunit TIM50	1,7	0,048
A0A0C4DGQ6	RPRD1A	Regulation of nuclear pre-mRNA domain-containing protein 1A	1,6	<0.001
O95816	BAG2	BAG family molecular chaperone regulator 2	1,6	<0.001
Q12955	ANK3	Ankyrin-3	1,6	<0.001
O75569	PRKRA	Interferon-inducible double-stranded RNA-dependent protein kinase activator A	1,6	<0.001
Q15365	PCBP1	Poly(rC)-binding protein 1	1,6	<0.001
Q9UQ80	PA2G4	Proliferation-associated protein 2G4	1,6	<0.001
P13797	PLS3	Plastin-3	1,6	<0.001
Q9BTE6	AARSD1	Alanyl-tRNA editing protein Aarsd1	1,6	<0.001
Q9UNY4	TTF2	Transcription termination factor 2	1,6	0,001
P33993	MCM7	DNA replication licensing factor MCM7	1,6	0,001
O00170	AIP	AH receptor-interacting protein	1,6	0,002
P30153	PPP2R1A	Serine/threonine-protein phosphatase 2A 65 kDa regulatory subunit A alpha isoform	1,6	0,002
Q01469	FABP5	Fatty acid-binding protein 5	1,6	0,002
Q9H2G2	SLK	STE20-like serine/threonine-protein kinase	1,6	0,003
P62241	RPS8	40S ribosomal protein S8	1,6	0,003
Q8NC51	SERBP1	Plasminogen activator inhibitor 1 RNA-binding protein	1,6	0,003
A0A0G2JH68	DIAPH1	Protein diaphanous homolog 1	1,6	0,003
Q8WXF1	PSPC1	Paraspeckle component 1	1,6	0,004
Q8IWX8	CHERP	Calcium homeostasis endoplasmic reticulum protein	1,6	0,004
P49588	AARS1	Alanine--tRNA ligase, cytoplasmic	1,6	0,004
P53618	COPB1	Coatomer subunit beta	1,6	0,004
Q9C0C9	UBE2O	(E3-independent) E2 ubiquitin-conjugating enzyme	1,6	0,005
P26368	U2AF2	Splicing factor U2AF 65 kDa subunit	1,6	0,006
Q15185	PTGES3	Prostaglandin E synthase 3	1,6	0,006
A0A1C7CYX9	DPYSL2	Dihydropyrimidinase-related protein 2	1,6	0,006
Q9BUF5	TUBB6	Tubulin beta-6 chain	1,6	0,006
Q9Y450	HBS1L	HBS1-like protein	1,6	0,008
P40937	RFC5	Replication factor C subunit 5	1,6	0,009
P47897	QARS1	Glutamine--tRNA ligase	1,6	0,009
P09543	CNP	2',3'-cyclic-nucleotide 3'-phosphodiesterase	1,6	0,01
Q8WWY3	PRPF31	U4/U6 small nuclear ribonucleoprotein Prp31	1,6	0,01
O43395	PRPF3	U4/U6 small nuclear ribonucleoprotein Prp3	1,6	0,011
Q2TAY7	SMU1	WD40 repeat-containing protein SMU1	1,6	0,012
O95861	BPNT1	3'(2'),5'-bisphosphate nucleotidase 1	1,6	0,014
Q5JRX3	PITRM1	Presequence protease, mitochondrial	1,6	0,014
O75152	ZC3H11A	Zinc finger CCCH domain-containing protein 11A	1,6	0,015
O75131	CPNE3	Copine-3	1,6	0,016

Q96RP9	GFM1	Elongation factor G, mitochondrial	1,6	0,016
Q9BWD1	ACAT2	Acetyl-CoA acetyltransferase, cytosolic	1,6	0,017
P08754	GNAI3	Guanine nucleotide-binding protein G(i) subunit alpha	1,6	0,017
Q92879	CELF1	CUGBP Elav-like family member 1	1,6	0,03
P54646	PRKAA2	5'-AMP-activated protein kinase catalytic subunit alpha-2	1,6	0,037
P42566	EPS15	Epidermal growth factor receptor substrate 15	1,6	0,046
Q6YN16	HSDL2	Hydroxysteroid dehydrogenase-like protein 2	1,5	<0.001
Q5JSZ5	PRRC2B	Protein PRRC2B	1,5	<0.001
Q8N0X7	SPART	Spartin	1,5	<0.001
Q6Y7W6	GIGYF2	GRB10-interacting GYF protein 2	1,5	<0.001
P26640	VARS1	Valine--tRNA ligase	1,5	0,001
O15371	EIF3D	Eukaryotic translation initiation factor 3 subunit D	1,5	0,001
O14802	POLR3A	DNA-directed RNA polymerase III subunit RPC1	1,5	0,001
P22102	GART	Trifunctional purine biosynthetic protein adenosine-3 [Includes: Phosphoribosylamine--glycine ligase	1,5	0,001
P62873	GNB1	Guanine nucleotide-binding protein G(I)/G(S)/G(T) subunit beta-1	1,5	0,001
Q96S44	TP53RK	EKC/KEOPS complex subunit TP53RK	1,5	0,002
O43159	RRP8	Ribosomal RNA-processing protein 8	1,5	0,002
M0R0F0	RPS5	40S ribosomal protein S5	1,5	0,003
F8WB06	ATXN2	Ataxin-2	1,5	0,003
Q15003	NCAPH	Condensin complex subunit 2	1,5	0,003
P05198	EIF2S1	Eukaryotic translation initiation factor 2 subunit 1	1,5	0,003
Q15042	RAB3GAP1	Rab3 GTPase-activating protein catalytic subunit	1,5	0,003
P78344	EIF4G2	Eukaryotic translation initiation factor 4 gamma 2	1,5	0,004
O95336	PGLS	6-phosphogluconolactonase	1,5	0,004
P62244	RPS15A	40S ribosomal protein S15a	1,5	0,005
O95573	ACSL3	Long-chain-fatty-acid--CoA ligase 3	1,5	0,005
P55795	HNRNPH2	Heterogeneous nuclear ribonucleoprotein H2	1,5	0,005
P55081	MFAP1	Microfibrillar-associated protein 1	1,5	0,007
Q9UBT2	UBA2	SUMO-activating enzyme subunit 2	1,5	0,007
Q13136	PPFIA1	Liprin-alpha-1	1,5	0,008
A0A0G2JNZ2	SCRIB	Protein scribble homolog	1,5	0,009
Q9NQT5	EXOSC3	Exosome complex component RRP40	1,5	0,01
Q9UJC3	HOOK1	Protein Hook homolog 1	1,5	0,014
A1X283	SH3PXD2B	SH3 and PX domain-containing protein 2B	1,5	0,014
Q8N1G4	LRRC47	Leucine-rich repeat-containing protein 47	1,5	0,014
Q86Y56	DNAAF5	Dynein assembly factor 5, axonemal	1,5	0,015
B4E1N1	ARMC6	Armadillo repeat-containing protein 6	1,5	0,016
Q00610	CLTC	Clathrin heavy chain 1	1,5	0,017
P20042	EIF2S2	Eukaryotic translation initiation factor 2 subunit 2	1,5	0,017
P04637	TP53	Cellular tumor antigen p53	1,5	0,018
P63165	SUMO1	Small ubiquitin-related modifier 1	1,5	0,018
Q9HB71	CACYBP	Calcyclin-binding protein	1,5	0,02
Q8WVM8	SCFD1	Sec1 family domain-containing protein 1	1,5	0,026
Q08J23	NSUN2	RNA cytosine C(5)-methyltransferase NSUN2	1,5	0,026
Q9Y696	CLIC4	Chloride intracellular channel protein 4	1,5	0,029
O75934	BCAS2	Pre-mRNA-splicing factor SPF27	1,5	0,031
Q8N9T8	KRI1	Protein KRI1 homolog	1,5	0,036
Q9BY32	ITPA	Inosine triphosphate pyrophosphatase	1,5	0,041
E9PGZ1	CALD1	Caldesmon	1,5	0,047
Q9BQG0	MYBBP1A	Myb-binding protein 1A	1,5	0,049
Q9NSD9	FARSB	Phenylalanine--tRNA ligase beta subunit	1,4	<0.001
Q8WUM4	PDCD6IP	Programmed cell death 6-interacting protein	1,4	<0.001
Q86TB9	PATL1	Protein PAT1 homolog 1	1,4	<0.001
O94826	TOMM70	Mitochondrial import receptor subunit TOM70	1,4	0,001
Q14151	SAFB2	Scaffold attachment factor B2	1,4	0,001
Q16658	FSCN1	Fascin	1,4	0,001
P17987	TCP1	T-complex protein 1 subunit alpha	1,4	0,001
Q96FW1	OTUB1	Ubiquitin thioesterase OTUB1	1,4	0,002
P25325	MPST	3-mercaptopyruvate sulfurtransferase	1,4	0,005
P52701	MSH6	DNA mismatch repair protein Msh6	1,4	0,011
Q7L2H7	EIF3M	Eukaryotic translation initiation factor 3 subunit M	1,4	0,015
O95782	AP2A1	AP-2 complex subunit alpha-1	1,4	0,02
Q96F45	ZNF503	Zinc finger protein 503	1,4	0,023
Q96N67	DOCK7	Dedicator of cytokinesis protein 7	1,4	0,023
P55265	ADAR	Double-stranded RNA-specific adenosine deaminase	1,4	0,023
Q9NR12	PDLIM7	PDZ and LIM domain protein 7	1,4	0,027
O00425	IGF2BP3	Insulin-like growth factor 2 mRNA-binding protein 3	1,4	0,031
Q8IYS1	PM20D2	Peptidase M20 domain-containing protein 2	1,4	0,031
Q9Y6G9	DYNC1LI1	Cytoplasmic dynein 1 light intermediate chain 1	1,4	0,034
Q9P258	RCC2	Protein RCC2	1,4	0,037
Q96I25	RBM17	Splicing factor 45	1,4	0,041
O75439	PMPCB	Mitochondrial-processing peptidase subunit beta	1,4	0,041
P62851	RPS25	40S ribosomal protein S25	1,4	0,041

P61163	ACTR1A	Alpha-centractin	1,4	0,042
Q99569	PKP4	Plakophilin-4	1,4	0,042
E9PD53	SMC4	Structural maintenance of chromosomes protein	1,4	0,044
P46821	MAP1B	Microtubule-associated protein 1B	1,4	0,049
P63173	RPL38	60S ribosomal protein L38	1,3	<0.001
Q96A33	CCDC47	Coiled-coil domain-containing protein 47	1,3	0,001
P11908	PRPS2	Ribose-phosphate pyrophosphokinase 2	1,3	0,001
Q16643	DBN1	Drebrin	1,3	0,001
P62195	PSMC5	26S proteasome regulatory subunit 8	1,3	0,001
P61158	ACTR3	Actin-related protein 3	1,3	0,001
Q13347	EIF3I	Eukaryotic translation initiation factor 3 subunit I	1,3	0,003
P46939	UTRN	Utrophin	1,3	0,003
P31948	STIP1	Stress-induced-phosphoprotein 1	1,3	0,003
O60343	TBC1D4	TBC1 domain family member 4	1,3	0,003
O75792	RNASEH2A	Ribonuclease H2 subunit A	1,3	0,004
P51114	FXR1	Fragile X mental retardation syndrome-related protein 1	1,3	0,004
Q8WYP5	AHCTF1	Protein ELYS	1,3	0,007
P13804	ETFA	Electron transfer flavoprotein subunit alpha, mitochondrial	1,3	0,007
Q9Y5A9	YTHDF2	YTH domain-containing family protein 2	1,3	0,007
Q14C86	GAPVD1	GTPase-activating protein and VPS9 domain-containing protein 1	1,3	0,007
P42696	RBM34	RNA-binding protein 34	1,3	0,007
P55060	CSE1L	Exportin-2	1,3	0,007
Q02252	ALDH6A1	Methylmalonate-semialdehyde dehydrogenase [acylating], mitochondrial	1,3	0,007
P63241	EIF5A	Eukaryotic translation initiation factor 5A-1	1,3	0,009
Q9Y2U8	LEMD3	Inner nuclear membrane protein Man1	1,3	0,011
P54136	RARS1	Arginine--tRNA ligase, cytoplasmic	1,3	0,011
Q96AG4	LRRC59	Leucine-rich repeat-containing protein 59	1,3	0,011
P46779	RPL28	60S ribosomal protein L28	1,3	0,012
Q9NZI8	IGF2BP1	Insulin-like growth factor 2 mRNA-binding protein 1	1,3	0,013
P45974	USP5	Ubiquitin carboxyl-terminal hydrolase 5	1,3	0,013
P35580	MYH10	Myosin-10	1,3	0,013
Q9BRX2	PELO	Protein pelota homolog	1,3	0,014
P49736	MCM2	DNA replication licensing factor MCM2	1,3	0,014
C9JRJ5	LIMD1	LIM domain-containing protein 1	1,3	0,014
P42285	MTREX	Exosome RNA helicase MTR4	1,3	0,016
H0Y5D5	CIZ1	Cip1-interacting zinc finger protein	1,3	0,017
Q9BPU6	DPYSL5	Dihydropyrimidinase-related protein 5	1,3	0,017
P18615	NELFE	Negative elongation factor E	1,3	0,018
Q14318	FKBP8	Peptidyl-prolyl cis-trans isomerase FKBP8	1,3	0,018
Q52LJ0	FAM98B	Protein FAM98B	1,3	0,02
P19367	HK1	Hexokinase-1	1,3	0,025
Q13509	TUBB3	Tubulin beta-3 chain	1,3	0,026
Q1KMD3	HNRNPUL2	Heterogeneous nuclear ribonucleoprotein U-like protein 2	1,3	0,026
P52272	HNRNPM	Heterogeneous nuclear ribonucleoprotein M	1,3	0,027
F8W0J6	NAP1L1	Nucleosome assembly protein 1-like 1	1,3	0,029
J3QR09	RPL19	Ribosomal protein L19	1,3	0,031
Q13526	PIN1	Peptidyl-prolyl cis-trans isomerase NIMA-interacting 1	1,3	0,031
Q9UBE0	SAE1	SUMO-activating enzyme subunit 1	1,3	0,034
Q9P0K7	RAI14	Ankycorbin	1,3	0,035
Q16543	CDC37	Hsp90 co-chaperone Cdc37	1,3	0,036
P62854	RPS26	40S ribosomal protein S26	1,3	0,041
Q9NR45	NANS	Sialic acid synthase	1,3	0,043
P25685	DNAJB1	DnaJ homolog subfamily B member 1	1,3	0,048
Q13045	FLII	Protein flightless-1 homolog	1,2	<0.001
Q9P2I0	CPSF2	Cleavage and polyadenylation specificity factor subunit 2	1,2	0,001
P42771	CDKN2A	Cyclin-dependent kinase inhibitor 2A	1,2	0,002
Q9HC35	EML4	Echinoderm microtubule-associated protein-like 4	1,2	0,003
A0A0A0MRM8	MYO6	Unconventional myosin-6	1,2	0,003
Q96C36	PYCR2	Pyrroline-5-carboxylate reductase 2	1,2	0,003
Q9UN37	VPS4A	Vacuolar protein sorting-associated protein 4A	1,2	0,004
Q9UMS4	PRPF19	Pre-mRNA-processing factor 19	1,2	0,006
Q9Y2Z0	SUGT1	Protein SGT1 homolog	1,2	0,008
P31939	ATIC	Bifunctional purine biosynthesis protein ATIC	1,2	0,008
K7EJL1	AP1M1	AP-1 complex subunit mu-1	1,2	0,008
F8VYE8	PPP1CC	Serine/threonine-protein phosphatase	1,2	0,008
Q9Y490	TLN1	Talin-1	1,2	0,009
Q96HC4	PDLIM5	PDZ and LIM domain protein 5	1,2	0,009
P98175	RBM10	RNA-binding protein 10	1,2	0,014
P49368	CCT3	T-complex protein 1 subunit gamma	1,2	0,015
P13489	RNH1	Ribonuclease inhibitor	1,2	0,017
Q9Y3S2	ZNF330	Zinc finger protein 330	1,2	0,017
Q9H0D6	XRN2	5'-3' exoribonuclease 2	1,2	0,018
Q12904	AIMP1	Aminoacyl tRNA synthase complex-interacting multifunctional protein 1	1,2	0,019

P36542	ATP5F1C	ATP synthase subunit gamma, mitochondrial	1,2	0,019
P36915	GNL1	Guanine nucleotide-binding protein-like 1	1,2	0,02
Q13907	IDI1	Isopentenyl-diphosphate Delta-isomerase 1	1,2	0,02
P37802	TAGLN2	Transgelin-2	1,2	0,021
A0A2R8YDQ9	SUCLA2	Succinate--CoA ligase [ADP-forming] subunit beta, mitochondrial	1,2	0,023
G5EA31	SEC24C	Protein transport protein Sec24C	1,2	0,027
Q07666	KHDRBS1	KH domain-containing, RNA-binding, signal transduction-associated protein 1	1,2	0,029
O43390	HNRNPR	Heterogeneous nuclear ribonucleoprotein R	1,2	0,029
P41240	CSK	Tyrosine-protein kinase CSK	1,2	0,033
Q9NW82	WDR70	WD repeat-containing protein 70	1,2	0,033
Q9NWH9	SLTM	SAFB-like transcription modulator	1,2	0,033
O94906	PRPF6	Pre-mRNA-processing factor 6	1,2	0,035
Q8WWQ0	PHIP	PH-interacting protein	1,2	0,035
P33176	KIF5B	Kinesin-1 heavy chain	1,2	0,036
P28838	LAP3	Cytosol aminopeptidase	1,2	0,037
P27540	ARNT	Aryl hydrocarbon receptor nuclear translocator	1,2	0,045
P39687	ANP32A	Acidic leucine-rich nuclear phosphoprotein 32 family member A	1,2	0,046
Q9BY44	EIF2A	Eukaryotic translation initiation factor 2A	1,2	0,047
P53384	NUBP1	Cytosolic Fe-S cluster assembly factor NUBP1	1,2	0,049
P29692	EEF1D	Elongation factor 1-delta	1,1	0,001
Q5JXI8	FHL1	Four and a half LIM domains protein 1	1,1	0,001
O43684	BUB3	Mitotic checkpoint protein BUB3	1,1	0,004
C9J0I9	ZC3HC1	Nuclear-interacting partner of ALK	1,1	0,004
Q13451	FKBP5	Peptidyl-prolyl cis-trans isomerase FKBP5	1,1	0,004
Q2TAM5	RELA	RELA protein	1,1	0,006
P43487	RANBP1	Ran-specific GTPase-activating protein	1,1	0,007
Q9H3K6	BOLA2	BolA-like protein 2	1,1	0,009
P30084	ECHS1	Enoyl-CoA hydratase, mitochondrial	1,1	0,009
P62701	RPS4X	40S ribosomal protein S4, X isoform	1,1	0,01
A0A1B0GWF2	STXBP1	Syntaxin-binding protein 1	1,1	0,01
P46778	RPL21	60S ribosomal protein L21	1,1	0,01
Q6ZN17	LIN28B	Protein lin-28 homolog B	1,1	0,01
P43246	MSH2	DNA mismatch repair protein Msh2	1,1	0,011
Q16527	CSRP2	Cysteine and glycine-rich protein 2	1,1	0,011
Q8IWS0	PHF6	PHD finger protein 6	1,1	0,012
Q5TDH0	DDI2	Protein DDI1 homolog 2	1,1	0,012
G3XAH6	PAPOLA	Poly(A) polymerase	1,1	0,012
P45973	CBX5	Chromobox protein homolog 5	1,1	0,012
Q15126	PMVK	Phosphomevalonate kinase	1,1	0,014
P84095	RHOG	Rho-related GTP-binding protein RhoG	1,1	0,014
Q02790	FKBP4	Peptidyl-prolyl cis-trans isomerase FKBP4	1,1	0,015
A0A087WXM6	RPL17	60S ribosomal protein L17	1,1	0,016
Q9UPQ9	TNRC6B	Trinucleotide repeat-containing gene 6B protein	1,1	0,017
M0R3C3	TECR	Very-long-chain enoyl-CoA reductase	1,1	0,017
Q99829	CPNE1	Copine-1	1,1	0,019
Q71RC2	LARP4	La-related protein 4	1,1	0,019
P60660	MYL6	Myosin light polypeptide 6	1,1	0,021
P49207	RPL34	60S ribosomal protein L34	1,1	0,021
Q10567	AP1B1	AP-1 complex subunit beta-1	1,1	0,023
P63092	GNAS	Guanine nucleotide-binding protein G(s) subunit alpha isoforms short	1,1	0,025
Q9UN86	G3BP2	Ras GTPase-activating protein-binding protein 2	1,1	0,027
P51116	FXR2	Fragile X mental retardation syndrome-related protein 2	1,1	0,027
H0YNW5	DUT	Deoxyuridine 5'-triphosphate nucleotidohydrolase	1,1	0,028
H7C5E4	XRN1	5'-3' exoribonuclease 1	1,1	0,031
P52294	KPNA1	Importin subunit alpha-5	1,1	0,031
P15880	RPS2	40S ribosomal protein S2	1,1	0,031
P31946	YWHAB	14-3-3 protein beta/alpha	1,1	0,036
O14893	GEMIN2	Gem-associated protein 2	1,1	0,037
K4DJ93	CUL4B	Cullin 4B, isoform CRA_e	1,1	0,042
Q9UKM9	RALY	RNA-binding protein Raly	1,1	0,043
P54578	USP14	Ubiquitin carboxyl-terminal hydrolase 14	1,1	0,046
C9J0J7	PFN2	Profilin	1,1	0,046
Q8IYI6	EXOC8	Exocyst complex component 8	1,1	0,048
P50991	CCT4	T-complex protein 1 subunit delta	1	0,007
P32322	PYCR1	Pyrroline-5-carboxylate reductase 1, mitochondrial	1	0,008
P07814	EPRS1	Bifunctional glutamate/proline--tRNA ligase	1	0,011
Q9NUQ9	CYRIB	CYFIP-related Rac1 interactor B	1	0,013
Q16576	RBBP7	Histone-binding protein RBBP7	1	0,017
A0A087WY55	VTA1	Chromosome 6 open reading frame 55, isoform CRA_b	1	0,022
Q7RTV0	PHF5A	PHD finger-like domain-containing protein 5A	1	0,022
P38117	ETFB	Electron transfer flavoprotein subunit beta	1	0,024
B5MCF9	PES1	Pescadillo homolog	1	0,024
A0A2R8Y855	SMARCE1	SWI/SNF-related matrix-associated actin-dependent regulator of chromatin subfamily E member 1	1	0,027

Q9UJ83	HACL1	2-hydroxyacyl-CoA lyase 1	1	0,029
Q9BZE9	ASPSCR1	Tether containing UBX domain for GLUT4	1	0,034
P55884	EIF3B	Eukaryotic translation initiation factor 3 subunit B	1	0,036
Q15370	ELOB	Elongin-B	1	0,04
Q9ULC4	MCTS1	Malignant T-cell-amplified sequence 1	1	0,043
P26358	DNMT1	DNA	1	0,045
A0A024RAC6	ELOA	Elongin-A	1	0,047
PRDX2 cysteine-dependent interactors				
Q9C0C2	TNKS1BP1	182 kDa tankyrase-1-binding protein	6,4	<0.001
Q9Y6A5	TACC3	Transforming acidic coiled-coil-containing protein 3	5,2	<0.001
Q8NFC6	BOD1L1	Biorientation of chromosomes in cell division protein 1-like 1	5,2	<0.001
P07355	ANXA2	Annexin A2	5,1	<0.001
Q7Z434	MAVS	Mitochondrial antiviral-signaling protein	4,9	<0.001
Q9NQX3	GPHN	Gephyrin [Includes: Molybdopterin adenylyltransferase	4,9	<0.001
E7EVA0	MAP4	Microtubule-associated protein	4,9	<0.001
Q9UHV9	PFDN2	Prefoldin subunit 2	4,5	<0.001
Q9BQA1	WDR77	Methylosome protein 50	4,2	<0.001
O60547	GMDS	GDP-mannose 4,6 dehydratase	4,2	<0.001
Q9Y266	NUDC	Nuclear migration protein nudC	4,1	<0.001
A0AVT1	UBA6	Ubiquitin-like modifier-activating enzyme 6	4,1	<0.001
P11802	CDK4	Cyclin-dependent kinase 4	4,1	<0.001
Q32MZ4	LRRFIP1	Leucine-rich repeat flightless-interacting protein 1	4,1	<0.001
Q9NPH2	ISYNA1	Inositol-3-phosphate synthase 1	4	<0.001
P22061	PCMT1	Protein-L-isoaspartate(D-aspartate) O-methyltransferase	4	<0.001
Q9HBH5	RDH14	Retinol dehydrogenase 14	4	0,004
P12955	PEPD	Xaa-Pro dipeptidase	3,9	0,001
P61289	PSME3	Proteasome activator complex subunit 3	3,9	0,005
B7Z7F3	RANBP3	Ran-binding protein 3	3,8	<0.001
O14744	PRMT5	Protein arginine N-methyltransferase 5	3,7	<0.001
A6NGP5	JPT2	Jupiter microtubule-associated homolog 2	3,7	<0.001
Q9ULW0	TPX2	Targeting protein for Xklp2	3,7	0,001
P46821	MAP1B	Microtubule-associated protein 1B	3,6	<0.001
Q14247	CTTN	Src substrate cortactin	3,6	<0.001
O00483	NDUFA4	Cytochrome c oxidase subunit NDUFA4	3,5	<0.001
Q96EA4	SPDL1	Protein Spindly	3,5	0,002
Q5T6F2	UBAP2	Ubiquitin-associated protein 2	3,4	<0.001
Q9H773	DCTPP1	dCTP pyrophosphatase 1	3,3	<0.001
Q8NC51	SERBP1	Plasminogen activator inhibitor 1 RNA-binding protein	3,3	<0.001
Q5SW79	CEP170	Centrosomal protein of 170 kDa	3,2	<0.001
Q96KB5	PBK	Lymphokine-activated killer T-cell-originated protein kinase	3,2	0,002
Q9BRP1	PDCD2L	Programmed cell death protein 2-like	3,1	0,001
P06132	UROD	Uroporphyrinogen decarboxylase	3,1	0,004
P07910	HNRNPC	Heterogeneous nuclear ribonucleoproteins C1/C2	3,1	0,042
Q9NUQ3	TXLNG	Gamma-taxilin	3	0,002
Q86V48	LUZP1	Leucine zipper protein 1	2,9	<0.001
O43809	NUDT21	Cleavage and polyadenylation specificity factor subunit 5	2,9	0,001
Q9H2U2	PPA2	Inorganic pyrophosphatase 2, mitochondrial	2,9	0,001
Q9NUP9	LIN7C	Protein lin-7 homolog C	2,9	0,002
P40222	TXLNA	Alpha-taxilin	2,9	0,002
P61758	VBP1	Prefoldin subunit 3	2,9	0,004
O60664	PLIN3	Perilipin-3	2,9	0,008
H0YNW5	DUT	Deoxyuridine 5'-triphosphate nucleotidohydrolase	2,8	<0.001
E7EPN9	PRRC2C	Protein PRRC2C	2,8	<0.001
Q8N3X1	FNBP4	Formin-binding protein 4	2,8	0,001
Q13541	EIF4EBP1	Eukaryotic translation initiation factor 4E-binding protein 1	2,8	0,006
O75223	GGCT	Gamma-glutamylcyclotransferase	2,8	0,011
P19174	PLCG1	1-phosphatidylinositol 4,5-bisphosphate phosphodiesterase gamma-1	2,7	0,002
O75381	PEX14	Peroxisomal membrane protein PEX14	2,7	0,004
E9PGZ1	CALD1	Caldesmon	2,7	0,004
Q8IYS1	PM20D2	Peptidase M20 domain-containing protein 2	2,7	0,004
Q8IWB7	WDFY1	WD repeat and FYVE domain-containing protein 1	2,7	0,004
P10599	TXN	Thioredoxin	2,6	<0.001
Q9P258	RCC2	Protein RCC2	2,6	<0.001
P26599	PTBP1	Polypyrimidine tract-binding protein 1	2,6	<0.001
P30041	PRDX6	Peroxiredoxin-6	2,6	0,002
O43143	DHX15	Pre-mRNA-splicing factor ATP-dependent RNA helicase DHX15	2,6	0,002
K7EJQ8	HDHD2	Haloacid dehalogenase-like hydrolase domain-containing protein 2	2,6	0,004
P30740	SERPINB1	Leukocyte elastase inhibitor	2,6	0,005
Q8WVC2	RPS21	40S ribosomal protein S21	2,6	0,006
Q16204	CCDC6	Coiled-coil domain-containing protein 6	2,6	0,011
H3BRL3	UBFD1	Ubiquitin domain-containing protein UBFD1	2,6	0,014
P52888	THOP1	Thimet oligopeptidase	2,5	<0.001
J3KN29	PSMD9	26S proteasome non-ATPase regulatory subunit 9	2,5	<0.001

Q9Y570	PPME1	Protein phosphatase methylesterase 1	2,5	<0.001
O14929	HAT1	Histone acetyltransferase type B catalytic subunit	2,5	<0.001
P48634	PRRC2A	Protein PRRC2A	2,5	<0.001
Q9HA64	FN3KRP	Ketosamine-3-kinase	2,5	0,002
Q8TAQ2	SMARCC2	SWI/SNF complex subunit SMARCC2	2,5	0,003
A0A087WTM1	ROBO1	Roundabout homolog 1	2,5	0,004
Q6IQ49	SDE2	Replication stress response regulator SDE2	2,5	0,004
Q6WKZ4	RAB11FIP1	Rab11 family-interacting protein 1	2,5	0,005
Q9P2B4	CTTNBP2NL	CTTNBP2 N-terminal-like protein	2,5	0,006
Q99598	TSNAX	Translin-associated protein X	2,5	0,008
P49903	SEPHS1	Selenide, water dikinase 1	2,5	0,009
K7ELV2	SEH1L	Nucleoporin SEH1	2,5	0,01
Q13542	EIF4EBP2	Eukaryotic translation initiation factor 4E-binding protein 2	2,5	0,045
F5GZS6	SLC3A2	4F2 cell-surface antigen heavy chain	2,4	<0.001
Q9BXJ9	NAA15	N-alpha-acetyltransferase 15, NatA auxiliary subunit	2,4	0,003
P35520	CBS	Cystathionine beta-synthase	2,3	<0.001
Q13428	TCOF1	Treacle protein	2,3	<0.001
P42771	CDKN2A	Cyclin-dependent kinase inhibitor 2A	2,3	<0.001
Q15019	SEPTIN2	Septin-2	2,3	0,009
Q9Y3B7	MRPL11	39S ribosomal protein L11, mitochondrial	2,3	0,017
Q8N6M0	OTUD6B	Deubiquitinase OTUD6B	2,3	0,017
Q49A26	GLYR1	Putative oxidoreductase GLYR1	2,3	0,037
P52907	CAPZA1	F-actin-capping protein subunit alpha-1	2,2	<0.001
Q13547	HDAC1	Histone deacetylase 1	2,2	0,002
Q14257	RCN2	Reticulocalbin-2	2,2	0,004
Q9UQE7	SMC3	Structural maintenance of chromosomes protein 3	2,2	0,006
Q5JRA6	MIA3	Transport and Golgi organization protein 1 homolog	2,2	0,007
E9PS17	SCYL1	N-terminal kinase-like protein	2,2	0,008
O00629	KPNA4	Importin subunit alpha-3	2,2	0,009
O94992	HEXIM1	Protein HEXIM1	2,2	0,01
Q96F45	ZNF503	Zinc finger protein 503	2,2	0,013
E7EV99	ADD1	Alpha-adducin	2,2	0,014
P38159	RBMX	RNA-binding motif protein, X chromosome	2,2	0,014
Q96GD0	PDXP	Pyridoxal phosphate phosphatase	2,2	0,015
E9PM92	C11orf58	Small acidic protein	2,2	0,017
A4D1S0	KLRG2	Killer cell lectin-like receptor subfamily G member 2	2,2	0,027
C9J0I9	ZC3HC1	Nuclear-interacting partner of ALK	2,1	<0.001
P35237	SERPINB6	Serpin B6	2,1	<0.001
P00492	HPRT1	Hypoxanthine-guanine phosphoribosyltransferase	2,1	0,004
Q9UBS4	DNAJB11	DnaJ homolog subfamily B member 11	2,1	0,014
Q9Y2R9	MRPS7	28S ribosomal protein S7, mitochondrial	2,1	0,015
O95104	SCAF4	SR-related and CTD-associated factor 4	2,1	0,016
F5H8D7	XRCC1	DNA repair protein XRCC1	2,1	0,016
Q9NVP1	DDX18	ATP-dependent RNA helicase DDX18	2,1	0,018
Q86WA6	BPHL	Valacyclovir hydrolase	2,1	0,026
Q6PKG0	LARP1	La-related protein 1	2	<0.001
Q06124	PTPN11	Tyrosine-protein phosphatase non-receptor type 11	2	<0.001
B1AK87	CAPZB	F-actin-capping protein subunit beta	2	<0.001
P54646	PRKAA2	5'-AMP-activated protein kinase catalytic subunit alpha-2	2	0,007
P41250	GARS1	Glycine--tRNA ligase	2	0,013
Q9H3S7	PTPN23	Tyrosine-protein phosphatase non-receptor type 23	2	0,014
Q9NXF7	DCAF16	DDB1- and CUL4-associated factor 16	2	0,016
O94903	PLPBP	Pyridoxal phosphate homeostasis protein	2	0,017
P29373	CRABP2	Cellular retinoic acid-binding protein 2	2	0,018
Q8IVM0	CCDC50	Coiled-coil domain-containing protein 50	2	0,021
O15143	ARPC1B	Actin-related protein 2/3 complex subunit 1B	2	0,025
P23588	EIF4B	Eukaryotic translation initiation factor 4B	2	0,049
Q16576	RBBP7	Histone-binding protein RBBP7	1,9	<0.001
Q93034	CUL5	Cullin-5	1,9	0,001
Q9C0C9	UBE2O	(E3-independent) E2 ubiquitin-conjugating enzyme	1,9	0,001
P52732	KIF11	Kinesin-like protein KIF11	1,9	0,002
Q8N6T3	ARFGAP1	ADP-ribosylation factor GTPase-activating protein 1	1,9	0,016
Q96K76	USP47	Ubiquitin carboxyl-terminal hydrolase 47	1,9	0,02
Q14240	EIF4A2	Eukaryotic initiation factor 4A-II	1,9	0,02
A1X283	SH3PXD2B	SH3 and PX domain-containing protein 2B	1,9	0,026
Q9Y3D0	CIAO2B	Cytosolic iron-sulfur assembly component 2B	1,9	0,031
P42574	CASP3	Caspase-3	1,9	0,042
Q16531	DDB1	DNA damage-binding protein 1	1,8	<0.001
P51452	DUSP3	Dual specificity protein phosphatase 3	1,8	<0.001
Q9Y3F4	STRAP	Serine-threonine kinase receptor-associated protein	1,8	<0.001
P31153	MAT2A	S-adenosylmethionine synthase isoform type-2	1,8	0,001
A0A1B0GW38	CBL	E3 ubiquitin-protein ligase CBL	1,8	0,003
Q9Y6Y8	SEC23IP	SEC23-interacting protein	1,8	0,005

Q12948	FOXC1	Forkhead box protein C1	1,8	0,014
Q12800	TFCP2	Alpha-globin transcription factor CP2	1,8	0,024
Q9HCN8	SDF2L1	Stromal cell-derived factor 2-like protein 1	1,8	0,026
Q2M1P5	KIF7	Kinesin-like protein KIF7	1,8	0,026
E9PQV9	DCUN1D5	DCN1-like protein	1,8	0,032
Q9BT25	HAUS8	HAUS augmin-like complex subunit 8	1,8	0,038
O60826	CCDC22	Coiled-coil domain-containing protein 22	1,8	0,047
Q06203	PPAT	Amidophosphoribosyltransferase	1,7	<0.001
Q96F86	EDC3	Enhancer of mRNA-decapping protein 3	1,7	0,004
Q9UBE0	SAE1	SUMO-activating enzyme subunit 1	1,7	0,006
A0A087X054	HYOU1	Hypoxia up-regulated protein 1	1,7	0,008
A0A3B3ISG5	IDE	Insulin-degrading enzyme	1,7	0,014
Q6P2Q9	PRPF8	Pre-mRNA-processing-splicing factor 8	1,7	0,014
P52788	SMS	Spermine synthase	1,7	0,023
E9PGT1	TSN	Component 3 of promoter of RISC	1,7	0,031
O43815	STRN	Striatin	1,7	0,039
Q6UN15	FIP1L1	Pre-mRNA 3'-end-processing factor FIP1	1,7	0,042
Q9BXP5	SRRT	Serrate RNA effector molecule homolog	1,7	0,045
Q92783	STAM	Signal transducing adapter molecule 1	1,7	0,048
Q5QPM7	PSMF1	Proteasome inhibitor PI31 subunit	1,6	<0.001
Q9UKG1	APPL1	DCC-interacting protein 13-alpha	1,6	<0.001
Q14C86	GAPVD1	GTPase-activating protein and VPS9 domain-containing protein 1	1,6	0,001
Q15393	SF3B3	Splicing factor 3B subunit 3	1,6	0,001
Q9UN37	VPS4A	Vacuolar protein sorting-associated protein 4A	1,6	0,004
O75663	TIPRL	TIP41-like protein	1,6	0,007
A0A087WTZ5	UBXN1	UBX domain-containing protein 1	1,6	0,01
P63000	RAC1	Ras-related C3 botulinum toxin substrate 1	1,6	0,018
O00165	HAX1	HCLS1-associated protein X-1	1,6	0,025
P49750	YLPM1	YLP motif-containing protein 1	1,6	0,038
O75533	SF3B1	Splicing factor 3B subunit 1	1,6	0,039
Q9Y265	RUVBL1	RuvB-like 1	1,5	0,001
P11413	G6PD	Glucose-6-phosphate 1-dehydrogenase	1,5	0,002
E9PLA9	CAPRIN1	Caprin-1	1,5	0,002
A0A087X2B5	BSG	Basigin	1,5	0,005
Q07666	KHDRBS1	KH domain-containing, RNA-binding, signal transduction-associated protein 1	1,5	0,01
Q9NYZ3	GTSE1	G2 and S phase-expressed protein 1	1,5	0,01
Q9BWJ5	SF3B5	Splicing factor 3B subunit 5	1,5	0,014
Q92667	AKAP1	A-kinase anchor protein 1, mitochondrial	1,5	0,022
P61106	RAB14	Ras-related protein Rab-14	1,5	0,035
O95347	SMC2	Structural maintenance of chromosomes protein 2	1,5	0,041
O60493	SNX3	Sorting nexin-3	1,5	0,047
Q96A33	CCDC47	Coiled-coil domain-containing protein 47	1,4	<0.001
Q8N5F7	NKAP	NF-kappa-B-activating protein	1,4	<0.001
Q13045	FLII	Protein flightless-1 homolog	1,4	<0.001
A0A0A0MRM8	MYO6	Unconventional myosin-6	1,4	0,001
Q92598	HSPH1	Heat shock protein 105 kDa	1,4	0,001
Q96HC4	PDLIM5	PDZ and LIM domain protein 5	1,4	0,002
O60343	TBC1D4	TBC1 domain family member 4	1,4	0,002
P20020	ATP2B1	Plasma membrane calcium-transporting ATPase 1	1,4	0,002
A0A024RCR6	BAG6	BCL2-associated athanogene 6	1,4	0,003
Q5BKZ1	ZNF326	DBIRD complex subunit ZNF326	1,4	0,003
Q9UNM6	PSMD13	26S proteasome non-ATPase regulatory subunit 13	1,4	0,003
P61981	YWHAG	14-3-3 protein gamma	1,4	0,005
P62333	PSMC6	26S proteasome regulatory subunit 10B	1,4	0,006
P15374	UCHL3	Ubiquitin carboxyl-terminal hydrolase isozyme L3	1,4	0,006
O00170	AIP	AH receptor-interacting protein	1,4	0,007
P35998	PSMC2	26S proteasome regulatory subunit 7	1,4	0,008
P50213	IDH3A	Isocitrate dehydrogenase [NAD] subunit alpha, mitochondrial	1,4	0,012
P31946	YWHAB	14-3-3 protein beta/alpha	1,4	0,013
Q7Z6Z7	HUWE1	E3 ubiquitin-protein ligase HUWE1	1,4	0,018
Q9UPN7	PPP6R1	Serine/threonine-protein phosphatase 6 regulatory subunit 1	1,4	0,024
O94905	ERLIN2	Erlin-2	1,4	0,028
O95801	TTC4	Tetratricopeptide repeat protein 4	1,4	0,03
Q96T23	RSF1	Remodeling and spacing factor 1	1,4	0,033
O14974	PPP1R12A	Protein phosphatase 1 regulatory subunit 12A	1,4	0,038
P13797	PLS3	Plastin-3	1,3	<0.001
P62191	PSMC1	26S proteasome regulatory subunit 4	1,3	0,001
Q9Y230	RUVBL2	RuvB-like 2	1,3	0,001
P25786	PSMA1	Proteasome subunit alpha type-1	1,3	0,001
O00151	PDLIM1	PDZ and LIM domain protein 1	1,3	0,002
Q7LBC6	KDM3B	Lysine-specific demethylase 3B	1,3	0,004
Q96D09	GPRASP2	G-protein coupled receptor-associated sorting protein 2	1,3	0,006
P08240	SRPRA	Signal recognition particle receptor subunit alpha	1,3	0,011

P55072	VCP	Transitional endoplasmic reticulum ATPase	1,3	0,012
Q9UJV9	DDX41	Probable ATP-dependent RNA helicase DDX41	1,3	0,021
Q92769	HDAC2	Histone deacetylase 2	1,3	0,023
P41214	EIF2D	Eukaryotic translation initiation factor 2D	1,3	0,024
A0MZ66	SHTN1	Shootin-1	1,3	0,024
A0A1C7CYX9	DPYSL2	Dihydropyrimidinase-related protein 2	1,3	0,025
Q15417	CNN3	Calponin-3	1,3	0,027
O00267	SUPT5H	Transcription elongation factor SPT5	1,3	0,027
P22314	UBA1	Ubiquitin-like modifier-activating enzyme 1	1,3	0,029
Q15276	RABEP1	Rab GTPase-binding effector protein 1	1,3	0,039
Q9H6S0	YTHDC2	3'-5' RNA helicase YTHDC2	1,3	0,044
Q9H0U4	RAB1B	Ras-related protein Rab-1B	1,3	0,046
Q9H9B4	SFXN1	Sideroflexin-1	1,2	0,001
Q6NUK1	SLC25A24	Calcium-binding mitochondrial carrier protein SCaMC-1	1,2	0,001
Q9UKX7	NUP50	Nuclear pore complex protein Nup50	1,2	0,002
Q15046	KARS1	Lysine--tRNA ligase	1,2	0,003
O00487	PSMD14	26S proteasome non-ATPase regulatory subunit 14	1,2	0,005
P06737	PYGL	Glycogen phosphorylase, liver form	1,2	0,005
Q9UJZ1	STOML2	Stomatin-like protein 2, mitochondrial	1,2	0,005
Q9UNF1	MAGED2	Melanoma-associated antigen D2	1,2	0,006
Q7Z4H7	HAUS6	HAUS augmin-like complex subunit 6	1,2	0,006
Q9UHD1	CHORDC1	Cysteine and histidine-rich domain-containing protein 1	1,2	0,01
P22695	UQCRC2	Cytochrome b-c1 complex subunit 2, mitochondrial	1,2	0,011
Q9GZT9	EGLN1	Egl nine homolog 1	1,2	0,012
Q9Y5A9	YTHDF2	YTH domain-containing family protein 2	1,2	0,013
O00273	DFFA	DNA fragmentation factor subunit alpha	1,2	0,014
P58546	MTPN	Myotrophin	1,2	0,02
P42677	RPS27	40S ribosomal protein S27	1,2	0,026
S4R3H4	ACIN1	Apoptotic chromatin condensation inducer in the nucleus	1,2	0,027
Q9BTE3	MCMBP	Mini-chromosome maintenance complex-binding protein	1,2	0,027
M0QY97	ZC3H4	Zinc finger CCCH domain-containing protein 4	1,2	0,028
Q14739	LBR	Delta(14)-sterol reductase LBR	1,2	0,03
P52701	MSH6	DNA mismatch repair protein Msh6	1,2	0,031
P22234	PAICS	Multifunctional protein ADE2 [Includes: Phosphoribosylaminoimidazole-succinocarboxamide synthase	1,2	0,035
P55265	ADAR	Double-stranded RNA-specific adenosine deaminase	1,2	0,04
Q8NI27	THOC2	THO complex subunit 2	1,2	0,046
P49790	NUP153	Nuclear pore complex protein Nup153	1,2	0,048
Q14137	BOP1	Ribosome biogenesis protein BOP1	1,2	0,049
P00387	CYB5R3	NADH-cytochrome b5 reductase 3	1,1	0,001
Q6P4A7	SFXN4	Sideroflexin-4	1,1	0,002
Q9Y295	DRG1	Developmentally-regulated GTP-binding protein 1	1,1	0,003
Q14566	MCM6	DNA replication licensing factor MCM6	1,1	0,003
P00338	LDHA	L-lactate dehydrogenase A chain	1,1	0,005
P49593	PPM1F	Protein phosphatase 1F	1,1	0,005
A0A0C4DGX4	CUL1	Cullin-1	1,1	0,006
Q13200	PSMD2	26S proteasome non-ATPase regulatory subunit 2	1,1	0,006
P22570	FDXR	NADPH:adrenodoxin oxidoreductase, mitochondrial	1,1	0,007
P13861	PRKAR2A	cAMP-dependent protein kinase type II-alpha regulatory subunit	1,1	0,007
E9PLK3	NPEPPS	Aminopeptidase	1,1	0,009
P05023	ATP1A1	Sodium/potassium-transporting ATPase subunit alpha-1	1,1	0,009
O95573	ACSL3	Long-chain-fatty-acid--CoA ligase 3	1,1	0,009
Q9NZB2	FAM120A	Constitutive coactivator of PPAR-gamma-like protein 1	1,1	0,012
Q96P70	IPO9	Importin-9	1,1	0,013
H0YDU8	PPP5C	Serine/threonine-protein phosphatase	1,1	0,014
Q04917	YWHAH	14-3-3 protein eta	1,1	0,016
Q96KR1	ZFR	Zinc finger RNA-binding protein	1,1	0,016
Q6UWP7	LCLAT1	Lysocardiolipin acyltransferase 1	1,1	0,018
Q8WWK9	CKAP2	Cytoskeleton-associated protein 2	1,1	0,021
Q9UIG0	BAZ1B	Tyrosine-protein kinase BAZ1B	1,1	0,024
A0A087WWP4	RBM15	RNA-binding protein 15	1,1	0,024
Q99504	EYA3	Eyes absent homolog 3	1,1	0,025
Q9H936	SLC25A22	Mitochondrial glutamate carrier 1	1,1	0,028
Q14694	USP10	Ubiquitin carboxyl-terminal hydrolase 10	1,1	0,028
Q9UBT2	UBA2	SUMO-activating enzyme subunit 2	1,1	0,038
P56385	ATP5ME	ATP synthase subunit e, mitochondrial	1,1	0,038
Q9NZL9	MAT2B	Methionine adenosyltransferase 2 subunit beta	1,1	0,04
O60832	DKC1	H/ACA ribonucleoprotein complex subunit DKC1	1,1	0,04
Q8WXF1	PSPC1	Paraspeckle component 1	1,1	0,041
P49588	AARS1	Alanine--tRNA ligase, cytoplasmic	1,1	0,043
P98175	RBM10	RNA-binding protein 10	1,1	0,049
P78346	RPP30	Ribonuclease P protein subunit p30	1	0,006
G8JLH9	STAT3	Signal transducer and activator of transcription	1	0,009
A0A087WUX8	APOOL	MICOS complex subunit	1	0,01

Q92597	NDRG1	Protein NDRG1	1	0,011
P46939	UTRN	Utrophin	1	0,014
Q2NKX8	ERCC6L	DNA excision repair protein ERCC-6-like	1	0,016
P09936	UCHL1	Ubiquitin carboxyl-terminal hydrolase isozyme L1	1	0,017
Q86YP4	GATAD2A	Transcriptional repressor p66-alpha	1	0,024
Q16512	PKN1	Serine/threonine-protein kinase N1	1	0,025
P60228	EIF3E	Eukaryotic translation initiation factor 3 subunit E	1	0,026
Q8ND82	ZNF280C	Zinc finger protein 280C	1	0,035
O95684	CEP43	Centrosomal protein 43	1	0,038
O43765	SGTA	Small glutamine-rich tetratricopeptide repeat-containing protein alpha	1	0,044
O43242	PSMD3	26S proteasome non-ATPase regulatory subunit 3	1	0,048
PRDX3 cysteine-dependent interactors				
P40616	ARL1	ADP-ribosylation factor-like protein 1	4,8	<0.001
Q5SZR4	TDRKH	Tudor and KH domain containing, isoform CRA_a	4,6	<0.001
P11766	ADH5	Alcohol dehydrogenase class-3	4,6	<0.001
F8VYE8	PPP1CC	Serine/threonine-protein phosphatase	4,4	<0.001
B3KUS5	USP30	Ubiquitin carboxyl-terminal hydrolase	4,1	<0.001
Q9NWV4	CZIB	CXXC motif containing zinc binding protein	4,1	<0.001
Q7L2H7	EIF3M	Eukaryotic translation initiation factor 3 subunit M	4	<0.001
Q07820	MCL1	Induced myeloid leukemia cell differentiation protein Mcl-1	3,9	<0.001
A0A0B4J1Z1	SRSF7	Serine/arginine-rich-splicing factor 7	3,9	<0.001
P05386	RPLP1	60S acidic ribosomal protein P1	3,9	<0.001
Q07021	C1QBP	Complement component 1 Q subcomponent-binding protein, mitochondrial	3,9	<0.001
H3BTA2	PPP4C	Serine/threonine-protein phosphatase	3,9	<0.001
P07355	ANXA2	Annexin A2	3,9	<0.001
Q14964	RAB39A	Ras-related protein Rab-39A	3,9	0,036
Q7Z434	MAVS	Mitochondrial antiviral-signaling protein	3,8	<0.001
Q9BS26	ERP44	Endoplasmic reticulum resident protein 44	3,7	0,001
Q8N5K1	CISD2	CDGSH iron-sulfur domain-containing protein 2	3,6	0,001
P22061	PCMT1	Protein-L-isoaspartate(D-aspartate) O-methyltransferase	3,6	0,001
C9JAW5	C9JAW5	HIG1 domain-containing protein	3,6	0,001
Q9BYN0	SRXN1	Sulfiredoxin-1	3,5	0,002
G5EA06	MRPS27	28S ribosomal protein S27, mitochondrial	3,5	0,009
Q6IBS0	TWF2	Twinfilin-2	3,4	<0.001
Q9HD26	GOPC	Golgi-associated PDZ and coiled-coil motif-containing protein	3,4	0,001
P06132	UROD	Uroporphyrinogen decarboxylase	3,4	0,001
P00492	HPRT1	Hypoxanthine-guanine phosphoribosyltransferase	3,4	0,001
O43809	NUDT21	Cleavage and polyadenylation specificity factor subunit 5	3,3	<0.001
P61106	RAB14	Ras-related protein Rab-14	3,3	<0.001
Q6DKI1	RPL7L1	60S ribosomal protein L7-like 1	3,3	0,001
P14174	MIF	Macrophage migration inhibitory factor	3,3	0,001
P19022	CDH2	Cadherin-2	3,3	0,001
Q9BQA1	WDR77	Methylosome protein 50	3,2	<0.001
Q92667	AKAP1	A-kinase anchor protein 1, mitochondrial	3,2	<0.001
P51809	VAMP7	Vesicle-associated membrane protein 7	3,2	0,006
Q9NQG6	MIEF1	Mitochondrial dynamics protein MID51	3,2	0,046
P47755	CAPZA2	F-actin-capping protein subunit alpha-2	3,1	<0.001
D6RA00	ENOPH1	Enolase-phosphatase E1	3,1	<0.001
P51148	RAB5C	Ras-related protein Rab-5C	3,1	0,008
Q16698	DECR1	2,4-dienoyl-CoA reductase, mitochondrial	3	0,001
P30041	PRDX6	Peroxiredoxin-6	3	0,002
O75600	GCAT	2-amino-3-ketobutyrate coenzyme A ligase, mitochondrial	3	0,002
Q9NS69	TOMM22	Mitochondrial import receptor subunit TOM22 homolog	3	0,002
Q96EA4	SPDL1	Protein Spindly	3	0,005
Q92990	GLMN	Glomulin	2,9	<0.001
Q9Y3D0	CIAO2B	Cytosolic iron-sulfur assembly component 2B	2,9	0,001
Q9BTE1	DCTN5	Dynactin subunit 5	2,9	0,002
Q8WVC2	RPS21	40S ribosomal protein S21	2,9	0,002
P02790	HPX	Hemopexin	2,9	0,007
Q15814	TBCC	Tubulin-specific chaperone C	2,9	0,03
Q9BSJ8	ESYT1	Extended synaptotagmin-1	2,8	<0.001
Q9Y5Y2	NUBP2	Cytosolic Fe-S cluster assembly factor NUBP2	2,8	0,001
Q5SY16	NOL9	Polynucleotide 5'-hydroxyl-kinase NOL9	2,8	0,001
Q15084	PDIA6	Protein disulfide-isomerase A6	2,8	0,001
Q9H9P8	L2HGDH	L-2-hydroxyglutarate dehydrogenase, mitochondrial	2,8	0,002
K7EJQ8	HDHD2	Haloacid dehalogenase-like hydrolase domain-containing protein 2	2,8	0,002
Q5T749	KPRP	Keratinocyte proline-rich protein	2,8	0,006
Q8N6T3	ARFGAP1	ADP-ribosylation factor GTPase-activating protein 1	2,7	0,001
M0R026	ILVBL	2-hydroxyacyl-CoA lyase 2	2,7	0,001
Q8IYS1	PM20D2	Peptidase M20 domain-containing protein 2	2,7	0,002
Q9NP61	ARFGAP3	ADP-ribosylation factor GTPase-activating protein 3	2,7	0,003
B4DJ81	NDUFS1	NADH-ubiquinone oxidoreductase 75 kDa subunit, mitochondrial	2,6	0,001
Q96S44	TP53RK	EKC/KEOPS complex subunit TP53RK	2,6	0,002

Q96IU4	ABHD14B	Protein ABHD14B	2,6	0,005
A0A087WU06	TUBGCP3	Gamma-tubulin complex component	2,6	0,007
Q96KB5	PBK	Lymphokine-activated killer T-cell-originated protein kinase	2,6	0,008
Q5VW32	BROX	BRO1 domain-containing protein BROX	2,6	0,011
P18669	PGAM1	Phosphoglycerate mutase 1	2,6	0,015
Q15388	TOMM20	Mitochondrial import receptor subunit TOM20 homolog	2,6	0,02
Q9NZ45	CISD1	CDGSH iron-sulfur domain-containing protein 1	2,6	0,025
O60566	BUB1B	Mitotic checkpoint serine/threonine-protein kinase BUB1 beta	2,6	0,035
Q9P287	BCCIP	BRCA2 and CDKN1A-interacting protein	2,5	0,001
Q96A49	SYAP1	Synapse-associated protein 1	2,5	0,002
P78346	RPP30	Ribonuclease P protein subunit p30	2,5	0,002
E9PJN0	ACOT8	Acyl-coenzyme A thioesterase 8	2,5	0,003
P54646	PRKAA2	5'-AMP-activated protein kinase catalytic subunit alpha-2	2,5	0,005
P30740	SERPINB1	Leukocyte elastase inhibitor	2,5	0,006
Q8N6M0	OTUD6B	Deubiquitinase OTUD6B	2,5	0,007
O95295	SNAPIN	SNARE-associated protein Snapin	2,5	0,007
Q8N6R0	EEF1AKNMT	eEF1A lysine and N-terminal methyltransferase	2,5	0,008
F5H008	VPS33B	Vacuolar protein sorting-associated protein 33B	2,5	0,009
Q9H840	GEMIN7	Gem-associated protein 7	2,5	0,009
Q16186	ADRM1	Proteasomal ubiquitin receptor ADRM1	2,5	0,021
Q5VUJ6	LRCH2	Leucine-rich repeat and calponin homology domain-containing protein 2	2,5	0,028
A6NDU8	C5orf51	UPF0600 protein C5orf51	2,5	0,034
Q7L5D6	GET4	Golgi to ER traffic protein 4 homolog	2,5	0,036
X6RM00	ERC1	ELKS/Rab6-interacting/CAST family member 1	2,4	0,003
Q9UKK9	NUDT5	ADP-sugar pyrophosphatase	2,4	0,004
Q9NYK5	MRPL39	39S ribosomal protein L39, mitochondrial	2,4	0,006
P56385	ATP5ME	ATP synthase subunit e, mitochondrial	2,4	0,008
Q86WA6	BPHL	Valacyclovir hydrolase	2,4	0,011
Q66PJ3	ARL6IP4	ADP-ribosylation factor-like protein 6-interacting protein 4	2,4	0,011
P63151	PPP2R2A	Serine/threonine-protein phosphatase 2A 55 kDa regulatory subunit B alpha isoform	2,4	0,016
P21796	VDAC1	Voltage-dependent anion-selective channel protein 1	2,4	0,026
Q9H6R0	DHX33	ATP-dependent RNA helicase DHX33	2,4	0,032
P11802	CDK4	Cyclin-dependent kinase 4	2,3	<0.001
Q9BQC3	DPH2	2-(3-amino-3-carboxypropyl)histidine synthase subunit 2	2,3	0,003
H3BV80	RNPS1	RNA-binding protein with serine-rich domain 1	2,3	0,005
Q8IVS2	MCAT	Malonyl-CoA-acyl carrier protein transacylase, mitochondrial	2,3	0,006
Q8IUF8	RIOX2	Ribosomal oxygenase 2	2,3	0,007
Q9ULX3	NOB1	RNA-binding protein NOB1	2,3	0,01
P57076	CFAP298	Cilia- and flagella-associated protein 298	2,3	0,011
Q9HCN8	SDF2L1	Stromal cell-derived factor 2-like protein 1	2,2	0,005
O14744	PRMT5	Protein arginine N-methyltransferase 5	2,2	0,006
O60547	GMDS	GDP-mannose 4,6 dehydratase	2,2	0,008
Q9NP97	DYNLRB1	Dynein light chain roadblock-type 1	2,2	0,011
Q9BPZ2	SPIN2B	Spindlin-2B	2,2	0,026
Q6UW78	UQCC3	Ubiquinol-cytochrome-c reductase complex assembly factor 3	2,2	0,045
P62879	GNB2	Guanine nucleotide-binding protein G(I)/G(S)/G(T) subunit beta-2	2,1	0,001
O43237	DYNC1LI2	Cytoplasmic dynein 1 light intermediate chain 2	2,1	0,007
A0A0A0MTB8	WDR36	WD repeat-containing protein 36	2,1	0,009
Q13509	TUBB3	Tubulin beta-3 chain	2,1	0,012
Q92785	DPF2	Zinc finger protein ubi-d4	2,1	0,014
Q16204	CCDC6	Coiled-coil domain-containing protein 6	2,1	0,037
Q9Y6Y8	SEC23IP	SEC23-interacting protein	2	0,001
Q14318	FKBP8	Peptidyl-prolyl cis-trans isomerase FKBP8	2	0,001
O95801	TTC4	Tetratricopeptide repeat protein 4	2	0,008
Q13257	MAD2L1	Mitotic spindle assembly checkpoint protein MAD2A	2	0,009
Q8NDI1	EHBP1	EH domain-binding protein 1	2	0,01
Q96BW9	TAMM41	Phosphatidate cytidylyltransferase, mitochondrial	2	0,01
Q9BZX2	UCK2	Uridine-cytidine kinase 2	2	0,011
Q9UQR0	SCML2	Sex comb on midleg-like protein 2	2	0,011
O43815	STRN	Striatin	2	0,015
Q9H974	QTRT2	Queuine tRNA-ribosyltransferase accessory subunit 2	2	0,016
Q15019	SEPTIN2	Septin-2	2	0,024
P49903	SEPHS1	Selenide, water dikinase 1	2	0,045
P35520	CBS	Cystathionine beta-synthase	1,9	0,003
Q9UI30	TRMT112	Multifunctional methyltransferase subunit TRM112-like protein	1,9	0,004
P52788	SMS	Spermine synthase	1,9	0,012
Q16718	NDUFA5	NADH dehydrogenase [ubiquinone] 1 alpha subcomplex subunit 5	1,9	0,013
Q15291	RBBP5	Retinoblastoma-binding protein 5	1,9	0,014
Q9Y679	AUP1	Lipid droplet-regulating VLDL assembly factor AUP1	1,9	0,014
Q8NBU5	ATAD1	ATPase family AAA domain-containing protein 1	1,9	0,016
P45954	ACADSB	Short/branched chain specific acyl-CoA dehydrogenase, mitochondrial	1,9	0,016
Q96AT9	RPE	Ribulose-phosphate 3-epimerase	1,9	0,018
Q9HB71	CACYBP	Calcyclin-binding protein	1,9	0,019

Q9UHD2	TBK1	Serine/threonine-protein kinase TBK1	1,9	0,022
O95551	TDP2	Tyrosyl-DNA phosphodiesterase 2	1,9	0,025
O75146	HIP1R	Huntingtin-interacting protein 1-related protein	1,9	0,036
Q96S59	RANBP9	Ran-binding protein 9	1,9	0,037
P62979	RPS27A	Ubiquitin-40S ribosomal protein S27a	1,8	0,002
P10599	TXN	Thioredoxin	1,8	0,011
Q9NQX3	GPHN	Gephyrin [Includes: Molybdopterin adenylyltransferase	1,8	0,025
P34896	SHMT1	Serine hydroxymethyltransferase, cytosolic	1,8	0,038
P17252	PRKCA	Protein kinase C alpha type	1,8	0,042
P18031	PTPN1	Tyrosine-protein phosphatase non-receptor type 1	1,7	0,007
Q9Y4B6	DCAF1	DDB1- and CUL4-associated factor 1	1,7	0,045
Q5QPM7	PSMF1	Proteasome inhibitor PI31 subunit	1,6	<0.001
Q8TDH9	BLOC1S5	Biogenesis of lysosome-related organelles complex 1 subunit 5	1,6	0,002
P21964	COMT	Catechol O-methyltransferase	1,6	0,003
Q9UH62	ARMCX3	Armadillo repeat-containing X-linked protein 3	1,6	0,006
Q2M2I8	AAK1	AP2-associated protein kinase 1	1,6	0,036
H7C155	RAF1	Non-specific serine/threonine protein kinase	1,6	0,047
O95831	AIFM1	Apoptosis-inducing factor 1, mitochondrial	1,5	0,002
Q96TC7	RMDN3	Regulator of microtubule dynamics protein 3	1,5	0,002
B4E1N1	ARMC6	Armadillo repeat-containing protein 6	1,5	0,007
Q9UL25	RAB21	Ras-related protein Rab-21	1,5	0,012
A0A0A0MR02	VDAC2	Outer mitochondrial membrane protein porin 2	1,5	0,014
Q16543	CDC37	Hsp90 co-chaperone Cdc37	1,5	0,016
O15269	SPTLC1	Serine palmitoyltransferase 1	1,5	0,018
P35268	RPL22	60S ribosomal protein L22	1,5	0,035
O75688	PPM1B	Protein phosphatase 1B	1,5	0,038
Q9Y266	NUDC	Nuclear migration protein nudC	1,5	0,047
O60825	PFKFB2	6-phosphofructo-2-kinase/fructose-2,6-bisphosphatase 2	1,5	0,049
Q16576	RBBP7	Histone-binding protein RBBP7	1,4	0,002
P60953	CDC42	Cell division control protein 42 homolog	1,4	0,002
Q8TC07	TBC1D15	TBC1 domain family member 15	1,4	0,005
Q9UGV2	NDRG3	Protein NDRG3	1,4	0,01
P62851	RPS25	40S ribosomal protein S25	1,4	0,01
Q5T760	SRSF11	Serine/arginine-rich-splicing factor 11	1,4	0,01
O75663	TIPRL	TIP41-like protein	1,4	0,034
Q9UL15	BAG5	BAG family molecular chaperone regulator 5	1,4	0,038
Q147X3	NAA30	N-alpha-acetyltransferase 30	1,4	0,047
Q8IXI1	RHOT2	Mitochondrial Rho GTPase 2	1,3	0,001
Q9GZS3	WDR61	WD repeat-containing protein 61	1,3	0,003
P51553	IDH3G	Isocitrate dehydrogenase [NAD] subunit gamma, mitochondrial	1,3	0,014
Q8TEX9	IPO4	Importin-4	1,3	0,024
Q5VT66	MTARC1	Mitochondrial amidoxime-reducing component 1	1,3	0,028
P19367	HK1	Hexokinase-1	1,3	0,035
P62820	RAB1A	Ras-related protein Rab-1A	1,3	0,04
Q9Y570	PPME1	Protein phosphatase methylesterase 1	1,3	0,047
P35237	SERPINB6	Serpin B6	1,2	0,002
O60784	TOM1	Target of Myb protein 1	1,2	0,006
P55072	VCP	Transitional endoplasmic reticulum ATPase	1,2	0,018
P20042	EIF2S2	Eukaryotic translation initiation factor 2 subunit 2	1,2	0,023
Q9NQT5	EXOSC3	Exosome complex component RRP40	1,2	0,026
P29558	RBMS1	RNA-binding motif, single-stranded-interacting protein 1	1,2	0,027
P26368	U2AF2	Splicing factor U2AF 65 kDa subunit	1,2	0,038
Q9H0U4	RAB1B	Ras-related protein Rab-1B	1,2	0,045
P62873	GNB1	Guanine nucleotide-binding protein G(I)/G(S)/G(T) subunit beta-1	1,1	0,009
Q15738	NSDHL	Sterol-4-alpha-carboxylate 3-dehydrogenase, decarboxylating	1,1	0,024
P31040	SDHA	Succinate dehydrogenase [ubiquinone] flavoprotein subunit, mitochondrial	1,1	0,027
P09211	GSTP1	Glutathione S-transferase P	1,1	0,027
Q53EL6	PDCD4	Programmed cell death protein 4	1,1	0,047
Q14126	DSG2	Desmoglein-2	1	0,012
Q96FW1	OTUB1	Ubiquitin thioesterase OTUB1	1	0,019
P56182	RRP1	Ribosomal RNA processing protein 1 homolog A	1	0,026
P50454	SERPINH1	Serpin H1	1	0,029
Q14498	RBM39	RNA-binding protein 39	1	0,035
P62081	RPS7	40S ribosomal protein S7	1	0,037
P16435	POR	NADPH--cytochrome P450 reductase	1	0,041
PRDX4 cysteine-dependent interactors				
Q12797	ASPH	Aspartyl/asparaginyl beta-hydroxylase	3,9	<0.001
I3L1P8	SLC25A11	Mitochondrial 2-oxoglutarate/malate carrier protein	3,5	<0.001
A0A0B4J1Z1	SRSF7	Serine/arginine-rich-splicing factor 7	3,1	0,002
F5H6E2	MYO1C	Unconventional myosin-Ic	2,9	0,001
O00469	PLOD2	Procollagen-lysine,2-oxoglutarate 5-dioxygenase 2	2,8	0,03
Q9NVP1	DDX18	ATP-dependent RNA helicase DDX18	2,6	0,007
Q9BSJ8	ESYT1	Extended synaptotagmin-1	2,5	0,003

Q9Y2R4	DDX52	Probable ATP-dependent RNA helicase DDX52	2,3	0,024
Q13618	CUL3	Cullin-3	2,2	0,013
Q9Y2R5	MRPS17	28S ribosomal protein S17, mitochondrial	2,2	0,03
D6RA00	ENOPH1	Enolase-phosphatase E1	2,1	0,017
P30154	PPP2R1B	Serine/threonine-protein phosphatase 2A 65 kDa regulatory subunit A beta isoform	2,1	0,021
O75592	MYCBP2	E3 ubiquitin-protein ligase MYCBP2	2,1	0,027
Q8NBS9	TXNDC5	Thioredoxin domain-containing protein 5	1,9	0,007
P84103	SRSF3	Serine/arginine-rich splicing factor 3	1,9	0,028
Q12905	ILF2	Interleukin enhancer-binding factor 2	1,9	0,032
P29372	MPG	DNA-3-methyladenine glycosylase	1,9	0,039
Q7KZ85	SUPT6H	Transcription elongation factor SPT6	1,9	0,043
Q92783	STAM	Signal transducing adapter molecule 1	1,8	0,041
Q66K74	MAP1S	Microtubule-associated protein 1S	1,8	0,049
A0A2R8Y7S2	SMARCA4	Transcription activator BRG1	1,7	0,008
B4DJ81	NDUFS1	NADH-ubiquinone oxidoreductase 75 kDa subunit, mitochondrial	1,7	0,039
Q8IUI8	CRLF3	Cytokine receptor-like factor 3	1,7	0,049
Q8WX93	PALLD	Palladin	1,7	0,049
Q14697	GANAB	Neutral alpha-glucosidase AB	1,6	0,001
P11802	CDK4	Cyclin-dependent kinase 4	1,6	0,011
A0A087X054	HYOU1	Hypoxia up-regulated protein 1	1,6	0,019
P49593	PPM1F	Protein phosphatase 1F	1,5	0,015
O75607	NPM3	Nucleoplasmin-3	1,5	0,022
Q14152	EIF3A	Eukaryotic translation initiation factor 3 subunit A	1,5	0,025
O14974	PPP1R12A	Protein phosphatase 1 regulatory subunit 12A	1,5	0,032
Q9BVP2	GNL3	Guanine nucleotide-binding protein-like 3	1,5	0,034
Q9C0C2	TNKS1BP1	182 kDa tankyrase-1-binding protein	1,5	0,043
Q9HCN8	SDF2L1	Stromal cell-derived factor 2-like protein 1	1,4	0,002
Q16513	PKN2	Serine/threonine-protein kinase N2	1,4	0,017
O43809	NUDT21	Cleavage and polyadenylation specificity factor subunit 5	1,4	0,028
Q92974	ARHGEF2	Rho guanine nucleotide exchange factor 2	1,3	0,002
Q5SW79	CEP170	Centrosomal protein of 170 kDa	1,3	0,013
Q9UQR0	SCML2	Sex comb on midleg-like protein 2	1,3	0,016
Q14318	FKBP8	Peptidyl-prolyl cis-trans isomerase FKBP8	1,3	0,02
P27824	CANX	Calnexin	1,3	0,022
P49411	TUFM	Elongation factor Tu, mitochondrial	1,3	0,022
Q9BWF3	RBM4	RNA-binding protein 4	1,3	0,038
Q16543	CDC37	Hsp90 co-chaperone Cdc37	1,3	0,039
A0A087WY71	AP2M1	AP-2 complex subunit mu	1,2	0,014
P18858	LIG1	DNA ligase 1	1,2	0,014
Q12904	AIMP1	Aminoacyl tRNA synthase complex-interacting multifunctional protein 1	1,2	0,019
P22234	PAICS	Multifunctional protein ADE2 [Includes: Phosphoribosylaminoimidazole-succinocarboxamide synthase	1,2	0,033
Q8TCG1	CIP2A	Protein CIP2A	1,2	0,04
P62249	RPS16	40S ribosomal protein S16	1,2	0,043
Q09666	AHNAK	Neuroblast differentiation-associated protein AHNAK	1,1	0,006
E7EPN9	PRRC2C	Protein PRRC2C	1,1	0,018
Q99567	NUP88	Nuclear pore complex protein Nup88	1,1	0,032
P30520	ADSS2	Adenylosuccinate synthetase isozyme 2	1,1	0,035
Q07020	RPL18	60S ribosomal protein L18	1,1	0,036
P13489	RNH1	Ribonuclease inhibitor	1	0,03
PRDX5 cysteine-dependent interactors				
P36551	CPOX	Oxygen-dependent coproporphyrinogen-III oxidase, mitochondrial	6,4	<0.001
Q6DKK2	TTC19	Tetratricopeptide repeat protein 19, mitochondrial	3,9	<0.001
Q96A49	SYAP1	Synapse-associated protein 1	3,9	<0.001
O00165	HAX1	HCLS1-associated protein X-1	3,7	<0.001
A0A0C4DGQ6	RPRD1A	Regulation of nuclear pre-mRNA domain-containing protein 1A	2,9	0,002
P78371	CCT2	T-complex protein 1 subunit beta	2,7	<0.001
P85037	FOXK1	Forkhead box protein K1	2,6	0,012
A0A024R442	A0A024R442	>tr|A0A024R442|A0A024R442_HUMAN Aspartyl aminopeptidase, isoform CRA_b OS=Homo sapiens OX=9606 GN=DNPEP PE=1 SV=1;>sp|Q9ULA0|DNPEP_HUMAN Aspartyl aminopeptidase OS=Homo sapiens OX=9606 GN=DNPEP PE=1 SV=1;>tr|E7ETB3|E7ETB3_HUMAN Aspartyl aminopeptidase, iso	2,6	0,012
P30740	SERPINB1	Leukocyte elastase inhibitor	2,3	0,016
Q2TAM5	RELA	RELA protein	2,2	0,013
Q10713	PMPCA	Mitochondrial-processing peptidase subunit alpha	2,2	0,018
A0A075B6R9	IGKV2D-24	Probable non-functional immunoglobulin kappa variable 2D-24	2,2	0,041
Q8NFC6	BOD1L1	Biorientation of chromosomes in cell division protein 1-like 1	2,1	<0.001
O95801	TTC4	Tetratricopeptide repeat protein 4	2,1	0,025
Q6PID6	TTC33	Tetratricopeptide repeat protein 33	2,1	0,043
Q96HS1	PGAM5	Serine/threonine-protein phosphatase PGAM5, mitochondrial	2	0,005
P13667	PDIA4	Protein disulfide-isomerase A4	2	0,018
O00483	NDUFA4	Cytochrome c oxidase subunit NDUFA4	2	0,025
Q96DH6	MSI2	RNA-binding protein Musashi homolog 2	2	0,044
P62979	RPS27A	Ubiquitin-40S ribosomal protein S27a	1,9	0,001
P07355	ANXA2	Annexin A2	1,9	0,007

E9PGZ1	CALD1	Caldesmon	1,8	0,023
O95831	AIFM1	Apoptosis-inducing factor 1, mitochondrial	1,6	0,001
Q9NZL9	MAT2B	Methionine adenosyltransferase 2 subunit beta	1,6	0,006
H7C128	BRD8	Bromodomain-containing protein 8	1,6	0,011
P48047	ATP5PO	ATP synthase subunit O, mitochondrial	1,6	0,013
P43304	GPD2	Glycerol-3-phosphate dehydrogenase, mitochondrial	1,6	0,015
P43686	PSMC4	26S proteasome regulatory subunit 6B	1,6	0,016
E5KLJ9	OPA1	Dynamin-like 120 kDa protein, form S1	1,5	0,004
P26599	PTBP1	Polypyrimidine tract-binding protein 1	1,5	0,006
Q13257	MAD2L1	Mitotic spindle assembly checkpoint protein MAD2A	1,5	0,02
Q96IZ0	PAWR	PRKC apoptosis WT1 regulator protein	1,4	0,013
A0A0A0MR02	VDAC2	Outer mitochondrial membrane protein porin 2	1,4	0,016
Q8N3X1	FNBP4	Formin-binding protein 4	1,3	0,009
C9J4Z3	RPL37A	60S ribosomal protein L37a	1,3	0,022
P31689	DNAJA1	DnaJ homolog subfamily A member 1	1,2	0,003
Q9HB71	CACYBP	Calcyclin-binding protein	1,2	0,018
Q8NC51	SERBP1	Plasminogen activator inhibitor 1 RNA-binding protein	1,2	0,028
P22234	PAICS	Multifunctional protein ADE2 [Includes: Phosphoribosylaminoimidazole-succinocarboxamide synthase	1,2	0,035
Q9NX63	CHCHD3	MICOS complex subunit MIC19	1,1	0,004
Q5QPM7	PSMF1	Proteasome inhibitor PI31 subunit	1,1	0,007
Q14C86	GAPVD1	GTPase-activating protein and VPS9 domain-containing protein 1	1,1	0,02
P40222	TXLNA	Alpha-taxilin	1,1	0,048

Table S4: all cysteine-dependent interactors (wild-type and C_KS)

uniprot ID	gene	protein	interaction
PRDX1 cysteine-dependent interactors			
P62273	RPS29	40S ribosomal protein S29	WT
P13667	PDIA4	Protein disulfide-isomerase A4	WT
O60762	DPM1	Dolichol-phosphate mannosyltransferase subunit 1	WT
Q15185	PTGES3	Prostaglandin E synthase 3	WT, C_2S
P31323	PRKAR2B	cAMP-dependent protein kinase type II-beta regulatory subunit	WT
P50570	DNM2	Dynamin-2	WT
Q13257	MAD2L1	Mitotic spindle assembly checkpoint protein MAD2A	WT
A0A3B3IUD2	MSTO1	Protein misato homolog 1	WT
Q96FV9	THOC1	THO complex subunit 1	WT
P15924	DSP	Desmoplakin	WT, C_2S
Q9Y2V2	CARHSP1	Calcium-regulated heat-stable protein 1	WT, C_2S
Q9H845	ACAD9	Complex I assembly factor ACAD9, mitochondrial	WT
P83731	RPL24	60S ribosomal protein L24	WT
Q9BY32	ITPA	Inosine triphosphate pyrophosphatase	WT, C_2S
O94760	DDAH1	N(G),N(G)-dimethylarginine dimethylaminohydrolase 1	WT
P62266	RPS23	40S ribosomal protein S23	WT
Q8WWH5	TRUB1	Probable tRNA pseudouridine synthase 1	WT
Q6P1L8	MRPL14	39S ribosomal protein L14, mitochondrial	WT
Q99961	SH3GL1	Endophilin-A2	WT
P08559	PDHA1	Pyruvate dehydrogenase E1 component subunit alpha, somatic form, mitochondrial	WT, C_2S
Q01082	SPTBN1	Spectrin beta chain, non-erythrocytic 1	WT
I3L2Z5	MAZ	Myc-associated zinc finger protein	WT
P49792	RANBP2	E3 SUMO-protein ligase RanBP2	WT, C_2S
Q14008	CKAP5	Cytoskeleton-associated protein 5	WT, C_2S
Q7L2E3	DHX30	ATP-dependent RNA helicase DHX30	WT
O14964	HGS	Hepatocyte growth factor-regulated tyrosine kinase substrate	WT
Q5JTH9	RRP12	RRP12-like protein	WT
P49841	GSK3B	Glycogen synthase kinase-3 beta	WT
P48735	IDH2	Isocitrate dehydrogenase [NADP], mitochondrial	WT
Q15149	PLEC	Plectin	WT, C_2S
E3W994	CLASP2	CLIP-associating protein 2	WT
Q16698	DECR1	2,4-dienoyl-CoA reductase, mitochondrial	WT
P48047	ATP5PO	ATP synthase subunit O, mitochondrial	WT, C_2S
E7EVH7	E7EVH7	Kinesin light chain	WT
Q15717	ELAVL1	ELAV-like protein 1	WT
P22626	HNRNPA2B1	Heterogeneous nuclear ribonucleoproteins A2/B1	WT
Q99615	DNAJC7	DnaJ homolog subfamily C member 7	WT, C_2S
Q7L1Q6	BZW1	Basic leucine zipper and W2 domain-containing protein 1	WT
Q01813	PFKP	ATP-dependent 6-phosphofructokinase, platelet type	WT
Q8N1F7	NUP93	Nuclear pore complex protein Nup93	WT
O95801	TTC4	Tetratricopeptide repeat protein 4	WT
P63165	SUMO1	Small ubiquitin-related modifier 1	WT, C_2S
P30048	PRDX3	Thioredoxin-dependent peroxide reductase, mitochondrial	WT, C_2S
D6RBD7	EEF1E1	Eukaryotic translation elongation factor 1 epsilon-1	WT
Q99543	DNAJC2	DnaJ homolog subfamily C member 2	WT

Q9NW13	RBM28	RNA-binding protein 28	WT
Q08211	DHX9	ATP-dependent RNA helicase A	WT
A0A1W2PRV5	SMN2	Survival motor neuron protein	WT
O60493	SNX3	Sorting nexin-3	WT
P62318	SNRPD3	Small nuclear ribonucleoprotein Sm D3	WT
Q9Y5K6	CD2AP	CD2-associated protein	WT
Q02241	KIF23	Kinesin-like protein KIF23	WT
P19623	SRM	Spermidine synthase	WT
P24534	EEF1B2	Elongation factor 1-beta	WT
Q9BV44	THUMPD3	THUMP domain-containing protein 3	WT
Q9BQG0	MYBBP1A	Myb-binding protein 1A	WT, C_2S
A0A0C4DGX4	CUL1	Cullin-1	WT
P51153	RAB13	Ras-related protein Rab-13	WT
Q8TCG1	CIP2A	Protein CIP2A	WT
P62851	RPS25	40S ribosomal protein S25	WT, C_2S
Q92879	CELF1	CUGBP Elav-like family member 1	WT, C_2S
O14617	AP3D1	AP-3 complex subunit delta-1	WT
P53582	METAP1	Methionine aminopeptidase 1	WT
Q71UI9	H2AZ2	Histone H2A.V	WT
Q96I25	RBM17	Splicing factor 45	WT, C_2S
O75369	FLNB	Filamin-B	WT
P43686	PSMC4	26S proteasome regulatory subunit 6B	WT
O43447	PPIH	Peptidyl-prolyl cis-trans isomerase H	WT
Q13595	TRA2A	Transformer-2 protein homolog alpha	WT
P36915	GNL1	Guanine nucleotide-binding protein-like 1	WT, C_2S
P24666	ACP1	Low molecular weight phosphotyrosine protein phosphatase	WT, C_2S
P61081	UBE2M	NEDD8-conjugating enzyme Ubc12	WT
P46940	IQGAP1	Ras GTPase-activating-like protein IQGAP1	WT, C_2S
P61011	SRP54	Signal recognition particle 54 kDa protein	WT, C_2S
Q13247	SRSF6	Serine/arginine-rich splicing factor 6	WT
Q9HAV4	XPO5	Exportin-5	WT
E9PD53	SMC4	Structural maintenance of chromosomes protein	WT, C_2S
O15446	POLR1G	DNA-directed RNA polymerase I subunit RPA34	WT
Q96N67	DOCK7	Dedicator of cytokinesis protein 7	WT, C_2S
A0A2R8YDQ9	SUCLA2	Succinate--CoA ligase [ADP-forming] subunit beta, mitochondrial	WT, C_2S
P49207	RPL34	60S ribosomal protein L34	WT, C_2S
Q9GZT3	SLIRP	SRA stem-loop-interacting RNA-binding protein, mitochondrial	WT, C_2S
Q8WTT2	NOC3L	Nucleolar complex protein 3 homolog	WT
P62280	RPS11	40S ribosomal protein S11	WT
P61160	ACTR2	Actin-related protein 2	WT
Q92615	LARP4B	La-related protein 4B	WT
A0A0A0MRM9	NOLC1	Nucleolar and coiled-body phosphoprotein 1	WT
O14974	PPP1R12A	Protein phosphatase 1 regulatory subunit 12A	WT
P49790	NUP153	Nuclear pore complex protein Nup153	WT, C_2S
Q9H6T3	RPAP3	RNA polymerase II-associated protein 3	WT
P07196	NEFL	Neurofilament light polypeptide	WT
P61313	RPL15	60S ribosomal protein L15	WT
A0A087WZ13	RAVER1	Ribonucleoprotein PTB-binding 1	WT, C_2S
O15305	PMM2	Phosphomannomutase 2	WT
E7EX90	DCTN1	Dynactin subunit 1	WT, C_2S
Q9H0C8	ILKAP	Integrin-linked kinase-associated serine/threonine phosphatase 2C	WT, C_2S
Q9BUQ8	DDX23	Probable ATP-dependent RNA helicase DDX23	WT
Q9BQ39	DDX50	ATP-dependent RNA helicase DDX50	WT
Q9UQE7	SMC3	Structural maintenance of chromosomes protein 3	WT, C_2S
Q9H2G2	SLK	STE20-like serine/threonine-protein kinase	WT, C_2S
Q13363	CTBP1	C-terminal-binding protein 1	WT
Q13813	SPTAN1	Spectrin alpha chain, non-erythrocytic 1	WT
A0A1B0GV47	KIF21A	Kinesin-like protein KIF21A	WT
O43707	ACTN4	Alpha-actinin-4	WT
Q8N9T8	KRI1	Protein KRI1 homolog	WT, C_2S
Q7Z434	MAVS	Mitochondrial antiviral-signaling protein	WT
P61163	ACTR1A	Alpha-centractin	WT, C_2S
A0A1W2PPZ5	TCEA1	Transcription elongation factor A protein 1	WT
F8W8I6	TIA1	Nucleolysin TIA-1 isoform p40	WT
P23258	TUBG1	Tubulin gamma-1 chain	WT, C_2S
Q02878	RPL6	60S ribosomal protein L6	WT
P25490	YY1	Transcriptional repressor protein YY1	WT
A0A2R8Y804	CTNNB1	Catenin beta-1	WT
B5MCF9	PES1	Pescadillo homolog	WT, C_2S
Q9NSK0	KLC4	Kinesin light chain 4	WT
Q96PK6	RBM14	RNA-binding protein 14	WT
Q9UHI6	DDX20	Probable ATP-dependent RNA helicase DDX20	WT, C_2S
H3BPE1	MACF1	Microtubule-actin cross-linking factor 1, isoforms 1/2/3/5	WT, C_2S

Q15813	TBCE	Tubulin-specific chaperone E	WT
Q8WVM8	SCFD1	Sec1 family domain-containing protein 1	WT, C_S
Q16352	INA	Alpha-internexin	WT
P19338	NCL	Nucleolin	WT
A0A087X2D5	MRPL45	39S ribosomal protein L45, mitochondrial	WT
A0A0A0MRT6	ABI1	Abl interactor 1	WT, C_S
P48507	GCLM	Glutamate--cysteine ligase regulatory subunit	WT
Q9H9A6	LRRC40	Leucine-rich repeat-containing protein 40	WT
P46060	RANGAP1	Ran GTPase-activating protein 1	WT, C_S
Q9ULV4	CORO1C	Coronin-1C	WT, C_S
F5GWT4	WNK1	Non-specific serine/threonine protein kinase	WT
A0A3B3ISG5	IDE	Insulin-degrading enzyme	WT
P14174	MIF	Macrophage migration inhibitory factor	WT, C_S
Q92974	ARHGEF2	Rho guanine nucleotide exchange factor 2	WT
Q13561	DCTN2	Dynactin subunit 2	WT, C_S
Q9H0B6	KLC2	Kinesin light chain 2	WT, C_S
Q9NR12	PDLIM7	PDZ and LIM domain protein 7	WT, C_S
Q14684	RRP1B	Ribosomal RNA processing protein 1 homolog B	WT, C_S
A5YKK6	CNOT1	CCR4-NOT transcription complex subunit 1	WT
P31942	HNRNPH3	Heterogeneous nuclear ribonucleoprotein H3	WT
P08243	ASNS	Asparagine synthetase [glutamine-hydrolyzing]	WT
Q96MU7	YTHDC1	YTH domain-containing protein 1	WT
P78316	NOP14	Nucleolar protein 14	WT
Q9NZB2	FAM120A	Constitutive coactivator of PPAR-gamma-like protein 1	WT
Q5JRX3	PITRM1	Presequence protease, mitochondrial	WT, C_S
Q96D71	REPS1	RalBP1-associated Eps domain-containing protein 1	WT
Q14683	SMC1A	Structural maintenance of chromosomes protein 1A	WT, C_S
Q9UG63	ABCF2	ATP-binding cassette sub-family F member 2	WT, C_S
Q5TDH0	DDI2	Protein DDI1 homolog 2	WT, C_S
P82921	MRPS21	28S ribosomal protein S21, mitochondrial	WT
O75717	WDHD1	WD repeat and HMG-box DNA-binding protein 1	WT
Q96KB5	PBK	Lymphokine-activated killer T-cell-originated protein kinase	WT
P27144	AK4	Adenylate kinase 4, mitochondrial	WT
E7ESP9	NEFM	160 kDa neurofilament protein	WT, C_S
Q9Y237	PIN4	Peptidyl-prolyl cis-trans isomerase NIMA-interacting 4	WT
F8WB06	ATXN2	Ataxin-2	WT, C_S
P54578	USP14	Ubiquitin carboxyl-terminal hydrolase 14	WT, C_S
P20042	EIF2S2	Eukaryotic translation initiation factor 2 subunit 2	WT, C_S
Q8WWK9	CKAP2	Cytoskeleton-associated protein 2	WT
P52948	NUP98	Nuclear pore complex protein Nup98-Nup96	WT
Q07666	KHDRBS1	KH domain-containing, RNA-binding, signal transduction-associated protein 1	WT, C_S
P46013	MKI67	Proliferation marker protein Ki-67	WT
P55084	HADHB	Trifunctional enzyme subunit beta, mitochondrial	WT, C_S
P18031	PTPN1	Tyrosine-protein phosphatase non-receptor type 1	WT
Q15654	TRIP6	Thyroid receptor-interacting protein 6	WT, C_S
Q9Y2Z4	YARS2	Tyrosine--tRNA ligase, mitochondrial	WT
Q14258	TRIM25	E3 ubiquitin/ISG15 ligase TRIM25	WT
O00425	IGF2BP3	Insulin-like growth factor 2 mRNA-binding protein 3	WT, C_S
P35659	DEK	Protein DEK	WT
O75592	MYCBP2	E3 ubiquitin-protein ligase MYCBP2	WT
O00273	DFFA	DNA fragmentation factor subunit alpha	WT
Q9H2U1	DHX36	ATP-dependent DNA/RNA helicase DHX36	WT
P29558	RBMS1	RNA-binding motif, single-stranded-interacting protein 1	WT
Q9BXP5	SRRT	Serrate RNA effector molecule homolog	WT
Q14974	KPNB1	Importin subunit beta-1	WT
Q96RP9	GFM1	Elongation factor G, mitochondrial	WT, C_S
Q02252	ALDH6A1	Methylmalonate-semialdehyde dehydrogenase [acylating], mitochondrial	WT, C_S
A0A024R4E5	HDLBP	High density lipoprotein binding protein	WT, C_S
Q9GZS1	POLR1E	DNA-directed RNA polymerase I subunit RPA49	WT
P38432	COIL	Coilin	WT
Q9ULT8	HECTD1	E3 ubiquitin-protein ligase HECTD1	WT
Q13838	DDX39B	Spliceosome RNA helicase DDX39B	WT
Q71RC2	LARP4	La-related protein 4	WT, C_S
Q9UGI8	TES	Testin	WT
Q02543	RPL18A	60S ribosomal protein L18a	WT
P78344	EIF4G2	Eukaryotic translation initiation factor 4 gamma 2	WT, C_S
P60174	TPI1	Triosephosphate isomerase	WT
O76003	GLRX3	Glutaredoxin-3	WT
O43252	PAPSS1	Bifunctional 3'-phosphoadenosine 5'-phosphosulfate synthase 1	WT
P55010	EIF5	Eukaryotic translation initiation factor 5	WT
Q9UQN3	CHMP2B	Charged multivesicular body protein 2b	WT
Q14677	CLINT1	Clathrin interactor 1	WT
Q13283	G3BP1	Ras GTPase-activating protein-binding protein 1	WT

P35249	RFC4	Replication factor C subunit 4	WT
Q9Y5X1	SNX9	Sorting nexin-9	WT
Q9NYJ8	TAB2	TGF-beta-activated kinase 1 and MAP3K7-binding protein 2	WT
P19367	HK1	Hexokinase-1	WT, C_S
Q9UNE7	STUB1	E3 ubiquitin-protein ligase CHIP	WT, C_S
E9PB90	HK2	Hexokinase	WT
Q7Z6Z7	HUWE1	E3 ubiquitin-protein ligase HUWE1	WT, C_S
F6T1Q0	PDE12	2',5'-phosphodiesterase 12	WT
Q5JTZ9	AARS2	Alanine--tRNA ligase, mitochondrial	WT
O14497	ARID1A	AT-rich interactive domain-containing protein 1A	WT
Q86U42	PABPN1	Polyadenylate-binding protein 2	WT
P37802	TAGLN2	Transgelin-2	WT, C_S
Q9BVJ6	UTP14A	U3 small nucleolar RNA-associated protein 14 homolog A	WT
Q8N163	CCAR2	Cell cycle and apoptosis regulator protein 2	WT
Q86VS8	HOOK3	Protein Hook homolog 3	WT
P39023	RPL3	60S ribosomal protein L3	WT, C_S
Q14161	GIT2	ARF GTPase-activating protein GIT2	WT
Q86UK7	ZNF598	E3 ubiquitin-protein ligase ZNF598	WT
P04637	TP53	Cellular tumor antigen p53	WT, C_S
O95453	PARN	Poly(A)-specific ribonuclease PARN	WT
Q86YP4	GATAD2A	Transcriptional repressor p66-alpha	WT
P22307	SCP2	Non-specific lipid-transfer protein	WT, C_S
Q15042	RAB3GAP1	Rab3 GTPase-activating protein catalytic subunit	WT, C_S
P23246	SFPQ	Splicing factor, proline- and glutamine-rich	WT
P00519	ABL1	Tyrosine-protein kinase ABL1	WT
Q9UI30	TRMT112	Multifunctional methyltransferase subunit TRM112-like protein	WT
P26373	RPL13	60S ribosomal protein L13	WT
A0A087WVZ9	POLR2E	DNA-directed RNA polymerase II subunit E	WT
M0R0F0	RPS5	40S ribosomal protein S5	WT, C_S
Q86WJ1	CHD1L	Chromodomain-helicase-DNA-binding protein 1-like	WT
Q14151	SAFB2	Scaffold attachment factor B2	WT, C_S
P28838	LAP3	Cytosol aminopeptidase	WT, C_S
P46777	RPL5	60S ribosomal protein L5	WT
O95782	AP2A1	AP-2 complex subunit alpha-1	WT, C_S
Q9H3U1	UNC45A	Protein unc-45 homolog A	WT
Q9H0H5	RACGAP1	Rac GTPase-activating protein 1	WT
Q01081	U2AF1	Splicing factor U2AF 35 kDa subunit	WT, C_S
O95239	KIF4A	Chromosome-associated kinesin KIF4A	WT
P12277	CKB	Creatine kinase B-type	WT
A0A087WY71	AP2M1	AP-2 complex subunit mu	WT
P55809	OXCT1	Succinyl-CoA:3-ketoacid coenzyme A transferase 1, mitochondrial	WT, C_S
C9JP00	MBNL1	Muscleblind-like protein 1	WT
P52732	KIF11	Kinesin-like protein KIF11	WT
Q14204	DYNC1H1	Cytoplasmic dynein 1 heavy chain 1	WT, C_S
Q13509	TUBB3	Tubulin beta-3 chain	WT, C_S
P46063	RECQL	ATP-dependent DNA helicase Q1	WT
P51114	FXR1	Fragile X mental retardation syndrome-related protein 1	WT, C_S
Q5HYI8	RABL3	Rab-like protein 3	WT
P42166	TMPO	Lamina-associated polypeptide 2, isoform alpha	WT
Q8TD19	NEK9	Serine/threonine-protein kinase Nek9	WT
Q7Z4H3	HDDC2	5'-deoxynucleotidase HDDC2	WT
Q9HD26	GOPC	Golgi-associated PDZ and coiled-coil motif-containing protein	WT, C_S
Q53H96	PYCR3	Pyrroline-5-carboxylate reductase 3	WT
Q9NPI6	DCP1A	mRNA-decapping enzyme 1A	WT
Q9BYN8	MRPS26	28S ribosomal protein S26, mitochondrial	WT
Q9NYZ3	GTSE1	G2 and S phase-expressed protein 1	WT
O94927	HAUS5	HAUS augmin-like complex subunit 5	WT
P57740	NUP107	Nuclear pore complex protein Nup107	WT, C_S
P54920	NAPA	Alpha-soluble NSF attachment protein	WT
P17252	PRKCA	Protein kinase C alpha type	WT
F8W8R3	POLD2	DNA polymerase delta subunit 2	WT
Q9H814	PHAX	Phosphorylated adapter RNA export protein	WT
P15170	GSPT1	Eukaryotic peptide chain release factor GTP-binding subunit ERF3A	WT, C_S
O43837	IDH3B	Isocitrate dehydrogenase [NAD] subunit beta, mitochondrial	WT, C_S
Q14966	ZNF638	Zinc finger protein 638	WT
Q7RTV0	PHF5A	PHD finger-like domain-containing protein 5A	WT, C_S
P53597	SUCLG1	Succinate--CoA ligase [ADP/GDP-forming] subunit alpha, mitochondrial	WT
Q9NR30	DDX21	Nucleolar RNA helicase 2	WT
E9PQV9	DCUN1D5	DCN1-like protein	WT
O00231	PSMD11	26S proteasome non-ATPase regulatory subunit 11	WT
P25786	PSMA1	Proteasome subunit alpha type-1	WT
P51570	GALK1	Galactokinase	WT
Q8NB90	SPATA5	ATPase family protein 2 homolog	WT

A0A3B3IRP5	CDC73	Parafibromin	WT, C,S
Q9H2P0	ADNP	Activity-dependent neuroprotector homeobox protein	WT
Q13464	ROCK1	Rho-associated protein kinase 1	WT
Q52LJ0	FAM98B	Protein FAM98B	WT, C,S
Q15233	NONO	Non-POU domain-containing octamer-binding protein	WT
Q9P2J5	LARS1	Leucine--tRNA ligase, cytoplasmic	WT, C,S
P60228	EIF3E	Eukaryotic translation initiation factor 3 subunit E	WT
C9JZR2	CTNND1	Catenin delta-1	WT, C,S
P49959	MRE11	Double-strand break repair protein MRE11	WT
P33240	CSTF2	Cleavage stimulation factor subunit 2	WT
Q16513	PKN2	Serine/threonine-protein kinase N2	WT, C,S
P15880	RPS2	40S ribosomal protein S2	WT, C,S
O43264	ZW10	Centromere/kinetochore protein zw10 homolog	WT
Q08752	PPID	Peptidyl-prolyl cis-trans isomerase D	WT
P35221	CTNNA1	Catenin alpha-1	WT
Q14669	TRIP12	E3 ubiquitin-protein ligase TRIP12	WT
P46778	RPL21	60S ribosomal protein L21	WT, C,S
P50213	IDH3A	Isocitrate dehydrogenase [NAD] subunit alpha, mitochondrial	WT
Q8N1G4	LRRC47	Leucine-rich repeat-containing protein 47	WT, C,S
O43237	DYNC1LI2	Cytoplasmic dynein 1 light intermediate chain 2	WT
Q14152	EIF3A	Eukaryotic translation initiation factor 3 subunit A	WT, C,S
Q6P2E9	EDC4	Enhancer of mRNA-decapping protein 4	WT, C,S
P23919	DTYMK	Thymidylate kinase	WT, C,S
P63272	SUPT4H1	Transcription elongation factor SPT4	WT, C,S
P52597	HNRNPF	Heterogeneous nuclear ribonucleoprotein F	WT
Q15785	TOMM34	Mitochondrial import receptor subunit TOM34	WT
P13804	ETFA	Electron transfer flavoprotein subunit alpha, mitochondrial	WT, C,S
Q10567	AP1B1	AP-1 complex subunit beta-1	WT, C,S
P47897	QARS1	Glutamine--tRNA ligase	WT, C,S
P62249	RPS16	40S ribosomal protein S16	WT
Q92616	GCN1	eIF-2-alpha kinase activator GCN1	WT
P19525	EIF2AK2	Interferon-induced, double-stranded RNA-activated protein kinase	WT, C,S
Q8NCW5	NAXE	NAD(P)H-hydrate epimerase	WT
Q16527	CSRP2	Cysteine and glycine-rich protein 2	WT, C,S
Q15637	SF1	Splicing factor 1	WT
P31689	DNAJA1	DnaJ homolog subfamily A member 1	WT, C,S
A0A087WXM6	RPL17	60S ribosomal protein L17	WT, C,S
Q9UG54	MAP3K7	Mitogen-activated protein kinase kinase kinase	WT, C,S
Q6Y7W6	GIGYF2	GRB10-interacting GYF protein 2	WT, C,S
P08708	RPS17	40S ribosomal protein S17	WT, C,S
K4DI93	CUL4B	Cullin 4B, isoform CRA_e	WT, C,S
P63010	AP2B1	AP-2 complex subunit beta	WT
Q9NZI8	IGF2BP1	Insulin-like growth factor 2 mRNA-binding protein 1	WT, C,S
P57772	EEFSEC	Selenocysteine-specific elongation factor	WT
Q96AG4	LRRC59	Leucine-rich repeat-containing protein 59	WT, C,S
P43246	MSH2	DNA mismatch repair protein Msh2	WT, C,S
Q13136	PPFIA1	Liprin-alpha-1	WT, C,S
O76021	RSL1D1	Ribosomal L1 domain-containing protein 1	WT, C,S
Q9UNM6	PSMD13	26S proteasome non-ATPase regulatory subunit 13	WT
A0A1B0GWF2	STXBP1	Syntaxin-binding protein 1	WT, C,S
Q08J23	NSUN2	RNA cytosine C(5)-methyltransferase NSUN2	WT, C,S
Q96F86	EDC3	Enhancer of mRNA-decapping protein 3	WT
O75569	PRKRA	Interferon-inducible double-stranded RNA-dependent protein kinase activator A	WT, C,S
A0A087X0K9	TJP1	Tight junction protein ZO-1	WT
J3QR09	RPL19	Ribosomal protein L19	WT, C,S
Q15154	PCM1	Pericentriolar material 1 protein	WT
O60701	UGDH	UDP-glucose 6-dehydrogenase	WT
D6R938	CAMK2D	Calcium/calmodulin-dependent protein kinase	WT
Q13451	FKBP5	Peptidyl-prolyl cis-trans isomerase FKBP5	WT, C,S
P62829	RPL23	60S ribosomal protein L23	WT, C,S
O75874	IDH1	Isocitrate dehydrogenase [NADP] cytoplasmic	WT, C,S
P56545	CTBP2	C-terminal-binding protein 2	WT
P30084	ECHS1	Enoyl-CoA hydratase, mitochondrial	WT, C,S
O75150	RNF40	E3 ubiquitin-protein ligase BRE1B	WT
Q9Y613	FHOD1	FH1/FH2 domain-containing protein 1	WT
H7C5E4	XRN1	5'-3' exoribonuclease 1	WT, C,S
Q15021	NCAPD2	Condensin complex subunit 1	WT
P50995	ANXA11	Annexin A11	WT
O43290	SART1	U4/U6.U5 tri-snRNP-associated protein 1	WT
P30153	PPP2R1A	Serine/threonine-protein phosphatase 2A 65 kDa regulatory subunit A alpha isoform	WT, C,S
Q15555	MAPRE2	Microtubule-associated protein RP/EB family member 2	WT
Q8WYP5	AHCTF1	Protein ELYS	WT, C,S
O43390	HNRNPR	Heterogeneous nuclear ribonucleoprotein R	WT, C,S

Q9Y2Z0	SUGT1	Protein SGT1 homolog	WT, C,S
Q96G46	DUS3L	tRNA-dihydrouridine(47) synthase [NAD(P)(+)]-like	WT
Q9ULX3	NOB1	RNA-binding protein NOB1	WT
Q14847	LASP1	LIM and SH3 domain protein 1	WT
O60783	MRPS14	28S ribosomal protein S14, mitochondrial	WT
P61586	RHOA	Transforming protein RhoA	WT
P08754	GNAI3	Guanine nucleotide-binding protein G(i) subunit alpha	WT, C,S
P49591	SARS1	Serine--tRNA ligase, cytoplasmic	WT
A0A087WY55	VTA1	Chromosome 6 open reading frame 55, isoform CRA_b	WT, C,S
P56192	MARS1	Methionine--tRNA ligase, cytoplasmic	WT
Q5SW79	CEP170	Centrosomal protein of 170 kDa	WT, C,S
Q9Y490	TLN1	Talin-1	WT, C,S
P42765	ACAA2	3-ketoacyl-CoA thiolase, mitochondrial	WT, C,S
Q9BY77	POLDIP3	Polymerase delta-interacting protein 3	WT
P55265	ADAR	Double-stranded RNA-specific adenosine deaminase	WT, C,S
B4DY08	HNRNPC	Heterogeneous nuclear ribonucleoproteins C1/C2	WT
Q92878	RAD50	DNA repair protein RAD50	WT
Q99569	PKP4	Plakophilin-4	WT, C,S
P42704	LRPPRC	Leucine-rich PPR motif-containing protein, mitochondrial	WT, C,S
Q9UPQ9	TNRC6B	Trinucleotide repeat-containing gene 6B protein	WT, C,S
O14654	IRS4	Insulin receptor substrate 4	WT
P33991	MCM4	DNA replication licensing factor MCM4	WT, C,S
Q9UHD8	SEPTIN9	Septin-9	WT
P00568	AK1	Adenylate kinase isoenzyme 1	WT, C,S
Q9BW92	TARS2	Threonine--tRNA ligase, mitochondrial	WT
Q96J01	THOC3	THO complex subunit 3	WT
Q9BXJ9	NAA15	N-alpha-acetyltransferase 15, NatA auxiliary subunit	WT
P46939	UTRN	Utrophin	WT, C,S
P11387	TOP1	DNA topoisomerase 1	WT, C,S
H0YDU8	PPP5C	Serine/threonine-protein phosphatase	WT
P49368	CCT3	T-complex protein 1 subunit gamma	WT, C,S
P18615	NELFE	Negative elongation factor E	WT, C,S
P27708	CAD	CAD protein [Includes: Glutamine-dependent carbamoyl-phosphate synthase	WT, C,S
J3KTA4	DDX5	DEAD box protein 5	WT
P60660	MYL6	Myosin light polypeptide 6	WT, C,S
O95785	WIZ	Protein Wiz	WT
A6NDG6	PGP	Glycerol-3-phosphate phosphatase	WT
P62269	RPS18	40S ribosomal protein S18	WT
A0A0U1RRM6	ENAH	Protein enabled homolog	WT, C,S
P38919	EIF4A3	Eukaryotic initiation factor 4A-III	WT
O75643	SNRNP200	U5 small nuclear ribonucleoprotein 200 kDa helicase	WT
Q9H840	GEMIN7	Gem-associated protein 7	WT, C,S
Q15424	SAFB	Scaffold attachment factor B1	WT
O15160	POLR1C	DNA-directed RNA polymerases I and III subunit RPAC1	WT, C,S
P55795	HNRNPH2	Heterogeneous nuclear ribonucleoprotein H2	WT, C,S
B1AK87	CAPZB	F-actin-capping protein subunit beta	WT, C,S
Q5QJE6	DNTTIP2	Deoxynucleotidyltransferase terminal-interacting protein 2	WT
Q8WXF1	PSPC1	Paraspeckle component 1	WT, C,S
Q9NTI5	PDS5B	Sister chromatid cohesion protein PDS5 homolog B	WT
O00571	DDX3X	ATP-dependent RNA helicase DDX3X	WT
Q8WX93	PALLD	Palladin	WT
Q99497	PARK7	Parkinson disease protein 7	WT, C,S
P62913	RPL11	60S ribosomal protein L11	WT
A0A1C7CYX9	DPYSL2	Dihydropyrimidinase-related protein 2	WT, C,S
P40939	HADHA	Trifunctional enzyme subunit alpha, mitochondrial	WT, C,S
A0A0A0MRM8	MYO6	Unconventional myosin-6	WT, C,S
P29144	TPP2	Tripeptidyl-peptidase 2	WT, C,S
Q9BWF3	RBM4	RNA-binding protein 4	WT
P35658	NUP214	Nuclear pore complex protein Nup214	WT, C,S
F8W0J6	NAP1L1	Nucleosome assembly protein 1-like 1	WT, C,S
O95347	SMC2	Structural maintenance of chromosomes protein 2	WT
Q99613	EIF3C	Eukaryotic translation initiation factor 3 subunit C	WT
P38117	ETFB	Electron transfer flavoprotein subunit beta	WT, C,S
A0A0A6YYL4	CORO7-PAM16	Coronin	WT
O75534	CSDE1	Cold shock domain-containing protein E1	WT
O15226	NKRF	NF-kappa-B-repressing factor	WT
P46776	RPL27A	60S ribosomal protein L27a	WT, C,S
P41252	IARS1	Isoleucine--tRNA ligase, cytoplasmic	WT, C,S
Q9NVH2	INTS7	Integrator complex subunit 7	WT
Q9GZL7	WDR12	Ribosome biogenesis protein WDR12	WT
P55060	CSE1L	Exportin-2	WT, C,S
P25325	MPST	3-mercaptopyruvate sulfurtransferase	WT, C,S
P61758	VBP1	Prefoldin subunit 3	WT

P51572	BCAP31	B-cell receptor-associated protein 31	WT
Q86Y56	DNAAF5	Dynein assembly factor 5, axonemal	WT, C$_2$S
Q13573	SNW1	SNW domain-containing protein 1	WT
P78371	CCT2	T-complex protein 1 subunit beta	WT
Q9P0K7	RAI14	Ankycorbin	WT, C$_2$S
Q9BTY7	HGH1	Protein HGH1 homolog	WT
Q13625	TP53BP2	Apoptosis-stimulating of p53 protein 2	WT
P09525	ANXA4	Annexin A4	WT
P52701	MSH6	DNA mismatch repair protein Msh6	WT, C$_2$S
Q14690	PDCD11	Protein RRP5 homolog	WT
P62633	CNBP	Cellular nucleic acid-binding protein	WT
P13861	PRKAR2A	cAMP-dependent protein kinase type II-alpha regulatory subunit	WT, C$_2$S
Q9BRX2	PELO	Protein pelota homolog	WT, C$_2$S
O60884	DNAJA2	DnaJ homolog subfamily A member 2	WT
P19105	MYL12A	Myosin regulatory light chain 12A	WT, C$_2$S
A0A087WVM4	MTHFD1L	Formyltetrahydrofolate synthetase	WT, C$_2$S
P10606	COX5B	Cytochrome c oxidase subunit 5B, mitochondrial	WT
Q99460	PSMD1	26S proteasome non-ATPase regulatory subunit 1	WT, C$_2$S
B4DLN1	B4DLN1	cDNA FLJ60124, highly similar to Mitochondrial dicarboxylate carrier	WT
Q9NXH9	TRMT1	tRNA	WT
P33176	KIF5B	Kinesin-1 heavy chain	WT, C$_2$S
P26640	VARS1	Valine--tRNA ligase	WT, C$_2$S
Q99959	PKP2	Plakophilin-2	WT, C$_2$S
P40227	CCT6A	T-complex protein 1 subunit zeta	WT
Q9UJU6	DBNL	Drebrin-like protein	WT
P46783	RPS10	40S ribosomal protein S10	WT
P29692	EEF1D	Elongation factor 1-delta	WT, C$_2$S
A0A2R8Y5F1	TSC2	Tuberin	WT
Q9NR45	NANS	Sialic acid synthase	WT, C$_2$S
A0A0G2JNZ2	SCRIB	Protein scribble homolog	WT, C$_2$S
P52272	HNRNPM	Heterogeneous nuclear ribonucleoprotein M	WT, C$_2$S
Q9P2R3	ANKFY1	Rabankyrin-5	WT
O75152	ZC3H11A	Zinc finger CCCH domain-containing protein 11A	WT, C$_2$S
O75792	RNASEH2A	Ribonuclease H2 subunit A	WT, C$_2$S
P62906	RPL10A	60S ribosomal protein L10a	WT, C$_2$S
A0A2R8Y880	RBBP6	E3 ubiquitin-protein ligase RBBP6	WT
P36578	RPL4	60S ribosomal protein L4	WT
Q9BZE9	ASPSCR1	Tether containing UBX domain for GLUT4	WT, C$_2$S
P52294	KPNA1	Importin subunit alpha-5	WT, C$_2$S
G5EA36	CDC27	Cell division cycle 27, isoform CRA_c	WT
Q9Y6G9	DYNC1LI1	Cytoplasmic dynein 1 light intermediate chain 1	WT, C$_2$S
Q13155	AIMP2	Aminoacyl tRNA synthase complex-interacting multifunctional protein 2	WT
P09110	ACAA1	3-ketoacyl-CoA thiolase, peroxisomal	WT, C$_2$S
P11172	UMPS	Uridine 5'-monophosphate synthase	WT
M0R3C3	TECR	Very-long-chain enoyl-CoA reductase	WT, C$_2$S
Q5TFE4	NT5DC1	5'-nucleotidase domain-containing protein 1	WT
P34897	SHMT2	Serine hydroxymethyltransferase, mitochondrial	WT
Q8IWB7	WDFY1	WD repeat and FYVE domain-containing protein 1	WT
Q9UBT2	UBA2	SUMO-activating enzyme subunit 2	WT, C$_2$S
Q8WVJ2	NUDCD2	NudC domain-containing protein 2	WT
Q7Z417	NUFIP2	Nuclear fragile X mental retardation-interacting protein 2	WT
Q02790	FKBP4	Peptidyl-prolyl cis-trans isomerase FKBP4	WT, C$_2$S
Q9NSV4	DIAPH3	Protein diaphanous homolog 3	WT
P07814	EPRS1	Bifunctional glutamate/proline--tRNA ligase	WT, C$_2$S
Q16658	FSCN1	Fascin	WT, C$_2$S
Q13148	TARDBP	TAR DNA-binding protein 43	WT
P53621	COPA	Coatomer subunit alpha	WT, C$_2$S
Q9Y3I0	RTCB	RNA-splicing ligase RtcB homolog	WT, C$_2$S
Q9BT25	HAUS8	HAUS augmin-like complex subunit 8	WT
O00399	DCTN6	Dynactin subunit 6	WT, C$_2$S
O43159	RRP8	Ribosomal RNA-processing protein 8	WT, C$_2$S
Q8IYI6	EXOC8	Exocyst complex component 8	WT, C$_2$S
A0A140T9R1	FLOT1	Flotillin	WT
K7EJL1	AP1M1	AP-1 complex subunit mu-1	WT, C$_2$S
Q92973	TNPO1	Transportin-1	WT, C$_2$S
Q5BKZ1	ZNF326	DBIRD complex subunit ZNF326	WT
Q15084	PDIA6	Protein disulfide-isomerase A6	WT, C$_2$S
C9JRJ5	LIMD1	LIM domain-containing protein 1	WT, C$_2$S
Q9Y2L1	DIS3	Exosome complex exonuclease RRP44	WT, C$_2$S
A0A0C4DGA6	HLTF	Helicase-like transcription factor	WT
Q14157	UBAP2L	Ubiquitin-associated protein 2-like	WT, C$_2$S
Q9Y5A9	YTHDF2	YTH domain-containing family protein 2	WT, C$_2$S
P25685	DNAJB1	DnaJ homolog subfamily B member 1	WT, C$_2$S

P50502	ST13	Hsc70-interacting protein	WT, C$_2$S
M0QXL5	FBL	rRNA 2'-O-methyltransferase fibrillarin	WT, C$_2$S
Q8WUM4	PDCD6IP	Programmed cell death 6-interacting protein	WT, C$_2$S
Q9UKF6	CPSF3	Cleavage and polyadenylation specificity factor subunit 3	WT
P62316	SNRPD2	Small nuclear ribonucleoprotein Sm D2	WT, C$_2$S
Q13435	SF3B2	Splicing factor 3B subunit 2	WT
P11177	PDHB	Pyruvate dehydrogenase E1 component subunit beta, mitochondrial	WT
Q9UQ35	SRRM2	Serine/arginine repetitive matrix protein 2	WT
O94979	SEC31A	Protein transport protein Sec31A	WT, C$_2$S
P37108	SRP14	Signal recognition particle 14 kDa protein	WT, C$_2$S
Q7Z406	MYH14	Myosin-14	WT, C$_2$S
G3V1C3	API5	Apoptosis inhibitor 5	WT, C$_2$S
P13807	GYS1	Glycogen [starch] synthase, muscle	WT, C$_2$S
E9PF10	NUP155	Nuclear pore complex protein Nup155	WT, C$_2$S
Q1KMD3	HNRNPUL2	Heterogeneous nuclear ribonucleoprotein U-like protein 2	WT, C$_2$S
P41240	CSK	Tyrosine-protein kinase CSK	WT, C$_2$S
O15020	SPTBN2	Spectrin beta chain, non-erythrocytic 2	WT
P35250	RFC2	Replication factor C subunit 2	WT
Q8WUH6	TMEM263	Transmembrane protein 263	WT, C$_2$S
P46779	RPL28	60S ribosomal protein L28	WT, C$_2$S
Q9BSD7	NTPCR	Cancer-related nucleoside-triphosphatase	WT
Q06210	GFPT1	Glutamine--fructose-6-phosphate aminotransferase [isomerizing] 1	WT
Q2TAL8	QRICH1	Glutamine-rich protein 1	WT
Q9BQ69	MACROD1	ADP-ribose glycohydrolase MACROD1	WT, C$_2$S
P48444	ARCN1	Coatomer subunit delta	WT, C$_2$S
Q16204	CCDC6	Coiled-coil domain-containing protein 6	WT, C$_2$S
Q15031	LARS2	Probable leucine--tRNA ligase, mitochondrial	WT
Q06124	PTPN11	Tyrosine-protein phosphatase non-receptor type 11	WT, C$_2$S
P14866	HNRNPL	Heterogeneous nuclear ribonucleoprotein L	WT
X1WI28	RPL10	60S ribosomal protein L10	WT, C$_2$S
Q9UGV2	NDRG3	Protein NDRG3	WT, C$_2$S
O95336	PGLS	6-phosphogluconolactonase	WT, C$_2$S
Q9C0C2	TNKS1BP1	182 kDa tankyrase-1-binding protein	WT, C$_2$S
Q07021	C1QBP	Complement component 1 Q subcomponent-binding protein, mitochondrial	WT, C$_2$S
P18583	SON	Protein SON	WT
Q6YN16	HSDL2	Hydroxysteroid dehydrogenase-like protein 2	WT, C$_2$S
Q92665	MRPS31	28S ribosomal protein S31, mitochondrial	WT
Q8IZ83	ALDH16A1	Aldehyde dehydrogenase family 16 member A1	WT
P62917	RPL8	60S ribosomal protein L8	WT
Q13618	CUL3	Cullin-3	WT
P31948	STIP1	Stress-induced-phosphoprotein 1	WT, C$_2$S
Q9HC35	EML4	Echinoderm microtubule-associated protein-like 4	WT, C$_2$S
P19022	CDH2	Cadherin-2	WT
B4DDF4	CNN2	Calponin	WT, C$_2$S
Q99426	TBCB	Tubulin-folding cofactor B	WT
Q5JXI8	FHL1	Four and a half LIM domains protein 1	WT, C$_2$S
Q9UKM9	RALY	RNA-binding protein Raly	WT, C$_2$S
P78347	GTF2I	General transcription factor II-I	WT
O95861	BPNT1	3'(2'),5'-bisphosphate nucleotidase 1	WT, C$_2$S
P50991	CCT4	T-complex protein 1 subunit delta	WT, C$_2$S
Q92597	NDRG1	Protein NDRG1	WT
A0A087X1A5	STAU1	Double-stranded RNA-binding protein Staufen homolog 1	WT, C$_2$S
P09622	DLD	Dihydrolipoyl dehydrogenase, mitochondrial	WT
O75131	CPNE3	Copine-3	WT, C$_2$S
P61158	ACTR3	Actin-related protein 3	WT, C$_2$S
O00267	SUPT5H	Transcription elongation factor SPT5	WT
P18858	LIG1	DNA ligase 1	WT
Q53EL6	PDCD4	Programmed cell death protein 4	WT
Q9H0E2	TOLLIP	Toll-interacting protein	WT
P39748	FEN1	Flap endonuclease 1	WT, C$_2$S
Q15750	TAB1	TGF-beta-activated kinase 1 and MAP3K7-binding protein 1	WT, C$_2$S
C9J4Z3	RPL37A	60S ribosomal protein L37a	WT
Q05048	CSTF1	Cleavage stimulation factor subunit 1	WT
Q00610	CLTC	Clathrin heavy chain 1	WT, C$_2$S
Q12904	AIMP1	Aminoacyl tRNA synthase complex-interacting multifunctional protein 1	WT, C$_2$S
Q96HC4	PDLIM5	PDZ and LIM domain protein 5	WT, C$_2$S
O43660	PLRG1	Pleiotropic regulator 1	WT, C$_2$S
O14980	XPO1	Exportin-1	WT
P53396	ACLY	ATP-citrate synthase	WT
Q9BV20	MRI1	Methylthioribose-1-phosphate isomerase	WT, C$_2$S
Q8IWS0	PHF6	PHD finger protein 6	WT, C$_2$S
P30520	ADSS2	Adenylosuccinate synthetase isozyme 2	WT, C$_2$S
Q14126	DSG2	Desmoglein-2	WT, C$_2$S

Q9BUF5	TUBB6	Tubulin beta-6 chain	WT, C$_2$S
P26368	U2AF2	Splicing factor U2AF 65 kDa subunit	WT, C$_2$S
O95232	LUC7L3	Luc7-like protein 3	WT
P27540	ARNT	Aryl hydrocarbon receptor nuclear translocator	WT, C$_2$S
Q2TAM5	RELA	RELA protein	WT, C$_2$S
F2Z2T2	XPA	DNA repair protein-complementing XP-A cells	WT
O94906	PRPF6	Pre-mRNA-processing factor 6	WT, C$_2$S
E7EPN9	PRRC2C	Protein PRRC2C	WT, C$_2$S
Q15003	NCAPH	Condensin complex subunit 2	WT, C$_2$S
Q9UPT5	EXOC7	Exocyst complex component 7	WT
P26639	TARS1	Threonine--tRNA ligase 1, cytoplasmic	WT
Q9UQ80	PA2G4	Proliferation-associated protein 2G4	WT, C$_2$S
O43615	TIMM44	Mitochondrial import inner membrane translocase subunit TIM44	WT
Q12849	GRSF1	G-rich sequence factor 1	WT, C$_2$S
P63241	EIF5A	Eukaryotic translation initiation factor 5A-1	WT, C$_2$S
B4E1N1	ARMC6	Armadillo repeat-containing protein 6	WT, C$_2$S
P46459	NSF	Vesicle-fusing ATPase	WT, C$_2$S
P16615	ATP2A2	Sarcoplasmic/endoplasmic reticulum calcium ATPase 2	WT, C$_2$S
P11388	TOP2A	DNA topoisomerase 2-alpha	WT, C$_2$S
Q5UIP0	RIF1	Telomere-associated protein RIF1	WT
Q15008	PSMD6	26S proteasome non-ATPase regulatory subunit 6	WT
Q9BR76	CORO1B	Coronin-1B	WT, C$_2$S
Q15075	EEA1	Early endosome antigen 1	WT, C$_2$S
O15294	OGT	UDP-N-acetylglucosamine--peptide N-acetylglucosaminyltransferase 110 kDa subunit	WT
P55884	EIF3B	Eukaryotic translation initiation factor 3 subunit B	WT, C$_2$S
O60684	KPNA6	Importin subunit alpha-7	WT, C$_2$S
F5H6E2	MYO1C	Unconventional myosin-Ic	WT, C$_2$S
Q5VYK3	ECPAS	Proteasome adapter and scaffold protein ECM29	WT, C$_2$S
Q13045	FLII	Protein flightless-1 homolog	WT, C$_2$S
Q9NWH9	SLTM	SAFB-like transcription modulator	WT, C$_2$S
Q8TAT6	NPLOC4	Nuclear protein localization protein 4 homolog	WT, C$_2$S
Q9NSD9	FARSB	Phenylalanine--tRNA ligase beta subunit	WT, C$_2$S
Q8ND24	RNF214	RING finger protein 214	WT
E7EVA0	MAP4	Microtubule-associated protein	WT, C$_2$S
Q9UHB6	LIMA1	LIM domain and actin-binding protein 1	WT, C$_2$S
Q8WWQ0	PHIP	PH-interacting protein	WT, C$_2$S
Q6IAA8	LAMTOR1	Ragulator complex protein LAMTOR1	WT, C$_2$S
A0A2R8Y855	SMARCE1	SWI/SNF-related matrix-associated actin-dependent regulator of chromatin subfamily E member 1	WT, C$_2$S
Q7Z478	DHX29	ATP-dependent RNA helicase DHX29	WT
P49327	FASN	Fatty acid synthase	WT
O15371	EIF3D	Eukaryotic translation initiation factor 3 subunit D	WT, C$_2$S
Q9HCD5	NCOA5	Nuclear receptor coactivator 5	WT
O15047	SETD1A	Histone-lysine N-methyltransferase SETD1A	WT
P12004	PCNA	Proliferating cell nuclear antigen	WT, C$_2$S
Q9Y3S2	ZNF330	Zinc finger protein 330	WT, C$_2$S
P42696	RBM34	RNA-binding protein 34	WT, C$_2$S
A0A0G2JH68	DIAPH1	Protein diaphanous homolog 1	WT, C$_2$S
Q5JSZ5	PRRC2B	Protein PRRC2B	WT, C$_2$S
O00487	PSMD14	26S proteasome non-ATPase regulatory subunit 14	WT, C$_2$S
Q09666	AHNAK	Neuroblast differentiation-associated protein AHNAK	WT, C$_2$S
Q14C86	GAPVD1	GTPase-activating protein and VPS9 domain-containing protein 1	WT, C$_2$S
Q8ND83	SLAIN1	SLAIN motif-containing protein 1	WT, C$_2$S
Q86TB9	PATL1	Protein PAT1 homolog 1	WT, C$_2$S
P30154	PPP2R1B	Serine/threonine-protein phosphatase 2A 65 kDa regulatory subunit A beta isoform	WT, C$_2$S
Q8IY81	FTSJ3	pre-rRNA 2'-O-ribose RNA methyltransferase FTSJ3	WT, C$_2$S
Q9BVP2	GNL3	Guanine nucleotide-binding protein-like 3	WT, C$_2$S
P62701	RPS4X	40S ribosomal protein S4, X isoform	WT, C$_2$S
Q9Y5Y2	NUBP2	Cytosolic Fe-S cluster assembly factor NUBP2	WT, C$_2$S
P48634	PRRC2A	Protein PRRC2A	WT, C$_2$S
Q9H7E9	C8orf33	UPF0488 protein C8orf33	WT, C$_2$S
Q9Y6Y8	SEC23IP	SEC23-interacting protein	WT, C$_2$S
Q9C0C9	UBE2O	(E3-independent) E2 ubiquitin-conjugating enzyme	WT, C$_2$S
P33993	MCM7	DNA replication licensing factor MCM7	WT, C$_2$S
P22102	GART	Trifunctional purine biosynthetic protein adenosine-3 [Includes: Phosphoribosylamine--glycine ligase	WT, C$_2$S
O00170	AIP	AH receptor-interacting protein	WT, C$_2$S
Q8IWZ3	ANKHD1	Ankyrin repeat and KH domain-containing protein 1	WT, C$_2$S
P51452	DUSP3	Dual specificity protein phosphatase 3	WT, C$_2$S
Q9NQT5	EXOSC3	Exosome complex component RRP40	WT, C$_2$S
O94826	TOMM70	Mitochondrial import receptor subunit TOM70	WT, C$_2$S
Q16543	CDC37	Hsp90 co-chaperone Cdc37	WT, C$_2$S
Q9UMS4	PRPF19	Pre-mRNA-processing factor 19	WT, C$_2$S
Q9UPN7	PPP6R1	Serine/threonine-protein phosphatase 6 regulatory subunit 1	WT, C$_2$S
Q9Y450	HBS1L	HBS1-like protein	WT, C$_2$S

H0Y5D5	CIZ1	Cip1-interacting zinc finger protein	WT, C$_2$S
E9PKP7	UBTF	Nucleolar transcription factor 1	WT, C$_2$S
Q9BSH4	TACO1	Translational activator of cytochrome c oxidase 1	WT, C$_2$S
O60832	DKC1	H/ACA ribonucleoprotein complex subunit DKC1	WT, C$_2$S
Q9NY93	DDX56	Probable ATP-dependent RNA helicase DDX56	WT, C$_2$S
Q13347	EIF3I	Eukaryotic translation initiation factor 3 subunit I	WT, C$_2$S
O95573	ACSL3	Long-chain-fatty-acid--CoA ligase 3	WT, C$_2$S
Q15370	ELOB	Elongin-B	C$_2$S
P62244	RPS15A	40S ribosomal protein S15a	WT, C$_2$S
Q00796	SORD	Sorbitol dehydrogenase	WT, C$_2$S
E9PGZ1	CALD1	Caldesmon	C$_2$S
P30566	ADSL	Adenylosuccinate lyase	WT, C$_2$S
P49736	MCM2	DNA replication licensing factor MCM2	WT, C$_2$S
Q15126	PMVK	Phosphomevalonate kinase	WT, C$_2$S
Q9BY44	EIF2A	Eukaryotic translation initiation factor 2A	C$_2$S
P25205	MCM3	DNA replication licensing factor MCM3	WT, C$_2$S
P55735	SEC13	Protein SEC13 homolog	WT, C$_2$S
Q9BWD1	ACAT2	Acetyl-CoA acetyltransferase, cytosolic	WT, C$_2$S
Q9UN86	G3BP2	Ras GTPase-activating protein-binding protein 2	WT, C$_2$S
Q9H0D6	XRN2	5'-3' exoribonuclease 2	WT, C$_2$S
O95816	BAG2	BAG family molecular chaperone regulator 2	WT, C$_2$S
Q8N0X7	SPART	Spartin	WT, C$_2$S
P62333	PSMC6	26S proteasome regulatory subunit 10B	WT, C$_2$S
Q96C36	PYCR2	Pyrroline-5-carboxylate reductase 2	WT, C$_2$S
Q8IWX8	CHERP	Calcium homeostasis endoplasmic reticulum protein	WT, C$_2$S
C9J0J7	PFN2	Profilin	C$_2$S
Q16822	PCK2	Phosphoenolpyruvate carboxykinase [GTP], mitochondrial	WT, C$_2$S
Q13144	EIF2B5	Translation initiation factor eIF-2B subunit epsilon	WT, C$_2$S
P45974	USP5	Ubiquitin carboxyl-terminal hydrolase 5	WT, C$_2$S
Q15417	CNN3	Calponin-3	WT, C$_2$S
A0A087WTZ5	UBXN1	UBX domain-containing protein 1	WT, C$_2$S
O43395	PRPF3	U4/U6 small nuclear ribonucleoprotein Prp3	WT, C$_2$S
Q8NCA5	FAM98A	Protein FAM98A	WT, C$_2$S
P27694	RPA1	Replication protein A 70 kDa DNA-binding subunit	WT, C$_2$S
Q13526	PIN1	Peptidyl-prolyl cis-trans isomerase NIMA-interacting 1	C$_2$S
P63092	GNAS	Guanine nucleotide-binding protein G(s) subunit alpha isoforms short	C$_2$S
O95747	OXSR1	Serine/threonine-protein kinase OSR1	WT, C$_2$S
P21964	COMT	Catechol O-methyltransferase	WT, C$_2$S
Q3ZCQ8	TIMM50	Mitochondrial import inner membrane translocase subunit TIM50	C$_2$S
Q5T7U1	GTF3C5	General transcription factor 3C polypeptide 5	WT, C$_2$S
Q86V48	LUZP1	Leucine zipper protein 1	WT, C$_2$S
P35579	MYH9	Myosin-9	WT, C$_2$S
P49321	NASP	Nuclear autoantigenic sperm protein	WT, C$_2$S
E5RGR0	LYPLA1	Acyl-protein thioesterase 1	C$_2$S
P54136	RARS1	Arginine--tRNA ligase, cytoplasmic	WT, C$_2$S
P50542	PEX5	Peroxisomal targeting signal 1 receptor	WT, C$_2$S
P54646	PRKAA2	5'-AMP-activated protein kinase catalytic subunit alpha-2	C$_2$S
Q9BZE4	GTPBP4	Nucleolar GTP-binding protein 1	WT, C$_2$S
Q13907	IDI1	Isopentenyl-diphosphate Delta-isomerase 1	WT, C$_2$S
E7ETK0	RPS24	40S ribosomal protein S24	WT, C$_2$S
P35580	MYH10	Myosin-10	WT, C$_2$S
P49588	AARS1	Alanine--tRNA ligase, cytoplasmic	WT, C$_2$S
Q9ULC4	MCTS1	Malignant T-cell-amplified sequence 1	C$_2$S
P52594	AGFG1	Arf-GAP domain and FG repeat-containing protein 1	C$_2$S
Q14247	CTTN	Src substrate cortactin	WT, C$_2$S
P45973	CBX5	Chromobox protein homolog 5	C$_2$S
P52788	SMS	Spermine synthase	WT, C$_2$S
P62195	PSMC5	26S proteasome regulatory subunit 8	WT, C$_2$S
Q9UN37	VPS4A	Vacuolar protein sorting-associated protein 4A	WT, C$_2$S
O75436	VPS26A	Vacuolar protein sorting-associated protein 26A	WT, C$_2$S
P17987	TCP1	T-complex protein 1 subunit alpha	WT, C$_2$S
Q9BTE6	AARSD1	Alanyl-tRNA editing protein Aarsd1	WT, C$_2$S
Q96GD0	PDXP	Pyridoxal phosphate phosphatase	WT, C$_2$S
Q15365	PCBP1	Poly(rC)-binding protein 1	WT, C$_2$S
Q7L0Y3	TRMT10C	tRNA methyltransferase 10 homolog C	WT, C$_2$S
Q9UNY4	TTF2	Transcription termination factor 2	WT, C$_2$S
O95373	IPO7	Importin-7	WT, C$_2$S
P36542	ATP5F1C	ATP synthase subunit gamma, mitochondrial	C$_2$S
Q6ZN17	LIN28B	Protein lin-28 homolog B	C$_2$S
O75934	BCAS2	Pre-mRNA-splicing factor SPF27	C$_2$S
Q99829	CPNE1	Copine-1	C$_2$S
P06132	UROD	Uroporphyrinogen decarboxylase	WT, C$_2$S
Q14166	TTLL12	Tubulin--tyrosine ligase-like protein 12	WT, C$_2$S

P43490	NAMPT	Nicotinamide phosphoribosyltransferase	WT, C, S
Q9BSJ8	ESYT1	Extended synaptotagmin-1	WT, C, S
O43143	DHX15	Pre-mRNA-splicing factor ATP-dependent RNA helicase DHX15	WT, C, S
P22314	UBA1	Ubiquitin-like modifier-activating enzyme 1	WT, C, S
P62241	RPS8	40S ribosomal protein S8	WT, C, S
O43719	HTATSF1	HIV Tat-specific factor 1	WT, C, S
O14893	GEMIN2	Gem-associated protein 2	C, S
P09543	CNP	2',3'-cyclic-nucleotide 3'-phosphodiesterase	WT, C, S
P13489	RNH1	Ribonuclease inhibitor	C, S
Q01469	FABP5	Fatty acid-binding protein 5	WT, C, S
E9PDU5	WDR6	WD repeat-containing protein 6	WT, C, S
Q92797	SYMPK	Symplekin	WT, C, S
Q13428	TCOF1	Treacle protein	WT, C, S
Q4KMP7	TBC1D10B	TBC1 domain family member 10B	WT, C, S
P26358	DNMT1	DNA	C, S
Q5T6F2	UBAP2	Ubiquitin-associated protein 2	WT, C, S
P43487	RANBP1	Ran-specific GTPase-activating protein	C, S
Q92667	AKAP1	A-kinase anchor protein 1, mitochondrial	WT, C, S
P98175	RBM10	RNA-binding protein 10	C, S
P31946	YWHAB	14-3-3 protein beta/alpha	C, S
P13797	PLS3	Plastin-3	WT, C, S
Q9UJC3	HOOK1	Protein Hook homolog 1	WT, C, S
Q9NW82	WDR70	WD repeat-containing protein 70	C, S
P43897	TSFM	Elongation factor Ts, mitochondrial	WT, C, S
Q9Y696	CLIC4	Chloride intracellular channel protein 4	C, S
P40937	RFC5	Replication factor C subunit 5	WT, C, S
P39687	ANP32A	Acidic leucine-rich nuclear phosphoprotein 32 family member A	C, S
Q9BYG3	NIFK	MKI67 FHA domain-interacting nucleolar phosphoprotein	WT, C, S
Q9Y2R4	DDX52	Probable ATP-dependent RNA helicase DDX52	C, S
Q86VP6	CAND1	Cullin-associated NEDD8-dissociated protein 1	WT, C, S
P48643	CCT5	T-complex protein 1 subunit epsilon	WT, C, S
A0A3B3IRI2	CTPS1	CTP synthase	WT, C, S
O00154	ACOT7	Cytosolic acyl coenzyme A thioester hydrolase	WT, C, S
P31939	ATIC	Bifunctional purine biosynthesis protein ATIC	C, S
Q9NQ88	TIGAR	Fructose-2,6-bisphosphatase TIGAR	C, S
Q14318	FKBP8	Peptidyl-prolyl cis-trans isomerase FKBP8	C, S
Q9UHB9	SRP68	Signal recognition particle subunit SRP68	WT, C, S
P51116	FXR2	Fragile X mental retardation syndrome-related protein 2	C, S
Q9UJ83	HACL1	2-hydroxyacyl-CoA lyase 1	C, S
P53618	COPB1	Coatomer subunit beta	WT, C, S
P42566	EPS15	Epidermal growth factor receptor substrate 15	C, S
O75439	PMPCB	Mitochondrial-processing peptidase subunit beta	C, S
G5EA31	SEC24C	Protein transport protein Sec24C	C, S
F8VYE8	PPP1CC	Serine/threonine-protein phosphatase	C, S
Q9NUQ9	CYRIB	CYFIP-related Rac1 interactor B	C, S
Q9BQ67	GRWD1	Glutamate-rich WD repeat-containing protein 1	WT, C, S
G3XAH6	PAPOLA	Poly(A) polymerase	C, S
P84095	RHOG	Rho-related GTP-binding protein RhoG	C, S
Q9NP97	DYNLRB1	Dynein light chain roadblock-type 1	WT, C, S
Q6PKG0	LARP1	La-related protein 1	WT, C, S
Q9HB71	CACYBP	Calcyclin-binding protein	C, S
Q12948	FOXC1	Forkhead box protein C1	WT, C, S
P62753	RPS6	40S ribosomal protein S6	WT, C, S
B7Z7F3	RANBP3	Ran-binding protein 3	WT, C, S
O43795	MYO1B	Unconventional myosin-Ib	C, S
P62258	YWHAE	14-3-3 protein epsilon	WT, C, S
P53384	NUBP1	Cytosolic Fe-S cluster assembly factor NUBP1	C, S
O75663	TIPRL	TIP41-like protein	C, S
P82673	MRPS35	28S ribosomal protein S35, mitochondrial	C, S
P68133	ACTA1	Actin, alpha skeletal muscle	WT, C, S
Q9NQX3	GPHN	Gephyrin [Includes: Molybdopterin adenylyltransferase	C, S
P32322	PYCR1	Pyrroline-5-carboxylate reductase 1, mitochondrial	C, S
Q2TAY7	SMU1	WD40 repeat-containing protein SMU1	C, S
Q96S44	TP53RK	EKC/KEOPS complex subunit TP53RK	C, S
Q9UHD1	CHORDC1	Cysteine and histidine-rich domain-containing protein 1	WT, C, S
Q53H12	AGK	Acylglycerol kinase, mitochondrial	WT, C, S
Q7LBC6	KDM3B	Lysine-specific demethylase 3B	WT, C, S
H0YNW5	DUT	Deoxyuridine 5'-triphosphate nucleotidohydrolase	C, S
P34949	MPI	Mannose-6-phosphate isomerase	C, S
Q16643	DBN1	Drebrin	C, S
Q6P587	FAHD1	Acylpyruvase FAHD1, mitochondrial	WT, C, S
Q8NFC6	BOD1L1	Biorientation of chromosomes in cell division protein 1-like 1	C, S
P42771	CDKN2A	Cyclin-dependent kinase inhibitor 2A	C, S

Q9UBE0	SAE1	SUMO-activating enzyme subunit 1	C, S
Q9UKD2	MRTO4	mRNA turnover protein 4 homolog	WT, C, S
Q9P2I0	CPSF2	Cleavage and polyadenylation specificity factor subunit 2	C, S
A0A024RAC6	ELOA	Elongin-A	C, S
Q96AC1	FERMT2	Fermitin family homolog 2	WT, C, S
A0A0C4DGQ6	RPRD1A	Regulation of nuclear pre-mRNA domain-containing protein 1A	C, S
P35268	RPL22	60S ribosomal protein L22	WT, C, S
Q9Y2U8	LEMD3	Inner nuclear membrane protein Man1	C, S
Q14694	USP10	Ubiquitin carboxyl-terminal hydrolase 10	C, S
O75533	SF3B1	Splicing factor 3B subunit 1	C, S
Q9BPU6	DPYSL5	Dihydropyrimidinase-related protein 5	C, S
E9PLK3	NPEPPS	Aminopeptidase	C, S
A1X283	SH3PXD2B	SH3 and PX domain-containing protein 2B	C, S
Q9Y2X3	NOP58	Nucleolar protein 58	C, S
P55081	MFAP1	Microfibrillar-associated protein 1	C, S
O60343	TBC1D4	TBC1 domain family member 4	C, S
P42285	MTREX	Exosome RNA helicase MTR4	C, S
Q96A33	CCDC47	Coiled-coil domain-containing protein 47	C, S
O14802	POLR3A	DNA-directed RNA polymerase III subunit RPC1	C, S
P63173	RPL38	60S ribosomal protein L38	C, S
P40222	TXLNA	Alpha-taxilin	C, S
Q8WWY3	PRPF31	U4/U6 small nuclear ribonucleoprotein Prp31	C, S
O00178	GTPBP1	GTP-binding protein 1	C, S
Q12955	ANK3	Ankyrin-3	C, S
Q9UHV9	PFDN2	Prefoldin subunit 2	WT, C, S
P62854	RPS26	40S ribosomal protein S26	C, S
O75832	PSMD10	26S proteasome non-ATPase regulatory subunit 10	WT, C, S
O75531	BANF1	Barrier-to-autointegration factor	WT, C, S
Q15061	WDR43	WD repeat-containing protein 43	C, S
Q8NC51	SERBP1	Plasminogen activator inhibitor 1 RNA-binding protein	C, S
Q13185	CBX3	Chromobox protein homolog 3	WT, C, S
O14744	PRMT5	Protein arginine N-methyltransferase 5	WT, C, S
Q96DH6	MSI2	RNA-binding protein Musashi homolog 2	WT, C, S
P11908	PRPS2	Ribose-phosphate pyrophosphokinase 2	C, S
Q96FW1	OTUB1	Ubiquitin thioesterase OTUB1	C, S
Q96P70	IPO9	Importin-9	C, S
Q15645	TRIP13	Pachytene checkpoint protein 2 homolog	C, S
Q9NXF7	DCAF16	DDB1- and CUL4-associated factor 16	C, S
Q32MZ4	LRRFIP1	Leucine-rich repeat flightless-interacting protein 1	WT, C, S
P05198	EIF2S1	Eukaryotic translation initiation factor 2 subunit 1	C, S
Q6P9B6	MEAK7	MTOR-associated protein MEAK7	C, S
O43684	BUB3	Mitotic checkpoint protein BUB3	C, S
P51553	IDH3G	Isocitrate dehydrogenase [NAD] subunit gamma, mitochondrial	C, S
Q9H3K6	BOLA2	BolA-like protein 2	C, S
Q9P258	RCC2	Protein RCC2	C, S
C9J0I9	ZC3HC1	Nuclear-interacting partner of ALK	C, S
Q96F45	ZNF503	Zinc finger protein 503	C, S
P62873	GNB1	Guanine nucleotide-binding protein G(I)/G(S)/G(T) subunit beta-1	C, S
O14929	HAT1	Histone acetyltransferase type B catalytic subunit	C, S
Q6WKZ4	RAB11FIP1	Rab11 family-interacting protein 1	C, S
P46821	MAP1B	Microtubule-associated protein 1B	C, S
Q16576	RBBP7	Histone-binding protein RBBP7	C, S
P27824	CANX	Calnexin	WT, C, S
A0A087X0M4	SLC4A1AP	Kanadaptin	C, S
Q8IYS1	PM20D2	Peptidase M20 domain-containing protein 2	C, S
P11802	CDK4	Cyclin-dependent kinase 4	C, S
Q9Y6A5	TACC3	Transforming acidic coiled-coil-containing protein 3	WT, C, S
O60784	TOM1	Target of Myb protein 1	C, S
Q7L2H7	EIF3M	Eukaryotic translation initiation factor 3 subunit M	C, S
Q9Y262	EIF3L	Eukaryotic translation initiation factor 3 subunit L	C, S
O00148	DDX39A	ATP-dependent RNA helicase DDX39A	C, S
P22061	PCMT1	Protein-L-isoaspartate(D-aspartate) O-methyltransferase	C, S
PRDX2 cysteine-dependent interactors			
Q9BQA1	WDR77	Methylosome protein 50	WT, C, S
Q6FI81	CIAPIN1	Anamorsin	WT
E9PGZ1	CALD1	Caldesmon	WT, C, S
O14744	PRMT5	Protein arginine N-methyltransferase 5	WT, C, S
O14965	AURKA	Aurora kinase A	WT
Q9H3K6	BOLA2	BolA-like protein 2	WT
P48507	GCLM	Glutamate--cysteine ligase regulatory subunit	WT
O60664	PLIN3	Perilipin-3	WT, C, S
Q9NQX3	GPHN	Gephyrin [Includes: Molybdopterin adenylyltransferase	WT, C, S
P10301	RRAS	Ras-related protein R-Ras	WT

Q96KB5	PBK	Lymphokine-activated killer T-cell-originated protein kinase	WT, C, S
Q9UL15	BAG5	BAG family molecular chaperone regulator 5	WT
E7EVA0	MAP4	Microtubule-associated protein	WT, C, S
Q9BTE6	AARSD1	Alanyl-tRNA editing protein Aarsd1	WT
Q5T4K5	CRTC2	CREB-regulated transcription coactivator 2	WT
Q8NC51	SERBP1	Plasminogen activator inhibitor 1 RNA-binding protein	WT, C, S
B4DDF4	CNN2	Calponin	WT
Q9NXV2	KCTD5	BTB/POZ domain-containing protein KCTD5	WT
A0A0A0MRN5	OGFR	Opioid growth factor receptor	WT
Q9Y570	PPME1	Protein phosphatase methylesterase 1	WT, C, S
O00566	MPHOSPH10	U3 small nucleolar ribonucleoprotein protein MPP10	WT
P53985	SLC16A1	Monocarboxylate transporter 1	WT
P35520	CBS	Cystathionine beta-synthase	WT, C, S
Q9H0S4	DDX47	Probable ATP-dependent RNA helicase DDX47	WT
P10599	TXN	Thioredoxin	WT, C, S
Q96IZ0	PAWR	PRKC apoptosis WT1 regulator protein	WT
P45985	MAP2K4	Dual specificity mitogen-activated protein kinase kinase 4	WT
Q13428	TCOF1	Treacle protein	WT, C, S
P85037	FOXK1	Forkhead box protein K1	WT
P07355	ANXA2	Annexin A2	WT, C, S
Q13541	EIF4EBP1	Eukaryotic translation initiation factor 4E-binding protein 1	WT, C, S
Q9ULX6	AKAP8L	A-kinase anchor protein 8-like	WT
O95816	BAG2	BAG family molecular chaperone regulator 2	WT
O96007	MOCS2	Molybdopterin synthase catalytic subunit	WT
Q9HA64	FN3KRP	Ketosamine-3-kinase	WT, C, S
Q15417	CNN3	Calponin-3	WT, C, S
O95104	SCAF4	SR-related and CTD-associated factor 4	WT, C, S
Q15365	PCBP1	Poly(rC)-binding protein 1	WT
Q9P2B4	CTTNBP2NL	CTTNBP2 N-terminal-like protein	WT, C, S
Q12948	FOXC1	Forkhead box protein C1	WT, C, S
Q96F45	ZNF503	Zinc finger protein 503	WT, C, S
O15511	ARPC5	Actin-related protein 2/3 complex subunit 5	WT
Q9NUQ3	TXLNG	Gamma-taxilin	WT, C, S
Q8WYA6	CTNNBL1	Beta-catenin-like protein 1	WT
Q9UI12	ATP6V1H	V-type proton ATPase subunit H	WT
P52888	THOP1	Thimet oligopeptidase	WT, C, S
Q16204	CCDC6	Coiled-coil domain-containing protein 6	WT, C, S
G3XAG1	ZNF512	Zinc finger protein 512	WT
Q9H7E9	C8orf33	UPF0488 protein C8orf33	WT
Q14247	CTTN	Src substrate cortactin	WT, C, S
P82921	MRPS21	28S ribosomal protein S21, mitochondrial	WT
P52907	CAPZA1	F-actin-capping protein subunit alpha-1	WT, C, S
P61758	VBP1	Prefoldin subunit 3	WT, C, S
P49790	NUP153	Nuclear pore complex protein Nup153	WT, C, S
Q8N806	UBR7	Putative E3 ubiquitin-protein ligase UBR7	WT
Q92945	KHSRP	Far upstream element-binding protein 2	WT
O00273	DFFA	DNA fragmentation factor subunit alpha	WT, C, S
P63167	DYNLL1	Dynein light chain 1, cytoplasmic	WT
Q13542	EIF4EBP2	Eukaryotic translation initiation factor 4E-binding protein 2	WT, C, S
Q9UNF1	MAGED2	Melanoma-associated antigen D2	WT, C, S
J3QQZ9	PNPO	Pyridoxal 5'-phosphate synthase	WT
E7EV99	ADD1	Alpha-adducin	WT, C, S
A0A1B0GW38	CBL	E3 ubiquitin-protein ligase CBL	WT, C, S
Q5QPM7	PSMF1	Proteasome inhibitor PI31 subunit	WT, C, S
F5H8D7	XRCC1	DNA repair protein XRCC1	WT, C, S
P26599	PTBP1	Polypyrimidine tract-binding protein 1	WT, C, S
Q16576	RBBP7	Histone-binding protein RBBP7	WT, C, S
Q06124	PTPN11	Tyrosine-protein phosphatase non-receptor type 11	WT, C, S
Q9UHD1	CHORDC1	Cysteine and histidine-rich domain-containing protein 1	WT, C, S
Q8IYS1	PM20D2	Peptidase M20 domain-containing protein 2	WT, C, S
O60826	CCDC22	Coiled-coil domain-containing protein 22	WT, C, S
Q5T6F2	UBAP2	Ubiquitin-associated protein 2	WT, C, S
A0A087WTM1	ROBO1	Roundabout homolog 1	WT, C, S
Q5SW79	CEP170	Centrosomal protein of 170 kDa	WT, C, S
Q7Z434	MAVS	Mitochondrial antiviral-signaling protein	WT, C, S
P49458	SRP9	Signal recognition particle 9 kDa protein	WT
Q9Y3F4	STRAP	Serine-threonine kinase receptor-associated protein	WT, C, S
Q6WKZ4	RAB11FIP1	Rab11 family-interacting protein 1	WT, C, S
P22314	UBA1	Ubiquitin-like modifier-activating enzyme 1	WT, C, S
P49321	NASP	Nuclear autoantigenic sperm protein	WT
Q8WWK9	CKAP2	Cytoskeleton-associated protein 2	WT, C, S
Q96F86	EDC3	Enhancer of mRNA-decapping protein 3	WT, C, S
Q96K76	USP47	Ubiquitin carboxyl-terminal hydrolase 47	WT, C, S

O00629	KPNA4	Importin subunit alpha-3	WT, C, S
Q68EM7	ARHGAP17	Rho GTPase-activating protein 17	WT
Q6PKG0	LARP1	La-related protein 1	WT, C, S
Q8N6M0	OTUD6B	Deubiquitinase OTUD6B	WT, C, S
Q93034	CUL5	Cullin-5	WT, C, S
Q96P47	AGAP3	Arf-GAP with GTPase, ANK repeat and PH domain-containing protein 3	WT
P11413	G6PD	Glucose-6-phosphate 1-dehydrogenase	WT, C, S
Q2NKX8	ERCC6L	DNA excision repair protein ERCC-6-like	WT, C, S
P22234	PAICS	Multifunctional protein ADE2 [Includes: Phosphoribosylaminoimidazole-succinocarboxamide synthase	WT, C, S
Q92783	STAM	Signal transducing adapter molecule 1	WT, C, S
Q86YP4	GATAD2A	Transcriptional repressor p66-alpha	WT, C, S
E7EPN9	PRRC2C	Protein PRRC2C	WT, C, S
P40222	TXLNA	Alpha-taxilin	WT, C, S
P35237	SERPINB6	Serpin B6	WT, C, S
P54646	PRKAA2	5'-AMP-activated protein kinase catalytic subunit alpha-2	WT, C, S
Q9BT25	HAUS8	HAUS augmin-like complex subunit 8	WT, C, S
Q96D09	GPRASP2	G-protein coupled receptor-associated sorting protein 2	WT, C, S
Q9NVP1	DDX18	ATP-dependent RNA helicase DDX18	WT, C, S
A0MZ66	SHTN1	Shootin-1	WT, C, S
P48634	PRRC2A	Protein PRRC2A	WT, C, S
P30740	SERPINB1	Leukocyte elastase inhibitor	WT, C, S
O60832	DKC1	H/ACA ribonucleoprotein complex subunit DKC1	C, S
O14974	PPP1R12A	Protein phosphatase 1 regulatory subunit 12A	WT, C, S
Q13200	PSMD2	26S proteasome non-ATPase regulatory subunit 2	WT, C, S
Q8IWB7	WDFY1	WD repeat and FYVE domain-containing protein 1	WT, C, S
Q6UN15	FIP1L1	Pre-mRNA 3'-end-processing factor FIP1	C, S
Q9UHV9	PFDN2	Prefoldin subunit 2	WT, C, S
C9J0I9	ZC3HC1	Nuclear-interacting partner of ALK	WT, C, S
Q9HCN8	SDF2L1	Stromal cell-derived factor 2-like protein 1	WT, C, S
Q92667	AKAP1	A-kinase anchor protein 1, mitochondrial	WT, C, S
P13797	PLS3	Plastin-3	WT, C, S
Q07666	KHDRBS1	KH domain-containing, RNA-binding, signal transduction-associated protein 1	WT, C, S
Q9ULW0	TPX2	Targeting protein for Xklp2	WT, C, S
P55265	ADAR	Double-stranded RNA-specific adenosine deaminase	C, S
E9PGT1	TSN	Component 3 of promoter of RISC	WT, C, S
Q92769	HDAC2	Histone deacetylase 2	WT, C, S
O00267	SUPT5H	Transcription elongation factor SPT5	C, S
P46939	UTRN	Utrophin	C, S
Q7Z6Z7	HUWE1	E3 ubiquitin-protein ligase HUWE1	WT, C, S
Q92597	NDRG1	Protein NDRG1	C, S
A4D1S0	KLRG2	Killer cell lectin-like receptor subfamily G member 2	WT, C, S
Q9H3S7	PTPN23	Tyrosine-protein phosphatase non-receptor type 23	WT, C, S
O95573	ACSL3	Long-chain-fatty-acid--CoA ligase 3	C, S
Q6P4A7	SFXN4	Sideroflexin-4	C, S
Q9UBT2	UBA2	SUMO-activating enzyme subunit 2	C, S
B1AK87	CAPZB	F-actin-capping protein subunit beta	WT, C, S
Q9NYZ3	GTSE1	G2 and S phase-expressed protein 1	WT, C, S
Q96HC4	PDLIM5	PDZ and LIM domain protein 5	WT, C, S
G8JLH9	STAT3	Signal transducer and activator of transcription	C, S
Q9UN37	VPS4A	Vacuolar protein sorting-associated protein 4A	WT, C, S
Q9H2U2	PPA2	Inorganic pyrophosphatase 2, mitochondrial	WT, C, S
Q5JRA6	MIA3	Transport and Golgi organization protein 1 homolog	WT, C, S
O75223	GGCT	Gamma-glutamylcyclotransferase	WT, C, S
Q7Z4H7	HAUS6	HAUS augmin-like complex subunit 6	C, S
Q9NXF7	DCAF16	DDB1- and CUL4-associated factor 16	WT, C, S
Q2M1P5	KIF7	Kinesin-like protein KIF7	C, S
Q9Y266	NUDC	Nuclear migration protein nudC	WT, C, S
Q14694	USP10	Ubiquitin carboxyl-terminal hydrolase 10	C, S
Q7LBC6	KDM3B	Lysine-specific demethylase 3B	C, S
O75663	TIPRL	TIP41-like protein	WT, C, S
E9PLA9	CAPRIN1	Caprin-1	WT, C, S
O00170	AIP	AH receptor-interacting protein	WT, C, S
Q14240	EIF4A2	Eukaryotic initiation factor 4A-II	WT, C, S
Q9C0C9	UBE2O	(E3-independent) E2 ubiquitin-conjugating enzyme	WT, C, S
O15143	ARPC1B	Actin-related protein 2/3 complex subunit 1B	C, S
Q96T23	RSF1	Remodeling and spacing factor 1	C, S
O60493	SNX3	Sorting nexin-3	C, S
Q9UKX7	NUP50	Nuclear pore complex protein Nup50	C, S
Q92598	HSPH1	Heat shock protein 105 kDa	WT, C, S
S4R3H4	ACIN1	Apoptotic chromatin condensation inducer in the nucleus	C, S
Q8ND82	ZNF280C	Zinc finger protein 280C	C, S
Q9UIG0	BAZ1B	Tyrosine-protein kinase BAZ1B	C, S
Q8NI27	THOC2	THO complex subunit 2	C, S

Q15276	RABEP1	Rab GTPase-binding effector protein 1	C,S
P49903	SEPHS1	Selenide, water dikinase 1	WT, C,S
Q8TAQ2	SMARCC2	SWI/SNF complex subunit SMARCC2	WT, C,S
Q9P258	RCC2	Protein RCC2	WT, C,S
J3KN29	PSMD9	26S proteasome non-ATPase regulatory subunit 9	WT, C,S
O00151	PDLIM1	PDZ and LIM domain protein 1	C,S
P13861	PRKAR2A	cAMP-dependent protein kinase type II-alpha regulatory subunit	C,S
Q5BKZ1	ZNF326	DBIRD complex subunit ZNF326	C,S
Q96KR1	ZFR	Zinc finger RNA-binding protein	C,S
Q9NPH2	ISYNA1	Inositol-3-phosphate synthase 1	WT, C,S
P50213	IDH3A	Isocitrate dehydrogenase [NAD] subunit alpha, mitochondrial	C,S
O60343	TBC1D4	TBC1 domain family member 4	WT, C,S
P49588	AARS1	Alanine--tRNA ligase, cytoplasmic	C,S
A0A3B3ISG5	IDE	Insulin-degrading enzyme	C,S
O43815	STRN	Striatin	C,S
A1X283	SH3PXD2B	SH3 and PX domain-containing protein 2B	C,S
Q6UWP7	LCLAT1	Lysocardiolipin acyltransferase 1	C,S
O95347	SMC2	Structural maintenance of chromosomes protein 2	C,S
P78346	RPP30	Ribonuclease P protein subunit p30	C,S
P63000	RAC1	Ras-related C3 botulinum toxin substrate 1	C,S
Q9NZB2	FAM120A	Constitutive coactivator of PPAR-gamma-like protein 1	C,S
P49750	YLPM1	YLP motif-containing protein 1	C,S
Q8N6T3	ARFGAP1	ADP-ribosylation factor GTPase-activating protein 1	C,S
Q9Y2R9	MRPS7	28S ribosomal protein S7, mitochondrial	C,S
E9PQV9	DCUN1D5	DCN1-like protein	C,S
Q9BXP5	SRRT	Serrate RNA effector molecule homolog	C,S
Q8N3X1	FNBP4	Formin-binding protein 4	WT, C,S
O43143	DHX15	Pre-mRNA-splicing factor ATP-dependent RNA helicase DHX15	WT, C,S
Q9Y5A9	YTHDF2	YTH domain-containing family protein 2	C,S
Q99598	TSNAX	Translin-associated protein X	WT, C,S
P00387	CYB5R3	NADH-cytochrome b5 reductase 3	C,S
P52701	MSH6	DNA mismatch repair protein Msh6	C,S
O94903	PLPBP	Pyridoxal phosphate homeostasis protein	C,S
P42677	RPS27	40S ribosomal protein S27	C,S
Q14739	LBR	Delta(14)-sterol reductase LBR	C,S
A0A024RCR6	BAG6	BCL2-associated athanogene 6	C,S
P51452	DUSP3	Dual specificity protein phosphatase 3	WT, C,S
Q8WVC2	RPS21	40S ribosomal protein S21	WT, C,S
Q9Y295	DRG1	Developmentally-regulated GTP-binding protein 1	C,S
Q6IQ49	SDE2	Replication stress response regulator SDE2	WT, C,S
M0QY97	ZC3H4	Zinc finger CCCH domain-containing protein 4	C,S
Q04917	YWHAH	14-3-3 protein eta	C,S
P52788	SMS	Spermine synthase	C,S
Q96A33	CCDC47	Coiled-coil domain-containing protein 47	C,S
P38159	RBMX	RNA-binding motif protein, X chromosome	C,S
P23588	EIF4B	Eukaryotic translation initiation factor 4B	C,S
A0A087WWP4	RBM15	RNA-binding protein 15	C,S
A0A087WTZ5	UBXN1	UBX domain-containing protein 1	C,S
Q9UQE7	SMC3	Structural maintenance of chromosomes protein 3	WT, C,S
P46821	MAP1B	Microtubule-associated protein 1B	WT, C,S
O95801	TTC4	Tetratricopeptide repeat protein 4	C,S
Q9UJV9	DDX41	Probable ATP-dependent RNA helicase DDX41	C,S
O00487	PSMD14	26S proteasome non-ATPase regulatory subunit 14	C,S
Q8N5F7	NKAP	NF-kappa-B-activating protein	C,S
A0A0A0MRM8	MYO6	Unconventional myosin-6	C,S
P49593	PPM1F	Protein phosphatase 1F	C,S
P25786	PSMA1	Proteasome subunit alpha type-1	C,S
O43809	NUDT21	Cleavage and polyadenylation specificity factor subunit 5	WT, C,S
Q13547	HDAC1	Histone deacetylase 1	WT, C,S
P56385	ATP5ME	ATP synthase subunit e, mitochondrial	C,S
H0YNW5	DUT	Deoxyuridine 5'-triphosphate nucleotidohydrolase	WT, C,S
P11802	CDK4	Cyclin-dependent kinase 4	WT, C,S
P55072	VCP	Transitional endoplasmic reticulum ATPase	C,S
P09936	UCHL1	Ubiquitin carboxyl-terminal hydrolase isozyme L1	C,S
P08240	SRPRA	Signal recognition particle receptor subunit alpha	C,S
P22695	UQCRC2	Cytochrome b-c1 complex subunit 2, mitochondrial	C,S
Q13045	FLII	Protein flightless-1 homolog	C,S
Q9C0C2	TNKS1BP1	182 kDa tankyrase-1-binding protein	WT, C,S
P98175	RBM10	RNA-binding protein 10	C,S
E9PLK3	NPEPPS	Aminopeptidase	C,S
Q8WXF1	PSPC1	Paraspeckle component 1	C,S
P62191	PSMC1	26S proteasome regulatory subunit 4	C,S
Q9GZT9	EGLN1	Egl nine homolog 1	C,S

Q9UPN7	PPP6R1	Serine/threonine-protein phosphatase 6 regulatory subunit 1	C,S
O75533	SF3B1	Splicing factor 3B subunit 1	C,S
Q9BRP1	PDCD2L	Programmed cell death protein 2-like	WT, C,S
Q86V48	LUZP1	Leucine zipper protein 1	WT, C,S
Q15019	SEPTIN2	Septin-2	C,S
Q99504	EYA3	Eyes absent homolog 3	C,S
Q9BWJ5	SF3B5	Splicing factor 3B subunit 5	C,S
A6NGP5	JPT2	Jupiter microtubule-associated homolog 2	WT, C,S
Q9BTE3	MCMBP	Mini-chromosome maintenance complex-binding protein	C,S
Q15046	KARS1	Lysine--tRNA ligase	C,S
Q96GD0	PDXP	Pyridoxal phosphate phosphatase	C,S
P61981	YWHAG	14-3-3 protein gamma	C,S
Q12800	TFCP2	Alpha-globin transcription factor CP2	C,S
Q06203	PPAT	Amidophosphoribosyltransferase	C,S
Q9H773	DCTPP1	dCTP pyrophosphatase 1	WT, C,S
A0A1C7CYX9	DPYSL2	Dihydropyrimidinase-related protein 2	C,S
P19174	PLCG1	1-phosphatidylinositol 4,5-bisphosphate phosphodiesterase gamma-1	WT, C,S
Q14566	MCM6	DNA replication licensing factor MCM6	C,S
Q9UNM6	PSMD13	26S proteasome non-ATPase regulatory subunit 13	C,S
P41214	EIF2D	Eukaryotic translation initiation factor 2D	C,S
H3BRL3	UBFD1	Ubiquitin domain-containing protein UBFD1	C,S
P60228	EIF3E	Eukaryotic translation initiation factor 3 subunit E	C,S
Q9NZL9	MAT2B	Methionine adenosyltransferase 2 subunit beta	C,S
P52732	KIF11	Kinesin-like protein KIF11	C,S
Q96P70	IPO9	Importin-9	C,S
Q14137	BOP1	Ribosome biogenesis protein BOP1	C,S
Q6NUK1	SLC25A24	Calcium-binding mitochondrial carrier protein SCaMC-1	C,S
O43765	SGTA	Small glutamine-rich tetratricopeptide repeat-containing protein alpha	C,S
Q16531	DDB1	DNA damage-binding protein 1	C,S
Q9Y230	RUVBL2	RuvB-like 2	C,S
P06737	PYGL	Glycogen phosphorylase, liver form	C,S
P05023	ATP1A1	Sodium/potassium-transporting ATPase subunit alpha-1	C,S
O14929	HAT1	Histone acetyltransferase type B catalytic subunit	WT, C,S
A0A087WUX8	APOOL	MICOS complex subunit	C,S
Q9Y6Y8	SEC23IP	SEC23-interacting protein	C,S
P58546	MTPN	Myotrophin	C,S
E9PS17	SCYL1	N-terminal kinase-like protein	C,S
P20020	ATP2B1	Plasma membrane calcium-transporting ATPase 1	C,S
O94992	HEXIM1	Protein HEXIM1	C,S
Q32MZ4	LRRFIP1	Leucine-rich repeat flightless-interacting protein 1	WT, C,S
O75381	PEX14	Peroxisomal membrane protein PEX14	C,S
Q15393	SF3B3	Splicing factor 3B subunit 3	C,S
Q8IVM0	CCDC50	Coiled-coil domain-containing protein 50	C,S
P42771	CDKN2A	Cyclin-dependent kinase inhibitor 2A	WT, C,S
O94905	ERLIN2	Erlin-2	C,S
H0YDU8	PPP5C	Serine/threonine-protein phosphatase	C,S
K7EJQ8	HDHD2	Haloacid dehalogenase-like hydrolase domain-containing protein 2	C,S
O43242	PSMD3	26S proteasome non-ATPase regulatory subunit 3	C,S
Q9H936	SLC25A22	Mitochondrial glutamate carrier 1	C,S
P30041	PRDX6	Peroxiredoxin-6	C,S
P15374	UCHL3	Ubiquitin carboxyl-terminal hydrolase isozyme L3	C,S
P29373	CRABP2	Cellular retinoic acid-binding protein 2	C,S
P61106	RAB14	Ras-related protein Rab-14	C,S
P00338	LDHA	L-lactate dehydrogenase A chain	C,S
Q9H6S0	YTHDC2	3'-5' RNA helicase YTHDC2	C,S
Q14C86	GAPVD1	GTPase-activating protein and VPS9 domain-containing protein 1	C,S
A0A0C4DGX4	CUL1	Cullin-1	C,S
Q9UBE0	SAE1	SUMO-activating enzyme subunit 1	C,S
P22570	FDXR	NADPH:adrenodoxin oxidoreductase, mitochondrial	C,S
P31946	YWHAB	14-3-3 protein beta/alpha	C,S
Q9UJZ1	STOML2	Stomatin-like protein 2, mitochondrial	C,S
P22061	PCMT1	Protein-L-isoaspartate(D-aspartate) O-methyltransferase	WT, C,S
Q9H9B4	SFXN1	Sideroflexin-1	C,S
Q9H0U4	RAB1B	Ras-related protein Rab-1B	C,S
P31153	MAT2A	S-adenosylmethionine synthase isoform type-2	C,S
Q6P2Q9	PRPF8	Pre-mRNA-processing-splicing factor 8	C,S
O95684	CEP43	Centrosomal protein 43	C,S
B7Z7F3	RANBP3	Ran-binding protein 3	WT, C,S
P42574	CASP3	Caspase-3	C,S
Q96EA4	SPDL1	Protein Spindly	WT, C,S
Q9UKG1	APPL1	DCC-interacting protein 13-alpha	C,S
F5GZS6	SLC3A2	4F2 cell-surface antigen heavy chain	C,S
P00492	HPRT1	Hypoxanthine-guanine phosphoribosyltransferase	C,S

P06132	UROD	Uroporphyrinogen decarboxylase	C,S
Q9BXJ9	NAA15	N-alpha-acetyltransferase 15, NatA auxiliary subunit	C,S
Q9Y265	RUVBL1	RuvB-like 1	C,S
P62333	PSMC6	26S proteasome regulatory subunit 10B	C,S
P12955	PEPD	Xaa-Pro dipeptidase	WT, C,S
P41250	GARS1	Glycine--tRNA ligase	C,S
Q9NUP9	LIN7C	Protein lin-7 homolog C	C,S
A0A087X054	HYOU1	Hypoxia up-regulated protein 1	C,S
Q9Y6A5	TACC3	Transforming acidic coiled-coil-containing protein 3	WT, C,S
Q9HBH5	RDH14	Retinol dehydrogenase 14	C,S
O60547	GMDS	GDP-mannose 4,6 dehydratase	WT, C,S
P35998	PSMC2	26S proteasome regulatory subunit 7	C,S
Q16512	PKN1	Serine/threonine-protein kinase N1	C,S
Q8NFC6	BOD1L1	Biorientation of chromosomes in cell division protein 1-like 1	WT, C,S
O00165	HAX1	HCLS1-associated protein X-1	C,S
A0AVT1	UBA6	Ubiquitin-like modifier-activating enzyme 6	WT, C,S
P61289	PSME3	Proteasome activator complex subunit 3	C,S
Q9Y3D0	CIAO2B	Cytosolic iron-sulfur assembly component 2B	C,S
Q86WA6	BPHL	Valacyclovir hydrolase	C,S
Q9UBS4	DNAJB11	DnaJ homolog subfamily B member 11	C,S
E9PM92	C11orf58	Small acidic protein	C,S
Q9Y3B7	MRPL11	39S ribosomal protein L11, mitochondrial	C,S
Q49A26	GLYR1	Putative oxidoreductase GLYR1	C,S
A0A087X2B5	BSG	Basigin	C,S
K7ELV2	SEH1L	Nucleoporin SEH1	C,S
P07910	HNRNPC	Heterogeneous nuclear ribonucleoproteins C1/C2	C,S
Q14257	RCN2	Reticulocalbin-2	C,S
O00483	NDUFA4	Cytochrome c oxidase subunit NDUFA4	C,S
PRDX3 cysteine-dependent interactors			
B7WPG3	HNRNPLL	Heterogeneous nuclear ribonucleoprotein L-like	WT
Q14161	GIT2	ARF GTPase-activating protein GIT2	WT
Q9Y4B6	DCAF1	DDB1- and CUL4-associated factor 1	WT, C,S
Q92804	TAF15	TATA-binding protein-associated factor 2N	WT
Q9UBE0	SAE1	SUMO-activating enzyme subunit 1	WT
F8W038	C17orf49	Chromosome 17 open reading frame 49	WT
Q6PKG0	LARP1	La-related protein 1	WT
Q15084	PDIA6	Protein disulfide-isomerase A6	WT, C,S
Q92785	DPF2	Zinc finger protein ubi-d4	WT, C,S
P51148	RAB5C	Ras-related protein Rab-5C	WT, C,S
Q9ULX3	NOB1	RNA-binding protein NOB1	WT, C,S
P04843	RPN1	Dolichyl-diphosphooligosaccharide--protein glycosyltransferase subunit 1	WT
Q86WA6	BPHL	Valacyclovir hydrolase	WT, C,S
A0A0A0MR02	VDAC2	Outer mitochondrial membrane protein porin 2	WT, C,S
O14828	SCAMP3	Secretory carrier-associated membrane protein 3	WT
Q5JRI1	SRSF10	Serine/arginine-rich-splicing factor 10	WT
G3V279	ERH	Enhancer of rudimentary homolog	WT
P10599	TXN	Thioredoxin	WT, C,S
Q8N5K1	CISD2	CDGSH iron-sulfur domain-containing protein 2	WT, C,S
A0A0A0MR09	PTPN9	Tyrosine-protein phosphatase non-receptor type 9	WT
Q9H6R0	DHX33	ATP-dependent RNA helicase DHX33	WT, C,S
Q15291	RBBP5	Retinoblastoma-binding protein 5	WT, C,S
H7BXI1	ESYT2	Extended synaptotagmin-2	WT
H3BRY6	INTS14	Integrator complex subunit 14	WT
Q5TDH0	DDI2	Protein DDI1 homolog 2	WT
P08240	SRPRA	Signal recognition particle receptor subunit alpha	WT
P27824	CANX	Calnexin	WT
P22695	UQCRC2	Cytochrome b-c1 complex subunit 2, mitochondrial	WT
Q16718	NDUFA5	NADH dehydrogenase [ubiquinone] 1 alpha subcomplex subunit 5	WT, C,S
Q14697	GANAB	Neutral alpha-glucosidase AB	WT
O75146	HIP1R	Huntingtin-interacting protein 1-related protein	WT, C,S
Q5VW32	BROX	BRO1 domain-containing protein BROX	WT, C,S
P05386	RPLP1	60S acidic ribosomal protein P1	WT, C,S
A6NDU8	C5orf51	UPF0600 protein C5orf51	WT, C,S
Q6DKI1	RPL7L1	60S ribosomal protein L7-like 1	WT, C,S
P30041	PRDX6	Peroxiredoxin-6	WT, C,S
Q9UKK9	NUDT5	ADP-sugar pyrophosphatase	WT, C,S
Q2M2I8	AAK1	AP2-associated protein kinase 1	WT, C,S
P57076	CFAP298	Cilia- and flagella-associated protein 298	WT, C,S
Q66PJ3	ARL6IP4	ADP-ribosylation factor-like protein 6-interacting protein 4	WT, C,S
Q15814	TBCC	Tubulin-specific chaperone C	WT, C,S
Q9NYK5	MRPL39	39S ribosomal protein L39, mitochondrial	WT, C,S
P78346	RPP30	Ribonuclease P protein subunit p30	WT, C,S
P06132	UROD	Uroporphyrinogen decarboxylase	WT, C,S

P62081	RPS7	40S ribosomal protein S7	WT, C,S
Q9UJS0	SLC25A13	Calcium-binding mitochondrial carrier protein Aralar2	WT
K7ERF1	EIF3K	Eukaryotic translation initiation factor 3 subunit K	WT
Q9H0E2	TOLLIP	Toll-interacting protein	WT
Q5SY16	NOL9	Polynucleotide 5'-hydroxyl-kinase NOL9	WT, C,S
O15269	SPTLC1	Serine palmitoyltransferase 1	WT, C,S
Q9Y5Y2	NUBP2	Cytosolic Fe-S cluster assembly factor NUBP2	WT, C,S
Q8IVS2	MCAT	Malonyl-CoA-acyl carrier protein transacylase, mitochondrial	WT, C,S
P50454	SERPINH1	Serpin H1	WT, C,S
Q9NP97	DYNLRB1	Dynein light chain roadblock-type 1	WT, C,S
Q9NS69	TOMM22	Mitochondrial import receptor subunit TOM22 homolog	WT, C,S
Q6UW78	UQCC3	Ubiquinol-cytochrome-c reductase complex assembly factor 3	C,S
A0A2R8YFH5	SEC23B	Protein transport protein SEC23	WT
Q9UHD2	TBK1	Serine/threonine-protein kinase TBK1	WT, C,S
P31040	SDHA	Succinate dehydrogenase [ubiquinone] flavoprotein subunit, mitochondrial	WT, C,S
Q8NBU5	ATAD1	ATPase family AAA domain-containing protein 1	WT, C,S
Q96AT9	RPE	Ribulose-phosphate 3-epimerase	WT, C,S
P35268	RPL22	60S ribosomal protein L22	WT, C,S
P19022	CDH2	Cadherin-2	WT, C,S
F8VYE8	PPP1CC	Serine/threonine-protein phosphatase	WT, C,S
Q6IBS0	TWF2	Twinfilin-2	WT, C,S
O60784	TOM1	Target of Myb protein 1	WT, C,S
P62873	GNB1	Guanine nucleotide-binding protein G(I)/G(S)/G(T) subunit beta-1	WT, C,S
Q13509	TUBB3	Tubulin beta-3 chain	WT, C,S
Q96EA4	SPDL1	Protein Spindly	WT, C,S
A0A0A0MTB8	WDR36	WD repeat-containing protein 36	WT, C,S
Q92990	GLMN	Glomulin	WT, C,S
Q9UL15	BAG5	BAG family molecular chaperone regulator 5	WT, C,S
O43815	STRN	Striatin	WT, C,S
Q9H0U4	RAB1B	Ras-related protein Rab-1B	WT, C,S
Q9UQR0	SCML2	Sex comb on midleg-like protein 2	WT, C,S
F5H008	VPS33B	Vacuolar protein sorting-associated protein 33B	WT, C,S
Q9BSJ8	ESYT1	Extended synaptotagmin-1	WT, C,S
P14174	MIF	Macrophage migration inhibitory factor	WT, C,S
P51809	VAMP7	Vesicle-associated membrane protein 7	WT, C,S
Q9NZ45	CISD1	CDGSH iron-sulfur domain-containing protein 1	WT, C,S
Q9BZX2	UCK2	Uridine-cytidine kinase 2	WT, C,S
Q8TDH9	BLOC1S5	Biogenesis of lysosome-related organelles complex 1 subunit 5	WT, C,S
Q9BQC3	DPH2	2-(3-amino-3-carboxypropyl)histidine synthase subunit 2	WT, C,S
O75663	TIPRL	TIP41-like protein	C,S
Q9GZS3	WDR61	WD repeat-containing protein 61	WT, C,S
O75688	PPM1B	Protein phosphatase 1B	C,S
P35237	SERPINB6	Serpin B6	WT, C,S
P62979	RPS27A	Ubiquitin-40S ribosomal protein S27a	WT, C,S
Q9NP61	ARFGAP3	ADP-ribosylation factor GTPase-activating protein 3	WT, C,S
H7C155	RAF1	Non-specific serine/threonine protein kinase	C,S
P54646	PRKAA2	5'-AMP-activated protein kinase catalytic subunit alpha-2	WT, C,S
P26368	U2AF2	Splicing factor U2AF 65 kDa subunit	C,S
Q9HB71	CACYBP	Calcyclin-binding protein	WT, C,S
A0A087WU06	TUBGCP3	Gamma-tubulin complex component	WT, C,S
Q8N6M0	OTUD6B	Deubiquitinase OTUD6B	WT, C,S
P62820	RAB1A	Ras-related protein Rab-1A	C,S
B4DJ81	NDUFS1	NADH-ubiquinone oxidoreductase 75 kDa subunit, mitochondrial	WT, C,S
Q8N6R0	EEF1AKNMT	eEF1A lysine and N-terminal methyltransferase	WT, C,S
P11802	CDK4	Cyclin-dependent kinase 4	WT, C,S
Q9H974	QTRT2	Queuine tRNA-ribosyltransferase accessory subunit 2	WT, C,S
P21964	COMT	Catechol O-methyltransferase	WT, C,S
Q9P287	BCCIP	BRCA2 and CDKN1A-interacting protein	WT, C,S
Q9UGV2	NDRG3	Protein NDRG3	C,S
P62879	GNB2	Guanine nucleotide-binding protein G(I)/G(S)/G(T) subunit beta-2	WT, C,S
H3BV80	RNPS1	RNA-binding protein with serine-rich domain 1	WT, C,S
Q8IYS1	PM20D2	Peptidase M20 domain-containing protein 2	WT, C,S
Q9HCN8	SDF2L1	Stromal cell-derived factor 2-like protein 1	WT, C,S
X6RM00	ERC1	ELKS/Rab6-interacting/CAST family member 1	WT, C,S
Q15738	NSDHL	Sterol-4-alpha-carboxylate 3-dehydrogenase, decarboxylating	C,S
Q9Y679	AUP1	Lipid droplet-regulating VLDL assembly factor AUP1	WT, C,S
P22061	PCMT1	Protein-L-isoaspartate(D-aspartate) O-methyltransferase	WT, C,S
Q7L2H7	EIF3M	Eukaryotic translation initiation factor 3 subunit M	WT, C,S
P18669	PGAM1	Phosphoglycerate mutase 1	WT, C,S
Q96S59	RANBP9	Ran-binding protein 9	C,S
O95295	SNAPIN	SNARE-associated protein Snapin	WT, C,S
Q15019	SEPTIN2	Septin-2	C,S
Q96BW9	TAMM41	Phosphatidate cytidylyltransferase, mitochondrial	WT, C,S

Q9BTE1	DCTN5	Dynactin subunit 5	WT, C,S
P18031	PTPN1	Tyrosine-protein phosphatase non-receptor type 1	WT, C,S
Q147X3	NAA30	N-alpha-acetyltransferase 30	C,S
Q9NQT5	EXOSC3	Exosome complex component RRP40	C,S
M0R026	ILVBL	2-hydroxyacyl-CoA lyase 2	WT, C,S
Q96FW1	OTUB1	Ubiquitin thioesterase OTUB1	C,S
Q9Y3D0	CIAO2B	Cytosolic iron-sulfur assembly component 2B	WT, C,S
P29558	RBMS1	RNA-binding motif, single-stranded-interacting protein 1	C,S
O95551	TDP2	Tyrosyl-DNA phosphodiesterase 2	C,S
Q5QPM7	PSMF1	Proteasome inhibitor PI31 subunit	WT, C,S
Q5VT66	MTARC1	Mitochondrial amidoxime-reducing component 1	C,S
P30740	SERPINB1	Leukocyte elastase inhibitor	WT, C,S
Q9H9P8	L2HGDH	L-2-hydroxyglutarate dehydrogenase, mitochondrial	WT, C,S
O43237	DYNC1LI2	Cytoplasmic dynein 1 light intermediate chain 2	WT, C,S
Q96IU4	ABHD14B	Protein ABHD14B	WT, C,S
H3BTA2	PPP4C	Serine/threonine-protein phosphatase	WT, C,S
P19367	HK1	Hexokinase-1	C,S
Q53EL6	PDCD4	Programmed cell death protein 4	C,S
Q07820	MCL1	Induced myeloid leukemia cell differentiation protein Mcl-1	WT, C,S
Q8N6T3	ARFGAP1	ADP-ribosylation factor GTPase-activating protein 1	WT, C,S
O43809	NUDT21	Cleavage and polyadenylation specificity factor subunit 5	WT, C,S
P17252	PRKCA	Protein kinase C alpha type	C,S
A0A0A0MS29	MFF	Mitochondrial fission factor	WT
Q16698	DECR1	2,4-dienoyl-CoA reductase, mitochondrial	WT, C,S
Q14318	FKBP8	Peptidyl-prolyl cis-trans isomerase FKBP8	WT, C,S
P16435	POR	NADPH--cytochrome P450 reductase	C,S
G5EA06	MRPS27	28S ribosomal protein S27, mitochondrial	WT, C,S
P35520	CBS	Cystathionine beta-synthase	WT, C,S
P52788	SMS	Spermine synthase	C,S
P07355	ANXA2	Annexin A2	WT, C,S
Q14126	DSG2	Desmoglein-2	C,S
O60566	BUB1B	Mitotic checkpoint serine/threonine-protein kinase BUB1 beta	C,S
Q16204	CCDC6	Coiled-coil domain-containing protein 6	C,S
P11766	ADH5	Alcohol dehydrogenase class-3	WT, C,S
Q9Y570	PPME1	Protein phosphatase methylesterase 1	C,S
P62851	RPS25	40S ribosomal protein S25	C,S
P61106	RAB14	Ras-related protein Rab-14	WT, C,S
Q8WVC2	RPS21	40S ribosomal protein S21	WT, C,S
P45954	ACADSB	Short/branched chain specific acyl-CoA dehydrogenase, mitochondrial	C,S
P34896	SHMT1	Serine hydroxymethyltransferase, cytosolic	C,S
Q16543	CDC37	Hsp90 co-chaperone Cdc37	C,S
Q07021	C1QBP	Complement component 1 Q subcomponent-binding protein, mitochondrial	WT, C,S
P55072	VCP	Transitional endoplasmic reticulum ATPase	C,S
D6RA00	ENOPH1	Enolase-phosphatase E1	WT, C,S
Q9UL25	RAB21	Ras-related protein Rab-21	C,S
Q7L5D6	GET4	Golgi to ER traffic protein 4 homolog	C,S
Q5T749	KPRP	Keratinocyte proline-rich protein	WT, C,S
Q9NQX3	GPHN	Gephyrin [Includes: Molybdopterin adenylyltransferase	C,S
Q96TC7	RMDN3	Regulator of microtubule dynamics protein 3	C,S
P09211	GSTP1	Glutathione S-transferase P	C,S
O14744	PRMT5	Protein arginine N-methyltransferase 5	C,S
Q16576	RBBP7	Histone-binding protein RBBP7	C,S
Q8IUF8	RIOX2	Ribosomal oxygenase 2	C,S
P60953	CDC42	Cell division control protein 42 homolog	C,S
Q8TEX9	IPO4	Importin-4	C,S
Q8TC07	TBC1D15	TBC1 domain family member 15	C,S
Q9Y266	NUDC	Nuclear migration protein nudC	C,S
Q9UI30	TRMT112	Multifunctional methyltransferase subunit TRM112-like protein	C,S
Q96A49	SYAP1	Synapse-associated protein 1	WT, C,S
P21796	VDAC1	Voltage-dependent anion-selective channel protein 1	C,S
P56182	RRP1	Ribosomal RNA processing protein 1 homolog A	C,S
Q96S44	TP53RK	EKC/KEOPS complex subunit TP53RK	WT, C,S
O95831	AIFM1	Apoptosis-inducing factor 1, mitochondrial	C,S
Q16186	ADRM1	Proteasomal ubiquitin receptor ADRM1	C,S
Q96KB5	PBK	Lymphokine-activated killer T-cell-originated protein kinase	C,S
Q9H840	GEMIN7	Gem-associated protein 7	C,S
Q9HD26	GOPC	Golgi-associated PDZ and coiled-coil motif-containing protein	WT, C,S
E9PJN0	ACOT8	Acyl-coenzyme A thioesterase 8	WT, C,S
Q15388	TOMM20	Mitochondrial import receptor subunit TOM20 homolog	C,S
Q8NDI1	EHBP1	EH domain-binding protein 1	C,S
Q9NWV4	CZIB	CXXC motif containing zinc binding protein	WT, C,S
P02790	HPX	Hemopexin	C,S
Q5T760	SRSF11	Serine/arginine-rich-splicing factor 11	C,S

Q9Y6Y8	SEC23IP	SEC23-interacting protein	C,S
O60825	PFKFB2	6-phosphofructo-2-kinase/fructose-2,6-bisphosphatase 2	C,S
P00492	HPRT1	Hypoxanthine-guanine phosphoribosyltransferase	WT, C,S
P51553	IDH3G	Isocitrate dehydrogenase [NAD] subunit gamma, mitochondrial	C,S
Q8IXI1	RHOT2	Mitochondrial Rho GTPase 2	C,S
O75600	GCAT	2-amino-3-ketobutyrate coenzyme A ligase, mitochondrial	WT, C,S
C9JAW5	C9JAW5	HIG1 domain-containing protein	WT, C,S
P40616	ARL1	ADP-ribosylation factor-like protein 1	WT, C,S
Q7Z434	MAVS	Mitochondrial antiviral-signaling protein	WT, C,S
P56385	ATP5ME	ATP synthase subunit e, mitochondrial	C,S
Q92667	AKAP1	A-kinase anchor protein 1, mitochondrial	WT, C,S
Q9UH62	ARMCX3	Armadillo repeat-containing X-linked protein 3	C,S
Q9BYN0	SRXN1	Sulfiredoxin-1	WT, C,S
Q5SZR4	TDRKH	Tudor and KH domain containing, isoform CRA_a	WT, C,S
B3KUS5	USP30	Ubiquitin carboxyl-terminal hydrolase	WT, C,S
Q14498	RBM39	RNA-binding protein 39	C,S
Q5VUJ6	LRCH2	Leucine-rich repeat and calponin homology domain-containing protein 2	C,S
Q9NQG6	MIEF1	Mitochondrial dynamics protein MID51	C,S
O60547	GMDS	GDP-mannose 4,6 dehydratase	C,S
O95801	TTC4	Tetratricopeptide repeat protein 4	C,S
Q9BQA1	WDR77	Methylosome protein 50	C,S
Q14964	RAB39A	Ras-related protein Rab-39A	C,S
P49903	SEPHS1	Selenide, water dikinase 1	C,S
Q13257	MAD2L1	Mitotic spindle assembly checkpoint protein MAD2A	C,S
Q9BS26	ERP44	Endoplasmic reticulum resident protein 44	C,S
Q9BPZ2	SPIN2B	Spindlin-2B	C,S
P20042	EIF2S2	Eukaryotic translation initiation factor 2 subunit 2	C,S
B4E1N1	ARMC6	Armadillo repeat-containing protein 6	C,S
P63151	PPP2R2A	Serine/threonine-protein phosphatase 2A 55 kDa regulatory subunit B alpha isoform	C,S
K7EJQ8	HDHD2	Haloacid dehalogenase-like hydrolase domain-containing protein 2	C,S
P47755	CAPZA2	F-actin-capping protein subunit alpha-2	C,S
A0A0B4J1Z1	SRSF7	Serine/arginine-rich-splicing factor 7	C,S
PRDX4 cysteine-dependent interactors			
Q96AC1	FERMT2	Fermitin family homolog 2	WT
Q9BS26	ERP44	Endoplasmic reticulum resident protein 44	WT
Q96DH6	MSI2	RNA-binding protein Musashi homolog 2	WT
Q9NW82	WDR70	WD repeat-containing protein 70	WT
P09110	ACAA1	3-ketoacyl-CoA thiolase, peroxisomal	WT
P22307	SCP2	Non-specific lipid-transfer protein	WT
F5GZS6	SLC3A2	4F2 cell-surface antigen heavy chain	WT
Q8NBS9	TXNDC5	Thioredoxin domain-containing protein 5	WT, C,S
P60174	TPI1	Triosephosphate isomerase	WT
P30041	PRDX6	Peroxiredoxin-6	WT
Q9BTZ2	DHRS4	Dehydrogenase/reductase SDR family member 4	WT
Q9Y2R5	MRPS17	28S ribosomal protein S17, mitochondrial	WT, C,S
Q96K76	USP47	Ubiquitin carboxyl-terminal hydrolase 47	WT
Q15084	PDIA6	Protein disulfide-isomerase A6	WT
Q13257	MAD2L1	Mitotic spindle assembly checkpoint protein MAD2A	WT
Q14739	LBR	Delta(14)-sterol reductase LBR	WT
Q86UP2	KTN1	Kinectin	WT
E9PGZ1	CALD1	Caldesmon	WT
Q9UHV9	PFDN2	Prefoldin subunit 2	WT
C9J9K3	RPSA	40S ribosomal protein SA	WT
P26599	PTBP1	Polypyrimidine tract-binding protein 1	WT
Q96I99	SUCLG2	Succinate--CoA ligase [GDP-forming] subunit beta, mitochondrial	WT
Q66K74	MAP1S	Microtubule-associated protein 1S	WT, C,S
P34897	SHMT2	Serine hydroxymethyltransferase, mitochondrial	WT
P10599	TXN	Thioredoxin	WT
P22234	PAICS	Multifunctional protein ADE2 [Includes: Phosphoribosylaminoimidazole-succinocarboxamide synthase	WT, C,S
P62249	RPS16	40S ribosomal protein S16	WT, C,S
I3L1P8	SLC25A11	Mitochondrial 2-oxoglutarate/malate carrier protein	WT, C,S
Q9Y4B6	DCAF1	DDB1- and CUL4-associated factor 1	WT
P15880	RPS2	40S ribosomal protein S2	WT
O15372	EIF3H	Eukaryotic translation initiation factor 3 subunit H	WT
P34949	MPI	Mannose-6-phosphate isomerase	WT
Q93034	CUL5	Cullin-5	WT
Q92783	STAM	Signal transducing adapter molecule 1	WT, C,S
P05388	RPLP0	60S acidic ribosomal protein P0	WT
P06576	ATP5F1B	ATP synthase subunit beta, mitochondrial	WT
P42345	MTOR	Serine/threonine-protein kinase mTOR	WT
P06733	ENO1	Alpha-enolase	WT
P18077	RPL35A	60S ribosomal protein L35a	WT
Q9HCD5	NCOA5	Nuclear receptor coactivator 5	WT

Q9BSJ8	ESYT1	Extended synaptotagmin-1	WT, C, S
P30154	PPP2R1B	Serine/threonine-protein phosphatase 2A 65 kDa regulatory subunit A beta isoform	WT, C, S
Q96C36	PYCR2	Pyrroline-5-carboxylate reductase 2	WT
B4DJ81	NDUFS1	NADH-ubiquinone oxidoreductase 75 kDa subunit, mitochondrial	WT, C, S
D6RA00	ENOPH1	Enolase-phosphatase E1	WT, C, S
O43809	NUDT21	Cleavage and polyadenylation specificity factor subunit 5	WT, C, S
Q13347	EIF3I	Eukaryotic translation initiation factor 3 subunit I	WT
P49411	TUFM	Elongation factor Tu, mitochondrial	WT, C, S
Q5SW79	CEP170	Centrosomal protein of 170 kDa	WT, C, S
Q9P2J5	LARS1	Leucine--tRNA ligase, cytoplasmic	WT
P62906	RPL10A	60S ribosomal protein L10a	WT
Q9UQR0	SCML2	Sex comb on midleg-like protein 2	WT, C, S
Q16513	PKN2	Serine/threonine-protein kinase N2	WT, C, S
P13489	RNH1	Ribonuclease inhibitor	WT, C, S
A0A087WY71	AP2M1	AP-2 complex subunit mu	WT, C, S
P18858	LIG1	DNA ligase 1	WT, C, S
O14974	PPP1R12A	Protein phosphatase 1 regulatory subunit 12A	WT, C, S
Q8IUI8	CRLF3	Cytokine receptor-like factor 3	C, S
F5H6E2	MYO1C	Unconventional myosin-Ic	WT, C, S
Q12904	AIMP1	Aminoacyl tRNA synthase complex-interacting multifunctional protein 1	WT, C, S
Q07020	RPL18	60S ribosomal protein L18	C, S
Q8WX93	PALLD	Palladin	C, S
Q14152	EIF3A	Eukaryotic translation initiation factor 3 subunit A	WT, C, S
Q14697	GANAB	Neutral alpha-glucosidase AB	WT, C, S
Q14318	FKBP8	Peptidyl-prolyl cis-trans isomerase FKBP8	C, S
Q9BWF3	RBM4	RNA-binding protein 4	C, S
A0A2R8Y7S2	SMARCA4	Transcription activator BRG1	WT, C, S
O75607	NPM3	Nucleoplasmin-3	C, S
O75592	MYCBP2	E3 ubiquitin-protein ligase MYCBP2	C, S
Q09666	AHNAK	Neuroblast differentiation-associated protein AHNAK	C, S
Q12905	ILF2	Interleukin enhancer-binding factor 2	C, S
P30520	ADSS2	Adenylosuccinate synthetase isozyme 2	C, S
Q9C0C2	TNKS1BP1	182 kDa tankyrase-1-binding protein	C, S
P84103	SRSF3	Serine/arginine-rich splicing factor 3	C, S
Q8TCG1	CIP2A	Protein CIP2A	C, S
Q9BVP2	GNL3	Guanine nucleotide-binding protein-like 3	C, S
A0A0B4J1Z1	SRSF7	Serine/arginine-rich-splicing factor 7	WT, C, S
E7EPN9	PRRC2C	Protein PRRC2C	C, S
Q16543	CDC37	Hsp90 co-chaperone Cdc37	C, S
Q13618	CUL3	Cullin-3	C, S
Q7KZ85	SUPT6H	Transcription elongation factor SPT6	C, S
Q92974	ARHGEF2	Rho guanine nucleotide exchange factor 2	C, S
Q9Y2R4	DDX52	Probable ATP-dependent RNA helicase DDX52	C, S
Q99567	NUP88	Nuclear pore complex protein Nup88	C, S
P49593	PPM1F	Protein phosphatase 1F	C, S
P27824	CANX	Calnexin	C, S
Q9HCN8	SDF2L1	Stromal cell-derived factor 2-like protein 1	C, S
P29372	MPG	DNA-3-methyladenine glycosylase	C, S
A0A087X054	HYOU1	Hypoxia up-regulated protein 1	C, S
P11802	CDK4	Cyclin-dependent kinase 4	C, S
Q12797	ASPH	Aspartyl/asparaginyl beta-hydroxylase	WT, C, S
O00469	PLOD2	Procollagen-lysine,2-oxoglutarate 5-dioxygenase 2	C, S
Q9NVP1	DDX18	ATP-dependent RNA helicase DDX18	C, S
PRDX5 cysteine-dependent interactors			
Q15388	TOMM20	Mitochondrial import receptor subunit TOM20 homolog	WT
Q9BS26	ERP44	Endoplasmic reticulum resident protein 44	WT
Q9H2P9	DPH5	Diphthine methyl ester synthase	WT
Q53GQ0	HSD17B12	Very-long-chain 3-oxoacyl-CoA reductase	WT
P63167	DYNLL1	Dynein light chain 1, cytoplasmic	WT
Q5T760	SRSF11	Serine/arginine-rich-splicing factor 11	WT
Q16822	PCK2	Phosphoenolpyruvate carboxykinase [GTP], mitochondrial	WT
Q16698	DECR1	2,4-dienoyl-CoA reductase, mitochondrial	WT
E9PGT1	TSN	Component 3 of promoter of RISC	WT
Q92990	GLMN	Glomulin	WT
Q9NT62	ATG3	Ubiquitin-like-conjugating enzyme ATG3	WT
Q99598	TSNAX	Translin-associated protein X	WT
A0A0B4J1Z1	SRSF7	Serine/arginine-rich-splicing factor 7	WT
P22061	PCMT1	Protein-L-isoaspartate(D-aspartate) O-methyltransferase	WT
Q15750	TAB1	TGF-beta-activated kinase 1 and MAP3K7-binding protein 1	WT
Q9Y266	NUDC	Nuclear migration protein nudC	WT
Q9BW92	TARS2	Threonine--tRNA ligase, mitochondrial	WT
P52888	THOP1	Thimet oligopeptidase	WT
Q9H773	DCTPP1	dCTP pyrophosphatase 1	WT

Q9P2N5	RBM27	RNA-binding protein 27	WT
Q6WKZ4	RAB11FIP1	Rab11 family-interacting protein 1	WT
F5GZS6	SLC3A2	4F2 cell-surface antigen heavy chain	WT
E9PJN0	ACOT8	Acyl-coenzyme A thioesterase 8	WT
Q9NQX3	GPHN	Gephyrin [Includes: Molybdopterin adenylyltransferase	WT
Q9GZU8	PSME3IP1	PSME3-interacting protein	WT
A0AVT1	UBA6	Ubiquitin-like modifier-activating enzyme 6	WT
Q12931	TRAP1	Heat shock protein 75 kDa, mitochondrial	WT
B7Z7F3	RANBP3	Ran-binding protein 3	WT
Q9UL15	BAG5	BAG family molecular chaperone regulator 5	WT
Q15061	WDR43	WD repeat-containing protein 43	WT
Q8NBU5	ATAD1	ATPase family AAA domain-containing protein 1	WT
Q13185	CBX3	Chromobox protein homolog 3	WT
P30041	PRDX6	Peroxiredoxin-6	WT
P26599	PTBP1	Polypyrimidine tract-binding protein 1	WT, C, S
P14174	MIF	Macrophage migration inhibitory factor	WT
O14929	HAT1	Histone acetyltransferase type B catalytic subunit	WT
Q9BQA1	WDR77	Methylosome protein 50	WT
Q9Y570	PPME1	Protein phosphatase methylesterase 1	WT
O14579	COPE	Coatomer subunit epsilon	WT
Q5T6F2	UBAP2	Ubiquitin-associated protein 2	WT
Q9C0C2	TNKS1BP1	182 kDa tankyrase-1-binding protein	WT
Q9BSJ8	ESYT1	Extended synaptotagmin-1	WT
P00492	HPRT1	Hypoxanthine-guanine phosphoribosyltransferase	WT
Q9Y6A5	TACC3	Transforming acidic coiled-coil-containing protein 3	WT
Q09666	AHNAK	Neuroblast differentiation-associated protein AHNAK	WT
H7BZM7	ZPR1	Zinc finger protein ZPR1	WT
P12955	PEPD	Xaa-Pro dipeptidase	WT
P22234	PAICS	Multifunctional protein ADE2 [Includes: Phosphoribosylaminoimidazole-succinocarboxamide synthase	WT, C, S
O60664	PLIN3	Perilipin-3	WT
Q9BRS2	RIOK1	Serine/threonine-protein kinase RIO1	WT
P11413	G6PD	Glucose-6-phosphate 1-dehydrogenase	WT
C9J9K3	RPSA	40S ribosomal protein SA	WT
Q14C86	GAPVD1	GTPase-activating protein and VPS9 domain-containing protein 1	WT, C, S
Q96RL1	UIMC1	BRCA1-A complex subunit RAP80	WT
O43815	STRN	Striatin	WT
Q9NQP4	PFDN4	Prefoldin subunit 4	WT
P15880	RPS2	40S ribosomal protein S2	WT
Q9HB71	CACYBP	Calcyclin-binding protein	WT, C, S
P40222	TXLNA	Alpha-taxilin	WT, C, S
Q15276	RABEP1	Rab GTPase-binding effector protein 1	WT
Q9UNM6	PSMD13	26S proteasome non-ATPase regulatory subunit 13	WT
Q66PJ3	ARL6IP4	ADP-ribosylation factor-like protein 6-interacting protein 4	WT
Q9H0E2	TOLLIP	Toll-interacting protein	WT
Q8NFC6	BOD1L1	Biorientation of chromosomes in cell division protein 1-like 1	WT, C, S
Q04446	GBE1	1,4-alpha-glucan-branching enzyme	WT
Q8N3X1	FNBP4	Formin-binding protein 4	WT, C, S
Q05655	PRKCD	Protein kinase C delta type	WT
P48047	ATP5PO	ATP synthase subunit O, mitochondrial	WT, C, S
Q5JRA6	MIA3	Transport and Golgi organization protein 1 homolog	WT
P43304	GPD2	Glycerol-3-phosphate dehydrogenase, mitochondrial	WT, C, S
Q9Y3F4	STRAP	Serine-threonine kinase receptor-associated protein	WT
Q16531	DDB1	DNA damage-binding protein 1	WT
H7C128	BRD8	Bromodomain-containing protein 8	WT, C, S
P05386	RPLP1	60S acidic ribosomal protein P1	WT
Q96A49	SYAP1	Synapse-associated protein 1	WT, C, S
P51665	PSMD7	26S proteasome non-ATPase regulatory subunit 7	WT
Q32MZ4	LRRFIP1	Leucine-rich repeat flightless-interacting protein 1	WT
Q8NC51	SERBP1	Plasminogen activator inhibitor 1 RNA-binding protein	WT, C, S
A0A0A0MR02	VDAC2	Outer mitochondrial membrane protein porin 2	WT, C, S
Q8N6M0	OTUD6B	Deubiquitinase OTUD6B	WT
Q9UI12	ATP6V1H	V-type proton ATPase subunit H	WT
O95801	TTC4	Tetratricopeptide repeat protein 4	WT, C, S
Q9BSD7	NTPCR	Cancer-related nucleoside-triphosphatase	WT
Q9BTY7	HGH1	Protein HGH1 homolog	WT
E7EVA0	MAP4	Microtubule-associated protein	WT
Q9Y277	VDAC3	Voltage-dependent anion-selective channel protein 3	WT
A0A087WUT6	EIF5B	Eukaryotic translation initiation factor 5B	WT
E7EV99	ADD1	Alpha-adducin	WT
E9PLA9	CAPRIN1	Caprin-1	WT
Q9H2U1	DHX36	ATP-dependent DNA/RNA helicase DHX36	WT
Q9BQ69	MACROD1	ADP-ribose glycohydrolase MACROD1	WT
P22570	FDXR	NADPH:adrenodoxin oxidoreductase, mitochondrial	WT

P43686	PSMC4	26S proteasome regulatory subunit 6B	WT, C_iS
Q02952	AKAP12	A-kinase anchor protein 12	WT
P62195	PSMC5	26S proteasome regulatory subunit 8	WT
P31689	DNAJA1	DnaJ homolog subfamily A member 1	WT, C_iS
Q2TAM5	RELA	RELA protein	WT, C_iS
P25398	RPS12	40S ribosomal protein S12	WT
P62333	PSMC6	26S proteasome regulatory subunit 10B	WT
P56385	ATP5ME	ATP synthase subunit e, mitochondrial	WT
A0A0C4DGQ6	RPRD1A	Regulation of nuclear pre-mRNA domain-containing protein 1A	WT, C_iS
P04843	RPN1	Dolichyl-diphosphooligosaccharide--protein glycosyltransferase subunit 1	WT
Q10713	PMPCA	Mitochondrial-processing peptidase subunit alpha	WT, C_iS
P46821	MAP1B	Microtubule-associated protein 1B	WT
F8W1A4	AK2	Adenylate kinase 2, mitochondrial	WT
Q6PID6	TTC33	Tetratricopeptide repeat protein 33	WT, C_iS
Q15645	TRIP13	Pachytene checkpoint protein 2 homolog	WT
O00483	NDUFA4	Cytochrome c oxidase subunit NDUFA4	WT, C_iS
P78371	CCT2	T-complex protein 1 subunit beta	WT, C_iS
P07355	ANXA2	Annexin A2	WT, C_iS
Q96IZ0	PAWR	PRKC apoptosis WT1 regulator protein	WT, C_iS
P62979	RPS27A	Ubiquitin-40S ribosomal protein S27a	WT, C_iS
E9PGZ1	CALD1	Caldesmon	WT, C_iS
C9J4Z3	RPL37A	60S ribosomal protein L37a	WT, C_iS
Q5QPM7	PSMF1	Proteasome inhibitor PI31 subunit	C_iS
Q9NZL9	MAT2B	Methionine adenosyltransferase 2 subunit beta	WT, C_iS
P85037	FOXK1	Forkhead box protein K1	WT, C_iS
Q9NX63	CHCHD3	MICOS complex subunit MIC19	C_iS
A0A024R442	A0A024R442	>tr|A0A024R442|A0A024R442_HUMAN Aspartyl aminopeptidase, isoform CRA_b OS=Homo sapiens OX=9606 GN=DNPEP PE=1 SV=1;>sp|Q9ULA0|DNPEP_HUMAN Aspartyl aminopeptidase OS=Homo sapiens OX=9606 GN=DNPEP PE=1 SV=1;>tr|E7ETB3|E7ETB3_HUMAN Aspartyl aminopeptidase, iso	WT, C_iS
P13667	PDIA4	Protein disulfide-isomerase A4	C_iS
Q96HS1	PGAM5	Serine/threonine-protein phosphatase PGAM5, mitochondrial	C_iS
O95831	AIFM1	Apoptosis-inducing factor 1, mitochondrial	C_iS
A0A075B6R9	IGKV2D-24	Probable non-functional immunoglobulin kappa variable 2D-24	C_iS
Q13257	MAD2L1	Mitotic spindle assembly checkpoint protein MAD2A	C_iS
E5KLJ9	OPA1	Dynamin-like 120 kDa protein, form S1	C_iS
P30740	SERPINB1	Leukocyte elastase inhibitor	C_iS
Q6DKK2	TTC19	Tetratricopeptide repeat protein 19, mitochondrial	WT, C_iS
O00165	HAX1	HCLS1-associated protein X-1	WT, C_iS
Q96DH6	MSI2	RNA-binding protein Musashi homolog 2	C_iS

Table S5. Amino acid motifs in C_i-SOH-mediated interactors

	motif	score	fold increase
1	..W.C..C.	319.4	15.3
2	.C..C..C.	315.7	7.6
3	.C..CG...	315.7	5.2
4	....C..CG	315.3	4.8
5	.H..C..C.	315.2	7.5
6	.C..C...I	311.7	4.5
7	.C..C...N	311.7	4.7
8	...KC..C.	311.6	3.7
9	.C..CQ...	310.5	3.6
10	.CD.C....	17.2	3.2
11	....CD.C.	16.4	3.3
12	L..LC..L.	16.2	2.7
13	.CV.C....	14	2.8
14	.A..C..C.	13	2.9
15	L...C..L.	12.3	1.6
16	F.Q.C....	11.6	2.6
17	.CG.C....	11.3	2.7
18	G...C..C.	10.1	2.8
19	V.K.C....	9.8	1.9
20	L..FC....	9.1	1.9
21	F..YC....	9.1	3
22	..E.C..L.	8.8	1.7
23	.L...C..D.	8.6	1.9
24	.I..C.E..	8.3	1.9
25	L.N.C....	8	1.8
26	V..VC....	7.9	1.9
27	....CI..N	7.9	2.8
28	I...C..Y.	7.6	2.4
29	L.E.C....	7.5	1.6
30	.C..C....	7.4	1.6
31	.G..C..C.	7	2.5
32	.V..C...A.	7	1.6
33	...GC.V..	6.9	1.8
34	.E..CR...	6.8	1.8
35	...LC..L.	6.8	1.6
36	I..FC....	6.7	2.2
37	F..IC....	6.7	2.2
38	..Y..C..L.	6.3	2.3
39	.V..C...P	6.2	1.8
40	.I..C..N.	6	2
41	I..AC....	6	1.9
42	....C.VI.	5.9	2
43	L.A.C....	5.8	1.6
44	..V.CL...	5.8	1.7
45	.V..C...Y	5.7	2.1
46	.LQ.C....	5.7	1.7
47	...HC...A	5.6	2.3
48	...VCR...	5.6	2.1
49	....CN.N.	5.6	2.9
50	....CFQ..	5.5	2.3
51	..A.CY...	5.5	2.4
52	.I..C..G.	5.4	1.8
53	V...C..L.	5.3	1.6
54	..I.CV...	5.3	2
55	...FC..V.	5.2	2
56	....CV..L	5.2	1.8
57	....CS.F.	5.2	2.4
58	F...C..P.	5	2.1
59	.Y..C...L	5	2.1
60	L...C..V.	4.9	1.6
61	...IC.A..	4.9	1.9
62	...DC...I	4.9	2.6
63	.V..C..R.	4.8	1.7
64	V...C...I	4.8	1.8
65	I...C..I.	4.8	2
66	...AC..A.	4.8	2
67	.S.AC....	4.7	1.9
68	...SCS...	4.6	1.9
69	.AL.C....	4.6	2.2
70	...LCG...	4.5	1.5
71	L..I.C....	4.5	1.5
72	.L...C...I	4.5	1.7
73	T...CS...	4.5	1.8
74	AA..C....	4.5	1.8
75	.P..C..P.	4.5	2.2
76	...FC.V..	4.4	2.1
77	G.I.C....	4.4	1.8
78	G.Y.C....	4.4	2.4
79	F...C..A.	4.3	1.9
80	....CRV..	4.3	2
81	L...C.I..	4.3	2.2
82	V...C..A.	4.3	2.4
83	L...C...F	4.2	2
84	....CRI..	4.2	2
85	...GCG...	4.2	1.9
86	..V.C.S..	4.2	2.1
87	V.R.C....	4.1	1.7
88	.I..CT...	4.1	1.9
89	.I.C..T.	4.1	2.1
90	..V.C..F.	4	1.9
91	.F..C.D..	4	2
92	.A..CI....	4	1.7
93	....C..TS	4	2.1
94	D...CF...	3.9	1.9
95	..V.CI...	3.9	1.8
96	K...C.L..	3.9	2
97	....C..SS	3.9	2.1
98	V...CI...	3.8	1.8
99	I...C...G	3.8	1.8
100	AI..C....	3.8	2
101	..L.C...V	3.8	1.7
102	.V..C...T	3.7	1.7
103	...ICD...	3.7	1.9
104	T...CL...	3.7	1.6
105	..G.C...D	3.7	1.9
106	.L..CK...	3.7	1.8
107	.L..C...Y	3.6	1.8
108	V...C...S	3.6	1.8
109	....C..C.	3.5	1.4
110	.L..C...L	3.4	1.4
111	F..LC....	3.4	1.8
112	.V.SC....	3.4	1.7
113	.I..C.D..	3.4	1.8
114	...LC..A.	3.3	1.5
115	...SCT...	3.3	1.7
116	L.V.C....	3.2	1.6
117	.L...CI...	3.2	1.7
118	.L..CE...	3	1.7
119	Y..C....	2.9	1.2
120	..G.C.L..	2.9	1.7
121	W...C....	2.5	1.4
122	....C..W.	2.1	1.3
123	H...C....	2.1	1.3
124	....CY...	2	1.2
125	.I.C....	2	1.2
126	....CF...	1.9	1.2
127	F...C....	1.9	1.2
128	.M..C....	1.9	1.3
129	...VC....	1.9	1.2
130	....C...M	1.9	1.4
131	....C...V	1.9	1.3
132	....C.L..	1.9	1.3
133	....C...W	1.8	1.4
134	..V.C....	1.8	1.2
135	.I..C....	1.8	1.3
136	....C..M.	1.7	1.2
137	....C..Y.	1.7	1.2
138	....CW...	1.7	1.3
139	...YC....	1.7	1.2
140	...FC....	1.7	1.2
141	I...C....	1.7	1.2
142	.L..C....	1.7	1.2
143	....CR...	1.7	1.3
144	...SC....	1.7	1.3
145	....CI...	1.7	1.3
146	....C...S	1.7	1.4
147	....C...P	1.7	1.5
148	.P..C....	1.7	1.6
149	....C.W..	1.6	1.4
150	.V..C....	1.6	1.2
151	.F..C....	1.6	1.2
152	....C..H.	1.6	1.3
153	..F.C....	1.6	1.2
154	....C...I	1.6	1.2
155	.Q..C....	1.6	1.2
156	....CS...	1.6	1.2
157	....CL...	1.6	1.2
158	..Q.C....	1.6	1.4
159	P...C....	1.6	1.5
160	....C...T	1.6	1.5
161	....C..F.	1.5	1.2
162	....C.V..	1.5	1.3
163	....C..V.	1.5	1.3
164	....C...A	1.5	1.3
165	...IC....	1.4	1.5
166	....CE...	1.4	1.4
167	....C.A..	1.3	1.3
168	....C.K..	1.3	1.3

Table S6. Amino acid motifs in C_R-S-S-C_R-mediated interactors

	motif	score	fold increase
1	....C..CG	322.2	9.4
2	.C..CG...	322	9.4
3	....CP.C.	313.4	7.1
4	.CP.C....	312.9	6.8
5	VC..C....	311.3	5.2
6	....C..CK	310.6	4.5
7	.C..CK...	18.7	4.6
8	....C..C.	15.2	2.1
9	L..LC....	11.5	1.9
10	.C..C....	9.9	1.9
11	..D..C.V..	9.4	2.3
12	V..LC....	7.9	2.1
13	..I.C..P.	7.7	4
14	..R.C..L.	7.3	2.1
15	..V.C.V..	7.1	2
16	L...C..F.	6.9	2
17	..V..CV...	6.3	2
18	..V.C..G.	6.3	2.1
19	L...C...N	6.1	2
20	..T.C.V..	5.7	2.1
21	..A.C.L..	5.4	2.2
22	...LC..L.	5.3	2.1
23	I..C...G	5.2	1.9
24	...ICD...	5.1	2.4
25	..V.CL...	5.1	1.9
26	....CP.I.	5	2.3
27	FL..C....	4.9	1.9
28	...RC..L.	4.9	1.9
29	.VI.C....	4.8	2.1
30	.L..C..V.	4.7	1.8
31	L..FC....	4.6	1.9
32	I...C..L.	4.5	1.8
33	.T..CL...	4.5	2.1
34	V...C.D..	4.2	2.1
35	.AS.C....	4.1	1.6
36	..V..CL...	4.1	1.8
37	.L...C..D.	4	1.9
38	L...C.V..	3.9	1.7
39	L.D.C....	3.9	1.8
40	....C.VL	3.7	1.9
41	.L..CV...	3.7	1.9
42	AA..C....	3.6	1.7
43	.A..C.L..	3.6	1.7
44	LA..C....	3.6	2.1
45	....CL..L	3.5	1.7
46	...VC...S	3.4	1.8
47	AL..C....	3.3	1.8
48	.L..C.L..	3.2	1.8
49	...FC....	2.6	1.3
50	....C.T..	2.6	1.4
51	...YC....	2.5	1.3
52	....CL...	2.4	1.3
53	....C.I..	2.3	1.2
54	...IC....	2.2	1.2
55	...HC....	2.2	1.3
56	.V..C....	2.2	1.4
57	I..C....	2.1	1.2
58	.L..C....	2.1	1.3
59	...WC....	2	1.5
60	...VC....	2	1.3
61	....C.F..	1.9	1.3
62	....C.V..	1.9	1.2
63	.H..C....	1.9	1.4
64	.F..C....	1.9	1.3
65	....C.S..	1.9	1.2
66	..E.C....	1.9	1.2
67	V...C....	1.8	1.2
68	..V.C....	1.8	1.2
69	.Y..C....	1.8	1.3
70	....CP...	1.6	1.2
71	....C...D	1.6	1.4
72	G...C....	1.5	1.2
73	....C.A..	1.4	1.2
74	....C.N..	1.4	1.3

REFERENCES

1. Sies, H.; Jones, D.P. Reactive Oxygen Species (ROS) as Pleiotropic Physiological Signalling Agents. *Nat Rev Mol Cell Biology* 2020, 1–21, doi:10.1038/s41580-020-0230-3.

2. Winterbourn, C.C. The Biological Chemistry of Hydrogen Peroxide. *Methods Enzymol* 2013, *528*, 3–25, doi:10.1016/b978-0-12-405881-1.00001-x.

3. Winterbourn, C.C.; Hampton, M.B. Thiol Chemistry and Specificity in Redox Signaling. *Free Radical Bio Med* 2008, *45*, 549 561, doi:10.1016/j.freeradbiomed.2008.05.004.

4. Winterbourn, C.C. Reconciling the Chemistry and Biology of Reactive Oxygen Species. *Nat Chem Biol* 2008, *4*, 278 286, doi:10.1038/nchembio.85.

5. Marinho, H.S.; Real, C.; Cyrne, L.; Soares, H.; Antunes, F. Hydrogen Peroxide Sensing, Signaling and Regulation of Transcription Factors. *Redox Biol* 2014, *2*, 535 562, doi:10.1016/j.redox.2014.02.006.

6. Winterbourn, C.C. Biological Production, Detection, and Fate of Hydrogen Peroxide. *Antioxid Redox Sign* 2017, *29*, ars.2017.7425, doi:10.1089/ars.2017.7425.

7. Wood, Z.A.; Poole, L.B.; Karplus, P.A. Peroxiredoxin Evolution and the Regulation of Hydrogen Peroxide Signaling. *Science* 2003, *300*, 650 653, doi:10.1126/science.1080405.

8. Delaunay, A.; Pflieger, D.; Barrault, M.-B.; Vinh, J.; Toledano, M.B. A Thiol Peroxidase Is an H2O2 Receptor and Redox-Transducer in Gene Activation. *Cell* 2002, *111*, 471–481, doi:10.1016/s0092-8674(02)01048-6.

9. Veal, E.A.; Findlay, V.J.; Day, A.M.; Bozonet, S.M.; Evans, J.M.; Quinn, J.; Morgan, B.A. A 2-Cys Peroxiredoxin Regulates Peroxide-Induced Oxidation and Activation of a Stress-Activated MAP Kinase. *Mol Cell* 2004, *15*, 129 139, doi:10.1016/j.molcel.2004.06.021.

10. Jarvis, R.M.; Hughes, S.M.; Ledgerwood, E.C. Peroxiredoxin 1 Functions as a Signal Peroxidase to Receive, Transduce, and Transmit Peroxide Signals in Mammalian Cells. *Free Radical Bio Med* 2012, *53*, 1522 1530, doi:10.1016/j.freeradbiomed.2012.08.001.

11. Sobotta, M.C.; Liou, W.; cker, S.S. ouml; Talwar, D.; Oehler, M.; Ruppert, T.; Scharf, A.N.D.; Dick, T.P. Peroxiredoxin-2 and STAT3 Form a Redox Relay for H2O2 Signaling. *Nat Chem Biol* 2014, *11*, 1 8, doi:10.1038/nchembio.1695.

12. Zito, E.; Melo, E.P.; Yang, Y.; Wahlander, Å.; Neubert, T.A.; Ron, D. Oxidative Protein Folding by an Endoplasmic Reticulum-Localized Peroxiredoxin. *Mol Cell* 2010, *40*, 787 797, doi:10.1016/j.molcel.2010.11.010.

13. Stöcker, S.; Maurer, M.; Ruppert, T.; Dick, T.P. A Role for 2-Cys Peroxiredoxins in Facilitating Cytosolic Protein Thiol Oxidation. *Nat Chem Biol* 2018, *14*, 148–155, doi:10.1038/nchembio.2536.

14. Brandstaedter, C.; Delahunty, C.; Schipper, S.; Rahlfs, S.; Yates, J.R.; Becker, K. The Interactome of 2-Cys Peroxiredoxins in Plasmodium Falciparum. *Sci Rep-uk* 2019, *9*, 13542, doi:10.1038/s41598-019-49841-3.

15. Karpievitch, Y.V.; Dabney, A.R.; Smith, R.D. Normalization and Missing Value Imputation for Label-Free LC-MS Analysis. *Bmc Bioinformatics* 2012, *13*, S5, doi:10.1186/1471-2105-13-s16-s5.

16. Ahlmann-Eltze, C.; Anders, S. ProDA: Probabilistic Dropout Analysis for Identifying Differentially Abundant Proteins in Label-Free Mass Spectrometry. *Biorxiv* 2019, 661496, doi:10.1101/661496.

17. Xiao, H.; Jedrychowski, M.P.; Schweppe, D.K.; Huttlin, E.L.; Yu, Q.; Heppner, D.E.; Li, J.; Long, J.; Mills, E.L.; Szpyt, J.; et al. A Quantitative Tissue-Specific Landscape of Protein Redox Regulation during Aging. *Cell* 2020, doi:10.1016/j.cell.2020.02.012.

18. Orre, L.M.; Vesterlund, M.; Pan, Y.; Arslan, T.; Zhu, Y.; Woodbridge, A.F.; Frings, O.; Fredlund, E.; Lehtiö, J. SubCellBarCode: Proteome-Wide Mapping of Protein Localization and Relocalization. *Mol Cell* 2019, *73*, 166-182.e7, doi:10.1016/j.molcel.2018.11.035.

19. Thul, P.J.; Åkesson, L.; Wiking, M.; Mahdessian, D.; Geladaki, A.; Blal, H.A.; Alm, T.; Asplund, A.; Björk, L.; Breckels, L.M.; et al. A Subcellular Map of the Human Proteome. *Science* 2017, *356*, eaal3321, doi:10.1126/science.aal3321.

20. Binder, J.X.; Pletscher-Frankild, S.; Tsafou, K.; Stolte, C.; O'Donoghue, S.I.; Schneider, R.; Jensen, L.J. COMPARTMENTS: Unification and Visualization of Protein Subcellular Localization Evidence. *Database* 2014, *2014*, bau012, doi:10.1093/database/bau012.

21. Bateman, A.; Martin, M.-J.; Orchard, S.; Magrane, M.; Alpi, E.; Bely, B.; Bingley, M.; Britto, R.; Bursteinas, B.; Busiello, G.; et al. UniProt: A Worldwide Hub of Protein Knowledge. *Nucleic Acids Res* 2018, *47*, gky1049-, doi:10.1093/nar/gky1049.

22. Rhee, S.G.; Kil, I.S. Multiple Functions and Regulation of Mammalian Peroxiredoxins. *Annu Rev Biochem* 2017, *86*, 749 775, doi:10.1146/annurev-biochem-060815-014431.

23. Paulsen, C.E.; Carroll, K.S. Cysteine-Mediated Redox Signaling: Chemistry, Biology, and Tools for Discovery. *Chem Rev* 2013, *113*, 4633–4679, doi:10.1021/cr300163e.

24. Wagih, O.; Sugiyama, N.; Ishihama, Y.; Beltrao, P. Uncovering Phosphorylation-Based Specificities through Functional Interaction Networks*. *Mol Cell Proteomics* 2016, *15*, 236–245, doi:10.1074/mcp.m115.052357.

25. Fu, L.; Li, Z.; Liu, K.; Tian, C.; He, J.; He, J.; He, F.; Xu, P.; Yang, J. A Quantitative Thiol Reactivity Profiling Platform to Analyze Redox and Electrophile Reactive Cysteine Proteomes. *Nat Protoc* 2020, 1–29, doi:10.1038/s41596-020-0352-2.

26. Bersweiler, A.; D'Autréaux, B.; Mazon, H.; Kriznik, A.; Belli, G.; Delaunay-Moisan, A.; Toledano, M.B.; Rahuel-Clermont, S. A Scaffold Protein That Chaperones a Cysteine-Sulfenic Acid in H2O2 Signaling. *Nat Chem Biol* 2017, *13*, 909 915, doi:10.1038/nchembio.2412.

27. Veal, E.A.; Ross, S.J.; Malakasi, P.; Peacock, E.; Morgan, B.A. Ybp1 Is Required for the Hydrogen Peroxide-Induced Oxidation of the Yap1 Transcription Factor. *J Biol Chem* 2003, *278*, 30896–30904, doi:10.1074/jbc.m303542200.

28. Talwar, D.; Messens, J.; Dick, T.P. A Role for Annexin A2 in Scaffolding the Peroxiredoxin 2–STAT3 Redox Relay Complex. *Nat Commun* 2020, *11*, 4512, doi:10.1038/s41467-020-18324-9.

29. Peskin, A.V.; Meotti, F.C.; Kean, K.M.; Göbl, C.; Peixoto, A.S.; Pace, P.E.; Horne, C.R.; Heath, S.G.; Crowther, J.M.; Dobson, R.C.J.; et al. Modifying the Resolving Cysteine Affects the Structure and Hydrogen Peroxide Reactivity of Peroxiredoxin 2. *J Biol Chem* 2021, 100494, doi:10.1016/j.jbc.2021.100494.

30. Putker, M.; Madl, T.; Vos, H.R.; Ruiter, H. de; Visscher, M.; Berg, M.C.W. van den; Kaplan, M.; Korswagen, H.C.; Boelens, R.; Vermeulen, M.; et al. Redox-Dependent Control of FOXO/DAF-16 by Transportin-1. *Mol Cell* 2013, *49*, 730 742, doi:10.1016/j.molcel.2012.12.014.

31. Perez-Riverol, Y.; Csordas, A.; Bai, J.; Bernal-Llinares, M.; Hewapathirana, S.; Kundu, D.J.; Inuganti, A.; Griss, J.; Mayer, G.; Eisenacher, M.; et al. The PRIDE Database and Related Tools and Resources in 2019: Improving Support for Quantification Data. *Nucleic Acids Res* 2018, *47*, gky1106-, doi:10.1093/nar/gky1106.

32. Conway, J.R.; Lex, A.; Gehlenborg, N. UpSetR: An R Package for the Visualization of Intersecting Sets and Their Properties. *Bioinformatics* 2017, *33*, 2938 2940, doi:10.1093/bioinformatics/btx364.

CHAPTER 3

THE BIOCHEMICAL CHARACTERIZATION OF TIPRL AS A REDOX-SENSITIVE PROTEIN

Loes van Dam[1], Marrit Putker[1], Robert M. van Es[1], Holger Rehmann[1], Michiel Vermeulen[1], Joppe Nieuwenhuis[1], Harmjan R. Vos[1], Boudewijn M. T. Burgering[1,2], Tobias Madl[3,4] and Tobias B. Dansen[1]

[1]Center for Molecular Medicine, Molecular Cancer Research, University Medical Center Utrecht, Universiteitsweg 100, 3584CG, Utrecht, The Netherlands
[2]Oncode Institute, University Medical Center Utrecht, Universiteitsweg 100, 3584CG, Utrecht, The Netherlands.
[3]Gottfried Schatz Research Center for Cell Signaling, Metabolism and Aging, Molecular Biology and Biochemistry, Medical University of Graz, 8010, Graz, Austria
[4]BioTechMed-Graz, Austria

Correspondence: t.b.dansen@umcutrecht.nl

KEYWORDS
redox signaling; cysteine oxidation; mTOR signaling; phosphatases, homodimerization

THE BIOCHEMICAL CHARACTERIZATION OF TIPRL AS A REDOX-SENSITIVE PROTEIN

ABSTRACT

Reactive oxygen species (ROS) have been shown to regulate the activity of many different proteins. Among these are protein phosphatases such as protein phosphatase 2A (PP2A), whose redox regulation allows for prolonged kinase signaling. PP2A is a ubiquitous protein phosphatase responsible for dephosphorylation of a broad spectrum of substrates and is implicated in the regulation of many signal transduction pathways. Here, we identify the PP2A regulating protein TIPRL as a redox-sensitive protein. We show that TIPRL is highly sensitive to oxidation and forms three different disulfide-dependent homodimers involving cysteines C14 and C87 in response to endogenous levels of H_2O_2. Preliminary data suggest that increased oxidation of TIPRL might suppress phosphatase activity of PP2A-C, without affecting the ability to bind PP2A-C. We explore the effects of redox-dependent homodimerization of TIPRL on PP2A and its downstream targets mTORC1 and PKB, as well as its role in oxidant-induced loss of viability and changes in metabolism. This is the first time TIPRL is described as a strong redox sensor, suggesting an important role for TIPRL in sensing the local redox state and enabling the cell to respond accordingly through redox regulation of cellular phosphatases.

INTRODUCTION

In order to function correctly and maintain homeostasis, cells must respond to their ever-changing environment. Cells do this by sensing changes in their environment and transducing these signals into a cellular response. The correct integration and amplification of different signals is crucial for the correct functioning of cells. For example, elevated ROS levels or low reducing power can create a more oxidizing local redox state, which leads to oxidative modifications on specific cysteines including reversible disulfide bonds. These modifications may lead to structural changes, thereby altering protein function and modifying signaling outcome. An example of this is the transient burst of H_2O_2 induced upon growth factor receptor activation through NADPH-dependent oxidases (NOXs) [1,2], which reversibly oxidizes a cysteine in the active site of protein tyrosine phosphatases (PTPs) and the lipid phosphatase PTEN [3,4]. The ROS-induced oxidation of these phosphatases leads to their inactivation and allows protein phosphorylation cascades to take place, required for sustained growth factor signaling [5,6].

Interestingly, protein phosphatase 2A (PP2A) is also reported to be a redox regulated phosphatase. Several studies reported PP2A thiol oxidation, resulting in the inhibition of PP2A catalytic activity [7–9], although details and implications of these modifications need to be further elucidated. PP2A enzymes constitute a large family of Ser-Thr phosphatases, with widespread functions in many cellular processes. The PP2A holoenzyme consists of the assembly of a catalytic C subunit (A or B isoform), one of two scaffolding subunits (subunit A) and a wide variety of regulatory subunits (subunit B, 26) that fine-tunes the substrate specificity, localization and phosphatase activity [10]. Together, there are more than 100 possibilities for the formation of the ternary PP2A complex. This is one of the reasons that PP2A is involved in practically any signaling pathway and mediates 30-50% of Ser-Thr dephosphorylation events [11].

A few other proteins have been described to regulate PP2A activity. For example, α4 and TIPRL (TOR signaling pathway regulator-like; TOR: Target of rapamycin) were suggested to be two of five PP2A modulators, serving to prevent aspecific phosphatase activity until the PP2A trimeric holoenzyme is assembled [12]. Unlike in yeast where the TIPRL homolog Tip41 induces PP2A activity (Sit4 in yeast) by blocking the binding of α4 orthologue and Sit4 inhibitor Tap42 [13], human TIPRL function is more ambiguous. Several publications report the formation of a ternary complex between TIPRL, α4 and PP2A, suggesting that the mutually exclusive interaction between α4 and TIPRL or PP2A is not conserved from yeast to humans [14,15]. Furthermore, while TIPRL stimulates PP2A activity in yeast, mammalian TIPRL has been reported to inhibit PP2A-C catalytic activity, thereby positively regulating mTOR signaling and downstream targets [14–17]. Furthermore, TIPRL has recently been suggested in another PP2A-independent process by interacting with and subsequent activation of eukaryotic initiation factor 2α (eIF2α) [18].

The protein TIPRL was identified as prone to cysteine oxidation in two mass-spectrometry-based screens for cysteine-dependent protein-protein interaction performed in our laboratory [19]. Here we further explore the function and redox regulation of TIPRL in human cells in relation to mTORC and PP2A dependent signaling. We provide evidence that TIPRL is highly sensitive to changes in the cellular redox state. Under more oxidizing conditions, it is readily oxidized on C14 and C87. This leads to the formation of three different TIPRL homodimers, linked though a disulfide between C14-C14, C87-C87 or C14-C87. Although the biological function of this cysteine-dependent control of TIPRL is not yet clear, our preliminary results suggest a role for redox-sensitive homodimerization of TIPRL in its regulation of PP2A-C and downstream PP2A targets mTORC1 and PKB.

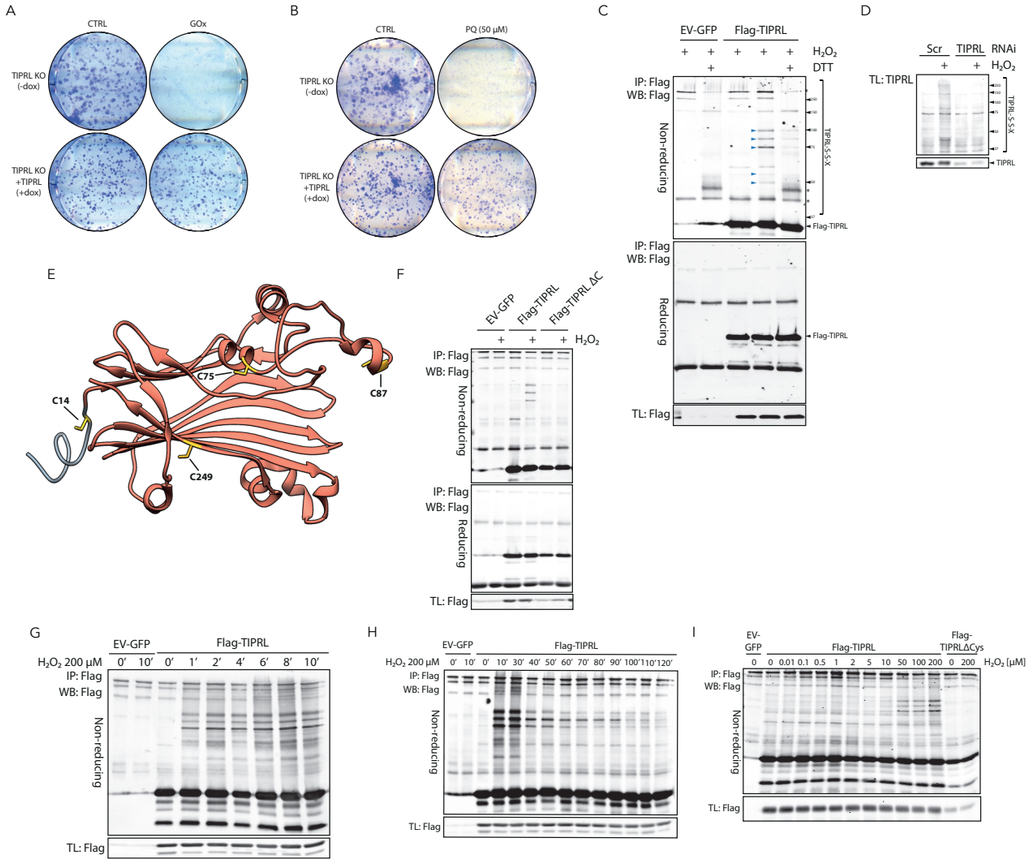

Figure 1. TIPRL is a redox-sensitive protein.
(**A-B**) Colony formation assay in doxycycline-inducible TIRPL knockout cells, showing that TIPRL is essential in protecting cells from redox stress. Both treatment with glucose oxidase (GO) as well as paraquat (PQ) lead to a decrease in colony outgrowth in TIPRL deficient cells. Re-expression of TIPRL can reverse the reduced colony outgrowth. (**C**) Oxidizing conditions (i.e. H_2O_2 exposure) induce a mass shift of a fraction of TIPRL. Parallel reducing and non-reducing SDS-PAGE and western blot analysis (WB) of Flag-TIPRL immunoprecipitations (IP). Cells were incubated with 200 µM of H_2O_2 for 15 minutes where indicated. Under non-reducing conditions, a fraction of TIPRL shows a H_2O_2-induced HMW band pattern (blue arrows). This band pattern is lost when samples were incubated with 10 mM DTT for 10 minutes prior to washing, or when samples are analyzed under reducing conditions (lower panel). (**D**) Endogenous TIPRL shows a HMW band pattern under oxidizing conditions (indicated by a smear). Cells were transfected with scrambled control (Scr) or TIPRL RNAi and incubated with 200 µM H_2O_2 for 15 minutes. Cells were lysed in non-reducing sample buffer and whole cell lysates were analyzed. Panels are from different exposures of the same membrane. (**E**) Cysteines (yellow) in the crystal structure of TIPRL (PDB ID: 5D9G). Residues 1-15 were removed for crystallization and are added manually, indicated in grey. The four cysteines 14, 75, 87 and 249 are indicated in yellow. (**F**) The TIPRL HMW band pattern is cysteine-dependent. Wild-type TIPRL and TIPRLΔC were immunoprecipitated and analyzed under reducing and non-reducing conditions. (**G**) The H_2O_2-induced, cysteine-dependent HMW band pattern is induced within 1 minute of H_2O_2 treatment, and diminishes after 30 minutes of H_2O_2 treatment (h). The HMW shift of TIPRL is induces H_2O_2 concentrations as low as 5 µM. Cells were incubated with different concentrations of H_2O_2 for 10 minutes prior to lysis.

RESULTS

TIPRL is a Redox-Sensitive Protein

We identified TIPRL as prone to cysteine oxidation in multiple mass-spectrometry-based screens for redox sensitive proteins. If oxidation of TIPRL is important in mediating the response to changes in the cellular redox state, loss of TIPRL could affect cell viability when cells are exposed to an oxidative challenge. To investigate this, we deleted the *TIPRL* gene from RPE cells using Crispr-Cas9, and introduced a doxycycline-inducible TIPRL expression construct. We then challenged cells with prolonged exposure to H_2O_2 generated by extracellular Glucose Oxidase (GOx), or treatment with the redox cycler paraquat (PQ) which generates superoxide. Cells that are knockout for TIPRL show strongly reduced colony outgrowth when challenged with these compounds. Re-expression of TIPRL can rescue this phenotype, indicating that it indeed stems from loss of TIPRL (Figure 1A-B). Flow cytometry experiments demonstrate that loss of colony outgrowth is not caused by differences in cell death (preliminary, data not shown), suggesting that a ROS-induced sustained cell cycle arrest might underlie the impaired outgrowth upon loss of TIPRL expression. These data suggest, for the first time, that TIPRL is important in resolving redox stress.

The observation that TIPRL is required for resistance to oxidants further led credence that TIPRL could be a bona fide hit in the aforementioned mass spectrometry screens for potentially redox-regulated proteins. To test if TIPRL is indeed a redox-sensitive protein (i.e. whether it undergoes reversible cysteine oxidation) we expressed and immunoprecipitated Flag-TIPRL before analysis under parallel reducing and non-reducing conditions. Exposure to H_2O_2 induces a mass shift of a fraction of TIPRL, as indicated by bands that migrate well above the MW of TIPRL (Figure 1C, blue arrows). There are five clearly visible bands; an intense triplet of bands at around 75, 85 and 100 kDa and two bands at 50 and 60 kDa. These TIRPL-containing complexes likely contain intermolecular disulfides judged by the large mass-shift and their reversibility upon treatment with the reducing agent DTT prior to washing (right lane). Furthermore, endogenous TIPRL also displays a H_2O_2-induced high molecular weight (HMW) band pattern (indicated by a smear), which is lost upon TIPRL knockdown (Figure 1D), suggesting that the HMW complexes also occur at endogenous TIPRL protein levels.

We next set out to identify which cysteines are involved in the formation of the disulfide induced mass shifts of TIPRL. TIPRL contains 4 cysteines (14, 75, 87, 249), of which C14 and C87 are surface exposed in an extended loop (Figure 1E). A cysteine-free mutant of TIPRL (TIPRL ΔC, in which its four cysteines were replaced with serines) no longer shift up on non-reducing SDS-PAGE, confirming that the HMW bands indeed represent disulfide-dependent complexes containing TIPRL (Figure 1F).

A time course of exposure to peroxide indicates that the oxidation of TIPRL occurs rapidly (within one minute) as well as transiently (Figure 1G-H. Furthermore, we show that the oxidation of TIPRL occurs upon exposure to peroxide levels as low as 10 µM (Figure 1I).

Together, these findings suggest that TIPRL is highly sensitive to oxidation and readily forms cysteine-dependent HMW complexes upon exposure to low levels of peroxide.

TIPRL Forms Disulfide-Dependent Homodimers Upon Oxidation

To dissect the nature of the HMW cysteine-dependent complexes containing TIPRL, we performed a diagonal SDS-PAGE on immunoprecipitated TIPRL (Figure 2A). With this technique, immunoprecipitated samples are separated under non-reducing conditions in the first dimension, followed by a second dimension under reducing conditions. Non-covalently bound proteins run in the diagonal in the second dimension, whereas covalent disulfide-dependent complex members run below the diagonal. As can be seen from the diagonal SDS-PAGE for wild-type TIPRL (for both the SimplyBlue-stained gel, top panel and Figure S1, and Flag-stained western blot, lower panel), the shifted HMW

bands indeed contain TIPRL, visible as distinct spots at the height of Flag-TIPRL below the diagonal (Figure 2B and S1). This indicates that the HMW bands indeed contain TIPRL. For Flag-TIPRLΔC these spots could indeed not be detected. However, no evidence of other proteins present in the complex was found below the diagonal at the predicted positions. This suggests that the HMW bands of TIPRL represent different cysteine-dependent TIPRL homo-oligomers.

To investigate this possibility further, Flag- and hemagglutinin (HA)-tagged TIPRL were co-expressed, followed by an IP for Flag-TIPRL and analysis under non-reducing and reducing conditions. HA-TIPRL is co-immunoprecipitated with Flag-TIPRL, indicating an interaction (Figure 2C). Like Flag-TIPRL, HA-TIPRL shows a H_2O_2-induced mass-shift under non-reducing conditions. The typical three-band pattern runs at (approximately) the same MW and could therefore be in the same complex. HA-TIPRL also binds to Flag-TIPRL independent of cysteines or H_2O_2 treatment, suggesting that TIPRL may already exist as complexes prior to disulfide formation.

To estimate the stoichiometry of the oligomeric TIPRL complexes, TIPRL-expressing cell lysates were fractionated on a size exclusion column (SEC), followed by immunoprecipitation and western blotting. The distinct HMW complexes of TIPRL elute from the column in one fraction, suggesting that these complexes have a similar molecular weight, about 40 kDa bigger than monomeric TIPRL (Figure 2D). These findings suggest that oxidized TIPRL can be found as homodimers of different shapes, potentially involving different disulfides.

To investigate which cysteines are involved in the formation of the different TIPRL homodimers we designed several TIPRL cysteine mutants (Figure 3A). These include the cysteine-free mutant of TIPRL (TIPRLΔC) that was described above. In addition, we generated four TIPRL mutants in which one of the four cysteines (Figure 3B) is mutated to a serine, and four mutants that contain only one of the four cysteines (e.g. TIPRL 14C contains a cysteine at position 14 and serines at positions 75, 87 and 249). There are several conclusions we can draw from IP experiments under parallel non-reducing and reducing conditions using these mutants.

First of all, the lower band of the HMW triplet is completely dependent on cysteine 14, as it is absent in the TIPRL-C14S pulldown, but detectable in the TIPRL-14C pulldown (Figure 3C). Similarly, the upper band of the triplet seems dependent on cysteine 87. Both cysteine 75 and 249 are not required for any HMW band. The middle band of the HMW triplet requires the presence of both cysteines 14 and 87, as evidenced by co-expressing TIPRL-14C or TIPRL-87C. Indeed, in these conditions we observe the formation of all three HMW bands (Figure 3D). Therefore, it seems like TIPRL forms at least three different disulfide-mediated homodimers involving C14 and C87: C14-C14, C87-C87 and C14-C87. Differences in migratory behavior of these homodimers could potentially be explained by the differential accessibility of SDS around the disulfide.

Closer inspection of the molecular packing of the TIPRL crystal structure as published in ref. [17] provides further evidence for the formation of homodimers. The N-terminal deletion, containing C14, was predicted to be a potential flexible region (Figure 3D, hypothetical N-terminus in grey), which could promote availability for homodimerization [17]. The crystal structure contains no evidence of a disulfide between C14-C87. The asymmetric unit of the TIPRL crystal structure seems to form a dimer through the N-terminal interface (containing C14), but this is not likely the case in cells, since the N-terminal residues of the purified protein are not native to TIPRL. Interestingly, a C87-C87-mediated disulfide between two TIPRL molecules was also modeled in the crystal packing of TIPRL, with a distance of 2.03 Å (Figure 3E), thereby confirming C87-C87-mediated homodimerization *in vitro*.

Together, our observations shows that TIPRL forms three different reversible disulfide-mediated homodimers upon exposure to H_2O_2, involving C14 and C87.

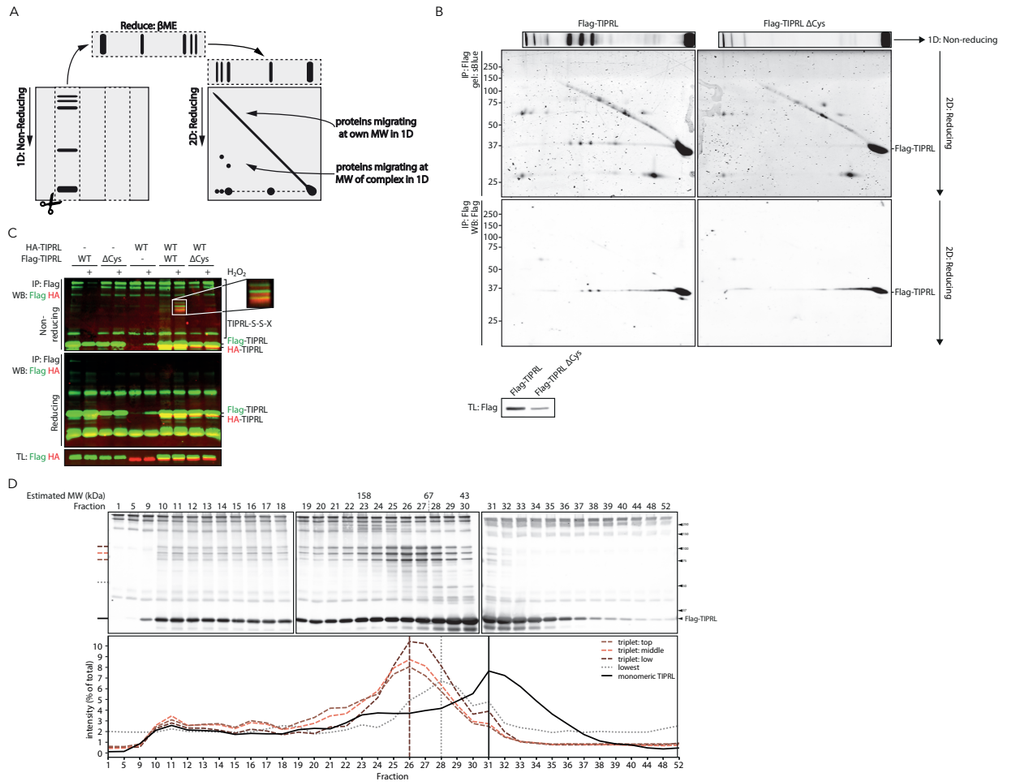

Figure 2. TIPRL forms disulfide-dependent homodimers upon oxidation.
(**A**) Schematic overview of diagonal (2D) SDS-PAGE. Immunoprecipitated samples are run under non-reducing conditions, so disulfide-mediated complexes migrate at their combined MW. The entire lane is excised and incubated in reducing sample buffer before running the second dimension, where disulfide-mediated complex members migrate at their own MW. Proteins migrating at their own MW in both the first and the second dimensions are shown on a diagonal, whereas disulfide-mediated complexes migrate below the diagonal in the second dimension. (**B**) TIPRL homodimerizes. The HMW bands indeed contain TIPRL, visible as distinct spots at the height of Flag-TIPRL below the diagonal. The absence of binding partners suggests that intermolecular disulfide bond formation between TIPRL and other proteins is not likely. (**C**) HMW HA-TIPRL co-immunoprecipitates with Flag-TIPRL, indicating homodimerization. Flag-TIPRL and Flag-TIPRLΔC (green) were co-expressed with HA-TIPRL (red), immunoprecipitated and analyzed under non-reducing conditions. (**D**) Size exclusion chromatography (SEC) of TIPRL. Flag-TIPRL expressing cells were treated with 200 μM of H_2O_2 for 15 minutes and their cell lysates were separated on a size-exclusion column. Flag-TIPRL was immunoprecipitated from the resulting 52 fractions, and analyzed under non-reducing conditions. Flag-TIPRL HMW bands were quantified from the resulting western blots (graph). HMW TIPRL are eluted from the column in one fraction, suggesting that TIPRL-containing complexes in all these bands have a similar molecular weight.

Functional Characterization of Redox-Dependent TIPRL Homodimerization

We next aimed to study whether cysteine-dependent homodimerization of TIPRL plays a role in the observed resistance to oxidants (Figure 1A). To this end, we stably expressed doxycycline-incudible TIPRL and TIPRLΔC in TIPRL knockout RPE cells and challenged these with prolonged exposure to H_2O_2 produced by GOx. No difference was found in colony outgrowth between wild-type and mutant TIPRL, suggesting that the ability of TIPRL to resolve redox stress is

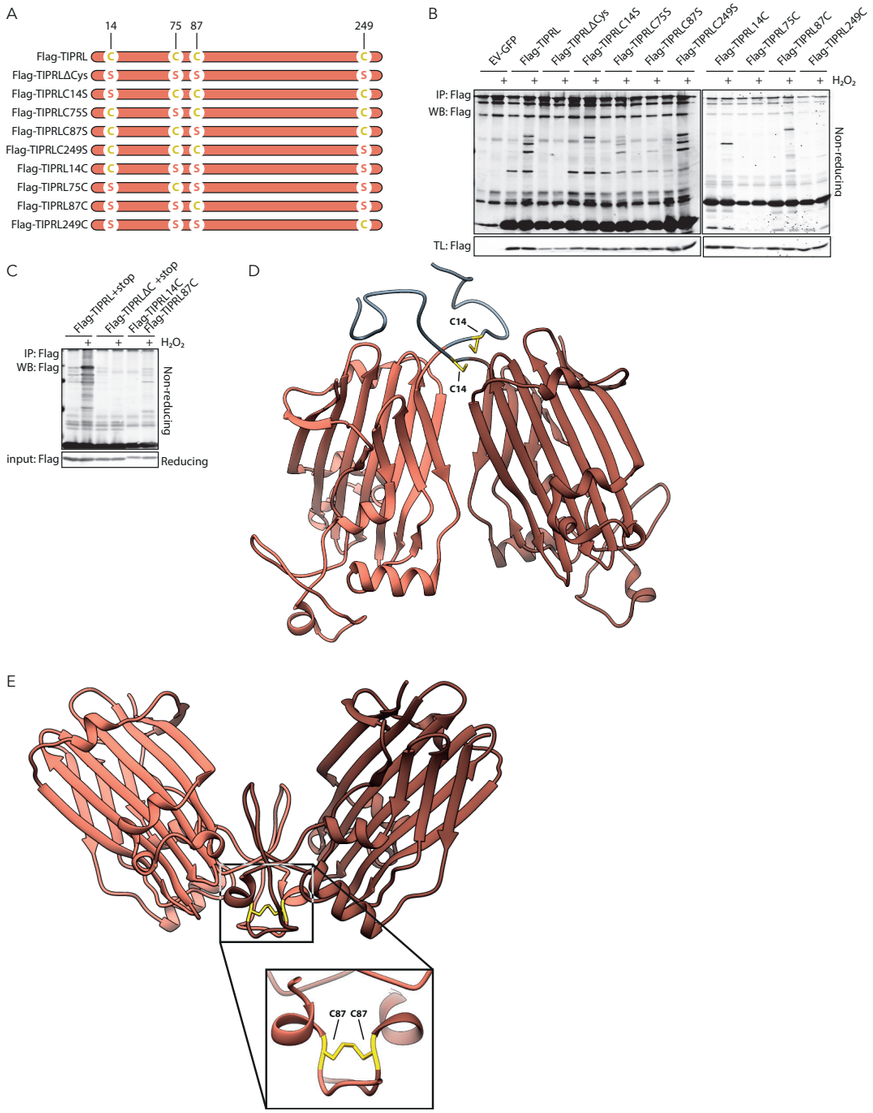

Figure 3. TIPRL forms three different disulfide-dependent homodimers upon oxidation.
(**A**) Schematic overview of TIPRL cysteine mutants that were used in our experiments. C, cysteine, S, serine. (**B**) HMW TIPRL is cysteine-specific. Different TIPRL cysteine mutants (see a) were used in immunoprecipitation and analysis under non-reducing conditions. The lower band of the HMW triplet is completely dependent on C14, the upper on C87, the middle on both C14 and C87. (**C**) Combining expression of TIPRL containing only C14 and only C87, respectively, results in the formation of all three disulfide-mediated HMW homodimeric complexes of TIPRL: C14-C14, C87-C87 and C14-C87. (**D**) Crystal packing of TIPRL (PDB ID: 5D9G), showing the N-terminal dimer interface in the asymmetric unit. Residues 1-15 were removed for crystallization and are added manually, indicated in grey. C14 is indicated in yellow. (**E**) Crystal packing of TIPRL (PDB ID: 5D9G), showing the C87-C87-mediated disulfide between two TIPRL molecules. C87 is indicated in yellow.

not dependent on its oxidation and subsequent dimerization (Figure 4A and S2).

The functional role of TIPRL in human cells is largely unclear. In order to see whether the interactome of TIPRL depends on its redox modifications we compared the interactome of wildtype (WT) and TIPRLΔC under oxidizing conditions in a label-free MS/MS-based approach. With this approach, we identify proteins that are significantly enriched in a H_2O_2- and cysteine-dependent manner (Figure 4B and Table 1-2). Interestingly, many of these are known redox-sensitive proteins, involved in the cellular ROS detoxification system, including thioredoxin (TRX) and peroxiredoxin 1, 2 and 5 (PRDX1, PRDX2 and PRDX5). We confirmed the complex formation with PRDX2 (general discussion). Other notable H_2O_2-induced, cysteine-dependent interactors of TIPRL are DJ1, SUMO, GAPDH and CDK4. However, experiments analyzing a possible functional role for these interactions have been inconclusive up to date. We also identified known interactors of TIPRL such as IGBP1 (α4), but their interaction with TIPRL seems not H_2O_2-induced (data not shown).

Interestingly, PP2A-C (PPP2CB) is significantly enriched in binding to wild-type TIPRL as compared to TIPRLΔC (Table 1), suggesting a role for oxidation and subsequent homodimerization of TIPRL in its regulation of PP2A-C. TIPRL binding to PP2A-C has been shown to inhibit the catalytic activity of the phosphatase [14–17], thereby positively regulating mTORC1 targets S6K and 4EBP1. We tested whether the absence of cysteines affects TIPRL binding to PP2A in an IP experiment (Figure 4C], but we observed no difference in the ability of TIPRL or TIPRLΔC to interact with PP2A-C. Similarly, the interaction between TIPRL and PP2A-C is not affected by oxidizing conditions. Since not all TIPRL homodimerizes under oxidizing conditions we might underestimate the effect of oxidation in these experiments, we investigated whether homodimerized TIPRL (HMW) is able to interact with PP2A-C. Indeed, HMW homodimerized TIPRL is co-immunoprecipitated with PP2A-C under non-reducing conditions (Figure 4D). These experiments suggest, in contrast to the mass spectrometry data, that oxidation and homodimerization of TIPRL do not affect its ability to bind PP2A-C.

It is, however, possible that not the binding but the ability of TIPRL to inhibit PP2A-C is affected by oxidation of TIPRL. To this end, we measured PP2A-C activity in combination with TIPRL or TIPRLΔC and in basal and oxidizing conditions in a preliminary experiment (Figure 4E). Indeed, overexpression of TIPRL inhibits PP2A-C phosphatase activity, as was described before. As controls, the PP2A-C inhibitor okadaic acid (OA) lowers PP2A-C activity, but activity is not affected by oxidizing conditions. Like wild-type TIPRL, cysteine-free TIPRL is also able to inhibit PP2A-C. Interestingly, more oxidizing conditions enhance the ability of TIPRL to inhibit PP2A-C, but not in the cysteine-free mutant of TIPRL. Although differences are small and this experiment needs to be repeated, this would suggest that oxidized TIPRL is more efficient at inhibiting PP2A-C than non-oxidized or TIPRLΔC is. We confirmed this by testing phosphatase activity of phosphatases bound to TIPRL. Although we might also measure activity of other phosphatases in this assay, we again see lower phosphatase activity in samples containing oxidized TIPRL compared to those with reduced or cysteine-free TIPRL (Figure 4F, preliminary data). An interesting observation is that although less PP2A-C is co-immunoprecipitated in samples with TIPRLΔC due to lower expression, more phosphatase activity is measured compared to wild-type TIPRL. Therefore, our results might be an underestimation of the effect of TIPRL oxidation on PP2A-C activity.

It has been shown that TIPRL facilitates amino acid-regulated mTORC1 signaling by inhibiting PP2A-C [15]. Combined with our previous results, this implies that oxidized TIPRL is more efficient at inhibiting PP2A-C in this context, leaving the mTORC1 target S6K phosphorylated. Indeed, preliminary experiments show that TIPRL overexpression results in sustained phosphorylation of S6K at T389, which seems dependent on TIPRL cysteines since TIPRLΔC does not show this effect (Figure 4G, preliminary data). In

this line, reducing the cellular environment by treating cells with β-mercaptoethanol limits the ability of TIPRL to sustain p-S6K phosphorylation (Figure 4H, preliminary data). Interestingly, H_2O_2 treatment completely diminishes S6K phosphorylation at T389, even when amino acids are added.

A major target of PP2A is PKB (Akt), which is dephosphorylated and inactivated at both T308 and S473 by PP2A [20–24]. Since TIPRL seems to inhibit PP2A activity, we examined whether TIPRL positively affects the phosphorylation status of PKB. Surprisingly, re-expression of TIPRL in TIPRL knockout cells lowers the phosphorylation of PKB at both T308 and S473 (Figure 4I-J, preliminary data). Inhibition of PP2A with OA does not abolish the observed dephosporylation of p-PKB, suggesting that the inhibitory effect of TIPRL on PKB does not involve the inactivation of PP2A (Figure 4J, preliminary data). Likewise, inhibition of mTORC1 by treatment with rapamycin does not affect this, which suggests mTORC1 activity is not required for TIPRL-dependent PKB inhibition.

Next, we wondered whether the inhibitory effect of TIPRL on PKB phosphorylation might be affected by oxidation of TIPRL. To this end, we treated TIPRL knockout cells and TIPRL expressing cells with H_2O_2. Oxidizing conditions seem to efficiently induce phosphorylation of PKB at both T308 and S473. Interestingly, the inhibitory effect of TIPRL on PKB phosphorylation that we observed under basal conditions is no longer present in more oxidizing conditions (Figure 4J, preliminary data). In summary, our preliminary data shows that the oxidation of TIPRL enhances its inhibitory effect on PP2A-C leading to more efficient inhibition of dephosphorylation of the mTORC1 target S6K. Furthermore, we observe an inhibitory effect of TIPRL on PKB (measured by phosphorylation at T308 and S473), although the oxidation of TIPRL itself does not seem to play a role in this. Of note, these data are preliminary and follow-up studies have to be done in order to confirm these findings.

DISCUSSION

The reversible oxidation of cysteines, which is indispensable for redox signaling, allows for the rapid respond to changes in the local redox environment, thereby integrating the cellular redox status with other signaling pathways. Cysteine oxidation can lead to reversible disulfide bond formation and subsequent structural rearrangements to modify signaling output. In this chapter, we describe TOR signaling pathway regulator-like (TIPRL) as a novel redox-sensitive protein, which is potentially involved in the control of PP2A and its downstream effects.

TIPRL rapidly forms disulfide-dependent homodimers via two of its cysteines, C14 and C87 upon treatment with low levels of H_2O_2, (Figure 1). For comparison, TIPRL oxidation occurs at H_2O_2 concentrations similar to those required for peroxiredoxin dimerization in tissue culture [25], both for ectopically expressed and endogenous TIPRL (Figure 1D).

Using mutational analysis, we show that three different homodimers can be formed with similar stoichiometry: C14-C14 C87-C87 and C14-C87. Interestingly, both C14 and C87 are surface exposed in an extended loop (Figure 1E). Closer inspection of the published crystal structure of TIPRL revealed that the C87-C87-mediated disulfide was also modeled in the crystal packing of TIPRL, with a distance of 2.03 Å (Figure 3E), which was not described by the authors [17]. In addition, TIPRL has been identified in several screens for redox-sensitive proteins [26–29]. Furthermore, recombinant TIPRL that is kept in reducing buffer *in vitro* rapidly turns over DTT present in the buffer (T. Madl, data not shown), suggesting that TIPRL cysteines are oxidized readily, or that TIPRL itself has an enzymatic redox acivity. On top of that, TIPRL maintains its structure upon oxidation in NMR spectroscopy and small-angle X-ray scattering experiments (T. Madl, data not shown). However, considerable caution should be taken when interpreting the results of these *in vitro* and NMR experiments, and they were variable and inconclusive.

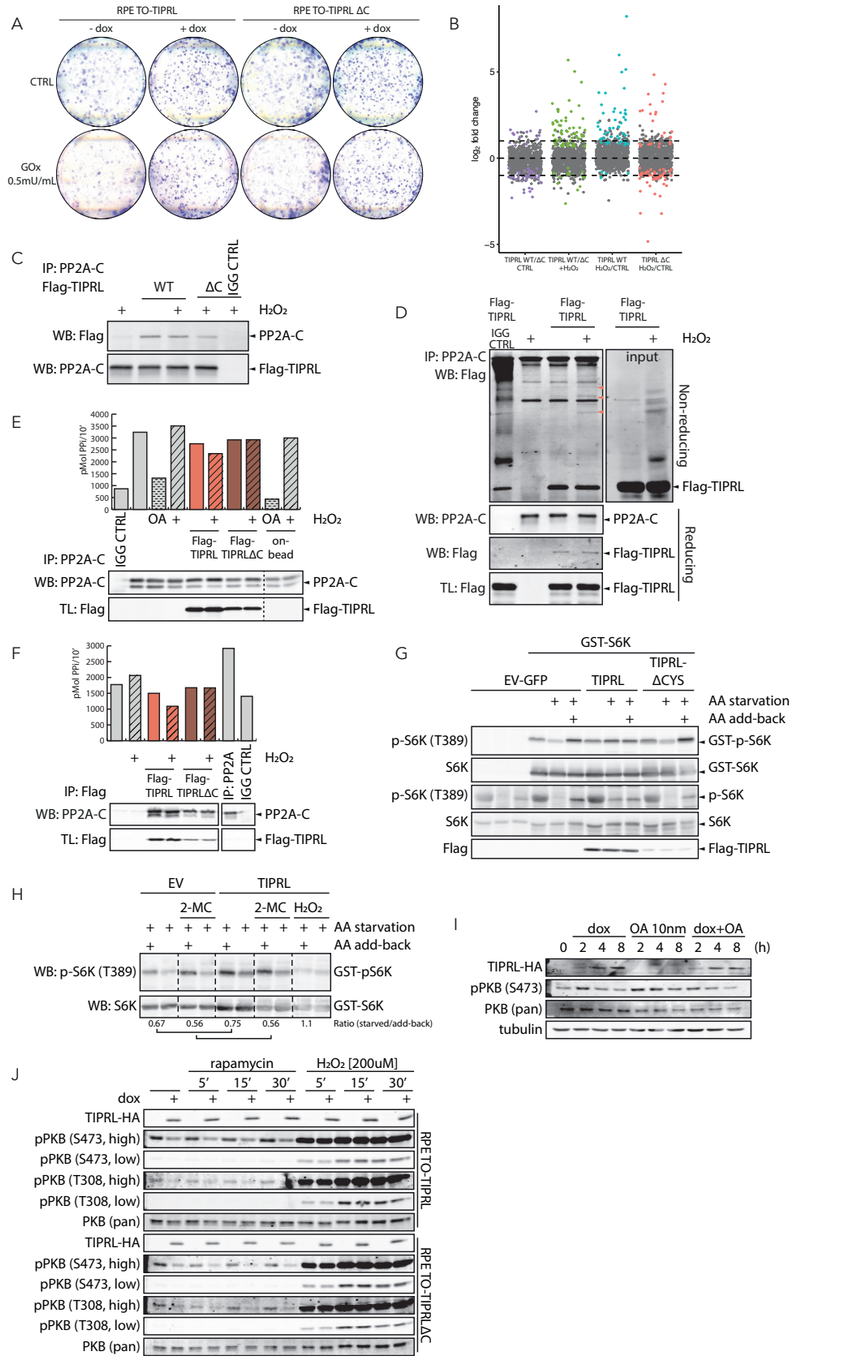

Figure 4. Functional characterization of TIPRL homodimerization. *(figure legend continues on next page)*

(**A**) Cysteine oxidation and homodimerization of TIPRL does not affect its ability to resolve redox stress. Colony formation assay in doxycycline-inducible TIRPL and TIPRLΔC cells with a TIPRL knockout background. TIPRL proficient cells are protected from GOx-induced redox stress. Removal of cysteines does not affect this. (**B**) Scatter plot of the mass spectrometry data, showing the $\log_2$ fold change of proteins within indicated conditions. Colored dots represent proteins with a p-value < 0.05 as calculated using inference of protein differential abundance by probabilistic dropout analysis (proDA). Horizontal dotted lines are positioned at $\log_2$ fold change of 1 and -1 (i.e. a 2-fold change). For the identity of specific TIPRL interactors see Tables 1-2. (**C**) Both Flag-TIPRL and Flag-TIPRLΔC interact with PP2A-C to a similar extent. Treatment with H_2O_2 does not affect this interaction. An IGG immunoprecipitation is used as a control. (**D**) Disulfide-dependent homodimers of TIPRL also interact with PP2A-C. PP2A-C was immunoprecipitated from cells expressing Flag-TIPRL and analysed under parallel reducing and non-reducing conditions. Total cell lysates are also shown (right panel, input) to indicate the MW of homodimerized TIPRL under non-reducing conditions. (**E**) Preliminary data. TIPRL inhibition of PP2A-C activity is increased under oxidizing conditions in a TIPRL cysteine-dependent manner. PP2A-C was immunoprecipitated from Flag-TIPRL and TIPRLΔC-expressing cells, which were treated as indicated with okadaic acid (OA) and H_2O_2 (the last two samples were treated on-bead). Immunoprecipitates were incubated on-bead with phosphorylated peptide and dephosphorylation (i.e. the release of PPi) was measured by colorimetric malachite green. Corresponding western blots show IP efficiency for PP2A-C and expression levels of Flag-TIPRL. Dotted lines indicate rearrangement of the same western blot. A typical experiment from a biological duplicate is shown. (**F**) Preliminary data. Phosphatases interacting with wild-type TIPRL show lower phosphatase activity is compared to those interacting with TIPRLΔC. This effect is cysteine-dependent. Overexpressed Flag-TIPRL and TIPRLΔC were immunoprecipitated from cells treated with H_2O_2 prior to lysis and phosphatase activity was measured using a malachite green detection method. Of note, less PP2A-C is co-immunoprecipitated in samples with TIPRLΔC due to lower expression, but more phosphatase activity is measured compared to wild-type TIPRL. n=1. (**G**) Preliminary data. TIPRL, but not TIPRLΔC overexpression results in sustained phosphorylation of (both endogenous and GST- overexpressed) S6K at T389 when cells are deprived of amino acids. Cells were starved from amino acids and growth factors for 1h, after which amino acids (AA) were replenished for 15 minutes and total cell lysates were analyzed on western blot. The antibody staining for endogenous p-S6K shows unspecific bands in non-starved cells, likely caused by the presence of BSA. (**H**) Preliminary data. Reducing the cellular environment reduces the ability of TIPRL to sustain p-S6K phosphorylation. Cells were treated with 100 μM β-mercaptoethanol during amino acid starvation. Dotted lines indicate rearrangement of the same western blot. The ratio of S6K phosphorylation in starved cells compared to AA addback represents the fraction of S6K phosphorylation that is retained upon amino acid starvation. (**I**) Preliminary data. TIPRL reduces the phosphorylation of PKB at S473. TIPRL expression was induced by doxycyclin treatment in TIPRL knockout cells for the indicated times. Cells were incubated with 10 nM of okadaic acid (OA) to inhibit PP2A for the indicated times. (**J**) Preliminary data. Both TIPRL and TIPRLΔC expression inhibit the phosphorylation of T308 and S473 in PKB, independent of mTORC1. Cells were treated with 50 nM rapamycin for indicated times. Oxidizing conditions, induced by treating cells with 200 μM of H_2O_2 for 10 minutes, induces phosphorylation of PKB.

Another prerequisite for reversible redox signaling is that the oxidation of cysteine thiols is transient, i.e. goes down after a period of time. Since not all TIPRL homodimers are reduced simultaneously (Figure 1H), it is possible that their reduction is enzymatically regulated. This idea is supported by the cysteine-dependent, H_2O_2-induced binding of thioredoxin (TRX) to TIPRL as shown in our mass spectrometry data (Table 2 and Figure 4B). Similar to observations such as the reduction of the disulfide-dependent complex between FOXO4 and p300 [30], it is possible that TXN in involved in actively reducing TIPRL disulfides, a process that requires the formation of a temporary mixed disulfide intermediate between TXN and TIPRL.

In addition to TXN, several peroxiredoxin isoforms (PRDX1, 2 and 5) seem to interact with TIPRL in a H_2O_2-induced, cysteine-dependent manner, as observed in our mass spectrometry experiment (Table 2). Peroxiredoxins are dedicated H_2O_2 scavengers, and are up to a million times more reactive with H_2O_2 than other known redox sensitive proteins. More importantly, they are also known to actively participate in the oxidation of proteins through redox relays. Further experiments need to be done to test whether peroxiredoxins are responsible for the oxidation of TIPRL through a redox relay. If this is the case, this would explain the high reactivity of TIPRL cysteines towards H_2O_2.

The oxidation-induced homodimerization of TIPRL occurs under near-physiological oxidizing conditions, suggesting a biological role for TIPRL oxidation. A number of studies have focused on a role for TIPRL in the inhibition of PP2A-C, although a precise role is unclear. For example, it has been suggested that TIPRL mediates binding between PP2A-C and its targets [31], but TIPRL overexpression was also reported to inhibit PP2A-C catalytic activity towards several targets, among which S6K and an ATM/ATR target [15,16]. The activity of TIPRL-bound PP2A-C was shown to be inhibited *in vitro*, and does not associate with the structural A- or regulatory B-subunits that are required for PP2A holoenzyme formation [14,15] . More recently, this was supported by the TIPRL protein structure, which provides evidence that TIPRL blocks the PP2A-C active site as well as the binding surface for the regulatory B-subunit [17]. In line with this, TIPRL was suggested to be one of five PP2A modulators, serving to prevent aspecific phosphatase activity until the PP2A trimeric holoenzyme is assembled [12]. Complementary to this, we find that TIPRL expression as well as binding inhibits the activity of PP2A-C (Figures 4E-F).

Our results also suggest that in addition to the association between PP2A-C and TIPRL, oxidation and subsequent homodimerization of TIPRL might affect the inhibitory effect of TIPRL on PP2A. Oxidizing conditions seem to further inhibit PP2A in a TIPRL cysteine-dependent manner, an observation that is lost when expressing the cysteine-free mutant of TIPRL.

The cysteine-free mutant of TIPRL is, however, still able to bind and inhibit PP2A in a redox-independent manner. Likely not all PP2A-C is bound by TIPRL and not all TIPRL is dimerized under more oxidizing conditions, so specific effects of oxidized-TIPRL-bound PP2A-C might be diluted by free PP2A-C and reduced TIPRL in these assays. In addition, TIPRL might not only affect PP2A-C catalytic activity, but instead regulate its activity towards specific targets. In line with this, examining the effects of TIPRL oxidation on the general phospho-proteome could provide evidence as to whether TIRPL oxidation indeed inhibits PP2A-C activity in cells, and if so to what extent. It is important to keep in mind that PP2A thiols are also thought to be subject to oxidation, leading to inhibition of PP2A catalytic activity [7–9], although we did not observe evidence for this in our experiments (Figures 4E-F).

TIPRL has been considered (and named after) an mTOR regulating protein because its yeast homolog, Tip41, inhibits TOR signaling by sequestration of the α4 ortholog Tap42. In contrast, however, human TIPRL has been reported to positively stimulate mTORC1 in response to amino acids [15]. We found that TIPRL overexpression results in sustained phosphorylation of S6K at T389, which seemed dependent on TIPRL oxidation since TIPRLΔC did not prevent dephosphorylation (Figure 4G, preliminary data). Interestingly, H_2O_2 treatment completely diminishes S6K phosphorylation at T389, even when amino acids are added (Figure 4H). This is in disagreement with observations that treating cells with oxidizing agents increases S6K phosphorylation, even when mTORC1 is inactivated by depleting cells from amino acids or treatment with rapamycin [32]. The molecular details underlying this discrepancy need to be further elucidated.

As discussed above, PP2A-C is a phosphatase with an extensive number of targets which is functionally involved in a diverse array of signaling pathways, sometimes in seemingly opposite manners. If PP2A-C catalytic activity were directly affected by its association with oxidized TIPRL, other targets downstream of PP2A-C would also be affected. A major target of PP2A is PKB (Akt), which is dephosphorylated and inactivated at both T308 and S473 by PP2A [20–24]. We tested whether TIPRL can induce the sustained phosphorylation of PKB. Surprisingly, TIPRL seems to negatively affect PKB phosphorylation at both T308 and S473, but this seemed not mediated though PP2A-C, suggesting a PP2A-independent role for TIPRL in the regulation of PKB. The notion that S473, an mTORC2 phosphorylation site [33], as well as T308, a PDK1-dependent phosphorylation site, are both affected, already suggests this is regulated more upstream of mTORC2 and PDK1.

When cells are also exposed to H_2O_2 to induce TIPRL oxidation and homodimerization, PKB is strongly phosphorylated at T308 and S473. This is consistent with findings that the PTEN phosphatase, well-known for its inhibition of the PI3K/PKB pathway, can also be oxidized and subsequently

inhibited [4]. Interestingly, the inhibitory effect of TIPRL on PKB phosphorylation that we observed under basal conditions is absent under oxidizing conditions (Figure 4J, preliminary data). Thus, H_2O_2 treatment seems to overrule the inhibitory effect of TIPRL on PKB phosphorylation.

Activation of PKB normally promotes glucose uptake and glycolysis. Indeed, inducible expression of TIPRL lowers both the basal glycolytic rates as well as the glycolytic capacity. However, again this seems not dependent on the ability of TIPRL to form disulfide-dependent homodimers, since re-expression of TIPRLΔC affects glycolytic function in a similar manner (Figure S3, preliminary data). Furthermore, the relative contribution to cellular bioenergetics of mitochondrial respiration and glycolysis (measured by %OCR/ECAR, data not shown) indicate a relative increase of mitochondrial activity in RPE cells expressing TIPRL, independent of cysteines.

Of note, PP2A is not the only phosphatase that seems to interact with TIPRL. Our mass spectrometry data suggest that, among others, related phosphatases PPP4 (catalytic and regulatory subunit), PPP6 (catalytic and regulatory subunits) and PPP1 (regulatory subunit) bind to TIPRL in a cysteine-dependent manner (Table 1). These interactions were also reported by others [16,34,35], and they suggest a more widespread role for TIPRL in the regulation of phosphatases. Future studies should therefore also focus on the effects of these interactions in order to elucidate the effect of TIPRL on these phosphatases.

Our results suggest that rather than affecting PP2A-C catalytic activity in general, the oxidation of TIPRL may affect pathways downstream of PP2A-C in different manners. However, we were so far unable to link the observed redox-dependent dimerization of TIPRL to newly discovered TIPRL-dependent phenotypes like oxidant-induced loss of viability or changes in metabolism. Further studies should aim at further elucidating a role for redox regulation of TIPRL.

MATERIALS AND METHODS

Cell Lines and Culturing

HEK293T were cultured in bicarbonate-buffered DMEM, supplemented with 10% FBS (Bodinco BDC-40506-C05), 2 mM L-glutamine (Lonza, BE17-605E) and 100 U/mL penicillin-streptomycin (Lonza, DE17-602E) and kept at 37°C and under a 6% CO^2 atmosphere. Transfections of HEK293T cells were carried out using PEI (Sigma-Aldrich, P3640) or Fugene-HD reagent (Promega, E2311) following the manufacturer's instructions. After two days, cells were harvested for further analysis. During amino acid starvation, cells were washed with PBS twice before they were incubated in amino acid free bicarbonate-buffered DMEM (Gibco) for 60 minutes. Amino acids (Bio Whitacker) were added back in the amino acid free medium for 15 minutes prior to lysis. CRISPR knockout lines were a kind gift of J. van den Berg and J. Nieuwenhuis. In short, 200k cells were plated with an siRNA for p53. After 8h, cells were transfected with pX330 (addgene plasmid ID 42230) and TIA-2A-Blast selection plasmids. Cells were selected with blasicidin and monoclonal knockout lines were verified by western blotting. Doxycylcin-inducible TIRPL or TIPRLΔC cells were transduced with lentivirus containing pINDUCER20-TIPRL or -TIPRLΔC and monoclonally selected for stable transduction using G418. TIPRL expression was confirmed by sequencing and western blotting.

For colony outgrowth assays, 1000 cells were seeded in a 6-wells plate. After allowing them to adhere for 4 hours, treatments were started as indicated. At 10 days post seeding, cells were fixed in methanol and stained with 0.5% crystal violet in 25% methanol. Plates were dried before imaging.

Plasmids and Reagents

Human TIPRL with *att* recombination sites were cloned from cDNA using the following primers: 5'-GGGGACAAGTTTGTACAAAAAAGCAGGCTTGATGATGATCCACGGCTTCCAG-3', R_5'-GGGGACCACTTTGTACAAGAAAGCTGGGTATTCCACTTGTGTACTTTTTTGTG-3'. Using Gateway technology (Invitrogen) entry clones were generated. The peroxidatic and resolving cysteine mutants of PRDX1-5 were created by site-directed mutagenesis PCR using the following primers: C14S_F_5'-GGGATTTCTCTTTCGGGCCCT-3', C14S_R_5'-AGGGCCCGAAAGAGAAATCCC-3', C75S_F_5'- TGCGTTAAGATCCGTAAACAACTAC-3', C75S_R_5'- GTAGTTGTTTACGGATCTTAACGCA-3', C87S_F_5'- AAAGTGGCCTCAGCTGHAAGAGT-3', C87S_R_5'- ACTCTTCAGCTGAGGCCACTTT-3', C249S_F_5'-GGGATTTCTCTTTCGGGCCCT-3', C249S_R_5'-AGGGCCCGAAAGAGAAATCCC-3', and verified by sequencing.

Gateway technology (Life Technologies) was used to create N-terminally tagged Flag-His, HA- and doxycylcin-inducible expression vectors (backbones pCDNA3 and pINDUCER20, Addgene #44012) from the resulting TIPRL cysteine mutant entry clones. The GST-S6K construct was a kind gift from Fried Zwartkruis. TIPRL sgRNA sequences are 5'-GACCCACATCATGAAGTCGG-3' and 5'-CATCATGAAGTCGGCGGATG-3' TIPRL knockdown was performed using smartpool RNAi oligos from Dharmacon (261726). β-mercaptoethanol was used in a concentration of 100 μM. Rapamycin was purchased from Biomol and used at 50 nM, okadaic acid was used at 500 nM unless stated otherwise. 30% H_2O_2 (Sigma 31642) was freshly diluted to a stock of 10 or 100 mM in H_2O for every experiment. Unless stated otherwise, H_2O_2 treatments were 200 for 10 minutes.

Co-Immunoprecipitations and Western Blotting

After treatment as indicated, cells were lysed using a buffer containing 50 mM Tris-HCl pH 7.5, 1% TX100, 1.5 mM MgCl2, 5 mM EDTA, 100 mM NaCl, NaF, Leupeptin and Aprotinin. 100 mM iodoacetamide was added to the lysis buffer to prevent post-lysis cysteine oxidation and to inactivate disulfide reducing enzymes. After centrifugation at 14000 rpm for 10 min, 5% of the supernatant was kept as input and the remaining supernatant was used for immunoprecipitation with anti-Flag-M2 affinity gel (Sigma A222). After a 2 h incubation whilst gently mixing, immunoprecipitates were washed 4 times with lysis buffer containing 1 M NaCl and samples were boiled for 5 min in sample buffer with or without the reducing agent β-mercaptoethanol. Samples were separated on a 10% polyacrylamide gel and transferred to immobilon-FL membranes (using standard protocols) before staining and antibody detection.

Antibodies that were used are Flag M2 (Sigma F3165), HA (12CA5, monoclonal from hybridoma cell lines and SC805), TIPRL (Abcam), S6K and pS6K (Cell signaling, CS2708 and CSS9205), PKB and p-PKB (Cell signaling, CS2920, CS4060 and CS13038), GST (SC138), anti-tubulin (Merck Millipore CP06), PP2A-C (Abcam ab188253). Detection of fluorescent secondary antibodies was performed using the LI-COR Biosciences Odyssey Infrared Imaging System or the Amersham Typhoon NIR Plus Biomolecular Imager (GE Healthcare), detection of secondary HRP-antibodies was performed on the FUJIFILM Luminescent Image Analyser LAS-3000.

2D Diagonal Electrophoresis

Immunoprecipitates were separated in the first dimension on a 10% SDS-PAGE gel and total protein content was stained using SimplyBlue. Gel lanes were cut out and incubated with 2x Laemmli sample buffer containing β-mercaptoethanol for 30' at room temperature. In the second dimension, reduced gel lanes were loaded on a second 10% SDS-PAGE gel at a right angle to the first dimension. Detection of proteins was done using SimplyBlue stain and using western blotting.

Mass Spectrometry

For the identification of TIPRL interactors the lysate of 4x20cm dishes were used for each pulldown on 75 ml of Flag-M2 beads similar to the immunoprecipitation experiments described above. All immunoprecipitations were performed using three biological replicates. After washing, beads were resuspended with 8M urea in 1M ammonium bicarbonate (ABC), reduced and alkylated in 10 mM TCEP and 40 mM chloroacetamide (CAA) for 30 minutes at RT. After fourfold dilution with 1M ABC, proteins were digested overnight on-bead with 250 ng Trypsin/LysC (Promega V5071) per sample

at 37°C. Samples were cleaned up with in-house-made C18 stagetips.

Mass spectrometry was performed as previously described [19]. Peptides were separated on a 30-cm pico-tip column (75 µm ID, New Objective) and were packed in-house with 3 µm aquapur gold C-18 material (Dr. Maisch) using a 140-min gradient (7–80% ACN 0.1% FA), delivered by an easy-nLC 1000 (LC120, Thermo Scientific), and electro-sprayed directly into an Orbitrap Fusion Tribrid Mass Spectrometer (Thermo Scientific). Raw files were analyzed with the MaxQuant software version 1.5.2.8 with oxidation of methionine, alkylation with N-ethylmaleimide and carbamidomethylation set as variable modifications. The Human protein database of UniProt was searched with both the peptide as well as the protein false discovery rate set to 1%. Downstream analysis was done using R version 4.0.2.

Data Analysis

A SummarizedExperiment object was created using LFQ data from the MaxQuant proteinGroups file and corresponding protein information. Proteins were filtered for reverse hits and standard contaminants. Next, we selected proteins that were identified with three or more unique peptides and were measured in at least one sample in 2 or more replicates. Data was $\log_2$-transformed and normalized using quantile normalization, which ensures overall intensity differences due to IP efficiency differences between samples are equalized while maintaining identical statistical distributions. ProDA model fitting was performed using sample names as design input and the number of proteins in the data as the number of subsamples. To test for differential protein abundance, the proDa fit object was used for comparing wild-type against mutant TIPRL or H_2O_2-treated against control conditions.

Size Exclusion Chromatography

20 million Flag-TIPRL transfected 293T cells were lysed in 1 ml of lysis buffer containing 100 mM iodoacetamide (desctibed abovetion). Lysates were cleared by sonication and centrifugation and subsequently fractionated in 52 fractions (1 ml per minute, 2 ml per fraction) on a HiLoad 16/60 Superdex 200 prep grade column (GE Healthcare) using lysis buffer without iodoacetamide as flow buffer. Upon fractionation, IPs were performed as described above. For quantification, band intensity was measured in ImageJ. The relative intensity was calculated per band and per fractions relative to the total protein intensity per band (e.g. the intensities of the monomeric TIPRL band in all fractions were added up), and the percentage of total per fraction was plotted. The peak of each data line (indicated with the vertical lines) represents the fraction in which the respective band was enriched the most.

PP2A Activity Assays

The activity of the catalytic PP2A-subunit was assayed according manufacturers protocol using the PP2A Immunoprecipitation Phosphatase Assay Kit (Upstate). In short, transfected 293T cells were lysed in phosphatase lysis buffer (20 mM imidazole-HCL, 2 mM EDTA, 2 mM EGTA pH 7.0 containing, aprotinin, leupeptin and 1 mM PMSF) and homogenized by sonication. PP2A-C or Flag-TIPRL was immunoprecipitated and washed with TBS and Ser/Thr assay buffer. Beads were incubated with phosphorylated peptide whilst shaking, and dephosphorylation (release of phosphate) was assayed by incubating the supernatant (taken of the beads) with a Malachite Green Phosphate Detection Solution. Absorbance values were measured at 655 nm and compared to the standard curve to determine the amount of released phosphate per sample.

SUPPLEMENTAL MATERIALS AND METHODS

Seahorse Flux Analysis

Extracellular consumption rates (ECAR) and oxygen consumption rates (OICR were measured using a Seahorse Bioscience XFe24 Analyzer in in mpH (milli pH) per min and pmol O2 per min, respectively. Cells were treated with doxycycline. After 24h, 40k cells were seeded in fibronectin-coated XF24 cell culture microplates (Seahorse Bioscience) and grown for 24h. Culture medium was replaced 1h before measurements and incubated at 37 °C. For the glycolysis stress test, culture medium was replaced by Sea-horse XF Base medium, supplemented with 2 mM L-glutamine and 26 µL NaOH (1M). During the test 10 mM glucose, 5 mM oligomycin and 100 mM 2-deoxyglucose (Sigma-Aldrich) were injected to each well after 18, 36 and 65 min, respectively. For the mitochondrial stress test, culture medium was replaced by Seahorse XF Base medium (Seahorse Bioscience), supplemented with 10 mM glucose (Sigma-Aldrich), 10 mM pyruvate (Sigma-Aldrich), 2 mM L-glutamine (Sigma-Aldrich), and 27 µL NaOH (1M). During the measurements, 1 µM oligomycin, 1 µM FCCP and µM of rotenone and antimycin A (all Sigma-Aldrich) were injected to each well after 18, 45 and 63cmin, respectively. After injections, plates were mixed for 4 minutes and measurements of 2 min were performed in triplicates, The first measurements after oligomycin injections were preceded by 5 min mixture time, followed by 8 min pause for the mitochondrial stress test and 5 min mixture time followed by 10 min pause for the glycolysis stress test. OCR and ECAR values per group were normalized to the total amount of protein present per well.

TABLES

Table 1. MSMS data corresponding to Figure 4B: Cysteine- and H_2O_2-dependent interactors of TIPRL and TIPRLΔC

Table 1. MSMS data corresponding to Figure 4B: Cysteine- and H_2O_2-dependent interactors of TIPRL and TIPRLΔC

gene	uniprot ID	protein	log ratio	p-value
interactors for TIPRLΔC, H_2O_2 vs. untreated				
Q92945-2	KHSRP	Far upstream element-binding protein 2	4.8	<0.001
Q06830	PRDX1	Peroxiredoxin-1	4.3	<0.001
E9PHK9	TCOF1	Treacle protein	3.8	0.004
Q6P2E9	EDC4	Enhancer of mRNA-decapping protein 4	3.7	0.003
P10599	TXN	Thioredoxin	3.3	<0.001
P32119	PRDX2	Peroxiredoxin-2	3.1	0.002
Q96F45	ZNF503	Zinc finger protein 503	2.8	0.012
Q4VCS5	AMOT	Angiomotin	2.7	<0.001
P04406	GAPDH	Glyceraldehyde-3-phosphate dehydrogenase	2.7	0.001
P49790	NUP153	Nuclear pore complex protein Nup153	2.6	0.001
Q9P258	RCC2	Protein RCC2	2.6	0.021
P05204	HMGN2	Non-histone chromosomal protein HMG-17	2.2	0.012
P26599	PTBP1	Polypyrimidine tract-binding protein 1	1.5	0.008
Q8IV96	DDX6	Probable ATP-dependent RNA helicase DDX6	1.5	0.011
H0Y5D5	CIZ1	Cip1-interacting zinc finger protein	1.3	0.019
Q9P2L0	ATAD2	ATPase family AAA domain-containing protein 2	1.2	0.013
E7ETK8	AARS	Alanine--tRNA ligase, cytoplasmic	1.2	0.021
P12270	TPR	Nucleoprotein TPR	1.0	0.037
interactors for H_2O_2-treated TIPRL, wild-type vs. ΔC				
P32119	PRDX2	Peroxiredoxin-2	5.7	<0.001
P30044-2	PRDX5	Peroxiredoxin-5, mitochondrial	5.0	0.001
Q06830	PRDX1	Peroxiredoxin-1	4.4	<0.001
P10599	TXN	Thioredoxin	3.3	<0.001
O95685	PPP1R3D	Protein phosphatase 1 regulatory subunit 3D	3.2	0.012
B4DJ60	PLS3	Plastin-3	3.0	0.001
C9J5L7	TNRC6B	Trinucleotide repeat-containing gene 6B protein	2.8	0.003
Q9UHD1	CHORDC1	Cysteine and histidine-rich domain-containing protein 1	2.7	<0.001
Q96M99	CTTN	Src substrate cortactin	2.7	0.011
E7EVA0	MAP4	Microtubule-associated protein	2.3	0.002
Q9H3K6	BOLA2	BolA-like protein 2	2.3	0.006
Q8TEQ6	GEMIN5	Gem-associated protein 5	2.2	<0.001
Q9UHV9	PFDN2	Prefoldin subunit 2	2.2	0.012
E9PH12	WAPAL	Wings apart-like protein homolog	2.2	0.035
E9PBS1	PAICS	Phosphoribosylaminoimidazole carboxylase, phosphoribosylaminoimidazole succinocarboxamide synthetase (Fragment)	2.1	0.006
Q32Q12	NME1-NME2	Nucleoside diphosphate kinase	2.1	0.039
E7ETK8	AARS	Alanine--tRNA ligase, cytoplasmic	2.0	0.001
E7EMC7	SQSTM1	Sequestosome-1	1.9	0.002
F8WA86	CNN3	Calponin-3	1.9	0.035
Q99497	PARK7	Protein DJ-1	1.8	0.001
Q9UEG4	ZNF629	Zinc finger protein 629	1.8	0.006
O00743-2	PPP6C	Isoform 2 of Serine/threonine-protein phosphatase 6 catalytic subunit	1.7	0.015
C9JRJ5	LIMD1	LIM domain-containing protein 1	1.6	0.008
Q9NY27	PPP4R2	Serine/threonine-protein phosphatase 4 regulatory subunit 2	1.6	0.008
P60510	PPP4C	Serine/threonine-protein phosphatase 4 catalytic subunit	1.6	0.033
B4DP17	CNBP	Cellular nucleic acid-binding protein	1.6	0.035
Q5JS25-5	PRRC2B	Protein PRRC2B	1.6	0.039
P11802	CDK4	Cyclin-dependent kinase 4	1.5	0.004
A8K8U5	TTK	Dual specificity protein kinase TTK	1.5	0.008
O15084	ANKRD28	Serine/threonine-protein phosphatase 6 regulatory ankyrin repeat subunit A	1.5	0.048
P13639	EEF2	Elongation factor 2	1.4	0.005
Q9UPN7	PPP6R1	Serine/threonine-protein phosphatase 6 regulatory subunit 1	1.4	0.024
O60566	BUB1B	Mitotic checkpoint serine/threonine-protein kinase BUB1 beta	1.4	0.035
F2Z3M7	PPP6R2	Serine/threonine-protein phosphatase 6 regulatory subunit 2	1.4	0.045
F5H012	TRIM21	E3 ubiquitin-protein ligase TRIM21	1.3	0.011
Q5W0B1	RNF219	RING finger protein 219	1.3	0.028
P48507	GCLM	Glutamate--cysteine ligase regulatory subunit	1.3	0.046
B1AHB1	MCM5	DNA replication licensing factor MCM5	1.2	0.016
P46781	RPS9	40S ribosomal protein S9	1.2	0.024
Q9H7E2-3	TDRD3	Tudor domain-containing protein 3	1.1	0.008
O14646-2	CHD1	Chromodomain-helicase-DNA-binding protein 1	1.1	0.008
O95239	KIF4A	Chromosome-associated kinesin KIF4A	1.1	0.010
Q15365	PCBP1	Poly(rC)-binding protein 1	1.1	0.023
C9J4Z3	RPL37A	60S ribosomal protein L37a	1.0	0.019
P62714	PPP2CB	Serine/threonine-protein phosphatase 2A catalytic subunit beta isoform	1.0	0.029
P04181	OAT	Ornithine aminotransferase, mitochondrial	1.0	0.049
interactors for wild-type TIPRL, H_2O_2 vs. untreated				
P32119	PRDX2	Peroxiredoxin-2	8.2	<0.001
Q06830	PRDX1	Peroxiredoxin-1	6.0	<0.001
Q92945-2	KHSRP	Far upstream element-binding protein 2	5.1	<0.001
P10599	TXN	Thioredoxin	5.0	<0.001
P30044-2	PRDX5	Peroxiredoxin-5, mitochondrial	4.1	0.005
E7ETK8	AARS	Alanine--tRNA ligase, cytoplasmic	3.8	<0.001
E9PHK9	TCOF1	Treacle protein	3.8	0.004
P04406	GAPDH	Glyceraldehyde-3-phosphate dehydrogenase	3.1	<0.001
B4DJ60	PLS3	Plastin-3	2.9	0.001
Q9H3K6	BOLA2	BolA-like protein 2	2.8	0.008
Q9P258	RCC2	Protein RCC2	2.7	0.024
P49790	NUP153	Nuclear pore complex protein Nup153	2.6	0.003
Q6P2E9	EDC4	Enhancer of mRNA-decapping protein 4	2.6	0.025
E7EVA0	MAP4	Microtubule-associated protein	2.6	0.030
B5MDQ0	ERCC6L	DNA excision repair protein ERCC-6-like	2.5	0.042
Q99497	PARK7	Protein DJ-1	2.4	0.001
Q9UHD1	CHORDC1	Cysteine and histidine-rich domain-containing protein 1	2.2	0.001
Q96M99	CTTN	Src substrate cortactin	2.2	0.026
O95239	KIF4A	Chromosome-associated kinesin KIF4A	2.1	0.001
P35659	DEK	Protein DEK	2.0	0.029
P26599	PTBP1	Polypyrimidine tract-binding protein 1	1.8	0.003
Q4VCS5	AMOT	Angiomotin	1.8	0.004
B4DP17	CNBP	Cellular nucleic acid-binding protein	1.8	0.020
Q8WWK9	CKAP2	Cytoskeleton-associated protein 2	1.7	0.002
P11802	CDK4	Cyclin-dependent kinase 4	1.7	0.005
E9PBS1	PAICS	Phosphoribosylaminoimidazole carboxylase, phosphoribosylaminoimidazole succinocarboxamide synthetase (Fragment)	1.7	0.025
Q8TEQ6	GEMIN5	Gem-associated protein 5	1.5	0.005
Q08945	SSRP1	FACT complex subunit SSRP1	1.4	0.017
A8K8U5	TTK	Dual specificity protein kinase TTK	1.4	0.036
P11387	TOP1	DNA topoisomerase 1	1.3	0.019
Q9Y5B9	SUPT16H	FACT complex subunit SPT16	1.3	0.027
Q15637-4	SF1	Splicing factor 1	1.2	0.008
P35520	CBS	Cystathionine beta-synthase	1.2	0.021
B7WNZ6	PRRC2C	Protein PRRC2C	1.1	0.006
B8ZZN6	SUMO1	Small ubiquitin-related modifier 1	1.1	0.030
B1AJY7	PSMD10	26S proteasome non-ATPase regulatory subunit 10	1.1	0.047
P78371	CCT2	T-complex protein 1 subunit beta	1.0	0.016
interactors for untreated TIPRL, wild-type vs. ΔC				
Q06830	PRDX1	Peroxiredoxin-1	2.7	<0.001
P10599	TXN	Thioredoxin	1.6	0.006
Q9NY27	PPP4R2	Serine/threonine-protein phosphatase 4 regulatory subunit 2	1.6	0.008
O15084	ANKRD28	Serine/threonine-protein phosphatase 6 regulatory ankyrin repeat subunit A	1.6	0.042
Q9UPN7	PPP6R1	Serine/threonine-protein phosphatase 6 regulatory subunit 1	1.5	0.017
P60510	PPP4C	Serine/threonine-protein phosphatase 4 catalytic subunit	1.5	0.044
E7EMC7	SQSTM1	Sequestosome-1	1.4	0.008
E7EPF0	ZCCHC17	Nucleolar protein of 40 kDa	1.4	0.015
O00743-2	PPP6C	Isoform 2 of Serine/threonine-protein phosphatase 6 catalytic subunit	1.3	0.048
Q14126	DSG2	Desmoglein-2	1.2	0.036
O14646-2	CHD1	Chromodomain-helicase-DNA-binding protein 1	1.1	0.024

Table 2. List of cysteine- and H_2O_2-dependent interactors of TIPRL

	uniprot ID	gene	protein
1	*P26599*	PTBP1	Polypyrimidine tract-binding protein 1
2	*Q6P2E9*	EDC4	Enhancer of mRNA-decapping protein 4
3	*Q8WWK9*	CKAP2	Cytoskeleton-associated protein 2
4	*Q9Y5B9*	SUPT16H	FACT complex subunit SPT16
5	*P35659*	DEK	Protein DEK
6	*P11387*	TOP1	DNA topoisomerase 1
7	*Q15637*	SF1	Splicing factor 1
8	*B8ZZN6*	SUMO1	Small ubiquitin-related modifier 1
9	*E9PHK9*	TCOF1	Treacle protein
10	*P49790*	NUP153	Nuclear pore complex protein Nup153
11	*P04406*	GAPDH	Glyceraldehyde-3-phosphate dehydrogenase
12	*Q08945*	SSRP1	FACT complex subunit SSRP1
13	*Q92945*	KHSRP	Far upstream element-binding protein 2
14	*P35520*	CBS	Cystathionine beta-synthase
15	*B5MDQ0*	ERCC6L	DNA excision repair protein ERCC-6-like
16	*Q9P258*	RCC2	Protein RCC2
17	*P78371*	CCT2	T-complex protein 1 subunit beta
18	*Q4VCS5*	AMOT	Angiomotin
19	*B7WNZ6*	PRRC2C	Protein PRRC2C
20	*B4DP17*	CNBP	Cellular nucleic acid-binding protein
21	*B1AJY7*	PSMD10	26S proteasome non-ATPase regulatory subunit 10
22	*Q96H99*	CTTN	Src substrate cortactin
23	*O95239*	KIF4A	Chromosome-associated kinesin KIF4A
24	*A8K8U5*	TTK	Dual specificity protein kinase TTK
25	*E9PBS1*	PAICS	Phosphoribosylaminoimidazole carboxylase, phosphoribosylaminoimidazole succinocarboxamide synthetase (Fragment)
26	*Q9H3K6*	BOLA2	BolA-like protein 2
27	*P11802*	CDK4	Cyclin-dependent kinase 4
28	*E7EVA0*	MAP4	Microtubule-associated protein
29	*E7ETK8*	AARS	Alanine--tRNA ligase, cytoplasmic
30	*Q99497*	PARK7	Protein DJ-1
31	*P30044*	PRDX5	Peroxiredoxin-5, mitochondrial
32	*B4DJ60*	PLS3	Plastin-3
33	*Q8TEQ6*	GEMIN5	Gem-associated protein 5
34	*Q9UHD1*	CHORDC1	Cysteine and histidine-rich domain-containing protein 1
35	*P10599*	TXN	Thioredoxin
36	*P32119*	PRDX2	Peroxiredoxin-2
37	*Q06830*	PRDX1	Peroxiredoxin-1

SUPPLEMENTARY FIGURES AND LEGENDS

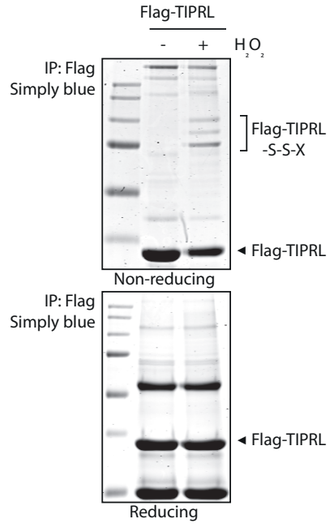

Figure S1. Simply blue-stained SDS-PAGE gel as was used for the experiment shown in Figure 2B (right lane).
Cells expressing Flag-TIPRL were exposed to 200 μM of H_2O_2 for 10 minutes and cells lysates were separated under reducing (lower panel) and non-reducing (upper panel) SDS-PAGE. SDS-PAGE gels were stained for total protein using Simply blue stain.

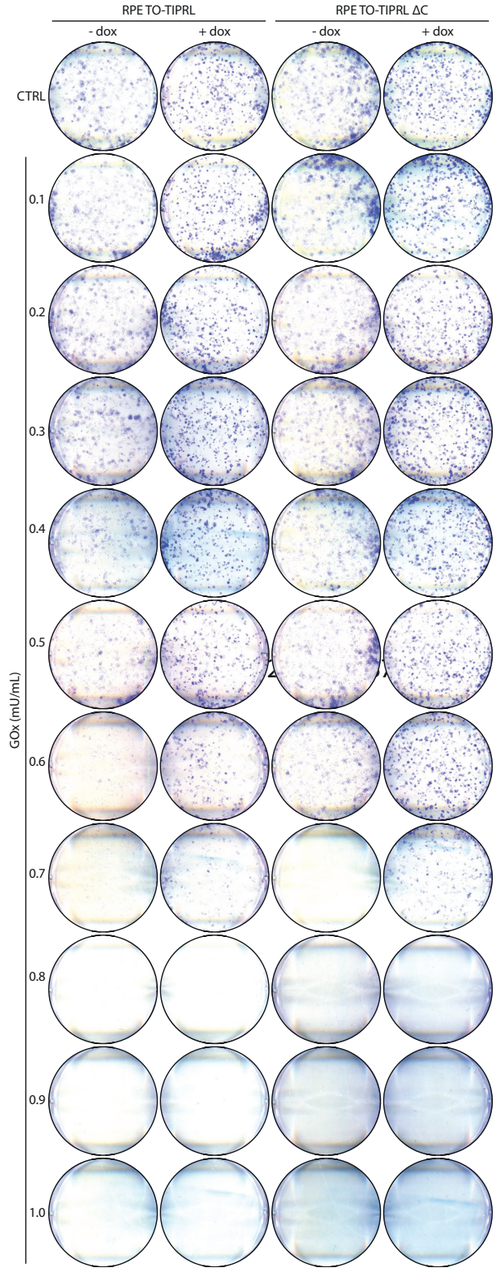

Figure S2. Extended figure corresponding to figure 4A.
Cysteine oxidation and homodimerization of TIPRL does not affect its ability to resolve redox stress. Colony formation assay in doxycycline-inducible TIRPL and TIPRLΔC cells with a TIPRL knockout background. TIPRL proficient cells are protected from GOx-induced redox stress. Removal of cysteines does not affect this.

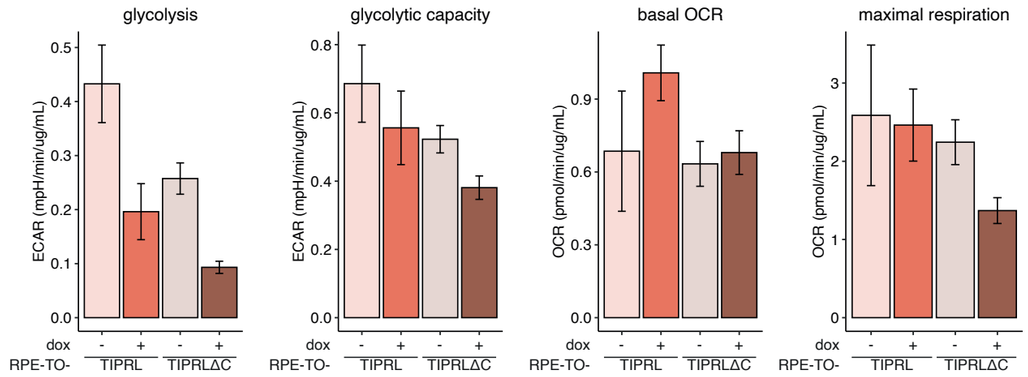

Figure S3. TIPRL decreases glycolytic capacity in a cysteine-independent manner.
ECAR (extracellular acidification rate) was determined in a glycolysis stress test and OCR (oxygen consumption rate) was determined in a mitochondrial stress test by Seahorse analysis of doxycyclin-inducible TIPRL or TIPRLΔC cells. TIRPL expression lowers both the basal glycolytic rates and maximal glycolysis. (n=3, mean and SD are plotted)

REFERENCES

1. Spencer, N.Y.; Engelhardt, J.F. The Basic Biology of Redoxosomes in Cytokine-Mediated Signal Transduction and Implications for Disease-Specific Therapies. *Biochemistry-us* **2014**, *53*, 1551–1564, doi:10.1021/bi401719r.

2. Mahadev, K.; Motoshima, H.; Wu, X.; Ruddy, J.M.; Arnold, R.S.; Cheng, G.; Lambeth, J.D.; Goldstein, B.J. The NAD(P)H Oxidase Homolog Nox4 Modulates Insulin-Stimulated Generation of H2O2 and Plays an Integral Role in Insulin Signal Transduction. *Mol Cell Biol* **2004**, *24*, 1844–1854, doi:10.1128/mcb.24.5.1844-1854.2004.

3. Tanner, J.J.; Parsons, Z.D.; Cummings, A.H.; Zhou, H.; Gates, K.S. Redox Regulation of Protein Tyrosine Phosphatases: Structural and Chemical Aspects. *Antioxid Redox Sign* **2011**, *15*, 77–97, doi:10.1089/ars.2010.3611.

4. Lee, S.-R.; Yang, K.-S.; Kwon, J.; Lee, C.; Jeong, W.; Rhee, S.G. Reversible Inactivation of the Tumor Suppressor PTEN by H2O2 *. *J Biol Chem* **2002**, *277*, 20336–20342, doi:10.1074/jbc.m111899200.

5. Frijhoff, J.; Dagnell, M.; Godfrey, R.; Östman, A. Regulation of Protein Tyrosine Phosphatase Oxidation in Cell Adhesion and Migration. *Antioxid Redox Sign* **2014**, *20*, 1994–2010, doi:10.1089/ars.2013.5643.

6. Czech, M.P.; Lawrence, J.C.; Lynn, W.S. Evidence for the Involvement of Sulfhydryl Oxidation in the Regulation of Fat Cell Hexose Transport by Insulin. *Proc National Acad Sci* **1974**, *71*, 4173–4177, doi:10.1073/pnas.71.10.4173.

7. Sommer, D.; Coleman, S.; Swanson, S.A.; Stemmer, P.M. Differential Susceptibilities of Serine/Threonine Phosphatases to Oxidative and Nitrosative Stress. *Arch Biochem Biophys* **2002**, *404*, 271–278, doi:10.1016/s0003-9861(02)00242-4.

8. Foley, T.D.; Kintner, M.E. Brain PP2A Is Modified by Thiol-Disulfide Exchange and Intermolecular Disulfide Formation. *Biochem Bioph Res Co* **2005**, *330*, 1224 1229, doi:10.1016/j.bbrc.2005.03.108.

9. Foley, T.D.; Petro, L.A.; Stredny, C.M.; Coppa, T.M. Oxidative Inhibition of Protein Phosphatase 2A Activity: Role of Catalytic Subunit Disulfides. *Neurochem Res* **2007**, *32*, 1957–1964, doi:10.1007/s11064-007-9394-x.

10. Eichhorn, P.J.A.; Creyghton, M.P.; Bernards, R. Protein Phosphatase 2A Regulatory Subunits and Cancer. *Biochimica Et Biophysica Acta Bba - Rev Cancer* **2009**, *1795*, 1–15, doi:10.1016/j.bbcan.2008.05.005.

11. Arnold, H.K.; Sears, R.C. A Tumor Suppressor Role for PP2A-B56α through Negative Regulation of c-Myc and Other Key Oncoproteins. *Cancer Metast Rev* **2008**, *27*, 147–158, doi:10.1007/s10555-008-9128-9.

12. Sents, W.; Ivanova, E.; Lambrecht, C.; Haesen, D.; Janssens, V. The Biogenesis of Active Protein Phosphatase 2A Holoenzymes: A Tightly Regulated Process Creating Phosphatase Specificity. *Febs J* **2013**, *280*, 644–661, doi:10.1111/j.1742-4658.2012.08579.x.

13. Jacinto, E.; Guo, B.; Arndt, K.T.; Schmelzle, T.; Hall, M.N. TIP41 Interacts with TAP42 and Negatively Regulates the TOR Signaling Pathway. *Mol Cell* **2001**, *8*, 1017–1026, doi:10.1016/s1097-2765(01)00386-0.

14. Smetana, J.H.C.; Zanchin, N.I.T. Interaction Analysis of the Heterotrimer Formed by the Phosphatase 2A Catalytic Subunit, A4 and the Mammalian Ortholog of Yeast Tip41 (TIPRL). *Febs J* **2007**, *274*, 5891 5904, doi:10.1111/j.1742-4658.2007.06112.x.

15. Nakashima, A.; Tanimura-Ito, K.; Oshiro, N.; Eguchi, S.; Miyamoto, T.; Momonami, A.; Kamada, S.; Yonezawa, K.; Kikkawa, U. A Positive Role of Mammalian Tip41-like Protein, TIPRL, in the Amino-Acid Dependent MTORC1-Signaling Pathway through Interaction with PP2A. *Febs Lett* **2013**, *587*, 2924 2929, doi:10.1016/j.febslet.2013.07.027.

16. McConnell, J.L.; Gomez, R.J.; McCorvey, L.R.A.; Law, B.K.; Wadzinski, B.E. Identification of a PP2A-Interacting Protein That Functions as a Negative Regulator of Phosphatase Activity in the ATM/ATR Signaling Pathway. *Oncogene* **2007**, *26*, 6021 6030, doi:10.1038/sj.onc.1210406.

17. Scorsato, V.; Lima, T.B.; Righetto, G.L.; Zanchin, N.I.T.; Brandão-Neto, J.; Sandy, J.; Pereira, H.D.; Ferrari, Á.J.R.; Gozzo, F.C.; Smetana, J.H.C.; et al. Crystal Structure of the Human Tip41 Orthologue, TIPRL, Reveals a Novel Fold and a Binding Site for the PP2Ac C-Terminus. *Sci Rep-uk* **2016**, *6*, 30813, doi:10.1038/srep30813.

18. Jeon, S.-J.; Ahn, J.-H.; Halder, D.; Cho, H.-S.; Lim, J.-H.; Jun, S.Y.; Lee, J.-J.; Yoon, J.-Y.; Choi, M.-H.; Jung, C.-R.; et al. TIPRL Potentiates Survival of Lung Cancer by Inducing Autophagy through the EIF2α-ATF4 Pathway. *Cell Death Dis* **2019**, *10*, 959, doi:10.1038/s41419-019-2190-0.

19. Putker, M.; Madl, T.; Vos, H.R.; Ruiter, H. de; Visscher, M.; Berg, M.C.W. van den; Kaplan, M.; Korswagen, H.C.; Boelens, R.; Vermeulen, M.; et al. Redox-Dependent Control of FOXO/DAF-16 by Transportin-1. *Mol Cell* **2013**, *49*, 730 742, doi:10.1016/j.molcel.2012.12.014.

20. Andjelković, M.; Jakubowicz, T.; Cron, P.; Ming, X.F.; Han, J.W.; Hemmings, B.A. Activation and Phosphorylation of a Pleckstrin Homology Domain Containing Protein Kinase (RAC-PK/PKB) Promoted by Serum and Protein Phosphatase Inhibitors. *Proc National Acad Sci* **1996**, *93*, 5699–5704, doi:10.1073/pnas.93.12.5699.

21. Meier, R.; Thelen, M.; Hemmings, B.A. Inactivation and Dephosphorylation of Protein Kinase Bα (PKBα) Promoted by Hyperosmotic Stress. *Embo J* **1998**, *17*, 7294–7303, doi:10.1093/emboj/17.24.7294.

22. Chen, D.; Fucini, R.V.; Olson, A.L.; Hemmings, B.A.; Pessin, J.E. Osmotic Shock Inhibits Insulin Signaling by Maintaining Akt/Protein Kinase B in an Inactive Dephosphorylated State. *Mol Cell Biol* **1999**, *19*, 4684–4694, doi:10.1128/mcb.19.7.4684.

23. Ivaska, J.; Nissinen, L.; Immonen, N.; Eriksson, J.E.; Kähäri, V.-M.; Heino, J. Integrin A2β1 Promotes Activation of Protein Phosphatase 2A and Dephosphorylation of Akt and Glycogen Synthase Kinase 3β. *Mol Cell Biol* **2002**, *22*, 1352–1359, doi:10.1128/mcb.22.5.1352-1359.2002.

24. Resjö, S.; Göransson, O.; Härndahl, L.; Zolnierowicz, S.; Manganiello, V.; Degerman, E. Protein Phosphatase 2A Is the Main Phosphatase Involved in the Regulation of Protein Kinase B in Rat Adipocytes. *Cell Signal* **2002**, *14*, 231–238, doi:10.1016/s0898-6568(01)00238-8.

25. Morgan, B.; Laer, K.V.; Owusu, T.N.E.; Ezeriņa, D.; Pastor-Flores, D.; Amponsah, P.S.; Tursch, A.; Dick, T.P. Real-Time Monitoring of Basal H2O2 Levels with Peroxiredoxin-Based Probes. *Nat Chem Biol* **2016**, *12*, 437 443, doi:10.1038/nchembio.2067.

26. Xiao, H.; Jedrychowski, M.P.; Schweppe, D.K.; Huttlin, E.L.; Yu, Q.; Heppner, D.E.; Li, J.; Long, J.; Mills, E.L.; Szpyt, J.; et al. A Quantitative Tissue-Specific Landscape of Protein Redox Regulation during Aging. *Cell* **2020**, doi:10.1016/j.cell.2020.02.012.

27. Weerapana, E.; Wang, C.; Simon, G.M.; Richter, F.; Khare, S.; Dillon, M.B.D.; Bachovchin, D.A.; Mowen, K.; Baker, D.; Cravatt, B.F. Quantitative Reactivity Profiling Predicts Functional Cysteines in Proteomes. *Nature* **2010**, *468*, 790 795, doi:10.1038/nature09472.

28. Wang, H.; Chen, X.; Li, C.; Liu, Y.; Yang, F.; Wang, C. Sequence-Based Prediction of Cysteine Reactivity Using Machine Learning. *Biochemistry-us* **2018**, *57*, 451 460, doi:10.1021/acs.biochem.7b00897.

29. Löwe, O.; Rezende, F.; Heidler, J.; Wittig, I.; Helfinger, V.; Brandes, R.P.; Schröder, K. BIAM Switch Assay Coupled to Mass Spectrometry Identifies Novel Redox Targets of NADPH Oxidase 4. *Redox Biol* **2019**, *21*, 101125, doi:10.1016/j.redox.2019.101125.

30. Dansen, T.B.; Smits, L.M.M.; Triest, M.H. van; Keizer, P.L.J. de; Leenen, D. van; Koerkamp, M.G.; Szypowska, A.; Meppelink, A.; Brenkman, A.B.; Yodoi, J.; et al. Redox-Sensitive Cysteines Bridge P300/CBP-Mediated Acetylation and FoxO4 Activity. *Nat Chem Biol* **2009**, *5*, 664 672, doi:10.1038/nchembio.194.

31. Song, I.S.; Jun, S.Y.; Na, H.J.; Kim, H.T.; Jung, S.Y.; Ha, G.H.; Park, Y.H.; Long, L.Z.; Yu, D.Y.; Kim, J.M.; et al. Inhibition of MKK7–JNK by the TOR Signaling Pathway Regulator-Like Protein Contributes to Resistance of HCC Cells to TRAIL-Induced Apoptosis. *Gastroenterology* **2012**, *143*, 1341 1351, doi:10.1053/j.gastro.2012.07.103.

32. Sarbassov, D.D.; Sabatini, D.M. Redox Regulation of the Nutrient-Sensitive Raptor-MTOR Pathway and Complex. *J Biol Chem* **2005**, *280*, 39505 39509, doi:10.1074/jbc.m506096200.

33. Sarbassov, D.D.; Guertin, D.A.; Ali, S.M.; Sabatini, D.M. Phosphorylation and Regulation of Akt/PKB by the Rictor-MTOR Complex. *Science* **2005**, *307*, 1098 1101, doi:10.1126/science.1106148.

34. Rosales, K.R.; Reid, M.A.; Yang, Y.; Tran, T.Q.; Wang, W.-I.; Lowman, X.; Pan, M.; Kong, M. TIPRL Inhibits Protein Phosphatase 4 Activity and Promotes H2AX Phosphorylation in the DNA Damage Response. *Plos One* **2015**, *10*, e0145938, doi:10.1371/journal.pone.0145938.

35. Gingras, A.-C.; Caballero, M.; Zarske, M.; Sanchez, A.; Hazbun, T.R.; Fields, S.; Sonenberg, N.; Hafen, E.; Raught, B.; Aebersold, R. A Novel, Evolutionarily Conserved Protein Phosphatase Complex Involved in Cisplatin Sensitivity* S. *Mol Cell Proteomics* **2005**, *4*, 1725–1740, doi:10.1074/mcp.m500231-mcp200.

GRAPHICAL ABSTRACT

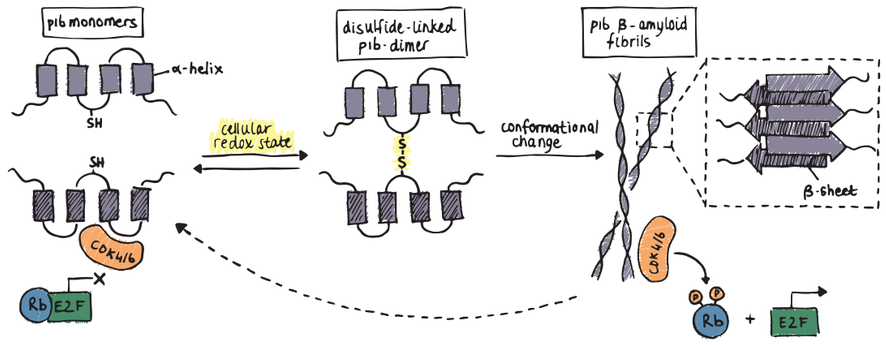

CHAPTER 4

CYSTEINE OXIDATION TRIGGERS AMYLOID FIBRIL FORMATION OF THE TUMOR SUPPRESSOR P16^{INK4A}

Christoph Göbl[1,2], Vanessa K. Morris[1,2]*, Loes van Dam[3]*, Marieke Visscher[3], Paulien E. Polderman[3], Christoph Hartlmüller[1,2], Hesther de Ruiter[3], Manuel Hora[1,2], Laura Liesinger[4,5], Ruth Birner-Gruenberger[4,5], Harmjan R. Vos[3], Bernd Reif[1,2], Tobias Madl[5,6], Tobias B. Dansen[1]*

[1]*Center for Integrated Protein Science Munich (CIPSM) at the Department of Chemistry Technische Universität München, Lichtenbergstr. 4, 85747, Garching, Germany*
[2]*Institute of Structural Biology, Helmholtz Zentrum München, 85764, Neuherberg, Germany*
[3]*Center for Molecular Medicine, Molecular Cancer Research, University Medical Center Utrecht, Universiteitsweg 100, 3584CG, Utrecht, The Netherlands*
[4]*Omics Center Graz, BioTechMed-Graz, Graz, Austria*
[5]*Gottfried Schatz Research Center for Cell Signaling, Metabolism and Aging, Molecular Biology and Biochemistry, Medical University of Graz, 8010, Graz, Austria*
[6]*BioTechMed-Graz, Austria*

Correspondence: t.b.dansen@umcutrecht.nl

**These authors contributed equally.*

PUBLISHED *in Redox Biol* 2019, *101316, https://doi.org/10.1016/j.redox.2019.101316*.

KEYWORDS

amyloids; protein aggregation; redox signaling; cysteine oxidation; structural biology; cell cycle; NMR

CYSTEINE OXIDATION TRIGGERS AMYLOID FIBRIL FORMATION OF THE TUMOR SUPPRESSOR P16^{INK4A}

ABSTRACT

The tumor suppressor p16^{INK4A} induces cell cycle arrest and senescence in response to oncogenic transformation and is therefore frequently lost in cancer. p16^{INK4A} is also known to accumulate under conditions of oxidative stress. Thus, we hypothesized it could potentially be regulated by reversible oxidation of cysteines (redox signaling). Here we report that oxidation of the single cysteine in p16^{INK4A} in human cells occurs under relatively mild oxidizing conditions and leads to disulfide-dependent dimerization. p16^{INK4A} is an all a-helical protein, but we find that upon cysteine-dependent dimerization, p16^{INK4A} undergoes a dramatic structural rearrangement and forms aggregates that have the typical features of amyloid fibrils, including binding of diagnostic dyes, presence of cross-β sheet structure, and typical dimensions found in electron microscopy. p16^{INK4A} amyloid formation abolishes its function as a Cyclin Dependent Kinase 4/6 inhibitor. Collectively, these observations mechanistically link the cellular redox state to the inactivation of p16^{INK4A} through the formation of amyloid fibrils.

INTRODUCTION

The *CDKN2A* gene-product p16^{INK4A} is an important cell-cycle regulator and acts as a tumor suppressor. It inhibits the D-type cyclin-dependent kinases CDK4 and CDK6 and hence prevents the downstream phosphorylation of the retinoblastoma (Rb) pocket protein [1]. This prevents release of E2 promoter binding factor 1 (E2F1), which is otherwise required for the transcriptional regulation of proteins that regulate entry into S-phase of the cell cycle [2]. Accumulation of p16^{INK4A} is observed upon exposure of cells to several stressors such as oxidative stress and is one of the earliest markers of oncogenic transformation [3]. The loss of p16^{INK4A} function, or loss of Rb downstream of CDK4/6, are some of the most frequently observed mutations in tumors [4]. Additionally, p16^{INK4A} plays an important role in aging, as clearance of p16^{INK4A}-expressing senescent cells has been shown to prolong lifespan in mice [5,6].

The molecular basis of p16^{INK4A}-mediated CDK4/6 inhibition is well established. p16^{INK4A} is a small, globular all-α-helical protein, that tightly binds into one side of the catalytic cleft of the CDK4/6 kinases. It efficiently distorts the cyclin D binding site, thereby blocking formation of the active CDK4/6-cyclin D complex, therefore preventing Rb phosphorylation [7,8]. Of particular relevance for this study, the single cysteine residue (C72) present in p16^{INK4A} is located on its surface and points away from the CDK4/6 kinase in the bound state; the residue is fully solvent accessible.

Reversible cysteine oxidation is the lynchpin in redox signaling, a form of signal transduction that is regulated by the cellular redox state. A more oxidizing cellular redox state, either due to elevated reactive oxygen species or a lack of reducing power, leads to oxidative modification of specific cysteine-thiols to form reversible disulfide (S-S) bridges. These oxidative modifications can lead to structural rearrangements and can both negatively and positively regulate protein function (for a review see [9]).

A number of observations spurred us to hypothesize that oxidation of p16^{INK4A} C72 could play a role in the regulation of p16^{INK4A} activity at the molecular level. Firstly, several studies have implicated a role for increased ROS in the oncogene-induced accumulation of p16^{INK4A} [10], but cysteine oxidation as the underlying mechanism has thus far not been considered nor excluded. Secondly, we identified p16^{INK4A} as prone to cysteine oxidation in a large mass-spectrometry based screen for redox sensitive proteins [11]. Here, we provide evidence that p16^{INK4A} itself is indeed sensitive to cysteine oxidation. We find that p16^{INK4A} is readily oxidized both *in vitro* and in cultured human cells to form a disulfide-dependent homodimer, and the oxidizing conditions required are well within the physiological range. Surprisingly, disulfide-dependent dimerization of p16^{INK4A} subsequently leads to the rapid formation of β-amyloid fibril structures, a state that has not been previously described for p16^{INK4A}. This transition subsequently leads to loss of CDK4/6 inhibitory capacity. Redox signaling-induced reversible disulfides have not previously been shown to induce β-amyloid fibrils in other proteins and hence adds to the repertoire of redox dependent protein regulation.

RESULTS

p16^{INK4A} is Oxidized to Form Disulfide Dependent Homodimers in Human Cells

To test whether p16^{INK4A} forms disulfide-dependent complexes under oxidizing conditions, immunoprecipitation followed by non-reducing SDS-PAGE was performed. Oxidation was induced using a concentration series of either hydrogen peroxide or the thiol-specific oxidant diamide (tetramethylazodicarboxamide) that ranged from subtoxic (5 μM) to mildly toxic (250 μM) in HEK293T cells. Flag-p16^{INK4A} readily formed intermolecular disulfide-dependent complexes (**Figure 1A**), as judged by the large mobility shift under non-reducing conditions, that was abolished when the samples were reduced prior to SDS-PAGE (last lanes). Note that only the Flag-p16^{INK4A} disulfide-dependent dimer band is observed and that its intensity increases upon exposure to increasing

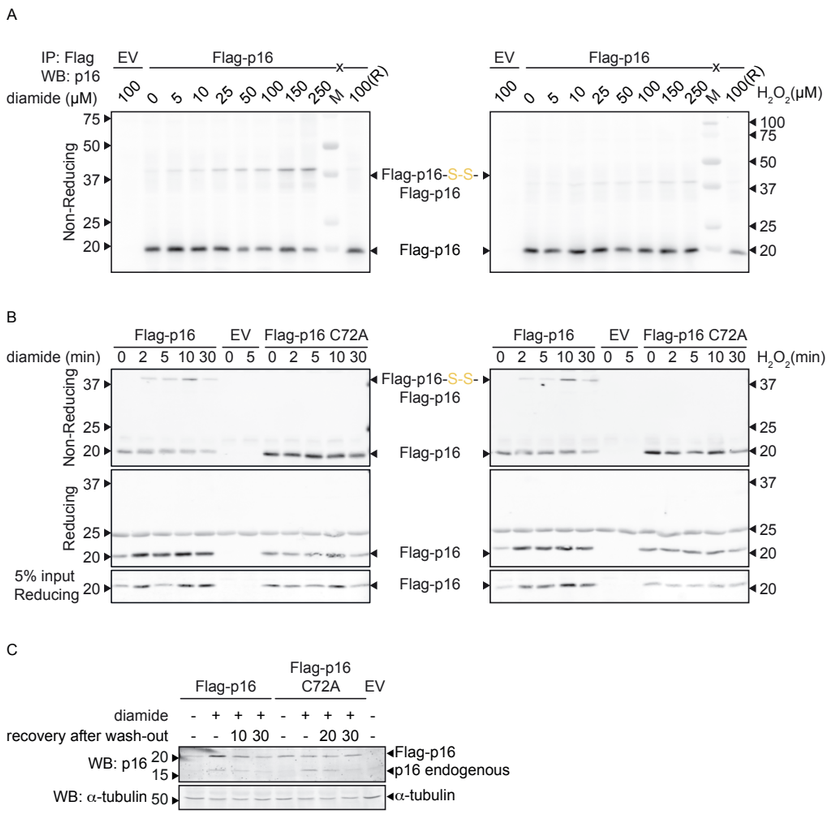

Figure 1. p16^{INK4A} forms intermolecular disulfides upon exposure to oxidants.
(**A**) Analysis of Immuno-precipitated Flag-p16^{INK4A} by non-reducing SDS-PAGE and Western Blot shows that part of the Flag-p16^{INK4A} migrates at about double the molecular weight upon 5 minutes treatment with low amounts of the thiol-specific oxidant diamide (left panel) or H_2O_2 (right panel). Reduction (R) prior to SDS-PAGE abolishes the shift in molecular weight, indicating that it is indeed due to an intermolecular disulfide (see also Figure S2A, S2B for confirmation that the high molecular weight form of p16^{INK4A} is an S-S-dependent homodimer). (**B**) S-S-dependent p16^{INK4A} homodimerization upon 200 μM diamide (left) or 200 μM H_2O_2 (right) occurs rapidly, coincides with accumulation of p16^{INK4A} protein levels and oxidation as well as accumulation are fully dependent on C72. (**C**) Endogenous p16^{INK4A} and over-expressed Flag-p16^{INK4A} accumulate in response to 200 μM diamide with similar kinetics. Note that p16^{INK4A}C72A does not accumulate whereas endogenous p16^{INK4A} does, suggesting that endogenous p16^{INK4A} levels are also regulated by cysteine-oxidation. (IP: immunoprecipitation, WB: Western Blot). All Western blots shown in Figure 1 are typical results of several repeats ($n^3$3 for all experiments).

oxidant concentration. We did not observe a "smear", which would be if p16^{INK4A} were to undergo random, nonspecific crosslinking to proteins. We then created p16^{INK4A} mutants in which the only cysteine was replaced by alanine (C72A) or serine (C72S). We opted to use p16^{INK4A} C72A for our further experiments in human cells in order to circumvent the potential effects of the introduction of a novel phosphorylation site in the C72S mutant. The C72A mutant is still functional as

a cell-cycle inhibitor and hence the mutation does not grossly affect protein function per se (Figure S1). To explore whether the observed intermolecular disulfide-dependent complexes are Flag-p16^{INK4A} homodimers, co-IP experiments were performed using combinations of wild-type (WT) p16^{INK4A} and C72A with short (Flag) and long (mCherry) N-terminal tags. Under non-reducing conditions, bands could be observed corresponding to disulfide-dependent dimers of Flag-p16^{INK4A}-S-S-Flag-p16^{INK4A} and of mCherry-p16^{INK4A}-S-S-Flag-p16^{INK4A} (Figure S2A) after Flag pull down. Furthermore, diagonal electrophoresis showed that after reduction (2nd dimension) Flag-p16^{INK4A} drops out of the diagonal as a single dot, whereas a heterodimer would have revealed a second Simply Blue stained protein with similar intensity dropping out of the diagonal (Figure S2B, see also Figure 2A in Chapter 3). To test the dynamics of the intermolecular disulfide-dependent dimerization of p16^{INK4A}, a time course of oxidant treatment was performed, using p16^{INK4A} C72A as a control. The oxidation of p16^{INK4A} was rapid, peaked after 10 minutes, was fully dependent on the only cysteine and was resolved upon boiling in reducing sample buffer (Figure 1B).

Concomitantly with its oxidation, p16^{INK4A} protein abundance increased, and this was again dependent on its single cysteine residue. Protein levels already increased after a few minutes of diamide treatment, excluding a role for gene transcription but suggestive of a role for decreased protein breakdown. The accumulation is best observed using reducing SDS-PAGE because all p16^{INK4A} then migrates in a single band (Figures 1B and 1C). The increased p16^{INK4A} protein levels rapidly returned to basal upon diamide wash-out with fresh media (Figure 1C). Endogenous p16^{INK4A} levels follow the same trend as Flag-p16^{INK4A} indicating that endogenous p16^{INK4A} is also regulated through cysteine oxidation. Taken together, both the increase in p16^{INK4A} levels as well as the oxidation are dependent on C72.

C72 of p16^{INK4A} is Readily Oxidized In Vitro

To study the reactivity of the p16^{INK4A} cysteine residue directly, we expressed and purified the isotope-labeled recombinant protein and confirmed its correct folding by solution nuclear magnetic resonance (NMR) spectroscopy. Upon treatment of the purified protein with oxidized glutathione (GSSG), we

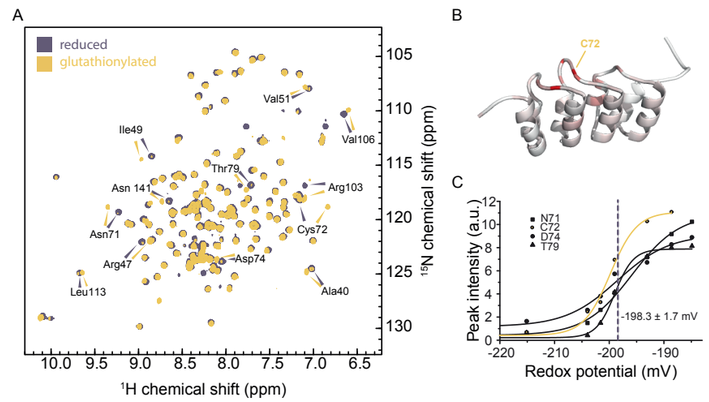

Figure 2. In vitro oxidation of p16INK4A.
(A) $_1H_{15}N$ HSQC solution NMR spectrum of recombinant p16^{INK4A} in the reduced state (magenta) and after S-glutathionylation (yellow). Amino acids with large chemical shift changes are labeled. (B) Cartoon representation of the p16^{INK4A} structure. A color gradient from white (unaffected) to red (strongly affected) shows the influence of S-glutathionylation on the chemical shift. (C) The redox potential of C72 is 198.3 ± 1.7 mV, as determined from intensity changes of four well-separated amino acids by titration of the reduced protein with oxidized glutathione.

observed chemical shift changes that occurred most strongly in proximity to the cysteine residue of $p16^{INK4A}$ (Figures 2A and 2B, Figure S3). These changes were reversed by addition of the reducing agent DTT, confirming the involvement of reversible cysteine oxidation. Mass spectrometric analysis of the intact protein showed that $p16^{INK4A}$ was S-glutathionylated (S-GSHylated) after treatment with GSSG (Figure S4). S-GSHylation of the protein does not change its monomeric state or overall fold, as indicated by identical peak line shapes and unchanged elution times in size exclusion chromatography. By titrating the reduced $p16^{INK4A}$ sample with increasing GSSG in a GSH/GSSG redox buffer we determined the redox potential of C72 using the Nernst equation [17] to be -198.3 +/- 1.7 meV (Figure 2C).

To study the structural role of the cysteine residue, we used the $p16^{INK4A}$C72S mutant, which is the most structurally conservative mutation, differing only by replacement of the sulfhydryl group with a hydroxyl group. This mutant showed monomeric behavior during purification and largely identical chemical shifts as compared to the wild-type protein (Figure S5), indicating that the mutation does not affect $p16^{INK4A}$ protein structure *per se*. Addition of GSSG to this mutant did not show any indications of interaction or covalent modification. Collectively, these experiments indicate that the $p16^{INK4A}$ C72 can be directly oxidized *in vitro* at physiologically occurring redox states.

Disulfide-Dependent Homo-Dimerization of $p16^{INK4A}$ Triggers Aggregation

The use of GSSG as an oxidant resulted in $p16^{INK4A}$ S-GSHylation *in vitro*, whereas experiments in human cells showed S-S-linked homodimerization (Figure 1) upon treatment with diamide or H_2O_2, even though both these agents lead to increased GSSG in cells. We therefore assessed whether H_2O_2 and diamide can directly oxidize $p16^{INK4A}$ *in vitro*. SDS-PAGE analysis revealed that disulfide-linked protein homodimers are also formed *in vitro*, similar to the pattern observed in the experiments in human cells (Figure S6A). Comparison of size exclusion chromatography traces of reduced and oxidized samples show that oxidation of $p16^{INK4A}$ causes a shift to high molecular mass, with the oxidized sample eluting in the void volume of the column (Figure S6B). In contrast to oxidation by GSSG, the addition of either H_2O_2 (Figure 3A) or diamide (Figures S6C and S6D) led to strong NMR chemical shift changes that indicated protein unfolding and aggregation. This indicates the formation of a multimeric species and the absence of monomeric $p16^{INK4A}$. Characterization of reduced and oxidized WT $p16^{INK4A}$ by Circular Dichroism (CD) spectroscopy revealed a transition to a less structured species, with some alpha-helical characteristics remaining (Figure S7A). Small-angle X-ray scattering (SAXS) on the oxidized samples indicates that the aggregates are larger than the detection limit of about 400 nm diameter (Figure S7B). S-Glutathionylation of $p16^{INK4A}$ C72 would abolish its reactivity towards diamide or H_2O_2. To exclude that the observed aggregation of $p16^{INK4A}$ stems from modifications other than C72, we also performed solution NMR spectroscopy on the S-glutathionylated $p16^{INK4A}$ (GS-$p16^{INK4A}$), as well as on the $p16^{INK4A}$ C72A mutant, treated with diamide or H_2O_2. No chemical shift changes were observed and the monomeric, S-glutathionylated protein sample as well as the $p16^{INK4A}$ C72A mutant were stable in presence of oxidizing agents (Figure S8). Together, these experiments indicate the formation of an aggregated $p16^{INK4A}$ species upon intermolecular disulfide bond formation *in vitro*.

Disulfide-Linked Homodimers of $p16^{ink4a}$ Form β-Amyloid Fibrils

Based on the indications of aggregation, transmission electron microscopy (EM) was employed to study the nature of the $p16^{INK4A}$ aggregates that formed upon oxidation. Interestingly, we found that the oxidized $p16^{INK4A}$ samples produced fibrillar structures (Figure 3B). One prominent group of fibrillar proteins are amyloid fibrils, which are characterized by a cross-β sheet core structure, meaning that β-strands run perpendicular to the fibril long axis [12,13]. To determine if $p16^{INK4A}$ fibrils are amyloid, we used the amyloid-specific dyes Thioflavin T (ThT) and Congo Red [14–16]. ThT assays showed an increase in fluorescence, which is characteristic for amyloids, when bound to oxidized $p16^{INK4A}$ (Figure 3C), while Congo

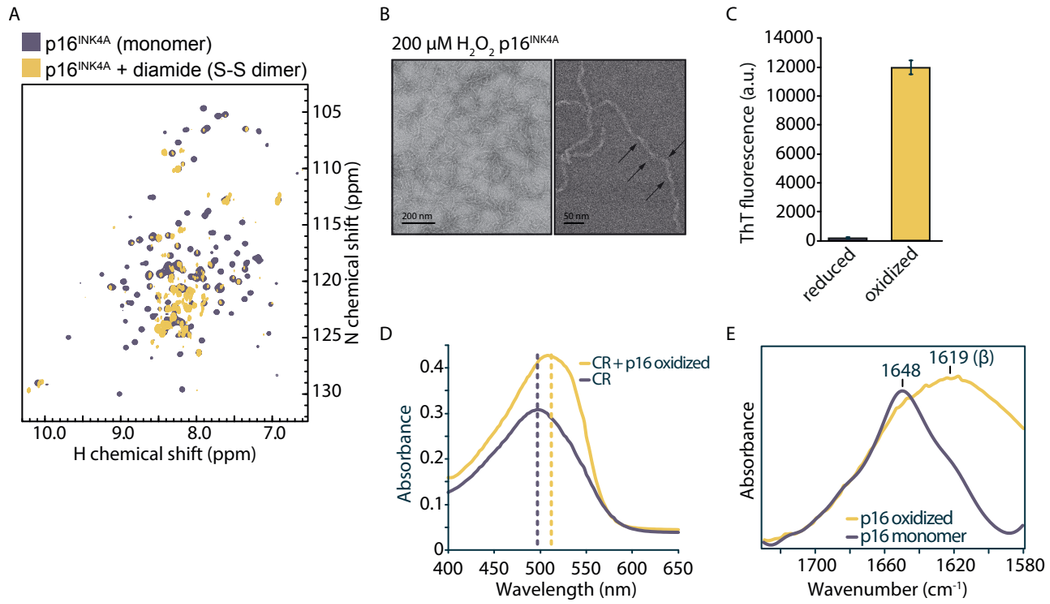

Figure 3. $p16^{INK4A}$ forms amyloid fibrils under oxidizing conditions. (A) $^{1}H,^{15}N$ HSQC solution NMR spectra of recombinant $p16^{INK4A}$ before (magenta) and after (yellow) oxidation with 50 mM H_2O_2 for 10 h at room temperature.
The collapse of the peaks to the center of the spectrum suggests formation of unstructured or aggregated protein. (**B**) Negative-stained transmission electron micrographs of diamide-treated $p16^{INK4A}$ showing the presence of amyloid fibrils. Right panel is at higher magnification, arrows highlight the twisted morphology which is typical of amyloid fibrils. (**C**) Fibril formation of $p16^{INK4A}$ monitored by thioflavin-T fluorescence measurement. Error bars represent standard deviation from four measurements. (**D**) Fibril formation of $p16^{INK4A}$ monitored by Congo red absorption. The absorption maximum shifts when bound to oxidized $p16^{INK4A}$, indicating the presence of amyloid fibrils. (**E**) Amide I region of the attenuated-total-reflectance Fourier-transform infrared spectra of $p16^{INK4A}$ monomer and fibrils. Peak maxima indicate that the structure contains primarily a-helix for monomers and cross-b sheet for fibrils.

Red absorbance measurements showed the red shift and increased absorbance characteristic of amyloid binding (Figure 3D). Fourier-transform infrared spectroscopy can distinguish cross β-sheets found in amyloid fibrils from β-sheets found in globular monomeric proteins [17,18]; in line with the dye-binding data, $p16^{INK4A}$ fibrils had a maximum at 1620 cm^{-1}, which falls within the typical amyloid β-sheet region, confirming the amyloid structure of the fibrils (Figure 3E). We performed a computational analysis using four fibril prediction algorithms [19–22] and all suggested a high propensity for β-amyloid formation in the region from residue no. 91-99 (Figure S9A).

Additionally, we recorded solid state NMR spectra on a uniformly ^{13}C-labeled $p16^{INK4A}$ sample to confirm the secondary structure of the aggregated state. Samples were prepared using the same conditions that were used for other experiments including electron microscopy, to ensure that results are comparable between experiments. In ^{13}C-^{13}C correlation spectra, only amino acid residues within a structured core are visible (Figure S9). The spectrum shows relatively few peaks compared to the 156 residues of full-length p16, suggesting that only specific parts of the sequence form the structural core of the amyloid fibrils. This is also indicated by the absence of certain residue types from the spectrum, for example isoleu-

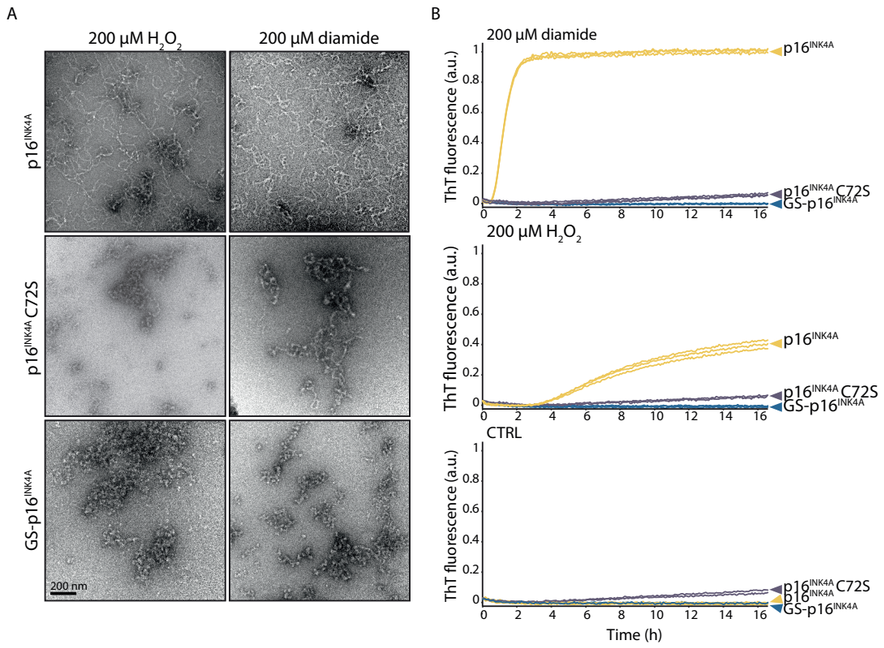

Figure 4. C72 is important for fibrillar morphology and ThT binding.
(**A**) Negative-stain transmission electron micrographs of p16^{INK4A} treated with 200 µM hydrogen peroxide (left) and 200 µM diamide (right). Top: WT p16^{INK4A}. Middle: p16^{INK4A}C72S. Bottom: GS-p16^{INKA}. (**B**) Thioflavin-T fluorescence kinetics assay of p16^{INK4A} samples (WT, C72S and GS) with 200 µM diamide addition (top) 200 µM H_2O_2 addition (middle) and without oxidizing agents (bottom). Three replicates were measured per sample and each are separately plotted.

cine (Figure S9B). Many of the peaks could be assigned to their amino-acid type due to their distinctive Cα and Cβ peak positions, which allowed for determination of the secondary structure. Nearly all assigned peaks have peak positions that are characteristic for β-sheet or random coil (Figure S9C), confirming that p16^{INK4A} aggregates have a β-sheet core and are therefore amyloid. These findings emphasize the dramatic structural rearrangement from the monomeric eight-a-helical bundle that is devoid of β-sheets.

Intermolecular p16^{INK4A} Disulfide Bond Formation is Essential for Amyloid Fibril Assembly

We further investigated the role of oxidation of the cysteine residue in fibril formation by comparing the p16^{INK4A} WT protein to p16^{INK4A}C72S. Electron microscopy revealed that upon treatment with as little as 200 µM H_2O_2 or diamide, WT samples formed large fibrillar structures (Figure 4A, top panels). There was no discernable difference between the morphology of fibrils formed with diamide or hydrogen peroxide treatment, or when higher concentrations of oxidizing agent were used. p16^{INK4A}C72S samples displayed a very different morphology, instead forming unordered, amorphous aggregates, as well as a small amount of short fibrillar species (Figure 4A, middle panels).

Glutathionylated-p16^{INK4A} (GS-p16^{INK4A}) samples were also analyzed by electron microscopy, and were found to form large, granular aggregates without any fibrils upon treatment with either H_2O_2 or diamide (Figure 4A, bottom panels). Although aggregates are seen by electron microscopy, the solution NMR spectra of GS-p16^{INK4A} indicate the sample is largely soluble and monomeric (Figure S7), suggesting that the aggregates seen by electron microscopy constitute only a small proportion of the total GS-p16^{INK4A} protein.

We next investigated the influence of intermolecular disulfide bond formation on the kinetics of fibril formation, by measuring the time- and oxidation-dependence of p16^{INK4A} WT, p16^{INK4A} C72S and GS-p16^{INK4A} variants using the ThT assay (Figure 4B). Upon treatment of WT p16^{INK4A} with oxidizing agents, the sample fluorescence rapidly increased as ThT-positive fibrils were formed, with maximum signal being achieved within 2 hours upon 200 µM diamide treatment (Figure 4B, top) and more than 16 hours for 200 µM H_2O_2 treatment (Figure 4B, middle), while no fibrils were formed in the absence of oxidizing agents (Figure 4B, bottom). The C72S mutant displayed only a very slight increase in fluorescence over time, and this was not affected by the presence or absence of oxidizing agents. GS-p16^{INK4A} did not form ThT-positive aggregates under any condition. The amyloids formed *in vitro* were reversible: boiling in non-reducing sample buffer for five minutes prior to SDS-PAGE resulted mainly in detection of the S-S-dependent dimers (Figure S10). The EM and ThT-kinetics data emphasize that the amorphous aggregates observed by EM for the p16^{INK4A}C72S and GS-p16^{INK4A} are not amyloid, both by morphology and by dye-binding properties. Therefore, we conclude that the intermolecular disulfide bond formation of p16^{INK4A} through C72 is critical for the formation of p16^{INK4A} amyloid fibrils.

p16^{INK4A} Cysteine Oxidation Triggers its Aggregation in Cultured Cells

Having shown that p16^{INK4A} forms amyloid fibrils upon oxidation *in vitro*, we investigated to what extent this behavior was conserved in cultured human cells. HEK293T cells expressing Flag-tagged p16^{INK4A} WT and p16^{INK4A} C72A mutant were exposed to diamide and processed for a filter trap assay: an assay that is commonly used to detect amyloids in cell extracts (Scheme top of Figure 5A). Exposure to diamide prior to lysis rapidly led to accumulation of the p16^{INK4A} homodimer in the solubilized pellet fraction and subsequent trapping of p16^{INK4A} on the filter membrane, and both were dependent on C72. Reduction of the protein lysates with DTT prior to washing abolished trapping, suggesting that the aggregation was reversible (Figure 5B). Clearance of p16^{INK4A} aggregates was observed over time after diamide treatment. After 120 minutes the aggregates were largely resolved (Figure 5C), reminiscent of turnover of the disulfide-linked homodimer in Figure 1C.

We also studied whether oxidation induced the aggregation of endogenous p16^{INK4A}, for which the expression levels are generally lower than those of transfected Flag-p16^{INK4A}. We found that endogenous p16^{INK4A} also forms disulfide-linked dimers upon oxidation and that part of these accumulate in the insoluble pellet fraction (Figure 5D). Similar amounts of endogenous p16^{INK4A} are found in the solubilized pellet fraction in the presence and absence of transfected Flag-p16^{INK4A}, suggesting that endogenous p16^{INK4A} levels are sufficient to form homodimers and aggregates (see reducing IP panels). The phase-transition from monomeric to the amyloid form of p16^{INK4A} would likely change its biochemical properties and protein-protein interactions. To test this, the interactomes of immunoprecipitated Flag-p16^{INK4A} and Flag-p16^{INK4A}C72A were investigated and compared by label-free quantitative mass spectrometry. Under basal conditions the interactomes were largely identical, but this changed dramatically upon diamide treatment (Figure S11). Diamide-treated WT p16^{INK4A} indeed showed a large number of binding partners not identified in diamide-treated p16^{INK4A} C72A pull-downs. The interaction with CDK4 and CDK6 was not affected by diamide treatment or the C72A mutation. Proteins that form amyloids are known to bind to chaperones and indeed several Heat Shock Proteins (HSPs) were found to interact with WT p16^{INK4A} upon diamide treatment, again indicative of aggregate formation.

p16^{INK4A} Cysteine Oxidation Restores CDK4/6 Kinase Activity

We then investigated how the p16^{INK4A} function as a CDK4/6 inhibitor would be affected by amyloid formation. CDK4/6

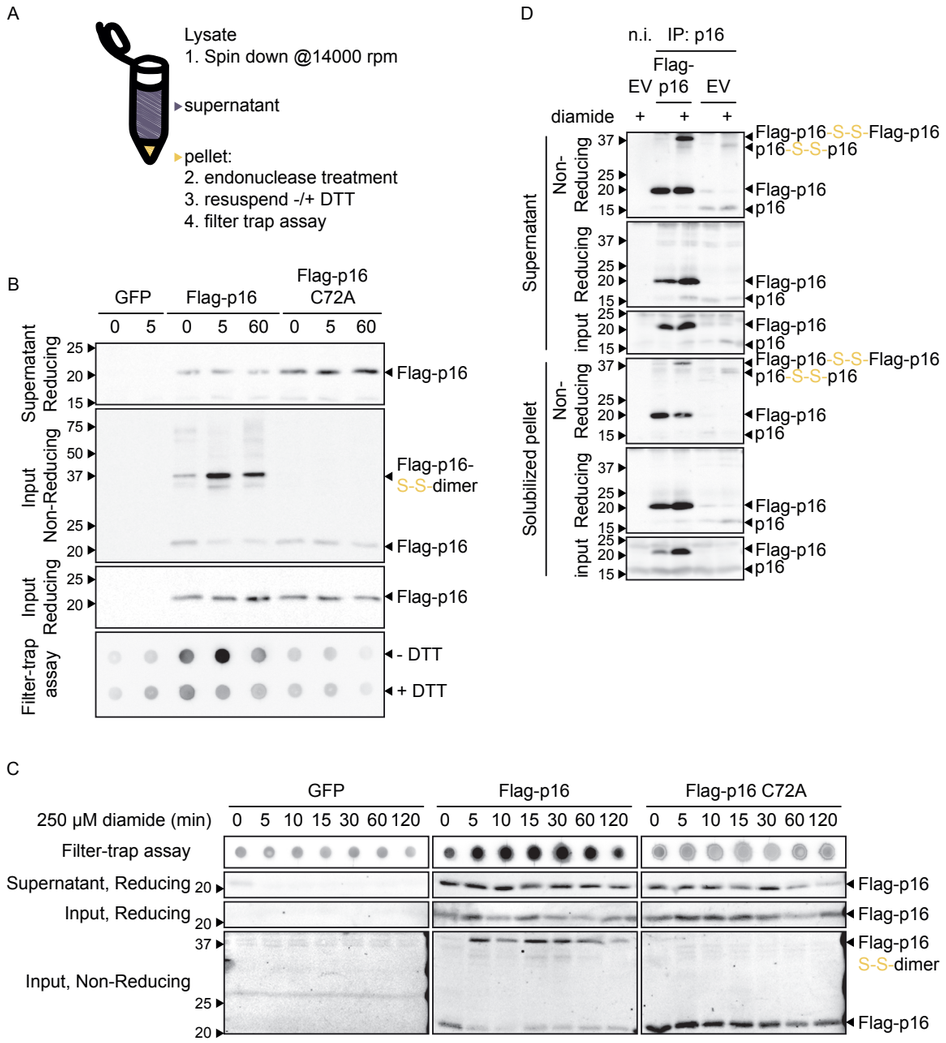

Figure 5. p16^{INK4A} Aggregates in Live Cells in Response to Oxidation.
(**A**) Set up for the filter trap assay for the detection of aggregates in cell lysates. (**B**) Results for the filter trap assay. Note that the majority of p16^{INK4A} in the pellet is in the form of S-S homodimers after lysis. p16^{INK4A}, but not p16^{INK4A}C72A, was trapped on the filter membrane upon treatment with 200 µM diamide and trapping was prevented by pretreatment with DTT. Equal amounts of p16^{INK4A} and p16^{INK4A} C72A were used as input for the filter trap assay. Note that the input for the filter trap assay runs mainly as a S-S-dependent dimer after boiling in non-reducing SDS-PAGE sample buffer. R: reducing, NR: non-reducing. (**C**) Aggregates of p16^{INK4A} peak around 30 minutes and are then cleared over time. (**D**) Endogenous p16^{INK4A} also forms S-S-linked dimers that (partially) form aggregates in the insoluble pellet fraction. Note that also mixed S-S-linked dimers of endogenous and overexpressed p16^{INK4A} can be observed in lanes where Flag-p16^{INK4A} was transfected. n.i: IP with non-immune serum as a control. p16(r): rabbit anti-p16^{INK4A}, p16(m): mouse anti-p16^{INK4A}, EV: empty vector, Red: reducing, Non-Red: non-reducing. All experiments were performed at least 3 times. Representative experiments are shown.

was co-immunoprecipitated with Flag-tagged p16^{INK4A}, and *in vitro* kinase assays were performed using a GST-tagged Rb fragment as a substrate (scheme Figure 6A). These experiments revealed that oxidation of WT p16^{INK4A} or p16^{INK4A}C72S did not greatly affect the binding to CDK4/6 (Figure 6A), which agrees with our observations in the MS experiments (Figure S11). The *in vitro* kinase assay showed that p16^{INK4A}-associated CDK4/6 was, as expected, inactive under basal conditions. CDK4/6 activity towards the GST-Rb fragment was regained when cells were exposed to diamide prior to lysis, despite the increased amount of p16^{INK4A} that was pulled down. The reactivation was strictly dependent on p16^{INK4A} C72. Taken together, these observations suggest that the amyloid form of p16^{INK4A} still interacts with CDK4/6 but in a manner that does not lead to kinase inhibition.

To test how p16^{INK4A} oxidation and aggregation impacts on the total CDK4/6 activity we performed qPCR analysis

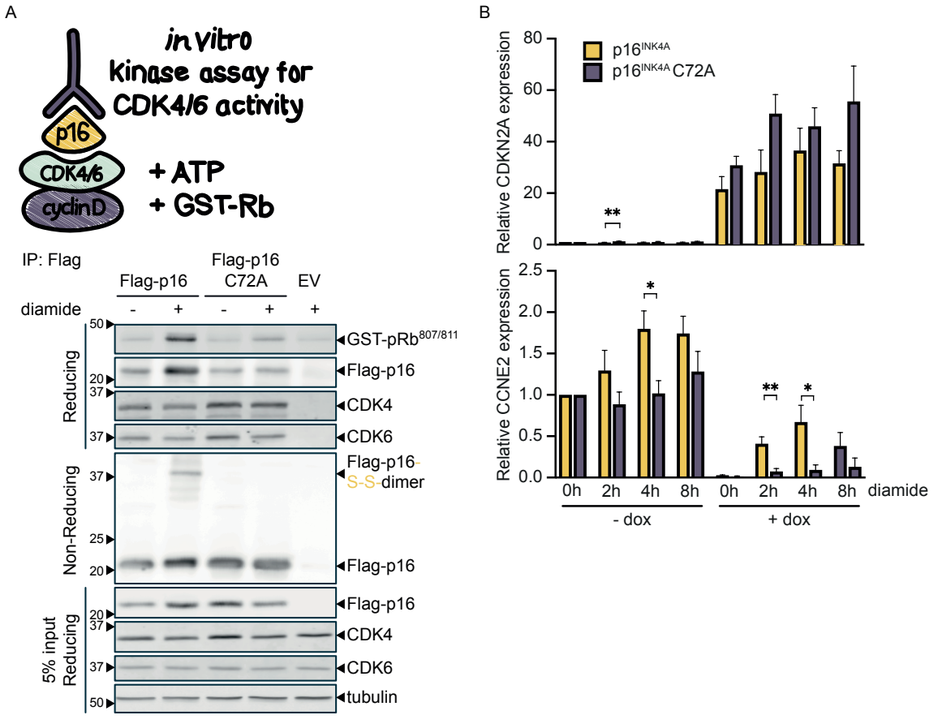

Figure 6. Oxidation of p16^{INK4A} impairs its inhibitory function towards CDK4/6.
(**A**) In vitro CDK4/6 kinase assay on WT p16^{INK4}A pulldowns shows that the oxidation of p16^{INK4A} C72 impairs its inhibitory function. Note that oxidation or mutation of C72 does not affect the amount of CDK4/6 that is co-immunoprecipitated. (R: Reducing, NR: Non-reducing). All Western blots shown in Figure 6 are typical results of several repeats (n=3 for all experiments). (**B**) qPCR analysis showing the expression of WT p16^{INK4A} or p16^{INK4A} C72A (top) in COLO-829 cells upon induction of expression from the respective pINDUCER20-p16INK4A construct. CCNE2 expression (bottom) is strongly repressed both by WT p16^{INK4A} and p16^{INK4A} C72A. Diamide treatment relieves this repression only in the WT p16^{INK4} expressing cell line. Note that the inducible system is somewhat leaky, which could explain induction of CCNE2 in the p16^{INK4A} WT cells by diamide in the absence of doxycycline. The mean plus SEM is displayed from n=5 biological replicates. * p<0.05, ** p<0.01, pairwise comparison using a two-sided t-test comparing cells carrying the inducible WT p16^{INK4} or p16^{INK4A} C72A construct in each condition.

on the expression of Cyclin E2 (CCNE2), which is a transcriptional target of E2F1 and hence should be upregulated by active CDK4/6. CCNE2 (**Figure 6B**, lower panel) was strongly repressed upon the doxycycline-induced p16^{INK4A} or p16^{INK4A} C72A expression (**Figure 6B**, top panel) in otherwise p16^{INK4A} deficient COLO829 melanoma cells. CCNE2 transcription was partially restored upon diamide treatment, but not in the cells expressing the p16^{INK4A} C72A redox-insensitive variant. The induction of CCNE2 by diamide in the absence of doxycycline in the p16^{INK4A} WT cell line is likely due to the fact that the inducible system is somewhat leaky. Although we did find evidence that CDK4/6 is indeed reactivated upon oxidation of p16^{INK4A}, and that this partially relieves E2F1 repression, we did not find evidence of perturbation of the S-phase checkpoint in cell-cycle analysis experiments using flow cytometry and video time-lapse microscopy (data not shown). This might be explained by the notion that substantial amounts of monomeric p16^{INK4A} persist under conditions where we find aggregated p16^{INK4A} in the insoluble pellet fraction of our lysates. The observed reactivation of CDK4/6 might therefore not be strong enough for full re-entry of the cell cycle under the tested conditions, but we cannot exclude that this might occur in other situations. Furthermore, treatment with oxidizing agents also affects the cell cycle through several other pathways, possibly obscuring p16^{INK4A} oxidation dependent effects.

Evolutionary Analysis of the Redox Sensitive Cysteine in p16^{INK4A}

Aggregation and inactivation of a tumor suppressor protein may seem a maladaptive response to oxidizing conditions, although we cannot exclude that it may support another currently unknown biological function. Conservation of evolutionarily-acquired cysteines at the surface of proteins can be indicative for a role in redox signaling, whereas the loss of acquired cysteines may indicate the cysteine hampers protein function [11,23]. We therefore investigated to what extent p16^{INK4A} C72 is conserved throughout evolution. The genes encoding p16^{INK4A} *(CDKN2A)* and p15^{INK4B} *(CDKN2B)* are the product of a gene duplication that occurred somewhere in evolution around the time that the mammalian branch of the evolutionary tree was formed [24] (see **Figure S12A** for reference). Strikingly, C72 in the human protein is not conserved in any of the protein sequences of the *CDKN2* orthologues in fish, birds, reptiles and amphibians. Yet, this cysteine is present in both p16^{INK4A} and p15^{INK4B} in almost all mammalian species for which sequence information is available in the ENSEMBL database [25], suggesting that acquisition of this cysteine occurred just before or coincided with the gene duplication of the ancestral *CDKN2* gene (**Figure 7A, B**). Further investigation of the protein sequences of the p16^{INK4A} and p15^{INK4B} orthologues revealed that the cysteine homologous to the human p16^{INK4A}-C72 was substituted later in evolution in several branches of mammalian species including some primates, rodentia and perissodactyla (see **Figures 7A, 7B** and **S12B**). The latter could indicate that redox regulation of the acquired cysteine homologous to human p16^{INK4A} C72 is not absolutely required for a p16^{INK4A} function and that C72 might be slightly deleterious and displays a weak purifying selection.

DISCUSSION

Amyloid fibrils are structures that can be formed by a wide variety of protein sequences [26]. These fibrils share common features, including an unbranched fibrillar morphology and a cross-β sheet core structure. Amyloids were previously thought to be largely disease-related, especially involved in neurodegenerative diseases, but there are increasing numbers of amyloid fibrils discovered that have a physiological function. Several mammalian examples have been reported in recent years, including the melanosome protein pMeL, amyloids involved in hormone storage, and the RIPK proteins, whose fibril formation appears to trigger necroptotic signaling pathways [27–30]. In this work we show that p16^{INK4A} can form fibrils under physiological conditions and in cell-based models, and that the formation is triggered by oxidation of the single cysteine residue and homodimerization. We presented evidence that p16^{INK4A} can form aggregates that have

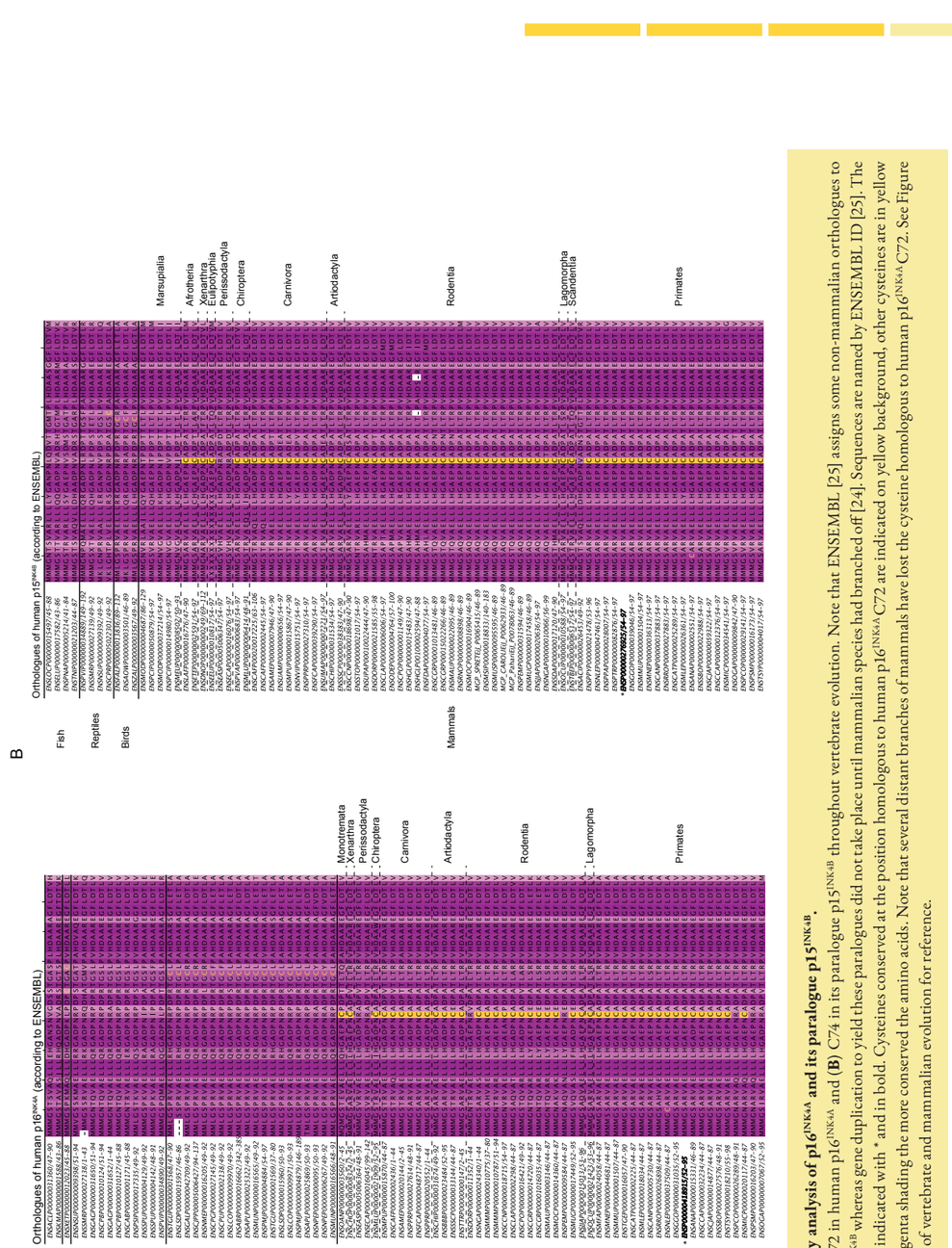

Figure 7. Evolutionary analysis of p16^{INK4A} and its paralogue p15^{INK4B}.
(A) Conservation of C72 in human p16^{INK4A} and **(B)** C74 in its paralogue p15^{INK4B} throughout vertebrate evolution. Note that ENSEMBL [25] assigns some non-mammalian orthologues to either p16^{INK4A} or p15^{INK4B} whereas gene duplication to yield these paralogues did not take place until mammalian species had branched off [24]. The human orthologues are indicated with * and in bold. Cysteines conserved at the position homologous to human p16^{INK4A} C72 are indicated in yellow background, other cysteines are in yellow text. The darker the magenta shading the more conserved the amino acids. Note that several distant branches of mammals have lost the cysteine homologous to human p16^{INK4A} C72. See Figure S12 for a schematic tree of vertebrate and mammalian evolution for reference.

the typical features of amyloid fibrils, including binding of diagnostic dyes, presence of cross-β sheet structure, and typical dimensions found in EM. The critical dependence of a disulfide cross-linked dimer as a subunit has not been observed so far and highlights the role of the cellular redox state as an important regulator of fibril formation.

The role of cysteine chemistry in amyloid formation has been discussed in detail previously [31]. Most commonly, disulfide bonds are found to stabilize a soluble, usually monomeric, form of the protein, preventing its un- or misfolding and aggregation. In many cases, blocking of disulfide bond formation by mutagenesis or chemistry generates proteins that are more prone to amyloid formation, such as has been demonstrated for lysozyme [32], SOD1 [33,34], insulin [35] and prion protein [36,37]. In contrast, oxidation of the single cysteine of $p16^{INK4A}$ is important for the transition of the monomeric protein to form amyloid fibrils, and modification of the cysteine by mutagenesis or S-glutathionylation prevents its amyloid formation. Proteins in which disulfide bonds have been postulated to be involved in stabilization of amyloid fibrils include the prion protein and RIPK fibrils, however disulfide bond formation itself is not required for conversion to amyloid in either of these cases [36–38].

Several properties of $p16^{INK4A}$ fibrils fit with those expected for functional amyloids, including their rapid formation (instead, disease-related amyloids can take days to form fibrils) [39,40], and their lack of clear polymorphism (no evidence of peak doubling in the solid-state NMR spectrum) [41,42]. We have shown that $p16^{INK4A}$ fibrils can be formed *in vitro* under relatively mild oxidizing conditions at physiological pH. In contrast to many other amyloid-forming proteins, $p16^{INK4A}$ does not require harsh treatments, such as extreme pH, high temperatures, high pressure or organic solvents, that are frequently used to destabilize folded proteins in order to convert them to amyloid fibrils in a practical time scale. One striking difference in the properties of $p16^{INK4A}$ amyloid fibrils, compared to classical disease-linked amyloids like amyloid-β and α-synuclein, is the apparent reversibility of the fibrillar state. Typical amyloids are highly stable and are not disaggregated by SDS buffers and do not run into SDS-PAGE gels [26,43,44]. Our results show that SDS is able to disaggregate $p16^{INK4A}$ fibrils into dimers, and that reducing-agent treatment further returns $p16^{INK4A}$ to a monomeric state. This was shown for both recombinantly-produced $p16^{INK4A}$ amyloid *in vitro*, as well as $p16^{INK4A}$ amyloid formed in a cellular model. Furthermore, we find that $p16^{INK4A}$ amyloids are transiently formed and do not persist in the cellular environment as judged by the filter trap assay. Clearance of the amyloids in cells could in principle proceed through degradation or disaggregation into monomers. There does not seem to be a clear increase of the monomeric form upon disappearance of the aggregates, which could suggest that the aggregates are being degraded rather than disaggregated. A recent study showed that $p16^{INK4A}$ also forms aggregates upon inhibition of autophagy [45], which is in line with this notion. The observation that $p16^{INK4A}$ amyloids are reversible and can be cleared from cells potentially adds to an emerging pattern of lability of amyloid fibrils that have functional roles in the cell. For example, RIPK1/3, and the phase-separating proteins FUS and hnRNPA2 are all reported to form functional amyloid fibrils, and are apparently SDS soluble [35,38]. This may be a hallmark for functional fibrils, which must be regulated and removed when the function is no longer needed. In contrast, highly stable, persistent aggregates may have toxic properties, such as in the case of Tau or TDP-43 aggregates, which are pathogenically related to various neurodegenerative diseases [46,47].

It is now generally accepted that the cellular redox environment contributes to various signaling pathways and that H_2O_2 can act as a secondary messenger molecule [9]. Cysteine residues are frequently found to be modified in large-scale analysis of the cysteinome and thousands of proteins are affected by redox regulation [48,49]. Redox potentials vary widely between cell types and specific compartments, ranging from -374 mV for the strongly reducing NADPH/$NADP^+$ redox couple in the liver cytosol to -180 mV from the GSH/GSSG couple in the oxidizing endoplasmic reticulum of B-cells [50].

In addition, the average redox potential varies greatly between cell cycle stages [51]. The redox potential of -198 mV that we found for the oxidation of C72 of $p16^{INK4A}$ is well within the physiological range. One difference between *in vitro* and cell culture oxidation of $p16^{INK4A}$ is that *in vitro* $p16^{INK4A}$ could be stably GSH-ylated whereas in cell cultures we only observed the disulfide-bonded homodimer. This might seem surprising, because there is ample GSH available in the cell and addition of micromolar ranges of diamide will likely react to form GSSG. Therefore, it may be unlikely that in cells diamide and H_2O_2 oxidize $p16^{INK4A}$ directly, but rather that its oxidation is the result of a redox relay or disulfide exchange mechanism, as has been proposed for other redox-sensitive proteins [52]. However, we cannot exclude that transient GSH-ylation of $p16^{INK4A}$ occurs in cells. Of note, tumor cells have been frequently reported to exhibit a more oxidizing milieu [53]. This could mean that $p16^{INK4A}$ would be more often in the dimerized and aggregated state, which could contribute to reactivation of CDK4/6 in tumors that express $p16^{INK4A}$. One might argue that $p16^{INK4A}$ inactivation by oxidizing conditions would be an inadequate response, that would be lost through evolutionary pressure. Evolutionary analysis indeed shows that the cysteine homologous to human $p16^{INK4A}$C72 was acquired recently: near or coinciding with the appearance of mammals and was then substituted again multiple times in several branches of mammalian evolution. However, this analysis would have to be further extended to be able to reject a potential beneficial biological role for $p16^{INK4A}$ amyloid formation, for instance to temporarily reactivate CDK4/6 in cells with high $p16^{INK4A}$ levels. Whether and how this indeed could also contribute to tumor progression remains to be established. Our pull-down experiments indicate that oxidation of $p16^{INK4A}$ leads to loss of its inhibitory activity towards CDK4/6 but that oxidized $p16^{INK4A}$ and CDK4/6 still bind. We speculate that the CDK4/6 interaction that we observe is of a different nature, which could underlie loss of inhibition of CDK4/6 upon oxidation of $p16^{INK4A}$. Amyloid formation-dependent inactivation of tumor suppressor proteins has been described before for p53 and also in this case amyloid formation was reversible [54].

Taken together, the presented work shows that redox signaling can trigger the formation of amyloid fibrils from an otherwise alpha-helical protein. Conversion of a protein from a soluble, monomeric and an insoluble, beta-amyloid fibrillar phase dependent on the cellular redox state has not been reported before. This could pose a more general mechanism in amyloid formation, as was recently shown for redox-dependent liquid-liquid phase-separation [55]. It also adds to the repertoire of structural alterations known to occur in response to redox signaling.

MATERIALS AND METHODS

Cell Lines, Plasmids, Antibodies and Compounds

Cells (HEK293T, COLO829) were cultured in DMEM low glucose supplemented with FCS (10%), L-glutamine (2mM) and Penicillin-Streptomycin (100 Units-0.1mg per ml medium) (all from Lonza). Cells were transfected using PEI (Sigma Aldrich) or X-tremeGENE 9 (Roche) according to manufacturer's instruction.

The vector containing the truncated form (Δ1–8) of wild type $p16^{INK4A}$ was a gift from R. Medema [56]. The cysteine mutant of $p16^{INK4A}$ was created by site-directed pcr mutagenesis. mCherry- (backbone pLV-CMV-bc) and Flag-His-tagged (backbone pCDNA3) and doxycycline-inducible (backbone pINDUCER20, Addgene #44012) $p16^{INK4A}$ constructs were created using gateway technology (Life Technologies). COLO-829 melanoma cells stably expressing doxycyline-inducible constructs were transduced with lentivirus containing pINDUCER20-$p16^{INK4A}$ or -$p16^{INK4A}$C72A. Cells were selected for stable transduction using geneticin and $p16^{INK4A}$ expression was confirmed by qPCR and western blotting. Subsequently, cells were transduced with lentivirus containing the FUCCI cell cycle probes mAG-hGeminin(1/110) / pCSII-EF (#RDB15268) and Fucci-G1 phase probe mKO2-hCdt1(30/120) / pCSII-EF (#RDB15267) (RIKEN BioResource Center), which were a kind gift from A. Miyawaki [57]. Cells

were selected for stable transduction using zeocin and made monoclonal by limiting dilution.

The following antibodies were used in this study: Flag (M2 F3165 Sigma Aldrich), p16^{INK4A} (10883 Proteintech), p16^{INK4A} (ab16123 Abcam), CDK4 (C-22 Santa Cruz), CDK6 (C-21 Santa Cruz), tubulin (CP06 Merck Millipore), Phospho-Rb Ser807/811 (9308 Cell Signaling). Solutions/compounds not mentioned elsewhere: 35% hydrogen peroxide (Merck).

Co-immunoprecipitation, SDS-PAGE and Western Blotting

Immuno-precipitation of endogenous p16 was done with rabbit anti-p16^{INK4A} (10883 Proteintech) using three 10 cm dishes of HEK293T cells per sample. Transfection was performed two days prior to sample preparation. Cells were scraped in 100 mM N-ethyl-maleimide in PBS (37 °C) to prevent post-lysis oxidation and collected by centrifugation at 1200 rpm for 3 minutes. Cells were lysed in a standard lysis buffer containing 50 mM Tris pH 7.5, 1% triton X-100, 1.5 mM $MgCl_2$, 5 mM EDTA, 100 mM NaCl supplemented with Aprotinin, Leupeptin and NaF. 100 mM iodoacetamide was added to to prevent post-lysis oxidation of cysteines. The cell lysates were subsequently centrifuged at 14000 rpm for 10 min. 50 µl of the supernatant was kept as input. For immunoprecipitation of endogenous p16^{INK4A} the pellet was resuspended in lysis buffer, sonicated and supplemented with 125U of benzonase and incubated for 1hr at 37 degrees. The remaining supernatant (and where indicated also the resolubilized pellet) was used for immunoprecipitation with the indicated antibody coupled to protein A-Agarose (Roche) or in case of transfected Flag-tagged constructs with anti-Flag M2 Affinity gel (Sigma Aldrich). After 2 h of incubation, beads were washed 3 times with standard lysis buffer supplemented with extra NaCl (1 M final concentration). After washing, samples were split into two parts, and sample buffer with or without a reducing agent (b-mercaptoethanol) was added. Samples were boiled for 5 min and separated on a 15% polyacrylamide gel. For Western Blotting, proteins were transferred to immobilon-FL membranes. For diagonal electrophoresis, non-reducing samples were separated on a 15% polyacrylamide gel, after which the entire protein containing lane was excised, reduced, and separated on a new 15% polyacrylamide gel. For visualization of diagonal electrophoresis proteins were stained by SimplyBlue.

Filter Trap Assay

HEK293T cells were transfected with Flag-p16^{INK4A}, Flag-p16^{INK4A} C72A or GFP as a control. After two days, cells were scraped in 100 mM N-ethyl-maleimide in PBS (37°C) to prevent post-lysis oxidation and collected by centrifugation at 1200 rpm for 3 minutes. Lysis buffer (50 mM Tris pH 7.5, 1% v/v Triton X-100, 1.5 mM $MgCl_2$, 5 mM EDTA, 100 mM NaCl, Protease inhibitors (Aprotinin + Leupeptin), NaF, 100 mM Iodoacetamide) added for 10 minutes followed by centrifugation for 15 minutes at 14000 rpm in an Eppendorf microfuge. The pellet was resuspended in benzonase buffer (50 mM Tris-HCL pH 8.0, 1 mM $MgCl_2$) and 125U of benzonase was added followed by incubation for 1hr at 37 degrees. The reaction was stopped by adding 2x termination buffer (40 mM EDTA, 0.2 % SDS, with or without 10 mM DTT). Protein content was measured using the BCA kit and 50 micrograms of protein per sample were loaded on a Bio Dot apparatus (Biorad) equipped with a 0.2 micron pore size nitrocellulose membrane soaked in buffer B (10 mM Tris-HCL pH 8.0, 150 mM NaCl, 2 % SDS) on top of two Whatmann paper filters soaked in Buffer A (10 mM Tris-HCL pH 8.0, 150 mM NaCl, 1 % SDS), after pre-washing the membrane with 100 µl of buffer A. Samples were pulled through the membrane using vacuum, followed by washing thrice with 100 µl of buffer A. The nitrocellulose membrane was further processed as for Western Blotting to detect trapped p16^{INK4A}.

Kinase Assay

The kinase assays in this study were performed with immunoprecipitated Flag-p16^{INK4A} or Flag-p16^{INK4A}C72A and the attached binding-partners. Beads were washed three times with standard lysis buffer followed by two washes with kinase buffer containing 25 mM Tris pH 7.5 and 10 mM $MgCl_2$. The beads were subsequently incubated for 30 min at 30 °C in 20 µl kinase buffer supplemented with 1 mM DTT, 1 µg human GST-Rb (48-378 Sigma Aldrich) as substrate and 0.2 mM ATP. Directly after the assay beads were boiled for 5 min in reducing sample buffer and loaded on a 15% polyacrylamide gel followed by Western Blotting.

RNA Extraction, cDNA Synthesis and qPCR

Doxycylcine-inducible p16^{INK4A} expressing Colo-829 cells were plated, and 24h before harvesting doxycline was added to induce expression of p16^{INK4A} or p16^{INK4A}C72A. Cells were treated as indicated. Cells were washed once with PBS and collected in RLT buffer. RNA was extracted using the RNeasy kit (Qiagen) according to the manufacturer's instructions. 1 ug RNA was used as input for cDNA synthesis using the iScript cDNA synthesis kit (Biorad). qPCR was performed with FastStart SYBR Green Master mix (Roche) using the CFX96 Touch Real-Time PCR Detection System. Relative gene expression was calculated using the ΔΔCt method [58] by normalization to HNRNPA1. Statistics were done with Graphpad Prism 8. Primer sequences: *p16^{INK4A}* forward (5′-CAACGCACCGAATAGTTACG-3′), *p16^{INK4A}* reverse (5′-ACCAGCGTGTCCAGGAAG-3′), *CCNE2* forward (5′-GGGGGATCAGTCCTTGCATT-3′), *CCNE2* reverse (5′-TCCCCAGCTTAAATCAGGCA-3′), *HNRNPA1* forward (5′-GGAAGCTACAGGTTACAACA-3′), *HNRNPA1* reverse (5′-AGTCACAAATACAGTCCTCG-3′).

Protein Expression and Purification

An *Escherichia coli* codon-optimized gene of *Homo sapiens* p16^{INK4} (UniProt ID: P42771) was cloned into a modified version of pETM-11 that includes a 6xHis, a protein A tag and a tobacco etch virus (TEV) protease cleavage site, leaving an additional glycine residue at the N-terminal cleavage site. For a glycerol stock solution, competent *E. coli* BL21 (DE3) cells were transformed with the p16^{INK4} harboring gene and inoculated in minimal medium in the presence of kanamycin (50 µg/l). After overnight incubation at 37 °C the cell suspension was mixed with glycerol to 50% (v/v) glycerol and stored at -80 °C. Uniformly ^{15}N-labeled protein samples were prepared from this stock by growing the cells in minimal medium containing $^{15}NH_4Cl$ as the only nitrogen source. The protein synthesis was induced by addition of 0.5 mM isopropyl-1-thio-D-galactopyranoside (IPTG) at an OD_{600} of 0.8 and cells were harvested after 14 h of induction at 19 °C. Cells were resuspended in purification buffer (110 mM potassium acetate, 20 mM HEPES [4-(2-hydroxyethyl)-1-piperazineethanesulfonic acid], pH 8.0, 2 mM $MgCl_2$, 2 mM β-mercaptoethanol (BME), 5% (v/v) glycerol and 20 mM imidazole) and ultrasonicated for lysis. The solution was applied to a gravity Ni-NTA agarose (QIAGEN) column following the manufacturer's instructions. After washing with purification buffer including 20 mM imidazole, the protein was eluted by using purification buffer including 200 mM imidazole and further purified by gel chromatography on an ÄKTA pure system equipped with a HiLoad 16/600 Superdex 75 pg column (GE Healthcare) running with purification buffer. The fractions containing the protein were pooled, incubated with 0.2 mg TEV protease overnight at 4 °C while dialyzed against purification buffer using a dialysis membrane with 5 kDa molecular weight cut-off (ZelluTrans, Roth). On the following day, the protein solution was applied to the Ni-NTA agarose column again to remove the cleaved tag, remaining undigested protein and the His_6-tagged TEV protease. The eluate was then buffer exchanged into purification buffer where BME was substituted with 1 mM DTT using dialysis. The protein solution was aliquoted, frozen in liquid nitrogen and stored at -80 °C. Solution NMR spectroscopy showed that no differences were observed after the freezing and thawing of the samples.

Solution NMR Spectroscopy

The protein stock was freshly buffer exchanged into NMR buffer (4 mM HEPES, 5 mM EDTA, pH 7.5) before measurement. Samples for protein characterization contained 1 mM DTT (dithiothreitol) whereas samples for redox-experiments did not. The protein concentration was 0.15 mM and contained 7% (vol/vol) ^2H_2O for the lock signal. Solution $^1H^{15}N$ HSQC NMR spectra were measured on an Avance III 600 Bruker NMR spectrometer equipped with a cryogenic triple resonance probe with gradients in the z-direction. The recycle

delay of the redox experiments performed (S-glutathionylation and hydrogen peroxide addition) was set to 1 s with a spectral window of 11/34 ppm in $^{1}H/^{15}N$ dimensions, 2048 points in the direct ^{1}H dimension, 128 complex data points in the indirect ^{15}N dimension, and with 8 or 16 scans per increment. Spectra were processed with the NMRPipe package [59] and analyzed by CcpNmr Analysis [60].

For determination of the S-glutathionylation redox potential, the concentration of GSSG in the sample buffer was gradually increased (0.2; 1.0; 2.3; 3.3; 3.9; 5.9; 7.8; 8.8; 9.8; 11.7 mM) by titrating from a 65 mM pH corrected stock solution while the concentration of the reduced form of GSH was kept constant at 4 mM. At each concentration point, a $^{1}H^{15}N$ HSQC NMR spectrum was recorded immediately after addition of the oxidation agent. For assignment of the S-GSHylated protein, HNCA and CBCACONH spectra were acquired. Determination of the redox potential was performed following the protocol of Piotukh *et al.* [61]. In summary, peak intensities of well isolated peaks (N71, C72, D74, T79) of the oxidized form were normalized to a non-affected asparagine side chain resonance and plotted against the redox potential of the buffer. This potential was determined from the standard half-cell potential of the glutathione redox couple (-240 mV at pH 7.0, 25 °C) after pH corrections [50]. The data were fitted to the sigmoidal decay function (equation 1):

$$y = A_2 + \frac{(A_1 - A_2)}{1 + e^{\frac{x - x_0}{dx}}} \quad , \qquad \text{(eq. 1)}$$

where A_1 and A_2 are the initial and final plateaus of the function, dx is the slope and x_0 refers to the desired parameter of the redox potential.

For oxidized samples of $p16^{INK4}$, a final concentration of 50 mM hydrogen peroxide (H_2O_2, from a 30% solution diluted with NMR buffer) or 100 µM diamide (from a freshly prepared 10 mM stock solution in H_2O) was added to the ^{15}N-labeled protein solution. $^{1}H^{15}N$ HSQC NMR spectra were acquired after the addition of the oxidizing agent in subsequent manner. After 10 h, no spectral changes were observed for WT protein anymore and the sample was applied to a size exclusion column (HiLoad 10/300 Superdex 75 pg column, GE Healthcare) and the dimeric fraction of about 50% of the total protein was pooled. The protein was applied to SDS gel electrophoresis in the presence and absence of BME.

CD Spectroscopy

Far-UV CD experiments were recorded on a J-715 spectrapolarimeter (Jasco, Tokyo, Japan). Spectra were acquired at room temperature with a response time of 1 s and a step resolution of 0.3 nm. Five scans were averaged and the signal was background corrected by subtraction of the buffer signal. The CD spectra were obtained from a 1 µM $p16^{INK4A}$ sample before and after oxidation with 200 µM hydrogen peroxide for 8 hours at room temperature and data were converted to molar ellipticity. Samples were freshly prepared and transferred into a 10 mM sodium phosphate buffer at pH 7.4 in the absence of reducing agents.

Small-Angle X-ray Scattering Measurements

SAXS data was recorded on an in-house SAXS instrument (SAXSess mc2, Anton Paar, Graz, Austria) equipped with a Kratky camera, a sealed X-ray tube and a two-dimensional Princeton Instruments PI•SCX:4300 (Roper Scientific) CCD camera. Measurements were performed with 90 min exposure time (540 frames of 10 s each) of three concentrations of 2.5 mg/ml, 1.25 mg/ml and 0.625 mg/ml in NMR buffer. The sample of reduced $p16^{INK4A}$ was measured immediately after purification and buffer exchange. The oxidized sample of $p16^{INK4A}$ was treated overnight with 50 mM H_2O_2 at room temperature. Next day, the sample was applied to size exclusion chromatography and the peak from 9-10 ml elution volume was pooled (see **Figure S6B**) and concentrated. Individual frames of the 90 min exposure were compared and no radiation damage was observed. A range of momentum transfer of $0.012 < s < 0.63$ Å^{-1} was covered ($s = 4\pi \sin(\theta)/\lambda$, where 2θ is the scattering angle and $\lambda = 1.5$ Å is the X-ray wavelength). SAXS data were analyzed with the package ATSAS version 2.8.1 [62]. Desmearing of the oxidized sample could not be performed because the scattering curve showed strong aggregation.

Thioflavin-T Fluorescence Assay

Samples of $p16^{INK4A}$ (20 µM) were prepared in buffer (4 mM HEPES, pH 7.5) with 20 µM ThT. Three replicates were measured for each sample. Samples were subjected to 1 mm orbital shaking for 2 min of every 5 min, in a 96-well, half-area, fluorescence plate (Corning) and measurements were taken every 5 min. Samples were excited at 440 nm and fluorescence emission was measured at 480 nm. Measurements were made using a Tecan GENios microplate reader.

Negative-stain Transmission Electron Microscopy

Protein samples were prepared by incubation of $p16^{INK4A}$ samples with or without oxidizing agents for 6–24 h at RT. Copper grids with 300 meshes coated with formvar/carbon film (Electron Microscopy Sciences, Hatfield, USA) were glow-discharged in argon atmosphere for 30 s at 3 mA. Grids were floated on a 5 µl drop of a 50 µM protein sample and incubated for 60 s. Grids were washed once with water, and then floated on 5 µl of uranyl acetate solution (2% w/v) for 30 s. Micrographs were taken on either a JEOL JEM 100CX transmission electron microscope or a JEOL JEM 1400 Plus transmission electron microscope (JEOL, Tokyo, Japan).

Prediction of Aggregation-Prone Regions

Four different aggregation prediction programs, TANGO [19], PASTA [20], Zyggregator [63]and Aggrescan [21] were used to identify putative regions responsible for the beta-aggregation of $p16^{INK4A}$ using the default settings.

Congo-Red Absorbance

Absorbance spectra were measured on samples of $p16^{INK4A}$ (20 µM) with Congo red (20 µM) in $p16^{INK4A}$ buffer. Spectra were recorded from 400–650 nm, with a resolution of 2 nm, on a Tecan Infinite 200Pro microplate reader in a 96-well, half-area, fluorescence plate (Corning).

Fourier-Transform Infrared Spectroscopy

$p16^{INK4A}$ (80 µM) samples were treated with 50 mM H_2O_2 overnight in $p16^{INK4A}$ buffer, then dialysed against water overnight. Spectra were recorded on a JASCO FT/IR-4100 FT-IR spectrometer with attenuated total reflectance (ATR) attachment. The samples were measured with 128 scans at a resolution of 2 cm^{-1} at room temperature.

Solid-State NMR Spectroscopy

Approximately 10 mg (150 µM) of ^{13}C-^{15}N labeled $p16^{INK4A}$ fibrils were prepared in $p16^{INK4A}$ buffer by addition of 50 mM H_2O_2 and incubation at 37 °C overnight. The sample was packed into a 3.2 mm MAS rotor by ultracentrifugation. Spectra were recorded on a Bruker Avance III 750 MHz spectrometer (Bruker BioSpin) equipped with a 3.2 mm triple-resonance MAS probe. A proton-driven spin diffusion (PDSD) spectrum [64] was recorded at 16.5 kHz MAS, with 50 ms mixing time, at a set temperature of 273 K, with 352 scans and 22 ms and 8 ms acquisition time in the direct and indirect dimensions, respectively. Experiments were acquired using Topspin 3.2 (Bruker Biospin) and analysed using CCPN Analysis 2 [60]. The secondary chemical shift was calculated as $[\delta(C\alpha_{observed}) - \delta(C\alpha_{random\ coil})] - [\delta(C\beta_{observed}) - \delta(C\beta_{random\ coil})]$ with random coil chemical shifts taken from [65].

Sample Preparation for Mass Spectrometry

HEK293T cells were transfected with Flag-$p16^{INK4A}$ or Flag-$p16^{INK4A}$ C72A. After two days, half of the dishes (3 full 15cm dishes per sample) were treated for 10 minutes with diamide (250 µM) (Sigma Aldrich) and subsequently harvested for immunoprecipitation with Flag beads as described before. After washing 2x with 1 M salt buffer and 3x with PBS to remove all soap, proteins were eluted from the beads by two times 5 minutes incubation with 75 µl 0.1 M glycine pH 2. The protein containing supernatant was transferred to a new tube and incubated for 20 minutes with 10 mM DTT and 2 M Urea (dissolved in 100 mM Tris pH 7.5), followed by 10 minutes incubation with iodoacetamide (50 mM). To digest the proteins, 0.25 µg trypsin (Promega) was added per sample and samples were incubated ON at 25 °C. The next day C18-stagetips were used for filtering and loading of the protein digest.

Mass Spectrometry and Data Analysis

The mass spectrometry was performed as previously described [11].

For the analysis MaxQuant software version 1.5.1.0 [66] was used. During the analysis, oxidation of methionine, alkylation of cysteines with iodoacetamide were set as variable modification. Proteins were identified by the IPI human V3.68 database and the relative amounts of protein in the separate experiments, the Intensity Based Absolute Quantification (IBAQ) [67], as well as the label free quantification [68] were calculated.

Further analysis was done using R version 3.4.0. The used code and description is currently being uploaded to GitHub. Proteins identified with two or more unique peptides were filtered for reverse hits, decoy hits and standard contaminants and samples that show aberrant clustering or low protein count were excluded. Subsequently the IBAQ data was Log2 transformed and normalized for IP efficiency. For p-value calculations, left-censored missing data was first imputed using a stochastic minimal value approach. Imputation was performed by random draws from a Gaussian distribution centered in the 10^{-4} quantile of the known data with a standard deviation that is same as the observed values [69]. A standard t-test was performed on the imputed data and p-values were adjusted for multiple testing using the Benjamini-Hochberg correction.

Mass Spectrometry of GS-p16^{INK4A}

The intact mass of p16^{INK4A} before and after oxidation by GSSG was obtained from LC-MS analysis, that was performed on recombinantly expressed protein (see protein expression and purification section). The sample was desalted using 10 kDa Amicon Ultra-0.5 centrifugal filter devices prior to measurement. 150 pmol of protein were injected into an Agilent 1200 system (Vienna, Austria) coupled to an LTQ-FT mass spectrometer (Thermo Fisher Scientific, Waltham, MA, USA). Separation was carried out on a monolithic PepSwift® column (500 µm x 5 cm Monolithic PS – DVB) at a flow rate of 20 µl/min using the following gradient, where solvent A is 0.05 % trifluoroacetic acid in water and solvent B is 0.05 % trifluoroacetic acid in acetonitrile: 0-5 min: 10 % B; 5-55 min: 10-100 % B; 55-65 min: 100 % B, 65-80 min: 10 % B. The sample was ionized in the electrospray source and analyzed using FT-MS operated in positive ion mode applying full scan MS (m/z 300 to 2000) with a resolution of 400,000. Acquired data were processed with the software Protein Deconvolution 2.0 SP2 (Thermo Fisher Scientific) using a S/N threshold of 5 and a relative abundance threshold of 20 %.

Flow Cytometry

Cell cycle analysis was performed using a combination of the FUCCI [57] system and DNA content staining. COLO-829 cells expressing the FUCCI constructs as well as pINDUCER20-p16^{INK4A} or p16^{INK4A} C72A were seeded and treated with doxycycline and LEE-011 for the indicated times and samples. Nocodazole was added 16h before harvest to capture cycling cells in mitosis to distinguish transient G1 from G1/G0 arrested cells. Cell culture medium was collected and cells were washed in PBS before trypsinization. Cells were fixed for 10 minutes at room temperature with 2% formalin in PBS. After 2 washes with PBS, cells were permeabilized with 70% ethanol for 30 minutes. Cells were resuspended in PBS with 0.1% BSA with DAPI and RNAse to stain the DNA. mKO2-hCtd1(30/120), mAG-hGeminin(1/110) and DAPI were measured using a BD FACSCelesta Flow Cytometer (BD Bioscience).

Evolutionary Analysis

Amino acid sequences of vertebrate orthologues of human p16^{INK4A} and p15^{INK4B} were downloaded from the ENSEMBL database [25]. Alignment and visualization of conservation was performed using JalView 2.10.1 software [70], with the Clustal plugin with default settings.

Data Availability

The datasets generated and/or analyzed in the current study are available from the corresponding authors upon reasonable request. The mass spectrometry proteomics data have been deposited to the ProteomeXchange Consortium via the PRIDE [71] partner repository with the dataset identifier PXD012353 and can be accessed using username: reviewer89417@ebi.ac.uk and password: fQ0pzPhh.

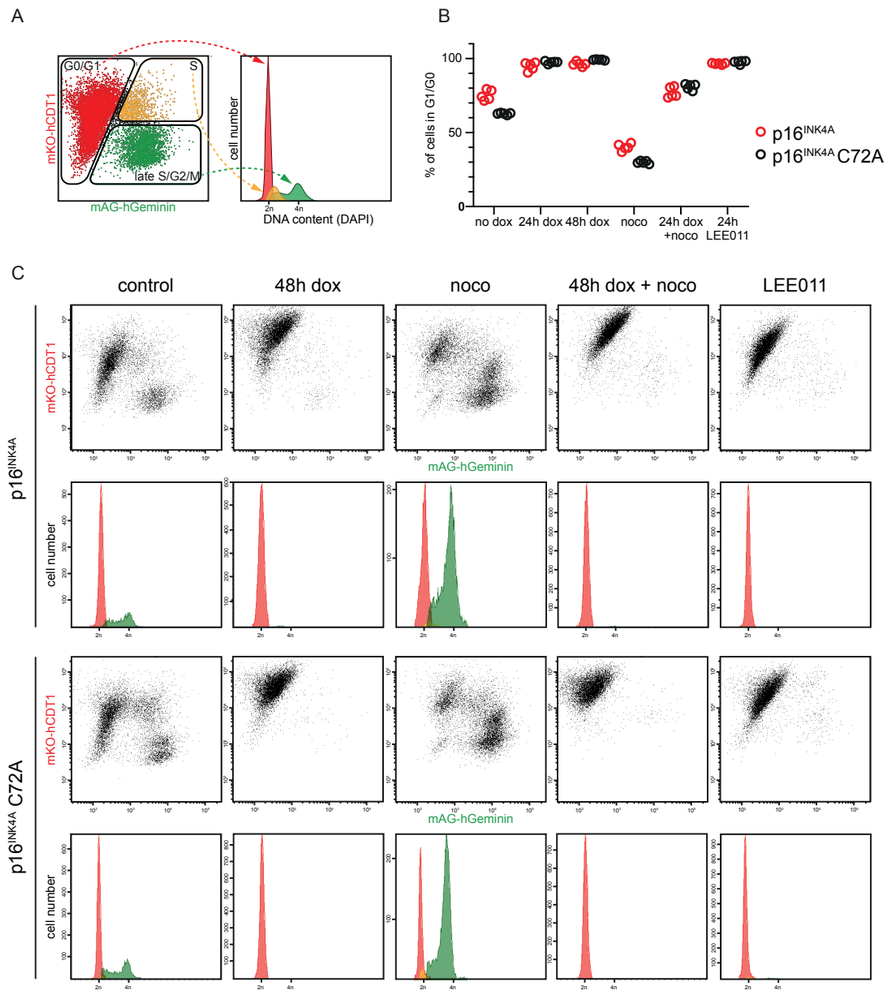

Figure S1. p16^{INK4A} C72 is dispensable for its role in cell cycle arrest.
(**A**) Cell-cycle profiling of COLO-829 cells expressing doxycycline inducible pINDUCER20-p16^{INK4A} wildtype or p16^{INK4A}C72A as well as the FUCCI cell cycle indicator system. Cells were trapped overnight in mitosis using Nocodazole to make G1/G0-arrested cells more obvious from those that were still cycling. The CDK4/6 inhibitor LEE011 was added to estimate to what extent CDK4/6 inhibition can induce cell cycle arrest in this cell line. The C72A mutation leaves the cell-cycle inhibitor function of p16^{INK4A} intact. (**B**) The graph shows the pooled results for the percentage of cells in G1/G0 phase of the cell cycle quantified from two experiments with at two or three replicates each. We conclude that p16^{INK4A}C72A is still able to induce a cell cycle arrest. (**C**) The FACS plots and histograms show typical results for each of the conditions.

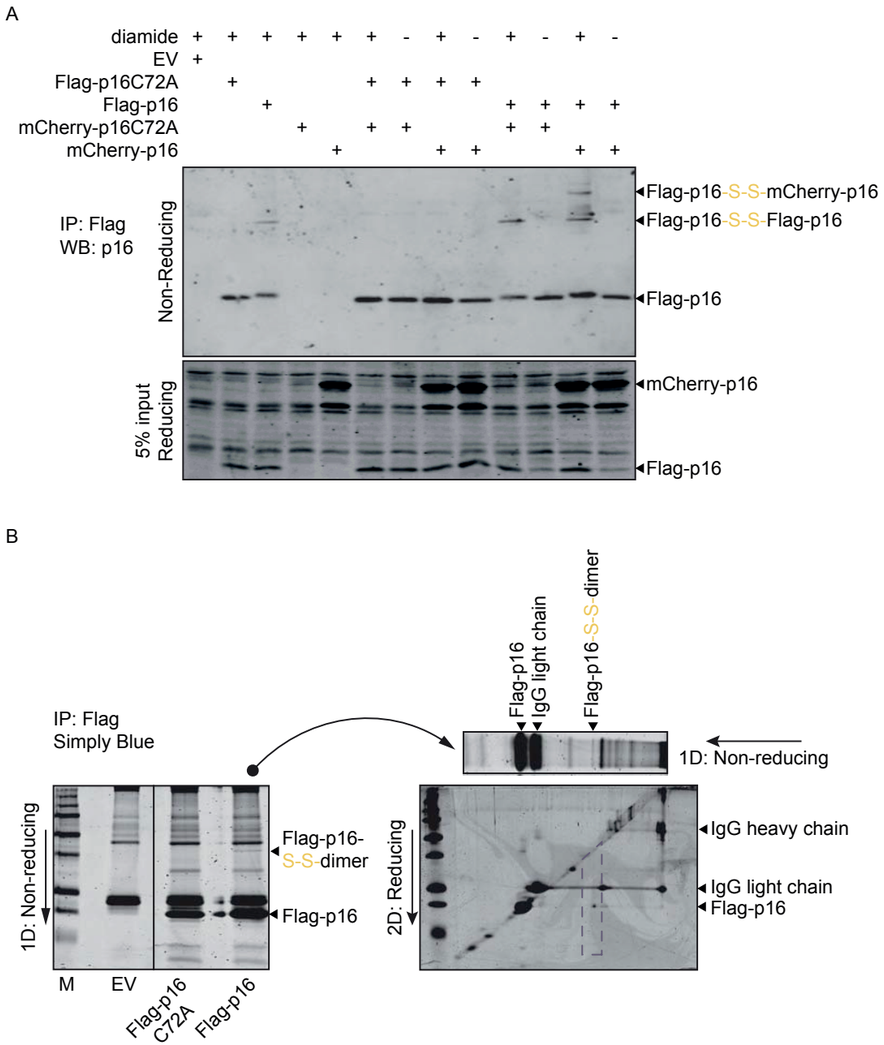

Figure S2. SDS-PAGE analysis of p16^{INK4A}.
(**A**) mCherry-p16^{INK4A} co-immunoprecipitates with Flag-p16^{INK4A} in a disulfide-dependent manner. Dimers consisting of both two Flag-p16^{INK4A} molecules or one Flag-p16^{INK4A} and one mCherry-p16^{INK4A} molecule can be detected. (**B**) Diagonal electrophoresis (non-reducing SDS-PAGE followed by reducing SDS-PAGE) shows that the high-molecular weight form of Flag-p16^{INK4A} separates in a single dot under the diagonal, confirming that the disulfide-containing high-molecular weight species of p16^{INK4A} consists of only p16^{INK4A} protein. Collectively, and because p16^{INK4A} has only one cysteine, these data must mean that the slow-migrating species of p16^{INK4A} detected under non-reducing conditions are indeed p16^{INK4A} homo-dimers. The experiments shown are typical results of at least two independent experiments. See also Figure 2A in Chapter 3.

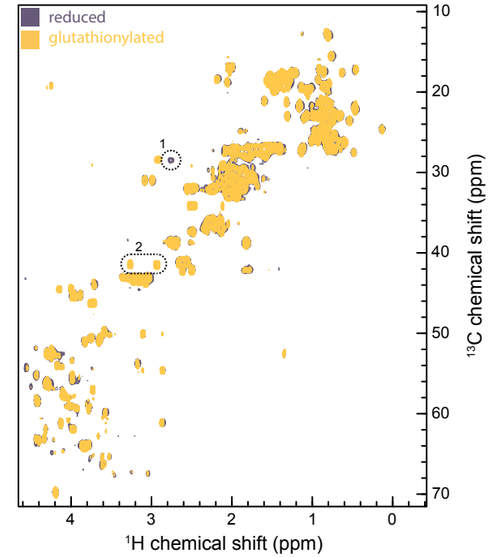

Figure S3. Overlap of ^{1}H^{13}C HSQC spectra in the reduced (magenta) and glutathionylated state (yellow).
The magenta peak labeled as (1) is the reduced C72 Cβ resonance. After titration with glutathione to the end point, the resonance disappears and the oxidized Cβ resonance appears at the position labeled as (2).

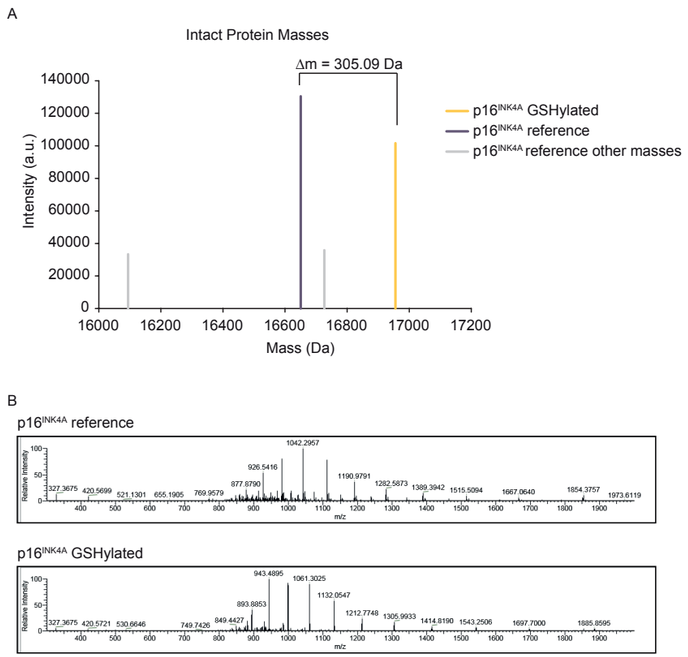

Figure S4. Mass spectrometry analysis of reduced and glutathionylated p16^{INK4A}. *(figure legend continues on next page)*

(**A**) Deconvoluted mass spectra of p16^{INK4A} treated with GSSG shows a mass-shift of 305 Da which is in agreement with the modification of p16^{INK4A} C72 with disulfide-linked glutathione (i.e. S-GSHylated p16^{INK4A}). (**B**) m/z spectra of the LC-MS analysis of recombinant p16^{INK4A} before and after S-GSHylation. The mass-spectrometric analysis to determine whether p16^{INK4A} was indeed S-GSHylated upon GSSG treatment was performed once.

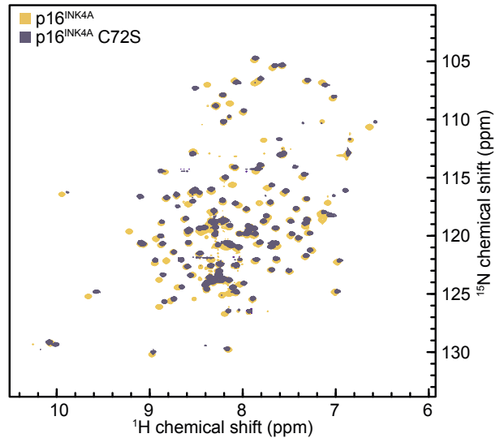

Figure S5. 1H15N HSQC solution NMR spectra of WT p16INK4A (blue) and p16INK4A C72S (orange).

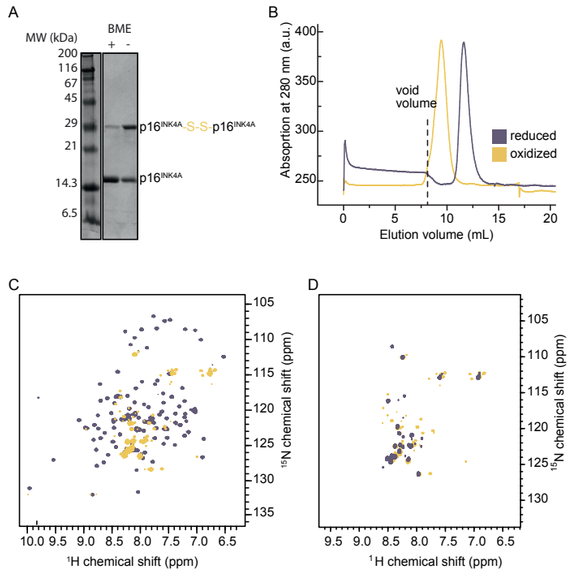

Figure S6. Analysis of oxidized p16^{INK4A}. *(figure legend continues on next page)*
(**A**) SDS-PAGE of wild-type p16^{INK4A} after hydrogen peroxide oxidation in the presence (left) and absence of the reducing agent BME in the sample buffer. A typical result is shown of at least 10 replicate experiments.
(**B**) Size exclusion chromatography of WT p16^{INK4A} before (magenta) and after (yellow) overnight oxidation with 50 mM hydrogen peroxide at room temperature. A typical result is shown of two replicate experiments. (**C**) Overlap of $^{1}H^{15}N$ HSQC solution spectra of reduced (magenta) WT p16^{INK4A} and after addition of diamide (yellow). A typical result is shown of five replicate experiments. (**D**) Overlap of $^{1}H^{15}N$ HSQC solution spectra of WT p16^{INK4A} oxidized with H_2O_2 (magenta) and diamide (yellow).

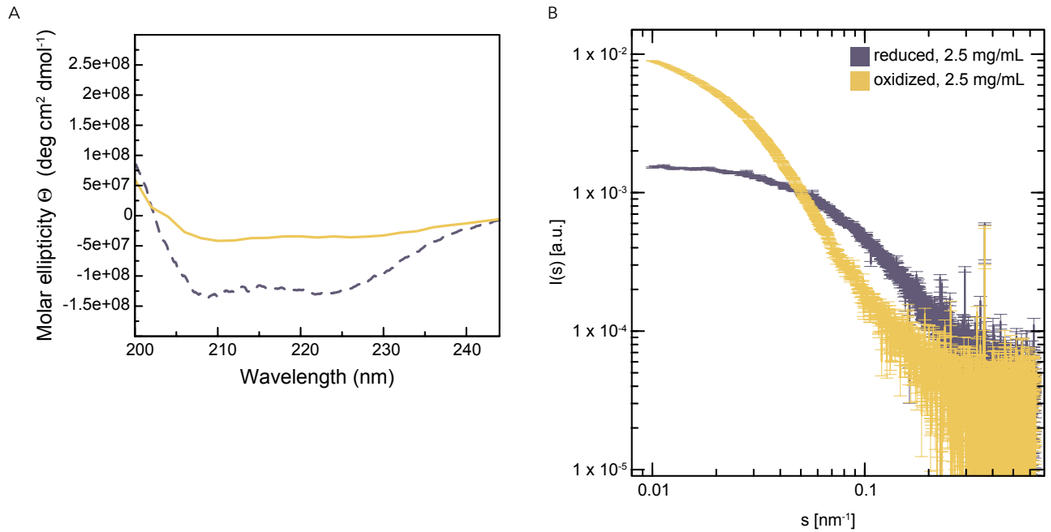

Figure S7. CD spectroscopy and SAXS curves of reduced and oxidized p16^{INK4A} samples.
(**A**) CD spectra of reduced (magenta) and oxidized (yellow) p16^{INK4A}. The experiment was performed twice and a typical result is shown.
(**B**) Scattering curves of reduced (magenta) and oxidized (yellow) p16^{INK4A}. Curves recorded using 2.5 mg/ml protein are presented. The oxidized sample displays typical characteristics of an aggregated protein state and could not be desmeared for detailed data analysis. The experiments were performed three times with varying concentrations showing the same trend and a single representative is shown.

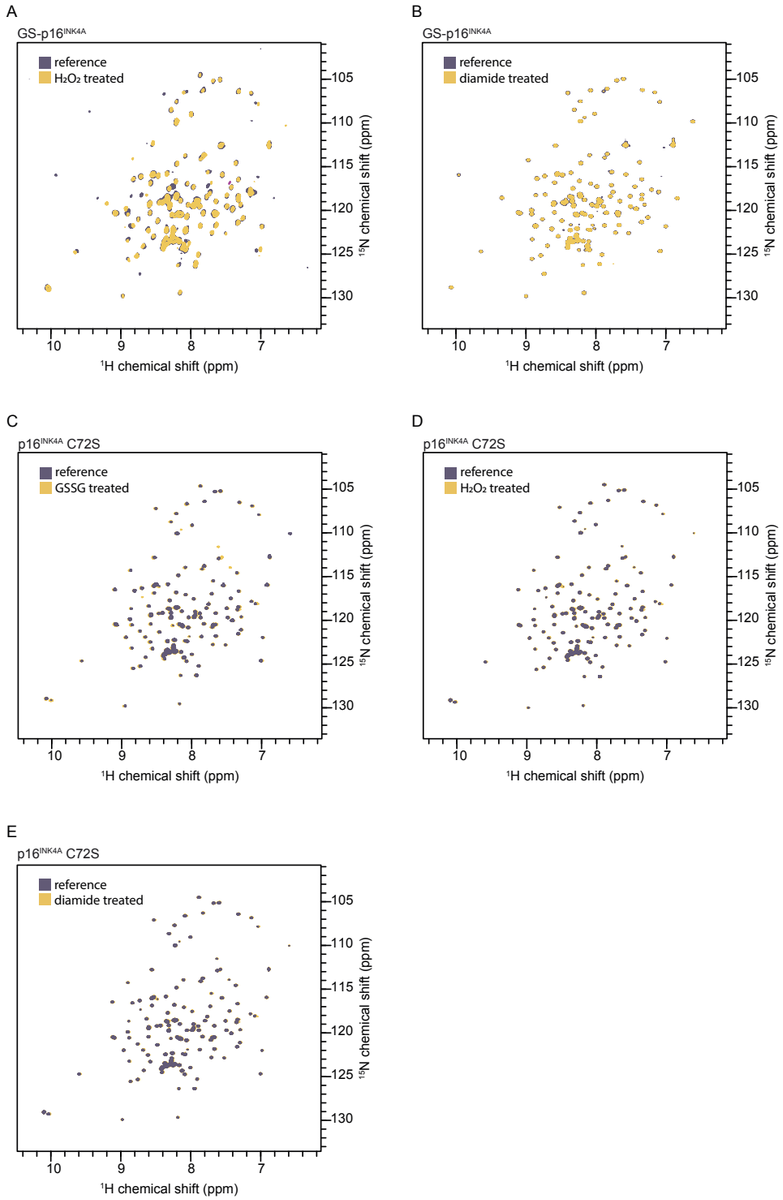

Figure S8. Effect of oxidizing agents on GS-p16^{INK4A} and p16^{INK4A} C72S.
(**A**) Overlap of $^{1}H^{15}N$ HSQC solution spectra of reduced (magenta) and H_2O_2 treated (yellow) GS-p16^{INK4A}. (**B**) Overlap of $^{1}H^{15}N$ HSQC solution spectra of reduced (magenta) and diamide treated (yellow) GS-p16^{INK4A}. (**C**) Overlap of $^{1}H^{15}N$ HSQC solution spectra of reduced (magenta) and GSSG treated (yellow) p16^{INK4A} C72S. (**D**) Overlap of $^{1}H^{15}N$ HSQC solution spectra of reduced (yellow) and H_2O_2 treated (magenta) p16^{INK4A} C72S. (**E**) Overlap of $^{1}H^{15}N$ HSQC solution spectra of reduced (magenta) and diamide treated (yellow) p16^{INK4A} C72S.

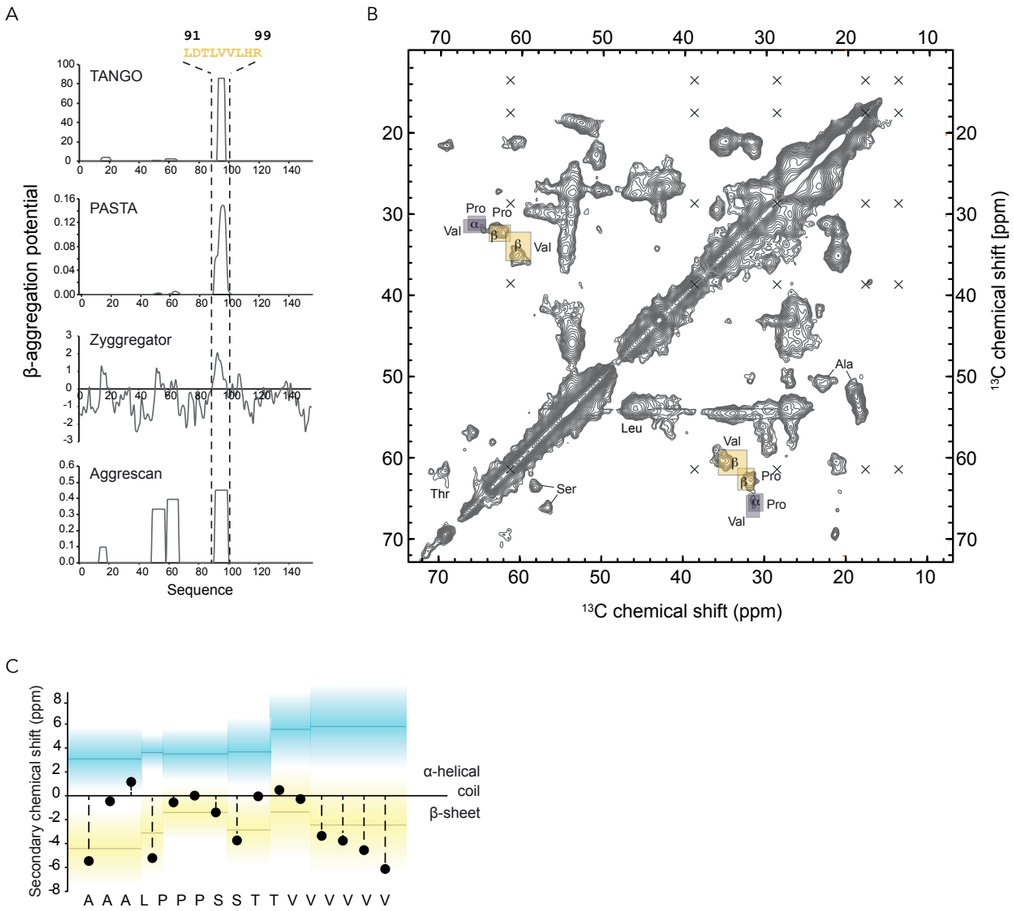

Figure S9. Prediction of p16^{INK4A} aggregation-prone regions.
(**A**) Four b-aggregation prediction algorithms predict that residues 90 to 99 of p16^{INK4A} have high aggregation propensity. (**B**) $^{13}C^{13}C$ solid state NMR spectrum of p16^{INK4A} fibrils showing the full aliphatic region. Crosses mark positions where peaks would be expected to arise from isoleucine residues. There are three isoleucines in the full p16^{INK4A} sequence, suggesting that these residues are absent from the folded b-sheet core of p16^{INK4A} fibrils. Peaks that correspond to amino acid types with distinct shifts are labeled. Boxes indicate the average shift expected for both secondary-structure types of proline and valine, within one standard deviation. (**C**) ^{13}C Secondary chemical shifts of uniquely assigned amino acid types showing the presence of β-sheet secondary structural elements. Horizontal lines indicate average values for secondary chemical shifts of alpha-helix (blue) and β-sheet (yellow), and regions are shaded to one standard deviation.

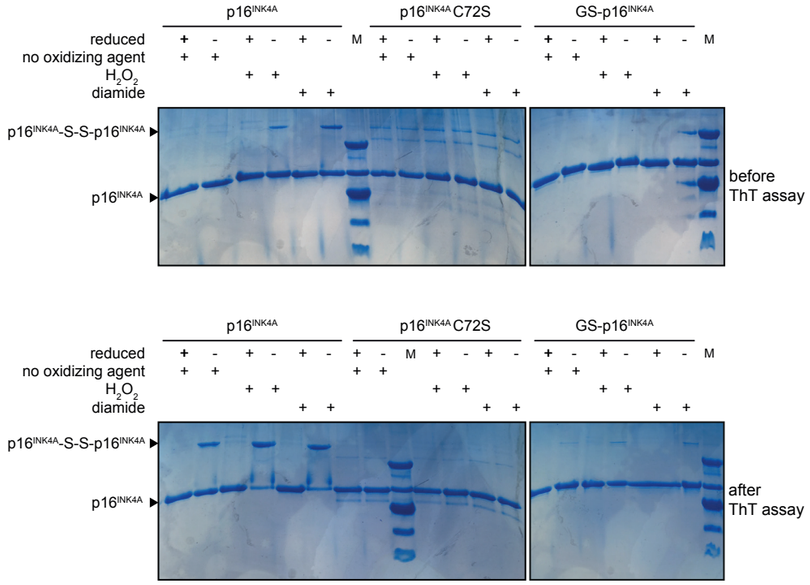

Figure S10. SDS-PAGE of p16^{INK4A} samples before and after ThT fibril formation assay.
Samples were taken before and after the ThT kinetics assay (see **Figure 4B**) and analyzed by SDS-PAGE. WT p16^{INK4A}, p16^{INK4A}C72S and GS-p16^{INK4A} were allowed to form fibrils in the absence or presence of oxidizing agents (H_2O_2 or diamide). Samples for gel analysis were incubated is SDS loading buffer with or without reducing agent (DTT). Dimer bands can be seen in non-reduced samples of oxidized WT p16^{INK4A}. Similar experiments (with slightly different loading and conditions) were performed at least 4 times. A typical result is shown.

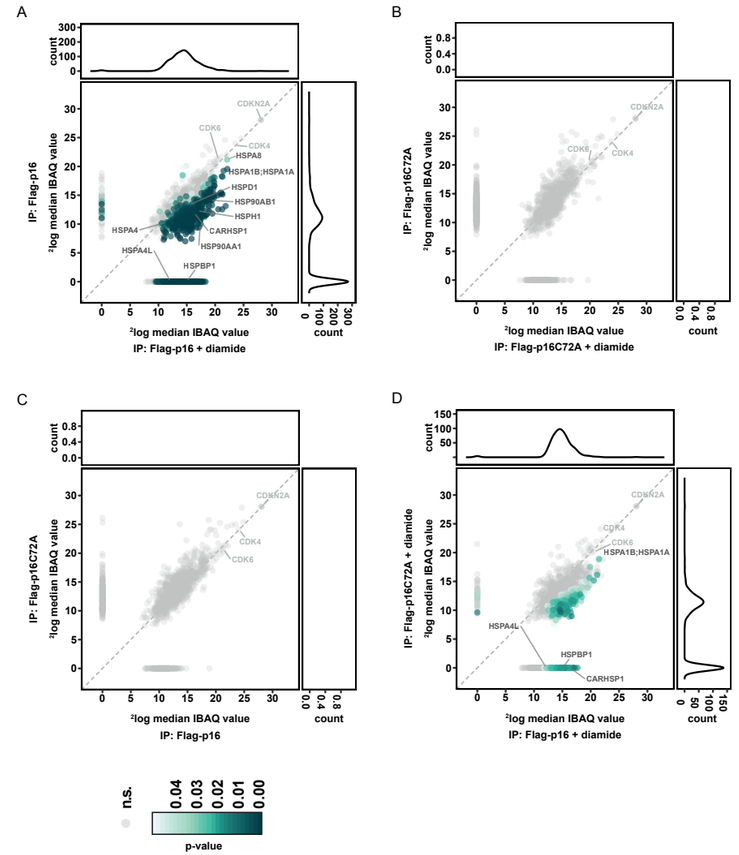

Figure S11. MS/MS analysis of the p16^{INK4A} interactome upon oxidation.
Diamide treatment (200 µM) induces large changes in the interaction profile of WT p16^{INK4A} and this largely depends on C72. (**A**) Comparison of the interactomes of WT p16^{INK4A} with or without diamide treatment. (**B**) Comparison of the interactomes of p16^{INK4A} C72A with or without diamide treatment. (**C**) Comparison of the interactomes of WT p16^{INK4A} and p16^{INK4A} C72A without diamide treatment. (**D**) Comparison of the interactomes of WT p16^{INK4A} and p16^{INK4A} C72A with diamide treatment. Note that the interaction with CDK4 and CDK6 is not altered by diamide treatment nor C72 dependent and that equal amounts of WT p16^{INK4A} and p16^{INK4A} C72A were pulled down. Several chaperone proteins can be found to interact upon oxidation. Log-transformed median IBAQ values are plotted, green colors represent proteins with adjusted p-values smaller than 0.05. Marginal plots represent the total number of significant proteins. N=6 biological replicates for WT p16^{INK4A} and p16^{INK4A} C72A, N=5 for p16^{INK4A} + diamide and N=4 for p16^{INK4A} C72A + diamide.

A

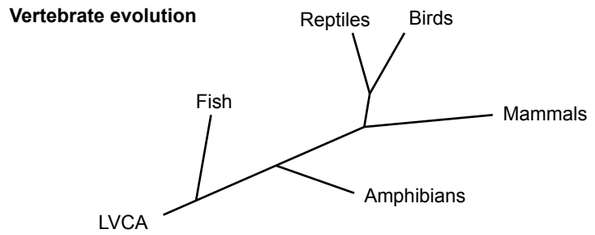

B

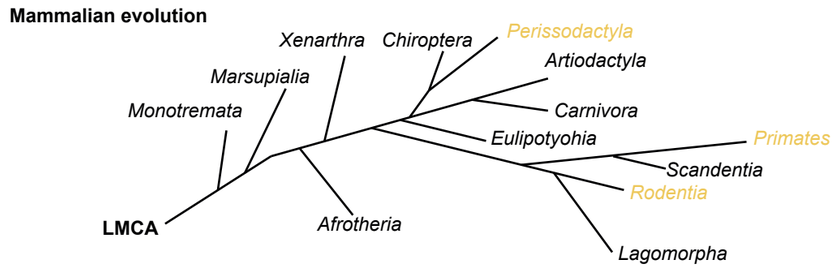

Figure S12. Evolutionary trees of vertebrate and mammalian evolution for reference.
(A) Evolutionary tree of vertebrate evolution for reference. LVCA: Last Vertebrate Common Ancestor. **(B)** Evolutionary tree of mammalian evolution for reference. LMCA: Last Mammalian Common Ancestor. Branches indicated in yellow color indicate branches in which some species have lost the cysteine homologous to human $p16^{INK4A}$ C72. Note that for some branches very few sequence information is available and that it cannot be excluded that also in the branches indicated in black color species might have lost the C homologous to human $p16^{INK4A}$ C72. Note that evolutionary trees in **(A)** and **(B)** are not to scale.

REFERENCES

1. Sherr, C.J. Cancer Cell Cycles. *Science* 1996, *274*, 1672–1677, doi:10.1126/science.274.5293.1672.
2. Johnson, D.G.; Schwarz, J.K.; Cress, W.D.; Nevins, J.R. Expression of Transcription Factor E2F1 Induces Quiescent Cells to Enter S Phase. *Nature* 1993, *365*, 349–352, doi:10.1038/365349a0.
3. Burd, C.E.; Sorrentino, J.A.; Clark, K.S.; Darr, D.B.; Krishnamurthy, J.; Deal, A.M.; Bardeesy, N.; Castrillon, D.H.; Beach, D.H.; Sharpless, N.E. Monitoring Tumorigenesis and Senescence In Vivo with a P16 INK4a -Luciferase Model. *Cell* 2013, *152*, 340–351, doi:10.1016/j.cell.2012.12.010.
4. Forbes, S.A.; Beare, D.; Boutselakis, H.; Bamford, S.; Bindal, N.; Tate, J.; Cole, C.G.; Ward, S.; Dawson, E.; Ponting, L.; et al. COSMIC: Somatic Cancer Genetics at High-Resolution. *Nucleic Acids Res* 2017, *45*, D777–D783, doi:10.1093/nar/gkw1121.
5. Baker, D.J.; Wijshake, T.; Tchkonia, T.; LeBrasseur, N.K.; Childs, B.G.; Sluis, B. van de; Kirkland, J.L.; Deursen, J.M. van Clearance of P16Ink4a-Positive Senescent Cells Delays Ageing-Associated Disorders. *Nature* 2011, *479*, 232–236, doi:10.1038/nature10600.
6. Childs, B.G.; Durik, M.; Wijers, M.E.; Sieben, C.J.; Zhong, J.; Saltness, R.A.; Jeganathan, K.B.; Verzosa, G.C.; Pezeshki, A.; Khazaie, K.; et al. Naturally Occurring P16Ink4a-Positive Cells Shorten Healthy Lifespan. *Nature* 2016, *530*, 184 189, doi:10.1038/nature16932.
7. Russo, A.A.; Tong, L.; Lee, J.-O.; Jeffrey, P.D.; Pavletich, N.P. Structural Basis for Inhibition of the Cyclin-Dependent Kinase Cdk6 by the Tumour Suppressor P16INK4a. *Nature* 1998, *395*, 237 243, doi:10.1038/26155.
8. Stepanova, L.; Leng, X.; Parker, S.B.; Harper, J.W. Mammalian P50Cdc37 Is a Protein Kinase-Targeting Subunit of Hsp90 That Binds and Stabilizes Cdk4. *Gene Dev* 1996, *10*, 1491–1502, doi:10.1101/gad.10.12.1491.
9. Holmström, K.M.; Finkel, T. Cellular Mechanisms and Physiological Consequences of Redox-Dependent Signalling. *Nat Rev Mol Cell Bio* 2014, *15*, 411–421, doi:10.1038/nrm3801.
10. Vurusaner, B.; Poli, G.; Basaga, H. Tumor Suppressor Genes and ROS: Complex Networks of Interactions. *Free Radical Bio Med* 2012, *52*, 7–18, doi:10.1016/j.freeradbiomed.2011.09.035.
11. Putker, M.; Madl, T.; Vos, H.R.; Ruiter, H. de; Visscher, M.; Berg, M.C.W. van den; Kaplan, M.; Korswagen, H.C.; Boelens, R.; Vermeulen, M.; et al. Redox-Dependent Control of FOXO/DAF-16 by Transportin-1. *Mol Cell* 2013, *49*, 730 742, doi:10.1016/j.molcel.2012.12.014.
12. Sunde, M.; Serpell, L.C.; Bartlam, M.; Fraser, P.E.; Pepys, M.B.; Blake, C.C.F. Common Core Structure of Amyloid Fibrils by Synchrotron X-Ray Diffraction11Edited by F. E. Cohen. *J Mol Biol* 1997, *273*, 729–739, doi:10.1006/jmbi.1997.1348.
13. Chiti, F.; Dobson, C.M. Protein Misfolding, Functional Amyloid, and Human Disease. *Annu Rev Biochem* 2006, *75*, 333–366, doi:10.1146/annurev.biochem.75.101304.123901.
14. LeVine, H. Quantification of β-Sheet Amyloid Fibril Structures with Thioflavin T. *Methods Enzymol* 1999, *309*, 274–284, doi:10.1016/s0076-6879(99)09020-5.
15. Klunk, W.E.; Pettegrew, J.W.; Abraham, D.J. Quantitative Evaluation of Congo Red Binding to Amyloid-like Proteins with a Beta-Pleated Sheet Conformation. *J Histochem Cytochem Official J Histochem Soc* 1989, *37*, 1273–1281, doi:10.1177/37.8.2666510.
16. Nilsson, M.R. Techniques to Study Amyloid Fibril Formation in Vitro. *Methods* 2004, *34*, 151–160, doi:10.1016/j.ymeth.2004.03.012.
17. Zandomeneghi, G.; Krebs, M.R.H.; McCammon, M.G.; Fändrich, M. FTIR Reveals Structural Differences between Native B-sheet Proteins and Amyloid Fibrils. *Protein Sci* 2004, *13*, 3314–3321, doi:10.1110/ps.041024904.
18. Sarroukh, R.; Goormaghtigh, E.; Ruysschaert, J.-M.; Raussens, V. ATR-FTIR: A "Rejuvenated" Tool to Investigate Amyloid Proteins. *Biochimica Et Biophysica Acta Bba - Biomembr* 2013, *1828*, 2328–2338, doi:10.1016/j.bbamem.2013.04.012.
19. Fernandez-Escamilla, A.-M.; Rousseau, F.; Schymkowitz, J.; Serrano, L. Prediction of Sequence-Dependent and Mutational Effects on the Aggregation of Peptides and Proteins. *Nat Biotechnol* 2004, *22*, 1302–1306, doi:10.1038/nbt1012.
20. Walsh, I.; Seno, F.; Tosatto, S.C.E.; Trovato, A. PASTA 2.0: An Improved Server for Protein Aggregation Prediction. *Nucleic Acids Res* 2014, *42*, W301–W307, doi:10.1093/nar/gku399.
21. Conchillo-Solé, O.; Groot, N.S. de; Avilés, F.X.; Vendrell, J.; Daura, X.; Ventura, S. AGGRESCAN: A Server for the Prediction and Evaluation of "Hot Spots" of Aggregation in Polypeptides. *Bmc Bioinformatics* 2007, *8*, 65, doi:10.1186/1471-2105-8-65.
22. Tartaglia, G.G.; Pawar, A.P.; Campioni, S.; Dobson, C.M.; Chiti, F.; Vendruscolo, M. Prediction of Aggregation-Prone Regions in Structured Proteins. *J Mol Biol* 2008, *380*, 425–436, doi:10.1016/j.jmb.2008.05.013.
23. Marino, S.M.; Gladyshev, V.N. Cysteine Function Governs Its Conservation and Degeneration and Restricts Its Utilization on Protein Surfaces. *J Mol Biol* 2010, *404*, 902–916, doi:10.1016/j.jmb.2010.09.027.
24. Regneri, J.; Klotz, B.; Wilde, B.; Kottler, V.A.; Hausmann, M.; Kneitz, S.; Regensburger, M.; Maurus, K.; Götz, R.; Lu, Y.; et al. Analysis of the Putative Tumor Suppressor Gene Cdkn2ab in Pigment Cells and Melanoma of Xiphophorus and Medaka. *Pigm Cell Melanoma R* 2019, *32*, 248–258, doi:10.1111/pcmr.12729.
25. Zerbino, D.R.; Achuthan, P.; Akanni, W.; Amode, M.R.; Barrell, D.; Bhai, J.; Billis, K.; Cummins, C.; Gall, A.; Girón, C.G.; et al. Ensembl 2018. *Nucleic Acids Res* 2018, *46*, D754–D761, doi:10.1093/nar/gkx1098.

26. Chiti, F.; Dobson, C.M. Protein Misfolding, Amyloid Formation, and Human Disease: A Summary of Progress Over the Last Decade. *Annu Rev Biochem* 2016, *86*, 1–42, doi:10.1146/annurev-biochem-061516-045115.

27. Fowler, D.M.; Koulov, A.V.; Alory-Jost, C.; Marks, M.S.; Balch, W.E.; Kelly, J.W. Functional Amyloid Formation within Mammalian Tissue. *Plos Biol* 2006, *4*, e6, doi:10.1371/journal.pbio.0040006.

28. Li, J.; McQuade, T.; Siemer, A.B.; Napetschnig, J.; Moriwaki, K.; Hsiao, Y.-S.; Damko, E.; Moquin, D.; Walz, T.; McDermott, A.; et al. The RIP1/RIP3 Necrosome Forms a Functional Amyloid Signaling Complex Required for Programmed Necrosis. *Cell* 2012, *150*, 339–350, doi:10.1016/j.cell.2012.06.019.

29. Maji, S.K.; Perrin, M.H.; Sawaya, M.R.; Jessberger, S.; Vadodaria, K.; Rissman, R.A.; Singru, P.S.; Nilsson, K.P.R.; Simon, R.; Schubert, D.; et al. Functional Amyloids As Natural Storage of Peptide Hormones in Pituitary Secretory Granules. *Science* 2009, *325*, 328–332, doi:10.1126/science.1173155.

30. Zhang, S.; Tang, M.; Luo, H.; Shi, C.; Xu, Y. Necroptosis in Neurodegenerative Diseases: A Potential Therapeutic Target. *Cell Death Dis* 2017, *8*, e2905–e2905, doi:10.1038/cddis.2017.286.

31. Li, Y.; Yan, J.; Zhang, X.; Huang, K. Disulfide Bonds in Amyloidogenesis Diseases Related Proteins. *Proteins Struct Funct Bioinform* 2013, *81*, 1862–1873, doi:10.1002/prot.24338.

32. Mossuto, M.F.; Bolognesi, B.; Guixer, B.; Dhulesia, A.; Agostini, F.; Kumita, J.R.; Tartaglia, G.G.; Dumoulin, M.; Dobson, C.M.; Salvatella, X. Disulfide Bonds Reduce the Toxicity of the Amyloid Fibrils Formed by an Extracellular Protein**. *Angewandte Chemie Int Ed Engl* 2011, *50*, 7048–7051, doi:10.1002/anie.201100986.

33. Chattopadhyay, M.; Durazo, A.; Sohn, S.H.; Strong, C.D.; Gralla, E.B.; Whitelegge, J.P.; Valentine, J.S. Initiation and Elongation in Fibrillation of ALS-Linked Superoxide Dismutase. *Proc National Acad Sci* 2008, *105*, 18663–18668, doi:10.1073/pnas.0807058105.

34. Furukawa, Y.; Kaneko, K.; Yamanaka, K.; O'Halloran, T.V.; Nukina, N. Complete Loss of Post-Translational Modifications Triggers Fibrillar Aggregation of SOD1 in the Familial Form of Amyotrophic Lateral Sclerosis*. *J Biol Chem* 2008, *283*, 24167–24176, doi:10.1074/jbc.m802083200.

35. Kato, M.; Han, T.W.; Xie, S.; Shi, K.; Du, X.; Wu, L.C.; Mirzaei, H.; Goldsmith, E.J.; Longgood, J.; Pei, J.; et al. Cell-Free Formation of RNA Granules: Low Complexity Sequence Domains Form Dynamic Fibers within Hydrogels. *Cell* 2012, *149*, 753–767, doi:10.1016/j.cell.2012.04.017.

36. Maiti, N.R.; Surewicz, W.K. The Role of Disulfide Bridge in the Folding and Stability of the Recombinant Human Prion Protein*. *J Biol Chem* 2001, *276*, 2427–2431, doi:10.1074/jbc.m007862200.

37. Honda, R. Role of the Disulfide Bond in Prion Protein Amyloid Formation: A Thermodynamic and Kinetic Analysis. *Biophys J* 2018, *114*, 885–892, doi:10.1016/j.bpj.2017.12.031.

38. Mompeán, M.; Li, W.; Li, J.; Laage, S.; Siemer, A.B.; Bozkurt, G.; Wu, H.; McDermott, A.E. The Structure of the Necrosome RIPK1-RIPK3 Core, a Human Hetero-Amyloid Signaling Complex. *Cell* 2018, *173*, 1244-1253.e10, doi:10.1016/j.cell.2018.03.032.

39. Ono, K.; Takahashi, R.; Ikeda, T.; Yamada, M. Cross-seeding Effects of Amyloid B-protein and A-synuclein. *J Neurochem* 2012, *122*, 883–890, doi:10.1111/j.1471-4159.2012.07847.x.

40. Ehrnhoefer, D.E.; Bieschke, J.; Boeddrich, A.; Herbst, M.; Masino, L.; Lurz, R.; Engemann, S.; Pastore, A.; Wanker, E.E. EGCG Redirects Amyloidogenic Polypeptides into Unstructured, off-Pathway Oligomers. *Nat Struct Mol Biol* 2008, *15*, 558–566, doi:10.1038/nsmb.1437.

41. Deshmukh, M.; Evans, M.L.; Chapman, M.R. Amyloid by Design: Intrinsic Regulation of Microbial Amyloid Assembly. *J Mol Biol* 2018, *430*, 3631–3641, doi:10.1016/j.jmb.2018.07.007.

42. Murray, D.T.; Kato, M.; Lin, Y.; Thurber, K.R.; Hung, I.; McKnight, S.L.; Tycko, R. Structure of FUS Protein Fibrils and Its Relevance to Self-Assembly and Phase Separation of Low-Complexity Domains. *Cell* 2017, *171*, 615-627.e16, doi:10.1016/j.cell.2017.08.048.

43. Makin, O.S.; Atkins, E.; Sikorski, P.; Johansson, J.; Serpell, L.C. Molecular Basis for Amyloid Fibril Formation and Stability. *P Natl Acad Sci Usa* 2005, *102*, 315–320, doi:10.1073/pnas.0406847102.

44. Baldwin, A.J.; Knowles, T.P.J.; Tartaglia, G.G.; Fitzpatrick, A.W.; Devlin, G.L.; Shammas, S.L.; Waudby, C.A.; Mossuto, M.F.; Meehan, S.; Gras, S.L.; et al. Metastability of Native Proteins and the Phenomenon of Amyloid Formation. *J Am Chem Soc* 2011, *133*, 14160–14163, doi:10.1021/ja2017703.

45. Coryell, P.R.; Goraya, S.K.; Griffin, K.A.; Redick, M.A.; Sisk, S.R.; Purvis, J.E. Autophagy Regulates the Localization and Degradation of P16INK4a. *Aging Cell* 2020, *19*, e13171, doi:10.1111/acel.13171.

46. Hanger, D.P.; Anderton, B.H.; Noble, W. Tau Phosphorylation: The Therapeutic Challenge for Neurodegenerative Disease. *Trends Mol Med* 2009, *15*, 112–119, doi:10.1016/j.molmed.2009.01.003.

47. Capitini, C.; Conti, S.; Perni, M.; Guidi, F.; Cascella, R.; Poli, A.D.; Penco, A.; Relini, A.; Cecchi, C.; Chiti, F. TDP-43 Inclusion Bodies Formed in Bacteria Are Structurally Amorphous, Non-Amyloid and Inherently Toxic to Neuroblastoma Cells. *Plos One* 2014, *9*, e86720, doi:10.1371/journal.pone.0086720.

48. Reest, J. van der; Lilla, S.; Zheng, L.; Zanivan, S.; Gottlieb, E. Proteome-Wide Analysis of Cysteine Oxidation Reveals Metabolic Sensitivity to Redox Stress. *Nat Commun* 2018, *9*, 1581 16, doi:10.1038/s41467-018-04003-3.

49. Yang, J.; Carroll, K.S.; Liebler, D.C. The Expanding Landscape of the Thiol Redox Proteome*. *Mol Cell Proteomics* 2016, *15*, 1–11, doi:10.1074/mcp.o115.056051.

50. Schafer, F.Q.; Buettner, G.R. Redox Environment of the Cell as Viewed through the Redox State of the Glutathione Disulfide/Glutathione Couple. *Free Radical Bio Med* 2001, *30*, 1191–1212, doi:10.1016/s0891-5849(01)00480-4.

51. Menon, S.G.; Goswami, P.C. A Redox Cycle within the Cell Cycle: Ring in the Old with the New. *Oncogene* 2007, *26*, 1101 1109, doi:10.1038/sj.onc.1209895.

52. Stöcker, S.; Maurer, M.; Ruppert, T.; Dick, T.P. A Role for 2-Cys Peroxiredoxins in Facilitating Cytosolic Protein Thiol Oxidation. *Nat Chem Biol* 2018, *14*, 148–155, doi:10.1038/nchembio.2536.

53. Gorrini, C.; Harris, I.S.; Mak, T.W. Modulation of Oxidative Stress as an Anticancer Strategy. *Nat Rev Drug Discov* 2013, *12*, 931 947, doi:10.1038/nrd4002.

54. Lee, A.S.; Galea, C.; DiGiammarino, E.L.; Jun, B.; Murti, G.; Ribeiro, R.C.; Zambetti, G.; Schultz, C.P.; Kriwacki, R.W. Reversible Amyloid Formation by the P53 Tetramerization Domain and a Cancer-Associated Mutant. *J Mol Biol* 2003, *327*, 699–709, doi:10.1016/s0022-2836(03)00175-x.

55. Kato, M.; Yang, Y.-S.; Sutter, B.M.; Wang, Y.; McKnight, S.L.; Tu, B.P. Redox State Controls Phase Separation of the Yeast Ataxin-2 Protein via Reversible Oxidation of Its Methionine-Rich Low-Complexity Domain. *Cell* 2019, *177*, 711-721.e8, doi:10.1016/j.cell.2019.02.044.

56. Medema, R.H.; Herrera, R.E.; Lam, F.; Weinberg, R.A. Growth Suppression by P16ink4 Requires Functional Retinoblastoma Protein. *Proc National Acad Sci* 1995, *92*, 6289–6293, doi:10.1073/pnas.92.14.6289.

57. Sakaue-Sawano, A.; Kurokawa, H.; Morimura, T.; Hanyu, A.; Hama, H.; Osawa, H.; Kashiwagi, S.; Fukami, K.; Miyata, T.; Miyoshi, H.; et al. Visualizing Spatiotemporal Dynamics of Multicellular Cell-Cycle Progression. *Cell* 2008, *132*, 487 498, doi:10.1016/j.cell.2007.12.033.

58. Livak, K.J.; Schmittgen, T.D. Analysis of Relative Gene Expression Data Using Real-Time Quantitative PCR and the 2−ΔΔC T Method. *Methods* 2001, *25*, 402–408, doi:10.1006/meth.2001.1262.

59. Delaglio, F.; Grzesiek, S.; Vuister, G.W.; Zhu, G.; Pfeifer, J.; Bax, A. NMRPipe: A Multidimensional Spectral Processing System Based on UNIX Pipes. *J Biomol Nmr* 1995, *6*, 277–293, doi:10.1007/bf00197809.

60. Vranken, W.F.; Boucher, W.; Stevens, T.J.; Fogh, R.H.; Pajon, A.; Llinas, M.; Ulrich, E.L.; Markley, J.L.; Ionides, J.; Laue, E.D. The CCPN Data Model for NMR Spectroscopy: Development of a Software Pipeline. *Proteins Struct Funct Bioinform* 2005, *59*, 687–696, doi:10.1002/prot.20449.

61. Piotukh, K.; Kosslick, D.; Zimmermann, J.; Krause, E.; Freund, C. Reversible Disulfide Bond Formation of Intracellular Proteins Probed by NMR Spectroscopy. *Free Radical Bio Med* 2007, *43*, 1263–1270, doi:10.1016/j.freeradbiomed.2007.06.010.

62. Franke, D.; Petoukhov, M.V.; Konarev, P.V.; Panjkovich, A.; Tuukkanen, A.; Mertens, H.D.T.; Kikhney, A.G.; Hajizadeh, N.R.; Franklin, J.M.; Jeffries, C.M.; et al. ATSAS 2.8: A Comprehensive Data Analysis Suite for Small-Angle Scattering from Macromolecular Solutions. *J Appl Crystallogr* 2017, *50*, 1212–1225, doi:10.1107/s1600576717007786.

63. Tartaglia, G.G.; Vendruscolo, M. The Zyggregator Method for Predicting Protein Aggregation Propensities. *Chem Soc Rev* 2008, *37*, 1395–1401, doi:10.1039/b706784b.

64. Szeverenyi, N.M.; Sullivan, M.J.; Maciel, G.E. Observation of Spin Exchange by Two-Dimensional Fourier Transform 13C Cross Polarization-Magic-Angle Spinning. *J Magnetic Reson 1969* 1982, *47*, 462–475, doi:10.1016/0022-2364(82)90213-x.

65. Wang, Y.; Jardetzky, O. Probability-based Protein Secondary Structure Identification Using Combined NMR Chemical-shift Data. *Protein Sci* 2002, *11*, 852–861, doi:10.1110/ps.3180102.

66. Cox, J.; Mann, M. MaxQuant Enables High Peptide Identification Rates, Individualized p.p.b.-Range Mass Accuracies and Proteome-Wide Protein Quantification. *Nat Biotechnol* 2008, *26*, 1367–1372, doi:10.1038/nbt.1511.

67. Schwanhäusser, B.; Busse, D.; Li, N.; Dittmar, G.; Schuchhardt, J.; Wolf, J.; Chen, W.; Selbach, M. Global Quantification of Mammalian Gene Expression Control. *Nature* 2011, *473*, 337–342, doi:10.1038/nature10098.

68. Luber, C.A.; Cox, J.; Lauterbach, H.; Fancke, B.; Selbach, M.; Tschopp, J.; Akira, S.; Wiegand, M.; Hochrein, H.; O'Keeffe, M.; et al. Quantitative Proteomics Reveals Subset-Specific Viral Recognition in Dendritic Cells. *Immunity* 2010, *32*, 279–289, doi:10.1016/j.immuni.2010.01.013.

69. Chich, J.-F.; David, O.; Villers, F.; Schaeffer, B.; Lutomski, D.; Huet, S. Statistics for Proteomics: Experimental Design and 2-DE Differential Analysis. *J Chromatogr B* 2007, *849*, 261–272, doi:10.1016/j.jchromb.2006.09.033.

70. Waterhouse, A.M.; Procter, J.B.; Martin, D.M.A.; Clamp, M.; Barton, G.J. Jalview Version 2—a Multiple Sequence Alignment Editor and Analysis Workbench. *Bioinformatics* 2009, *25*, 1189–1191, doi:10.1093/bioinformatics/btp033.

71. Vizcaíno, J.A.; Csordas, A.; del-Toro, N.; Dianes, J.A.; Griss, J.; Lavidas, I.; Mayer, G.; Perez-Riverol, Y.; Reisinger, F.; Ternent, T.; et al. 2016 Update of the PRIDE Database and Its Related Tools. *Nucleic Acids Res* 2016, *44*, D447–D456, doi:10.1093/nar/gkv1145.

CHAPTER 5

CROSSTALK BETWEEN REDOX SIGNALING AND PROTEIN AGGREGATION

Loes van Dam[1] and Tobias B. Dansen[1]

[1]Center for Molecular Medicine, Molecular Cancer Research, University Medical Center Utrecht, Universiteitsweg 100, 3584CG, Utrecht, The Netherlands

Correspondence: t.b.dansen@umcutrecht.nl

PUBLISHED *in Biochem Soc Trans* 2020, *https://doi.org/10.1042/BST20190054*.

KEYWORDS

protein aggregation; redox signaling; cysteine oxidation; structural biology; protein stability; amyloids

CROSSTALK BETWEEN REDOX SIGNALING AND PROTEIN AGGREGATION

ABSTRACT

It is well established that both an increase in Reactive Oxygen Species (ROS: i.e. $O_2^{\cdot-}$, H_2O_2 and OH) as well as protein aggregation accompany aging and proteinopathies such as Parkinson's and Alzheimer's disease. However, it is far from clear whether there is a causal relation between the two. This review describes how protein aggregation can be affected both by redox signaling (downstream of H_2O_2), as well as by ROS-induced damage, and aims to give an overview of the current knowledge of how redox signaling affects protein aggregation and vice versa. Redox signaling has been shown to play roles in almost every step of protein aggregation and amyloid formation, from aggregation initiation to the rapid oligomerization of large amyloids, which tend to be less toxic than oligomeric prefibrillar aggregates. We explore the hypothesis that age-associated elevated ROS production could be part of a redox signaling dependent-stress-response in an attempt to curb protein aggregation and minimize toxicity.

INTRODUCTION

Both the loss of proteostasis and ROS production as a consequence of mitochondrial dysfunction are among the hallmarks of aging [1]. While there is plenty of evidence that these two hallmarks are tightly intertwined, their cause and effect relationships remain unclear. This might be partly due to the fact that ROS, in the form of H_2O_2, itself plays a dual role. While at lower levels H_2O_2 acts as a second messenger in redox signaling, which is absolutely required for physiology and for lifespan extension in model systems [2], at higher levels H_2O_2 and other ROS could lead to random damage including for instance protein unfolding and aggregation, and the latter has been proposed to accelerate the aging process [3–10]. But there is also evidence of functional redox signaling dependent protein aggregation, for instance providing a means to (temporarily) inactivate or alter function of proteins. Redox-dependent protein aggregation is also often reversible. But there are also many examples of protein aggregation-induced enhanced ROS production, which may eventually contribute to cellular dysfunction and cell death.

An hypothesis that could unite both H_2O_2 as a signaling molecule and ROS as a driver of age-related protein aggregation was posed by Hekimi et al. [2]. It proposes that age-related damage triggers stress-response pathways that could depend on redox signaling and hence produce H_2O_2 (either directly or indirectly through $O2^{\cdot-}$ followed by dismutation) as a second messenger in an attempt to regain homeostasis. Over time, when more damage accumulates, H_2O_2 produced to further boost this stress response surpasses levels that are merely involved in signaling, leading to a build-up H_2O_2 and ROS associated damage. This eventually would lead to a vicious cycle in which ROS-dependent damage triggers a redox signaling-dependent stress-response, leading to a further increase in ROS. This hypothesis would also fit with the observations that several types of aggregates can trigger ROS production.

In this review we will focus on examples of the interplay between redox signaling and protein aggregation. We review the current knowledge and try to illuminate possible relationships between redox signaling and proteostasis.

Protein Folding

Proteins are synthesized as linear peptide chains on ribosomes and must fold into 3D structures to execute their biological functions. Protein folding is driven for a large part by the spontaneous burial of nonpolar amino acids in the folding core, but also guided by hydrogen bonds, van der Waals- and electrostatic interactions. The many weak, noncovalent and often distant (in sequence) interaction possibilities complicate the conformational possibilities. The stability of natively folded proteins depends on local environmental factors such as pH and temperature.

Most (~70%) protein folding takes place at the ribosome during translation. Several mechanisms are in place to ensure correct folding: the sequential folding of domains emerging from the ribosome, the spatial restrictions of the ribosomal exit channel, the rate of translation as well as the ribosome-associated chaperones RAC and NAC (ribosome-associated complex and nascent-chain associated complex, respectively) [11,12]. More downstream of the ribosome, the HSP70 system of chaperones prevents undesirable domain interactions. Moreover, HSP70 functions as a binding interface for other chaperones like HSP90 and chaperonins, which aid in de novo folding by recognizing exposed hydrophobic residues and promoting ATP-dependent refolding.

Proteins need to overcome considerable energy barriers to reach their final, stable conformation, inherently leading to accumulation of folding intermediates (**Figure 1**) [13]. Examples of slow steps in protein folding include disulfide bond formation and prolyl isomerization [14]. Partially folded proteins are at high risk of misfolding and aggregation, due to non-native interactions through for instance the exposure of hydrophobic residues [15,16]. Other reasons for faulty protein accumulation are mutations or polymorphisms, translation errors and the structurally dynamic characteristic of proteins. Misfolded conformations are quasi-stable, making them more

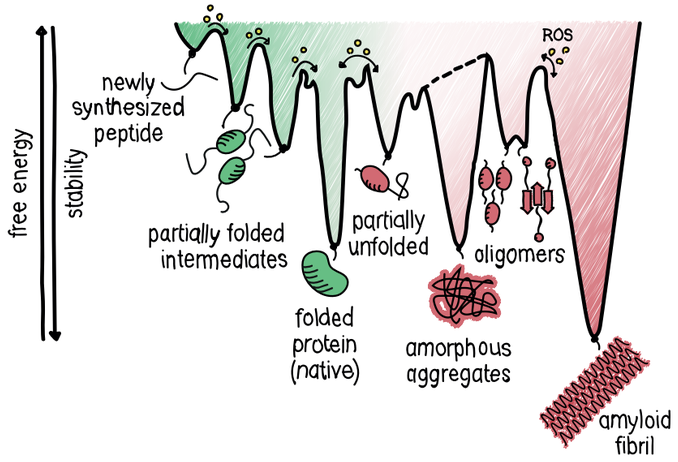

Figure 1. Energy landscape in proteostasis
Newly synthesized peptides sample different conformations during protein folding, on their way downhill to the most thermodynamically favorable state. Energetically trapped, partially unfolded or sub-optimally folded intermediates may accumulate as they need to cross energy barriers to reach their native, low energy state. Non-native interactions may lead to protein aggregation, thereby interfering with the protein folding process. The proteostasis network can assist in lowering energy barriers and preventing non-native interactions. As indicated by the yellow circles, H_2O_2-mediated redox signaling or ROS-dependent damage helps to overcome the transition state between intermediates of the proteostasis network.

prone to aggregation when proteostasis control systems are saturated. The latter happens increasingly during aging [17]. The high plasticity of partially folded intermediates is in contrast to extremely structured aggregates like amyloid fibrils.

Another hallmark of aging, the failure to maintain proteostasis, presents itself as an accumulation of misfolded proteins and aggregates. Like folding, aggregation is predominantly driven by hydrophobic interactions, which is why aggregation prone regions (APRs) in proteins are generally distinguished by their high hydrophobicity, low net charge and high β-sheet propensity [18,19]. During aggregation, the hydrophobic interactions are mostly intermolecular, and therefore aggregation is concentration dependent. Due to the similarity between the composition of APRs and protein regions driving hydrophobic core formation during folding, aggregation and folding pathways constantly compete. Aggregation has long been considered only as a sign of degeneration and dysfunction. However, despite strong selective pressure against protein aggregation, numerous APRs remain in the proteome, which is in line with the notion that protein aggregation can play a functional or regulatory role [20,21]. The number of possible conformations for aggregation intermediates is large, and they need to overcome free energy barriers on their way to mature aggregates. This means that aggregation intermediates are energetically trapped and thus accumulate (Figure 1), allowing more non-native interactions to occur. Typically, these nonspecific interactions between polypeptides form a disordered assembly without a specified shape termed amorphous aggregates.

While most aggregates are amorphous, examples of more structured aggregate types are oligomeric aggregates and the extremely structured β-amyloid fibrils, and the latter are characterized by a cross-β-structure (in which β-strands lie perpendicular to the fibril axis). Amyloid fibrillization consists of a slow lag phase directed by intermolecular interactions during which misfolded polypeptides congregate into nuclei and form oligomers containing β-sheets. During the subsequent exponential growth phase oligomers cluster further with these nuclei and grow rapidly into prefibrils and protofibrils with a cross-β-structure. During the final saturation phase 2-6 protofibrils assemble into mature multistrand amyloid fibrils which can adopt several polymorphic structures by twisting or lateral association [22]. Amyloid fibrils are one of the most thermodynamically stable and stiff protein arrangements known [23].

Amyloids are a hallmark of (age-related) proteinopathies such as ALS, Alzheimer's, prion disease and cataract. Early studies focused on the mature aggregate deposits as toxic species. The toxicity of amyloids is complex however, and several intermediates and oligomers but also mature amyloid fibrils have now been linked to pathogenesis [11–13]. Some reports even suggest an inverse correlation between oligomer size and toxicity of aggregates [24–27]. This complexity is also thought to be one of the reasons for clinical trial failures in proteinopathies, with hardly any effective therapy available for treatment [13,28]. Adding to the complexity is the fact that many types of amyloids are shown to be functional with roles reported in chemical storage, structure, signaling and inactivation of the soluble protein [29]. Another type of functional aggregation is controlled by protein domains lacking rigid 3D structures under physiological conditions, present in 15-30% of proteins. These intrinsically disordered regions (IDRs) have a high conformational plasticity and susceptibility to modifications, enabling a multitude of interactions [30]. With these interactions, IDRs drive misfolding and aggregation of (partially) disordered proteins as well as liquid-liquid phase separation (LLPS), thereby forming membrane-less compartments which are important for the concentration and segregation of biochemical reactions [31]. However, LLPS condensates have also been reported to catalyze amyloid fibrillization [32,33].

Clearance of Protein Aggregates

There are three quality control networks to ensure continuous surveillance of the proteome: (i) chaperones that mediate (re)folding, (ii) the ubiquitin-proteasome system (UPS) and (iii) autophagy to clear misfolded proteins and aggregates.

As mentioned previously, chaperones aid in *de novo* protein folding by lowering energy barriers between folding intermediates. During aggregation, chaperones instead raise the energy barriers toward aggregation by preventing intermolecular interactions. Besides preventing aggregation, chaperones play an important role in active disaggregation [34]. Recent reports show that almost all types of aggregates are reversible [35,36]. The coordinated action of small HSPs (sHSPs), HSP40, HSP70 and HSP110 can even disaggregate amyloid fibrils by fragmentation and depolymerization into both monomeric and oligomeric species. The activity of chaperones is therefore twofold: on the one hand to prevent aggregation, on the other to disaggregate (intermediate) aggregates.

One of the major protein degradation systems is the ubiquitin-proteasome system (UPS). There are several constitutions of the proteasome, but the 20S and 26S are most prominent. Ubiquitinated proteins and insoluble aggregates are pulled through the proteasomal ring-like structure, to be broken down by proteolysis. Not surprisingly, proteasomal dysfunction is associated with aging and leads to the accumulation of aggregates [5–7,9,10], catalyzing a chain reaction in which aggregates block the proteasome which causes further dysfunction [37].

A third mechanism by which cells can clear and recycle cellular components is by autophagy. Many types of protein aggregates are cleared by autophagy, including tau, Aβ, α-synuclein, huntingtin, SOD1 and $p16^{INK4A}$ [38–43], with autophagy defects leading to neurodegenerative disease [44,45].

Defects in and decreased activity of any of these proteostasis surveillance systems are associated with aging and proteinopathies, underpinning their importance in maintaining proteostasis.

Redox Signaling

Increased markers for ROS-induced damage and mitochondrial ROS generation have long been associated with age and neurodegenerative disorders, which has often been regarded as

evidence for a causal link between oxidative damage and aging [46–54]. This is in contrast with the unexpected observation that increased ROS levels may extend lifespan in yeast and C. elegans [55,56], while increased ROS does not accelerate aging in mice [57]. The key to resolve this apparent paradox probably lies in the notion that ROS in the form of H_2O_2 has become widely recognized as second messenger in so-called redox signaling, which has been shown to be involved in a plethora of cellular responses [46]. Central to redox signaling is the reversible oxidation/reduction of the nucleophilic thiol side chain of specific cysteine residues. Oxidation of cysteines in proteins commonly causes structural changes and functional interactions through disulfide bond formation, such as (hetero)dimerization, oligomerization, and even aggregation, and thereby provides an important molecular switch for protein activity or function. For a comprehensive review see [58].

Compared to superoxide anions and hydroxyl radicals, the other main cellular ROS, H_2O_2, has a relatively low reactivity and allows for specific rather than random oxidation of dedicated cysteines. Redox signaling starts with the production of H_2O_2: either directly (i.e. by DUOX enzymes or ERO1-dependent protein folding in the ER) or after dismutation of superoxide produced by leakage of electrons from complex I and III of the electron transport chain during mitochondrial respiration, or by NADPH-dependent oxidases (NOXs). For a comprehensive review on subcellular sources of ROS see [59].

Superoxide and H_2O_2 are efficiently scavenged by antioxidant systems and the balance between ROS production and antioxidant capacity determines the redox state of cellular compartments [60,61]. When the amount of ROS surpasses the levels required for signaling, non-specific cellular damage (oxidative stress) can occur due to their high reactivity with biomolecules. Furthermore, H_2O_2 may be converted by more reactive species in the presence of transition metal ions, thereby changing its role from messenger to damaging agent. In line with this, it has been suggested that oxidative damage exists merely as a side product of cellular signaling, and that ROS are in fact part of the stress response to for instance proteotoxic stress [2,62]. A good distinction between ROS as a signaling molecule versus ROS as oxidative stress has been proposed by Sies et al. [59]. Throughout this review we will try to use the term 'ROS' in case the exact species is unclear or in the case of random damage rather than signaling, whereas redox signaling and reversible cysteine oxidation are considered regulated processes downstream of H_2O_2.

Other amino acid side chains besides cysteine and methionine are also subject to oxidation. For example, Tyr and Trp phenoxyl radicals, carbonylated Lys/His/Cys, SNO-/SSG-modifications as well as lipid peroxidation and its aldehyde byproduct 4-hydroxynonenal (HNE) are all ROS-induced and have been associated with proteinopathies [63,64]. Collectively, the dual roles of H_2O_2/ROS in signaling and damage make it difficult to understand whether the increase in ROS in aging represents a causal link with oxidative damage, redox signaling or both. In this review we will focus mostly on the effects of reversible cysteine oxidation dependent redox signaling but will also include examples of how random oxidative damage affects protein aggregation.

REDOX SIGNALING AND PROTEIN AGGREGATION

Protein aggregation can be affected or directly regulated by redox signaling or the cellular redox state. In general, cysteine oxidation results in structural changes, for instance through disulfide formation, that affect protein function [58]. These structural changes can also provide a molecular switch to partially unfold and subsequently aggregate. Interestingly, many proteins are predicted to contain conditionally disordered regions that could be redox sensitive and thereby facilitate the transition from disorder-to-order or order-to-disorder dependent on oxidation or reduction [65]. Similar to IDPs, this transition is driven by the multiplicity of possible interactions. Conversely, it is also known that misfolded proteins are more sensitive to oxidation, which has been suggested to tag proteins for proteolysis [66].

Functional Redox-Dependent Aggregation

As mentioned earlier, several amyloid fibrils have functional roles in humans. Amyloid fibril formation can also be reversible [67,68] and reversible oxidation of cysteines can provide the molecular switch that regulates fibrillization. For example, the tumor suppressor $p16^{INK4A}$ is readily oxidized on its only cysteine in an oxidizing environment, causing disulfide-linked homodimerization and subsequent rapid but reversible β-amyloid fibrillization. This redox-dependent change from a soluble monomeric protein into insoluble but reversible β-amyloid fibrils leads to the inactivation of the protein, allowing reactivation of CDK4/6 proteins otherwise inactivated by high $p16^{INK4A}$ expression [69]. These observations fit with the notion that redox signaling can regulate S-phase entry and cellular proliferation [70,71].

Another illustration of redox-dependent functional protein aggregation is provided by tryptophan hydroxylase 2 (TPH2), the rate-limiting enzyme in serotonin neurotransmitter production. TPH2 aggregates upon oxidation of any out of 13 cysteines and subsequent intra- and intermolecular disulfide bond formation, thereby reversibly inhibiting protein activity. TPH2 catalytic activity correlates directly with the number of cysteines that are oxidized [72,73]. Although the direct purpose for redox regulation of serotonin biosynthesis is unknown, it provides a link between neurological function and redox signaling, a concept that is widely accepted in the molecular regulation of circadian rhythm [74].

In a similar way, redox status is linked to intracellular calcium concentrations through oxidation-dependent protein aggregation of visinin-like protein-1 (VSNL1), a neuronal calcium sensor important that can activate guanylyl cyclase (GC). Under low calcium concentrations, GC produces the second messenger cGMP that can activate calcium channels. When bound to calcium, structural rearrangements in VSNL1 make the C-terminal C187 available for reversible oxidation and subsequent homodimerization and aggregation. These disulfide-crosslinked aggregates are reversible upon treatment with reducing agents. As a result of aggregation, functional levels of VSNL1 are decreased, possibly providing a second mechanism to keep GC inactive besides calcium levels. Furthermore, VSNL1 aggregates are found in ALS-associated deposits, linking them to neuronal impairment [75–79].

Conversely, there are also examples where cysteine oxidation prevents functional aggregation rather than trigger it. For example, yeast ataxin2 spontaneously forms liquid-like droplets that can convert to β-amyloid fibrils. Oxidation of ataxin1 regulates this process by melting the droplets, a process that can be reversed by methionine sulfoxide reductases [80]. Phase-separated ataxin2 is an inhibitor of TORC1 during respiratory growth, thereby stimulating autophagy. Reactivation of TORC1 under oxidizing conditions though regulation of ataxin2, in combination with nutrient starvation thereby allows coupling of mitochondrial function to TORC1-mediated metabolism [81].

This combination of findings suggests a more general mechanism, where reversible redox-regulated protein aggregation directly dictates protein activity. It also has significant implications for our understanding of aggregated proteins, which are not solely a waste product of misfolded proteins but rather a temporary conformation linked to protein activity.

Cysteine Oxidation-Driven Protein Aggregation in Disease

Cysteine oxidation is also involved in toxic protein aggregation. This is illustrated by the amorphous aggregation of γ-crystallins, known to cause cataract. Reduced antioxidant capacity induces formation of an intramolecular disulfide bond between C32 and C41, which is both necessary and sufficient to induce irreversible aggregation through destabilization of the N-terminus [82,83]. This is especially interesting in an age-related context since the reducing capacity of the eye diminishes with age [84].

Another detrimental type of aggregation is caused by mutations resulting in an uneven number of cysteines in the transmembrane receptor NOTCH3. NOTCH3 contains a highly

conserved even number of cysteines forming disulfide bridges that maintain structural integrity. Any unpaired cysteine stimulates multimerization and aggregation through loss of a structural disulfides and exposure of an oxidation-prone cysteine that can form non-native disulfide [85,86]. Aggregated NOTCH3 accumulates in the vascular wall, leading to the rare systemic vasculopathology CASADIL.

Oxidation can also occur on other amino acids like methionine which can drastically alter protein structure. In this way, oxidation of a surface-exposed vital residue results in misfolding and aggregation. Several proteins follow this order of events. Examples include: GAPDH [87], γ-synuclein [88], interferon β1a [89], human growth hormone [90], κ-casein [91], FasL [92], transthyretin [93], apolipoprotein AI [94], AMPK [95], PrP [96] and huntingtin [97].

Interestingly, oxidation also triggers the aggregation of direct redox modulators. Cu,Zn-superoxide dismutase (SOD1) is an enzyme important for the dismutation of superoxide to H_2O_2 and O_2, and its misfolding and fibrillization plays a crucial role in the etiology of the familial form of amyotrophic lateral sclerosis (ALS). The enzymatic product of SOD1, H_2O_2, can directly oxidize the surface-exposed C111 in SOD1 which triggers its amyloid fibrillization. In a different manner, higher concentrations of H_2O_2 overoxidize C111 to $SO_{2/3}H$ causing

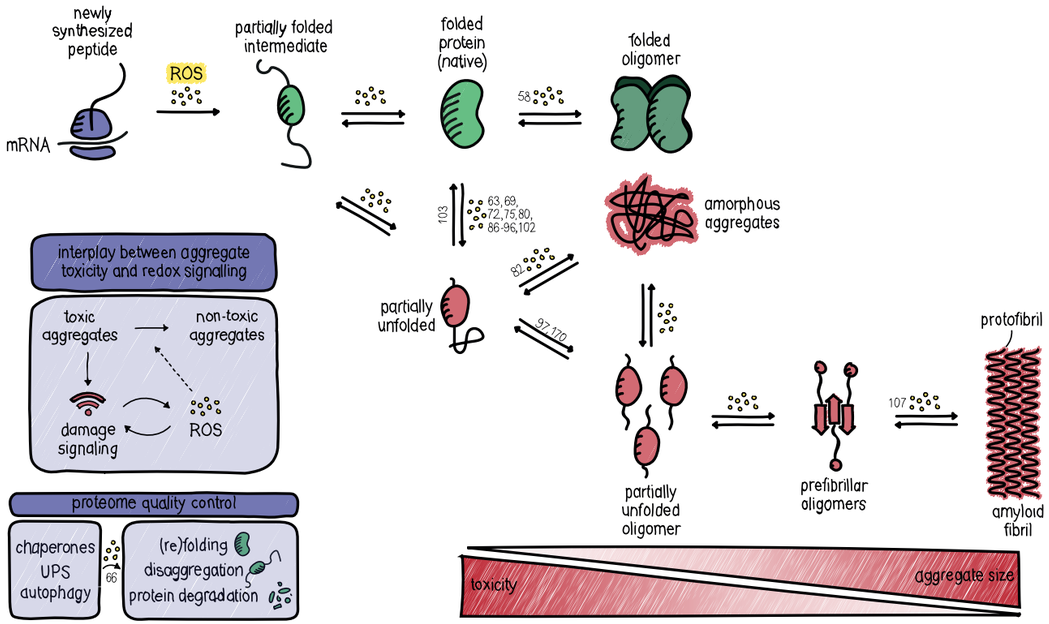

Figure 2. The proteostasis network
Cells employ several mechanisms to maintain proteins integrity and minimize non-native or harmful protein conformations. Mechanisms are in place for proteome quality control. Redox signaling participates in proteostasis by modulating the folding, misfolding, (dis)aggregation and the extent of toxicity of protein aggregates. References to examples of the various steps are indicated in numbers. Note that in some cases it is not clear from the literature what exact step in aggregation is affected, or whether multiple steps are affected, and in this case the reference is denoted at the first transition from native to partially unfolded.

amorphous aggregation [98–102]. Additionally, mutations causing conformational changes in SOD1 expose its four cysteines, making the structural disulfide bond between C57 and C146 accessible to reduction by the TRX and GSH-GRX systems [101]. Subsequent oxidation leads to the formation of non-native disulfides that cause formation of insoluble SOD1 multimers and aggregates. Contributing to the cytotoxicity of SOD1 aggregates, SOD1 oxidation has been shown to co-occur with cytoplasmic mislocalization and fibrillization of TAR-DNA-binding protein TDP-43, thereby inducing apoptosis [102].

Besides facilitating aggregation, cysteine oxidation can also prevent it. This is evident for human amylin (hIAPP), which forms a disulfide bridge between C2 and C7 upon oxidation. Oxidized hIAPP stabilizes an α-helical structure at the N-terminus, protecting the peptide from amyloid formation and safeguarding its activity in insulin and glucagon secretion as well as reducing food intake and gastric emptying [103,104]. A similar mechanism has been published for β-microglobulin and endostatin, for which two disulfide bonds guard its native folded conformation [105–107].

Furthermore, oxidation does not only trigger aggregation. Post-aggregation oxidation of proteins seems to be widespread, changing the structural conformation of established aggregates of proteins including huntingtin and β-microglobulin [106,107]. Besides providing an explanation for the abundance of oxidative modifications found in aggregate deposits, this finding suggests that insoluble aggregates are not inert protein disposals but can still alter their structure and interactions due to redox-dependent post-aggregation modifications. This view is supported by the concept that distinct structures of aggregated proteins also cause distinct phenotypes [108,109]. Targeting post-misfolding oxidation might also offer therapeutic opportunities. For example, thiol-reactive compounds can force refolding and reactivation of mutant p53 tumor-suppressor (be it direct or indirect) [110,111], a concept that could be meaningful in proteinopathies.

The previously described cases of protein aggregation and dysfunction induced by cysteine oxidation seem in line with a causal role for ROS in proteinopathies. However, it has been suggested that there is an inverse correlation between the size and toxicity of aggregates, meaning that an increase in size from toxic oligomeric intermediates to insoluble aggregates means a decrease in detrimental effects (Figure 2). In that line of reasoning, stimulating formation of insoluble aggregates might be a cellular means to confine toxic oligomers. In accordance with this, several types of smaller soluble oligomeric aggregates (including Aβ, α-synuclein and huntingtin) actually impair the 20S/26S proteasome by stabilizing its closed conformation [37]. This could mean that formation of the more toxic soluble oligomers from natively folded proteins triggers a unidirectional switch, forming insoluble aggregates due to the inability of the proteasome to break down misfolded proteins. Redox signaling-dependent protein oxidation could therefore be a facilitator of aggregation and actually partake in the proteotoxic stress response. In support of this it was shown that promoting formation of large insoluble aggregates is protective against amyloid-induced ROS production [112].

In summary, the cellular redox environment and protein aggregation show a strong association. With examples of protein oxidation both inducing and preventing aggregation (summarized in Table 1), having functional as wells as pathological consequences and occurring both before and after aggregation, there seems no unifying role for protein oxidation in protein aggregation. However, many proteins do seem to follow the same sequence of events upon oxidation, which includes a partial unfolding and subsequent aggregation step.

EFFECTS OF AGGREGATION ON THE CELLULAR REDOX STATE

Protein aggregation can also modulate the cellular redox state, and, as mentioned, this could either be part of the proteotoxic stress response, cellular dysfunction as a result of the accu-

mulation of protein aggregates, or both. For example, based on thiol-disulfide redox couples and redox sensors it has been determined that under basal conditions mitochondria, the cytosol and nucleus are in a relatively reduced state as compared to the ER. This reverses radically when protein aggregation induces proteasomal dysfunction, resulting in a more oxidizing cytosol and reducing ER [60,113]. S-nitrosylation could be a possible contributor to this change due to the overactivation of the N-methyl-D-aspartate receptor (NMDAR, an inducer of neuronal nitric oxide synthase (nNOS)) or Aβ-dependent iNOS activation in neurons and glial cells of AD patients [114–116]. A shift to a more oxidizing cellular redox state upon proteotoxic stress is further supported by many reversible cysteine modifications that change in models for proteinopathies like AD [117,118].

A more direct explanation for the redox changes that occur upon aggregation can be found in the direct redox-dependent aggregation of redox modulators. As discussed above, SOD1 aggregation is directly triggered by oxidation of C111, thereby inactivating its function. This leads to the accumulation of superoxide at the expense of H_2O_2, where the former is more associated with random damage and the latter with redox signaling.

Another effect of aggregation on the cellular redox state is exemplified by the transmembrane Aβ protein precursor (AβPP), which is the precursor for the archetypical amyloidogenic Aβ peptide and the main component of amyloid plaques in brains of AD-patients. Interestingly, monomeric Aβ is suggested to have an antioxidant activity by hydrophilic chelation of transition metals, thereby preventing lipoprotein oxidation [119–122]. However, this chelation of metals also promotes the aggregation of Aβ, and redox-active metal ions like Cu(II) and Fe(III) can catalyze the production of ROS when bound to aggregated Aβ. Aβ binding results in the reduction of the metal's oxidation state, which then converts O_2 into H_2O_2, superoxide and hydroxyl radicals via Fenton chemistry [123–126]. Hence, the binding of Aβ to metals changes its properties from an antioxidant to a pro-oxidant [120]. ROS-induced o,o'-dityrosine covalent crosslinking then catalyzes further aggregation of Aβ [127]. Interestingly, a similar interplay between metals and oligomers has been reported for α-synuclein [128], pointing potentially at a more general mechanism in which misfolded oligomeric proteins in conjunction with metal ions induce the production of ROS. Metal concentrations, aggregation as well as ROS production all increase with age and even without knowing the exact cause, the consequence is faster neurodegeneration [129].

Furthermore, many aggregates can directly cause mitochondrial dysfunction, resulting in metabolic stress, enhanced ROS production and eventually cell death. For example, amyloid oligomers are well-known for their permeabilization of membranes, which is considered a main toxicity event. A rapid influx of intracellular Ca^{2+} as well as the direct permeabilization of the mitochondrial membrane causes an increase in mitochondrial ROS production [130–133].

When unfolded proteins accumulate in the ER, a condition called ER stress triggers the unfolded protein response (UPR) in an attempt to restore homeostasis. Protein aggregates like oligomeric Aβ have been shown to trigger ER stress and the UPR [134,135]. Prolonged ER stress is known to evoke intracellular ROS production at the ER through several mechanisms. These include overactivation of Ero1 oxidoreductases through a futile cycle of forming and repairing mismatched disulfides, thereby producing H_2O_2 and oxidizing GSH, respectively [132,136,137]. In addition, ER stress causes superoxide production though activation of NOXs and the release of Ca^{2+} which increases electron leakage from mitochondria (for a review see [138]). Hence, since ROS are both a trigger and a consequence of ER stress, this further aggravates the imbalance accompanying ER stress [139].

REDOX REGULATION OF AGGREGATE CLEARANCE

To cope with the challenges caused by protein aggregation, cells are equipped with several mechanisms aimed at the clearance of misfolded proteins and aggregates, which themselves are also shown to be redox-regulated, adding another level of the complex interdependency of proteostasis and ROS.

Besides their role in folding of newly synthesized proteins, molecular chaperones are also part of this cellular disaggregation machinery. There are many types of chaperones, but a general initial step seems to be the initial coverage of aggregates with HSP70 [140]. An example of the redox regulation of HSPs is through the reversible oxidation of MGE1, a mitochondrial nucleotide exchange factor of HSP70, on M155. The consequential structural change from an active homodimer to monomer leads to MGE1 amyloid formation, which prevents activation of HSP70. Interestingly, oxidized MGE1 is suggested to increases binding affinity of the inactive HSP70 for unfolded substrates. As HSP70 is essential in protein folding and proteostasis, MGE1 might act as an initial sensor of protein aggregation, priming the chaperone system for resolution of protein aggregates [141,142].

Peroxiredoxins are more unconventional chaperones. With their abundance and exceptional reactivity to H_2O_2, peroxiredoxins are important H_2O_2 scavengers. Their highly conserved active site consists of 2 catalytic cysteine residues. Besides their antioxidant activity, peroxiredoxins are known for their ability to oxidize protein thiols by a redox relay as well as for their chaperone activity [143]. Assembled as a high molecular weight complex, peroxiredoxins can form ring-like chaperone structures with holdase activity that bind and prevent aggregation of unfolded proteins [144,145]. Among others, hyperoxidation of the peroxiredoxin catalytic cysteine particularly stimulates an oligomeric chaperone structure, whereas glutathionylation inhibits it [146–149]. Thereby peroxiredoxins can sense high and low ROS levels and switch their function accordingly from antioxidant and redox signaling mediator to chaperone.

Redox control of the UPS is complex, with studies claiming both inhibitory and activating effects. In general, the 20S, but not 26S proteasome is thought to specifically degrade oxidized proteins [150–152]. Elevated ROS and mitochondrial dysfunction shift the proteasome population from 26S to 20S, thereby adapting to the proteolytic need for clearance of oxidized substrates [153]. In support of this, proteasomal degradation has been shown to be stimulated >10-fold upon exposure to H_2O_2 or superoxide, while simultaneously abolishing 26S-mediated degradation [154–156]. The proteasome is also subject to direct redox modifications. For example, the 20S proteasome can be glutathionylated, resulting in its opening and activation [156,157]. Thus, under oxidizing conditions the 20S proteasome is stimulated to clear oxidized substrates, but this shift away from 26S permits the accumulation of otherwise misfolded proteins. This, however, has been debated by the notion that a high NAD+/NADH ratio, correlating with an oxidizing cellular state, opens and activates the 26S proteasome [158,159]. Also, the lipid peroxidation byproduct HNE was found to inhibit proteasomal activity for the breakdown of oxidized proteins [160,161]. In summary, oxidizing conditions result in a shift to the 20S proteasome, accompanied by a possible decrease in 26S activity. This might favor the accumulation of non-oxidized misfolded proteins. Moreover, the interaction between the cellular redox state and the proteasome is bidirectional. Blockage of the proteasome for instance, leads to an increase in ROS, which in its turn might cause a vicious cycle of protein oxidation and aggregation [162,163].

It has been suggested that both aggregation and cellular redox state are coupled through their regulation of autophagy [164]. Autophagy is thought to be activated in more oxidizing conditions [165–168], although this might not always be straightforward as glutathione reductase loss, resulting in oxidizing conditions, was recently shown to suppress autophagy and enhance aggregation [169]. The recruitment of ubiquitinylated substrates to autophagosomes is mediated

by receptors like SQSTM1/p62. Interestingly, components of the autophagy system have also been found to aggregate in a redox-dependent manner themselves. For example, oxidation of p62 at C105/113 in the N-terminal disordered region causes oligomerization and subsequent aggregation of p62. This stimulates autophagy in response to ROS, possibly in an attempt to maintain cellular homeostasis [170]. In addition, aggregated p62 occupies the NRF2-binding site in KEAP1, allowing stabilization of NRF2. NRF2 nuclear translocation causes expression of antioxidant- and stress response genes, among which p62 itself [171]. Redox-dependent p62 aggregation therefore ensures a robust stress response involving both autophagy and antioxidant response. Accordingly, mutations perturbing the redox-sensitivity of the NRF2 pathway are linked to ALS. Of note, mutant KRAS induced lung tumors in mice have been shown to depend on the NRF2 pathway for their survival and outgrowth [172], likely because it facilitates antioxidant- and autophagy-dependent clearance of cancer-associated proteotoxic and metabolic stress.

Taken together, protein aggregation has been shown to modulate ROS levels in several ways. Some of the increases in ROS production upon the gradual accumulation of aggregates might therefore be an attempt to regain homeostasis through modulation of the stress response. This eventually reaches a turning point when ROS reaches toxic levels and triggers a stress-response on its own [2]. The notion that oxidation by ROS can facilitate protein aggregation and that amyloids themselves can trigger ROS production could in principle also constitute a feed forward loop in which a small change in either ROS or protein aggregation could rapidly lead to a toxic cellular catastrophe, making redox-regulated protein aggregation an irreversible process [173]. But extensive random damage induced by ROS production either from an overactive stress response or from gross cellular dysfunction resulting in for instance lipid peroxidation might also have an evolutionary benefit and serve to actively eliminate damaged cells through the induction of ferroptosis [174].

CONCLUSIONS

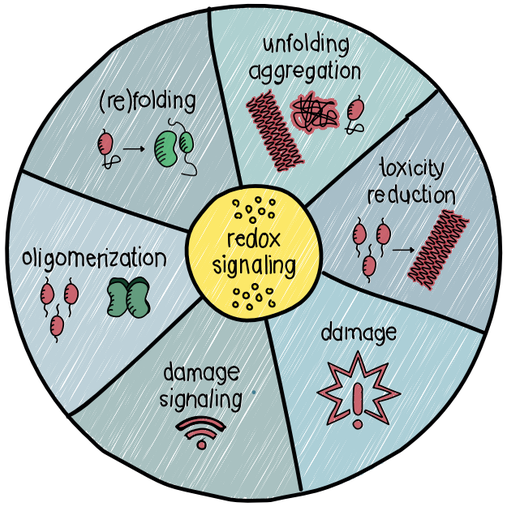

Figure 3. Redox regulation of proteostasis
Redox signaling modulates proteostasis in many ways. Among its roles are the regulation of protein folding, unfolding/aggregation, toxicity reduction and damage response.

In this review, we have discussed the reciprocal regulation of redox signaling and protein aggregation. In short, oxidation of specific residues causes conformational changes and causes partial unfolding of a protein. This exposes residues that can participate in non-native interactions. Further structural rearrangements drive the oligomerization and subsequent formation of insoluble aggregates. We can distinguish two types of cysteine residues here: structural residues that form disulfide bonds for correct protein folding, and cysteines that can be reversibly oxidized which serve as important signaling switches. When reversible disulfide bond formation changes the protein structure such that it directly corresponds to protein function, it can be both a structural and a regulatory residue. Although the underlying processes seem somewhat similar, the functional consequences of redox-dependent protein aggregation are not. Besides simply resulting in toxic protein aggregates, oxidative aggregation can result in reversible (in)activation of a protein which allows regulation. This can alter protein function and may serve as a protective or pro-survival mechanism. Although little is known about functional aggregation, it is thought that most aggregates are actually reversible, benefiting the regulatory possibilities. This is also reflected in the suggestion that insoluble aggregates are not inert protein disposals but can still alter its structure and morphology according to redox-dependent post-aggregation modifications and that distinct structures of aggregated proteins also cause distinct phenotypes.

On the other hand, there is the hypothesis that ROS-induced aggregation might be a cellular strategy to clear the more toxic soluble aggregates. Many of the examples we discussed in this review support this; they are part of a positive feedback system in which high ROS levels promote aggregation and the aggregates themselves promote ROS production. In this way, redox signaling creates a bistable switch between functional proteins and insoluble aggregates without the accumulation of toxic intermediates. Therefore, modulating ROS levels to promote rather than inhibit aggregation could be a more sensible therapeutic approach.

Almost all processes involved in protein aggregation are redox regulated (Figure 3). However, it is hard to determine whether altered redox signaling is a cause or consequence of protein aggregation. Often times it seems like it is both: altered redox signaling favors aggregation, but the mutual amplification of the systems also provides a feed forward loop, consequently altering the cellular redox state. One clue might lie in the hypothesis stating that H_2O_2 is produced as a signaling molecule in response to damage, such as an accumulation of aggregates. A gradual increase in aggregation is accompanied by an increased H_2O_2 production, which intensifies over time. Eventually, the H_2O_2 might reach toxic levels, which itself may lead to damage. Understanding whether H_2O_2 is produced as a stress-response in order to regain homeostasis might change our view of proteinopathies.

Why aggregation is so much more prominent in aged individuals is not entirely clear. The age-dependent increase of aggregation, oxidation and mitochondrial dysfunction, together with a decline in multiple aggregation clearance systems could cumulatively cause a destabilizing environment from which protein aggregates can no longer recover [175,176]. The diverse effects of oxidative aggregation on proteins suggests that in order to regulate proteins by oxidative aggregation, reversibility of the process is essential in some cases. Little is known about reversibility of oxidized aggregates. For example, when the reducing capacity of a cell is restored, can the aggregates fall apart into functional monomers again by reduction of the oxidative modifications? It is also not clear if and how cellular systems to clear protein aggregates such as the proteasome and autophagy can distinguish between 'functional' aggregates that are a temporary, regulated protein state, and toxic protein aggregates that need clearance

PERSPECTIVES

- **Importance of the field**: Both redox signaling and correct protein folding are essential for maintaining healthy cellular homeostasis. Accordingly, loss of proteostasis and ROS production as a consequence of mitochondrial dysfunction have been described as hallmarks of aging. This becomes especially clear in proteinopathies, where both aberrant redox signaling and protein aggregation are associated with severe neurodegenerative problems.
- **Summary of the current thinking:** Collectively, these studies outline complex relationship between ROS, redox signaling and proteostasis, where cause and consequence are often hard to differentiate. Whereas protein oxidation can trigger aggregation, increases in H_2O_2 production upon the gradual accumulation of aggregates might be a stress-response by itself. A small change in redox state or aggregation can in this way rapidly lead to a feed-forward

loop, making redox-regulated protein aggregation an irreversible process.

- **Future directions:** Going forward, it is important to better understand whether or not H2O2 is produced as a signal in response to proteotoxic stress in order to restore homeostasis, and whether increased H2O2 levels promote aggregation as a cellular strategy to clear the more toxic oligomeric aggregates. Understanding the multifaceted mechanisms regulating protein aggregation will pave the way for novel therapeutic windows to combat proteinopathies.

TABLES

Table 1. Summary of redox-regulated protein aggregates

Protein	Abbreviation	Normal function	Involved Residue (Cys)	Modification	Consequence(s)	Type of Aggregation	Related Pathologies	Reference
AMP-activated protein kinase	AMPK-alpha	Energy metabolism	C130 and C174	disulfde	Inactivation	soluble aggregates	Cardiopathologies, energy starvation	[95]
Apolipoprotein A-I	APOA1	Cholesterol transport	methionines	methionine oxidation	Partial unfolding, fibrillization and inactivation	amyloid	APOA1 amyloidoses and atherosclerosis	[94]
APP/Amyloid-β	Aβ	Unknown	M35	methionine oxidation	Required for pro-oxidative activity	amyloid	Alzheimer's	[119]
Ataxin-2	ATXN2	TORC1 inhibition	methionines	methionine oxidation	Oxidation reverses aggregation, fuctional regulation of activity	LLPS, amyloid	Spinocerebellar atrophy, ALS	[80]
Cellular prion protein	PrP^{C} and PrP^{SC}	Synaptic function	C179 and C214	disulfde exchange	Reduction of PrP^{C} induces agrgegation of PrP^{SC} polymer	amyloid	Transmissable spongiform encelopathies	[96]
Cyclin-dependent kinase inhibitor 2A	$p16^{INK4A}$	Cell cycle regulation, senescence	C72	homodimerization	Inactivation	amyloid	Cancer	[69]
Endostatin	COL18A1	Angiogenesis inhibition	C33, C135, C165 and C173	disulfde	Prevents aggregation	amyloid	Alzheimer's	[105]
Fas ligand	FasL	Apoptosis, inflammation	methionines	methionine oxidation	Multimerization and aggregation, enhanced biological activity	unknown	Acute lung injury	[92]
Glyceraldehyde-3-phosphate dehydrogenase	GAPDH	Glycolysis	M46	methionine oxidation, disulfdes	Local conformational change promotes disulfde crosslinking and aggregation	amyloid	Alzheimer's, motor neuron disease	[87]
Growth hormone (recombinant)	hGH	(Therapeutic protein production)	M14 and M125	methionine oxidation	Lower stability	unknown	GH deficiency	[90]
human Islet Amyloid Polypeptide	hIAPP	Insulin/glucagon secretion, gastric emptying	C2 and C7	disulfde	Prevents aggregation	amyloid	Type 2 diabetes	[103]
Huntingtin	HTT	Unknown	M8	post-aggregation methionine oxidation	Controls interaction between aggregates	amyloid	Huntington disease	[106]
			C115 and C119	disulfde mediated oligomerization	Oxidation-dependent soluble toxic oligomers, slower clearance	soluble oligomeric aggregates		[97]
Interferon-β1a (recombinant)	IFNβ1a	(Therapeutic protein production)	many residues (M, H, F, W, Y)	crosslinking	Lower stability	unknown		[89]

Table 1. Continued.

Protein	Abbreviation	Normal function	Involved Residue (Cys)	Modification	Consequence(s)	Type of Aggregation	Related Pathologies	Reference
Mitochondrial GrpE protein homolog	MGE1	Proteostasis, HSP70 cochaperone	M155	methionine oxidation	Inactive HSP70 but targeting it to unfolded proteins	amyloid	Myopathies	[141]
Sequestosome-1	SQSTM1/p62	Autophagy	C105 and C113	disulfde mediated oligomerization	More autophagy, cell survival	insoluble aggregates, LLPS	ALS	[170]
Superoxide dismutase 1	SOD1	Dismutation of superoxide	C111	disulfde-linked dimerization	Oligomerization and subsequent fibril formation	oligomeric, amyloid and amorphous	ALS	[102]
Transthyretin	TTR	Thyroid hormone binding	C10, M1 and M13	cysteine solfonic acid, methionine sulfoxide	Tetramer dissociation and aggregation	amyloid	Senile systemic amyloidosis	[93]
Tryptophan hydroxylase 2	TPH2	Serotonin biosynthesis	any out of 13 cysteines	disulfde, crosslinking	Misfolding, intra- and intermolecular disulfde bond formation, protein inactivation	unknown, disulfde crosslinked oligomers	Parkinson's	[72]
Vinisin-like protein 1	VSNL1	Calcium sensing	C187	disulfde-linked homodimerization	Reduced levels of functional protein	amyloid, disulfde crosslinked oligomers	ALS, AD	[75]
γ-synuclein	SNCG	Neurofilament network integrity	M38 and Y39	oxidation-dependent oligomerization	Aggregation and seeding for α-synuclein aggregation	amyloid	Parkinson's	[88]
β2-microglobulin	β2M	MHCI light chain	C25 and C80	disulfde reduction, disulfde exchange, post aggregation oxidation	Aggregation, post-aggregation stabilization	amyloid	Haemodialysis-related amyloidosis	[107]
γ-crystallins	CRYG	Lens transparency	C32 and C41	intramolecular disulfde	Destabilizes its N-terminal domain, stabilizes an intermediate which is prone to aggregation	amorphous	Cataract	[82]
κ-casein	CSN3	Milk protein	M95 and M106	methionine oxidation	Increased aggregation, increased toxicity	amyloid	Corpora amylacea	[91]

REFERENCES

1. Lopez-Otin, C.; Blasco, M.A.; Partridge, L.; Serrano, M.; Kroemer, G. The Hallmarks of Aging. *Cell* 2013, *153*, 1194–1217. doi:10.1016/j.cell.2013.05.039.
2. Hekimi, S.; Lapointe, J.; Wen, Y. Taking a "Good" Look at Free Radicals in the Aging Process. *Trends Cell Biol* 2011, *21*, 569–576. doi:10.1016/j.tcb.2011.06.008.
3. Hipp, M.S.; Kasturi, P.; Hartl, F.U. The Proteostasis Network and Its Decline in Ageing. *Nat Rev Mol Cell Bio* 2019, *20*, 421–435. doi:10.1038/s41580-019-0101-y.
4. Walther, D.M.; Kasturi, P.; Zheng, M.; Pinkert, S.; Vecchi, G.; Ciryam, P.; Morimoto, R.I.; Dobson, C.M.; Vendruscolo, M.; Mann, M.; et al. Widespread Proteome Remodeling and Aggregation in Aging C. Elegans. *Cell* 2015, *161*, 919–932. doi:10.1016/j.cell.2015.03.032.
5. Matsui, H.; Ito, H.; Taniguchi, Y.; Inoue, H.; Takeda, S.; Takahashi, R. Proteasome Inhibition in Medaka Brain Induces the Features of Parkinson's Disease. *J Neurochem* 2010, *115*, 178–187. doi:10.1111/j.1471-4159.2010.06918.x.
6. Kitajima, Y.; Tashiro, Y.; Suzuki, N.; Warita, H.; Kato, M.; Tateyama, M.; Ando, R.; Izumi, R.; Yamazaki, M.; Abe, M.; et al. Proteasome Dysfunction Induces Muscle Growth Defects and Protein Aggregation. *J Cell Sci* 2014, *127*, 5204–5217. doi:10.1242/jcs.150961.
7. Wang, R.; Zhao, J.; Zhang, J.; Liu, W.; Zhao, M.; Li, J.; Lv, J.; Li, Y. Effect of Lysosomal and Ubiquitin-Proteasome System Dysfunction on the Abnormal Aggregation of α-Synuclein in PC12 Cells. *Exp Ther Med* 2015, *9*, 2088–2094. doi:10.3892/etm.2015.2432.
8. Koga, H.; Kaushik, S.; Cuervo, A.M. Protein Homeostasis and Aging: The Importance of Exquisite Quality Control. *Ageing Res Rev* 2011, *10*, 205–215. doi:10.1016/j.arr.2010.02.001.
9. Visscher, M.; Henata, S.D.; Wildschut, M.H.E.; Es, R.M. van; Dhondt, I.; Michels, H.; Kemmeren, P.; Nollen, E.A.; Brackeman, B.P.; Burgering, B.M.T.; et al. Proteome-Wide Changes in Protein Turnover Rates in C. Elegans Models of Longevity and Age-Related Disease. *Cell Reports* 2016, *16*, 3041 3051. doi:10.1016/j.celrep.2016.08.025.
10. Kumar, V.; Singh, D.; Singh, B.K.; Singh, S.; Mittra, N.; Jha, R.R.; Patel, D.K.; Singh, C. Alpha-Synuclein Aggregation, Ubiquitin Proteasome System Impairment, and l-Dopa Response in Zinc-Induced Parkinsonism: Resemblance to Sporadic Parkinson's Disease. *Mol Cell Biochem* 2018, *444*, 149–160. doi:10.1007/s11010-017-3239-y.
11. Wilson, D.N.; Beckmann, R. The Ribosomal Tunnel as a Functional Environment for Nascent Polypeptide Folding and Translational Stalling. *Curr Opin Struc Biol* 2011, *21*, 274–282. doi:10.1016/j.sbi.2011.01.007.
12. Balchin, D.; Hayer-Hartl, M.; Hartl, F.U. In Vivo Aspects of Protein Folding and Quality Control. *Science* 2016, *353*, aac4354, doi:10.1126/science.aac4354.
13. Brockwell, D.J.; Radford, S.E. Intermediates: Ubiquitous Species on Folding Energy Landscapes? *Curr Opin Struc Biol* 2007, *17*, 30–37, doi:10.1016/j.sbi.2007.01.003.
14. Brakmann, I.; Hebert, D.N. Protein Folding in the Endoplasmic Reticulum. *Csh Perspect Biol* 2013, *5*, a013201, doi:10.1101/cshperspect.a013201.
15. Weids, A.J.; Ibstedt, S.; Tamás, M.J.; Grant, C.M. Distinct Stress Conditions Result in Aggregation of Proteins with Similar Properties. *Sci Rep-uk* 2016, *6*, srep24554, doi:10.1038/srep24554.
16. Uversky, V.N.; Fink, A.L. Conformational Constraints for Amyloid Fibrillation: The Importance of Being Unfolded. *Biochimica Et Biophysica Acta Bba - Proteins Proteom* 2004, *1698*, 131–153. doi:10.1016/j.bbapap.2003.12.008.
17. Gupta, R.; Kasturi, P.; Bracher, A.; Loew, C.; Zheng, M.; Villella, A.; Garza, D.; Hartl, F.U.; Raychaudhuri, S. Firefly Luciferase Mutants as Sensors of Proteome Stress. *Nat Methods* 2011, *8*, 879–884, doi:10.1038/nmeth.1697.
18. Bouziane, H.; Chouarfia, A. Sequence- and Structure-Based Prediction of Amyloidogenic Regions in Proteins. *Soft Comput* 2019, 1–24, doi:10.1007/s00500-019-04087-z.
19. Chiti, F.; Stefani, M.; Taddei, N.; Ramponi, G.; Dobson, C.M. Rationalization of the Effects of Mutations on Peptide and Protein Aggregation Rates. *Nature* 2003, *424*, 805. doi:10.1038/nature01891.
20. Monsellier, E.; Chiti, F. Prevention of Amyloid-like Aggregation as a Driving Force of Protein Evolution. *Embo Rep* 2007, *8*, 737–742, doi:10.1038/sj.embor.7401034.
21. Levy, E.D.; De, S.; Teichmann, S.A. Cellular Crowding Imposes Global Constraints on the Chemistry and Evolution of Proteomes. *Proc National Acad Sci* 2012, *109*, 20461–20466, doi:10.1073/pnas.1209312109.
22. Annamalai, K.; Gührs, K.; Koehler, R.; Schmidt, M.; Michel, H.; Loos, C.; Gaffney, P.M.; Sigurdson, C.J.; Hegenbart, U.; Schönland, S.; et al. Polymorphism of Amyloid Fibrils In Vivo. *Angewandte Chemie Int Ed* 2016, *55*, 4822–4825, doi:10.1002/anie.201511524.
23. Knowles, T.P.; Fitzpatrick, A.W.; Meehan, S.; Mott, H.R.; Vendruscolo, M.; Dobson, C.M.; Welland, M.E. Role of Intermolecular Forces in Defining Material Properties of Protein Nanofibrils. *Science* 2007, *318*, 1900–1903, doi:10.1126/science.1150057.
24. Sengupta, U.; Nilson, A.N.; Kayed, R. The Role of Amyloid-β Oligomers in Toxicity, Propagation, and Immunotherapy. *Ebiomedicine* 2016, *6*, 42–49. doi:10.1016/j.ebiom.2016.03.035.
25. Lambert, M.P.; Barlow, A.K.; Chromy, B.A.; Edwards, C.; Freed, R.; Liosatos, M.; Morgan, T.E.; Rozovsky, I.; Trommer, B.; Viola, K.L.; et al. Diffusible, Nonfibrillar Ligands Derived from Aβ1–42 Are Potent Central Nervous System Neurotoxins. *Proc National Acad Sci* 1998, *95*, 6448–6453. doi:10.1073/pnas.95.11.6448.

26. Glabe, C.G. Common Mechanisms of Amyloid Oligomer Pathogenesis in Degenerative Disease. *Neurobiol Aging* 2006, *27*, 570–575, doi:10.1016/j.neurobiolaging.2005.04.017.

27. Soeda, Y.; Saito, M.; Maeda, S.; Ishida, K.; Nakamura, A.; Kojima, S.; Takashima, A. Methylene Blue Inhibits Formation of Tau Fibrils but Not of Granular Tau Oligomers: A Plausible Key to Understanding Failure of a Clinical Trial for Alzheimer's Disease. *J Alzheimer's Dis* 2019, *Preprint*, 1–10, doi:10.3233/jad-181001.

28. Mijnders, M.; Kleizen, B.; Braakman, I. Correcting CFTR Folding Defects by Small-Molecule Correctors to Cure Cystic Fibrosis. *Curr Opin Pharmacol* 2017, *34*, 83–90, doi:10.1016/j.coph.2017.09.014.

29. Otzen, D.; Riek, R. Functional Amyloids. *Csh Perspect Biol* 2019, a033860, doi:10.1101/cshperspect.a033860.

30. Uversky, V.N.; Oldfield, C.J.; Dunker, A.K. Intrinsically Disordered Proteins in Human Diseases: Introducing the D2 Concept. *Annu Rev Biophys* 2008, *37*, 215–246, doi:10.1146/annurev.biophys.37.032807.125924.

31. Banani, S.F.; Lee, H.O.; Hyman, A.A.; Rosen, M.K. Biomolecular Condensates: Organizers of Cellular Biochemistry. *Nat Rev Mol Cell Bio* 2017, *18*, 285–298, doi:10.1038/nrm.2017.7.

32. Peskett, T.R.; Rau, F.; O'Driscoll, J.; Patani, R.; Lowe, A.R.; Saibil, H.R. A Liquid to Solid Phase Transition Underlying Pathological Huntingtin Exon1 Aggregation. *Mol Cell* 2018, *70*, 588-601.e6, doi:10.1016/j.molcel.2018.04.007.

33. Ambadipudi, S.; Biernat, J.; Riedel, D.; Mandelkow, E.; Zweckstetter, M. Liquid–Liquid Phase Separation of the Microtubule-Binding Repeats of the Alzheimer-Related Protein Tau. *Nat Commun* 2017, *8*, 275, doi:10.1038/s41467-017-00480-0.

34. Wentink, A.; Nussbaum-Krammer, C.; Bukau, B. Modulation of Amyloid States by Molecular Chaperones. *Csh Perspect Biol* 2019, *11*, a033969, doi:10.1101/cshperspect.a033969.

35. Gao, X.; Carroni, M.; Nussbaum-Krammer, C.; Mogk, A.; Nillegoda, N.B.; Szlachcic, A.; Guilbride, D.L.; Saibil, H.R.; Mayer, M.P.; Bukau, B. Human Hsp70 Disaggregase Reverses Parkinson's-Linked α-Synuclein Amyloid Fibrils. *Mol Cell* 2015, *59*, 781–793, doi:10.1016/j.molcel.2015.07.012.

36. Cereghetti, G.; Saad, S.; Dechant, R.; Peter, M. Reversible, Functional Amyloids: Towards an Understanding of Their Regulation in Yeast and Humans. *Cell Cycle* 2018, *17*, 1545–1558, doi:10.1080/15384101.2018.1480220.

37. Thibaudeau, T.A.; Anderson, R.T.; Smith, D.M. A Common Mechanism of Proteasome Impairment by Neurodegenerative Disease-Associated Oligomers. *Nat Commun* 2018, *9*, 1097, doi:10.1038/s41467-018-03509-0.

38. Caccamo, A.; Ferreira, E.; Branca, C.; Oddo, S. P62 Improves AD-like Pathology by Increasing Autophagy. *Mol Psychiatr* 2016, *22*, 865, doi:10.1038/mp.2016.139.

39. Cho, M.-H.; Cho, K.; Kang, H.-J.; Jeon, E.-Y.; Kim, H.-S.; Kwon, H.-J.; Kim, H.-M.; Kim, D.-H.; Yoon, S.-Y. Autophagy in Microglia Degrades Extracellular β-Amyloid Fibrils and Regulates the NLRP3 Inflammasome. *Autophagy* 2014, *10*, 1761–1775, doi:10.4161/auto.29647.

40. Cuervo, A.M.; Stefanis, L.; Fredenburg, R.; Lansbury, P.T.; Sulzer, D. Impaired Degradation of Mutant α-Synuclein by Chaperone-Mediated Autophagy. *Science* 2004, *305*, 1292–1295, doi:10.1126/science.1101738.

41. Ravikumar, B.; Duden, R.; Rubinsztein, D.C. Aggregate-Prone Proteins with Polyglutamine and Polyalanine Expansions Are Degraded by Autophagy. *Hum Mol Genet* 2002, *11*, 1107–1117, doi:10.1093/hmg/11.9.1107.

42. Yung, C.; Sha, D.; Li, L.; Chin, L.-S. Parkin Protects Against Misfolded SOD1 Toxicity by Promoting Its Aggresome Formation and Autophagic Clearance. *Mol Neurobiol* 2016, *53*, 6270–6287, doi:10.1007/s12035-015-9537-z.

43. Coryell, P.R.; Goraya, S.K.; Griffin, K.A.; Redick, M.A.; Sisk, S.R.; Purvis, J.E. Autophagy Regulates the Localization and Degradation of P16INK4a. *Biorxiv* 2019, 521682, doi:10.1101/521682.

44. Chen, Y.; Liu, H.; Guan, Y.; Wang, Q.; Zhou, F.; Jie, L.; Ju, J.; Pu, L.; Du, H.; Wang, X. The Altered Autophagy Mediated by TFEB in Animal and Cell Models of Amyotrophic Lateral Sclerosis. *American journal of translational research* 2015, *7*, 1574–1587.

45. Bordi, M.; Berg, M.J.; Mohan, P.S.; Peterhoff, C.M.; Alldred, M.J.; Che, S.; Ginsberg, S.D.; Nixon, R.A. Autophagy Flux in CA1 Neurons of Alzheimer Hippocampus: Increased Induction Overburdens Failing Lysosomes to Propel Neuritic Dystrophy. *Autophagy* 2016, *12*, 2467–2483, doi:10.1080/15548627.2016.1239003.

46. Stadtman, E.R. Protein Modification in Aging. *J Gerontology* 1988, *43*, B112–B120, doi:10.1093/geronj/43.5.b112.

47. Evans, A.R.; Gu, L.; Guerrero, R.; Robinson, R.A.S. Global CPILOT Analysis of the APP/PS-1 Mouse Liver Proteome. *Proteom - Clin Appl* 2015, *9*, 872–884, doi:10.1002/prca.201400149.

48. Abdul, H.M.; Sultana, R.; Clair, D.K.S.; Markesbery, W.R.; Butterfield, D.A. Oxidative Damage in Brain from Human Mutant APP/PS-1 Double Knock-in Mice as a Function of Age. *Free Radic Biology Medicine* 2008, *45*, 1420–1425, doi:10.1016/j.freeradbiomed.2008.08.012.

49. Sinclair, A.J.; Bayer, A.J.; Johnston, J.; Warner, C.; Maxwell, S.R.J. Altered Plasma Antioxidant Status in Subjects with Alzheimer's Disease and Vascular Dementia. *Int J Geriatr Psych* 1998, *13*, 840–845, doi:10.1002/(sici)1099-1166(1998120)13:12<840::aid-gps877>3.0.co;2-r.

50. Smith, M.A.; Rottkamp, C.A.; Nunomura, A.; Raina, A.K.; Perry, G. Oxidative Stress in Alzheimer's Disease. *Biochimica Et Biophysica Acta Bba - Mol Basis Dis* 2000, *1502*, 139–144, doi:10.1016/s0925-4439(00)00040-5.

51. Gu, L.; Robinson, R.A.S. High-Throughput Endogenous Measurement of S -Nitrosylation in Alzheimer's Disease Using Oxidized Cysteine-Selective CPILOT. *Analyst* 2016, *141*, 3904 3915, doi:10.1039/c6an00417b.

52. Robinson, R.A.S.; Cao, Z.; Williams, C. Oxidative Stress in CD90+ T-Cells of AβPP/PS-1 Transgenic Mice. *J Alzheimer's Dis* 2013, *37*, 661–666, doi:10.3233/jad-130665.

53. Sohal, R.S.; Sohal, B.H. Hydrogen Peroxide Release by Mitochondria Increases during Aging. *Mech Ageing Dev* 1991, *57*, 187–202, doi:10.1016/0047-6374(91)90034-w.

54. Asensi, M.; Sastre, J.; Pallardo, F.V.; Lloret, A.; Lehner, M.; Asuncion, J.G.; Viña, J. [23] Ratio of Reduced to Oxidized Glutathione as Indicator of Oxidative Stress Status and DNA Damage. *Methods Enzymol* 1999, *299*, 267–276, doi:10.1016/s0076-6879(99)99026-2.

55. Raamsdonk, J.M.V.; Hekimi, S. Deletion of the Mitochondrial Superoxide Dismutase Sod-2 Extends Lifespan in Caenorhabditis Elegans. *Plos Genet* 2009, *5*, e1000361, doi:10.1371/journal.pgen.1000361.

56. Mesquita, A.; Weinberger, M.; Silva, A.; Sampaio-Marques, B.; Almeida, B.; Leão, C.; Costa, V.; Rodrigues, F.; Burhans, W.C.; Ludovico, P. Caloric Restriction or Catalase Inactivation Extends Yeast Chronological Lifespan by Inducing H2O2 and Superoxide Dismutase Activity. *Proc National Acad Sci* 2010, *107*, 15123–15128, doi:10.1073/pnas.1004432107.

57. Pérez, V.I.; Remmen, H.V.; Bokov, A.; Epstein, C.J.; Vijg, J.; Richardson, A. The Overexpression of Major Antioxidant Enzymes Does Not Extend the Lifespan of Mice. *Aging Cell* 2009, *8*, 73–75, doi:10.1111/j.1474-9726.2008.00449.x.

58. Holmström, K.M.; Finkel, T. Cellular Mechanisms and Physiological Consequences of Redox-Dependent Signalling. *Nat Rev Mol Cell Bio* 2014, *15*, 411–421, doi:10.1038/nrm3801.

59. Sies, H.; Berndt, C.; Jones, D.P. Oxidative Stress. *Annu Rev Biochem* 2017, *86*, 715–748, doi:10.1146/annurev-biochem-061516-045037.

60. Go, Y.-M.; Jones, D.P. Redox Compartmentalization in Eukaryotic Cells. *Biochimica Et Biophysica Acta Bba - Gen Subj* 2008, *1780*, 1273–1290, doi:10.1016/j.bbagen.2008.01.011.

61. Kaludercic, N.; Deshwal, S.; Lisa, F.D. Reactive Oxygen Species and Redox Compartmentalization. *Front Physiol* 2014, *5*, 285, doi:10.3389/fphys.2014.00285.

62. Wang, Y.; Hekimi, S. Mitochondrial Dysfunction and Longevity in Animals: Untangling the Knot. *Science* 2015, *350*, 1204–1207, doi:10.1126/science.aac4357.

63. Cheignon, C.; Tomas, M.; Bonnefont-Rousselot, D.; Faller, P.; Hureau, C.; Collin, F. Oxidative Stress and the Amyloid Beta Peptide in Alzheimer's Disease. *Redox Biol* 2018, *14*, 450–464, doi:10.1016/j.redox.2017.10.014.

64. Sultana, R.; Perluigi, M.; Butterfield, D.A. Lipid Peroxidation Triggers Neurodegeneration: A Redox Proteomics View into the Alzheimer Disease Brain. *Free Radical Bio Med* 2013, *62*, 157–169, doi:10.1016/j.freeradbiomed.2012.09.027.

65. Erdős, G.; Mészáros, B.; Reichmann, D.; Dosztányi, Z. Large-Scale Analysis of Redox-Sensitive Conditionally Disordered Protein Regions Reveals Their Widespread Nature and Key Roles in High-Level Eukaryotic Processes. *Proteomics* 2019, *19*, 1800070, doi:10.1002/pmic.201800070.

66. Dukan, S.; Farewell, A.; Ballesteros, M.; Taddei, F.; Radman, M.; Nyström, T. Protein Oxidation in Response to Increased Transcriptional or Translational Errors. *Proc National Acad Sci* 2000, *97*, 5746–5749, doi:10.1073/pnas.100422497.

67. Audas, T.E.; Audas, D.E.; Jacob, M.D.; Ho, J.J.D.; Khacho, M.; Wang, M.; Perera, J.K.; Gardiner, C.; Bennett, C.A.; Head, T.; et al. Adaptation to Stressors by Systemic Protein Amyloidogenesis. *Dev Cell* 2016, *39*, 155–168, doi:10.1016/j.devcel.2016.09.002.

68. Saad, S.; Cereghetti, G.; Feng, Y.; Picotti, P.; Peter, M.; Dechant, R. Reversible Protein Aggregation Is a Protective Mechanism to Ensure Cell Cycle Restart after Stress. *Nat Cell Biol* 2017, *19*, 1202–1213, doi:10.1038/ncb3600.

69. Göbl, C.; Morris, V.K.; Dam, L. van; Visscher, M.; Polderman, P.E.; Hartlmüller, C.; Ruiter, H. de; Hora, M.; Liesinger, L.; Birner-Gruenberger, R.; et al. Cysteine Oxidation Triggers Amyloid Fibril Formation of the Tumor Suppressor P16INK4A. *Redox Biol* 2019, 101316, doi:10.1016/j.redox.2019.101316.

70. Pervaiz, S.; Clement, M.-V. Superoxide Anion: Oncogenic Reactive Oxygen Species? *Int J Biochem Cell Biology* 2007, *39*, 1297–1304, doi:10.1016/j.biocel.2007.04.007.

71. Hoffman, A.; Spetner, L.M.; Burke, M. Ramifications of a Redox Switch within a Normal Cell: Its Absence in a Cancer Cell. *Free Radical Bio Med* 2008, *45*, 265–268, doi:10.1016/j.freeradbiomed.2008.03.025.

72. Kuhn, D.M.; Sykes, C.E.; Geddes, T.J.; Jaunarajs, K.L.E.; Bishop, C. Tryptophan Hydroxylase 2 Aggregates through Disulfide Cross-linking upon Oxidation: Possible Link to Serotonin Deficits and Non-motor Symptoms in Parkinson's Disease. *J Neurochem* 2011, *116*, 426–437, doi:10.1111/j.1471-4159.2010.07123.x.

73. Kuhn, D.M.; Geddes, T.J. Peroxynitrite Inactivates Tryptophan Hydroxylase via Sulfhydryl Oxidation. *J Biol Chem* 1999, *274*, 29726–29732, doi:10.1074/jbc.274.42.29726.

74. Bothwell, M.Y.; Gillette, M.U. Circadian Redox Rhythms in the Regulation of Neuronal Excitability. *Free Radical Bio Med* 2018, *119*, 45–55, doi:10.1016/j.freeradbiomed.2018.01.025.

75. Liebl, M.P.; Kaya, A.M.; Tenzer, S.; Mittenzwei, R.; Koziollek-Drechsler, I.; Schild, H.; Moosmann, B.; Behl, C.; Clement, A.M. Dimerization of Visinin-like Protein 1 Is Regulated by Oxidative Stress and Calcium and Is a Pathological Hallmark of Amyotrophic Lateral Sclerosis. *Free Radical Bio Med* 2014, *72*, 41 54, doi:10.1016/j.freeradbiomed.2014.04.008.

76. Groblewska, M.; Muszyński, P.; Wojtulewska-Supron, A.; Kulczyńska-Przybik, A.; Mroczko, B. The Role of Visinin-Like Protein-1 in the Pathophysiology of Alzheimer's Disease. *J Alzheimer's Dis* 2015, *47*, 17–32, doi:10.3233/jad-150060.

77. Youn, H.; Jeoung, M.K.; Koo, Y.; Ji, H.; Markesbery, W.R.; Ji, I.; Ji, T.H. Kalirin Is Under-Expressed in Alzheimer's Disease Hippocampus. *J Alzheimer's Dis* 2007, *11*, 385 397, doi:10.3233/jad-2007-11314.

78. Lederer, C.W.; Torrisi, A.; Pantelidou, M.; Santama, N.; Cavallaro, S. Pathways and Genes Differentially Expressed in the Motor Cortex of Patients with Sporadic Amyotrophic Lateral Sclerosis. *Bmc Genomics* 2007, *8*, 26 26, doi:10.1186/1471-2164-8-26.

79. Braunewell, K.; Riederer, P.; Spilker, C.; Gundelfinger, E.D.; Bogerts, B.; Bernstein, H.G. Abnormal Localization of Two Neuronal Calcium Sensor Proteins, Visinin-like Proteins (Vilips)-1 and -3, in Neocortical Brain Areas of Alzheimer Disease Patients. *Dement Geriatr Cogn* 2001, *12*, 110 116, doi:10.1159/000051244.

80. Kato, M.; Yang, Y.-S.; Sutter, B.M.; Wang, Y.; McKnight, S.L.; Tu, B.P. Redox State Controls Phase Separation of the Yeast Ataxin-2 Protein via Reversible Oxidation of Its Methionine-Rich Low-Complexity Domain. *Cell* 2019, *177*, 711-721.e8, doi:10.1016/j.cell.2019.02.044.

81. Yang, Y.-S.; Kato, M.; Wu, X.; Litsios, A.; Sutter, B.M.; Wang, Y.; Hsu, C.-H.; Wood, N.E.; Lemoff, A.; Mirzaei, H.; et al. Yeast Ataxin-2 Forms an Intracellular Condensate Required for the Inhibition of TORC1 Signaling during Respiratory Growth. *Cell* 2019, *177*, 1 32, doi:10.1016/j.cell.2019.02.043.

82. Serebryany, E.; Woodard, J.C.; Adkar, B.V.; Shabab, M.; King, J.A.; Shakhnovich, E.I. An Internal Disulfide Locks a Misfolded Aggregation-Prone Intermediate in Cataract-Linked Mutants of Human ΓD-Crystallin. *J Biol Chem* 2016, *291*, 19172–19183, doi:10.1074/jbc.m116.735977.

83. Thorn, D.C.; Grosas, A.B.; Mabbitt, P.D.; Ray, N.J.; Jackson, C.J.; Carver, J.A. The Structure and Stability of the Disulfide-Linked ΓS-Crystallin Dimer Provide Insight into Oxidation Products Associated with Lens Cataract Formation. *J Mol Biol* 2018, *431*, 483–497, doi:10.1016/j.jmb.2018.12.005.

84. Lou, M.F. Redox Regulation in the Lens. *Prog Retin Eye Res* 2003, *22*, 657–682, doi:10.1016/s1350-9462(03)00050-8.

85. Duering, M.; Karpinska, A.; Rosner, S.; Hopfner, F.; Zechmeister, M.; Peters, N.; Kremmer, E.; Haffner, C.; Giese, A.; Dichgans, M.; et al. Co-Aggregate Formation of CADASIL-Mutant NOTCH3: A Single-Particle Analysis. *Hum Mol Genet* 2011, *20*, 3256–3265, doi:10.1093/hmg/ddr237.

86. Wollenweber, F.A.; Hanecker, P.; Bayer-Karpinska, A.; Malik, R.; Bäzner, H.; Moreton, F.; Muir, K.W.; Müller, S.; Giese, A.; Opherk, C.; et al. Cysteine-Sparing CADASIL Mutations in NOTCH3 Show Proaggregatory Properties in Vitro. *Stroke J Cereb Circulation* 2015, *46*, 786–792, doi:10.1161/strokeaha.114.007472.

87. Samson, A.L.; Knaupp, A.S.; Kass, I.; Kleifeld, O.; Marijanovic, E.M.; Hughes, V.A.; Lupton, C.J.; Buckle, A.M.; Bottomley, S.P.; Medcalf, R.L. Oxidation of an Exposed Methionine Instigates the Aggregation of Glyceraldehyde-3-Phosphate Dehydrogenase. *J Biol Chem* 2014, *289*, 26922–26936, doi:10.1074/jbc.m114.570275.

88. Surgucheva, I.; Sharov, V.S.; Surguchov, A. γ-Synuclein: Seeding of α-Synuclein Aggregation and Transmission between Cells. *Biochemistry-us* 2012, *51*, 4743–4754, doi:10.1021/bi300478w.

89. Torosantucci, R.; Sharov, V.S.; Beers, M. van; Brinks, V.; Schöneich, C.; Jiskoot, W. Identification of Oxidation Sites and Covalent Cross-Links in Metal Catalyzed Oxidized Interferon Beta-1a: Potential Implications for Protein Aggregation and Immunogenicity. *Mol Pharmaceut* 2013, *10*, 2311–2322, doi:10.1021/mp300665u.

90. Mulinacci, F.; Poirier, E.; Capelle, M.A.H.; Gurny, R.; Arvinte, T. Influence of Methionine Oxidation on the Aggregation of Recombinant Human Growth Hormone. *Eur J Pharm Biopharm* 2013, *85*, 42–52, doi:10.1016/j.ejpb.2013.03.015.

91. Koudelka, T.; Dehle, F.C.; Musgrave, I.F.; Hoffmann, P.; Carver, J.A. Methionine Oxidation Enhances κ-Casein Amyloid Fibril Formation. *J Agr Food Chem* 2012, *60*, 4144–4155, doi:10.1021/jf205168t.

92. Herrero, R.; Kajikawa, O.; Matute-Bello, G.; Wang, Y.; Hagimoto, N.; Mongovin, S.; Wong, V.; Park, D.R.; Brot, N.; Heinecke, J.W.; et al. The Biological Activity of FasL in Human and Mouse Lungs Is Determined by the Structure of Its Stalk Region. *J Clin Invest* 2011, *121*, 1174–1190, doi:10.1172/jci43004.

93. Zhao, L.; Buxbaum, J.N.; Reixach, N. Age-Related Oxidative Modifications of Transthyretin Modulate Its Amyloidogenicity. *Biochemistry-us* 2013, *52*, 1913–1926, doi:10.1021/bi301313b.

94. Wong, Y.Q.; Binger, K.J.; Howlett, G.J.; Griffin, M.D.W. Methionine Oxidation Induces Amyloid Fibril Formation by Full-Length Apolipoprotein A-I. *Proc National Acad Sci* 2010, *107*, 1977–1982, doi:10.1073/pnas.0910136107.

95. Shao, D.; Oka, S.; Liu, T.; Zhai, P.; Ago, T.; Sciarretta, S.; Li, H.; Sadoshima, J. A Redox-Dependent Mechanism for Regulation of AMPK Activation by Thioredoxin1 during Energy Starvation. *Cell Metab* 2014, *19*, 232 245, doi:10.1016/j.cmet.2013.12.013.

96. Sideri, T.C.; Stojanovski, K.; Tuite, M.F.; Grant, C.M. Ribosome-Associated Peroxiredoxins Suppress Oxidative Stress–Induced de Novo Formation of the [PSI+] Prion in Yeast. *Proc National Acad Sci* 2010, *107*, 6394–6399, doi:10.1073/pnas.1000347107.

97. Fox, J.H.; Connor, T.; Stiles, M.; Kama, J.; Lu, Z.; Dorsey, K.; Lieberman, G.; Sapp, E.; Cherny, R.A.; Banks, M.; et al. Cysteine Oxidation within N-Terminal Mutant Huntingtin Promotes Oligomerization and Delays Clearance of Soluble Protein. *J Biol Chem* 2011, *286*, 18320–18330, doi:10.1074/jbc.m110.199448.

98. Cozzolino, M.; Amori, I.; Pesaresi, M.G.; Ferri, A.; Nencini, M.; Carrì, M.T. Cysteine 111 Affects Aggregation and Cytotoxicity of Mutant Cu,Zn-Superoxide Dismutase Associated with Familial Amyotrophic Lateral Sclerosis. *J Biol Chem* 2008, *283*, 866–874, doi:10.1074/jbc.m705657200.

99. Karch, C.M.; Prudencio, M.; Winkler, D.D.; Hart, P.J.; Borchelt, D.R. Role of Mutant SOD1 Disulfide Oxidation and Aggregation in the Pathogenesis of Familial ALS. *Proc National Acad Sci* 2009, *106*, 7774 7779, doi:10.1073/pnas.0902505106.

100. Chen, X.; Shang, H.; Qiu, X.; Fujiwara, N.; Cui, L.; Li, X.M.; Gao, T.M.; Kong, J. Oxidative Modification of Cysteine 111 Promotes Disulfide Bond-Independent Aggregation of SOD1. *Neurochem Res* 2012, *37*, 835 845, doi:10.1007/s11064-011-0679-8.

101. Álvarez-Zaldiernas, C.; Lu, J.; Zheng, Y.; Yang, H.; Blasi, J.; Solsona, C.; Holmgren, A. Cellular Redox Systems Impact the Aggregation of Cu,Zn Superoxide Dismutase Linked to Familial Amyotrophic Lateral Sclerosis. *J Biol Chem* 2016, *291*, 17197–17208, doi:10.1074/jbc.m115.708230.

102. Xu, W.-C.; Liang, J.-Z.; Li, C.; He, Z.-X.; Yuan, H.-Y.; Huang, B.-Y.; Liu, X.-L.; Tang, B.; Pang, D.-W.; Du, H.-N.; et al. Pathological Hydrogen Peroxide Triggers the Fibrillization of Wild-Type SOD1 via Sulfenic Acid Modification of Cys-111. *Cell Death Dis* 2018, *9*, 67, doi:10.1038/s41419-017-0106-4.

103. Camargo, D.C.R.; Tripsianes, K.; Buday, K.; Franko, A.; Göbl, C.; Hartlmüller, C.; Sarkar, R.; Aichler, M.; Mettenleiter, G.; Schulz, M.; et al. The Redox Environment Triggers Conformational Changes and Aggregation of HIAPP in Type II Diabetes. *Sci Rep-uk* 2017, *7*, 1 11, doi:10.1038/srep44041.

104. Paulsson, J.F.; Andersson, A.; Westermark, P.; Westermark, G.T. Intracellular Amyloid-like Deposits Contain Unprocessed pro-Islet Amyloid Polypeptide (ProIAPP) in Beta Cells of Transgenic Mice Overexpressing the Gene for Human IAPP and Transplanted Human Islets. *Diabetologia* 2006, *49*, 1237 1246, doi:10.1007/s00125-006-0206-7.

105. He, Y.; Zhou, H.; Tang, H.; Luo, Y. Deficiency of Disulfide Bonds Facilitating Fibrillogenesis of Endostatin. *J Biol Chem* 2006, *281*, 1048–1057, doi:10.1074/jbc.m507745200.

106. Mitomi, Y.; Nomura, T.; Kurosawa, M.; Nukina, N.; Furukawa, Y. Post-Aggregation Oxidation of Mutant Huntingtin Controls the Interactions between Aggregates. *J Biol Chem* 2012, *287*, 34764–34775, doi:10.1074/jbc.m112.387035.

107. Liu, C.; Sawaya, M.R.; Eisenberg, D. B2-Microglobulin Forms Three-Dimensional Domain-Swapped Amyloid Fibrils with Disulfide Linkages. *Nat Struct Mol Biol* 2011, *18*, 49, doi:10.1038/nsmb.1948.

108. Tanaka, M.; Chien, P.; Naber, N.; Cooke, R.; Weissman, J.S. Conformational Variations in an Infectious Protein Determine Prion Strain Differences. *Nature* 2004, *428*, 323, doi:10.1038/nature02392.

109. Nekooki-Machida, Y.; Kurosawa, M.; Nukina, N.; Ito, K.; Oda, T.; Tanaka, M. Distinct Conformations of in Vitro and in Vivo Amyloids of Huntingtin-Exon1 Show Different Cytotoxicity. *Proc National Acad Sci* 2009, *106*, 9679–9684, doi:10.1073/pnas.0812083106.

110. Zhang, Q.; Bykov, V.J.N.; Wiman, K.G.; Zawacka-Pankau, J. APR-246 Reactivates Mutant P53 by Targeting Cysteines 124 and 277. *Cell Death Dis* 2018, *9*, 439, doi:10.1038/s41419-018-0463-7.

111. Zhang, Q.; Bergman, J.; Wiman, K.G.; Bykov, V.J.N. Role of Thiol Reactivity for Targeting Mutant P53. *Cell Chem Biol* 2018, *25*, 1219-1230.e3, doi:10.1016/j.chembiol.2018.06.013.

112. Carija, A.; Navarro, S.; Groot, N.S. de; Ventura, S. Protein Aggregation into Insoluble Deposits Protects from Oxidative Stress. *Redox Biol* 2017, *12*, 699–711, doi:10.1016/j.redox.2017.03.027.

113. Kirstein, J.; Morito, D.; Kakihana, T.; Sugihara, M.; Minnen, A.; Hipp, M.S.; Nussbaum-Krammer, C.; Kasturi, P.; Hartl, F.U.; Nagata, K.; et al. Proteotoxic Stress and Ageing Triggers the Loss of Redox Homeostasis across Cellular Compartments. *Embo J* 2015, *34*, 2334–2349, doi:10.15252/embj.201591711.

114. Combs, C.K.; Karlo, J.C.; Kao, S.-C.; Landreth, G.E. β-Amyloid Stimulation of Microglia and Monocytes Results in TNFα-Dependent Expression of Inducible Nitric Oxide Synthase and Neuronal Apoptosis. *J Neurosci* 2001, *21*, 1179–1188, doi:10.1523/jneurosci.21-04-01179.2001.

115. Zhao, Q.-F.; Yu, J.-T.; Tan, L. S-Nitrosylation in Alzheimer's Disease. *Mol Neurobiol* 2015, *51*, 268–280, doi:10.1007/s12035-014-8672-2.

116. Floden, A.M.; Li, S.; Combs, C.K. β-Amyloid-Stimulated Microglia Induce Neuron Death via Synergistic Stimulation of Tumor Necrosis Factor α and NMDA Receptors. *J Neurosci* 2005, *25*, 2566–2575, doi:10.1523/jneurosci.4998-04.2005.

117. Correani, V.; Francesco, L.D.; Cera, I.; Mignogna, G.; Giorgi, A.; Mazzanti, M.; Fumagalli, L.; Fabrizi, C.; Maras, B.; Schininà, M.E. Reversible Redox Modifications in the Microglial Proteome Challenged by Beta Amyloid. *Mol Biosyst* 2015, *11*, 1584–1593, doi:10.1039/c4mb00703d.

118. Gu, L.; Robinson, R.A.S. A Simple Isotopic Labeling Method to Study Cysteine Oxidation in Alzheimer's Disease: Oxidized Cysteine-Selective Dimethylation (OxcysDML). *Anal Bioanal Chem* 2016, *408*, 2993 3004, doi:10.1007/s00216-016-9307-4.

119. Kontush, A.; Berndt, C.; Weber, W.; Akopyan, V.; Arlt, S.; Schippling, S.; Beisiegel, U. Amyloid-β Is an Antioxidant for Lipoproteins in Cerebrospinal Fluid and Plasma. *Free Radical Bio Med* 2001, *30*, 119–128, doi:10.1016/s0891-5849(00)00458-5.

120. Kontush, A. Amyloid-β: An Antioxidant That Becomes a pro-Oxidant and Critically Contributes to Alzheimer's Disease. *Free Radical Bio Med* 2001, *31*, 1120–1131, doi:10.1016/s0891-5849(01)00688-8.

121. Atwood, C.S.; Obrenovich, M.E.; Liu, T.; Chan, H.; Perry, G.; Smith, M.A.; Martins, R.N. Amyloid-β: A Chameleon Walking in Two Worlds: A Review of the Trophic and Toxic Properties of Amyloid-β. *Brain Res Rev* 2003, *43*, 1–16, doi:10.1016/s0165-0173(03)00174-7.

122. Baruch-Suchodolsky, R.; Fischer, B. Aβ 40 , Either Soluble or Aggregated, Is a Remarkably Potent Antioxidant in Cell-Free Oxidative Systems. *Biochemistry-us* 2009, *48*, 4354–4370, doi:10.1021/bi802361k.

123. Huang, X.; Atwood, C.S.; Hartshorn, M.A.; Multhaup, G.; Goldstein, L.E.; Scarpa, R.C.; Cuajungco, M.P.; Gray, D.N.; Lim, J.; Moir, R.D.; et al. The Aβ Peptide of Alzheimer's Disease Directly Produces Hydrogen Peroxide through Metal Ion Reduction. *Biochemistry-us* 1999, *38*, 7609–7616, doi:10.1021/bi990438f.

124. Hensley, K.; Carney, J.M.; Mattson, M.P.; Aksenova, M.; Harris, M.; Wu, J.F.; Floyd, R.A.; Butterfield, D.A. A Model for Beta-Amyloid Aggregation and Neurotoxicity Based on Free Radical Generation by the Peptide: Relevance to Alzheimer Disease. *Proc National Acad Sci* 1994, *91*, 3270–3274, doi:10.1073/pnas.91.8.3270.

125. Smith, D.G.; Cappai, R.; Barnham, K.J. The Redox Chemistry of the Alzheimer's Disease Amyloid β Peptide. *Biochimica Et Biophysica Acta Bba - Biomembr* 2007, *1768*, 1976–1990, doi:10.1016/j.bbamem.2007.02.002.

126. Barnham, K.J.; Ciccotosto, G.D.; Tickler, A.K.; Ali, F.E.; Smith, D.G.; Williamson, N.A.; Lam, Y.-H.; Carrington, D.; Tew, D.; Kocak, G.; et al. Neurotoxic, Redox-Competent Alzheimer's β-Amyloid Is Released from Lipid Membrane by Methionine Oxidation. *J Biol Chem* 2003, *278*, 42959–42965, doi:10.1074/jbc.m305494200.

127. Atwood, C.S.; Perry, G.; Zeng, H.; Kato, Y.; Jones, W.D.; Ling, K.-Q.; Huang, X.; Moir, R.D.; Wang, D.; Sayre, L.M.; et al. Copper Mediates Dityrosine Cross-Linking of Alzheimer's Amyloid-β †. *Biochemistry-us* 2004, *43*, 560–568, doi:10.1021/bi0358824.

128. Deas, E.; Cremades, N.; Angelova, P.R.; Ludtmann, M.H.R.; Yao, Z.; Chen, S.; Horrocks, M.H.; Banushi, B.; Little, D.; Devine, M.J.; et al. Alpha-Synuclein Oligomers Interact with Metal Ions to Induce Oxidative Stress and Neuronal Death in Parkinson's Disease. *Antioxid Redox Sign* 2016, *24*, 376–391, doi:10.1089/ars.2015.6343.

129. Lovell, M.A.; Robertson, J.D.; Teesdale, W.J.; Campbell, J.L.; Markesbery, W.R. Copper, Iron and Zinc in Alzheimer's Disease Senile Plaques. *J Neurol Sci* 1998, *158*, 47–52, doi:10.1016/s0022-510x(98)00092-6.

130. Hashimoto, M.; Rockenstein, E.; Crews, L.; Masliah, E. Role of Protein Aggregation in Mitochondrial Dysfunction and Neurodegeneration in Alzheimer's and Parkinson's Diseases. *Neuromol Med* 2003, *4*, 21–35, doi:10.1385/nmm:4:1-2:21.

131. Schubert, D.; Behl, C.; Lesley, R.; Brack, A.; Dargusch, R.; Sagara, Y.; Kimura, H. Amyloid Peptides Are Toxic via a Common Oxidative Mechanism. *Proc National Acad Sci* 1995, *92*, 1989–1993, doi:10.1073/pnas.92.6.1989.

132. Brookes, P.S.; Yoon, Y.; Robotham, J.L.; Anders, M.W.; Sheu, S.-S. Calcium, ATP, and ROS: A Mitochondrial Love-Hate Triangle. *Am J Physiol-cell Ph* 2004, *287*, C817–C833, doi:10.1152/ajpcell.00139.2004.

133. Curtain, C.C.; Ali, F.; Volitakis, I.; Cherny, R.A.; Norton, R.S.; Beyreuther, K.; Barrow, C.J.; Masters, C.L.; Bush, A.I.; Barnham, K.J. Alzheimer's Disease Amyloid-β Binds Copper and Zinc to Generate an Allosterically Ordered Membrane-Penetrating Structure Containing Superoxide Dismutase-like Subunits. *J Biol Chem* 2001, *276*, 20466–20473, doi:10.1074/jbc.m100175200.

134. Casas-Tinto, S.; Zhang, Y.; Sanchez-Garcia, J.; Gomez-Velazquez, M.; Rincon-Limas, D.E.; Fernandez-Funez, P. The ER Stress Factor XBP1s Prevents Amyloid-Beta Neurotoxicity. *Hum Mol Genet* 2011, *20*, 2144–2160, doi:10.1093/hmg/ddr100.

135. Gerakis, Y.; Hetz, C. Emerging Roles of ER Stress in the Aetiology and Pathogenesis of Alzheimer's Disease. *Febs J* 2017, *285*, 995–1011, doi:10.1111/febs.14332.

136. Haynes, C.M.; Titus, E.A.; Cooper, A.A. Degradation of Misfolded Proteins Prevents ER-Derived Oxidative Stress and Cell Death. *Mol Cell* 2004, *15*, 767–776, doi:10.1016/j.molcel.2004.08.025.

137. Peng, T.; Jou, M. Oxidative Stress Caused by Mitochondrial Calcium Overload. *Ann Ny Acad Sci* 2010, *1201*, 183–188, doi:10.1111/j.1749-6632.2010.05634.x.

138. Santos, C.X.C.; Tanaka, L.Y.; Wosniak, J.; Laurindo, F.R.M. Mechanisms and Implications of Reactive Oxygen Species Generation During the Unfolded Protein Response: Roles of Endoplasmic Reticulum Oxidoreductases, Mitochondrial Electron Transport, and NADPH Oxidase. *Antioxid Redox Sign* 2009, *11*, 2409–2427, doi:10.1089/ars.2009.2625.

139. Malhotra, J.D.; Kaufman, R.J. Endoplasmic Reticulum Stress and Oxidative Stress: A Vicious Cycle or a Double-Edged Sword? *Antioxid Redox Sign* 2007, *9*, 2277–2294, doi:10.1089/ars.2007.1782.

140. Mogk, A.; Bukau, B.; Kampinga, H.H. Cellular Handling of Protein Aggregates by Disaggregation Machines. *Mol Cell* 2018, *69*, 214–226, doi:10.1016/j.molcel.2018.01.004.

141. Karri, S.; Singh, S.; Paripati, A.K.; Marada, A.; Krishnamoorthy, T.; Guruprasad, L.; Balasubramanian, D.; Sepuri, N.B.V. Adaptation of Mge1 to Oxidative Stress by Local Unfolding and Altered Interaction with Mitochondrial Hsp70 and Mxr2. *Mitochondrion* 2018, *46*, 140–148, doi:10.1016/j.mito.2018.04.003.

142. Miyata, Y.; Rauch, J.N.; Jinwal, U.K.; Thompson, A.D.; Srinivasan, S.; Dickey, C.A.; Gestwicki, J.E. Cysteine Reactivity Distinguishes Redox Sensing by the Heat-Inducible and Constitutive Forms of Heat Shock Protein 70. *Chem Biol* 2012, *19*, 1391–1399, doi:10.1016/j.chembiol.2012.07.026.

143. Stöcker, S.; Maurer, M.; Ruppert, T.; Dick, T.P. A Role for 2-Cys Peroxiredoxins in Facilitating Cytosolic Protein Thiol Oxidation. *Nat Chem Biol* 2017, *14*, doi:10.1038/nchembio.2536.

144. Weids, A.J.; Grant, C.M. The Yeast Peroxiredoxin Tsa1 Protects against Protein-Aggregate-Induced Oxidative Stress. *J Cell Sci* 2014, *127*, 1327–1335, doi:10.1242/jcs.144022.

145. Teixeira, F.; Tse, E.; Castro, H.; Makepeace, K.A.T.; Meinen, B.A.; Borchers, C.H.; Poole, L.B.; Bardwell, J.C.; Tomás, A.M.; Southworth, D.R.; et al. Chaperone Activation and Client Binding of a 2-Cysteine Peroxiredoxin. *Nat Commun* 2019, *10*, 659, doi:10.1038/s41467-019-08565-8.

146. Jang, H.H.; Kim, S.Y.; Park, S.K.; Jeon, H.S.; Lee, Y.M.; Jung, J.H.; Lee, S.Y.; Chae, H.B.; Jung, Y.J.; Lee, K.O.; et al. Phosphorylation and Concomitant Structural Changes in Human 2-Cys Peroxiredoxin Isotype I Differentially Regulate Its Peroxidase and Molecular Chaperone Functions. *Febs Lett* 2006, *580*, 351–355, doi:10.1016/j.febslet.2005.12.030.

147. Saccoccia, F.; Di Micco, P.; Boumis, G.; Brunori, M.; Koutris, I.; Miele, A.E.; Morea, V.; Sriratana, P.; Williams, D.L.; Bellelli, A.; et al. Moonlighting by Different Stressors: Crystal Structure of the Chaperone Species of a 2-Cys Peroxiredoxin. *Structure* 2012, *20*, 429–439, doi:10.1016/j.str.2012.01.004.

148. Park, J.W.; Piszczek, G.; Rhee, S.G.; Chock, P.B. Glutathionylation of Peroxiredoxin I Induces Decamer to Dimers Dissociation with Concomitant Loss of Chaperone Activity. *Biochemistry-us* 2011, *50*, 3204–3210, doi:10.1021/bi101373h.

149. Barranco-Medina, S.; Lázaro, J.-J.; Dietz, K.-J. The Oligomeric Conformation of Peroxiredoxins Links Redox State to Function. *Febs Lett* 2009, *583*, 1809 1816, doi:10.1016/j.febslet.2009.05.029.

150. Shringarpure, R.; Grune, T.; Davies, K.J.A. Protein Oxidation and 20S Proteasome-Dependent Proteolysis in Mammalian Cells. *Cell Mol Life Sci Cmls* 2001, *58*, 1442–1450, doi:10.1007/pl00000787.

151. Shringarpure, R.; Grune, T.; Mehlhase, J.; Davies, K.J.A. Ubiquitin Conjugation Is Not Required for the Degradation of Oxidized Proteins by Proteasome. *J Biol Chem* 2003, *278*, 311–318, doi:10.1074/jbc.m206279200.

152. Grune, T.; Merker, K.; Sandig, G.; Davies, K.J.A. Selective Degradation of Oxidatively Modified Protein Substrates by the Proteasome. *Biochem Bioph Res Co* 2003, *305*, 709–718, doi:10.1016/s0006-291x(03)00809-x.

153. Livnat-Levanon, N.; Kevei, É.; Kleifeld, O.; Krutauz, D.; Segref, A.; Rinaldi, T.; Erpapazoglou, Z.; Cohen, M.; Reis, N.; Hoppe, T.; et al. Reversible 26S Proteasome Disassembly upon Mitochondrial Stress. *Cell Reports* 2014, *7*, 1371–1380, doi:10.1016/j.celrep.2014.04.030.

154. Davies, K.J.; Goldberg, A.L. Oxygen Radicals Stimulate Intracellular Proteolysis and Lipid Peroxidation by Independent Mechanisms in Erythrocytes. *J Biological Chem* 1987, *262*, 8220–8226.

155. Reinheckel, T.; Ullrich, O.; Sitte, N.; Grune, T. Differential Impairment of 20S and 26S Proteasome Activities in Human Hematopoietic K562 Cells during Oxidative Stress. *Archives of Biochemistry and Biophysics* 2000, *377*, 65–68.

156. Silva, G.M.; Netto, L.E.S.; Simões, V.; Santos, L.F.A.; Gozzo, F.C.; Demasi, M.A.A.; Oliveira, C.L.P.; Bicev, R.N.; Klitzke, C.F.; Sogayar, M.C.; et al. Redox Control of 20S Proteasome Gating. *Antioxid Redox Sign* 2012, *16*, 1183–1194, doi:10.1089/ars.2011.4210.

157. Jung, T.; Höhn, A.; Grune, T. The Proteasome and the Degradation of Oxidized Proteins: Part III—Redox Regulation of the Proteasomal System. *Redox Biol* 2014, *2*, 388–394, doi:10.1016/j.redox.2013.12.029.

158. Tsvetkov, P.; Myers, N.; Eliav, R.; Adamovich, Y.; Hagai, T.; Adler, J.; Navon, A.; Shaul, Y. NADH Binds and Stabilizes the 26S Proteasomes Independent of ATP. *J Biol Chem* 2014, *289*, 11272–11281, doi:10.1074/jbc.m113.537175.

159. Cagnetta, A.; Cea, M.; Calimeri, T.; Acharya, C.; Fulciniti, M.; Tai, Y.-T.; Hideshima, T.; Chauhan, D.; Zhong, M.Y.; Patrone, F.; et al. Intracellular NAD+ Depletion Enhances Bortezomib-Induced Anti-Myeloma Activity. *Blood* 2013, *122*, 1243–1255, doi:10.1182/blood-2013-02-483511.

160. Jenner, P. Oxidative Stress in Parkinson's Disease. *Ann Neurol* 2003, *53*, S26–S38, doi:10.1002/ana.10483.

161. Shringarpure, R.; Grune, T.; Sitte, N.; Davies*, K.J.A. 4-Hydroxynonenal-Modified Amyloid-β Peptide Inhibits the Proteasome: Possible Importance in Alzheimer's Disease*. *Cell Mol Life Sci Cmls* 2000, *57*, 1802–1809, doi:10.1007/pl00000660.

162. Lee, M.; Hyun, D.; Jenner, P.; Halliwell, B. Effect of Proteasome Inhibition on Cellular Oxidative Damage, Antioxidant Defences and Nitric Oxide Production. *J Neurochem* 2001, *78*, 32–41, doi:10.1046/j.1471-4159.2001.00416.x.

163. Ling, Y.-H.; Liebes, L.; Zou, Y.; Perez-Soler, R. Reactive Oxygen Species Generation and Mitochondrial Dysfunction in the Apoptotic Response to Bortezomib, a Novel Proteasome Inhibitor, in Human H460 Non-Small Cell Lung Cancer Cells. *J Biol Chem* 2003, *278*, 33714–33723, doi:10.1074/jbc.m302559200.

164. Mehta, N.J.; Marwah, P.K.; Njus, D. Are Proteinopathy and Oxidative Stress Two Sides of the Same Coin? *Cells* 2019, *8*, 59, doi:10.3390/cells8010059.

165. Scherz-Shouval, R.; Shvets, E.; Fass, E.; Shorer, H.; Gil, L.; Elazar, Z. Reactive Oxygen Species Are Essential for Autophagy and Specifically Regulate the Activity of Atg4. *Embo J* 2007, *26*, 1749–1760, doi:10.1038/sj.emboj.7601623.

166. Bensaad, K.; Cheung, E.C.; Vousden, K.H. Modulation of Intracellular ROS Levels by TIGAR Controls Autophagy. *Embo J* 2009, *28*, 3015–3026, doi:10.1038/emboj.2009.242.

167. Chen, Y.; Azad, M.B.; Gibson, S.B. Superoxide Is the Major Reactive Oxygen Species Regulating Autophagy. *Cell Death Differ* 2009, *16*, 1040–1052, doi:10.1038/cdd.2009.49.

168. Dodson, M.; Darley-Usmar, V.; Zhang, J. Cellular Metabolic and Autophagic Pathways: Traffic Control by Redox Signaling. *Free Radical Bio Med* 2013, *63*, 207–221, doi:10.1016/j.freeradbiomed.2013.05.014.

169. Guerrero-Gómez, D.; Mora-Lorca, J.A.; Sáenz-Narciso, B.; Naranjo-Galindo, F.J.; Muñoz-Lobato, F.; Parrado-Fernández, C.; Goikolea, J.; Cedazo-Minguez, Á.; Link, C.D.; Neri, C.; et al. Loss of Glutathione Redox Homeostasis Impairs Proteostasis by Inhibiting Autophagy-Dependent Protein Degradation. *Cell Death Differ* 2019, *26*, 1545–1565, doi:10.1038/s41418-018-0270-9.

170. Carroll, B.; Otten, E.G.; Manni, D.; Stefanatos, R.; Menzies, F.M.; Smith, G.R.; Jurk, D.; Kenneth, N.; Wilkinson, S.; Passos, J.F.; et al. Oxidation of SQSTM1/P62 Mediates the Link between Redox State and Protein Homeostasis Available online: https://www.nature.com/articles/s41467-017-02746-z.pdf.

171. Komatsu, M.; Kurokawa, H.; Waguri, S.; Taguchi, K.; Kobayashi, A.; Ichimura, Y.; Sou, Y.-S.; Ueno, I.; Sakamoto, A.; Tong, K.I.; et al. The Selective Autophagy Substrate P62 Activates the Stress Responsive Transcription Factor Nrf2 through Inactivation of Keap1. *Nat Cell Biol* 2010, *12*, 213–223, doi:10.1038/ncb2021.

172. Kerr, E.M.; Gaude, E.; Turrell, F.K.; Frezza, C.; Martins, C.P. Mutant Kras Copy Number Defines Metabolic Reprogramming and Therapeutic Susceptibilities. *Nature* 2016, *531*, 110–113, doi:10.1038/nature16967.

173. Paola, D.; Domenicotti, C.; Nitti, M.; Vitali, A.; Borghi, R.; Cottalasso, D.; Zaccheo, D.; Odetti, P.; Strocchi, P.; Marinari, U.M.; et al. Oxidative Stress Induces Increase in Intracellular Amyloid β-Protein Production and Selective Activation of BI and BII PKCs in NT2 Cells. *Biochem Bioph Res Co* 2000, *268*, 642–646, doi:10.1006/bbrc.2000.2164.

174. Stockwell, B.R.; Angeli, J.P.F.; Bayir, H.; Bush, A.I.; Conrad, M.; Dixon, S.J.; Fulda, S.; Gascón, S.; Hatzios, S.K.; Kagan, V.E.; et al. Ferroptosis: A Regulated Cell Death Nexus Linking Metabolism, Redox Biology, and Disease. *Cell* 2017, *171*, 273–285, doi:10.1016/j.cell.2017.09.021.

175. Palikaras, K.; Tavernarakis, N. Mitophagy in Neurodegeneration and Aging. *Frontiers Genetics* 2012, *3*, 297, doi:10.3389/fgene.2012.00297.

176. Violi, F.; Loffredo, L.; Carnevale, R.; Pignatelli, P.; Pastori, D. Atherothrombosis and Oxidative Stress: Mechanisms and Management in Elderly. *Antioxid Redox Sign* 2017, *27*, 1083–1124, doi:10.1089/ars.2016.6963.

CHAPTER 6

THE BIOCHEMICAL CHARACTERIZATION OF CDK4 AS A REDOX-SENSITIVE PROTEIN

Loes van Dam[1], Paulien E. Polderman[1], María Benavente Díaz[1], Suda Ratnasingam[1], Matthijs Baars[1], Boudewijn M. T. Burgering[1,2], Tobias B. Dansen[1]

[1]Center for Molecular Medicine, Molecular Cancer Research, University Medical Center Utrecht, Universiteitsweg 100, 3584CG, Utrecht, The Netherlands
[2]Oncode Institute, University Medical Center Utrecht, Universiteitsweg 100, 3584CG, Utrecht, The Netherlands.

Correspondence: t.b.dansen@umcutrecht.nl

KEYWORDS
redox signaling; cysteine oxidation; cell cycle; CDK4; CDK6; cyclin D; ribociclib; LEE011

THE BIOCHEMICAL CHARACTERIZATION OF CDK4 AS A REDOX-SENSITIVE PROTEIN

ABSTRACT

Cyclin-dependent kinases (CDKs), together with their corresponding regulatory cyclin control the timely progression through the cell cycle. CDK4, and its paralog CDK6, stimulate the transition of G1 to S-phase upon binding to the D-type cyclins. Reactive oxygen species (ROS) can both stimulate and inhibit cell cycle progression, and this is at least in part mediated through the reversible oxidation of cysteine residues in key regulatory proteins. In this chapter, we show that CDK4 and cyclin D form a temporary covalently linked complex under oxidizing conditions. This is mediated by the formation of a disulfide bond involving cysteine 135 in CDK4, which stabilizes the otherwise hydrostatic non-covalent interaction between these proteins. Moreover, disulfide formation leads to an increased kinase activity of the CDK4-cyclin D complex. We further characterize the disulfide-dependent CDK4/cyclin D complex with respect to differential binding partners and substrates. The identification of the redox sensitive C135 at the CDK4/cyclin D interface could provide a potential target for novel covalent cytostatic drugs.

INTRODUCTION

Eukaryotic cells divide when they are stimulated with proliferative signals such as growth factors and hormones [1–3]. Proliferative signals are opposed by stress signals, which can activate cell cycle checkpoints [4,5]. Communication between signaling pathways that regulate cell division, metabolic status and genome integrity, but also cell-cell contacts or cytoskeletal integrity are crucial for the decision to enter the cell cycle [6]. Cell division is a major metabolic commitment, and especially in metazoans comes with the risk of the acquisition of oncogenic mutations. Sustained proliferative signaling is indeed a universal hallmark for cancer cells [7]. One of the ways cells integrate these signals is through signal transduction mediated by the reversible oxidation of specific cysteines, known as redox signaling [8]. This was elegantly illustrated in a recent study that shows that oscillatory H_2O_2-dependent protein thiol oxidation is essential for the coupling of cell division and metabolism in yeast [9]. The correlation of the cellular oxidation state with cell cycle phase was also demonstrated in a study that uses genetically encoded fluorescent redox sensors [10]. Furthermore, cell fate decisions regarding proliferation and differentiation during embryonic development are driven by hypoxic and oxidative environments, respectively [11]. Loss of redox control of the cell cycle can result in inappropriate re-entry into the cell cycle, resulting in developmental defects, cancer or neurodegenerative diseases [12].

Prolonged exposure to higher levels of reactive oxygen species (ROS) triggers a cell cycle arrest, for instance through the activation of the p53 tumor suppressor (reviewed in ref. [13]), replication fork stalling [14] and accumulation of $p16^{INK4A}$, which inhibits the D-cyclin type CDKs CDK4 and CDK6[15]. But besides the growth arrest in response to high levels of oxidants, stimulation of growth factor receptors results in the production of H_2O_2 (generated by NADPH oxidase (NOX) enzymes), which further enables proliferative growth factor receptor signaling through inhibition of protein tyrosine phosphatases. Indeed, exogenous H_2O_2 has long been recognized as a mimetic of for instance insulin, PDGF and EGF [16,17]. The combined action of the growth factor receptor tyrosine kinase and NOX-derived H_2O_2 eventually culminates in the expression of cyclin D and stimulation of cell cycle entry from G0 to G1 [18–20]. ROS therefore both activates and inactivates CDK4 and CDK6 activity through upstream signaling. Furthermore, our laboratory previously described the disulfide-dependent association of CDK4 with FOXO3 and FOXO4 under oxidizing conditions, suggesting that CDK4 contains (a) redox-sensitive cysteine(s). In the present study we explore whether the activity of the CDK4-cyclin D complex is also regulated by oxidation of cysteines.

The kinase activity of most cyclin-dependent kinases is largely controlled by binding of the appropriate cyclins, the levels of which fluctuate throughout the cell cycle. CDK4 and CDK6 associate with D-type cyclins D1, D2 and D3, resulting in a protein complex that is required for cells to transition from G1 into S-phase during cell proliferation. While levels of most cyclins fluctuate throughout the cell cycle, cyclin D levels are regulated by the levels of mitogens and growth factors [21–23]. Although redox changes are thought to control the cell cycle in several ways [8,24] and D-type cyclins have been described to be redox-regulated [18], limited evidence exists to date describing direct redox control of CDKs [25].

Here, we show that an oxidizing cellular environment triggers the formation of an intermolecular disulfide between CDK4 and any of the D-type cyclin isoforms D1, D2 and D3, that otherwise bind through non-covalent interactions. This disulfide involves cysteine 135 in CDK4, which is in close proximity to cysteine 7 in cyclin D. These results suggest that the stabilized interaction enhances the kinase activity of the complex under oxidizing conditions.

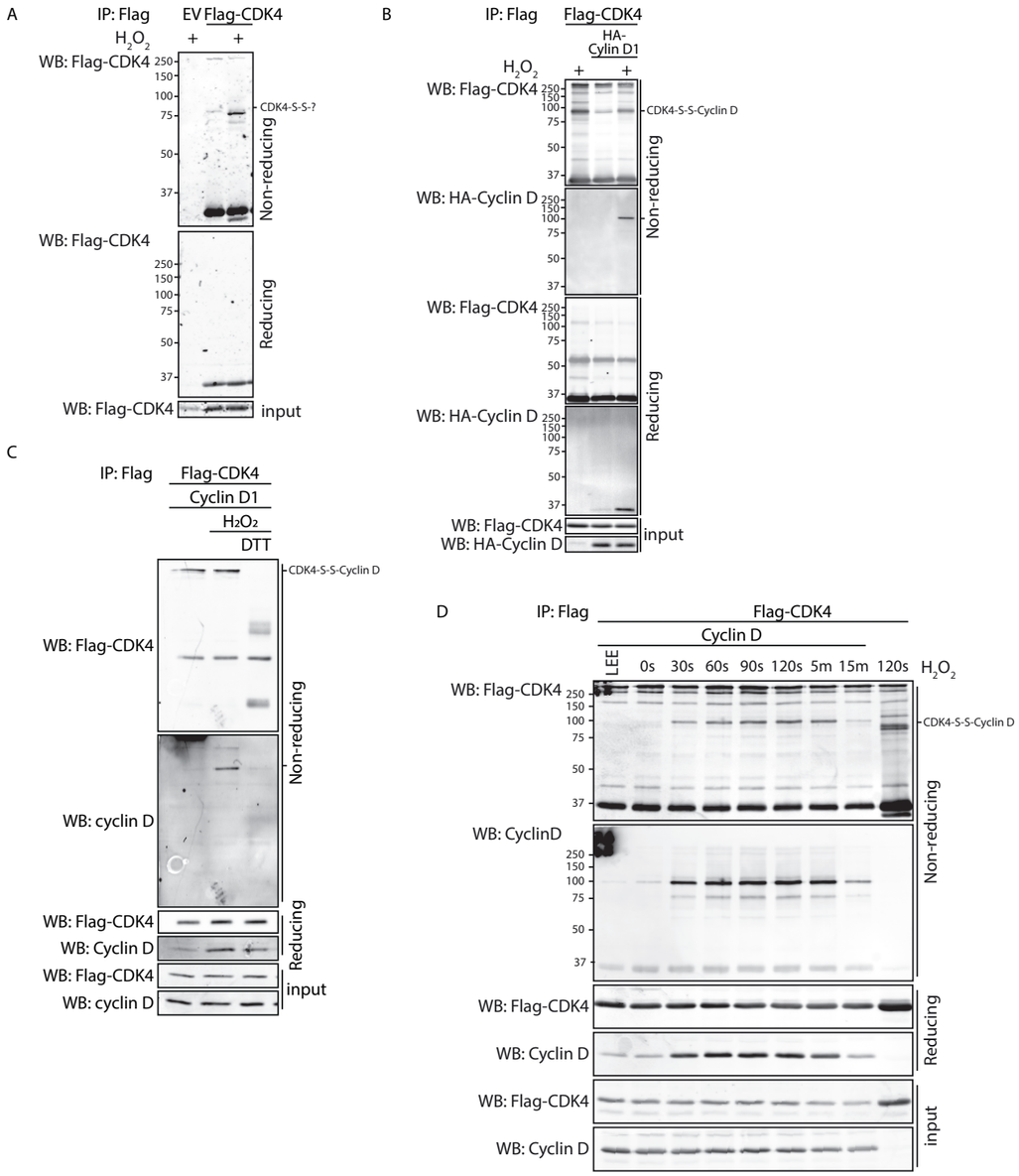

Figure 1. CDK4 forms a disulfide-dependent complex with Cyclin D. *(figure legend continues on next page)*
(**A**) Parallel reducing and non-reducing SDS-PAGE and western blot analysis (WB) of Flag-CDK4. Cells were incubated with 200 μM of H_2O_2 for 2 minutes where indicated. Exposure of 293T cells to H_2O_2 induces a mass shift of a fraction of CDK4. (**B**) Parallel reducing and non-reducing SDS-PAGE and western blot analysis (WB) of Flag-CDK4 immunoprecipitates (IP). Flag-CDK4 and HA-tagged cyclin D1 were expressed in 293T cells and exposed to 200 μM of H_2O_2 for 2 minutes. CDK4 and cyclin D form an intermolecular disulfide-dependent complex upon exposure to H_2O_2, and migrate as a single band under non-reducing conditions. (**C**) The intermolecular disulfide-dependent complex between CDK4 and cyclin D is lost when samples were incubated with 20 mM DTT for 10 minutes prior to washing. (**D**) The H_2O_2-induced, cysteine-dependent complex between CDK4 and cyclin D is induced within 30 seconds of H_2O_2 treatment, and diminishes after 5 minutes of H_2O_2 treatment.

RESULTS

CDK4 Forms a Disulfide-Dependent Complex with Cyclin D

CDK4 was identified in multiple mass-spectrometry-based screens for redox sensitive proteins (see ref [25] and **chapters 3** and **5**). To study whether CDK4 is indeed prone to cysteine oxidation in the form of intermolecular disulfide formation, we expressed Flag-CDK4 in HEK293T cells followed by immunopurification and SDS-PAGE under parallel reducing and non-reducing conditions. Exposure of these cells to H_2O_2 causes a fraction of CDK4 to shift to a higher molecular weight (HMW) of 75-100 kDa, which indicates that indeed cysteines in CDK4 become oxidized (**Figure 1A**). Moreover, CDK4 seems to form intermolecular disulfides since the observed large mass shift is reversible and absent in reduced samples (middle panel).

To investigate whether CDK4 is able to form a disulfide-dependent complex with its regulatory binding partner cyclin D1 upon exposure to H_2O_2, HA-tagged cyclin D1 was co-expressed with Flag-CDK4. Indeed, CDK4 and cyclin D form an intermolecular disulfide-dependent complex upon exposure to H_2O_2, and migrate as a single band under non-reducing conditions (**Figure 1B**). This CDK4-cyclin D complex is resistant to washing with a buffer supplemented with 1M NaCl, as can be expected for a covalent interactions such as disulfide bridges. The disulfide-dependent complex between CDK4 and cyclin D is sensitive to reduction, as both proteins migrate at their own molecular weight when IP samples are incubated with the reducing agent DTT (**Figure 1C**) before washing. Furthermore, the complex between CDK4 and Cyclin D is induced rapidly (within 20s) upon exposure to H_2O_2 (**Figure 1D**). The complex is transient as its abundance decreases after 5 minutes, and after 15 minutes it is almost non-detectable.

In summary, CDK4 is able to form a disulfide-dependent complex with cyclin D1 upon H_2O_2 exposure, that is rapidly and transiently formed under oxidizing conditions.

CDK4 Cysteine 135 is Required for the Interaction Between CDK4 and Cyclin D

CDK4 contains 4 cysteines at positions 78, 135, 202 and 215. The published crystal structures of CDK4 in complex with cyclin D1 reveals that C135 is situated at the cyclin D1 binding interface [26]. Two cysteines in cyclin D1 (C7/C8) are in close proximity of CDK4 C135 (**Figure 2A** and **S1** in more detail). Mutational analysis showed that the H_2O_2-induced interaction between CDK4 and cyclin D1 indeed depends on C135 (**Figure 2B**). Note that CDK4 also forms another disulfide-mediated complex mediated by cysteines C78 and C202, indicated by the bands detected with the anti-flag antibody that run slightly lower than CDK4-cyclin D. It is possible this band contains S-S-dependent CDK4 homodimers mediated by C78 and C202, as it involves two CDK4 cysteines. Together, the observation of a C135-dependent complex between CDK4 and cyclin D1 seems to be in agreement with the positioning of cysteines as shown in the crystal structure of the CDK4-cyclin D1 complex.

While CDK4 is widely reported to interact with cyclin D1, relatively little is known about its interaction with the other cyclin D isoforms [28,29]. To find out whether the other cyclin D isoforms are also capable of forming a disulfide-dependent complex with CDK4, Flag-CDK4 and HA-cyclin D1, D2 or D3 were co-expressed in HEK293T and stimulated with H_2O_2. Both cyclin D2 and -D3 form a H_2O_2- dependent high-molecular weight complex with CDK4, similar to cyclin D1. However, the induction of the disulfide-dependent interaction with CDK4 by H_2O_2 is much less strong as compared to cyclin D1 (**Figure 2C**, non-reducing IP). (**Figure 2C**, reducing IP). Of note, in these experiments we observe a considerable fraction of cyclin D binding non-covalently to CDK4 before H_2O_2 treatment, suggesting that a pre-existing non-covalent interaction serves as the starting point for the covalent interaction between CDK4-cyclin D. The observation that H_2O_2 also increases the amount of total cyclin D1 binding could be due to loss of non-covalently bound cyclin D1 in the washing steps of the immunoprecipitation protocol. The total amount of cyclin D2 and D3 pulled down by CDK4

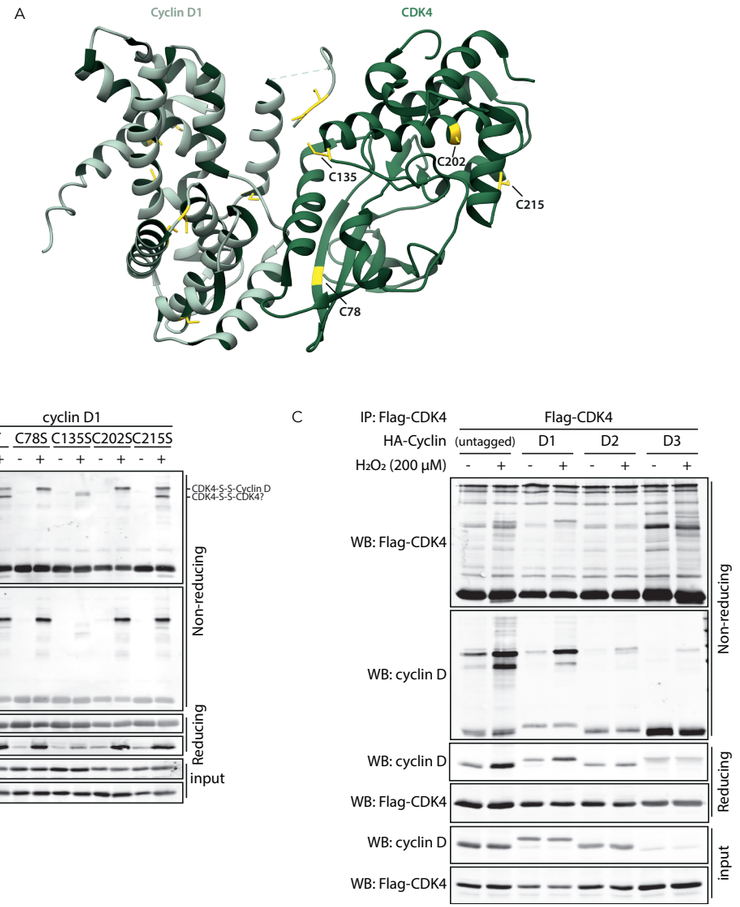

Figure 2. CDK4 Cysteine 135 is required for the interaction between CDK4 and Cyclin D.
(**A**) Crystal structure of CDK4 in complex with cyclin D1 (PDB ID: 2W96) visualized using UCSF Chimera. The four CDK cysteines 78, 135, 202 and 215 are indicated in yellow. (**B**) Cells expressing Flag-CDK4 cysteine mutants and cyclin D were subjected to H_2O_2 for 2 minutes. Samples were used in a Flag-CDK4 immunoprecipitation and subjected to analysis under non-reducing and reducing conditions. The complex between CDK4 and cyclin D is dependent on C135. (**C**) Cells expressing Flag-CDK4 and HA-cyclin D1, D2 or D3 were subjected to H_2O_2 for 2 minutes before Flag-CDK4 immunoprecipitation. Samples were analyzed under non-reducing and reducing conditions.

is however not much affected by H_2O_2. We speculate that the non-covalent interaction of CDK4 with cyclin D2 and D3 is more resistant to washing during IP, and that these two cyclin D isoforms form a disulfide-dependent complex with CDK4 to a lesser extent than cyclin D1. Of the cysteines of cyclin D in proximity to CDK4-C135, only the cysteine homologous to C7 in Cyclin D1 (C5 in cyclin D2 and D3) is conserved in all three cyclin D isoforms, and is therefore likely to be involved in the disulfide-dependent interaction with CDK4. In summary, all cyclin D isoforms (D1, D2 and D3) are able to form a disulfide-dependent complex with CDK4, which is dependent on C135 in CDK4.

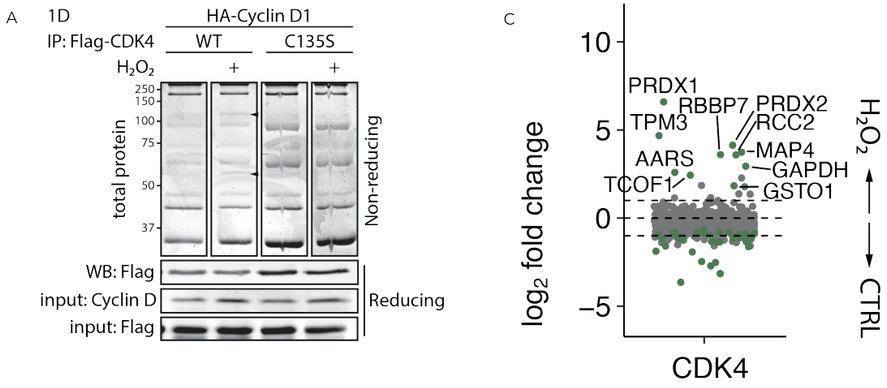

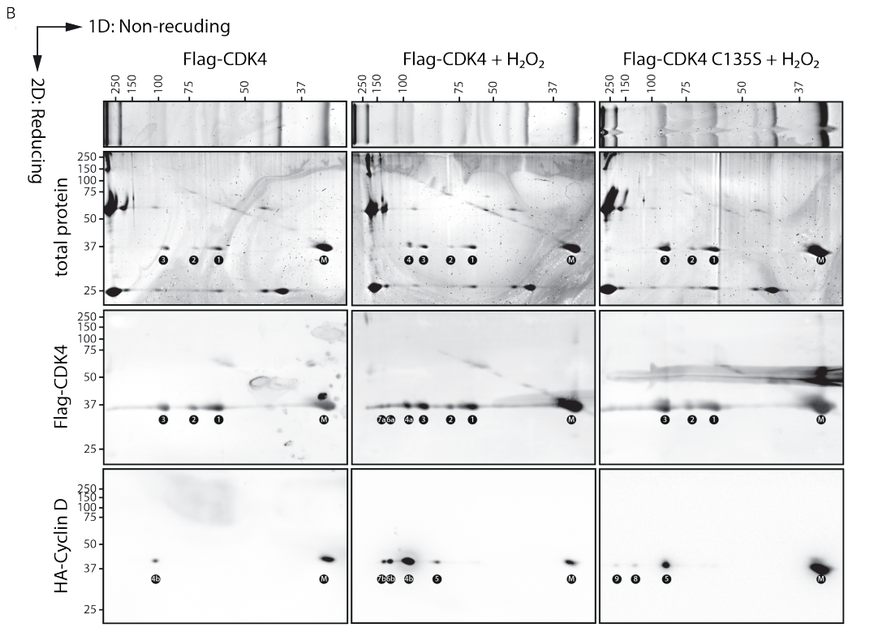

Figure 3. Characterization of CDK4 redox-dependent covalent complexes.
(**A**) Flag-CDK4 was immunoprecipitated from cells co-expressing Flag-CDK4 and HA-cyclin D. Samples are separated using SDS-PAGE under non-reducing conditions in the first dimension, so disulfide-mediated complexes migrate at their combined MW. (**B**) The entire lane is excised and incubated in reducing sample buffer before separation by SDS-PAGE in the second dimension, where disulfide-mediated complex members migrate at their own MW. Proteins migrating at their own MW in both the first and the second dimensions are shown on a diagonal, whereas disulfide-mediated complexes migrate below the diagonal in the second dimension. Gels were either stained for total protein or immunoblotted and stained using anti-Flag(-CDK4) or anti-HA(-cyclin D) antibodies. M: monomeric protein (Flag-CDK4 anf HA-cyclin D). (**C**) Scatter plot of the mass spectrometry data from cells expressing Flag-CDK4, showing the $\log_2$ fold change of proteins in H_2O_2 treated cells versus control. Colored dots represent proteins with a p-value < 0.05 as calculated using inference of protein differential abundance by probabilistic dropout analysis (proDA). Horizontal dotted lines are positioned at $\log_2$ fold change of 1 and -1 (i.e. a 2-fold change). For the identity of specific interactors see **Table 1**.

Characterization of CDK4 Redox-Dependent Covalent Complexes

To investigate the possibility that CDK4 forms also other cysteine-dependent protein complexes we immunoprecipitated CDK4 and subjected it to diagonal SDS-PAGE and western blotting (see chapter 3, Figure 2A for a schematic overview of this method). A large number of disulfide-dependent complexes containing CDK4 is visible. Note that 1) CDK4 and cyclin D have a similar molecular weight (~34 kDa without affinity tags) and that 2) migratory properties of proteins on SDS-PAGE may be different than expected when samples are analyzed under non-reducing conditions due to SDS accessibility. Spots 1-3 (~60, ~75 and ~100 kDa, **Figure 3B**) are already present before H_2O_2 treatment and contain CDK4 but not cyclin D (or other proteins as judged by the absence of spots of similar intensities at the same vertical position in the simply blue stained gel). These spots therefore most likely stem from S-S-dependent CDK4 homodimers. The differential horizontal poistion could be due to oligomerization or alternative disulfide linkage, similar to what we observed for TIPRL (see **chapter 3**). The intensities of these spots does not increase with H_2O_2. and are independent of C135. We cannot fully exclude that spots 1-3 are caused by some background signal, corresponding with their low intenities in the first dimension and absence in previous experiments.

The S-S-dependent CDK4-cyclin D complex observed in Figures 1 and 2 is clearly visible and indicated as spot 4 on both western blots**.** It is also lightly visible under endogenous conditions (cyclin D western blot only, spot 4b), suggesting that a small amount of cyclin D already interacts without H_2O_2 treatment. Indeed, spot 4 is absent in the experiment using the CDK4 C135S mutant, corroborating our previous observation. Spot 6 and 7 likely derive from disulfide formation between cyclin D and one of the redox-dependent CDK4 complexes that gave rise to spots 1-3. That would be in accordance with the idea that cyclin D binds CDK4 C135, and that this cysteine is not involved in CDK4 S-S-homodimerization.

The complex that falls apart in spot 5 is best visible in the cyclin D blot, but there could be some signal for CDK4 as well**.** Strikingly, the staining for cyclin D in this spot is much more prominent in the CDK4 C135S pulldown. There are several possible explanations for this observation. i) Perhaps the absence of CDK4 C135 leaves the cysteine in cyclin D availalble for the formation of a disulfide dependent complex with another binding partner. Since the experiment uses Flag-CDK4 C135S as a bait, this disulfide-containing complex of cyclin D and another protein still interacts with CDK4 non-covalently. ii) When CDK4 is unable to form a S-S-dependent CDK4-cyclin D complex, it will start forming non-native interactions. This is supported by our data in Figure 2B, where the band pattern in the CDK C135S mutant (non-reducing) is different from that in WT CDK. iii) Cyclin D is also capable of forming S-S-dependent homodimers, which in their turn bind non-covalently to CDK4. Because CDK4 and cyclin D have a similar molecular weight, this S-S-dependent cyclin D homodimer will end up around the same MW as would CDK4-cyclin D (spot 4). Although these findings need to be interpreted with caution, this data suggests CDK4 forms disulfides mainly with cyclin D through C135 upon exposure of cells to H_2O_2.

We next aimed to identify potential new interaction partners of the CDK4-cyclin D covalent complexes. We therefore performed a preliminary label-free MS/MS experiment to identify proteins that interact with CDK4 in a H_2O_2-dependent manner (**Figure 3C** and **Table 1**). Interestingly, we identify proteins that are known to be involved in redox signaling, such as the cytosolic peroxiredoxins 1 and 2 (PRDX1-2), GAPDH, the redox-sensitive glycolytic enzyme GAPDH and the thioltransferase enzyme GSTO1. Although these interactions need to be verified in more detail, these observations suggest that CDK4 can form several redox-dependent interactions.

Functional Characterization of Redox-Dependent Complexes of CDK4 and cyclin D

To answer the question whether the disulfide-mediated interaction affects the activity of the CDK4-cyclin D complex, a kinase assay was performed. Interestingly, CDK4 immunoprecipitated from H_2O_2-treated cells displays a higher activity in a subsequent in vitro kinase assay using recombinant GST-Rb fragment as a substrate (**Figure 4A**). However, the increase in Rb1 phosphorylation at S807/811 is not dependent on the disulfide-mediated complex between CDK4 and cyclin D as we also observe this effect in the C135S mutant. This is further corroborated by the observation that when we incubate the samples with DTT to reduce the covalent interaction between CDK4 and cyclin D, the H_2O_2-induced increase in kinase activity is not affected (**Figure 4B**). Surprisingly, the kinase activity of CDK4 in complex with cyclin D3 is much stronger as compared to cyclins D1 and D2, irrespective of the cellular redox state (supplementary **Figure S4**). Togeth-

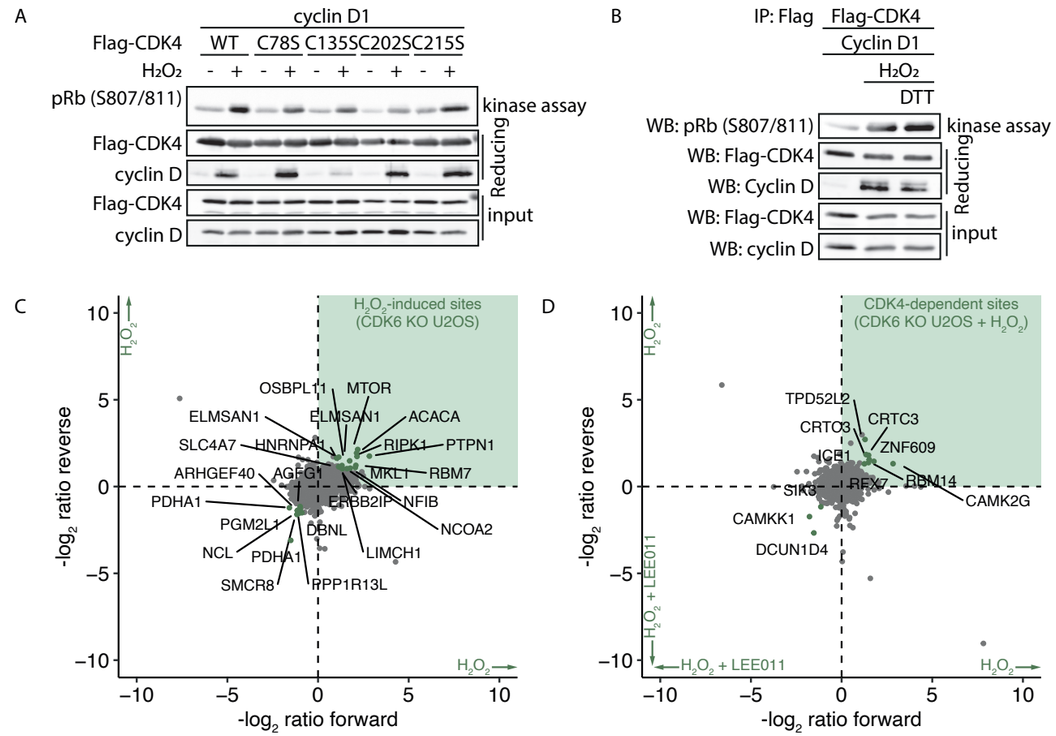

Figure 4. Functional characterization of redox-dependent complexes of CDK4 and cyclin D.
(**A**) *In vitro* kinase assay using immunoprecipitated Flag-CDK4 mutants from cells subjected to H_2O_2 for 2 minutes. Immunoprecipitates were washed with kinase buffer followed by incubation with ATP and recombinant GST-Rb fragment as a substrate. Rb phosphorylation increases upon treatment with H_2O_2. (**B**) *In vitro* kinase assay using immunoprecipitated Flag-CDK4 from cells subjected to H_2O_2 for 2 minutes. Where incubated, immunoprecipitates were incubated with 20 mM DTT for 10 minutes prior to washing. (**C**) Phosphoproteomics results for CDK6-knockout U2OS cells upon treatment with H_2O_2 Colored dots represent proteins with p-values < 0.05. Colored dots in the green quadrant with $-\log_2$ ratios >1 or < -1 are listed in Table 2. (**D**) Phosphoproteomics results for H_2O_2-treated CDK6-knockout U2OS cells upon treatment LEE011 Colored dots represent proteins with p-values < 0.05. Colored dots in the green quadrant with $-\log_2$ ratios >1 or < -1 are listed in Table 2.

er, these results indicate that the kinase activity of the disulfide-bound CDK4-cyclin D complex is not redox regulated even though H_2O_2 stimulates the covalent CDK4-cyclin D interaction.

It is possible that the formation of the covalent complex of oxidized CDK4 and cyclin D can determine substrate specificity. The observation that the kinase activity for Rb1 is not dependent on the disulfide-mediated interaction between CDK4 and cyclin D does not mean there there are no changes in kinase activity per se. One reason could be an altered substrate specificity of the complex, phosphorylating substrates other than Rb1. As a preliminary experiment, we performed phosphopeptide enrichment mass-spectrometry. CDK4 and closely related CDK6 are considered largely redundant. In addition, in contrast to CDK4, the closely related CDK6 does not contain a cysteine around position C135, suggesting that CDK6 is unable to form a disulfide-dependent complex with cyclin D. Therefore, we knocked out CDK6 and CDK4 in U2OS cell lines using CRISPR-Cas9 technology and stimulated H_2O_2-treated cells with the CDK4/6 inhibitor LEE011 (ribociclib). To accurately quantify relative levels of phosphorylated proteins we made use of Stable Isotope Labelling by Amino acids in Cell Culture (SILAC), followed by phosphopeptide enrichment. Firstly, multiple phosphorylation sites are detected that change in CDK6-knockout U2OS cells upon treatment with H_2O_2 (**Figure 4C** and **Table 2**). Phosphorylation on sites that are specific for CDK4 should be inhibited by treatment with LEE011. Using these criteria, a H_2O_2-dependent and CDK4-specific phosphorylation site was detected in TNIK (a kinase involved in JNK and Wnt pathway activation), and multiple sites were detected in CAMK2G and OSBPL10 (a calcium/calmodulin-dependent kinase and a lipid receptor, respectively) from this preliminary experiment (**Figure 4D** and **Table 2**). It is possible that these substrates are indeed disulfide-dependent substrates of CDK4, since these sites do not change significantly in the CDK4 KO cells treated with H_2O_2 (**Table 3**), and since CDK6 does not contain a cysteine around position C135. Future experiments will be needed to confirm these preliminary results, and focus on establishing the effect of these phosphorylations.

DISCUSSION

The activity of CDK family members is strictly dependent on association with their complementary cyclins, the abundance of which is regulated in a cell cycle-phase dependent manner, or by the levels of mitogens and growth factors. D-type cyclins associate with CDK4 and CDK6 to enable cell cycle progression from G1 to S-phase by phosphorylating members of the retinoblastoma (Rb) family proteins, thereby releasing their inhibitory effect on the E2F1 transcription factor [30,31].

Here, and based on earlier observations pointing in that direction [25], we aimed to assess whether CDK4 could be redox sensitive. We show that the complex between CDK4 and cyclin D can be covalently linked through the formation of a disulfide bond, which is induced by a more oxidative cellular environment (i.e. H_2O_2 treatment). We provide evidence that this interaction is mediated by cysteine 135 of CDK4. All three cyclin D isoforms D1, D2 and D2 are able to form this interaction. Additionally, the data suggest that the kinase activity of the complex is increased under oxidizing conditions, although this seems to occur independently of disulfide formation between CDK4-cyclin D.

The interaction between CDK4 and cyclin D is well documented. Consistent with literature, we observe a variable fraction of cyclin D interacting with CDK4 even without exposure to H_2O_2 (see e.g. **Figure 1B**, reducing IP). This disulfide-independent interaction could support the hypothesis that pre-existing complexes between CDK4-cyclin D can be crosslinked under oxidizing conditions through the formation of a disulfide bond. If this is indeed the case, low-affinity interactions can be locked in a high affinity complex through this mechanism, similar to what was shown for FOXO4 and TNPO1 [32]. The fraction of disulfide-independent bound cyclin D in the experiments is somewhat variable, possibly due to variation in the levels of overexpression which affects the stoichiometry of the complex. Furthermore, the IP protocol used to identify disulfide-dependent interactions includes a high-salt washing step that could lead to loss of non-covalent interactions. Future experiments should therefore be performed using a more stable cell expression system or CDK4 knockout cell lines for more comparable results.

The diagonal SDS-PAGE experiment also provides evidence for the disulfide-dependent dimerization of CDK4 with cyclin D, as well as different S-S-dependent CDK4 homodimers. (**Figure 3B**).

The kinase activity of the disulfide-bound CDK4-cyclin D complex is not directly affected by the disulfide bond between CDK4-cyclin D (**Figure 4A, 4B** and **Supplementary Figure S4**), even though overall kinase activity is increased under oxidizing conditions. The reason for this is not entirely clear, but it is possible that there is still plenty cyclin D remaining in the samples even after stringent washing with 1M NaCl, and that this remaining cyclin D pool can phosphorylate Rb1. The same washing conditions are also reason for the loss of non-covalently bound cyclin D1 in conditions not treated with H_2O_2. Possibly, kinase activity this is dependent on the molecular and cellular context. For example, the stoichiometry of CDK4 and cyclin D overexpression might influence kinase activity of the complex. On top of that, the cellular context including dephosphorylation events by phosphatases such as PP1 [33] and cyclin E expression can affect kinase activity of the covalent CDK4-cyclin D complex, albeit not in short timescales like those used in this study. It has been described that phosphorylation of CDK4 on T172 by the CDK-activating kinase CDK7 stimulates kinase activity [34]. A next step could be to test the CDK4 phosphorylation state of T172 upon oxidation and its subsequent kinase activity.

We recently showed that the CDK4/6 inhibitor and tumor suppressor $p16^{INK4A}$ can also be oxidized, upon which it forms amyloid-like fibrils and it loses its ability to inhibit CDK4/6 (**chapter 1** and [39]). The observation that CDK4 itself can also be oxidized, and the increased kinase activity of CDK4 upon H_2O_2 stimulation would seem to corroborate the findings on $p16^{INK4A}$, since both processes stimulate CDK4 kinase activity and potentially cell cycle progression from G1 to S-phase. Because of the low stoichiometry of the CDK4-cyclin D complex it is still possible that the complex is inactivated by H_2O_2, but this effect is obscured by the inactivation of $p16^{INK4A}$ (and this activation of CDK4/6). We are currently in the process of assessing the effects of $p16^{INK4A}$ and CDK4 oxidation on the cell cycle, and whether and how exactly the disulfide-bound CDK4-cyclin D complex influences Rb phosphorylation and S-phase entry.

As most of the experiments were performed in the presence of cyclin D, it is possible that we overlook any effects of CDK4 oxidation that are independent of cyclin D. As an example, mutational analysis of CDK4 reveals another disulfide-mediated complex dependent on two CDK4 cysteines C78 and C202, possibly containing S-S-dependent CDK4 homodimers.

In the proteomics experiment, we identify a number of H_2O_2-induced interaction partners for CDK4. Many of these are known-redox-sensitive proteins such as peroxiredoxins 1 and 2. Peroxiredoxins are dedicated H_2O_2 scavengers, but, more importantly, they are also known to actively participate in the oxidation of proteins through redox relays [35,36]. Further experiments need to be done to test whether peroxiredoxins are responsible for the oxidation of CDK4 through a redox relay. In addition, we identify GSTO1 as an interaction partner of CDK4. GSTO1 catalyzes thioltransferase reactions using glutathione as a cofactor, which opens up the possibility that oxidized CDK4 is reduced by GSTO1. It is important to keep in mind that the proteomics experiment was performed in with endogenoud cyclin D in order to enrich for potential new interaction partners, and that these cells (293T) have inactive Rb. However, it is possible that new interaction partners bind only as a trimeric complex – when cyclin D is also present.

In order to assess whether the formation of the covalent complex of oxidized CDK4 and cyclin D can determine substrate specificity we set up preliminary phosphoproteomics experiments, which were perfomed in the presence of overexpressed cyclin D and in an Rb-proficient U2OS cell line. If the oxidation of CDK4-cyclin D indeed affects substrate specificity, these results offer a starting point for the identification of new substrates. In line with this, new functions of CDK4/6 besides their well-documented role in cell cycle progression through Rb phosphorylation are starting to emerge. For example, CDK6-cyclin D3 has been shown to act as a rate-limiting regulator of carbon flow into the pentose phosphate- and serine pathways [37].

CDK6 is related to CDK4 and their structures are highly similar. Although CDK6 contains two extra cysteines in an extended loop that is not present in CDK4, CDK6 does not contain a homologous cysteine at C135. Furthermore, there is no other cysteine present at the binding interface with cyclin D (data not shown). This raises the question if CDK6 is also subject to oxidation and disulfide-dependent dimerization with cyclin D. Interestingly, like CDK4, CDK6 is also able to form a disulfide-linked complex with cyclin D and also shows increased kinase activity upon stimulation with H_2O_2 (supplementary **Figure S2**). In a preliminary experiment, the interaction between CDK6 and cyclin D seems dependent on C306 (data not shown). CDK6 does not have any cysteine

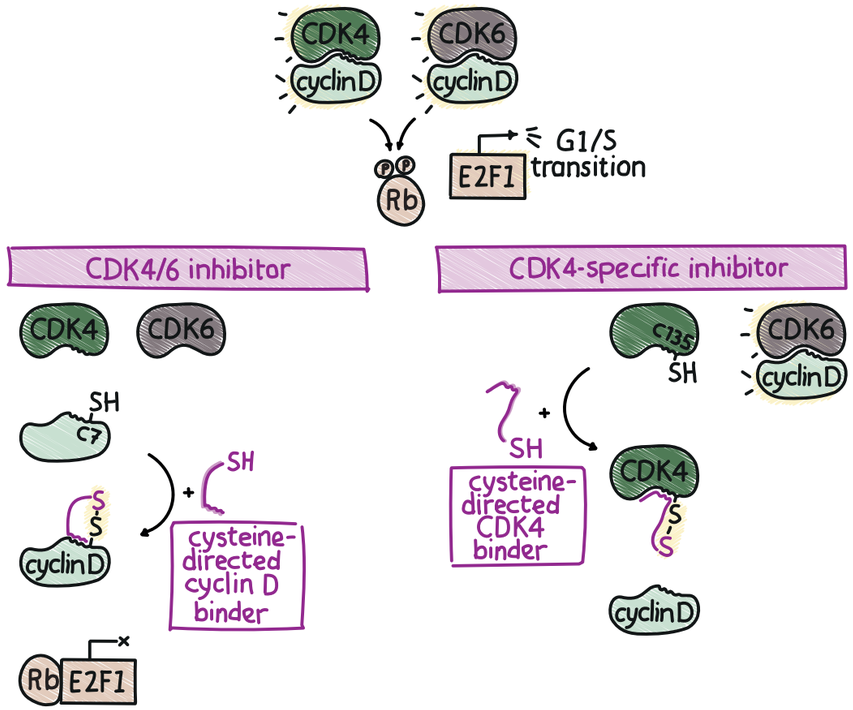

Figure 5.
The region around CDK4 C135 could serve as a template for the design of a cysteine-directed covalent cyclin D binder to prevent complex formation of cyclin D with both CDK4 and CDK6 and inhibit their activity (left panel). If indeed the reactive cysteine in cyclin D1 is C7, the region around this cysteine could serve as a template for the design of a covalent, CDK4-specific inhibitor that targets C135 and does not also target CDK6.

around the cyclin D binding interface like CDK4 does (C135). This would seem to suggest that the covalent interaction between CDK6 and D-type cyclins is of a different nature than their canonical, non-covalent interaction, and different from the interaction between CDK4-cyclin D. Therefore, uncovering the exact properties of the interaction CDK4/6 surface with cyclin D is a vital issue for future research. While the CDK4-cyclinD1 and CDK6-cyclin D3 complexes are the most characterized (e.g. [38]), the data suggests that both CDK4 and CDK6 can interact with cyclins D1, D2 and D3 in a disulfide-linked complex. Expression patterns of D-type cyclins vary between tissue types, and any differences in the preference for a cyclin D isoform, as well as differences in their redox regulation would be interesting because this would allow for a context-dependent response.

This research shows that CDK4 is a redox-sensitive protein. The observation that CDK4 and cyclin D can interact covalently upon oxidizing conditions is especially interesting, since this potentially links the cellular redox state to the decision to commit to the cell cycle transition from G1 to S-phase. By linking pre-existing CDK4-cyclin D complexes, low levels of H_2O_2 can potentially contribute to Rb phosphorylation and cell cycle progression from G1 to S-phase. Taken together, the data suggest that more oxidizing conditions can potentially stimulate cell cycle entry though oxidation of CDK4 and subsequent covalent complex formation between CDK4 and cyclin D. Hypothetically, this regulation could be part of a larger mechanism of finetuning of cellular processes by H_2O_2, depending on the concentration and duration of oxidants exposure, as well as the oxidation of context-dependent and cell-specific target proteins. More specifically, low levels of could H_2O_2 stimulate proliferation, amongst others thought the oxidation and activation of CDK4 and inactivation of $p16^{INK4A}$, whereas higher or prolonged levels of H_2O_2 cause oxidative stress and cell cycle arrest.

The redox regulation of CDK4 could also be of importance as a potential new drug target, regardless of the functional effect of CDK4 oxidation. CDK4/6 activity is frequently upregulated in cancers, and CDK4 inhibitors are currently being exploited in the clinic (i.e. Palbociclib). These inhibitors are small molecule ATP-analogs that bind to the ATP-binding pocket. Since all kinases bind ATP, ATP-analogs are prone to off-target binding which could result in a limited response and /or adverse side effects [40]. There is a recent surge in the development of cysteine-directed, covalent drugs. The here described identification of a disulfide at the interface of CDK4 and Cyclin D could be a starting point for the design novel CDK4/6 inhibitors that are not based on the ATP-binding pocket. The region around CDK4 C135 could serve as a template for the design of a cysteine-directed covalent cyclin D binder to prevent complex formation with both CDK4 and CDK6 and inhibit their activity (**Figure 5**, left panel). Conversely, if we can confirm that the reactive cysteine in cyclin D1 is indeed C7, the region around this cysteine in cyclin D1 could serve as a template for the design of a covalent, CDK4 inhibitor that targets C135 (**Figure 5**, right panel).. This could be the first CDK4-specific inhibitor (i.e. that does not also target CDK6), since CDK6 does not contain a cysteine on its interaction surface with cyclin D.

MATERIALS AND METHODS

Cell Lines and Culturing

HEK293T and U2OS cells were cultured in bicarbonate-buffered DMEM, supplemented with 10% FBS (Bodinco BDC-40506-C05), 2 mM L-glutamine (Lonza, BE17-605E) and 100 U/mL penicillin-streptomycin (Lonza, DE17-602E) and kept at 37°C and under a 6% CO^2 atmosphere. Transfections were carried out using PEI (Sigma-Aldrich, P3640) or FugeneHD reagent (Promega, E2311) following the manufacturer's instructions. After two days, cells were harvested for further analysis. CRISPR knockout lines were created by plating 200k U2OS cells. After 24h, cells were transfected with pX458 (addgene plasmid ID 48138) containing a gRNA against CDK6. The top 15% GFP-expressing cells were sorted in 96-wells plates, and monoclonal knockout lines were verified by western blotting and sequencing.

Plasmids and Reagents

Full length human CDK4 and CDK6 were a kind gift from Sander van den Heuvel (Utrecht University), Addgene plasmid ID 1866 and 1874, respectively. Constructs with *att* recombination sites were were amplified from full-length CDK4 and CDK6 using the following primers: CDK4_F_5'-GGGGACAAGTTTGTACAAAAAAG-CAGGCTTCGCTACCTCTCGATATGAGCCAG-3', CDK4_R_5'-GGGGACCACTTTGTACAAGAAAGCT-GGGTCTCACTCCGGATTACCTTCATCC-3', CDK6_F_5'-GGGGACAAGTTTGTACAAAAAAG-CAGGCTTCGAGAAGGACGGCCTGTGCCGCG-3', CDK6_R_5'-GGGGACCACTTTGTACAAGAAAGCT-GGGTCTTAAACGGCTGTATTCAGCTCC-3'. Using Gateway technology (Invitrogen) entry clones were generated. CDK4 cysteine mutants were created by site-directed mutagenesis PCR using the following primers:

CDK4_C78S_F_5'-GCTGATGGACGT-CAGTGCCACATCCCGAACTGACDK4-3', CDK4_C78S_C78S_R_5'-GTCAGTTCGG-GATGTGGCACTGACGTCCATCACDK4-3', CDK4_C135S_F_5'-TTTCCTTCATGCCAATAGCATC-GTTCACCGAGATCTGAAGCDK4-3', CDK4_C135S_R_5'-CTTCAGATCTCGGTGAAC-GATGCTATTGGCATGAAGGAAACDK4-3', CDK4_C202S_F_5'-ACATGTGGAGTGTTGG-CAGTATCTTTGCAGAGATGTTTCGCDK4-3', CDK4_C202S_R_5'-CGAAACATCTCTGCAAAGA-TACTGCCAACACTCCACATGTCDK4-3', CDK4_C215S_F_5'-TCGAAAGCCTCTCTTCAGT-GGAAACTCTGAAGCCGACCDK4-3', CDK4_C215S_R_5'-GTCGGCTTCAGAGTTTCCACT-GAAGAGAGGCTTTCGA-3', and verified by sequencing. Gateway technology (Life Technologies) was used to create N-terminally tagged Flag-His and HA-expression vectors (backbones pCDNA3) from the resulting CDK4 cysteine mutant entry clones. HrA-tagged Cyclin-D1-3 constructs were purchased from Addgene (plasmid IDs 8948, 8950 and 10912, respectively). CDK6 sgRNA sequences are 5'-CCGC-CACGCATTCGTACTGC-3' and 5'-CGCGCTTCAACG-CCACGAAA-3'. β-mercaptoethanol was used in a concentration of 100 µM. 30% H_2O_2 (Sigma 31642) was freshly diluted to a stock of 10 or 100 mM in H_2O for every experiment. Unless stated otherwise, H_2O_2 treatments were 200µM for 2 minutes. LEE011 (ribociclib) was used at a concentration of 10µM for 30 minutes.

Co-immunoprecipitations, in vitro Kinase Assay and Western Blotting

After treatment as indicated, cells were lysed using a buffer containing 50 mM Tris-HCl pH 7.5, 1% TX100, 1.5 mM MgCl2, 5 mM EDTA, 100 mM NaCl, NaF, Leupeptin and Aprotinin. 100 mM iodoacetamide was added to the lysis buffer to prevent post-lysis cysteine oxidation and to inactivate disulfide reducing enzymes. After centrifugation at 14000 rpm for 10 min, 5% of the supernatant was kept as input and the remaining supernatant was used for immunoprecipitation with anti-Flag-M2 affinity gel (Sigma A222). After a 2 h incubation whilst gently mixing, immunoprecipitates were washed 4 times with lysis buffer containing 1 M NaCl and samples were boiled for 5 min in sample buffer with or without the reducing agent β-mercaptoethanol. Where stated, samples were incubated with 20 mM DTT. Samples were separated on a 10% polyacrylamide gel and transferred to immobilon-FL membranes (using standard protocols) before staining and antibody detection. Samples for *in vitro* kinase assays were taken after high salt wash of the immunoprecipitates. Samples were incubated with 1 µg of recombinant GST-Rb1 (Sigma-Aldrich SRP0256) each, in a kinase buffer consisting of 200 µM ATP, 1 mM DTT, and 0.1 mM Oxaloacetate for 30 minutes at 30°C.

Antibodies that were used are Flag M2 (Sigma F3165), HA (12CA5, monoclonal from hybridoma cell lines and SC805), CDK4 (Transduction Laboratories C18720), CDK6 (Santa Cruz SC-177), cyclin D1 (Abcam ab134175) and phospho-Rb S807/811 (Cell Signaling Technology CS9308). Detection of fluorescent secondary antibodies was performed using the LI-COR Biosciences Odyssey Infrared Imaging System or the Amersham Typhoon NIR Plus Biomolecular Imager (GE Healthcare), detection of secondary HRP-antibodies was performed on the FUJIFILM Luminescent Image Analyser LAS-3000.

2D Diagonal Electrophoresis

Immunoprecipitates were separated in the first dimension on a 10% SDS-PAGE gel and total protein content was stained using SimplyBlue. Gel lanes were cut out and incubated with 2x Laemmli sample buffer containing β-mercaptoethanol for 30' at room temperature. In the second dimension, reduced gel lanes were loaded on a second 10% SDS-PAGE gel at a right angle to the first dimension. Detection of proteins was done using SimplyBlue stain and using western blotting.

Mass Spectrometry

For the identification of CDK4 interactors the lysate of 4x20cm dishes were used for each pulldown on 75 ml of Flag-M2 beads similar to the immunoprecipitation experiments described above. All immunoprecipitations were performed using three biological replicates. After washing, beads were resuspended with 8M urea in 1M ammonium bicarbonate (ABC), reduced and alkylated in 10 mM TCEP and 40 mM chloroacetamide (CAA) for 30 minutes at RT. After fourfold dilution with 1M ABC, proteins were digested overnight on-bead with 250 ng Trypsin/LysC (Promega V5071) per sample at 37°C. Samples were cleaned up with in-house-made C18 stagetips.

Mass spectrometry was performed as previously described [32]. Peptides were separated on a 30-cm pico-tip column (75 µm ID, New Objective) and were packed in-house with 3 µm aquapur gold C-18 material (Dr. Maisch) using a 140-min gradient (7–80% ACN 0.1% FA), delivered by an easy-nLC 1000 (LC120, Thermo Scientific), and electro-sprayed directly into an Orbitrap Fusion Tribrid Mass Spectrometer (Thermo Scientific). Raw files were analyzed with the MaxQuant software version 1.5.2.8 with oxidation of methionine, alkylation with N-ethylmaleimide and carbamidomethylation set as variable modifications. The Human protein database of UniProt was searched with both the peptide as well as the protein false discovery rate set to 1%. Downstream analysis was done using R version 4.0.2.

A SummarizedExperiment object was created using LFQ data from the MaxQuant proteinGroups file and corresponding protein information. Proteins were filtered for reverse hits and standard contaminants. Next, we selected proteins that were identified with three or more unique peptides and were measured in at least one sample in 2 or more replicates. Data was log_2-transformed and normalized using quantile normalization, which ensures overall intensity differences due to IP efficiency differences between samples are equalized while maintaining identical statistical distributions. ProDA model fitting was performed using sample names as design input and the number of proteins in the data as the number of subsamples. To test for differential protein abundance, the proDa fit object was used for comparing wild-type against mutant TIPRL or H_2O_2-treated against control conditions.

Stable Isotope Labelling by Amino acids in Cell Culture (SILAC) and Phosphopeptide Enrichment

U2OS cells were grown in SILAC medium containing DMEM without arginine and lysine (PAA), supplemented with mM L-glutamine (Lonza, BE17-605E) and 100 U/mL penicillin-streptomycin (Lonza, DE17-602E), 10% dialized FBS (Gibco), 73µg/mL light/K0 (Sigma) or heavy/K8 (Sigma or Silantes) L-Lysine and 29.4µg/mL light/R0 (Sigma) or heavy/R0 (Sigma or Silantes) L-arginine. Labelling efficiency was confirmed >95%. After transfection and treatments, cells were washed twice with cold PBS. Cells were lysed in a buffer containing 8M Urea, 1M Ammonium Bicarbonate, 40mM CAA, 10mM TCEP and phosphatase inhibitor cocktail 2 and 3 (both Sigma-Aldrich). Lysates were boiled to 95°C for 5 minutes, cooled on ice for 15 minutes, and sonicated using a probe sonicator (Heilscher) for 30 seconds at 70% amplitude/0.5 cycle. Samples were heated to 95°C for 5 minutes and cooled on ice for 15 minutes again, then samples were diluted four times with a 2M Ammonium Bicarbonate solution. Heavy and light lysates were mixed 1:1 (as determined

using the Bradford Protein Assay, Bio-Rad). Samples were digested overnight at 37°C with Lys-C (Promega). Phosphopeptides were enriched using TiO2 as described in [41]. A second phosphopeptide enrichment was performed with TiO2 beads on C8 stagetips made in-house.

Mass spectrometry was performed as follows: peptides were separated on a 30 cm column (75 µm ID fused silica capillary with emitter tip (New Objective)) packed with 3 µm aquapur gold C-18 material (dr. Maisch) using a 140-minute gradient (7% to 80% ACN 0.1% FA), delivered by an easy-nLC 1000 (Thermo). Peptides were electro-sprayed directly into a Thermo Scientific Orbitrap Fusion Tribrid Mass Spectrometer and analyzedin Top Speed data dependent mode with the resolution of the full scan set at 240000 and an intensity threshold of 5000 ions. Most intense ions were isolated by the quadrupole and fragmented with a HCD collision energy of 30%. The maximum injection time of the iontrap was set to 35 milliseconds.

Mass spectrometry data was processed using MaxQuant and further analyzed using Perseus 1.5.5.3 and and R. Sites were filtered for potential contaminants and reverse identification. SignA values were calculated, phosphosites with SignA values smaller than 0.05 are considered significant. Sites were filtered for localization precision value > 0.75.

TABLES

Table 1. MSMS data corresponding to Figure 3B: H_2O_2-dependent interactors of CDK4

uniprot ID	gene	protein	log_2 ratio	*p*-value
Q06830	PRDX1	Peroxiredoxin-1	6.6	<0.001
Q5VU66	TPM3	Tropomyosin alpha-3 chain	4.7	0.001
P32119	PRDX2	Peroxiredoxin-2	4.1	0.004
E7EVA0	MAP4	Microtubule-associated protein	3.7	0.011
Q9P258	RCC2	Protein RCC2	3.6	0.006
E9PFM2	RBBP7	Histone-binding protein RBBP7	3.6	0.006
P04406	GAPDH	Glyceraldehyde-3-phosphate dehydrogenase	2.9	<0.001
E7ETK8	AARS	Alanine--tRNA ligase, cytoplasmic	2.6	0.010
E9PHK9	TCOF1	Treacle protein	2.4	0.012
P78417	GSTO1	Glutathione S-transferase omega-1	1.8	0.006

Table 2. Posphorylation site affected by H2O2 - and LEE11 sites in CDK4 knockout sells

uniprot ID	gene	protein	site	log_2 ratio
sites for CDK4KO + H_2O_2 versus CDK4KO				
Q53EU6	AGPAT9	Glycerol-3-phosphate acyltransferase 3	S68	3.3
P18031	PTPN1	Tyrosine-protein phosphatase non-receptor type 1	S50	3.3
Q13085	ACACA	Acetyl-CoA carboxylase 1	S80	2.6
P42345	MTOR	Serine/threonine-protein kinase mTOR	S1261	2.5
O75592-2	MYCBP2	E3 ubiquitin-protein ligase MYCBP2	S3440	2.4
F6RU81	ELMSAN1	ELM2 and SANT domain-containing protein 1	T628	2.3
B3KSY4	hCG_1787779	Coronin	S245	2.3
F6RU81	ELMSAN1	ELM2 and SANT domain-containing protein 1	S636	2.2
Q8WW12	PCNP	PEST proteolytic signal-containing nuclear protein	S77	2.2
Q13546-2	RIPK1	Receptor-interacting serine/threonine-protein kinase 1	S274	2.2
C9JXL3	SLC4A7	Sodium bicarbonate cotransporter 3	S255	2.1
Q9H8S9	MOB1B	MOB kinase activator 1B	T35	1.9
C9JXL3	SLC4A7	Sodium bicarbonate cotransporter 3	S258	1.9
F5GXJ4	STIM2	Stromal interaction molecule 2	S748	1.9
O60716-5	CTNND1	Catenin delta-1	S352	1.7
F8VRZ2	MAPKAPK5	MAP kinase-activated protein kinase 5	S15	1.7
P30622-2	CLIP1	CAP-Gly domain-containing linker protein 1	S143	1.6
C9K0J5	RAPH1	Ras-associated and pleckstrin homology domains-containing protein 1	S623	1.6
Q9Y580	RBM7	RNA-binding protein 7	S136	1.6
Q01082	SPTBN1	Spectrin beta chain, non-erythrocytic 1	T2187	1.6
H0Y4W2	TRRAP	Transformation/transcription domain-associated protein	S1799	1.6
B1AMS2	38961	Septin-6	T418	1.5
C9J167	PMS2	Mismatch repair endonuclease PMS2	S495	1.5
P12270	TPR	Nucleoprotein TPR	T2137	1.5
F5H6Z0	CDK17	Cyclin-dependent kinase 17	S39	1.4
Q9UNI6	DUSP12	Dual specificity protein phosphatase 12	S335	1.4
Q9BXB4	OSBPL11	Oxysterol-binding protein-related protein 11	S189	1.4
B4DDG8	PARN	Poly(A)-specific ribonuclease PARN	S496	1.4
C9J167	PMS2	Mismatch repair endonuclease PMS2	S497	1.4
Q86YV5	SGK223	Tyrosine-protein kinase SgK223	S694	1.4
Q9UQ35	SRRM2	Serine/arginine repetitive matrix protein 2	S2692	1.4
Q15208	STK38	Serine/threonine-protein kinase 38	S264	1.4
E7ENL7	TRAPPC12	Trafficking protein particle complex subunit 12	S167	1.4
Q9UPN4-3	CEP131	Centrosomal protein of 131 kDa	S47	1.3
Q9H4G0-4	EPB41L1	Band 4.1-like protein 1	S467	1.3
Q9H307	PNN	Pinin	S66	1.3
F5H774	RTN3	Reticulon-3	S204	1.3
Q6IN85-4	SMEK1	Serine/threonine-protein phosphatase 4 regulatory subunit 3A	S498	1.3
Q6IN85-4	SMEK1	Serine/threonine-protein phosphatase 4 regulatory subunit 3A	S502	1.3
Q9UHR4	BAIAP2L1	Brain-specific angiogenesis inhibitor 1-associated protein 2-like protein 1	S331	1.2
Q96B23-2	C18orf25	Uncharacterized protein C18orf25	S67	1.2
G8JL86	COBLL1	Cordon-bleu protein-like 1	S371	1.2
O75420	GIGYF1	PERQ amino acid-rich with GYF domain-containing protein 1	S862	1.2
Q15154-2	PCM1	Pericentriolar material 1 protein	S93	1.2
Q01082	SPTBN1	Spectrin beta chain, non-erythrocytic 1	T2328	1.2
Q9H1K0	ZFYVE20	Rabenosyn-5	S226	1.2

Q9H1K0	ZFYVE20	Rabenosyn-5	S226	1.2
P49674	CSNK1E	Casein kinase I isoform epsilon	S354	1.1
E9PG60	IQSEC1	IQ motif and SEC7 domain-containing protein 1	S75	1.1
B7Z6Y0	MELK	Maternal embryonic leucine zipper kinase	S142	1.1
Q9BXB4	OSBPL11	Oxysterol-binding protein-related protein 11	S174	1.1
Q2KHR3-2	QSER1	Glutamine and serine-rich protein 1	S376	1.1
Q13573	SNW1	SNW domain-containing protein 1	S224	1.1
P53814-5	SMTN	Smoothelin	S523	1.0
P08559-3	PDHA1	Pyruvate dehydrogenase E1 component subunit alpha, somatic form, mitochondrial	S269	-2.3
Q6PCE3	PGM2L1	Glucose 1,6-bisphosphate synthase	S175	-1.8
O75179-2	ANKRD17	Ankyrin repeat domain-containing protein 17	S1939	-1.3
Q8WUF5	PPP1R13L	RelA-associated inhibitor	S84	-1.3
Q8TER5-4	ARHGEF40	Rho guanine nucleotide exchange factor 40	T371	-1.2
Q8WUF5	PPP1R13L	RelA-associated inhibitor	S280	-1.2
Q8WUF5	PPP1R13L	RelA-associated inhibitor	S81	-1.2
C9K0X4	ABLIM1	Actin-binding LIM protein 1	S382	-1.1
C9J2I0	AGFG1	Arf-GAP domain and FG repeat-containing protein 1	T99	-1.1
P08559-3	PDHA1	Pyruvate dehydrogenase E1 component subunit alpha, somatic form, mitochondrial	S201	-1.1
P39023	RPL3	60S ribosomal protein L3	S13	-1.1
P42677	RPS27L	40S ribosomal protein S27	S78	-1.0
sites for CDK4KO + H_2O_2 versus CDK4KO + H_2O_2 + LEE011				
F5H6G1	RB1	Retinoblastoma-associated protein	S834	5.0
F5H564	EIF4G3	Eukaryotic translation initiation factor 4 gamma 3	S760	1.9
P50750-2	CDK9	Cyclin-dependent kinase 9	S464	1.7
H0YLX2	RFX7	DNA-binding protein RFX7	S321	1.4
O15014	ZNF609	Zinc finger protein 609	S1055	1.2
F5H6Z0	CDK17	Cyclin-dependent kinase 17	S39	1.1

Table 3. Phosphoproteomics data corresponding to Figures 3C-D : H_2O_2 - and LEE11-affected sites in CDK6 knockout cells

uniprot ID	gene	protein	site	log_2 ratio
tes for CDK6 KO H_2O_2 versus CDK6 KO				
18031	PTPN1	Tyrosine-protein phosphatase non-receptor type 1	S50	2.3
13085	ACACA	Acetyl-CoA carboxylase 1	S80	2.1
42345	MTOR	Serine/threonine-protein kinase mTOR	S1261	2.0
9Y580	RBM7	RNA-binding protein 7	S136	1.8
13546-2	RIPK1	Receptor-interacting serine/threonine-protein kinase 1	S274	1.8
6RU81	ELMSAN1	ELM2 and SANT domain-containing protein 1	T628	1.6
9BXB4	OSBPL11	Oxysterol-binding protein-related protein 11	S174	1.5
6RU81	ELMSAN1	ELM2 and SANT domain-containing protein 1	S636	1.4
7ER32	MKL1	MKL/myocardin-like protein 1	S312	1.4
5VW31	NFIB	Nuclear factor 1	S12	1.4
7EWM1	NCOA2	Nuclear receptor coactivator 2	S771	1.3
8VXY0	HNRNPA1	Heterogeneous nuclear ribonucleoprotein A1	S95	1.2
7EPK0	LIMCH1	LIM and calponin homology domains-containing protein 1	S334	1.2
96RT1-6	ERBB2IP	Protein LAP2	S872	1.1
9JXL3	SLC4A7	Sodium bicarbonate cotransporter 3	S258	1.1
08559-3	PDHA1	Pyruvate dehydrogenase E1 component subunit alpha, somatic form, mitochondrial	S269	-2.4
6PCE3	PGM2L1	Glucose 1,6-bisphosphate synthase	S175	-1.5
19338	NCL	Nucleolin	T121	-1.4
08559-3	PDHA1	Pyruvate dehydrogenase E1 component subunit alpha, somatic form, mitochondrial	S201	-1.4
8TEV9-2	SMCR8	Smith-Magenis syndrome chromosomal region candidate gene 8 protein	S498	-1.4
8TER5-4	ARHGEF40	Rho guanine nucleotide exchange factor 40	T371	-1.3
8WUF5	PPP1R13L	RelA-associated inhibitor	S84	-1.3
9UJU6	DBNL	Drebrin-like protein	S274	-1.2
C9J2I0	AGFG1	Arf-GAP domain and FG repeat-containing protein 1	S101	-1.1
sites for CDK6 KO + H_2O_2 versus CDK6 KO + H_2O_2 + LEE011				
Q9UKE5-2	TNIK	TRAF2 and NCK-interacting protein kinase	S519	1.4
Q13555-6	CAMK2G	Calcium/calmodulin-dependent protein kinase type II subunit gamma	S321	1.3
Q96PK6	RBM14	RNA-binding protein 14	S520	1.3
Q13555-6	CAMK2G	Calcium/calmodulin-dependent protein kinase type II subunit gamma	S320	1.2
Q9BXB5	OSBPL10	Oxysterol-binding protein-related protein 10	S199	1.2
Q9BXB5	OSBPL10	Oxysterol-binding protein-related protein 10	S201	1.1

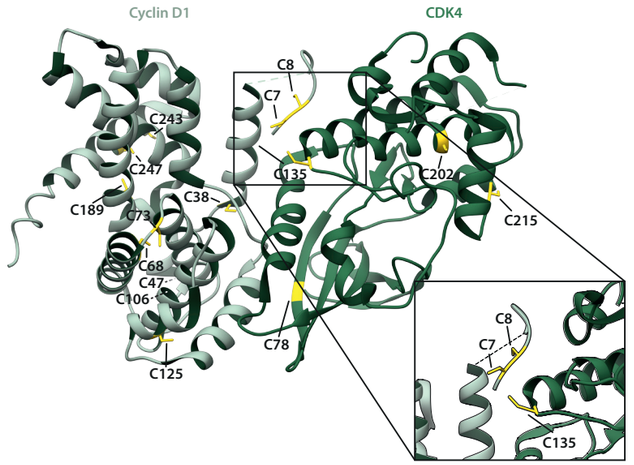

Figure S1. Crystal structure of CDK4 in complex with cyclin D1.
Crystal structure of CDK4 in complex with cyclin D1 (PDB ID: 2W96) visualized using UCSF Chimera, including an enlargement of part of the binding interface between CDK4 and cyclin D1. The four CDK4 cysteines 78, 135, 202 and 215 and cyclin D cysteines 7, 8, 38, 47, 68, 73, 106, 125, 189, 239, 243, and 247 are indicated in yellow. C285 of cyclin D is not present in the crystal structure, dashed lines are cysteines not clearly visible in this angle of representation.

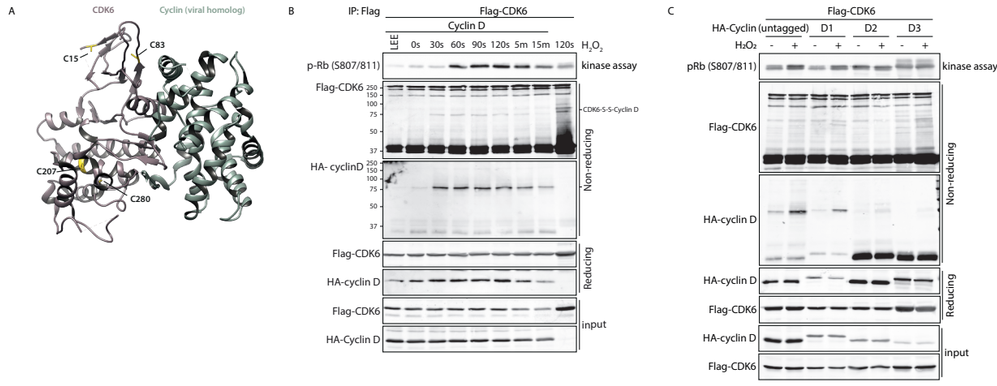

Figure S2. *(figure legend continues on next page)*
(**A**) Crystal structure of CDK6 in complex with a viral cyclin (PDB ID: 1JOW) visualized using UCSF Chimera. CDK6 cysteines 15, 83, 207 and 280 are indicated in yellow. C7 and C306 of CDK6 is not present in the crystal structure. (**B**) Parallel reducing and non-reducing SDS-PAGE and western blot analysis (WB) of Flag-CDK6 immunoprecipitates (IP) and a complementary *in vitro* kinase assay using recombinant GST-Rb as a substrate. Flag-CDK6 and cyclin D1 were expressed in 293T cells and exposed to 200 μM of H_2O_2 for the indicated time. CDK6 and cyclin D form an intermolecular disulfide-dependent complex upon exposure to H_2O_2, and migrate as a single band under non-reducing conditions. The H_2O_2-induced complex between CDK6 and cyclin D is induced within 30 seconds of H_2O_2 treatment, and decreases after 5 minutes of H_2O_2 treatment. (**C**) Cells expressing Flag-CDK6 and HA-cyclin D1, D2 or D3 were subjected to H_2O_2 for 2 minutes before Flag-CDK6 immunoprecipitation and *in vitro* kinase assay. Samples were analyzed under non-reducing and reducing conditions.

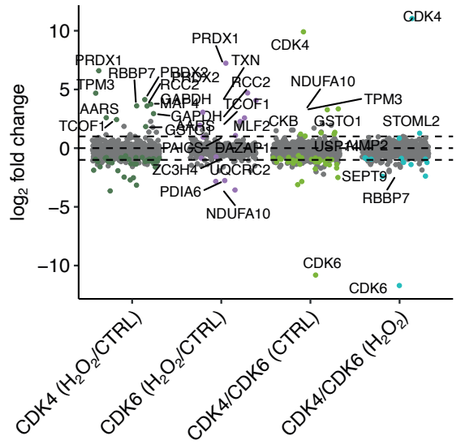

Figure S3
Scatter plot of the mass spectrometry data from cells expressing Flag-CDK4 or Flag-CDK6, showing the $\log_2$ fold change of proteins in H_2O_2 treated cells versus untreated control for the first two conditions, or CDK4 versus CDK6 in the last 2 conditions. Colored dots represent proteins with a p-value < 0.05 as calculated using inference of protein differential abundance by probabilistic dropout analysis (proDA). Horizontal dotted lines are positioned at $\log_2$ fold change of 1 and -1 (i.e. a 2-fold change).

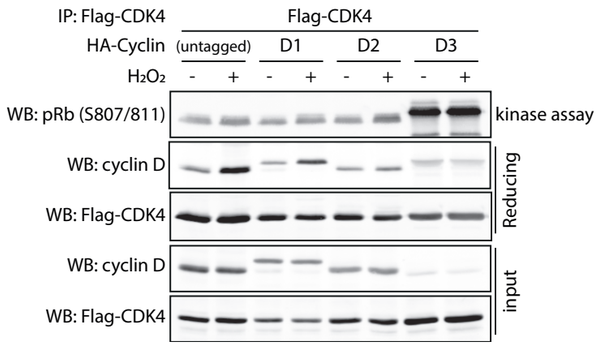

Figure S4
Parallel reducing and non-reducing SDS-PAGE and western blot analysis (WB) of Flag-CDK4 immunoprecipitates (IP) and a complementary *in vitro* kinase assay using recombinant GST-Rb as a substrate. 293T cells expressing Flag-CDK4 and HA-cyclin D1, D2 or D3 were and exposed to 200 μM of H_2O_2 2 minutes. Kinase activity of CDK4 in complex with cyclin D3 is greatly enhanced compared to cyclins D1 and D2.

REFERENCES

1. Malumbres, M.; Barbacid, M. To Cycle or Not to Cycle: A Critical Decision in Cancer. *Nat Rev Cancer* **2001**, *1*, 222–231, doi:10.1038/35106065.
2. Pardee, A.B. A Restriction Point for Control of Normal Animal Cell Proliferation. *Proc National Acad Sci* **1974**, *71*, 1286–1290, doi:10.1073/pnas.71.4.1286.
3. Meloche, S.; Pouysségur, J. The ERK1/2 Mitogen-Activated Protein Kinase Pathway as a Master Regulator of the G1- to S-Phase Transition. *Oncogene* **2007**, *26*, 3227–3239, doi:10.1038/sj.onc.1210414.
4. Yang, H.W.; Chung, M.; Kudo, T.; Meyer, T. Competing Memories of Mitogen and P53 Signalling Control Cell-Cycle Entry. *Nature* **2017**, *549*, 404–408, doi:10.1038/nature23880.
5. Heldt, F.S.; Barr, A.R.; Cooper, S.; Bakal, C.; Novák, B. A Comprehensive Model for the Proliferation–Quiescence Decision in Response to Endogenous DNA Damage in Human Cells. *Proc National Acad Sci* **2018**, *115*, 201715345, doi:10.1073/pnas.1715345115.
6. Spiller, D.G.; Wood, C.D.; Rand, D.A.; White, M.R.H. Measurement of Single-Cell Dynamics. *Nature* **2010**, *465*, 736–745, doi:10.1038/nature09232.
7. Hanahan, D.; Weinberg, R.A. Hallmarks of Cancer: The next Generation. *Cell* **2011**, *144*, 646 674, doi:10.1016/j.cell.2011.02.013.
8. Burhans, W.C.; Heintz, N.H. The Cell Cycle Is a Redox Cycle: Linking Phase-Specific Targets to Cell Fate. *Free Radical Bio Med* **2009**, *47*, 1282 1293, doi:10.1016/j.freeradbiomed.2009.05.026.
9. Amponsah, P.S.; Yahya, G.; Zimmermann, J.; Mai, M.; Mergel, S.; Mühlhaus, T.; Storchova, Z.; Morgan, B. Peroxiredoxins Couple Metabolism and Cell Division in an Ultradian Cycle. *Nat Chem Biol* **2021**, 1–8, doi:10.1038/s41589-020-00728-9.
10. Huang, B.K.; Ali, S.; Stein, K.T.; Sikes, H.D. Interpreting Heterogeneity in Response of Cells Expressing a Fluorescent Hydrogen Peroxide Biosensor. *Biophys J* **2015**, *109*, 2148–2158, doi:10.1016/j.bpj.2015.08.053.
11. Dennery, P.A. Oxidative Stress in Development: Nature or Nurture? *Free Radical Bio Med* **2010**, *49*, 1147–1151, doi:10.1016/j.freeradbiomed.2010.07.011.
12. Sarsour, E.H.; Kumar, M.G.; Chaudhuri, L.; Kalen, A.L.; Goswami, P.C. Redox Control of the Cell Cycle in Health and Disease. *Antioxid Redox Sign* **2009**, *11*, 2985–3011, doi:10.1089/ars.2009.2513.
13. Shi, T.; Dansen, T.B. Reactive Oxygen Species Induced P53 Activation: DNA Damage, Redox Signaling, or Both? *Antioxid Redox Sign* **2020**, *33*, 839–859, doi:10.1089/ars.2020.8074.
14. Hornsveld, M.; Feringa, F.M.; Krenning, L.; Berg, J. van den; Smits, L.M.M.; Nguyen, N.B.T.; Rodríguez-Colman, M.J.; Dansen, T.B.; Medema, R.H.; Burgering, B.M.T. A FOXO-Dependent Replication Checkpoint Restricts Proliferation of Damaged Cells. *Cell Reports* **2021**, *34*, 108675, doi:10.1016/j.celrep.2020.108675.
15. Vurusaner, B.; Poli, G.; Basaga, H. Tumor Suppressor Genes and ROS: Complex Networks of Interactions. *Free Radical Bio Med* **2012**, *52*, 7–18, doi:10.1016/j.freeradbiomed.2011.09.035.
16. Lennicke, C.; Cochemé, H.M. Redox Regulation of the Insulin Signalling Pathway. *Redox Biol* **2021**, *42*, 101964, doi:10.1016/j.redox.2021.101964.
17. Goldkorn, T.; Balaban, N.; Matsukuma, K.; Chea, V.; Gould, R.; Last, J.; Chan, C.; Chavez, C. EGF-Receptor Phosphorylation and Signaling Are Targeted by H2O2 Redox Stress. *Am J Resp Cell Mol* **1998**, *19*, 786–798, doi:10.1165/ajrcmb.19.5.3249.
18. Burch, P.M.; Heintz, N.H. Redox Regulation of Cell-Cycle Re-Entry: Cyclin D1 as a Primary Target for the Mitogenic Effects of Reactive Oxygen and Nitrogen Species. *Antioxid Redox Sign* **2005**, *7*, 741–751, doi:10.1089/ars.2005.7.741.
19. Lee, S.-R.; Kwon, K.-S.; Kim, S.-R.; Rhee, S.G. Reversible Inactivation of Protein-Tyrosine Phosphatase 1B in A431 Cells Stimulated with Epidermal Growth Factor*. *J Biol Chem* **1998**, *273*, 15366–15372, doi:10.1074/jbc.273.25.15366.
20. Frijhoff, J.; Dagnell, M.; Godfrey, R.; Östman, A. Regulation of Protein Tyrosine Phosphatase Oxidation in Cell Adhesion and Migration. *Antioxid Redox Sign* **2014**, *20*, 1994–2010, doi:10.1089/ars.2013.5643.
21. Matsushime, H.; Roussel, M.F.; Sherr, C.J. Novel Mammalian Cyclins (CYL Genes) Expressed during G1. *Cold Spring Harb Sym* **1991**, *56*, 69–74, doi:10.1101/sqb.1991.056.01.010.
22. Matsushime, H.; Roussel, M.F.; Ashmun, R.A.; Sherr, C.J. Colony-Stimulating Factor 1 Regulates Novel Cyclins during the G1 Phase of the Cell Cycle. *Cell* **1991**, *65*, 701–713, doi:10.1016/0092-8674(91)90101-4.
23. Matsushime, H.; Ewen, M.E.; Strom, D.K.; Kato, J.-Y.; Hanks, S.K.; Roussel, M.F.; Sherr, C.J. Identification and Properties of an Atypical Catalytic Subunit (P34PSK-J3/Cdk4) for Mammalian D Type G1 Cyclins. *Cell* **1992**, *71*, 323–334, doi:10.1016/0092-8674(92)90360-o.
24. Latimer, H.R.; Veal, and E.A. Peroxiredoxins in Regulation of MAPK Signalling Pathways; Sensors and Barriers to Signal Transduction. *Mol Cells* **2016**, *39*, 40 45, doi:10.14348/molcells.2016.2327.
25. Putker, M.; Vos, H.R.; Dorenmalen, K. van; Ruiter, H. de; Duran, A.G.; Snel, B.; Burgering, B.M.T.; Vermeulen, M.; Dansen, T.B. Evolutionary Acquisition of Cysteines Determines FOXO Paralog-Specific Redox Signaling. *Antioxid Redox Sign* **2015**, *22*, 15 28, doi:10.1089/ars.2014.6056.
26. Day, P.J.; Cleasby, A.; Tickle, I.J.; O'Reilly, M.; Coyle, J.E.; Holding, F.P.; McMenamin, R.L.; Yon, J.; Chopra, R.; Lengauer, C.; et al. Crystal Structure of Human CDK4 in Complex with a D-Type Cyclin. *Proc National Acad Sci* **2009**, *106*, 4166 4170, doi:10.1073/pnas.0809645106.
27. Tchakarska, G.; Sola, B. The Double Dealing of Cyclin D1. *Cell Cycle* **2019**, *19*, 1–16, doi:10.1080/15384101.2019.1706903.

28. Mullany, L.K.; White, P.; Hanse, E.A.; Nelsen, C.J.; Goggin, M.M.; Mullany, J.E.; Anttila, C.K.; Greenbaum, L.E.; Kaestner, K.H.; Albrecht, J.H. Distinct Proliferative and Transcriptional Effects of the D-Type Cyclins in Vivo. *Cell Cycle* **2008**, *7*, 2215–2224, doi:10.4161/cc.7.14.6274.

29. Ely, S.; Liberto, M.D.; Niesvizky, R.; Baughn, L.B.; Cho, H.J.; Hatada, E.N.; Knowles, D.M.; Lane, J.; Chen-Kiang, S. Mutually Exclusive Cyclin-Dependent Kinase 4/Cyclin D1 and Cyclin-Dependent Kinase 6/Cyclin D2 Pairing Inactivates Retinoblastoma Protein and Promotes Cell Cycle Dysregulation in Multiple Myeloma. *Cancer Res* **2005**, *65*, 11345–11353, doi:10.1158/0008-5472.can-05-2159.

30. Kato, J.; Matsushime, H.; Hiebert, S.W.; Ewen, M.E.; Sherr, C.J. Direct Binding of Cyclin D to the Retinoblastoma Gene Product (PRb) and PRb Phosphorylation by the Cyclin D-Dependent Kinase CDK4. *Gene Dev* **1993**, *7*, 331–342, doi:10.1101/gad.7.3.331.

31. Lundberg, A.S.; Weinberg, R.A. Functional Inactivation of the Retinoblastoma Protein Requires Sequential Modification by at Least Two Distinct Cyclin-Cdk Complexes. *Mol Cell Biol* **1998**, *18*, 753–761, doi:10.1128/mcb.18.2.753.

32. Putker, M.; Madl, T.; Vos, H.R.; Ruiter, H. de; Visscher, M.; Berg, M.C.W. van den; Kaplan, M.; Korswagen, H.C.; Boelens, R.; Vermeulen, M.; et al. Redox-Dependent Control of FOXO/DAF-16 by Transportin-1. *Mol Cell* **2013**, *49*, 730 742, doi:10.1016/j.molcel.2012.12.014.

33. Nelson, D.A.; Krucher, N.A.; Ludlow, J.W. High Molecular Weight Protein Phosphatase Type 1 Dephosphorylates the Retinoblastoma Protein*. *J Biol Chem* **1997**, *272*, 4528–4535, doi:10.1074/jbc.272.7.4528.

34. Kato, J.Y.; Matsuoka, M.; Strom, D.K.; Sherr, C.J. Regulation of Cyclin D-Dependent Kinase 4 (Cdk4) by Cdk4-Activating Kinase. *Mol Cell Biol* **1994**, *14*, 2713–2721, doi:10.1128/mcb.14.4.2713.

35. Stöcker, S.; Maurer, M.; Ruppert, T.; Dick, T.P. A Role for 2-Cys Peroxiredoxins in Facilitating Cytosolic Protein Thiol Oxidation. *Nat Chem Biol* **2017**, *14*, doi:10.1038/nchembio.2536.

36. Dam, L. van; Pagès-Gallego, M.; Polderman, P.E.; Es, R.M. van; Burgering, B.M.T.; Vos, H.R.; Dansen, T.B. The Human 2-Cys Peroxiredoxins Form Widespread, Cysteine-Dependent- and Isoform-Specific Protein-Protein Interactions. *Antioxidants* **2021**, *10*, 627, doi:10.3390/antiox10040627.

37. Wang, H.; Nicolay, B.N.; Chick, J.M.; Gao, X.; Geng, Y.; Ren, H.; Gao, H.; Yang, G.; Williams, J.A.; Suski, J.M.; et al. The Metabolic Function of Cyclin D3–CDK6 Kinase in Cancer Cell Survival. *Nature* **2017**, *546*, 426 430, doi:10.1038/nature22797.

38. Anders, L.; Ke, N.; Hydbring, P.; Choi, Y.J.; Widlund, H.R.; Chick, J.M.; Zhai, H.; Vidal, M.; Gygi, S.P.; Braun, P.; et al. A Systematic Screen for CDK4/6 Substrates Links FOXM1 Phosphorylation to Senescence Suppression in Cancer Cells. *Cancer Cell* **2011**, *20*, 620 634, doi:10.1016/j.ccr.2011.10.001.

39. Göbl, C.; Morris, V.K.; Dam, L. van; Visscher, M.; Polderman, P.E.; Hartlmüller, C.; Ruiter, H. de; Hora, M.; Liesinger, L.; Birner-Gruenberger, R.; et al. Cysteine Oxidation Triggers Amyloid Fibril Formation of the Tumor Suppressor P16INK4A. *Redox Biol* **2019**, 101316, doi:10.1016/j.redox.2019.101316.

40. Álvarez-Fernández, M.; Malumbres, M. Mechanisms of Sensitivity and Resistance to CDK4/6 Inhibition. *Cancer Cell* **2020**, *37*, 514–529, doi:10.1016/j.ccell.2020.03.010.

41. Urbaniak, M.D.; Martin, D.M.A.; Ferguson, M.A.J. Global Quantitative SILAC Phosphoproteomics Reveals Differential Phosphorylation Is Widespread between the Procyclic and Bloodstream Form Lifecycle Stages of Trypanosoma Brucei. *J Proteome Res* **2013**, *12*, 2233–2244, doi:10.1021/pr400086y.

CHAPTER 7

GENERAL DISCUSSION

GENERAL DISCUSSION

Redox signaling is a crucial mechanism for cells to maintain homeostasis. The underlying basis for redox signaling is the reversible oxidation of specific protein thiols, which can alter protein functionality, activity and availability for protein-protein interactions by inducing conformational changes. Downstream effects include modulation of phosphorylation pathways, altered gene expression by activation or inhibition of transcription factors, regulation of cell cycle progression, energy metabolism, cytoskeletal organization and ion transport, and is therefore considered a major cell signaling mechanism [1–4]. A more oxidizing cellular environment due to increased levels of reactive oxygen species (ROS) leads to the reversible oxidation of cysteine thiols in proteins to a sulfenic acid (-SOH). Sulfenic acids are generally transient intermediates, that, upon condensation form a disulfide with a nearby thiol, and hence covalently links two cysteine side chains. A decreased reducing power can lead to the prolonged existence of these disulfides [5].

Although rapid advances are made in detecting thiol oxidation [6,7], determination of oxidative modifications on cysteines is a challenging task given the short lifetime of and similarities between several of the cysteine oxidation states. In addition, most detection methods are based on differential alkylation techniques before and after reduction, which is unsuitable to distinguish different reversible modifications. These limitations are part of the reason that disulfide-mediated complexes are underexplored. The goal of the research described in this thesis is to understand molecular mechanisms that underlie redox signal propagation and how changes in the cellular redox state affect signaling pathways. In chapter 2, we studied how the oxidation of proteins is achieved both efficiently and specifically. In chapters 3, 4 and 6 of this thesis, we explored several signaling pathways that proceed through the reversible oxidation of cysteine residues. Finally, in chapters 4 and 5 we examined how redox regulation can affect protein aggregation. These themes will contribute understanding the various kinds of redox signaling mechanisms and their relative contributions cellular signaling and homeostasis.

REACTIVITY AND SPECIFICITY IN REDOX SIGNALING

As discussed extensively in this thesis, the reversible oxidation of proteins downstream of H_2O_2 is considered a major cell signaling mechanism. There are numerous examples of signaling pathways that proceed through the reversible oxidation of cysteine residues, of which we described several in chapters 3, 4 and 6. It has been difficult to explain how H_2O_2 as a second messenger achieves the reactivity (i.e. how it reacts with low abundant targets) and specificity (i.e. reacting with specific thiols on specific proteins) required for proper signal transduction (see also Figure 5 in chapter 1).

Firstly, most protein thiols in general have been found to have a low reactivity with H_2O_2 [8,9]. On top of that, the two cytosolic PRDXs (PRDX1 and PRDX2) are expected to scavenge more than 99% of cytosolic H_2O_2 [10]. Together with the abundance and reactivity of GPXs and other peroxidases, most H_2O_2 is converted or cleared at rates that are hard to beat [11–13]. This means that cysteine thiols in H_2O_2 effector proteins are generally outcompeted by peroxiredoxins for the reaction with H_2O_2.

Thirdly, H_2O_2 is undoubtedly an inherently unspecific oxidant because it lacks complexity, and it is poorly understood how H_2O_2 causes the oxidation of specific redox-sensitive proteins in particular pathways in the context of virtually limitless potential targets in a cell. Any redox-regulated signal transduction protein should be able to react selectively despite the competition of extremely reactive enzymes like peroxiredoxins. Only this will ensure the signal specificity required for the proper response to a certain stimulus [13].

There are several proposed explanations for this problem, which are not mutually exclusive [5]. These models are elaborately discussed in the first chapter of this thesis (General Introduction). For some proteins it has been shown that the poor reactivity-based disadvantage can be overcome by a 'redox relay' in which peroxiredoxins (or other peroxidases) initially react with H_2O_2 and then oxidize a target [14–19]. In chapter 2, we explored this peroxiredoxin-based relay on a proteome-wide scale, and investigated whether it provides the required reactivity and specificity for cysteine-oxidation based redox signaling. As mentioned, mammalian cells express five 2-cys peroxiredoxin isoforms, each with their own localization, oxidation kinetics and structural differences around their catalytic sites. Widespread peroxiredoxin-based redox relay could therefore not only explain the reactivity but could also grant selectivity in H_2O_2-dependent redox signaling.

We show that the different 2-cys peroxiredoxin isoforms indeed participate in the formation of such mixed disulfide intermediates, and that they each have their own subset of targets.

Oxidized peroxiredoxins could in principle relay oxidizing equivalents to other thiols via two molecular mechanisms: C_P-SOH and C_P-S-S-C_R-mediated (Figure 1, left). Our results suggest that there are large differences between peroxiredoxin isoforms in terms of their preferred relay mechanisms, allowing for a layer of specificity. The percentage of C_P-S-S-C_R-mediated binders ranges from 21% to 16% for PRDX2 and PRDX3, 44% and 58% for PRDX1 and PRDX4, and, as much as 73% of PRDX5, respectively. The preference for either mechanism might come from different oxidation kinetics between peroxiredoxin isoforms. For example, the rate constant for disulfide formation is 13 s^{-1} for PRDX1 and only 0.6 s^{-1} for PRDX2, resulting in a longer lifetime of the PRDX2 sulfenic acid. Different sensitivities to overoxidation also underlie persistence of the C_P-SOH [20]. A longer C_P-SOH lifetime allows peroxiredoxins to react with a different set of protein thiols involving the C_P-SOH mechanism, whereas a longer lifetime of the disulfide would promote interaction with via the C_P-S-S-C_R-mediated mechanism. It is likely one of the underlying causes for the differences in the preferred mechanism between isoforms, as reflected in the percentage of C_P-S-S-C_R-mediated interactors.

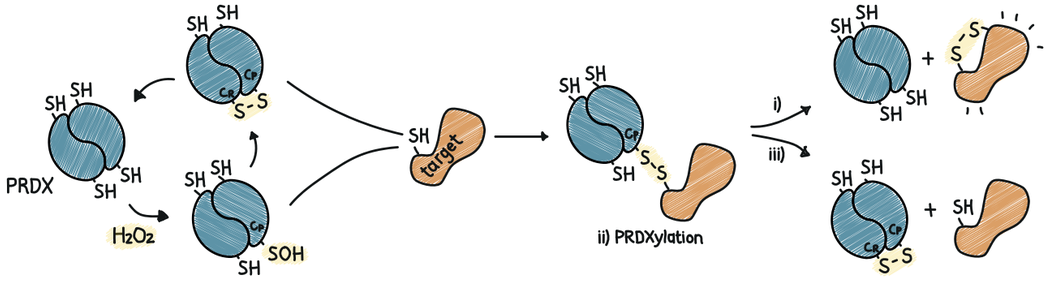

Figure 1. Possible outcomes of the intermolecular disulfide formation between a peroxiredoxin and a target protein.
i) The disulfide is resolved via a disulfide exchange reaction with another nearby cysteine from the target protein (complex), forming an intra- or intermolecular disulfide bond in the target protein and leaving peroxiredoxin in a reduced state. **ii)** The intermolecular disulfide between the peroxiredoxin and its target protein is the final product, representing a novel post-translational modification (PTM) on cysteine which we call 'S-peroxiredoxinylation' (S-PRDXylation). The disulfide can still take part in a disulfide exchange reaction with the peroxiredoxin resolving cysteine (C_R), thereby reducing the target and forming the canonical disulfide C_P-S-S-C_R. **iii)** The recycling of the PRDXylated target protein could require the TRX system.

Peroxiredoxins are predicted to switch from mostly reduced to mostly oxidized within a very narrow range of H_2O_2 concentrations [20]. Since each peroxiredoxin isoform has a unique combination of rate constants for each step in the peroxiredoxin catalytic cycle (sulfenic acid formation, sulfenic acid condensation and disulfide reduction), it is possible that peroxiredoxin isoforms switch from mostly reduced to mostly oxidized at distinct peroxide concentrations. The accumulation of C_P-SOH and C_P-S-S-C_R at distinct concentrations of H_2O_2 per peroxiredoxin isoform may differentially modulate H_2O_2-mediated redox signaling.

Another layer of specificity of PRDX1-5 interactors might result from amino acids surrounding the cysteine in a target protein. As C_P-SOH and C_P-S-S-C_R are structurally distinct, the local environment of an interacting cysteine could determine whether an interaction is favorable. Likewise, the local amino acid composition around the peroxiredoxin catalytic center might influence the affinity for targets. In **chapter 2**, we explore possible differences in the local amino acid composition of peroxiredoxin targets separated by their interaction mechanism and by the peroxiredoxin isoform they interact with.

Our mass-spectrometry data also suggest that different peroxiredoxin isoforms interact with each other in a cysteine-dependent manner. The nature of these interactions in terms of their cysteine-dependency and macromolecular composition is not entirely clear. It is possible that peroxiredoxins form multimeric complexes involving two different monomeric isoforms forming form heterodimeric complexes, or perhaps a homodimer interacting with another monomeric isoform. Since peroxiredoxins interact with a diverse set of proteins, including many redox relay target proteins, thioredoxin (TRX) and glutathione S-transferase pi (πGST, for PRDX6, an isoform that is structurally similar to PRDX1-5) it is possible that a heterodimeric peroxiredoxin complex has yet another subset of target proteins [21,22]. Although further work needs to be carried out to elucidate the nature of these interactions, this could further expand the repertoire of peroxiredoxin-based redox signaling.

So far, the end-product of peroxiredoxin-dependent cysteine oxidation is unknown. There are multiple possible outcomes following the intermolecular disulfide formation between a peroxiredoxin and a target protein (**Figure 1**). These include:

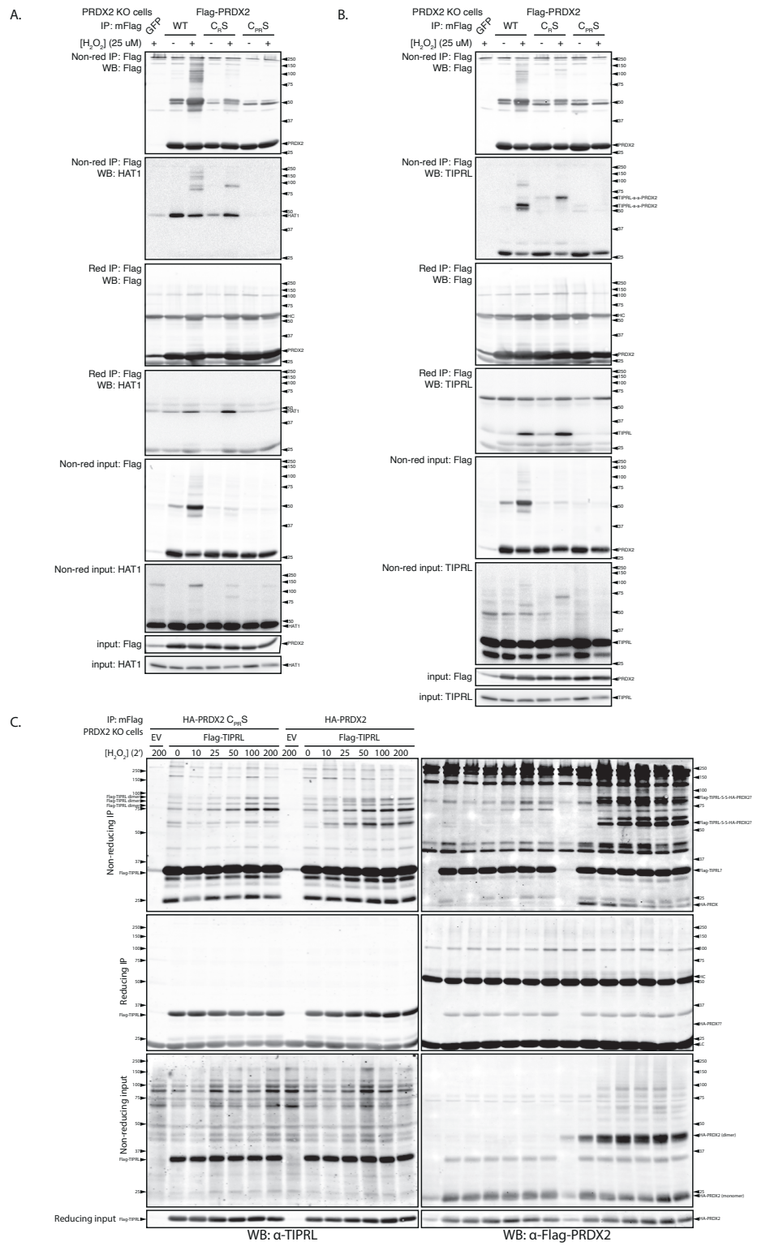

Figure 2. *(figure legend continues on next page)*
A) The interaction between PRDX2 and its binding partner histone acetyltransferase 1 (HAT1). PRDX2 knockout 293T cells were transfected with Flag-PRDX2 and cysteines mutants. Oxidizing conditions induce a mass shift of a fraction of PRDX2. Parallel reducing and non-reducing SDS-PAGE and western blot analysis (WB) of Flag-PRDX2 immunoprecipitations (IP). Cells were incubated with 25 μM of H_2O_2 for 2 minutes where indicated. Under non-reducing conditions, HAT1 shows a H_2O_2 induced mass-

shift. This mass-shift is less pronounced in conditions with PRDX2 cysteine mutants, and is lost when samples are analyzed under reducing conditions. **B)** interaction between PRDX2 and its binding partner TIPRL. PRDX2 knockout cells were transfected with Flag-PRDX2 and cysteines mutants as in A). Oxidizing conditions induce a mass shift of a fraction of PRDX2. Parallel reducing and non-reducing SDS-PAGE and western blot analysis (WB) of Flag-PRDX2 immunoprecipitations (IP). Cells were incubated with 25 μM of H_2O_2 for 2 minutes where indicated. Under non-reducing conditions, PRDX2 is able to form several disulfide-dependent heterodimers with TIPRL upon stimulation with H_2O_2, as indicated by a mass-shift. This mass-shift is less not there in conditions with PRDX2 cysteine mutants, and is lost when samples are analyzed under reducing conditions. **C)** TIPRL and PRDX2 oxidation kinetics. PRDX2 knockout cells were transfected with HA-PRDX2 and cysteines mutants, and Flag-TIPRL. Cells were incubated with different concentrations of H_2O_2 for 2 minutes as indicated, before harvesting and analysis of samples under reducing and non-reducing conditions. There is no clear difference in the extent of TIPRL disulfide formation in the presence or absence of PRDX2.

i) The disulfide is resolved via a disulfide exchange reaction with another nearby cysteine in the target protein (complex), forming an intra- or intermolecular disulfide bond in the target protein and releasing peroxiredoxin in a reduced state. This has been shown for the relay between PRDX2 and STAT3 [16].
ii) The intermolecular disulfide between the peroxiredoxin and its target protein is the final product, representing a novel post-translational modification (PTM) on cysteine which we refer to as 'S-peroxiredoxinylation' (S-PRDXylation). Like other PTMs, S-PRDXylation could alter the target protein's conformation, protein function, activity, etc. Alternatively, PRDXylation might protect proteins from undesired (thiol) oxidation. Besides a role as a post-translational modification impacting the function of specific proteins, widespread PRDXylation could in principle also serve as a redox buffer. Importantly, the mixed disulfide between peroxiredoxin and the PRDXylated target protein can still take part in a disulfide exchange reaction with the peroxiredoxin resolving cysteine (C_R), thereby reducing and releasing the target and forming the canonical disulfide C_P-S-S-C_R.
iii) The recycling of the PRDXylated target protein could require the TRX system. If this is the case, the use of TRX-based disulfide exchange interactions as a readout for protein thiol oxidation as used in ref. [17] can not distinguish between PRDXylated proteins and disulfide bonds in proteins as described under i).

Of note, our mass spectrometry-based screen does not distinguish between these different types of end-products described above. The possible outcomes of the peroxiredoxin-based redox relay described above are not mutually exclusive and may act in parallel. In an attempt to characterize a few peroxiredoxin interactors, we investigated the interaction between PRDX2 and its binding partner histone acetyltransferase 1 (HAT1). In PRDX2-deficient cells, restoring PRDX2 levels with wild-type PRDX2 induces HAT1 oxidation in the form of disulfides, as described in i) (**Figure 2A**, non-reducing input). Similar behavior was observed for mutant PRDX2-C_RS, albeit to a lesser extent, but addback of PRDX2-C_{PR}S barely induces HAT1 disulfide formation. This suggests that PRDX2 facilitates HAT1 disulfide formation, and that the relay intermediate between PRDX2 and HAT1 is resolved via a disulfide exchange reaction with another nearby cysteine, resulting in the formation of intermolecular HAT1 disulfide bonds, according to the scenario described above at i).

We found that PRDX2 is able to form several disulfide-dependent heterodimers with TIPRL upon stimulation with H_2O_2 (**Figure 2B**). However, we did not observe differences in the extent of TIPRL disulfide formation in the presence or absence of active peroxiredoxins. This suggests that the interaction between TIPRL and PRDX2 does not result in additional disulfide bonds in TIPRL, and that TIPRL is PRDXylated by PRDX2 as described in iii). Interestingly, even though the oxidation of TIPRL is not catalyzed by a PRDX2-dependent relay, TIPRL forms disulfide-dependent dimers with similar kinetics as peroxiredoxins (**Figure 2C**). Despite the strong redox-regulated interaction between PRDX2 and TIPRL, it is of course possible that TIPRL oxidation is catalyzed by other peroxiredoxin isoforms.

An important implication of a redox relay is that it allows redox signaling to gradually change into oxidative damage with increasing H_2O_2 levels. As described in section B), the floodgate model suggests that both redox signaling and random oxidative damage do not occur until H_2O_2 levels are high enough to cause overoxidation of peroxiredoxins. In other words, redox signaling and random oxidative damage would occur approximately simultaneously, after the hyperoxidation of peroxiredoxins. This is in contrast to peroxiredoxin-based redox relays, which can only take place when peroxiredoxins are catalytically active and not hyperoxidized. H_2O_2-dependent signaling would thus occur at concentrations below those required for overoxidation of peroxiredoxins. At higher [H_2O_2], peroxiredoxin overoxidation would thus inactivate redox signaling and change H_2O_2 from a signaling to a damaging agent. Peroxiredoxin-based redox relays thus allow for a concentration-dependent H_2O_2 effect in which redox signaling precedes oxidative damage.

Interestingly, it has been shown that oxidized glutaredoxins (GRX) can also be reduced by target proteins such as the rxYFP-Grx1p and Grx1-roGFP2 fusion protein-based redox probes as well as peroxiredoxins [23–25]. This could be described as a GRX-based redox relay, analogous with a PRDX-based redox relay.

It should also be noted that all typical post-translational modifications (PTMs) are controlled by enzymes that catalyze the addition of the PTM, but also by enzymes that catalyze the inverse reaction; the removal of the PTM. For example, protein phosphorylation is catalyzed by kinases whereas phosphatases catalyze dephosphorylation reactions. It seems obvious that also thiol oxidation is controlled bidirectionally in order to function in signaling [5,26]. Assuming that is also the case for peroxiredoxin-based redox relays, there should be enzymes that actively remove oxidative modifications from peroxiredoxin target proteins.

We find a fair number of proteins in our screen that interact with specific peroxiredoxin isoforms independent of the peroxiredoxin catalytic cysteines (**chapter 2**). The specific set of binders per peroxiredoxin isoform led us to hypothesize that some of these could function as adaptor proteins that facilitate the peroxiredoxin-based redox relay. Adaptor proteins have been shown to be involved in peroxidase-dependent redox relays. For example, the PRDX2-STAT3 redox relay has recently been shown to depend on association with the membrane-associated scaffold protein ANXA2 [27]. Likewise, Orp1-dependent Yap1 oxidation is dependent on the presence of the adapter protein Ybp1, shielding oxidized Orp1 from reduction [28,29]. Scaffold proteins may recruit target proteins and bring them in close proximity to peroxiredoxins, before peroxiredoxins react with H_2O_2 to form C_P-SOH and C_P-S-S-C_R (**Figure 3E**). Alternatively, redox relay targets and peroxiredoxins may form scaffold dependent complexes prior to peroxiredoxin oxidation, facilitating efficient transfer of oxidizing equivalents directly upon oxidation. A scaffold protein would not only increase the chances that a peroxiredoxin finds a target, but could also provide another means of achieving specificity, coming from the interaction of specific peroxiredoxin isoforms (and their targets) with specific adaptors for the relay of oxidation to subsets of target proteins.

REDOX CONTROL OF CELLULAR SIGNALING

TIPRL

Redox-dependent inactivation of protein tyrosine phosphatases is known to facilitate growth factor signaling upon the activation of growth factor receptors, allowing for sustained phosphorylation-mediated signaling [30,31]. In **chapter 3**, we identified the protein phosphatase 2A (PP2A)-regulatory protein TIPRL (TOR signaling pathway regulator-like; TOR: Target of rapamycin) as a redox-sensor. A slightly more oxidizing cellular redox state rapidly causes the oxidation of cysteines C14 and C87, upon which TIPRL forms three differentially linked homodimers with a disulfide between C14-C14, C87-C87 or C14-C87. Our preliminary experiments suggest that the redox-dependent homodimerization

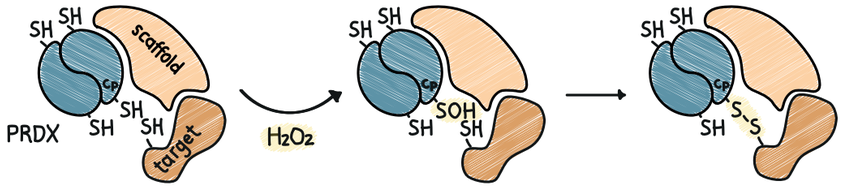

Figure 3.
Scaffold proteins may recruit target proteins and bring them in close proximity to peroxiredoxins, before peroxiredoxins react with H_2O_2 to form C_P-SOH and C_P-S-S-C_R. Alternatively, redox relay targets and peroxiredoxins may form scaffold dependent complexes prior to peroxiredoxin oxidation, facilitating efficient transfer of oxidizing equivalents directly upon oxidation.

of TIPRL might play a role in its regulation of PP2A-C and downstream PP2A targets mTORC1 and PKB.

Although the reversible oxidation of the catalytic cysteine of protein tyrosine phosphatases has emerged as a mechanism of activity regulation, the Ser/Thr phosphatase PP2A does not contain a catalytic cysteine. Nevertheless, PP2A is redox regulated in several manners. For example, the cysteines 266 and 269 of PP2A, comprising a potentially redox -active CXXC-motif, have been shown to be sensitive to oxidation, resulting in the inhibition of PP2A catalytic activity [32,33]. Furthermore, H_2O_2 has been shown to inhibit PP2A catalytic activity by increased levels of oxidized glutathione (GSSG), suggesting that PP2A can be glutathionylated [34]. In contradiction with these studies, it was reported that PP2A is activated rather than inactivated in response to H_2O_2, leading to the dephosphorylation of the Rb, p130 and p107 pocket proteins [35]. Finally, hypoxia is also thought to influence PP2A activity, although depending on the context, this may lead to either activation or inactivation of phosphatase activity [36–38]. In all cases, however, the exact nature of the modifications and the mechanism underlying PP2A (in)activation requires further research.

We described in **chapter 3** that TIPRL is required for resistance to prolonged exposure to oxidants. However, the ability of TIPRL to resolve redox stress is not dependent on its oxidation and subsequent dimerization. It was suggested that TIPRL can function as a scaffold protein mediating the interaction of PP2A with MKK7, thereby inhibiting TRAIL-induced apoptosis [39]. Investigating the role of TIPRL in redox stress resistance in the light of MKK7 regulation could be a direction for future work.

Our results suggest that oxidized TIPRL is more potent at inhibiting PP2A catalytic function even though we were unable to find a direct role downstream of the oxidation of TIPRL. Moreover, TIPRL-bound PP2A was described to lack A- and B- subunits *in vitro* [40], which suggests a mechanism for reduced phosphatase activity. The selective (dis)assembly of the PP2A holoenzyme could allow for target-specific redox regulation of PP2A phosphatase activity. Furthermore, rather than affecting PP2A-C catalytic activity in general, oxidation of TIPRL may affect pathways downstream of PP2A in different ways. This is in line with the literature discussed above (reviewed in ref. [41]), which suggests a context-dependent effect of a more oxidizing cellular environment on PP2A activity. This potentially allows fine-tuning of PP2A-mediated activity by separating dephosphorylation events regulated by the redox state from those that are not. Notwithstanding the requirement for further studies, we hypothesize that the redox sensitivity of TIPRL may facilitate and fine-tune the redox regulation of PP2A.

Redox Control of the G1-S Cell Cycle Transition

The transition of the G1 to S phase of the cell cycle is under control of the closely related CDK4 and CDK6, both of which depend on the D-type cyclins for activity and can be inactivated by $p16^{INK4A}$.

In **chapter 4**, we described how mild oxidizing conditions can cause the oxidation of the only cysteine in the $p16^{INK4A}$ tumor suppressor, resulting in its disulfide-dependent homodimerization. This triggers a dramatic structural rearrangement, resulting in the formation of amyloid-like aggregates (termed 'oxaggregation') and its inactivation as a CDK4/6 inhibitor. In **chapter 6**, we described how cysteine C135 of cyclin-dependent kinase 4 (CDK4) is subject to oxidation, leading to the formation of a covalently linked complex with its classical interaction partner cyclin D, as well as increased kinase activity of the complex.

It is possible that both processes complement each other, i.e. the oxidation-dependent inactivation of $p16^{INK4A}$ as well as -activation of CDK4-cyclin D potentially result in the phosphorylation of Rb, thereby releasing the E2F1 transcription factor and thus stimulating cells to progress from G1 to S.

Whether, how and in which situations these two mechanisms complement each other, is still unclear. $P16^{INK4A}$ is an important cell cycle regulator and tumor suppressor and its expression in healthy cycling cells is normally low. Accumulation of $p16^{INK4A}$ is a marker for senescence and aging that is induced upon several types of cellular stress, ensuring a cell cycle arrest under those conditions, thus preventing cell cycle progression under unfavorable circumstances and/or of damaged cells. As a result, loss of $p16^{INK4A}$ function, or loss of downstream Rb, are one of the most frequent markers of oncogenic transformation [42]. Although the CDK4-cyclin D complex is associated with proliferation, CDK4-cyclin D in complex with $p21^{CIP1}$ also accumulates in senescent cells [43–46]. Since senescent cells also exhibit elevated $p16^{INK4A}$ levels, it is thus possible that the redox regulation of the $p16^{INK4A}$ and the CDK4-cyclin D pathways might converge in senescent cells. Interestingly, the p21-CDK4-cyclin D complexes are functionally active in senescent cells, yet Rb is in a hypophosphorylated state, suggesting that kinase activity is directed at a substrate other than Rb in the context of senescence [47,48]. In other words, the reactivation of CDK4 in senescent cells could affect different CDK4 substrates than Rb and affect CDK4 signaling in a different manner. On the other hand, CDK4 is expressed more broadly than $p16^{INK4A}$, suggesting that the redox regulation of CDK4-cyclin D is more ubiquitous than that of $p16^{INK4A}$. Of course, in our experiments for both the oxidation of $p16^{INK4A}$ and the oxidation of CDK4-cyclin D, not all of the total $p16^{INK4A}$/CDK4-cyclin D protein pool is oxidized, leaving a fraction for 'canonical' regulation. This could also be a possible explanation for why $p16^{INK4A}$ is still functional as a cell-cycle inhibitor after treating cells with oxidants (see **Figure S1**, **chapter 4**). Although we did find evidence that CDK4/6 is reactivated upon oxidation of $p16^{INK4A}$, and that this partially relieves E2F1 repression, we did not find evidence of perturbation of the S-phase checkpoint in additional cell-cycle analysis experiments using flow cytometry and video time-lapse microscopy (data not shown). The reactivation of CDK4/6 that we observed might therefore not be strong enough for full re-entry of the cell cycle under the tested conditions, but we cannot exclude that this might occur in other situations. Additionally, treatment with oxidizing agents also inhibits the cell cycle through several other pathways, possibly obscuring cell cycle re-entry downstream of $p16^{INK4A}$ oxidation. For example, oxidizing conditions activate p53 through the p38-MAPK pathway, thereby triggering a p53-dependent cell cycle arrest and cell death [49].

In this sense, a comparison can be drawn with the regulation of signaling by protein phosphorylation. The direct effects of phosphatase activity depend on the phosphorylation state within the cell. In other words, a phosphatase can dephosphorylate its targets only if they are available, which depends on the kinases that are active within a system, This can result in different effects of increased phosphatase activity between cell types. For example, the SHP2 tyrosine phosphatase is shown to act as a tumor suppressor in hepatocytes, whereas

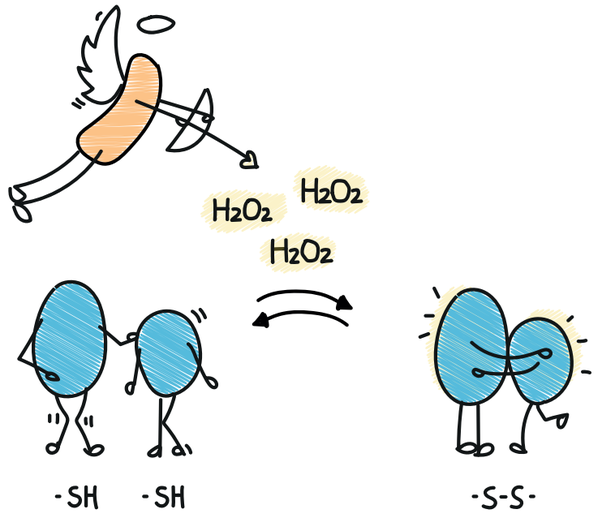

Figure 4. Disulfides can serve as molecular staples that direct and crosslink pre-existing protein complexes.

it is thought to promote tumorigenesis in monocytes [50,51], and this may stem from a differential phosphorylated crucial target in these cells. Likewise, cell type, redox status, p16-expression, ROS type, cell cycle phase, and much more will likely dictate the effect of $p16^{INK4A}$ oxaggregation.

We can only speculate if and why cells require CDK4/6 (re) activation and cell cycle progression in oxidizing conditions (in cells expressing $p16^{INK4A}$). The observation that $p16^{INK4A}$ is highly prone to oxidation even under physiological levels of H_2O_2 may suggest that $p16^{INK4A}$ oxaggregation plays a role under mild oxidative conditions. This would be in good agreement with a large body of literature on how low levels of ROS can dramatically increase the rate of proliferation, even though this is not in the context of high $p16^{INK4A}$ levels (reviewed in refs [1,52]). Exposing cells to prolonged or high levels of H_2O_2 caused by perturbations of the redox balance triggers the activation of cell cycle checkpoints and cell cycle arrest, thus leading to the opposite effect.

Together, it is possible that the oxidation of cell cycle regulators ensures the fine-tuning of the redox control of the cell cycle. One might imagine that, as a prerequisite for proliferation, ROS stimulate cell cycle entry though the activation of CDK4-cyclin D and inactivation of $p16^{INK4A}$. As the cell cycle progresses, it is important that ROS do not exceed concentrations that might cause random damage and oxidative distress. When they do exceed the physiological levels, cell cycle checkpoints are activated and the cell cycle is halted. Complementary redox-regulated mechanisms that might play a role in fine-tuning the redox control of the cell cycle are the ROS-dependent activation of the p53 tumor suppressor, activation of the G1/S checkpoint and the ROS-induced arrest in S phase via PP2A-dependent pRB dephosphorylation [53]. The adequate calibration of the cell cycle machinery in light of the redox state is crucial for an appropriate response to changes in ROS levels. For example, it is possible that cells require low levels of ROS to enter the cell cycle and stimulate proliferation, but at the same time require the reducing power to prevent proliferation. This would ensure a 'break' on the cell cycle if the reducing capacity of the cell is inadequate. This could prevent potentially hazardous levels of ROS can jeopardize the proper progression of the cell cycle, leading to for instance oncogenic mutations or a permanent cell cycle arrest. This is a more common concept in biology. For example, the Myc transcription factor activates proliferation as well as apoptosis, only stimulates proliferation if specific signals block the apoptotic pathway [54]. In this line of reasoning, it can be assumed that the oxidation-mediated inactivation of $p16^{INK4A}$ and -activation of CDK4-cyclin D could be part of a larger mechanism that adjusts the cell cycle so that it exclusively proceeds under favorable redox conditions.

Interestingly, tumor cells are characterized by increased levels of ROS [55], meaning that both $p16^{INK4A}$ and CDK4-cyclin D are more often in the oxidized state, thereby promoting proliferation of cancer cells. Whether the redox regulation of $p16^{INK4A}$ and/or CDK4-cyclin D indeed contribute to cancer progression remains to be addressed. As discussed in chapter 1, the single cysteine in $p16^{INK4A}$ is likely acquired recently in terms of evolution, and was substituted thereafter multiple times in several branches of mammalian evolution. This supports the hypothesis that there is evolutionary pressure against the redox dependent inactivation of $p16^{INK4A}$.

The non-covalent interaction between CDK4 and cyclin D is well established. It may well serve as the starting point for the covalent interaction between CDK4-cyclin D, in which the preassembled complex is poised for oxidation and covalent interaction through disulfide bond formation. There is an increasing number of examples that suggest that a pre-existing protein complex can become covalentltly linked in this manner, thereby stabilizing an otherwise weak interaction or three-dimensional conformation. This context, the disulfide bond is functioning as a 'molecular staple' (**Figure 4**). For example, disulfides are thought to crosslink the pre-existing complex between the FOXO4 transcription factor and the nuclear import factor Transportin 1 (TNPO1), which is required for nuclear import and activation of FOXO4 by increased oxidizing conditions [56]. To what extent this is a general mechanism in redox-regulated pathways is unclear and is an issue that should be addressed in further research. Moreover, the potential role for scaffold proteins in facilitating these interactions should be examined.

CROSSTALK BETWEEN REDOX SIGNALING AND PROTEIN HOMEOSTASIS

High levels of ROS can lead to random damage to proteins, including protein unfolding and aggregation, processes that have been associated with aging. As discussed, low levels of H_2O_2 act as an essential second messenger and are associated with healthy cell physiology [57]. In **chapter 5**, we discussed how these seemingly opposite effects of H_2O_2 as a signaling molecule and H_2O_2 as a driver of age-related protein aggregation can be united in one hypothesis [57,58]. In an attempt to regain homeostasis, age-related damage might trigger stress response pathways that partially depend on redox signaling, and thus are accompanied by the production of H_2O_2 as a signaling molecule. Gradually, more damage accumulates, again accompanied by a further increase in H_2O_2 levels to boost the stress response pathways. As a result, H_2O_2 levels accumulate and lead to ROS-associated damage. This creates a vicious cycle, in which ROS-dependent damage triggers redox-dependent stress-response pathways which in turn lead to more ROS production. We discuss many examples of the interplay between redox signaling and protein stability.

A question that emerges from this overview is whether altered redox signaling is a cause or consequence of protein aggregation, and whether the vicious cycle described above applies also here. It is clear that there is a complex relationship between ROS, redox signaling and proteostasis. Whereas protein oxidation can trigger aggregation, increases in H_2O_2 production upon the gradual accumulation of aggregates might be a stress response by itself. A small change in redox state or aggregation can in this way rapidly lead to a feed-forward loop, making redox-regulated protein aggregation an irreversible process.

In **chapter 4**, we described how $p16^{INK4A}$ can form fibrils under physiological conditions, triggered by oxidation of the single cysteine residue and subsequent S-S-dependent homodimerization. We present evidence that $p16^{INK4A}$ can form

aggregates that have the typical features of amyloid fibrils, including the binding of diagnostic dyes, presence of a cross-β sheet structure, and typical dimensions found in EM. To our knowledge, this is the first report of the critical dependence on a reversible disulfide cross-linked dimer as a subunit for fibril formation, which highlights the role of the cellular redox state as an important regulator of fibril formation.

From a structural point of view, it is interesting to identify the starting point for the redox-induced conformational changes of $p16^{INK4A}$, i.e. is sulfenylation of C72 sufficient for $p16^{INK4A}$ aggregation, or is disulfide formation required to induce β-amyloid formation? The starting point for conformational changes could provide insights for other proteins that possibly follow this mechanism, for example the availability of a secondary cysteine to allow for disulfide formation can be a determining factor in case disulfide formation is required. A major difficulty in answering this question is that it is nearly impossible to separate -S-S- from -SOH in an experimental setting, since disulfide formation is always preceded by sulfenylation. In an attempt to answer this question nonetheless, we collaborated with Agnieszka Bronowska (Newcastle University) who performed *in silico* simulations of how different C72 oxidation states affect $p16^{INK4A}$ conformational stability using all-atom and steered molecular dynamics (MD) simulations and constant force pulling simulations and metadynamics. Both non-oxidized ($p16^{INK4A}$-SH) $p16^{INK4A}$ as well as glutathionylated $p16^{INK4A}$ ($p16^{INK4A}$-SSG) maintain their secondary structure when challenged with mechanical forces (data not shown). In accordance, the NMR structure of $p16^{INK4A}$-SSG showed no signs of aggregation (**Figure 2A** in **chapter 4**), GSHylation indeed prevented amyloid formation. However, when sulfenylated $p16^{INK4A}$ ($p16^{INK4A}$-SOH) or $p16^{INK4A}$-hydrazine (an adduct of diamide before disulfide formation) was used in the simulations, fewer residues maintained their secondary structure compared to $p16^{INK4A}$-SH or -SSG, and more residues adopted a β-sheet structure. Furthermore, residues 67-115 within the normally α-helical core structure of $p16^{INK4A}$ are the first to change their conformation following the sulfenylation of $p16^{INK4A}$, as suggested also by the algorithms used for prediction of aggregation prone regions (**Figure S9A** in **chapter 4**). The alpha-helix in this region contains two adjacent valine residues V95, V96, which are considered thermodynamically less favorable in alpha-helices due to steric hindrance [59]. Indeed, V96 seems especially important in this conformational change, since its *in silico* mutation into alanine (V96A) maintains a high number of structured residues. Whether this residue is indeed important in $p16^{INK4A}$ oxaggregation, and whether mutant $p16^{INK4A}$-V96A is indeed resistant to oxaggregation needs to be examined in an experimental setup. But it is striking to note that, like also observed for the single cysteine at position 72, several vertebrate species including mammals have changes in V95, V96 or both, that are more favorable in helices. Although speculative, these adaptations could be a means to omit redox-dependent aggregation of $p16^{INK4A}$.

It is possible that the oxaggregation of $p16^{INK4A}$ is initiated through a peroxiredoxin-catalyzed redox relay leading to $p16^{INK4A}$ C72 oxidation. We have made a start to investigate the effect of peroxiredoxins on the aggregation of $p16^{INK4A}$, and we tested whether tethering of PRDX1 to $p16^{INK4A}$ affects its oxidation-induced aggregation. HEK293T cells expressing Flag-tagged PRDX1 WT and catalytic dead mutant $C_{PR}S$ tethered to $p16^{INK4A}$ were exposed to oxidants and processed for a filter trap assay for the detection of protein aggregates in cell extracts (see also the scheme in **Figure 5A** in **chapter 4**). The tethering of $p16^{INK4A}$ to PRDX1 together with exposure to H_2O_2 drastically increases the trapping of $p16^{INK4A}$ on the filter membrane, indicative of protein aggregation (**Figure 5A**). This seems dependent on the oxidation by H_2O_2 as well as the catalytic activity of PRDX1, as mutation of the PRDX1 catalytic cysteines diminishes filter trapping. This is in contrast with the reported chaperone function of peroxiredoxins (discussed below), and this preliminary experiment suggests that PRDX1 promotes $p16^{INK4A}$ aggregation in a H_2O_2- and cysteine-dependent manner. $P16^{INK4A}$ aggregation is dependent on oxidation and dimerization (**chapter 4**). Therefore, although we do not clearly observe dimer formation of $p16^{INK4A}$ when tethered to PRDX1, this experiment also

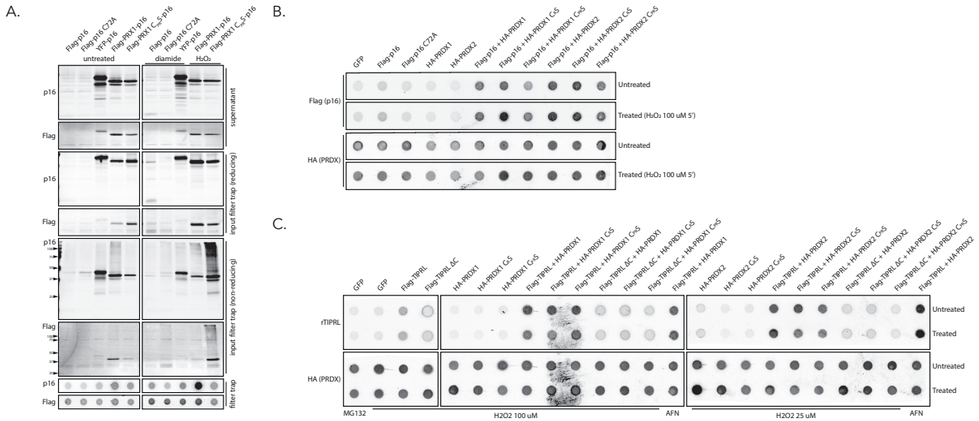

Figure 5. The effect of peroxiredoxins on the aggregation of $p16^{INK4A}$.
A) Tethering $p16^{INK4A}$ to PRDX1 and exposure to H_2O_2 increases the trapping of $p16^{INK4A}$ on the filter trap membrane. Flag-$p16^{INK4A}$, YFP-$p16^{INK4A}$ and Flag-PRDX1 tethered to $p16^{INK4A}$ were expressed in 293T cells knockout for PRDX1 and PRDX2, and treated with 250 μM diamide or 100 μM H_2O_2. Samples were analyzed under parallel reducing and non-reducing conditions and subjected to a filter trap assay. Due to low expression of Flag-p16 constructs, Flag-p16 dimerization is not detectable and Flag-p16 is only detected on the filter trap membrane. Equal amounts of protein were used as input for the filter trap assay. **B)** Co-expression of HA-PRDX1 and HA-PRDX2 with Flag-p16 and exposure to H_2O_2 increases the trapping of $p16^{INK4A}$ on the filter trap membrane. **C** The recycling of the PRDXylated target protein could require the TRX system. Co-expression of Flag-TIPRL with HA-PRDX1 or HA-PRDX2 also promote the aggregation of TIPRL.

suggests that PRDX1 promotes $p16^{INK4A}$ oxidation. Of note, the cysteine mutant of PRDX1 tethered to p16 results in a smear on the SDS-PAGE (non-reducing input), but there is no increase in filter trapping in these conditions. This could be an indication for unfolding and random intermolecular disulfide formation of this protein.

$P16^{INK4A}$ aggregation is also affected by PRDX2 in a cysteine-dependent manner, and also occurs when peroxiredoxin is co-expressed rather than tethered to $p16^{INK4A}$ (**Figure 5B**). This observation is supported by the identification of $p16^{INK4A}$ as a cysteine-dependent interactor for PRDX2 in our screen in **chapter 2** [21]. Interestingly, co-expression of $p16^{INK4A}$ with the resolving cysteine mutant of peroxiredoxin PRDX2 C_RS, is also capable of promoting aggregation of $p16^{INK4A}$, suggesting that the interaction might proceed via the C_p-SOH mediated mechanism as described in **chapter 2**. Note that these experiments are performed in wild-type HEK293T cells which also express endogenous, wildtype peroxiredoxins, which could obscure mutant-specific effects. Technically, it remains to be verified whether the peroxiredoxin-dependent aggregation of $p16^{INK4A}$ is indeed also dependent on C72 in $p16^{INK4A}$, but the combined observations seem to point in that direction

There are several quality control networks in place to maintain a healthy proteome. These include the clearance of (misfolded) proteins by the ubiquitin-proteasome system (UPS) and autophagy, and chaperone-mediated protein (re)folding. Redox signaling can also regulate proteostasis through the chaperone function of peroxiredoxins. Depending on their redox status as well as post-translational modifications, 2-cys peroxiredoxins are known to oligomerize into a decameric or dodecameric doughnut-like structure [60,61]. For example, PRDX2 was shown to exist in an equilibrium of dimers and decamers in solution, in which the oxidation of PRDX2 by H_2O_2 and subsequent disulfide formation promotes dissociation into dimers, whereas overoxidation of PRDX2 in a

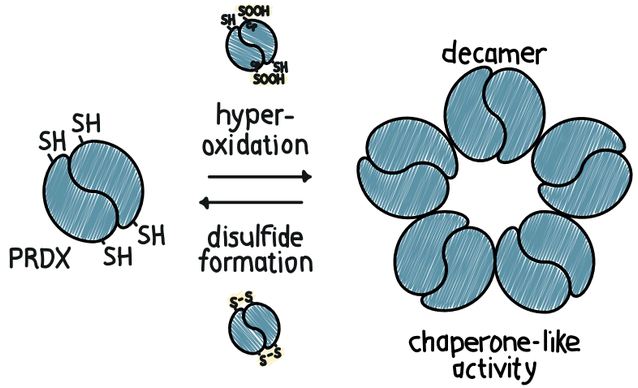

Figure 6. Peroxiredoxins exist in an equilibrium of dimers and decamers in solution.
Decamers have chaperone-like activity. The oxidation of PRDX2 by H_2O_2 and subsequent disulfide formation promotes dissociation into dimers, whereas overoxidation of PRDX2 promotes the formation of the decameric form.

more oxidizing environment promotes the formation of the decameric form (Figure 6) [62,63]. Since a lack in reductive power can likely stabilize existing disulfides but not cause overoxidation of peroxiredoxins (own data, not shown and refs. [64,65]), it is likely that a lack of reductive power results in dissociation into dimers, whereas a more oxidizing environment can cause overoxidation of peroxiredoxins and lead to decameric chaperones. This chaperone structure of 2-cys peroxiredoxins has been shown to inhibit protein aggregation, thus providing a redox-dependent protective mechanism that maintains proteostasis under oxidative stress conditions [66].

The coordinated action of small HSPs is thought to disaggregate amyloid fibrils (chapter 5) [58]. Considering the redox-dependent chaperone function of peroxiredoxins, it is possible that dodecameric peroxiredoxins resolve the aggregation and amyloid formation of $p16^{INK4A}$ in concert with small HSPs. Hypothetically, this could even be linked to the cell cycle, in which low [H_2O_2] causes $p16^{INK4A}$ oxaggregation and possibly reactivation of the cell cycle, whereas high [H_2O_2] promote disaggregation and reactivation of $p16^{INK4A}$ through the chaperone function of peroxiredoxins, thereby blocking the cell cycle. Alternatively, it is possible that $p16^{INK4A}$ is actively oxidized via a redox relay by peroxiredoxins, thereby promoting the oxidation and subsequent β-amyloid formation. Of note, these two hypotheses are not mutually exclusive, as these mechanisms might be activated under distinct redox conditions. Since peroxiredoxins are more often in an overoxidized state in a more oxidizing environment (but not with a lack of reductive capacity), this in turn stimulates the toroid formation and chaperone function of peroxiredoxins [62,63]. It is possible that the chaperone function is only activated upon high levels of H_2O_2 in an attempt to relieve proteotoxic stress. If this is the case, it is possible that oxaggregation is regulated over a range of oxidation states. This could hypothetically even link cell cycle progression to H_2O_2-concentrations: low levels of H_2O_2 could cause peroxiredoxin-mediated oxaggregation and inactivation of $p16^{INK4A}$ and allow cell cycle progression from G1 to S-phase, whereas at higher H_2O_2 levels the peroxiredoxin chaperone function could resolve the $p16^{INK4A}$ aggregates, thereby inducing a cell cycle arrest.

It is unknown whether peroxiredoxin-dependent protein aggregation is a more general feature of peroxiredoxins and involves the aggregation of other proteins besides $p16^{INK4A}$. We therefore examined the effect of PRDX1 and PRDX2 expression on TIPRL, a protein for which there is no evidence that it tends to aggregate. TIPRL aggregation is also promoted by the presence of PRDX1 and PRDX2 in a manner similar to $p16^{INK4A}$, although this does not seem to depend on PRDX catalytic activity (Figure 5C). This preliminary experiment was performed in HEK293T cells that are knockout for PRDX1 and PRDX2 (DKO), suggesting that TIPRL is not able to aggregate without the presence of PRDX1/2. Furthermore, TIPRL aggregation is likely fully dependent on TIPRL cysteines. Interestingly, these findings seem to be in contrast with our earlier findings in Figure 2, in which we showed that TIPRL homodimerization is not dependent on peroxiredoxins. Why aggregation does seem dependent on the presence of peroxiredoxins is not clear from these experiments. A possible explanation for this dependency on peroxiredoxins may be that only the PRDXylated form of TIPRL aggregates. These findings raise the following questions for future research: How widespread is protein oxaggregation?, Which proteins does it affect?, What type of aggregates are formed? Is a peroxiredoxin-dependent redox-relay always involved?

A remarkable, but casual observation is that in our laboratory for a wide selection of proteins, the cysteine mutant constructs seem more difficult to express at high levels than their wild-type counterparts. This is at least the case for most proteins discussed in this thesis – TIPRL, $p16^{INK4A}$, CDK4 and CDK6, and PRDX1-5 as well as other examples from our lab such as p53. There are several possible explanations for this observation. It is possible that proteins can prevent permanent damage as a result of a highly oxidizing environment through the formation of disulfide bonds (for instance through PRDXylation) and thereby prevent their degradation. A prerequisite for this would be that these disulfide bonds are reversible in order to restore normal protein conformation and functionality. Further experimental studies are required to substantiate or reject this hypothesis, or to investigate whether it applies to a subset of redox-sensitive proteins. A first step could be to investigate in silico whether aggregation-prone proteins are depleted or enriched in exposed cysteines, or to investigate the insoluble protein fraction upon an oxidant stimulus using mass spectrometry.

CONCLUDING REMARKS

In this thesis we have presented several signaling pathways that proceed through the reversible oxidation of cysteine residues on the proteins $p16^{INK4A}$, TIPRL, CDK4/CDK6 and cyclin D and PRDX1-5. It is clear that the redox regulation of these proteins contributes to essential cellular functions such as cell cycle arrest, phosphatase signaling, G1-to-S transition and protein stability. For all these proteins mentioned above, it is obvious that context matters a great deal. There are many possible outcomes of H_2O_2-induced cysteine oxidation in many different pathways, which suggests a level of specificity and fine-tuning of the response to changes in the cellular redox environment. The outcome of H_2O_2-dependent signaling may depend on, for example, the strength and source

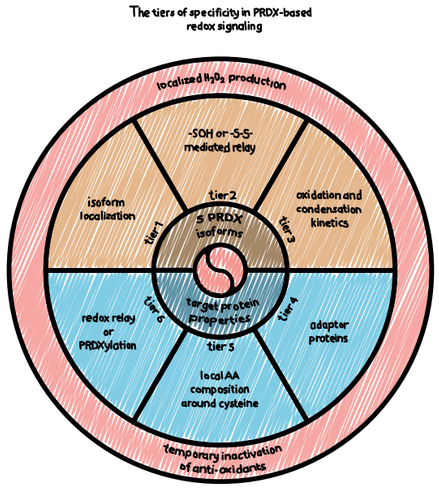

Figure 7. The tiers of PRDX-mediated specificity in H_2O_2-signaling.
Divided in the aspects determined by peroxiredoxins themselves and those determined by target proteins. Independent of peroxiredoxin properties, the localized production of H_2O_2 as well as the floodgate mechanism might contribute to H_2O_2-signaling specificity.

of H_2O_2 generation, its duration, the subcellular location as well as cell state, tissue type, the presence of cofactors, etc. Finetuning the response to redox conditions is of importance since it would ensure cellular integrity. For example, a proper cellular judgement of whether ROS levels are either adequate or too high for cells to enter the cell cycle would contribute to the maintenance of genomic integrity. Although the architecture of many redox-regulated protein networks has been mapped, their dynamic function and integration of different networks often remains unclear. It will be challenging to understand the integration of different redox-regulated networks with respect to their sensitivity to oxidation and the hierarchy in forwarding of signals to execute cell fate decisions.

One approach to tackling such challenges might be to make use of localized, inducible production of H_2O_2 rather than an extracellular bolus of H_2O_2. This can be achieved by targeting the genetically encoded H_2O_2 generating enzyme D-amino acid oxidase (DAAO) to specific sites [67].

H_2O_2 is unequivocally a small molecule without much handles to discriminate what thiols it reacts with, which means that molecular features that can explain sensitivity and selectivity for reacting with H2O2 must be present in its targets in order to achieve specific signal propagation. An enigma in H_2O_2-mediated signaling is how redox regulated proteins are oxidized specifically when their intrinsic reactivity with H_2O_2 is low. Above, we discussed different manners in which this reactivity and specificity could be achieved (summarized in **Figure 7**). Most likely, all mechanisms mentioned play a role to some extent, since examples can be found for all. Additionally, the differential localization of the peroxiredoxin isoforms might contribute to increased scavenging of H_2O_2 in specific compartments to prevent a local H_2O_2 build-up, or alternatively it might ensure a redox-relay to local isoform-specific targets – or both. It is unclear what determines the more dominant mechanism in the case of two seemingly competing ones (such as direct oxidation and peroxiredoxin-based redox relays). Nevertheless, it is clear that peroxiredoxin-based redox regulation is important in cytosolic protein oxidation. Simultaneous deletion of cytosolic PRDX1 and PRDX2 results in a decrease – rather than an increase – of overall cytosolic protein thiol oxidation, which is in agreement with thiol oxidation being predominantly catalyzed by peroxiredoxins [17].

From a pathological viewpoint, the precise role of H_2O_2-mediated thiol oxidation is mostly unknown. Are increased levels of oxidants promoting or protecting against tumorigenesis? Does protein oxidation stimulate or prevent the build-up of toxic protein aggregates? The answer to these questions is beginning to look ambiguous, with examples emerging supporting both sides. For example, the deregulation of peroxiredoxins has been associated with several pathologies [68,69], but it is unclear whether these are due to the pro-oxidative or anti-oxidative function of peroxiredoxins. Nonetheless it would be useful in the future to be able to generate targeted interventions to specific thiol oxidations, more so because of the advantages that come with covalent targeting of substrates.

REFERENCES

1. Burhans, W.C.; Heintz, N.H. The Cell Cycle Is a Redox Cycle: Linking Phase-Specific Targets to Cell Fate. *Free Radical Bio Med* **2009**, *47*, 1282 1293, doi:10.1016/j.freeradbiomed.2009.05.026.
2. Finkel, T. Signal Transduction by Reactive Oxygen Species. *J Cell Biology* **2011**, *194*, 7–15, doi:10.1083/jcb.201102095.
3. Rhee, S.G.; Kil, I.S. Multiple Functions and Regulation of Mammalian Peroxiredoxins. *Annu Rev Biochem* **2017**, *86*, 749 775, doi:10.1146/annurev-biochem-060815-014431.
4. Young, D.; Pedre, B.; Ezeriņa, D.; Smet, B.D.; Lewandowska, A.; Tossounian, M.-A.; Bodra, N.; Huang, J.; Rosado, L.A.; Breusegem, F.V.; et al. Protein Promiscuity in H2O2 Signaling. *Antioxid Redox Sign* **2018**, *30*, 1285–1324, doi:10.1089/ars.2017.7013.
5. Stöcker, S.; Laer, K.V.; Mijuskovic, A.; Dick, T.P. The Conundrum of Hydrogen Peroxide Signaling and the Emerging Role of Peroxiredoxins as Redox Relay Hubs. *Antioxid Redox Sign* **2017**, *28*, 558–573, doi:10.1089/ars.2017.7162.
6. Alcock, L.J.; Perkins, M.V.; Chalker, J.M. Chemical Methods for Mapping Cysteine Oxidation. *Chem Soc Rev* **2018**, *47*, 231–268, doi:10.1039/c7cs00607a.
7. Shi, Y.; Carroll, K.S. Activity-Based Sensing for Site-Specific Proteomic Analysis of Cysteine Oxidation. *Accounts Chem Res* **2020**, *53*, 20–31, doi:10.1021/acs.accounts.9b00562.
8. Winterbourn, C.C. The Biological Chemistry of Hydrogen Peroxide. *Methods Enzymol* **2013**, *528*, 3–25, doi:10.1016/b978-0-12-405881-1.00001-x.
9. Marinho, H.S.; Real, C.; Cyrne, L.; Soares, H.; Antunes, F. Hydrogen Peroxide Sensing, Signaling and Regulation of Transcription Factors. *Redox Biol* **2014**, *2*, 535 562, doi:10.1016/j.redox.2014.02.006.
10. Winterbourn, C.C.; Hampton, M.B. Thiol Chemistry and Specificity in Redox Signaling. *Free Radical Bio Med* **2008**, *45*, 549 561, doi:10.1016/j.freeradbiomed.2008.05.004.
11. Toppo, S.; Flohé, L.; Ursini, F.; Vanin, S.; Maiorino, M. Catalytic Mechanisms and Specificities of Glutathione Peroxidases: Variations of a Basic Scheme. *Biochimica Et Biophysica Acta Bba - Gen Subj* **2009**, *1790*, 1486–1500, doi:10.1016/j.bbagen.2009.04.007.
12. Klug, D.; Rabani, J.; Fridovich, I. A Direct Demonstration of the Catalytic Action of Superoxide Dismutase through the Use of Pulse Radiolysis. *J Biological Chem* **1972**, *247*, 4839–4842.
13. Brigelius-Flohé, R.; Flohé, L. Basic Principles and Emerging Concepts in the Redox Control of Transcription Factors. *Antioxid Redox Sign* **2011**, *15*, 2335–2381, doi:10.1089/ars.2010.3534.
14. Delaunay, A.; Pflieger, D.; Barrault, M.-B.; Vinh, J.; Toledano, M.B. A Thiol Peroxidase Is an H2O2 Receptor and Redox-Transducer in Gene Activation. *Cell* **2002**, *111*, 471–481, doi:10.1016/s0092-8674(02)01048-6.
15. Veal, E.A.; Findlay, V.J.; Day, A.M.; Bozonet, S.M.; Evans, J.M.; Quinn, J.; Morgan, B.A. A 2-Cys Peroxiredoxin Regulates Peroxide-Induced Oxidation and Activation of a Stress-Activated MAP Kinase. *Mol Cell* **2004**, *15*, 129 139, doi:10.1016/j.molcel.2004.06.021.
16. Sobotta, M.C.; Liou, W.; cker, S.S. ouml; Talwar, D.; Oehler, M.; Ruppert, T.; Scharf, A.N.D.; Dick, T.P. Peroxiredoxin-2 and STAT3 Form a Redox Relay for H2O2 Signaling. *Nat Chem Biol* **2014**, *11*, 1 8, doi:10.1038/nchembio.1695.
17. Stöcker, S.; Maurer, M.; Ruppert, T.; Dick, T.P. A Role for 2-Cys Peroxiredoxins in Facilitating Cytosolic Protein Thiol Oxidation. *Nat Chem Biol* **2017**, *14*, doi:10.1038/nchembio.2536.
18. Brandstaedter, C.; Delahunty, C.; Schipper, S.; Rahlfs, S.; Yates, J.R.; Becker, K. The Interactome of 2-Cys Peroxiredoxins in Plasmodium Falciparum. *Sci Rep-uk* **2019**, *9*, 13542, doi:10.1038/s41598-019-49841-3.
19. Barata, A.G.; Dick, T.P. A Role for Peroxiredoxins in H2O2- and MEK-Dependent Activation of the P38 Signaling Pathway. *Redox Biol* **2020**, *28*, 101340, doi:10.1016/j.redox.2019.101340.
20. Portillo-Ledesma, S.; Randall, L.M.; Parsonage, D.; Rizza, J.D.; Karplus, P.A.; Poole, L.B.; Denicola, A.; Ferrer-Sueta, G. Differential Kinetics of Two-Cysteine Peroxiredoxin Disulfide Formation Reveal a Novel Model for Peroxide Sensing. *Biochemistry-us* **2018**, *57*, acs.biochem.8b00188, doi:10.1021/acs.biochem.8b00188.
21. Dam, L. van; Pagès-Gallego, M.; Polderman, P.E.; Es, R.M. van; Burgering, B.M.T.; Vos, H.R.; Dansen, T.B. The Human 2-Cys Peroxiredoxins Form Widespread, Cysteine-Dependent- and Isoform-Specific Protein-Protein Interactions. *Antioxidants* **2021**, *10*, 627, doi:10.3390/antiox10040627.
22. Zhou, S.; Sorokina, E.M.; Harper, S.; Li, H.; Ralat, L.; Dodia, C.; Speicher, D.W.; Feinstein, S.I.; Fisher, A.B. Peroxiredoxin 6 Homodimerization and Heterodimerization with Glutathione S-Transferase Pi Are Required for Its Peroxidase but Not Phospholipase A2 Activity. *Free Radical Bio Med* **2016**, *94*, 145–156, doi:10.1016/j.freeradbiomed.2016.02.012.
23. Schwarzländer, M.; Dick, T.P.; Meye, A.J.; Morgan, B. Dissecting Redox Biology Using Fluorescent Protein Sensors. *Antioxid Redox Sign* **2015**, *24*, 15041308401700 7 12, doi:10.1089/ars.2015.6266.
24. Gutscher, M.; Pauleau, A.-L.; Marty, L.; Brach, T.; Wabnitz, G.H.; Samstag, Y.; Meyer, A.J.; Dick, T.P. Real-Time Imaging of the Intracellular Glutathione Redox Potential. *Nat Methods* **2008**, *5*, 553–559, doi:10.1038/nmeth.1212.
25. Peskin, A.V.; Pace, P.E.; Behring, J.B.; Paton, L.N.; Soethoudt, M.; Bachschmid, M.M.; Winterbourn, C.C. Glutathionylation of the Active Site Cysteines of Peroxiredoxin 2 and Recycling by Glutaredoxin. *J Biol Chem* **2015**, *291*, jbc.M115.692798, doi:10.1074/jbc.m115.692798.

26. Netto, L.E.S.; Oliveira, M.A. de; Tairum-Jr, C.; Neto, J.F. da S. Conferring Specificity in Redox Pathways by Enzymatic Thiol/Disulfide Exchange Reactions. *Free Radical Res* **2015**, *50*, 1 99, doi:10.3109/10715762.2015.1120864.

27. Talwar, D.; Messens, J.; Dick, T.P. A Role for Annexin A2 in Scaffolding the Peroxiredoxin 2–STAT3 Redox Relay Complex. *Nat Commun* **2020**, *11*, 4512, doi:10.1038/s41467-020-18324-9.

28. Bersweiler, A.; D'Autréaux, B.; Mazon, H.; Kriznik, A.; Belli, G.; Delaunay-Moisan, A.; Toledano, M.B.; Rahuel-Clermont, S. A Scaffold Protein That Chaperones a Cysteine-Sulfenic Acid in H2O2 Signaling. *Nat Chem Biol* **2017**, *13*, 909 915, doi:10.1038/nchembio.2412.

29. Veal, E.A.; Ross, S.J.; Malakasi, P.; Peacock, E.; Morgan, B.A. Ybp1 Is Required for the Hydrogen Peroxide-Induced Oxidation of the Yap1 Transcription Factor. *J Biol Chem* **2003**, *278*, 30896–30904, doi:10.1074/jbc.m303542200.

30. Frijhoff, J.; Dagnell, M.; Godfrey, R.; Östman, A. Regulation of Protein Tyrosine Phosphatase Oxidation in Cell Adhesion and Migration. *Antioxid Redox Sign* **2014**, *20*, 1994–2010, doi:10.1089/ars.2013.5643.

31. Czech, M.P.; Lawrence, J.C.; Lynn, W.S. Evidence for the Involvement of Sulfhydryl Oxidation in the Regulation of Fat Cell Hexose Transport by Insulin. *Proc National Acad Sci* **1974**, *71*, 4173–4177, doi:10.1073/pnas.71.10.4173.

32. Sommer, D.; Coleman, S.; Swanson, S.A.; Stemmer, P.M. Differential Susceptibilities of Serine/Threonine Phosphatases to Oxidative and Nitrosative Stress. *Arch Biochem Biophys* **2002**, *404*, 271–278, doi:10.1016/s0003-9861(02)00242-4.

33. Foley, T.D.; Petro, L.A.; Stredny, C.M.; Coppa, T.M. Oxidative Inhibition of Protein Phosphatase 2A Activity: Role of Catalytic Subunit Disulfides. *Neurochem Res* **2007**, *32*, 1957–1964, doi:10.1007/s11064-007-9394-x.

34. Rao, R.K.; Clayton, L.W. Regulation of Protein Phosphatase 2A by Hydrogen Peroxide and Glutathionylation. *Biochem Bioph Res Co* **2002**, *293*, 610 616, doi:10.1016/s0006-291x(02)00268-1.

35. Cicchillitti, L.; Fasanaro, P.; Biglioli, P.; Capogrossi, M.C.; Martelli, F. Oxidative Stress Induces Protein Phosphatase 2A-Dependent Dephosphorylation of the Pocket Proteins PRb, P107, and P130*. *J Biol Chem* **2003**, *278*, 19509–19517, doi:10.1074/jbc.m300511200.

36. Conza, G.D.; Cafarello, S.T.; Loroch, S.; Mennerich, D.; Deschoemaeker, S.; Matteo, M.D.; Ehling, M.; Gevaert, K.; Prenen, H.; Zahedi, R.P.; et al. The MTOR and PP2A Pathways Regulate PHD2 Phosphorylation to Fine-Tune HIF1α Levels and Colorectal Cancer Cell Survival under Hypoxia. *Cell Reports* **2017**, *18*, 1699–1712, doi:10.1016/j.celrep.2017.01.051.

37. Heikkinen, P.T.; Nummela, M.; Leivonen, S.-K.; Westermarck, J.; Hill, C.S.; Kähäri, V.-M.; Jaakkola, P.M. Hypoxia-Activated Smad3-Specific Dephosphorylation by PP2A2. *J Biol Chem* **2010**, *285*, 3740–3749, doi:10.1074/jbc.m109.042978.

38. Raghuraman, G.; Rai, V.; Peng, Y.; Prabhakar, N.R.; Kumar, G.K. Pattern-Specific Sustained Activation of Tyrosine Hydroxylase by Intermittent Hypoxia: Role of Reactive Oxygen Species-Dependent Downregulation of Protein Phosphatase 2A and Upregulation of Protein Kinases. *Antioxid Redox Sign* **2009**, *11*, 1777–1789, doi:10.1089/ars.2008.2368.

39. Song, I.S.; Jun, S.Y.; Na, H.J.; Kim, H.T.; Jung, S.Y.; Ha, G.H.; Park, Y.H.; Long, L.Z.; Yu, D.Y.; Kim, J.M.; et al. Inhibition of MKK7–JNK by the TOR Signaling Pathway Regulator-Like Protein Contributes to Resistance of HCC Cells to TRAIL-Induced Apoptosis. *Gastroenterology* **2012**, *143*, 1341 1351, doi:10.1053/j.gastro.2012.07.103.

40. Nakashima, A.; Tanimura-Ito, K.; Oshiro, N.; Eguchi, S.; Miyamoto, T.; Momonami, A.; Kamada, S.; Yonezawa, K.; Kikkawa, U. A Positive Role of Mammalian Tip41-like Protein, TIPRL, in the Amino-Acid Dependent MTORC1-Signaling Pathway through Interaction with PP2A. *Febs Lett* **2013**, *587*, 2924 2929, doi:10.1016/j.febslet.2013.07.027.

41. Raman, D.; Pervaiz, S. Redox Inhibition of Protein Phosphatase PP2A: Potential Implications in Oncogenesis and Its Progression. *Redox Biol* **2019**, *27*, 101105, doi:10.1016/j.redox.2019.101105.

42. Forbes, S.A.; Beare, D.; Boutselakis, H.; Bamford, S.; Bindal, N.; Tate, J.; Cole, C.G.; Ward, S.; Dawson, E.; Ponting, L.; et al. COSMIC: Somatic Cancer Genetics at High-Resolution. *Nucleic Acids Res* **2017**, *45*, D777–D783, doi:10.1093/nar/gkw1121.

43. Atadja, P.; Wong, H.; Veillette, C.; Riabowol, K. Overexpression of Cyclin D1 Blocks Proliferation of Normal Diploid Fibroblasts. *Exp Cell Res* **1995**, *217*, 205–216, doi:10.1006/excr.1995.1080.

44. Stein, G.H.; Drullinger, L.F.; Soulard, A.; Dulić, V. Differential Roles for Cyclin-Dependent Kinase Inhibitors P21 and P16 in the Mechanisms of Senescence and Differentiation in Human Fibroblasts. *Mol Cell Biol* **1999**, *19*, 2109–2117, doi:10.1128/mcb.19.3.2109.

45. Leontieva, O.V.; Lenzo, F.; Demidenko, Z.N.; Blagosklonny, M.V. Hyper-Mitogenic Drive Coexists with Mitotic Incompetence in Senescent Cells. *Cell Cycle* **2012**, *11*, 4642–4649, doi:10.4161/cc.22937.

46. Ye, C.; Zhang, X.; Wan, J.; Chang, L.; Hu, W.; Bing, Z.; Zhang, S.; Li, J.; He, J.; Wang, J.; et al. Radiation-Induced Cellular Senescence Results from a Slippage of Long-Term G2 Arrested Cells into G1 Phase. *Cell Cycle* **2013**, *12*, 1424–1432, doi:10.4161/cc.24528.

47. Brookes, S.; Gagrica, S.; Sanij, E.; Rowe, J.; Gregory, F.J.; Hara, E.; Peters, G. Evidence for a CDK4-Dependent Checkpoint in a Conditional Model of Cellular Senescence. *Cell Cycle* **2015**, *14*, 1164–1173, doi:10.1080/15384101.2015.1010866.

48. Duff, M.L.; Gouju, J.; Jonchère, B.; Guillon, J.; Toutain, B.; Boissard, A.; Henry, C.; Guette, C.; Lelièvre, E.; Coqueret, O. Regulation of Senescence Escape by the Cdk4–EZH2–AP2M1 Pathway in Response to Chemotherapy. *Cell Death Dis* **2018**, *9*, 199, doi:10.1038/s41419-017-0209-y.

49. Shi, T.; Soest, D.M.K. van; Polderman, P.E.; Burgering, B.M.T.; Dansen, T.B. DNA Damage and Oxidant Stress Activate P53 through Differential Upstream Signaling Pathways. *Free Radical Bio Med* **2021**, *172*, 298–311, doi:10.1016/j.freeradbiomed.2021.06.013.

50. Bard-Chapeau, E.A.; Li, S.; Ding, J.; Zhang, S.S.; Zhu, H.H.; Princen, F.; Fang, D.D.; Han, T.; Bailly-Maitre, B.; Poli, V.; et al. Ptpn11/Shp2 Acts as a Tumor Suppressor in Hepatocellular Carcinogenesis. *Cancer Cell* **2011**, *19*, 629–639, doi:10.1016/j.ccr.2011.03.023.

51. Loh, M.L.; Vattikuti, S.; Schubbert, S.; Reynolds, M.G.; Carlson, E.; Lieuw, K.H.; Cheng, J.W.; Lee, C.M.; Stokoe, D.; Bonifas, J.M.; et al. Mutations in PTPN11 Implicate the SHP-2 Phosphatase in Leukemogenesis. *Blood* **2004**, *103*, 2325–2331, doi:10.1182/blood-2003-09-3287.

52. Chiu, J.; Dawes, I.W. Redox Control of Cell Proliferation. *Trends Cell Biol* **2012**, *22*, 592 601, doi:10.1016/j.tcb.2012.08.002.

53. Ranjan, P.; Heintz, N.H. S-Phase Arrest by Reactive Nitrogen Species Is Bypassed by Okadaic Acid, an Inhibitor of Protein Phosphatases PP1/PP2A Available online: https://www-sciencedirect-com.proxy.library.uu.nl/science/article/pii/S0891584905005307?casa_token=w8tF1l0F-hdkAAAAA:C2jHD9ch-41ThQAcmdU8iyMzlWFOBTO5UT9Lvd-1MWs5o82jA08KYeC1x_BE7e_cacShYKdUwVZk (accessed on 13 May 2021).

54. Harrington, E.A.; Bennett, M.R.; Fanidi, A.; Evan, G.I. C-Myc-induced Apoptosis in Fibroblasts Is Inhibited by Specific Cytokines. *Embo J* **1994**, *13*, 3286–3295, doi:10.1002/j.1460-2075.1994.tb06630.x.

55. Cairns, R.A.; Harris, I.S.; Mak, T.W. Regulation of Cancer Cell Metabolism. *Nat Rev Cancer* **2011**, *11*, 85–95, doi:10.1038/nrc2981.

56. Putker, M.; Madl, T.; Vos, H.R.; Ruiter, H. de; Visscher, M.; Berg, M.C.W. van den; Kaplan, M.; Korswagen, H.C.; Boelens, R.; Vermeulen, M.; et al. Redox-Dependent Control of FOXO/DAF-16 by Transportin-1. *Mol Cell* **2013**, *49*, 730 742, doi:10.1016/j.molcel.2012.12.014.

57. Hekimi, S.; Lapointe, J.; Wen, Y. Taking a "Good" Look at Free Radicals in the Aging Process. *Trends Cell Biol* **2011**, *21*, 569–576, doi:10.1016/j.tcb.2011.06.008.

58. Dam, L. van; Dansen, T.B. Cross-Talk between Redox Signalling and Protein Aggregation. *Biochem Soc Trans* **2020**, doi:https://doi.org/10.1042/BST20190054.

59. Lyu, P.C.; Liff, M.I.; Marky, L.A.; Kallenbach, N.R. Side Chain Contributions to the Stability of Alpha-Helical Structure in Peptides. *Science* **1990**, *250*, 669–673, doi:10.1126/science.2237416.

60. Parsonage, D.; Youngblood, D.S.; Sarma, G.N.; Wood, Z.A.; Karplus, and P.A.; Poole, L.B. *Analysis of the Link between Enzymatic Activity and Oligomeric State in AhpC, a Bacterial Peroxiredoxin†,‡*; Biochemistry; American Chemical Society, 2005; Vol. 44; ISBN 44-31-10583.

61. Wood, Z.A.; Poole, L.B.; Hantgan, R.R.; Karplus, P.A. Dimers to Doughnuts: Redox-Sensitive Oligomerization of 2-Cysteine Peroxiredoxins †,‡. *Biochemistry-us* **2002**, *41*, 5493 5504, doi:10.1021/bi012173m.

62. Schröder, E.; Littlechil*, J.A.; Lebedev, A.A.; Errington, N.; Vagin, A.A.; Isupov, M.N. Crystal Structure of Decameric 2-Cys Peroxiredoxin from Human Erythrocytes at 1.7Å Resolution. *Structure* **2000**, *8*, 605–615, doi:10.1016/s0969-2126(00)00147-7.

63. Pastor-Flores, D.; Talwar, D.; Pedre, B.; Dick, T.P. Real-Time Monitoring of Peroxiredoxin Oligomerization Dynamics in Living Cells. *Proc National Acad Sci* **2020**, *117*, 16313–16323, doi:10.1073/pnas.1915275117.

64. Fernandez-Caggiano, M.; Schröder, E.; Cho, H.-J.; Burgoyne, J.; Barallobre-Barreiro, J.; Mayr, M.; Eaton, P. Oxidant-Induced Interprotein Disulfide Formation in Cardiac Protein DJ-1 Occurs via an Interaction with Peroxiredoxin 2. *J Biol Chem* **2016**, *291*, 10399 10410, doi:10.1074/jbc.m115.699850.

65. Matte, A.; Low, P.S.; Turrini, F.; Bertoldi, M.; Campanella, M.E.; Spano, D.; Pantaleo, A.; Siciliano, A.; Franceschi, L.D. Peroxiredoxin-2 Expression Is Increased in β-Thalassemic Mouse Red Cells but Is Displaced from the Membrane as a Marker of Oxidative Stress. *Free Radical Bio Med* **2010**, *49*, 457–466, doi:10.1016/j.freeradbiomed.2010.05.003.

66. Jang, H.H.; Lee, K.O.; Chi, Y.H.; Jung, B.G.; Park, S.K.; Park, J.H.; Lee, J.R.; Lee, S.S.; Moon, J.C.; Yun, J.W.; et al. Two Enzymes in One Two Yeast Peroxiredoxins Display Oxidative Stress-Dependent Switching from a Peroxidase to a Molecular Chaperone Function. *Cell* **2004**, *117*, 625–635, doi:10.1016/j.cell.2004.05.002.

67. Saravi, S.S.S.; Eroglu, E.; Waldeck-Weiermair, M.; Sorrentino, A.; Steinhorn, B.; Belousov, V.; Michel, T. Differential Endothelial Signaling Responses Elicited by Chemogenetic H2O2 Synthesis. *Redox Biol* **2020**, *36*, 101605, doi:10.1016/j.redox.2020.101605.

68. Perkins, A.; Poole, L.B.; Karplus, P.A. Tuning of Peroxiredoxin Catalysis for Various Physiological Roles. *Biochemistry-us* **2014**, *53*, 7693 7705, doi:10.1021/bi5013222.

69. Park, M.H.; Jo, M.; Kim, Y.R.; Lee, C.-K.; Hong, J.T. Roles of Peroxiredoxins in Cancer, Neurodegenerative Diseases and Inflammatory Diseases. *Pharmacol Therapeut* **2016**, *163*, 1–23, doi:10.1016/j.pharmthera.2016.03.018.

APPENDICES

NEDERLANDSE SAMENVATTING

Het menselijk lichaam bestaat uit een geschatte 38 biljoen cellen, met een enorme diversiteit aan morfologieën en functies [1]. Ondanks deze diversiteit en complexiteit zijn alle cellen opgebouwd uit dezelfde bouwstenen. Cellen worden omringd door een celmembraan, gevuld met onder andere water, suikers, eiwitten en eiwitfabrieken (ribosomen), erfelijk materiaal in de vorm van DNA, energiecentrales (mitochondriën) en nog veel meer. Eiwitten zijn de functionele bouwstenen van de cellen in ons lichaam. In onze cellen zijn veel verschillende taken te vervullen, en daarom zijn er veel verschillende eiwitten, ieder met een eigen functie. Ons lichaam kent 21 aminozuren waar alle eiwitten uit zijn opgebouwd. De lengte van eiwitten kan variëren van enkele tot duizenden aminozuren. Dit betekent dat je met slechts tien aminozuren al verschillende ketens kunt maken, en met een gemiddeld formaat eiwit van 300 aminozuren .

Het totale aantal verschillende eiwitten (het proteoom) is niet precies bekend, maar schattingen variëren van minimaal 20.000, tot maar liefst zo veel als 400.000.

Cellen maken eiwitten op basis van een genetische code die is opgeslagen in het DNA. Ieder eiwit heeft een eigen DNA code (een gen). Alle lichaamscellen hebben in principe een complete set van het DNA tot hun beschikking, en kunnen dus theoretische alle eiwitten maken. Het produceren van eiwitten wordt geregeld door 'genregulatie'; hiermee worden bepaalde genen aan- of uit uitgezet. Om ervoor te zorgen dat een cel zijn specifieke functie kan uitvoeren, moeten alleen die genen aan staan die de cel nodig heeft. Een bètacel in de alvleesklier moet bijvoorbeeld eiwitten produceren die belangrijk zijn voor de glucosehuishouding (insuline), maar heeft geen eiwitten nodig die specifiek zijn voor bijvoorbeeld levercellen. Van een actief gen wordt de DNA-code eerst gekopieerd tot mRNA, een proces dat transcriptie heet. De mRNA-code wordt vervolgens afgelezen in eiwitfabrieken, die er een eiwit van maken. Dit proces heet translatie. De functie van een eiwit wordt bepaald door de structuur van het eiwit. Eiwitten worden gemaakt als een lange streng van aminozuren, en worden daarna gevouwen in driedimensionale structuren.

Bovenop de functionele diversiteit van cellen zijn deze cellen onderworpen aan constante veranderingen in de interne en externe omgeving. Omdat cellen en organismen alleen levensvatbaar zijn binnen relatief beperkte condities, proberen cellen en organismen continu om hun toestand stabiel te houden ondanks de veranderingen in hun omgeving. Dit concept staat bekend als 'homeostase'. Cellen handhaven bijvoorbeeld een constante temperatuur, zuurgraad en hoeveelheid voedingsstoffen. Zodra er veranderingen in het evenwicht plaatsvinden, neemt de cel deze signalen waar met behulp van sensoren en reageert erop door eiwitten aan of uit te zetten die de balans kunnen herstellen. Door de grote diversiteit aan eiwitten en cellen is het aantal mogelijke combinaties aan reacties bijna oneindig. De reeks aan signalen die wordt doorgegeven om intern en tussen verschillende cellen te communiceren heet 'signaaltransductie'. Als cellen niet goed in staat zijn homeostase te waarborgen, kan dit leiden tot in een verstoring van cellulaire processen en kan het bijdragen aan het ontstaan van ziekten zoals kanker, neurodegeneratieve aandoeningen en diabetes [2].

Één manier waarop cellen reageren op veranderingen in hun omgeving is door het aan- of uitzetten van genen die coderen voor eiwitten die helpen de balans te herstellen. Een andere manier is door kleine wijzigingen aan te brengen op al bestaande eiwitten, die daardoor actief of minder actief worden of een iets andere functie krijgen, en zo signaaltransductie in gang zetten. Dit noem je post-translationele modificaties (PTMs).

De reversibele oxidatie van het aminozuur cysteïne door reactieve vormen van zuurstof (reactive oxygen species, ROS) is een voorbeeld van een PTM. Het ROS-molecuul dat hiervoor verantwoordelijk is, is waterstofperoxide (H_2O_2). H_2O_2 kan het aminozuur cysteïne oxideren via een redoxreactie (reductie-oxidatie), wat zorgt voor een 'oxidatieve modificatie' (zie ook **Figuur 4** in **hoofdstuk 1**). Deze manier van signalen doorgeven in cellen wordt redox-signaaltransductie genoemd.

Een oxidatieve modificatie van een eiwit veroorzaakt een wijziging in de structuur van dat eiwit, die op zijn beurt een effect kan hebben op het functioneren van dat eiwit. Op die manier kunnen redox-gereguleerde structuurveranderingen in een eiwit functioneren als schakelaar.

Redox-signaaltransductie is een fundamentele vorm van signaaltransductie, cruciaal voor cellen om homeostase te handhaven en dus voor al het leven op aarde. Het doel van het onderzoek beschreven in dit proefschrift is om de moleculaire mechanismen te begrijpen die ten grondslag liggen aan redox-signaaltransductie, en welk effect veranderingen in de redox status van een cel hebben op signaaltransductie.

Dit proefschrift behandelt drie belangrijke thema's, opgedeeld in zeven hoofdstukken. Ten eerste onderzoeken we hoe de oxidatie van cysteïnes door H_2O_2 efficiënt en specifiek kan gebeuren. Ten tweede kijken we naar wat oxidatie door H_2O_2 doet op de functie van bepaalde eiwitten in de cel. We bekijken ook wat deze functieveranderingen voor effect hebben op het gedrag van cellen. Ten derde onderzoeken we welk effect redoxregulatie heeft op het ontvouwen van eiwitten en eiwitaggregatie.

Een belangrijk vraagstuk over hoe H_2O_2 werkt als signaaltransductiemolecuul is hoe het kan dat H_2O_2 specifieke cysteïnes kan oxideren in signaaltransductieroutes, in de context van een vrijwel ongelimiteerd aantal potentiele doelwitten in een cel. H_2O_2 reageert alleen met de juiste cysteïnes in de juiste eiwitten om een bepaald signaal door te geven, terwijl er ook heel veel andere eiwitten met cysteïnes in de cel aanwezig zijn. Cellen zijn uitgerust met een sterk systeem van antioxidanten; abundante eiwitten (zoals peroxiredoxins) waarvan verwacht wordt dat ze >99% van alle cellulaire H_2O_2 weghalen [3]. Ten tweede hebben de meeste cysteïnes in eiwitten een lage reactiviteit met H_2O_2 [4,5]. Hoe het mogelijk is dat H_2O_2 tóch kan leiden tot oxidatie van specifieke, laag abundante eiwitten is niet goed duidelijk (zie ook **Figuur 5** in **hoofdstuk 1**).

Er zijn verschillende hypotheses die (deels) kunnen verklaren hoe H_2O_2 de benodigde reactiviteit en specificiteit kan behalen. Eén van die hypotheses komt van de observatie dat peroxiredoxin eiwitten, die normaal als antioxidant H_2O_2 weghalen, óók als peroxidases kunnen werken [6–11]. Hierbij reageert H_2O_2 eerst met de extreem reactieve cysteïne van peroxiredoxin, waarna de geoxideerde peroxiredoxin een disulfide intermediair vormt met een minder reactief cysteïne in een doeleiwit (zie ook **Figuur 6D** in **hoofdstuk 1**). Geoxideerde peroxiredoxins kunnen zo de oxidatie van andere eiwitten faciliteren via disulfide uitwisselingsreacties. Dit mechanisme wordt een 'peroxiredoxin-afhankelijke redox relay' genoemd. Onderzoekers hebben laten zien dat deze peroxiredoxin-afhankelijke redox relay ook op grotere schaal voorkomt [10,11]. Dit kan verklaren hoe zoveel intrinsiek niet-reactieve eiwitten tóch geoxideerd worden als respons op H_2O_2-afhankelijke signaaltransductie, ondanks de aanwezigheid van een abundant en reactief antioxidantsysteem.

Hoewel dit model de *reactiviteit* van H_2O_2 verklaart, is het nog onduidelijk hoe de oxidatie van *specifieke* eiwitten kan worden bereikt in H_2O_2-afhankelijke signaaltransductie. Dit is nodig omdat cellen een specifieke respons nodig hebben om te reageren op een verandering in hun cellulaire omgeving door middel van relevante biologische signalen. De zogenaamde 2-cys peroxiredoxins hebben vijf verschillende isovormen in zoogdieren, ieder met een eigen subcellulaire lokalisatie, oxidatiekinetiek en structurele verschillen rond hun katalytische centrum. Onze hypothese is daarom dat de verschillende peroxiredoxin-eiwitten ook kunnen zorgen voor de benodigde selectiviteit in redox-signaaltransductie.

In **hoofdstuk 2** onderzoeken we peroxiredoxin- afhankelijke redox relay op een proteoom-brede schaal. We gebruiken een grootschalige systematische analyse m.b.v. massa-spectrometrie om cysteïne-afhankelijke bindingspartners te identificeren van de vijf 2-cys peroxiredoxin isovormen. We laten zien

dat alle isovormen van peroxiredoxins cysteïne-afhankelijke heterodimeren kunnen vormen met talloze andere eiwitten, en dat iedere isovorm een voorkeur heeft voor een andere subset van deze disulfide-afhankelijke bindingspartners. We bestuderen welke isovorm-specifieke eigenschappen ten grondslag kunnen liggen aan deze observaties en we laten zien dat peroxiredoxin-afhankelijke redox relays via twee verschillende moleculaire mechanismen kunnen verlopen. Dit is een sterke aanwijzing dat peroxiredoxins een rol kunnen spelen in het faciliteren van niet alleen reactiviteit maar ook selectiviteit in de signaaltransductie van H_2O_2, om zo een specifiek signaal te genereren.

Hoofstukken 3, 4 en **6** gaan verder in op cysteïne-afhankelijke redox regulatie van verschillende signaaltransductieeiwitten. In **hoofdstuk 3** bestuderen we het eiwit TIPRL, een eiwit waar niet veel over bekend is. TIPRL is betrokken bij de regulatie van PP2A, dat verantwoordelijk is voor het verwijderen van fosfaatgroepen van eiwitten. Fosforylering van eiwitten (ook een PTM) is een belangrijke vorm van signaaltransductie in een cel, waarbij fosfaatgroepen op eiwitten worden geplaatst. Het is belangrijk dat de fosfaatgroepen op het juiste moment worden verwijderd. We laten zien dat TIPRL-cysteïnes erg gevoelig zijn voor de oxidatie door H_2O_2. Na de oxidatie van TIPRL kunnen twee TIPRL-eiwitten elkaar binden via een zwavelbrug, en zo een homodimeer vormen. TIPRL vormt drie verschillende zwavelbrug-afhankelijke homodimeren via cysteïnes C14 en C87 (C14-C14, C87-C87 en C14-C87). Onze resultaten suggereren ook dat TIPRL normaal gesproken PP2A inhibeert en zo het verwijderen van fosfaatgroepen vertraagt, en dat de oxidatie en dimerisatie van TIPRL ervoor zorgen dat deze inhibitie van PP2A nóg efficiënter verloopt. Toekomstig onderzoek is nodig om uit te wijzen welk effect dit precies heeft op de cel.

Hoofstuk 4 beschrijft de oxidatie en daaropvolgende zwavelbrug-afhankelijke dimerisatie van het tumorsuppressoreiwit $p16^{INK4A}$. Dit zorgt ervoor dat het eiwit een drastische structurele verandering ondergaat en β-amyloïde fibrillen vormt, eiwitaggregaten die kenmerkend zijn voor amyloïdoses zoal Parkinson en Alzheimer. $P16^{INK4A}$ zorgt er normaal voor dat een cel stopt met delen door de eiwitten CDK4 en CDK6 te remmen. De amyloïdevorming van $p16^{INK4A}$ zorgt ervoor dat CDK4 en CDK6 niet meer geremd worden. We gebruiken de term 'oxaggregatie' voor de kritieke afhankelijkheid van een zwavelbrug-afhankelijke dimeer als subeenheid voor fibrilvorming. Deze observaties brengen de cellulaire redox status in verband met de regulatie van de celcyclus via de formatie van β-amyloïde fibrillen.

In hoge concentraties reageren ROS niet alleen met cysteïnes, maar ook met andere willekeurige moleculen. Dit kan eiwitschade veroorzaken, zoals eiwitontvouwing en -aggregatie. Opstapeling van kapotte eiwitten speelt een rol bij veroudering en ouderdomsziekten zoals de ziekte van Alzheimer. Daarentegen functioneert H_2O_2 zoals genoemd als een belangrijk signaaltransductiemolecuul dat belangrijk is voor het gezond functioneren van cellen. In **hoofdstuk 5** bediscussieren we hoe deze schijnbaar tegenovergestelde effecten van H_2O_2 - als signaalmolecuul, en als drijfveer van eiwitaggregatie tijdens veroudering – verenigd kunnen worden in één hypothese. We geven een overzicht van de literatuur over de complexe relatie tussen redox-signaaltransductie en eiwitaggregatie.

In **hoofdstuk 6** beschrijven we een voorbeeld van hoe de cellulaire redox status samenhangt met de voortgang van de celcyclus [12]. Een van de belangrijkste kenmerken van kanker is de ontsporing van celdeling. We laten zien dat de celdelingsregulatoreiwitten CDK4 en cycline D tijdelijk een covalent gebonden eiwitcomplex vormen onder invloed van ROS. Dit covalente eiwitcomplex wordt veroorzaakt door de oxidatie van cysteïne C135 in CDK4 en de vorming van een zwavelbrug tussen CDK4 en cycline D. Deze interactie stabiliseert op die manier een normaal gesproken hydrostatische, niet-covalente interactie, vergelijkbaar met een moleculair nietje (de zwavelbrug) in twee vellen papier (de eiwitten). We laten zien dat de zwavelbrug-afhankelijke binding de activiteit van het CDK4-cycline D complex verhoogt, en zo potentieel de celdeling kan versnellen. Dit onderzoek geeft aan dat de redoxgevoelige cysteïne C135 in het CDK4-cycline D complex een goed aanknopingspunt zou kunnen zijn voor nieuwe medicijnen tegen kanker.

Ten slotte vatten we het werk in dit proefschrift samen in **hoofdstuk 7.** We bespreken de vernieuwende concepten en mogelijke implicaties van dit werk.

REFERENTIES

1. Sender, R.; Fuchs, S.; Milo, R. Revised Estimates for the Number of Human and Bacteria Cells in the Body. *Plos Biol* 2016, *14*, e1002533, doi:10.1371/journal.pbio.1002533.
2. Galluzzi, L.; Yamazaki, T.; Kroemer, G. Linking Cellular Stress Responses to Systemic Homeostasis. *Nat Rev Mol Cell Bio* 2018, *19*, 731–745, doi:10.1038/s41580-018-0068-0.
3. Winterbourn, C.C. Biological Production, Detection, and Fate of Hydrogen Peroxide. *Antioxid Redox Sign* 2017, *29*, ars.2017.7425, doi:10.1089/ars.2017.7425.
4. Winterbourn, C.C. The Biological Chemistry of Hydrogen Peroxide. *Methods Enzymol* 2013, *528*, 3–25, doi:10.1016/b978-0-12-405881-1.00001-x.
5. Marinho, H.S.; Real, C.; Cyrne, L.; Soares, H.; Antunes, F. Hydrogen Peroxide Sensing, Signaling and Regulation of Transcription Factors. *Redox Biol* 2014, *2*, 535 562, doi:10.1016/j.redox.2014.02.006.
6. Delaunay, A.; Pflieger, D.; Barrault, M.-B.; Vinh, J.; Toledano, M.B. A Thiol Peroxidase Is an H2O2 Receptor and Redox-Transducer in Gene Activation. *Cell* 2002, *111*, 471–481, doi:10.1016/s0092-8674(02)01048-6.
7. Veal, E.A.; Findlay, V.J.; Day, A.M.; Bozonet, S.M.; Evans, J.M.; Quinn, J.; Morgan, B.A. A 2-Cys Peroxiredoxin Regulates Peroxide-Induced Oxidation and Activation of a Stress-Activated MAP Kinase. *Mol Cell* 2004, *15*, 129 139, doi:10.1016/j.molcel.2004.06.021.
8. Sobotta, M.C.; Liou, W.; cker, S.S. ouml; Talwar, D.; Oehler, M.; Ruppert, T.; Scharf, A.N.D.; Dick, T.P. Peroxiredoxin-2 and STAT3 Form a Redox Relay for H2O2 Signaling. *Nat Chem Biol* 2014, *11*, 1 8, doi:10.1038/nchembio.1695.
9. Barata, A.G.; Dick, T.P. A Role for Peroxiredoxins in H2O2- and MEKK-Dependent Activation of the P38 Signaling Pathway. *Redox Biol* 2020, *28*, 101340, doi:10.1016/j.redox.2019.101340.
10. Stöcker, S.; Maurer, M.; Ruppert, T.; Dick, T.P. A Role for 2-Cys Peroxiredoxins in Facilitating Cytosolic Protein Thiol Oxidation. *Nat Chem Biol* 2018, *14*, 148–155, doi:10.1038/nchembio.2536.
11. Brandstaedter, C.; Delahunty, C.; Schipper, S.; Rahlfs, S.; Yates, J.R.; Becker, K. The Interactome of 2-Cys Peroxiredoxins in Plasmodium Falciparum. *Sci Rep-uk* 2019, *9*, 13542, doi:10.1038/s41598-019-49841-3.
12. Burhans, W.C.; Heintz, N.H. The Cell Cycle Is a Redox Cycle: Linking Phase-Specific Targets to Cell Fate. *Free Radical Bio Med* 2009, *47*, 1282 1293, doi:10.1016/j.freeradbiomed.2009.05.026.
13. Erdős, G.; Mészáros, B.; Reichmann, D.; Dosztányi, Z. Large-Scale Analysis of Redox-Sensitive Conditionally Disordered Protein Regions Reveals Their Widespread Nature and Key Roles in High-Level Eukaryotic Processes. *Proteomics* 2019, *19*, 1800070, doi:10.1002/pmic.201800070.

CURRICULUM VITAE

Loes van Dam was born on the 23rd of March 1989 in Rotterdam, the Netherlands. She attended College Den Hulster in Venlo, the Netherlands where she passed her VWO and International Baccalaureate exams in 2007. After a gap year of working and traveling, she moved to Utrecht to start a Bachelor's in Biomedical Sciences at the University Utrecht, the Netherlands in 2008. After receiving her Bachelor Diploma in 2011, she continued her education in the Master's Programme Cancer, Genomics and Developmental Biology at the Graduate School of Life Sciences at Utrecht University. During this time, Loes completed several internships. During her first internship she studied TOR signaling pathway regulator-like (TIPRL) as a cysteine-dependent redox-sensor in the lab of Dr. Tobias Dansen (University Medical Center, Utrecht) and under the supervision of Dr. Marrit Putker. She wrote her thesis on the reciprocal regulation between metabolism and the cell cycle machinery under the supervision of Dr. Joanna Kaplon in the lab of Prof. Dr. Daniel Peeper (Netherlands Cancer Insitute, the Netherlands). During her last internship she studied the role of ASS1 in the chemoresistance of malignant pleural mesothelioma in the lab of Prof. Dr Courtney Broaddus (University of California, San Fancisco, USA) under the supervision of Dr. Dario Barbone. She received her Master's degree *cum laude* in 2014.

In 2015, she started her PhD in the group of dr. Tobias Dansen in the Department of Molecular Cancer Research (MCR) at the University Medical Center, Utrecht, the results of which are described in this thesis.

Loes will continue her scientific career as a postdoctoral researcher to explore the gastronomic and textural properties of filamentous fungi under the supervision of Dr. Leonie Johanna Jahn and Prof. Morten Otto Alexander Sommer at the Novo Nordisk Foundation Center for Biosustainability at the Technical University of Denmark (DTU).

PUBLICATIONS

(Most recent on top)

L. van Dam, M. Pagès-Gallego, P.E. Polderman, R.M. van Es, B.M.T. Burgering, H.R. Vos, T.B. Dansen
The Human 2-Cys Peroxiredoxins Form Widespread, Cysteine-Dependent- and Isoform-Specific Protein-Protein Interactions.
Antioxidants **2021**, *10*, 627, doi:10.3390/antiox10040627.

L. van Dam, T.B. Dansen
Cross-Talk between Redox Signalling and Protein Aggregation.
Biochem Soc Trans **2020**, doi:10.1042/BST20190054.

C. Göbl*, V.K. Morris*, L. van Dam*, M. Visscher, P.E. Polderman, C. Hartlmüller, H. de Ruiter, M. Hora, L. Liesinger, R. Birner-Gruenberger, H.R. Vos, B. Reif, T. Madl, T.B. Dansen
Cysteine Oxidation Triggers Amyloid Fibril Formation of the Tumor Suppressor $P16^{INK4A}$.
Redox Biol **2019**, 101316, doi:10.1016/j.redox.2019.101316.

J. Kaplon*, L. van Dam*, D. Peeper
Two-Way Communication between the Metabolic and Cell Cycle Machineries: The Molecular Basis.
Cell Cycle **2015**, *14*, 2022–2032, doi:10.1080/15384101.2015.1044172.

*equal contributions

ACKNOWLEDGEMENTS

An end of an era: that is what it feels like after years in the Stratenum. It took some time, but here it is: my thesis. I am thankful and proud to have my name on the cover, but I am honored to have worked with a great amount of amazing people. Without them, my time at the Stratenum and this thesis would not be the same. I can safely say that I am really happy that I chose to do my PhD in this environment. There were many highs and lows, and I am genuinely grateful for all people that helped me along the way. I have worked with so many people and I will try to thank you all (and probably fail, so hereby: thank you all!).

The one person I cannot thank enough is my supervisor **Tobias**. T, jouw onuitputbare enthousiasme voor experimenten en data maakt dat het lab een inspirerende plek is om te werken en leren. Zélfs na mijn licht ontvlambare stage mocht ik bij je komen werken. Je begeleiding, steun, geduld (vooral tijdens de laatste fase), peptalks en eindeloze kennis waren cruciaal voor mijn ontwikkeling. De vrijheid die je je mensen weet te bieden is bijzonder, dat heb ik erg gewaardeerd. Jouw wetenschappelijke mening is een belangrijke maatstaf voor me. Ik ben je onwijs dankbaar dat je me hebt geleerd hoe goede experimenten eruitzien (controles en meer controles!), en hoe ik kritisch kan zijn op wetenschappelijk onderzoek – een onmisbare vaardigheid. Ondanks mijn neiging resultaten nogal eens negatiever te interpreteren dan ze zijn, was ik na een overleg met jou altijd weer enthousiast over mijn project. Ook op persoonlijk vlak heb ik je gedurende de jaren steeds beter leren kennen, ik heb veel plezier beleefd aan onze niet-wetenschappelijke discussies. Dank voor alles, ik ga al je woordgrappen missen.

Boudewijn, ik heb enorme bewondering voor jouw manier van werken en leiding geven. De vrijheid en kansen die je voor de mensen om je heen creëert is bijzonder. Ik kan zeker nog veel leren van jouw relaxte houding en humor in het leven. Die houding heeft ook het Stratenum en de groep gemaakt tot wat die is. Ik heb veel plezier beleefd aan de koffiemomentjes in de mancave, en uiteraard alle borrels. Enorm bedankt voor alles. Hopelijk kunnen we nog vaker een biertje drinken op Down the Rabbit Hole!

I would also like to thank the members of my reading committee that approved my thesis and allow me to defend my thesis. **Madelon Maurice**, **Willianne Vonk**, **Sander van den Heuvel**, **Marc Baldus** en **Harm Kampinga**: thank you for taking the time to go through my scientific ramblings.

En dan: mijn lieve partynimfen en mancavegenoten **Sasha** en **Harmjan**. Allereerst heel erg bedankt dat jullie aan mijn zijde staan tijdens mijn verdediging. Wat was het fijn dat ik met jullie een kamer mocht delen. Op die manier hebben we een hoop highs en lows kunnen meegemaakt van elkaar, en dat kunnen delen maakt alles fijner. **Sasha**, we zijn ongeveer tegelijk begonnen en hebben samen afscheid genomen van het Stratenum. Je was echt mijn maatje, en we hebben enorm veel lol gehad samen, van redoxcongres tot vage gaybar op ADE en van sollicitatiefrustratie (mooi woord!) tot Veni-champagne. Ik ben een vriend rijker. Ik wacht ook nog steeds op de dag dat ik een woede-uitbarsting van je meemaak, alhoewel ik eigenlijk wel besef dat die dag nooit gaat komen. **Harmjan**, ondanks dat je in jezelf praat (en hárd) had ik je nóóit willen missen als kamergenoot en collega. Ik mis onze vaste koffiemomenten en ouwehoersessies. Bedankt ook dat ik je als schietschijf mocht gebruiken voor al mijn vragen over mass-spec/scheikunde/Stratenum-geschiedenis/random onderwerpen. Je kennis en aanwezigheid (en slechte humor) in het lab zijn van enorme waarde. Hopelijk komen jullie me opzoeken in Kopenhagen.

Guest of honor **Paulien**, ik heb zó'n ongelofelijke bewondering voor hoe jij in het leven staat. Je positiviteit en bizarre mensenkennis zijn heel belangrijk voor me geweest tijdens mijn PhD, maar zijn ook onmisbaar voor het lab (en eigenlijk voor iedereen om jou heen) en mogen niet onderschat worden; zeker niet door jezelf. Ik heb genoten van het samen proeven doen en samenwerken. Daarnaast hadden we natuurlijk Up/Pinot aan jou te danken, we missen hem nog steeds heel erg. Ik hoop dat we contact houden.

Next up: the other Dansen lab members. **Marc**, you were my knight in shining armor when I started programming. I don't know how I would have survived without you. You are incredibly good at explaining, thank you for your patience and help on the peroxiredoxin paper. I also had load of fun with you outside the lab (especially when we got you drunk!). Also: I'm still waiting to try your pasta 'salad'! **Daan**, ik heb genoten van je nuchterheid en van alle koffiemomentjes. Je straalt een aanstekelijke relaxtheid uit waardoor het lijkt alsof alles je heel makkelijk afgaat (hoewel ik ook wel weet dat dat niet altijd zo is). Hou dat vast! Ik ben benieuwd naar je werk, keep me posted! **Tao**, it was so great to have you in the lab, and to see you develop into a skilled scientist. I learned a lot from you, also as a person. I hope we can stay in touch. Lots of luck for you and Xiaogang at UPenn, you'll do great!

The rest of the mancave: **Tianshu**, I am honored to call you my friend! Thank you for all the fun moments, and for teaching me some Chinese culture. I hope we can keep up our annual bevrijdingsdag parties, and ik geloof dat we voortaan ook gewoon Nederlands kunnen praten. Het beste voor de toekomst! **Maojie**, I hope you enjoy the daddy-life! Although not physically in the mancave anymore, you are there in spirit! I laughed a lot with you, especially when you have breakfast with smelly French cheese early in the morning. **Paula**, unfortunately we didn't overlap more, but the short time we worked together was fun. Is the plant still alive? Enjoy your time in the lab, and keep the guys under control! **Marten**, ik zet je gewoon hierbij, yolo. Het was enorm chill om jou als collega te hebben vanwege je passie voor wetenschap, humor en directheid. Het was zeker even wennen toen je weg was. Des te beter dat we als oud-collega dat biertje af en toe hebben volgehouden.

Dan het onmisbare dreamteam van analisten: Lydia, Miranda en Paulien. Zonder jullie als stabiele factor zijn we nergens. Ik mis de interactie met jullie heel erg. **Lydia**, bedankt dat je altijd voor me klaarstond, en altijd alles in goede banen wist te leiden. **Miranda**, officieel niet meer een Burgering, maar daar kun je natuurlijk nooit helemaal mee stoppen. Succes bij Sakia en bedankt voor alles!

Marlies, bedankt voor je positieve energie. Tof om samen veel te organiseren zoals de retreat (en natuurlijk Denkkracht). Ik kon altijd goed met je praten en we zaten meestal op één lijn. Succes met afronden, en we houden contact.

Andere leden van het stratenum: **Maria**, thank you for all (scientific and non-scientific) advice, I admire your hard work and it's good to have you around! **Robert**, bedankt voor je mass-spec hulp, en je sarcasme. Ik ben benieuwd of dat ei nog steeds op je bureau ligt. **Nguyen**: remember to take a break once in a while! All the best. **Jasmin**, we kennen elkaar al van een bachelorcursus, maar in SF heb ik je pas echt goed leren kennen. Wat een lol hebben we gehad (loose-jaw). Jammer dat je bulderende lach niet meer op het stratenum te horen is, die werkt erg aanstekelijk. Het was een eer om je paranimf te zijn. **Mirjam**, heerlijk om af en toe lekker samen te bashen op iedereen. Fijn om ook veel samen te organiseren, je bent lekker daadkrachtig. Bedankt voor alles. Heel veel succes met het afronden, en ik kom graag je vernieuwde paleisje nog eens bekijken. **Lisa**, ik kan me nog goed ons eerste uitje herinneren naar de Parade – and it did not end well haha. Heel veel geluk in Londen! **Sjors**, George, het bierteam. Ik denk dat wij de aller-allerbelangrijkste taak in het hele stratenum hadden (belangrijker dan koffie nog)! Het was lachen om je zo te leren kennen, en via jou nog veel andere leden van je groep. **WJ**, bedankt voor alle biertjes die we mochten delen, en voor je grappen bij de koffie. Ook bedankt aan het eerste Genoom-team: **Marc**, **Myrthe**, **Francis** en **Bob**. Wat was het heftig hè, zo in het diepe gegooid worden. Gedeelde smart is halve smart zullen we maar zeggen. Francis ook bedankt dat je me erop wees dat je in R niet alles in de console hoef te doen, maar het kunt opslaan als script. In my defense: ik had nog nooit eerder iets in R gedaan. Bob: bijna tegelijk begonnen (eigenlijk al in de bachelor!) en bijna tegelijk afgerond, we lopen lekker synchroon! **Joske**, op jou kon ik rekenen wat borrels betreft! Tof om je (werk) te leren kennen, en het testweekje met Boete werkte aanstekelijk!

PI's of the center: **Maria**, **Peter**, **Yvonne**, **Jurian**, **Fried**, **Saskia**, **Madelon**, **Hugo**, **Martijn**, **Aniek**, **Eric**, **Suzanne**, **Antoine** en **Jeroen**: thank you for all questions, input and comments

thought my PhD and all work discussions. A critical audience is one of the most important things in science, and you contributed greatly to that. **Fried**, Friedje, wat vond ik het lachen om met jou te ouwehoeren in de celkweek. Dat maakt die uren die we daar beide door hebben gebracht toch iets leuker! Dank ook voor al je wetenschappelijke input. **Yvonne**, fijn om unne mede-Limbo rond te hebben lopen op het lab.

All other (former) colleagues of the CMM labs Lens/Maurice/Snippert/Gloerich/De Keizer/Schuijers/Kalkhoven/Van Mil/Cuppen/De Ridder: thanks for your input during our shared workdiscussions and for the great atmosphere, especially during all our social events. I have always enjoyed the LSD's, theme borrels, retreats and Friday-afternoon-beers a lot. Special thanks to **Boekhout, Suzanne, Ingrid V, Bas, Sander, Christina, Jooske, Susan, Denise, Marjolein V, Nizar, Lotte, Koen, Maria, Stephanie, Imogen, Miguel, Mojtaba, Neeraj, Marjolein B, Johannes, Diana, Rana, Ingrid J, Jeroen, Joep Felix, Ronja, Joanna von B, Joanna W, Roy, Ingrid A, Sippe, Maaike, Bram, Jose, John, Marieke, Sabina, Lipeng, Lily, Marjoleine, David, Lucas, Vittoria. Marrit,** bedankt voor de introductie in het lab – ooit komt het TIPRL verhaal nog tot een eind. Michael Hadders: bedankt voor je hulp bij de het 'ontdekken' van de stiekeme zwavelbrug in de TIPRL structuur. Holger, bedankt voor je oneindige kennis en geduld, en je bijdrage aan het TIPRL stuk. Maaike, te gek hoe jij in je eentje de seahorse wist te temmen, en fijn om je als collega te hebben.

Cristina, bedankt voor van alles en nogwat. Jouw organisatietalent is eindeloos, en vooral de masterclass was altijd geniaal. Ik kom nog een keer jullie paleisje bekijken! Ook **Marianne** bedankt voor alle antwoorden op mijn vragen.

Marjoleine, **Cheuk**, **Marcel**, **Huub**, **Livio,** onze liefste **schoonmakers** en de **helden van de ICT**. Jullie zijn onmisbaar om heel veel redenen. Heel erg bedankt voor alles dat jullie voor me hebben gedaan. Wim, Marc Eric, Dick en collega's, bedankt voor het fixen van mijn problemen als ik de neiging had mijn laptop uit het raam te smijten (of er gewoon koffie op had gemorst). **Lenie**, we missen je nog steeds op het stratenum. Bedankt voor de talloze opruimsessie na een uit de hand gelopen vrijdagborrel.

Oud-studenten: **Esmé**, **Zoïe**, **Matthijs** en **Suda**, bedankt voor alle proeven die jullie voor en met me hebben gedaan. Ik heb veel van jullie geleerd. Matthijs: bedankt voor je werk aan het CDK stuk, en succes met je promotie!

Ik wil ook mensen van buiten de academische wereld bedanken voor hun indirecte bijdrage aan dit proefschrift. Door jullie kon ik de onvermijdelijke tegenslagen die gemoeid gaan met het doen van onderzoek relativeren. Soms kom je juist op de beste ideeën als je even niet met je onderzoek bezig bent. Jullie zorgden er ook voor dat ik alles in perspectief kon zetten als dat nodig was, ook al begrepen jullie er vaak de ballen van.

Allereerst mijn lieve studievrienden, de lieve vriendjes en vriendinnetjes van de U4L: **Bart, Bren, Celine, Dieke, El, Eric, Eva, Jer, Johan, Joost, Jop, Jos, Juan Luis, Kim, Lars, Len, Leo, Lot, Marina, Mark, Marleen, Mathieu, Roos, Ruud** en **Saar**. Dank voor alles dat we samen hebben beleefd en gedeeld: kroegavonden, weekendjes, Réflüflöps, feestjes, etentjes, festivals, fietstochtjes, hulp bij moeilijke keuzes, wijnproeverijen en -reizen maar vooral vriendschap. Lieve Saar, bedankt voor onze hechte vriendschap vanaf dag één van de studie. El, het was een eer om met jou Huize Hulst te delen. Smulpapen Joppe, Lotte, Jeroen, Marina, Eric, Eva, Johan en Kjos: zonder jullie had ik niet durven solliciteren voor mijn huidige baan, ik heb genoten van onze avonden en al het lekkers er te eten/drinken/koken valt. Team Aad: wat hebben we lekker kunnen nerden over onze reis.

Lieve **Soto**: jullie zijn letterlijk de énige reden dat ik de eerste lockdown heb overleefd. Leo en Rudie: superbijzonder om met jullie in de buurt een nieuw leven op te kunnen bouwen in Kopenhagen. Joost en Leo: ons traject is toch iets anders, bedankt voor het delen van jullie herkenbare promotieperikelen. Gedeelde smart is halve smart!

Verder ook **Ingriii, Renske, Rinske, Lies, Taar, Marijne, Paul, Bren, Tinus** en **Noor** bedankt. Noor, bedankt voor de prachtige omslag.

Lieve **Schattepuumelkes**, alde sjoenkelaers! Het is bijzonder om zoveel vrienden te hebben uit een vorige levensfase (of drie). Ik hoop op nog veel meer joeksigheid, frieteier, zachte lammetjes en shub met jullie, dat maakt het leven leuk!

Tot slot een woord aan mijn lieve familie: de mensen die ik het langste ken en er altijd zijn geweest. Zonder jullie aanmoediging en thuishonk had ik dit nooit kunnen doen, en was ik niet geworden wie ik nu ben. **Mama**, bedankt voor je steun en bezorgdheid van de afgelopen jaren. Het is verdrietig dat papa er niet bij kan zijn, hij had dit een bijzonder moment gevonden en zou vast trots zijn. **Hanneke**, zussie, dank voor je steun, maar ook je humor, bezorgdheid en luisterend oor de laatste jaren. Ik ben trots op je. Ik zeg het niet vaak genoeg. **Peet**, dank je wel voor je interesse in mijn werk. Als bioloog kan ik zelfs inhoudelijk met je over mijn werk praten, dat is heel fijn. Ook **Kitty** bedankt voor je steun. **Daan**, **Willemijn** en de meiden+1, bedankt voor jullie voorbeeld en gezelligheid. Ook mijn lieve schoonfamilie **Anke**, **Ton**, **Lidwine**, **Jasper** en **Ivar**: bedankt voor jullie support.

Faab, de laatste woorden zijn natuurlijk voor jou. Afgelopen jaren waren af en toe best heftig. We hebben enorm veel avontuur beleefd samen. Sterker nog: we zitten midden in ons nieuwste avontuur! Bedankt voor het aanhoren van soms onbegrijpelijk gebrabbel, voor je onvoorwaardelijke steun, geduld en begrip gedurende mijn PhD. Je hebt me geleerd hoe ik sommige dingen kan aanpakken op werk, en helpt me mijn soms chaotische gedachten te beteugelen. Ik prijs me enorm rijk met jou aan mijn zijde. Je blijft me verbazen. En 'verblijden' met slechte grappen. Dank je wel voor alles.

Loes

COLOFON
Achieving specificity in redox signaling and redox regulation of protein function
PhD thesis, Utrecht University, the Netherlands
ISBN/EAN: 978-90-393-7461-0

Cover art: Beyond trees by Noortje Haegens
Layout: Yasmin Katlich
Printing: Ipskamp printing